

# **Minimum Detectable Concentrations with Typical Radiation Survey for Instruments for Various Contaminants and Field Conditions**

## AVAILABILITY OF REFERENCE MATERIALS IN NRC PUBLICATIONS

### NRC Reference Material

As of November 1999, you may electronically access NUREG-series publications and other NRC records at NRC's Library at [www.nrc.gov/reading-rm.html](http://www.nrc.gov/reading-rm.html). Publicly released records include, to name a few, NUREG-series publications; *Federal Register* notices; applicant, licensee, and vendor documents and correspondence; NRC correspondence and internal memoranda; bulletins and information notices; inspection and investigative reports; licensee event reports; and Commission papers and their attachments.

NRC publications in the NUREG series, NRC regulations, and Title 10, "Energy," in the *Code of Federal Regulations* may also be purchased from one of these two sources.

#### 1. The Superintendent of Documents

U.S. Government Publishing Office  
Washington, DC 20402-0001  
Internet: [bookstore.gpo.gov](http://bookstore.gpo.gov)  
Telephone: (202) 512-1800  
Fax: (202) 512-2104

#### 2. The National Technical Information Service

5301 Shawnee Road  
Alexandria, VA 22312-0002  
[www.ntis.gov](http://www.ntis.gov)  
1-800-553-6847 or, locally, (703) 605-6000

A single copy of each NRC draft report for comment is available free, to the extent of supply, upon written request as follows:

Address: **U.S. Nuclear Regulatory Commission**  
Office of Administration  
Multimedia, Graphics, and Storage &  
Distribution Branch  
Washington, DC 20555-0001  
E-mail: [distribution.resource@nrc.gov](mailto:distribution.resource@nrc.gov)  
Facsimile: (301) 415-2289

Some publications in the NUREG series that are posted at NRC's Web site address [www.nrc.gov/reading-rm/doc-collections/nuregs](http://www.nrc.gov/reading-rm/doc-collections/nuregs) are updated periodically and may differ from the last printed version. Although references to material found on a Web site bear the date the material was accessed, the material available on the date cited may subsequently be removed from the site.

### Non-NRC Reference Material

Documents available from public and special technical libraries include all open literature items, such as books, journal articles, transactions, *Federal Register* notices, Federal and State legislation, and congressional reports. Such documents as theses, dissertations, foreign reports and translations, and non-NRC conference proceedings may be purchased from their sponsoring organization.

Copies of industry codes and standards used in a substantive manner in the NRC regulatory process are maintained at—

#### The NRC Technical Library

Two White Flint North  
11545 Rockville Pike  
Rockville, MD 20852-2738

These standards are available in the library for reference use by the public. Codes and standards are usually copyrighted and may be purchased from the originating organization or, if they are American National Standards, from—

#### American National Standards Institute

11 West 42nd Street  
New York, NY 10036-8002  
[www.ansi.org](http://www.ansi.org)  
(212) 642-4900

Legally binding regulatory requirements are stated only in laws; NRC regulations; licenses, including technical specifications; or orders, not in NUREG-series publications. The views expressed in contractor prepared publications in this series are not necessarily those of the NRC.

The NUREG series comprises (1) technical and administrative reports and books prepared by the staff (NUREG-XXXX) or agency contractors (NUREG/CR-XXXX), (2) proceedings of conferences (NUREG/CP-XXXX), (3) reports resulting from international agreements (NUREG/IA-XXXX), (4) brochures (NUREG/BR-XXXX), and (5) compilations of legal decisions and orders of the Commission and Atomic and Safety Licensing Boards and of Directors' decisions under Section 2.206 of NRC's regulations (NUREG-0750).

**DISCLAIMER:** This report was prepared as an account of work sponsored by an agency of the U.S. Government. Neither the U.S. Government nor any agency thereof, nor any employee, makes any warranty, expressed or implied, or assumes any legal liability or responsibility for any third party's use, or the results of such use, of any information, apparatus, product, or process disclosed in this publication, or represents that its use by such third party would not infringe privately owned rights.

# **Minimum Detectable Concentrations with Typical Radiation Survey for Instruments for Various Contaminants and Field Conditions**

Manuscript Completed: August 2020

Date Published: August 2020

Prepared by:  
E.W. Abelquist\*  
J.P. Clements  
A.M. Huffert  
D.A. King\*  
T.J. Vitkus\*  
B.A. Watson

Division of Decommissioning, Uranium Recovery,  
and Waste Programs  
Office of Nuclear Material Safety and Safeguards  
U.S. Nuclear Regulatory Commission  
Washington, DC 20555-0001

\*Oak Ridge Associated Universities  
1299 Bethel Valley Road Oak Ridge, TN 37830

John Clements, NRC Project Manager

Office of Nuclear Material Safety and Safeguards



## ABSTRACT

This document describes and quantitatively evaluates the effects of various factors on the detection sensitivity of commercially available portable field instruments being used to conduct radiological surveys in support of decommissioning. Facilities licensed by the U.S. Nuclear Regulatory Commission (NRC) must demonstrate that residual radioactivity at their site meets radiological dose-based criteria for license termination, such as the criterion of 25 millirem per year for unrestricted release in “Radiological Criteria for License Termination” (the License Termination Rule), Subpart E to Title 10 of the Code of Federal Regulations Part 20, “Standards for Protection against Radiation.” These dose-based criteria are often expressed as concentration-based screening values for structural surface contamination in units of disintegrations per minute per 100 square centimeters and for surface soil contamination in units of picocuries per gram. As described in NUREG-1575, Revision 1, “Multi-Agency Radiation Site Survey and Investigation Manual (MARSSIM),” issued August 2000, radiological survey instruments are used to measure radiation levels that are then directly compared to the release criteria.

Since publication of the original NUREG-1507 in 1998, licensees have increasingly used additional survey instrumentation and data capture tools, including global positioning system (GPS) and geographic information system (GIS) technologies. Survey techniques and calculation methodologies have changed over the interim period along with the introduction of advanced radiation survey instruments. This document introduces some concepts related to GPS/GIS based techniques and methodologies along with considerations for detection efficiency calculations, background interferences, signal degradation, and other topics associated with radiation survey instrumentation.

The purpose of this document is three-fold. First, the data were used to determine the validity of the theoretical minimum detectable concentrations that licensees calculate by using traditional *a priori* decision rules and to discuss GPS/GIS technologies that support *a posteriori* decision rules. Second, the results of the study provide guidance to licensees for (a) selection and proper use of portable survey instruments and (b) understanding the effect of field conditions and the limitations and capabilities of those instruments. Third, the NUREG emphasizes the use of data quality objectives that are developed while considering project- and instrument-specific inputs.

### Paperwork Reduction Act

This NUREG provides voluntary guidance for implementing the mandatory information collections in 10 CFR Parts 20 and 50 that are subject to the Paperwork Reduction Act of 1995 (44 U.S.C. 3501 et. seq.). These information collections were approved by the Office of Management and Budget, approval numbers 3150-0014 and 3150-0011. Send comments regarding this information collection to the Information Services Branch (T6-A10M), U.S. Nuclear Regulatory Commission, Washington, DC 20555-0001, or by e-mail to [Infocollects.Resource@nrc.gov](mailto:Infocollects.Resource@nrc.gov), and to the OMB reviewer at: OMB Office of Information and Regulatory Affairs (3150-0014 and 3150-0011), Attn: Desk Officer for the Nuclear Regulatory Commission, 725 17th Street, NW Washington, DC 20503; e-mail: [oira\\_submission@omb.eop.gov](mailto:oira_submission@omb.eop.gov).

**Public Protection Notification**

The NRC may not conduct or sponsor, and a person is not required to respond to, a collection of information unless the document requesting or requiring the collection displays a currently valid OMB control number.

# TABLE OF CONTENTS

|   |             |
|---|-------------|
| <b>ABSTRACT .....</b>   | <b>iii</b>  |
| <b>TABLE OF CONTENTS.....</b>   | <b>v</b>    |
| <b>LIST OF FIGURES.....</b>   | <b>ix</b>   |
| <b>LIST OF TABLES .....</b>   | <b>xiii</b> |
| <b>ACKNOWLEDGMENTS .....</b>  | <b>xix</b>  |
| <b>ABBREVIATIONS AND ACRONYMS .....</b>   | <b>xxi</b>  |
| <b>1 INTRODUCTION.....</b>  | <b>1-1</b>  |
| 1.1 Background .....  | 1-1         |
| 1.2 Need for this Report .....  | 1-2         |
| 1.3 Scope .....   | 1-2         |
| 1.4 Methodology.....  | 1-3         |
| <b>2 INSTRUMENTATION.....</b>   | <b>2-1</b>  |
| 2.1 Gas Proportional Detectors .....  | 2-1         |
| 2.2 Geiger-Mueller Detectors .....  | 2-1         |
| 2.3 Zinc Sulfide Scintillation Detectors .....                                      | 2-1         |
| 2.4 Plastic Scintillation Detectors .....   | 2-1         |
| 2.5 Sodium Iodide Scintillation Detectors .....                                     | 2-2         |
| 2.6 Nonplanar Detectors .....   | 2-2         |
| 2.7 Ratemeter-Scalers .....   | 2-2         |
| 2.8 Pressurized Ionization Chamber .....  | 2-2         |
| 2.9 Dose Ratemeters .....   | 2-2         |
| 2.10 Portable Gamma Spectrometer.....   | 2-3         |
| 2.10.1 Low-Resolution Spectrometers .....   | 2-3         |
| 2.10.2 High-Resolution Spectrometers .....  | 2-3         |
| 2.11 Laboratory Instrumentation .....   | 2-4         |
| 2.12 Additional Instrumentation.....  | 2-4         |
| <b>3 STATISTICAL INTERPRETATIONS OF MINIMUM<br/>DETECTABLE CONCENTRATIONS .....</b> | <b>3-1</b>  |
| 3.1 Fundamental Concepts of MDC .....   | 3-1         |
| 3.2 Review of Expressions of MDC.....   | 3-5         |
| <b>4 VARIABLES AFFECTING INSTRUMENT MINIMUM DETECTABLE<br/>CONCENTRATIONS.....</b>  | <b>4-1</b>  |
| 4.1 Radionuclide Sources for Calibration .....                                      | 4-7         |
| 4.2 Source-to-Detector Distance .....   | 4-8         |
| 4.3 Window Density Thickness .....  | 4-9         |
| 4.4 Source Geometry Factors .....   | 4-10        |
| 4.5 Ambient Background Count Rate.....  | 4-11        |

|          |   |            |
|----------|---|------------|
| <b>5</b> | <b>VARIABLES AFFECTING MINIMUM DETECTABLE CONCENTRATIONS<br/>IN THE FIELD .....</b>                       | <b>5-1</b> |
| 5.1      | Background Count Rates for Various Materials .....  | 5-1        |
| 5.2      | Backscatter Effects.....  | 5-2        |
| 5.3      | Effects of Surface Condition on Detection Sensitivity .....   | 5-3        |
| 5.3.1    | Surface Preparation .....   | 5-3        |
| 5.3.2    | Measurement Results for Various Surface Types.....  | 5-4        |
| 5.4      | Attenuation Effects of Overlaying Material (Self-Absorption) .....  | 5-6        |
| 5.4.1    | Methodology.....  | 5-6        |
| 5.4.2    | Measurement of Various Surface Coatings .....   | 5-7        |
| 5.5      | Use of Alpha and/or Beta Measurements to Assess Surface Activity .....                                    | 5-10       |
| 5.6      | The Effects of Radon Progeny and Beryllium-7 on Detection Sensitivity .....                               | 5-13       |
| 5.6.1    | Interferences from Radon Decay Products .....   | 5-13       |
| 5.6.2    | Interferences from Beryllium-7 .....  | 5-15       |
| 5.7      | Potential Impacts of Signal Degradation .....   | 5-15       |
| 5.7.1    | Signal Degradation Investigation Design .....   | 5-16       |
| 5.7.2    | Plateauing Overview .....   | 5-16       |
| 5.7.3    | Signal Degradation Investigation Results—Peak Voltage.....  | 5-17       |
| 5.7.4    | Signal Degradation Investigation Results—900 Volts .....  | 5-17       |
| 5.7.5    | Results Using Peak Voltage for Detector Setup .....   | 5-18       |
| 5.7.6    | Discussion of Detector Signal Loss.....   | 5-18       |
| 5.7.7    | Conclusions and Recommendations.....  | 5-19       |
| <b>6</b> | <b>SCANNING SENSITIVITY .....</b>   | <b>6-1</b> |
| 6.1      | Introduction.....   | 6-1        |
| 6.2      | Human Factors and <i>A Priori</i> Scan MDC Calculations .....   | 6-2        |
| 6.2.1    | Index of Sensitivity .....  | 6-3        |
| 6.2.2    | Surveyor Efficiency .....   | 6-4        |
| 6.2.3    | Observation Interval .....  | 6-5        |
| 6.2.4    | <i>A Priori</i> Scan MDCs for Building and Structure Surfaces.....  | 6-6        |
| 6.2.5    | <i>A Priori</i> Scan MDCs for Land Areas.....   | 6-11       |
| 6.3      | <i>A Posteriori</i> Decisions Using an Investigation Level .....  | 6-16       |
| 6.3.1    | <i>A Posteriori</i> Investigation Levels .....  | 6-24       |
| 6.3.2    | <i>A Priori</i> MDCRs Versus <i>A Posteriori</i> Investigation Levels Using<br>Radiation Survey Data..... | 6-28       |
| 6.3.3    | <i>A Posteriori</i> Assessment of Surveyor Efficiency .....   | 6-29       |
| 6.4      | Decommissioning Planning and Data Quality Objectives .....  | 6-32       |
| 6.5      | Conclusions and Recommendations.....  | 6-33       |
| <b>7</b> | <b>IN SITU GAMMA SPECTROMETRY AND EXPOSURE RATE<br/>MEASUREMENTS .....</b>                                | <b>7-1</b> |
| 7.1      | Detection Technologies.....   | 7-1        |
| 7.2      | Collimation.....  | 7-2        |
| 7.3      | Efficiency Software.....  | 7-2        |
| 7.4      | Sensitivity Measurements for ISGS Systems.....  | 7-3        |
| 7.5      | Geometric Issues for ISGS Measurements.....   | 7-4        |
| 7.5.1    | Depth Distribution.....   | 7-5        |
| 7.5.2    | Discrete Particles .....  | 7-5        |
| 7.6      | ISGS Measurements in Outdoor Test Area.....   | 7-7        |
| 7.7      | Exposure Rate Measurements in Outdoor Test Area .....   | 7-8        |



|                   |   |             |
|-------------------|---|-------------|
| 7.8               | ISGS Measurement of Scrap Metal.....  | 7-9         |
| <b>8</b>          | <b>LABORATORY INSTRUMENTATION DETECTION LIMITS .....</b>  | <b>8-1</b>  |
| 8.1               | Review of Analytical MDCs.....  | 8-1         |
| 8.2               | Background Activities for Various Soil Types .....  | 8-1         |
| 8.3               | Effects of Soil Condition on MDC .....  | 8-2         |
| 8.3.1             | Effects of Soil Moisture on MDC .....   | 8-3         |
| 8.3.2             | Effects of Soil Density on MDC .....  | 8-3         |
| 8.3.3             | Effects of High-Z Materials on MDC.....   | 8-4         |
| <b>9</b>          | <b>REFERENCES.....</b>  | <b>9-1</b>  |
| <b>10</b>         | <b>NUREG-1507 GLOSSARY .....</b>  | <b>10-1</b> |
| <b>APPENDIX A</b> | <b>CASE STUDY—DETECTOR CALIBRATIONS FOR MIXED<br/>SOURCE/COMPLEX DECAY SERIES CONTAMINATION<br/>FIELDS, METHODS, AND EXAMPLES .....</b> | <b>A-1</b>  |



## LIST OF FIGURES

|             |  |      |
|-------------|--|------|
| Figure 3-1  | Critical Level, $L_C$ .....  | 3-7  |
| Figure 3-2  | Detection Limit, $L_D$ .....   | 3-7  |
| Figure 4-1  | MDCs for Gas Proportional Detector ( $\alpha+\beta$ ) Mode for Various Radionuclides .....         | 4-20 |
| Figure 4-2  | MDCs for GM Detector for Various Radionuclides .....   | 4-20 |
| Figure 4-3  | Source-to-Detector Distance Effects on MDC for Higher Energy Beta Emitters .....                   | 4-21 |
| Figure 4-4  | Source-to-Detector Distance Effects on MDC for Lower Energy Beta Emitters .....                    | 4-21 |
| Figure 4-5  | Source-to-Detector Distance Effects on MDC for Alpha-Emitters .....                                | 4-22 |
| Figure 4-6  | Effects of Window Density Thickness on Total Efficiency for Higher Energy Beta-Emitters .....      | 4-22 |
| Figure 4-7  | Effects of Window Density Thickness on Total Efficiency for Lower Energy Beta Emitters .....       | 4-23 |
| Figure 4-8  | Effects of Window Density Thickness on MDC for Higher Energy Beta Emitters .....                   | 4-23 |
| Figure 4-9  | Effects of Window Density Thickness on MDC for Lower Energy Beta Emitters .....                    | 4-24 |
| Figure 4-10 | Effects of Ambient Background on MDC Calculation .....   | 4-24 |
| Figure 5-1  | Effect of Surface Material on Gas Proportional Detector ( $\alpha$ Only) MDC.....                  | 5-53 |
| Figure 5-2  | Effect of Surface Material on Gas Proportional Detector ( $\beta$ Only) MDC.....                   | 5-53 |
| Figure 5-3  | Effects of Oil Density Thickness on Source Efficiency for Various Sources.....                     | 5-54 |
| Figure 5-4  | Effects of Oil Density Thickness on MDC.....   | 5-54 |
| Figure 5-5  | Effects of Paint Density Thickness on Source Efficiency (Gas Proportional— $\alpha+\beta$ ) .....  | 5-55 |
| Figure 5-6  | Effects of Paint Density Thickness on Source Efficiency (Gas Proportional— $\alpha$ -only).....    | 5-55 |
| Figure 5-7  | Effects of Paint Density Thickness on Source Efficiency (Gas Proportional— $\beta$ -Only).....     | 5-56 |
| Figure 5-8  | Effects of Paint Density Thickness on Source Efficiency (GM Detector).....                         | 5-56 |
| Figure 5-9  | Effects of Paint Density Thickness on Source Efficiency (ZnS Scintillation Detector).....          | 5-57 |
| Figure 5-10 | Effects of Dust Density Thickness on Source Efficiency (Gas Proportional— $\alpha + \beta$ ) ..... | 5-57 |
| Figure 5-11 | Effects of Dust Density Thickness on Source Efficiency (Gas Proportional— $\alpha$ -only).....     | 5-58 |

|             |  |      |
|-------------|--|------|
| Figure 5-12 | Effects of Dust Density Thickness on Source Efficiency (Gas Proportional— $\beta$ -Only).....  | 5-58 |
| Figure 5-13 | Effects of Dust Density Thickness on Source Efficiency (GM Detector).....  | 5-59 |
| Figure 5-14 | Effects of Dust Density Thickness on Source Efficiency (ZnS Scintillation Detector).....   | 5-59 |
| Figure 5-15 | Effects of Water Density Thickness on Source Efficiency (Gas Proportional— $\alpha + \beta$ ) .....  | 5-60 |
| Figure 5-16 | Effects of Water Density Thickness on Source Efficiency (Gas Proportional— $\alpha$ -only).....  | 5-60 |
| Figure 5-17 | Effects of Water Density Thickness on Source Efficiency (Gas Proportional— $\beta$ only).....  | 5-61 |
| Figure 5-18 | Effects of Water Density Thickness on Source Efficiency (GM Detector) .....  | 5-61 |
| Figure 5-19 | Effects of Water Density Thickness on Source Efficiency (ZnS Scintillation Detector).....  | 5-62 |
| Figure 5-20 | Effects of Dust Density Thickness on MDC for Various Sources Using the Gas Proportional Detector in $\alpha + \beta$ and $\alpha$ -Only Modes.....                   | 5-62 |
| Figure 5-21 | Effects of Dust Density Thickness on MDC for Various Sources Using the Gas Proportional Detector in $\beta$ -Only Mode.....  | 5-63 |
| Figure 5-22 | Effects of Dust Density Thickness on MDC for Various Sources Using the GM Detector .....   | 5-63 |
| Figure 5-23 | Effects of Dust Density Thickness on MDC for an Alpha Source Using the ZnS Scintillation Detector .....  | 5-64 |
| Figure 5-24 | Overall Effects of Paint, Dust, and Water Density Thickness on Source Efficiency for Various Sources Using the Gas Proportional Detector in $\beta$ -Only Mode ..... | 5-65 |
| Figure 5-25 | Apparatus for Controlling Detector-to-Source Distances.....  | 5-66 |
| Figure 5-26 | Example Voltage Plateau for a New Detector .....   | 5-66 |
| Figure 5-27 | Example Voltage Plateau for a New Detector with a Degraded Signal .....  | 5-67 |
| Figure 5-28 | Example Voltage Plateau for a Detector with a Damaged Crystal .....  | 5-67 |
| Figure 5-29 | Peak Voltages by Subpopulation .....   | 5-68 |
| Figure 5-30 | Quartile Plot of Voltages Producing Peak Detector Responses .....  | 5-68 |
| Figure 5-31 | Counts per Minute for Am-241 by Subpopulation at 900 Volts.....  | 5-69 |
| Figure 5-32 | Counts per Minute for Cs-137 by Subpopulation at 900 Volts.....  | 5-70 |
| Figure 5-33 | Counts per Minute for Co-60 by Subpopulation at 900 Volts .....  | 5-71 |
| Figure 5-34 | Quartile Plot of Response for Am-241 at 900 Volts .....  | 5-72 |
| Figure 5-35 | Quartile Plot of Response for Cs-137 at 900 Volts .....  | 5-73 |
| Figure 5-36 | Quartile Plot of Response for Co-60 at 900 Volts.....  | 5-74 |
| Figure 5-37 | Counts Obtained at Peak Voltage, Cs-137 Source .....   | 5-75 |

|             |   |      |
|-------------|---|------|
| Figure 5-38 | Quartile Plot of Response for Cs-137 at Peak Voltage .....  | 5-76 |
| Figure 5-39 | Counts Obtained at Cs-137 Peak Voltage, Co-60 Source .....  | 5-77 |
| Figure 5-40 | Counts Obtained at Cs-137 Peak Voltage, Am-241 Source.....  | 5-78 |
| Figure 5-41 | Gamma Detection Using an NaI Scintillator and a PMT (Hamamatsu,<br>2007) .....  | 5-78 |
| Figure 6-1  | Signal Detection Theory Measures of Sensitivity ( $d'$ ) and Criterion Shown<br>Relative to Assumed Underlying Distributions..... | 6-50 |
| Figure 6-2  | Example NaI Scintillation Detector Response as a Function of Gamma<br>Energy .....  | 6-50 |
| Figure 6-3  | Example Histogram of Normally Distributed Background Dataset .....  | 6-51 |
| Figure 6-4  | Example Q-Q Plot of Normally Distributed Background Dataset.....  | 6-51 |
| Figure 6-5  | Example Q-Q Plot of Bimodal Distributed Background Dataset.....   | 6-52 |
| Figure 6-6  | Example Background Frequency Distribution .....   | 6-52 |
| Figure 6-7  | Example Background and Background Plus Signal at the Initial<br>3,000 cpm-to-Concentration Ratio.....                             | 6-53 |
| Figure 6-8  | Example Background and Background Plus Signal at the Initial<br>5,000 cpm-to-Concentration Ratio.....                             | 6-54 |
| Figure 6-9  | Example Background and Background Plus Signal at the Initial<br>2,000 cpm-to-Concentration Ratio.....                             | 6-55 |
| Figure 6-10 | Example 1 Background Population and Investigation Level.....  | 6-56 |
| Figure 6-11 | Example 2 Medium-Specific Populations and Investigation Levels.....   | 6-56 |
| Figure 6-12 | Example 3 Background Population and Investigation Level.....  | 6-57 |
| Figure 6-13 | Example 4 Site Data Populations and Associated Investigation Levels.....  | 6-57 |
| Figure 6-14 | Hidden Source Identified Using Background or Site Data To Establish<br>Investigation Levels .....                                 | 6-58 |
| Figure 6-15 | Gross MDCRs and Investigation Levels for $i = 1$ and $p = 0.5$ .....  | 6-59 |
| Figure 6-16 | Gross MDCRs and Investigation Levels for $i = 1$ and $p = 0.75$ .....   | 6-60 |
| Figure 6-17 | Gross MDCRs and Investigation Levels for $i = 2$ and $p = 0.5$ .....  | 6-61 |
| Figure 6-18 | Gross MDCRs and Investigation Levels for $i = 2$ and $p = 0.75$ .....   | 6-62 |
| Figure 7-1  | Hexagonal Circle Packing and Reduced Center-to-Center Distances to<br>Increase Overlap of FOVs .....                              | 7-18 |
| Figure 7-2  | Co-60 ISGS Results in Outdoor Test Area .....   | 7-18 |
| Figure 7-3  | Exposure Rate Measurements in the Outdoor Test Area.....  | 7-19 |
| Figure 8-1  | Efficiency versus Energy for Various Densities .....  | 8-7  |
| Figure A-1  | Example Alpha Detector Source Calibration Curve .....   | A-22 |
| Figure A-2  | Example Beta Detector Source Calibration Curve .....  | A-23 |
| Figure A-3  | Exhibit 1. C-14 and Tc-99, Beta-Only, Gas Proportional Detector.....  | A-41 |

|             |  |      |
|-------------|--|------|
| Figure A-4  | Exhibit 2. Ni-63, Co-60 and Cs-137, Beta-Only, Gas Proportional Detector ....                    | A-43 |
| Figure A-5  | Exhibit 3a. Am-241, H-3, Cs-137 and SrY-90, Alpha Plus Beta, Plastic Scintillator Detector ..... | A-45 |
| Figure A-6  | Exhibit 3b - Alpha. Am-241, H-3, Cs-137 and SrY-90, Alpha-Only, Gas Proportional Detector .....  | A-47 |
| Figure A-7  | Exhibit 3b - Beta. Am-241, H-3, Cs-137, and SrY-90, Beta-Only, Gas Proportional Detector .....   | A-49 |
| Figure A-8  | Exhibit 4a. Th-232 Plus Decay Series, Alpha Plus Beta, Gas Proportional Detector.....            | A-51 |
| Figure A-9  | Exhibit 4b. Th-232 Plus Decay Series, Beta-Only, Gas Proportional Detector.....                  | A-53 |
| Figure A-10 | Exhibit 4c. Th-232 Plus Decay Series, Alpha-Only, Gas Proportional Detector.....                 | A-55 |
| Figure A-11 | Exhibit 5a. Processed U-Aged Yellow Cake, Alpha-Only, ZnS Detector.....                          | A-57 |
| Figure A-12 | Exhibit 5b. Processed U-Aged Yellow Cake, Beta-Only, GM Detector .....                           | A-59 |
| Figure A-13 | Exhibit 5c. Processed U-Pregnant Lixiviant, Alpha-Only, Dual Phoswich (ZnS) Detector.....        | A-61 |
| Figure A-14 | Exhibit 5d. Processed U-Pregnant Lixiviant, Beta-Only, Dual Phoswich (Plastic Scintillator)..... | A-63 |
| Figure A-15 | Exhibit 5e. Unprocessed U Ore, Alpha Plus Beta, Gas Proportional Detector .....                  | A-65 |
| Figure A-16 | Exhibit 6a. Enriched U, Alpha-Only, Gas Proportional Detector .....                              | A-67 |
| Figure A-17 | Exhibit 6b. Enriched U and Tc-99, Alpha Plus Beta, Gas Proportional Detector.....                | A-69 |
| Figure A-18 | Exhibit 7a. Processed U Tailings, Alpha Plus Beta, Gas Proportional Detector.....                | A-71 |
| Figure A-19 | Exhibit 7b. Processed U Tailings, Beta-Only, GM Detector .....                                   | A-73 |
| Figure A-20 | Exhibit 8a. Ra-226 Plus Decay Series, Alpha Plus Beta, Gas Proportional Detector.....            | A-75 |
| Figure A-21 | Exhibit 8b. Ra-226 Plus Decay Series, Alpha Plus Beta, Gas Proportional Detector .....           | A-77 |

## LIST OF TABLES

|            |   |      |
|------------|---|------|
| Table 3-1  | MDC Results for Data Obtained from Gas Proportional Detector Using Various MDC Expressions .....            | 3-6  |
| Table 4-1  | Characteristics of Radionuclide Sources Used for Calibration and Static Measurements .....                  | 4-12 |
| Table 4-2  | Average Total Efficiencies for Various Detectors and Radionuclides .....                                    | 4-12 |
| Table 4-3  | MDCs for Various Detectors and Radionuclides .....  | 4-13 |
| Table 4-4  | Instrument Efficiencies .....   | 4-14 |
| Table 4-5  | Source-to-Detector Distance Effects for Beta-Emitters .....   | 4-14 |
| Table 4-6  | Source-to-Detector Distance Effects for Beta-Emitters .....   | 4-15 |
| Table 4-7  | MDCs for Various Source-to-Detector Distances for Beta-Emitters .....                                       | 4-15 |
| Table 4-8  | MDCs for Various Source-to-Detector Distances for Alpha-Emitters .....                                      | 4-16 |
| Table 4-9  | Window Density Thickness Effects for Beta-Emitters .....  | 4-16 |
| Table 4-10 | Window Density Thickness Effects for Beta-Emitters .....  | 4-17 |
| Table 4-11 | Source Geometry Effects on Instrument Efficiency .....  | 4-18 |
| Table 4-12 | Ambient Background Effects .....  | 4-19 |
| Table 5-1  | Background Count Rate for Various Materials .....   | 5-20 |
| Table 5-2  | MDCs for Various Materials .....  | 5-21 |
| Table 5-3  | Efficiencies and Backscatter Factors for SrY-90 .....   | 5-21 |
| Table 5-4  | Surface Material Effects on Source Efficiency for Tc-99 Distributed on Various Surfaces .....               | 5-22 |
| Table 5-5  | Surface Material Effects on Source Efficiency for Th-230 Distributed on Various Surfaces .....              | 5-23 |
| Table 5-6  | Surface Material Effects on MDC for Tc-99 and Th-230 Distributed on Various Surfaces .....                  | 5-24 |
| Table 5-7  | Effects of Oil Density Thickness on Source Efficiency and MDC (Gas Proportional— $\alpha + \beta$ ) .....   | 5-25 |
| Table 5-8  | Effects of Paint Density Thickness on Source Efficiency and MDC (Gas Proportional— $\alpha + \beta$ ) ..... | 5-26 |
| Table 5-9  | Effects of Paint Density Thickness on Source Efficiency and MDC .....                                       | 5-27 |
| Table 5-10 | Effects of Paint Density Thickness on Source Efficiency and MDC (Gas Proportional— $\beta$ Only) .....      | 5-28 |
| Table 5-11 | Effects of Paint Density Thickness on Source Efficiency and MDC (GM Detector) .....                         | 5-29 |
| Table 5-12 | Effects of Paint Density Thickness on Source Efficiency and MDC .....                                       | 5-30 |
| Table 5-13 | Effects of Dust Density Thickness on Source Efficiency and MDC (Gas Proportional— $\alpha + \beta$ ) .....  | 5-31 |

|            |  |      |
|------------|--|------|
| Table 5-14 | Effects of Dust Density Thickness on Source Efficiency and MDC (Gas Proportional— $\alpha$ -Only) .....  | 5-32 |
| Table 5-15 | Effects of Dust Density Thickness on Source Efficiency and MDC (Gas Proportional— $\beta$ -Only) .....   | 5-33 |
| Table 5-16 | Effects of Dust Density Thickness on Source Efficiency and MDC (GM Detector) .....   | 5-34 |
| Table 5-17 | Effects of Dust Density Thickness on Source Efficiency and MDC (ZnS Scintillation Detector) .....  | 5-35 |
| Table 5-18 | Effects of Water Density Thickness on Source Efficiency and MDC (Gas Proportional— $\alpha+\beta$ /C-14) .....   | 5-36 |
| Table 5-19 | Effects of Water Density Thickness on Source Efficiency and MDC (Gas Proportional— $\alpha+\beta$ /Tc-99) .....  | 5-37 |
| Table 5-20 | Effects of Water Density Thickness on Source Efficiency and MDC (Gas Proportional— $\alpha+\beta$ /SrY-90) .....   | 5-38 |
| Table 5-21 | Effects of Water Density Thickness on Source Efficiency and MDC (Gas Proportional— $\alpha$ Only) .....  | 5-39 |
| Table 5-22 | Effects of Water Density Thickness on Source Efficiency and MDC (Gas Proportional— $\beta$ Only/C-14) .....  | 5-40 |
| Table 5-23 | Effects of Water Density Thickness on Source Efficiency and MDC (Gas Proportional— $\beta$ Only/Tc-99) .....   | 5-41 |
| Table 5-24 | Effects of Water Density Thickness on Source Efficiency and MDC (Gas Proportional— $\beta$ Only/SrY-90) .....  | 5-42 |
| Table 5-25 | Effects of Water Density Thickness on Source Efficiency and MDC (GM Detector/C-14) .....   | 5-43 |
| Table 5-26 | Effects of Water Density Thickness on Source Efficiency and MDC (GM Detector/Tc-99) .....  | 5-44 |
| Table 5-27 | Effects of Water Density Thickness on Source Efficiency and MDC (GM Detector/SrY-90) .....   | 5-45 |
| Table 5-28 | Effects of Water Density Thickness on Source Efficiency and MDC (ZnS Scintillation Detector) .....   | 5-46 |
| Table 5-29 | Total Efficiencies for Detectors Used To Assess Uranium Surface Activity .....   | 5-47 |
| Table 5-30 | Normalized Total Efficiencies for Processed Uranium with Various Absorber Thicknesses .....  | 5-48 |
| Table 5-31 | Detector Efficiency for Low-Enriched Uranium (3 Percent) Using a 126-cm <sup>2</sup> Proportional Detector with a 0.4-mg/cm <sup>2</sup> Window (Gas Proportional— $\alpha + \beta$ ) .... | 5-48 |
| Table 5-32 | Detector Efficiency for Low-Enriched Uranium (3 Percent) Using a 126-cm <sup>2</sup> Proportional Detector with a 3.8-mg/cm <sup>2</sup> Window (Gas Proportional— $\beta$ only) .....     | 5-48 |
| Table 5-33 | Raw Voltages Producing the Peak Response by Subpopulation .....  | 5-49 |
| Table 5-34 | Statistical Analysis for Peak Response Investigation .....   | 5-50 |
| Table 5-35 | Raw Results for 900-Volt Default Setting .....   | 5-50 |



|            |  |      |
|------------|--|------|
| Table 5-36 | Statistical Analysis for 900-Volt Default Investigation—Am-241 Source .....  | 5-51 |
| Table 5-37 | Statistical Analysis for 900-Volt Default Investigation—Cs-137 Source .....  | 5-52 |
| Table 5-38 | Statistical Analysis for 900-Volt Default Investigation—Co-60 Source .....   | 5-52 |
| Table 5-39 | Statistical Analysis for Peak Voltage Investigation—Cs-137 Source.....   | 5-52 |
| Table 6-1  | Values of d' for Selected True Positive and False Positive Proportions .....   | 6-35 |
| Table 6-2  | Scanning Sensitivity (MDCR) of the Ideal Observer for Various Background<br>Levels.....  | 6-35 |
| Table 6-3  | NaI Scintillation Detector Count Rate versus Exposure Rate (cpm per $\mu$ R/h).....  | 6-36 |
| Table 6-4  | Activity Fraction Estimates for Various Enrichments of Uranium.....  | 6-37 |
| Table 6-5  | NaI Scintillation Detector Scan MDCs for Common Radiological<br>Contaminants—Example 1 .....                                       | 6-38 |
| Table 6-6  | NaI Scintillation Detector Scan MDCs for Common Radiological<br>Contaminants—Example 2 .....                                       | 6-39 |
| Table 6-7  | NaI Scintillation Detector Scan MDCs for Common Radiological<br>Contaminants—Example 3.....  | 6-40 |
| Table 6-8  | NaI Scintillation Detector Scan MDCs ERC and CPMR Input Values .....   | 6-41 |
| Table 6-9  | Land Surveys without Headphones .....  | 6-42 |
| Table 6-10 | Land Surveys with Headphones .....   | 6-42 |
| Table 6-11 | Wall Surveys without Headphones .....  | 6-43 |
| Table 6-12 | Wall Surveys with Headphones .....   | 6-44 |
| Table 6-13 | Test Results for Headphones versus No Headphones.....  | 6-45 |
| Table 6-14 | Correlations Comparing Time, Coverage, and Percent Found.....  | 6-46 |
| Table 6-15 | Parallel DQOs for Hypothetical Radium Sites .....  | 6-47 |
| Table 7-1  | Important Parameters for ISGS Measurements .....   | 7-11 |
| Table 7-2  | Discrete Source MDAs at 1-Meter Detector Height .....  | 7-14 |
| Table 7-3  | Discrete Source MDAs at 2-Meter Detector Height .....  | 7-15 |
| Table 7-4  | ISGS Data from Outdoor Test Area.....  | 7-16 |
| Table 7-5  | Exposure Rate Measurements from Outdoor Test Area.....   | 7-16 |
| Table 7-6  | Calculated Total Activity for Selected Radionuclides Using Mass-Based,<br>Critical Group Dose Factors for Steel (106 grams).....   | 7-17 |
| Table 7-7  | Efficiency and MDA Summary for ISGS Measurements of Scrap Steel<br>Pallet with a 10-Minute Count Time .....                        | 7-17 |
| Table 7-8  | Calculated Total Activity for Selected Radionuclides Using Mass-Based,<br>Critical Group Dose Factors for Copper (106 grams) ..... | 7-17 |
| Table 7-9  | Efficiency and MDA Summary for ISGS Measurements of Scrap Copper<br>Pallet with a 30-Minute Count Time .....                       | 7-17 |

|            |  |      |
|------------|--|------|
| Table 8-1  | Typical Radionuclide Concentrations Found in Background Soil Samples in the United States.....                         | 8-5  |
| Table 8-2  | Effects of Moisture Content on Gamma Spectrometry Analyses.....  | 8-5  |
| Table 8-3  | Effects of High-Z Content on Gamma Spectrometry Analyses.....  | 8-6  |
| Table A-1  | ROC, Calibration Source, Detector Specifications, and Efficiency Calculations.....                                     | A-5  |
| Table A-2  | ROC, Calibration Source, Detector Specifications, and Efficiency Calculations for Newly Processed Natural Uranium..... | A-6  |
| Table A-3  | ROC, Calibration Source, Detector Specifications, and Efficiency Calculations for Aged Processed Natural Uranium.....  | A-8  |
| Table A-4  | Comparative Relative RFs for Surface Activity Result Reporting for Aged Processed Natural Uranium.....                 | A-10 |
| Table A-5  | ROC, Efficiency Calculations for Aged Processed Natural Uranium.....   | A-11 |
| Table A-6  | ROC, Efficiency Calculations for Aged Processed Natural Uranium.....   | A-12 |
| Table A-7  | Exhibit Number and Radionuclides of Concern.....   | A-17 |
| Table A-8  | Case-Specific Radionuclides, Radiations, and Instrument Inputs.....  | A-18 |
| Table A-9  | Radiation Data for Beta-Emitters.....  | A-19 |
| Table A-10 | Radiation Data for Alpha Emitters.....   | A-20 |
| Table A-11 | Calculation Rules Based on the Form of the I/A Levels.....   | A-21 |
| Table A-12 | Calibration Source Data.....   | A-22 |
| Table A-13 | Activity Reporting Options for Thorium Series.....   | A-27 |
| Table A-14 | Radiation Data for Uranium (U-238 and U-235) Decay Series (Unprocessed Ore).....                                       | A-30 |
| Table A-15 | Processed Uranium Ore: Uranium-238 Chain.....  | A-31 |
| Table A-16 | Pregnant Lixiviant.....  | A-31 |
| Table A-17 | Tailings Chain.....  | A-33 |
| Table A-18 | Radon Chain.....   | A-36 |
| Table A-19 | Exhibit 1. C-14 and Tc-99, Beta-Only, Gas Proportional Detector.....   | A-40 |
| Table A-20 | Exhibit 2. Ni-63, Co-60 and Cs-137, Beta-Only, Gas Proportional Detector.....  | A-42 |
| Table A-21 | Exhibit 3a. Am-241, H-3, Cs-137 and SrY-90, Alpha Plus Beta, Plastic Scintillator Detector.....                        | A-44 |
| Table A-22 | Exhibit 3b - Alpha. Am-241, H-3, Cs-137 and SrY-90, Alpha-Only, Gas Proportional Detector.....                         | A-46 |
| Table A-23 | Exhibit 3b - Beta. Am-241, H-3, Cs-137, and SrY-90, Beta-Only, Gas Proportional Detector.....                          | A-48 |
| Table A-24 | Exhibit 4a. Th-232 Plus Decay Series, Alpha Plus Beta, Gas Proportional Detector.....                                  | A-50 |

|            |  |      |
|------------|--|------|
| Table A-25 | Exhibit 4b. Th-232 Plus Decay Series, Beta-Only, Gas Proportional Detector.....                  | A-52 |
| Table A-26 | Exhibit 4c. Th-232 Plus Decay Series, Alpha-Only, Gas Proportional Detector.....                 | A-54 |
| Table A-27 | Exhibit 5a. Processed U-Aged Yellow Cake, Alpha-Only, ZnS Detector.....                          | A-56 |
| Table A-28 | Exhibit 5b. Processed U-Aged Yellow Cake, Beta-Only, GM Detector .....                           | A-58 |
| Table A-29 | Exhibit 5c. Processed U-Pregnant Lixiviant, Alpha-Only, Dual Phoswich (ZnS) Detector.....        | A-60 |
| Table A-30 | Exhibit 5d. Processed U-Pregnant Lixiviant, Beta-Only, Dual Phoswich (Plastic Scintillator)..... | A-62 |
| Table A-31 | Exhibit 5e. Unprocessed U Ore, Alpha Plus Beta, Gas Proportional Detector.....                   | A-64 |
| Table A-32 | Exhibit 6a. Enriched U, Alpha-Only, Gas Proportional Detector .....                              | A-66 |
| Table A-33 | Exhibit 6b. Enriched U and Tc-99, Alpha Plus Beta, Gas Proportional Detector.....                | A-68 |
| Table A-34 | Exhibit 7a. Processed U Tailings, Alpha Plus Beta, Gas Proportional Detector.....                | A-70 |
| Table A-35 | Exhibit 7b. Processed U Tailings, Beta-Only, GM Detector .....                                   | A-72 |
| Table A-36 | Exhibit 8a. Ra-226 Plus Decay Series, Alpha Plus Beta, Gas Proportional Detector.....            | A-74 |
| Table A-37 | Exhibit 8b. Ra-226 Plus Decay Series, Alpha Plus Beta, Gas Proportional Detector.....            | A-76 |



## ACKNOWLEDGMENTS

### *Revision 0 (1998) Acknowledgments*

This report was a collaborative effort by the staff of the Environmental Survey and Site Assessment Program (ESSAP) of the Oak Ridge Institute for Science and Education, Brookhaven National Laboratory, and the Nuclear Regulatory Commission. In addition to writing certain sections, Eric Abelquist, working closely with Tony Huffert and George Powers of the NRC, was responsible for the overall planning and management of this project. Dr. William Brown, Brookhaven National Laboratory, provided input on the human factors associated with scanning and wrote the bulk of Section 6. Many of the detection sensitivity experiments conducted in this report were designed and performed by Elmer Bjelland and Lea Mashburn, while Jim Payne and Scott Potter performed many measurements during development of the feasibility study. Other technical contributors included Wade Adams, Armin Ansari, William L. (Jack) Beck, Dale Condra, Ray Morton, Ann Payne, Steven King, Tim Vitkus, and Duane Quayle. Elaine Waters, Robyn Ellis, Debi Herrera, Tabatha Fox, and Debbie Adams provided much of the word processing support, while Teresa Bright and Dean Herrera produced all of the graphics.

Special thanks to Jim Berger, George Chabot, Bobby Coleman, Ken Swinth, and Ed Walker who performed valuable reviews of the report and provided thoughtful comments, and to all the computer simulation and field survey test participants.

### *Revision 1 (2020) Acknowledgments*

The first revision to this report was again a collaborative effort between the Oak Ridge Associated Universities (ORAU) and the Nuclear Regulatory Commission (NRC). David King of ORAU worked closely with John Clements of the NRC on the planning and management of this revision. Several of the original team members from the 1998 report also provided valuable input to this revision, including Eric Abelquist and Tim Vitkus at ORAU, and Tony Huffert at the NRC.

Many thanks go to numerous reviewers within the NRC and ORAU, and a special thanks goes to Nadine Aridi for her assistance in formatting the final document.



## ABBREVIATIONS AND ACRONYMS

|              |   |
|--------------|---|
| AL           | action level  |
| ANSI         | American National Standards Institute                           |
| ANOVA        | analysis of variance  |
| BEGe         | broad-energy germanium  |
| BTV          | background threshold value                                      |
| c/dis        | counts per disintegration                                       |
| CFR          | Code of Federal Regulations                                     |
| cpm          | counts per minute   |
| CPMR         | count-rate-to-exposure-rate ratio                               |
| DCGL         | derived concentration guideline level                           |
| DQO          | data quality objective  |
| dpm          | disintegrations per minute                                      |
| EFF          | efficiency  |
| EMC          | elevated measurement comparison                                 |
| EPA          | U.S. Environmental Protection Agency                            |
| ERC          | exposure-rate-to-concentration ratio                            |
| ERG          | Environmental Restoration Group                                 |
| FIDLER       | Field Instrument for the Detection of Low Energy Radiation      |
| FOV          | field of view   |
| FR           | Federal Register  |
| GEIS         | generic environmental impact statement                          |
| GeLi         | lithium-drifted germanium                                       |
| GIS          | geographic information system                                   |
| GM           | Geiger-Mueller  |
| GPS          | global positioning system                                       |
| HPGe         | high-purity germanium   |
| IL           | Investigation level   |
| ILPP         | <i>a posteriori</i> investigation level for post processed data |
| ISGS         | in situ gamma spectrometry                                      |
| ISO          | International Organization for Standardization                  |
| keV          | kiloelectron volt   |
| LaBr3        | lanthanum bromide   |
| LTR          | License Termination Rule  |
| MARSSIM      | “Multi-Agency Radiation Site Survey and Investigation Manual”   |
| MD           | minimum detectable  |
| MDA          | minimum detectable activity                                     |
| MDC          | minimum detectable concentration                                |
| MDCR         | minimum detectable count rate                                   |
| MDCRsurveyor | surveyor-specific MDCR  |

|        |   |
|--------|---|
| MeV    | megaelectron volt   |
| NaI    | sodium iodide   |
| NCRP   | National Council on Radiation Protection and Measurements |
| NIST   | National Institute of Standards and Technology            |
| NRC    | U.S. Nuclear Regulatory Commission                        |
| ORAU   | Oak Ridge Associated Universities                         |
| PIC    | pressurized ionization chamber                            |
| PMT    | photo-multiplier tube                                     |
| REGe   | reverse electrode germanium                               |
| RF     | relative fraction   |
| ROI    | region of interest  |
| SP     | subpopulation   |
| SrY    | strontium/yttrium (in secular equilibrium)                |
| UPL    | upper prediction limit                                    |
| USL    | upper simultaneous limit                                  |
| USRADS | ultrasonic ranging and data system                        |
| UTL    | upper tolerance limit                                     |
| WF     | weighting factor  |
| WH     | Wilson Hilferty   |
| ZnS    | zinc sulfide  |



# 1 INTRODUCTION

## 1.1 Background

Facilities licensed by the U.S. Nuclear Regulatory Commission (NRC) are required to demonstrate that residual radioactivity at their site meets the applicable release criteria before the associated license can be terminated. The NRC completed a decommissioning rulemaking effort that culminated in a Federal Register (FR) notice on July 21, 1997 (62 FR 39058), and publication of the final rule as Subpart E, "Radiological Criteria for License Termination" (the License Termination Rule [LTR]) to Title 10 of the Code of Federal Regulations (10 CFR) Part 20, "Standards for Protection against Radiation." The LTR establishes residual contamination criteria for release of facilities for unrestricted and restricted use, as described in 10 CFR 20.1402 and 10 CFR 20.1403, respectively.

The NRC published supplemental information regarding implementation of the LTR in the Federal Register on November 18, 1998 (63 FR 64132); December 7, 1999 (64 FR 68395); and June 13, 2000 (65 FR 37186). This supplemental information establishes concentration-based screening values for structural surface contamination in units of disintegrations per minute per 100 square centimeters (dpm/100 cm<sup>2</sup>) and for surface soil contamination in units of picocuries per gram (pCi/g). These screening values correspond to levels of radionuclide contamination that would be deemed to comply with the dose limit of 25 mrem/yr in 10 CFR 20.1402, "Radiological Criteria for Unrestricted Use," but there are specific conditions under which the screening values can be applied (as discussed in 65 FR 37186). Additional information on the criteria for conducting screening dose modeling evaluations can be found in Appendix H of NUREG-1757, Volume 2, Revision 1. If the criteria for conducting screening dose modeling evaluations are not able to be met, the licensee may also calculate site-specific concentration-based limits. In either case, the radionuclide-specific values that correspond to the dose limit are defined as derived concentration guideline levels (DCGLs).

Licensees decommissioning their facilities are required to demonstrate to the NRC that residual contamination will comply with the NRC dose limit. This demonstration typically includes the collection of radiation survey and sample data that are directly compared to DCGLs. An important factor affecting the radiological survey design is the minimum detectable concentration (MDC) of field survey instruments in relation to the DCGL(s). The MDC may apply to either the concentration of radioactivity on a material surface or within a volume of material. If the DCGLs are lower than the MDC of field survey instruments, extensive additional measurements and/or samples with laboratory analysis may be necessary, significantly impacting the overall cost and schedule of decommissioning projects.

Many terms are used to describe concentration-based decommissioning decision limits (e.g., pCi/g for soil or dpm/100 cm<sup>2</sup> on surfaces). Examples of terms include "cleanup goals," "remediation goals," "release limits," and "authorized limits." This NUREG uses the term DCGL for consistency with NUREG-1575, Revision 1, "Multi-Agency Radiation Survey and Site Investigation Manual (MARSSIM)," issued August 2000, which addresses the decommissioning of land areas and fixed structures (i.e., real property). The release of materials and equipment could become necessary as a result of site decommissioning, and many of the strategies from this NUREG may apply to those cases as well. As stated above, the DCGLs are dose-based residual radioactivity limits applicable to the current LTR. As discussed in MARSSIM and NUREG-1757, "Consolidated Decommissioning Guidance" Volume 1 (Revision 2) and Volume 2

(Revision 1), issued September 2006, the DCGLs may be either site-specific or established screening values. More specifically, there is the  $DCGL_w$ , which is the allowable average concentration over a defined large survey unit (e.g., a land parcel or building surface), and the  $DCGL_{EMC}$ , which is the allowable concentration in a small area of elevated activity (e.g., a hotspot).

As later sections will show, it is important to understand the relationship between radiological contaminant detectability (the MDC) and some action level. For example, data quality objectives (DQOs) are developed during the planning phase of a decommissioning project, and the design should consider whether a detector's MDC is below a required action level, meaning that surveyors can detect concentrations below the limit. If the MDC is higher than the action level, the surveyor should consider alternate detectors, detector configurations, or survey designs. Therefore, this NUREG presents guidance for calculating MDCs that optimize the ability to demonstrate compliance with an applicable action level. This document uses "DCGL" as the single term for the concentration in  $dpm/100\text{ cm}^2$  or  $pCi/g$  that corresponds to the action level.

## **1.2 Need for this Report**

The primary purpose of this NUREG is to provide guidance to licensees for selection and proper use of portable survey instruments. It also aims to give licensees an understanding of the field conditions under which the capabilities of those instruments can be limited and the extent of the limitations.

## **1.3 Scope**

The major emphasis of this study was the evaluation of detection sensitivity for field survey instruments in both the static and scanning modes of operation. The parameters studied for their effects on detection sensitivity included variables that determine the instrument MDC (e.g., probe surface area, radionuclide energy, window density thickness, source to detector geometry) and variables that can affect the instrument detection efficiency in the field (e.g., various surface types and coatings, including painted, scabbled, or wet surfaces). The authors did not expect to obtain empirical data for every possible combination of variables; rather, the emphasis was on establishing the necessary baseline data so that an instrument's response could be accurately predicted under a variety of possible field conditions.

Additionally, the study presents several case studies to demonstrate methods for developing site-specific weighted efficiencies and MDCs for projects that involve mixtures of multiple contaminants and/or radionuclides with complex decay schemes. The methods described should be considered as acceptable for multisource calibrations in lieu of the availability of custom, contaminant-specific calibration sources.

Section 2 describes all instrumentation used in this study. The types of instruments commonly used in the field radiological surveys evaluated in this study include gas proportional, Geiger-Mueller (GM), zinc sulfide ( $ZnS[Ag]$  or  $ZnS$ ) scintillation, and sodium iodide ( $NaI[Tl]$  or  $NaI$ ) scintillation detectors. The study did not intend to compare field survey instruments from different manufacturers (e.g., Ludlum, Eberline, Bicon). In general, the specific instruments used for these measurements are representative of their type; one notable exception is the pressurized ionization chamber (PIC) described in Section 2.8.

Scan MDCs were evaluated for both structural surfaces and land areas. The approach used to determine *a priori* scan MDCs coupled the detector and contamination characteristics with

human factors. That is, if a surveyor can discern a significant increase in a detector's count rate response (i.e., the number of "clicks"), that increase will presumably represent the signal (over noise) associated with a radiological contaminant. Some decommissioning projects do not, however, rely on the surveyors' decisionmaking abilities. These projects may instruct surveyors during the planning phase of a decommissioning project to perform surveys without listening and without attempting to locate hotspots in real time. Data capture technologies are used to record detector response, the date and time of measurements, and the location (i.e., coordinates) of each measurement. Captured data are processed and mapped, and follow-up investigation decisions are made on the basis of actual, rather than predicted, outcomes. This study evaluates methods for making *a posteriori* assessment phase decisions and recommends ways to harmonize *a priori* and *a posteriori* decisionmaking.

This study also addressed the detection sensitivity of some commonly used laboratory procedures. Because most of the information on laboratory procedures and thermoluminescence dosimeters is already available, this information takes the form of a literature review. However, the authors expected that some laboratory measurements would be needed to address specific objectives of the study.

Finally, this report is not intended to be a complete evaluation of the performance of portable survey instrumentation. Several available references give comprehensive information on the performance of health physics instrumentation. One such study (Swinth & Kenoyer, 1985) involves the evaluation of ionization chambers, GM detectors, alpha survey meters, and neutron dose equivalent survey meters according to the draft American National Standards Institute (ANSI) Standard N42.17, "Performance Specifications for Health Physics Instrumentation," issued November 1985. These instruments were subjected to a broad array of testing, including general characteristics, electronic and mechanical requirements, radiation response, interfering responses, and environmental factors. An important result of the cited study was the susceptibility of air- and gas-flow proportional counters to environmental factors such as humidity, elevations, and temperature. The study also concluded that the alpha scintillation detector is relatively stable under variable environmental conditions.

Another study summarized the regulatory requirements and practices of NRC licensees regarding the use of accredited calibration laboratories. That report concluded that more definitive guidance is needed to describe how to perform and document the calibration of survey instruments to demonstrate compliance with the regulatory requirements in NUREG/CR-6062, "Performance of Portable Radiation Survey Instruments," issued December 1993. Other guidance provides design and performance criteria, test and calibration requirements, and operating instruction requirements for portable radiation detection instruments (e.g., ANSI N42.33-2006, "American National Standard for Portable Radiation Detection Instrumentation for Homeland Security," and International Organization for Standardization [ISO] 7503-1, "Evaluation of Surface Contamination—Part 1: Beta Emitters and Alpha Emitters" [1988] and ISO 7503-3:2016, "Measurement of Radioactivity—Measurement and Evaluation of Surface Contamination—Part 3: Apparatus Calibration [2016]).

#### **1.4 Methodology**

During radiological surveys in support of decommissioning, field instruments are generally used to scan surface areas for elevated levels of radiation and to directly measure total surface activity at particular locations. Although the surface scans and direct measurements can be made with the same instruments, the two procedures have very different MDCs. Scanning can have a much higher MDC than a static count, depending on scanning speed, distance of the

probe to the surface, and other instrument factors. The “human factor,” described in Section 6.2, also affects the scanning MDC. Therefore, when applicable, this study determined the MDC of each instrument for both the scanning and static modes of operation.

Several statistical interpretations of the MDC concept can result in different MDC values for an instrument, even for the same set of data. In this study, the specific approach for statistical interpretation of the data was selected after a thorough review of the relevant literature. This work also includes a sensitivity study, evaluating the quantitative effects of various statistical treatments on the MDC (Section 3).

Oak Ridge Associated Universities (ORAU) in Oak Ridge, TN, performed most of the studies. A measurement hood, constructed of Plexiglas, provided a controlled environment in which to obtain measurements with minimal disturbances from ambient airflow. The Plexiglas measurement hood, measuring 93 centimeters in length, 60 centimeters in height, and 47 centimeters in depth, was equipped with a barometer and thermometer to measure ambient pressure and temperature within the chamber. Measurements were performed within the measurement hood using a detector source jig to ensure that the detector to source geometry was reproducible for all parameters studied. Various field conditions were simulated, under well-controlled and reproducible conditions. Special sources were constructed and characterized in ORAU laboratories to meet the specific objectives of this study. On the basis of the empirical results of these studies, sets of normalized curves were constructed that would indicate instrument response as a function of source energy, geometry, background radiation level, and other parameters, including source-to-detector distance, window density thickness, and density thickness of overlaying material.

The quantitative data were treated and reported in accordance with U.S. Environmental Protection Agency (EPA) guidance in HPSR-1, “Upgrading Environmental Radiation Data” issued August 1980. Data were reported with an unambiguous statement of the uncertainty. The assessment of the uncertainty included an estimate of the combined overall uncertainty. Random uncertainties associated with measurement parameters (e.g., number of counts, weight, volume) were propagated to determine an overall uncertainty. It was generally assumed that measurement parameters were statistically independent; therefore, the propagation of errors did not consider any covariance terms. Uncertainties were also propagated in the MDC determination to provide a measure of the overall uncertainty in the MDC from both counting errors and other sources of error (e.g., detector efficiency, source efficiency, calibration source activity).

Guidance from the ISO 7503 standards (1988 and 2016) was utilized in the development of this report. The 2016 update to the ISO 7503 series occurred during the drafting of Revision 1 of this NUREG. As such, a comparison of the 1988 and 2016 ISO 7503 standards was performed in order to determine if it is necessary to update methods and terminology for the sake of Revision 1, while recognizing that many of the MDC methods, equations, and terminology currently used in practice were directly resultant from the 1988 series. As a result, this NUREG considers aspects from both the original and revised ISO 7503 series (1988 and 2016, respectively). For example, many of the traditional definitions, such as detector and source efficiency, found in ISO 7503-1:1988, are used to be consistent with current industry methods also presented in MARSSIM and other references commonly used during a decommissioning action. Additionally, this NUREG considers weighted efficiency calculations similar to those described in ISO 7503-3:2016 to more accurately predict detector responses. A more detailed discussion of the ISO 7503 series comparison is provided in Section 4 of this report. (Note: Further references to ISO 7503 will include the appropriate publication year [1988 or 2016].)

Experts at several other facilities were contacted to discuss various aspects of this study, such as the statistical approaches to MDC measurements and methods for construction of calibration sources, and to obtain calibration sources already constructed that could be used in this study. These institutions included the National Institute of Standards and Technology (NIST), the U.S. Department of Energy's Environmental Measurements Laboratory, Argonne National Laboratory, Pacific Northwest National Laboratory, and Oak Ridge National Laboratory. ORAU also collaborated with Brookhaven National Laboratory to address the "human factor" in performing radiological scan surveys (Section 6.2).



## 2 INSTRUMENTATION

### 2.1 Gas Proportional Detectors

Gas proportional detectors are used for detecting both alpha and beta radiation. This study used Ludlum model 43 68 detectors, with a physical probe area of 126 cm<sup>2</sup> (the effective probe area is 100 cm<sup>2</sup>, which accounts for the fraction of the probe area covered by the protective screen). Gas proportional detectors with larger probe surfaces, such as the Ludlum model 43-37 detectors with a physical probe area of 573 cm<sup>2</sup>, are suitable for scanning large surface areas. The detector cavity in these instruments is filled with P 10 gas (90 percent argon, 10 percent methane). Alpha or beta particles, or both, enter the cavity through an aluminized Mylar window. The density thickness of this window is one factor that can affect the detector efficiency and thus the MDC of the instrument. The instrument can be used to detect (1) only alpha radiation by using a low operating voltage, (2) alpha-plus-beta radiation by using a higher operating voltage, or (3) only beta radiation by using a thicker Mylar window to block the alpha particles in a mixed alpha/beta field. Instrument response was evaluated using all three modes of operation.

### 2.2 Geiger-Mueller Detectors

Colloquially referred to as “pancake” detectors, these are used for detecting beta and gamma radiation (these detectors can also respond to alpha radiation to varying degrees). This study used Eberline model HP-260 detectors, which have a physical probe area of approximately 20 cm<sup>2</sup> (with an effective probe area of 15.5 cm<sup>2</sup>). The detector tube is filled with readily ionizable inert gas, which is a mixture of argon, helium, neon, and a halogen-quenching gas. Incident radiation enters this cavity through a mica window. The density thickness of the window can vary between 1.4 and 2.0 milligrams per square centimeter (mg/cm<sup>2</sup>), affecting detection sensitivity. A digital ratemeter-scaler with a set threshold value registers the output pulses.

### 2.3 Zinc Sulfide Scintillation Detectors

Alpha scintillation detectors use scintillators instead of gas as detection media. A commonly used detector is the zinc sulfide scintillation detector, which uses silver-activated zinc sulfide, ZnS(Ag). This study used the Eberline model AC-3-7, with a physical probe area of 74 cm<sup>2</sup> (and an effective probe area of 59 cm<sup>2</sup>). Alpha particles enter the scintillator through an aluminized Mylar window. The Mylar window prevents ambient light from activating the photomultiplier but is still thin enough to allow penetration by alpha radiation without significant energy degradation. The light pulses are amplified by a photomultiplier, converted to voltage pulses, and counted on a digital scaler/ratemeter with a set threshold value.

### 2.4 Plastic Scintillation Detectors

Plastic scintillation detectors have many advantages over other hand-held radiation detectors including high light output and the ability to be shaped into almost any desired form with a high degree of durability. This study used a Ludlum model 44-142 “beta scintillator,” which has an active probe area of 100 cm<sup>2</sup> (effective probe area of 88 cm<sup>2</sup>) and an aluminized Mylar window thickness of 1.2 mg/cm<sup>2</sup>. ORAU has demonstrated that the Ludlum model 44-142, though marketed as a beta scintillator, has alpha radiation detection efficiencies similar to those of the Ludlum model 43-68 gas proportional detector. An additional 3.8 mg/cm<sup>2</sup> Mylar shield can be incorporated on the detector’s surface to block alpha particle interaction in a mixed alpha/beta field. The aluminized Mylar window allows beta particles to enter the scintillator while preventing

ambient light from interacting with the photomultiplier. The scintillator creates light pulses that are amplified by the photomultiplier and then converted into measurable voltage pulses and counted on a digital ratemeter-scaler with a set threshold value.

## **2.5 Sodium Iodide Scintillation Detectors**

For detection of gamma radiation, thallium-activated sodium iodide (NaI(Tl)) scintillation detectors are widely used. Primarily, these detectors are useful for scanning surface areas for elevated gamma radiation. This study used the Victoreen model 489-55 with a 3.2 cm × 3.8-cm (1.25" × 1.5") NaI(Tl) crystal and the Ludlum model 44-10 with a 5.1 cm × 5.1-cm (2" × 2") NaI(Tl) crystal. The scan MDC discussion in Chapter 6 considers other crystal sizes, specifically the 2.5 cm × 2.5 cm (1" × 1") and 7.6 cm × 7.6 cm (3" × 3") that licensees may use to scan surfaces for gamma-emitting radionuclides. The output voltage pulse is recorded on a ratemeter or ratemeter-scaler.

## **2.6 Nonplanar Detectors**

Nonplanar detectors are used to detect beta and gamma radiation on nonplanar surfaces (i.e., extended lengths of heating, ventilation, and air conditioning ductwork and process piping). Common models of the nonplanar detectors incorporate variations of traditional GM-based and NaI(Tl) and cesium iodide scintillation technologies. Unlike many traditional beta and gamma detectors, which typically measure contamination on a 180-degree planar (or  $2\pi$ ) field of view, these nonplanar instruments can identify radioactivity in a 360-degree (or  $4\pi$ ) geometry about the detector. This field of view may also be achieved by arraying together other planar detectors into one that has a 360-degree field of view.

## **2.7 Ratemeter-Scalers**

The detectors described above are used in conjunction with ratemeter-scalers. The detector response is recorded as an integrated count, noted as a count rate, or both. This study evaluated both modes of operation for the following instrument combinations: Ludlum model 2221 ratemeter-scaler with Ludlum 43-68, Ludlum 44-10, Eberline HP 260, and Eberline AC-3-7 detectors; and Ludlum model 12 ratemeter-scaler with the Victoreen 489 55 and Ludlum 44-10 detectors.

## **2.8 Pressurized Ionization Chamber**

The PIC can be used to monitor "real-time" direct gamma-ray levels and record exposure rates. Ionization chambers operate by collecting ions within a cavity chamber filled with pressurized argon gas. The current generated is proportional to the amount of ionization produced in the chamber. Quantitative measurements of exposure rate are made and recorded in microrentgens per hour ( $\mu\text{R/h}$ ).

## **2.9 Dose Ratemeters**

Dose ratemeters can be used to collect dose rate measurements (in units of rem per hour or similar) and cross-calibrated with other gamma-measuring instruments. Commonly used dose ratemeters include the Thermo Scientific™ MicroRem/Sievert Tissue Equivalent Survey Meter (MicroRem) for radiation fields less than 200 milliroentgens per hour, and the Ludlum Model 9-4 portable ion chamber for radiation fields in the range of milliroentgens to roentgens per hour. Benefits of the MicroRem instrument include a linear response to all energies within the



operational range, a tissue equivalent scintillator with a nearly flat energy response, and gamma and x-ray detection from tissue equivalent photon response.

## **2.10 Portable Gamma Spectrometer**

Portable gamma spectrometers can be used to identify and quantify gamma-emitting radionuclides in a variety of settings and in situ measurement environments. Instruments in this category use an electronics package called a multichannel analyzer to perform pulse height analysis to determine photon energy. Each time a gamma ray deposits its energy in the detector, an electronic pulse is produced. The pulse height in volts is used to identify photon energy. Activity is determined by the number of counts of a particular pulse height. Counting statistics for gamma spectroscopy systems are more complicated than those of other detector types largely because background conditions are different at different energy locations on the spectrum. The vendor documentation for each specific instrument includes detailed descriptions of minimum detectable activity (MDA) calculations and other equations.

These portable instruments are generally divided into two categories: low resolution and high resolution. Resolution for gamma spectroscopy equipment is a measure of peak width in kiloelectron volts (keV) of a specified gamma ray energy expressed as the full width at half maximum. Systems with wide peaks (i.e., low resolution) may have trouble differentiating gamma rays of similar energy.

### **2.10.1 Low-Resolution Spectrometers**

Most gamma spectroscopy field units use low-resolution scintillation detectors. NaI(Tl) and cerium (Ce)-activated lanthanum bromide (LaBr<sub>3</sub>(Ce)) spectrometers are portable, operate at room temperature, and require little maintenance compared to other technologies. For low-resolution systems, the resolution is measured as the relative percent full width at half maximum for a 662-keV gamma ray. Resolution varies depending on the configuration with typical values of 7 percent for NaI(Tl) and 2.7 percent for LaBr<sub>3</sub>(Ce). Low-resolution spectrometers are best used when the radioactive contaminants are known and simple energy spectra. Portable scintillation spectrometers typically use 2.5-cm × 2.5-cm (1" × 1") to 5.1-cm × 5.1-cm (2" × 2") cylindrical crystals, but many different configurations are available.

### **2.10.2 High-Resolution Spectrometers**

High-resolution gamma spectroscopy systems use semiconductor detectors. The best identification capabilities are provided by high-purity germanium (HPGe) crystals. Resolution is normally measured using two or more gamma rays spanning the useful range of the spectrum. A resolution of 1.6 to 2.0 keV for the 1332.5-keV cobalt (Co)-60 gamma ray is typical. Though not commonly performed, a relative percent resolution of 0.15 percent at 662 keV could be compared against 7 percent (NaI) and 2.7 percent (LaBr<sub>3</sub>) scintillator resolution values. The superior resolution of HPGe spectrometers provides a powerful tool for identifying and quantifying unknown radionuclides with complex energy spectra. Different detector designs of crystal shape, electrode configuration, and window thickness are available to meet the specific needs of the project. Germanium detectors must be cryogenically cooled either with an attached liquid nitrogen dewar or a mechanical chiller, which increases the complexity of operations and limits field use. Specialized HPGe detector systems using Monte Carlo simulations can accommodate *in situ* assessments of soils, waste packages, and other objects.

## **2.11 Laboratory Instrumentation**

The study of field survey instruments was extended to include a limited number of measurements using laboratory instrumentation. The following laboratory instrumentation was used:

- Canberra 3100 VAX workstation connected to intrinsic germanium detectors (Oxford Instruments and EG&G ORTEC) with extended range capability for low-energy x-rays
- Canberra 3100 VAX workstation connected to solid-state alpha detectors (Canberra and Oxford Instruments)
- Low-background alpha/beta gas flow proportional counters (Oxford Instruments)
- Liquid scintillation counter (Packard Instrument)

## **2.12 Additional Instrumentation**

Additional survey instrumentation commonly used for decommissioning surveys that were not evaluated in this report include the following:

- The dual phosphor alpha-plus-beta detector consists of ZnS(Ag) adhered to a plastic scintillation material. This detector allows for the simultaneous assessment of alpha and beta radiation at each survey location. Cross-talk between the alpha and beta channels should be carefully considered when evaluating the data.
- Berkeley Nucleonics SAM 940 hand-held spectrometer has a 7.6 centimeter (3-inch) NaI detector. Global positioning system (GPS) capability is available.
- The RS-700 system from Radiation Solutions, Inc., has two 10.2-cm × 10.2-cm × 40.6-cm (4" x 4" x 16" - 4L) NaI detectors and uses Radiation Solution's RadAssist software as the operating software. The system operates at a nominal scan rate of 1–2 meters per second (m/s), acquires one 1024 channel gamma spectrum per second, continually displays the spectra on the system computer, and saves data for offline use.

Other important instrumentation not studied in this report includes the following:

- Devices such as the ultrasonic ranging and data system (USRADS) that track both the position and output of radiation detectors have been used for many years. USRADS (from ChemRad Tennessee Corporation) provides a documented survey by correlating the location and magnitude of the instrument response at 1-second intervals. Similarly, the Thermo Nutech laser-assisted ranging and data system combines radiological data acquisition and spatial identification to help collect and present radiological survey data. Both systems eliminate subjective interpretation of the data by the surveyor and verify the survey area coverage.
- Advanced positioning products by Trimble® and other manufacturers enhance survey capabilities through the use of GPS, laser, optical and inertial technologies with application software and wireless communications. Trimble® offers products like

the GeoXH and associated software linked to satellites for recording real-time geospatial data with the survey instrument output. In addition to exterior GPS technologies, Trimble® has products like the Robotic Total Station with three-dimensional mapping and positioning capabilities for surveys of a facility's interior. The hand-held products can be used with the Microsoft Windows platform, which also allows the use of additional independent data-logging software when geospatial-related data recording is not feasible. The flexibility of the Trimble® products permits them to be used in many different applications and with a variety of radiation detection instruments.

- A floor monitor developed by Shonka Research Associates, Inc., uses position-sensitive proportional counter-based radiation detectors. The position sensitive proportional counter allows one detector to act as the equivalent of hundreds of individual detectors, which results in the collection of vast amounts of data. Process software saves the survey data at very high rates and correlates the data as a function of survey location. The system provides completely documented radiation surveys and allows visualization of the survey results in a real-time mode.
- Indoor floor and wall survey monitors developed by Environmental Restoration Group (ERG) use an ERG model 102F and 102W built on the functionality of the Ludlum model 239-1F with a standalone indoor positioning system (no external beacons) that are accurate within less than an inch. The systems can be used to perform alpha and beta-gamma surveys via the ZnS plastic scintillator detectors. Both 102 systems also incorporate a stepper motor, which allows for variable speed control to achieve the desired MDC. The ERG software processes accumulated survey data. The software calculates and exports data in multiple file formats including three-dimensional geographic information systems (GIS) Shapefile (.shp), Excel, or raw text. Data limits can be tailored to visually identify observed measurements exceeding a given threshold. In the six-zone ZnS plastic scintillator floor monitor, each zone has an area of 100 cm<sup>2</sup> to optimize the scanning area for faster results on the Models 102F and 102W



### 3 STATISTICAL INTERPRETATIONS OF MINIMUM DETECTABLE CONCENTRATIONS

Detection limits for field survey instrumentation are an important criterion in the selection of appropriate instrumentation and measurement procedures. For the most part, detection limits need to be determined to evaluate whether a particular instrument and measurement procedure can detect residual activity at the regulatory release criteria (DCGLs). Compliance with decommissioning criteria can be demonstrated by performing surface activity measurements and directly comparing the results to the surface activity DCGLs. However, before any measurements are made, the survey instrument and measurement procedures should be shown to have sufficient detection capabilities relative to the surface activity DCGLs (i.e., the detection limit of the survey instrument should be less than the appropriate surface activity DCGL).

The measurement of residual radioactivity during surveys in support of decommissioning often involves evaluating residual radioactivity at near-background levels. Thus, the minimum amount of radioactivity that a given survey instrument and measurement procedure can detect must be determined. In general, the MDC is the minimum activity concentration on a surface or within a material volume that an instrument is expected to detect (e.g., activity expected to be detected with 95 percent confidence). However, this activity concentration, or the MDC, is determined *a priori*; that is, before survey measurements are conducted.

As generally defined, the detection limit, which may be a count or count rate, is independent of field conditions such as scabbled, wet, or dusty surfaces. That is, the detection limit is based on the number of counts and does not necessarily equate to measured activity under field conditions. These field conditions do, however, affect the instrument's "detection sensitivity" or MDC. Therefore, the terms "MDC" and "detection limit" should not be used interchangeably.

For this study, the MDC corresponds to the smallest activity concentration measurement that is practically achievable with a given instrument and type of measurement procedure. That is, the MDC depends not only on the particular instrument characteristics (instrument efficiency, background, integration time, etc.), but also on the factors involved in the survey measurement process (EPA, 1980), which include surface type, source-to-detector geometry, and source efficiency (backscatter and self-absorption).

#### 3.1 Fundamental Concepts of MDC

This report does not present a rigorous derivation of MDC concepts but does offer sufficient theory to acquaint the reader with the fundamental concepts. The detection limits discussed here are based on counting statistics alone and do not include other sources of error. NUREG/CR-4007, "Lower Limit of Detection: Definition and Elaboration of a Proposed Position for Radiological Effluent and Environmental Measurements," issued September 1984, and ANSI N13.30, "Performance Criteria for Radiobioassay," issued 2011, address systematic uncertainties in the measurement process. Although the following statistical formulation assumes a normal distribution of net counts, between sample and blank, this may not be the case for low blank total counts. However, because of the advantage of having a single, simple MDC expression, and because deviations from the normality assumption do not affect the MDC expression in this report as severely as had been expected (Brodsky, 1992), the authors decided that the normality assumption was proper for purposes of this report. That is, the MDC concepts discussed below should be considered as providing information on the general

detection capability of the measurement system and not as absolute levels of activity that can or cannot be detected (National Council on Radiation Protection and Measurements [NCRP] 58, "A Handbook of Radioactivity Measurements Procedures," dated February 1, 1985).

The MDC concepts discussed in this document derive from statistical hypothesis testing, in which a decision is made on the presence of activity. Specifically, a choice is made between the null hypothesis ( $H_0$ ) and the alternative hypothesis ( $H_a$ ). The null hypothesis is generally stated as "no net activity is present in the sample" (i.e., observed counts are not greater than background), while the alternative hypothesis states that the observed counts are greater than background, and thus, "net activity is present in the sample." In this context "sample" has a general meaning; it may apply to direct measurements of surface activity, laboratory analyses of samples, and other entities.

A first step in understanding the MDC concepts is to consider an appropriate blank (background) distribution for the medium to be evaluated. Currie (1968) defines the blank as the signal resulting from a sample that is identical, in principle, to the sample of interest, except that the residual activity is absent. This determination must be made under the same geometry and counting conditions as used for the sample (Brodsky & Gallagher, 1991). In the context of this report, an example of this medium may be an unaffected concrete surface that is considered representative of the surfaces to be measured in the remediated area. (This report uses the terms "blank" and "background" interchangeably.)

In this statistical framework, one must consider the distribution of counts obtained from measurements of the blank, which may be characterized by a population mean ( $\mu_B$ ) and standard deviation ( $\sigma_B$ ). In the measurement of a sample known to be free of residual activity, this zero-activity (background) sample has a mean count ( $C_B$ ) and standard deviation ( $s_B$ ). The net count (and, subsequently, residual activity) can be determined by subtracting the blank counts from the sample counts. This results in a zero-mean count frequency distribution that is approximately normally distributed (Figure 3-1). The standard deviation of this distribution ( $\sigma_0$ ) is obtained by propagating the individual errors (standard deviations) associated with both the blank ( $\sigma_B$ ) and the zero-activity samples ( $s_B$ ):

$$\sigma_0 = \sqrt{\sigma_B^2 + s_B^2} \quad (\text{Eq. 3.1})$$

A critical level may then be determined from this distribution and used as a tool to decide when activity is present. The critical level ( $L_C$ ) is that net count in a zero-mean count distribution having a probability, denoted by  $\alpha$ , of being exceeded (Figure 3-1). It is common practice to set  $\alpha$  equal to 0.05 and to accept a 5-percent probability of incorrectly concluding that activity is present when it is not. That is, if the observed net count is less than the critical level, the surveyor correctly concludes that no net activity is present. When the net count exceeds  $L_C$ , the null hypothesis is rejected in favor of its alternative, and the surveyor falsely concludes that net activity is present in the blank sample. It should also be noted that  $L_C$  is equivalent to a given probability (e.g., 5 percent) of committing a Type I error (false positive detection). The expression for  $L_C$  is generally given as the following:

$$L_C = k_\alpha \sigma_0 \quad (\text{Eq. 3.2})$$

where  $k_\alpha$  is the value of the standard normal deviate corresponding to a one-tailed probability level of  $1-\alpha$ . As stated previously, the usual choice for  $\alpha$  is 0.05, and the corresponding value for  $k_\alpha$  is 1.645. For an appropriate blank counted under the same conditions as the sample, the

assumption may be made that the standard deviations of the blank and zero-activity sample are equal (i.e.,  $\sigma_B$  equals  $s_B$ ). Thus, the critical level may be expressed as the following:

$$L_C = 1.645 \sqrt{2 s_B^2} = 2.33 s_B \quad (\text{Eq. 3.3})$$

The  $L_C$  value determined above is in terms of net counts, and thus, the  $L_C$  value should be added to the background count if comparisons are to be made to the directly observable instrument gross count.

The detection limit ( $L_D$ ) is defined to be the number of mean net counts obtained from samples for which the observed net counts are almost always certain to exceed the critical level (Figure 3-2).  $L_D$  is the mean of a net count distribution. The detection limit is positioned far enough above zero so that there is a probability, denoted by  $\beta$ , that the  $L_D$  will result in a signal less than  $L_C$ . It is common practice to set  $\beta$  equal to 0.05 and to accept a 5-percent probability of incorrectly concluding that no activity is present, when it is indeed present (Type II error). That is, the surveyor has already agreed to conclude that no net activity is present for an observed net count that is less than the critical level; however, an amount of residual activity that would yield a mean net count of  $L_D$  is expected to produce a net count less than the critical level 5 percent of the time. This is equivalent to missing residual activity when it is present.

The expression for  $L_D$  is generally given as follows:

$$L_D = L_C + k_\beta \sigma_D \quad (\text{Eq. 3.4})$$

where  $k_\beta$  is the value of the standard normal deviate corresponding to a one-tailed probability level of  $1-\beta$  for detecting the presence of net activity, and  $\sigma_D$  is the standard deviation of the net sample count ( $C_S$ ) when  $C_S$  equals  $L_D$ . For clarification, consider the measurement of a sample that provides a gross count given by  $C_{S+B}$ , at the detection level. The net sample count,  $C_S$ , is calculated by subtracting the mean blank count ( $\mu_B$ ) from the gross count. The detection limit may be written as follows, recognizing that  $C_S$  equals  $L_D$ :

$$L_D = C_S + (C_B - \mu_B) \quad (\text{Eq. 3.5})$$

The standard deviation of the net sample ( $\sigma_D$ ) is obtained by propagating the error in the gross count and from the background when the two are subtracted to obtain  $L_D$ . As previously noted, the standard deviation of this distribution ( $\sigma_0$ ) is obtained by propagating the uncertainties associated with both the blank ( $C_B$ ) and the zero-activity samples ( $\mu_B$ ); therefore, the following applies:

$$\sigma_D = \sqrt{C_S + \sigma_0^2} = \sqrt{L_D + \sigma_0^2} \quad (\text{Eq. 3.6})$$

This expression for  $\sigma_D$  may be substituted into Equation 3.4 and the equation solved for  $L_D$ .

As stated previously, the usual choice for  $\beta$  is 0.05, and the corresponding value for  $k_\beta$  is 1.645. If it is assumed that  $\sigma_D$  is approximately equal to the standard deviation of the background, then for the case of paired observations of the background and sample  $\sigma_0^2$  equals  $2s_B^2$ . Following considerable algebraic manipulation, the detection limit may be expressed as follows:

$$L_D = 2.71 + 4.65 s_B \quad (\text{Eq. 3.7})$$

The assumption that the standard deviation of the count ( $\sigma_D$ ) is approximately equal to that of the background greatly simplifies the expression for  $L_D$  and is usually valid for total counts greater than 70 for each sample and blank count (Brodsky, 1992). Examination of this expression determined that in the limit of very low background counts,  $s_B$  would be zero and the constant 2.71 should be 3, based on a Poisson count distribution (Brodsky & Gallagher, 1991). Thus, the expression for the detection limit becomes the following:

$$L_D = 3 + 4.65 s_B \quad (\text{Eq. 3.8})$$

The detection limit calculated above may be stated as the net count having a 95-percent probability of being detected when a sample contains activity at  $L_D$ , with a maximum 5-percent probability of falsely interpreting sample activity as activity resulting from background (false negative or Type II error).

The MDC of a sample follows directly from the detection limit concepts. It is a level of radioactivity, either on a surface or within a volume of material, that is practically achievable by an overall measurement process (EPA, 1980). The expression for MDC may be given as follows:

$$MDC = \frac{3 + 4.65 s_B}{KT} \quad (\text{Eq. 3.9})$$

where  $K$  is a proportionality constant that relates the detector response to the activity level in a sample for a given set of measurement conditions, and  $T$  is the counting time. The factor  $K$  typically encompasses the detector efficiency, self-absorption factors, and probe area corrections.

This expression of the MDC equation was derived assuming equivalent (paired) observations of the sample and blank (i.e., equal counting intervals for the sample and background), in contrast to the MDC expression that results when taking credit for repetitive observations of the well-known blank. There is some debate concerning the appropriateness of taking credit for repetitive observations of the blank because of the uncertainties associated with using a well-known blank for many samples when there may be instrument instabilities or changes in the measurement process not detected by the surveyor (Brodsky & Gallagher, 1991). Therefore, it is desirable to obtain repetitive measurements of background, simply to provide a better estimate of the background value that must be subtracted from each gross count in the determination of surface activity. Thus, the background is typically well known for purposes other than reducing the corresponding MDC, such as to improve the accuracy of the background value. This report uses the following expression for MDC:

$$MDC = \frac{3 + 4.65\sqrt{C_B}}{KT} \quad (\text{Eq. 3.10})$$

where  $C_B$  is the background count in time ( $T$ ) for paired observations of the sample and blank. For example, if 10 1-minute repetitive observations of background were performed,  $C_B$  is equal to the average of the 10 observations and  $T$  is equal to 1 minute. The quantities encompassed by the proportionality constant ( $K$ ), such as the detection efficiency and probe geometry, should also be average, "well-known" values for the instrument. For assessing MDC for surface activity measurements, the MDC is given in units of dpm/100 cm<sup>2</sup>.



For cases in which the background and sample are counted for different time intervals, the MDC becomes the following:

$$MDC = \frac{3 + 3.29 \sqrt{R_B T_{S+B} \left(1 + \frac{T_{S+B}}{T_B}\right)}}{K T_{S+B}} \quad (\text{Eq. 3.11})$$

where  $R_B$  is the background counting rate, and  $T_{S+B}$  and  $T_B$  are the sample and background counting times, respectively (Strom & Stansbury, 1992).

One difficulty with the MDC expression in Equation 3.10 is that all uncertainty is attributed to Poisson counting errors, which can result in an overestimate of the detection capabilities of a measurement process. The proportionality constant ( $K$ ) embodies measurement parameters that have associated uncertainties that may be significant compared to the Poisson counting errors. A conservative solution to this problem has been to replace the parameter values (specifically, the mean parameter values) that determine  $K$  with lower bound values that represent a 95-percent probability that the parameter values are higher than that bound (NUREG/CR-4007; ANSI N13.30). In this case, the MDC equation becomes:

$$MDC = \frac{3 + 4.65 \sqrt{C_B}}{K_{0.05} T} \quad (\text{Eq. 3.12})$$

where  $K_{0.05}$  is the lower bound value that represents a 95-percent probability that values of  $K$  are higher than that bound (ANSI N13.30). For example, if the detector efficiency in a specified measurement process was experimentally determined to be  $0.20 \pm 0.08$  ( $2\sigma$  error), the value of the detector efficiency that would be used in Equation 3.10 is 0.12. This would have the effect of increasing the MDC by a factor of 1.7 (using 0.12 instead of 0.20). Therefore, it is important to understand the magnitude of the uncertainty associated with each of the parameters used in the MDC determination. In this context, errors associated with each measurement parameter were propagated in the MDC determination. The magnitude of the uncertainty in the MDC may then be used as a decision tool for determining the need to implement some methodology for adjusting the MDC for uncertainties in  $K$ .

### **3.2 Review of Expressions of MDC**

A significant aspect of this study involved the review of the relevant literature on statistical interpretations of MDC. One approach, suited for this application of the MDC concept, was selected and used throughout the entire study for consistency. However, a sensitivity study considered other statistical approaches. That is, several statistical treatments of the data used the same set of measurement results to calculate the MDC. The tabulated results provided the range of MDC values calculated using the various approaches.

The data used to perform the MDC sensitivity analysis were obtained by performing static measurements under ideal laboratory conditions with a gas proportional detector, operated in the beta-only mode, on a strontium/yttrium (SrY)-90 source (this part of the study did not evaluate the expressions for scanning sensitivity). For purposes of comparison, both the background and sample counting times were 1 minute long (i.e., paired observations). Ten repetitive measurements of background were obtained, and the mean and standard deviation were calculated to be 354 and 18 counts, respectively. The total efficiency of the detector was determined to be 0.34 counts per disintegration (c/dis), and a probe area correction for the 126 cm<sup>2</sup> detector was made.

The study reviewed several expressions of MDC (or the various terms used to convey detection limit) in the literature. The measurement results determined above were used to determine the values for the various expressions of MDC. The average background from the repetitive observations was used in the MDC equations that required a background value, while the standard deviation of the background distribution was used for others. Table 3-1 illustrates the variations in MDC that may be calculated from the same set of measurement results. The MDC values ranged from 146 to 211 dpm/100 cm<sup>2</sup> for the gas proportional detectors calibrated to SrY-90.

This limited sensitivity study demonstrates that the MDC expressions widely referenced in the literature produce very consistent MDC results. The smallest value of MDC results from the expression that allows credit for the “well-known” blank (Currie, 1968). Due to the general level of agreement among the MDC results, it is unlikely that any of these results would lead to a situation where the instrumentation is deemed to have insufficient detection capabilities relative to a surface activity release limit (e.g., DCGL).

**Table 3-1 MDC Results for Data Obtained from Gas Proportional Detector Using Various MDC Expressions**

| MDC Expression <sup>a, b</sup>   | MDC Result <sup>c</sup> (dpm/100 cm <sup>2</sup> ) | Reference                 |
|--|--|---------------------------|
| $2.71 + 4.65 \sqrt{B}$   | 210  | NCRP 58; EPA, 1980        |
| $2.71 + 4.65 \sigma_B$   | 204  | Currie, 1968              |
| $2.71 + 3.29 \sigma_B$   | 146  | Currie, 1968              |
| $3 + 4.65 \sqrt{B}$  | 211  | Brodsky & Gallagher, 1991 |
| $\frac{3 + 3.29 \sqrt{R_B T_{S+B} \left(1 + \frac{T_{S+B}}{T_B}\right)}}{KT_{S+B}}$ <sup>d</sup> | 211  | Strom & Stansbury, 1992   |

<sup>a</sup>The data used in each MDC expression were obtained from a Ludlum model 43-68 gas proportional detector and SrY-90 source. Average background counts (B) of 354 in 1 minute, standard deviation of 18, probe area correction for 126-cm<sup>2</sup> detector, and detector efficiency of 0.34 c/dis were obtained.

<sup>b</sup>Each MDC expression is written using symbols that may be different from the ones presented in their respective references. However, the meaning of each has been preserved.

<sup>c</sup>Each MDC result was presented in terms of dpm/100 cm<sup>2</sup> to facilitate comparison of the different MDC expressions. This involved correcting the MDC expression for probe area and detector efficiency.

<sup>d</sup>The terms  $R_B$ ,  $T_{S+B}$ , and  $T_B$  refer to the background counting rate, gross count time, and background counting time, respectively. Using  $T_{S+B}$  equal to  $T_B$  (1 minute) resulted in the same expression as that of Brodsky and Gallagher (1991).

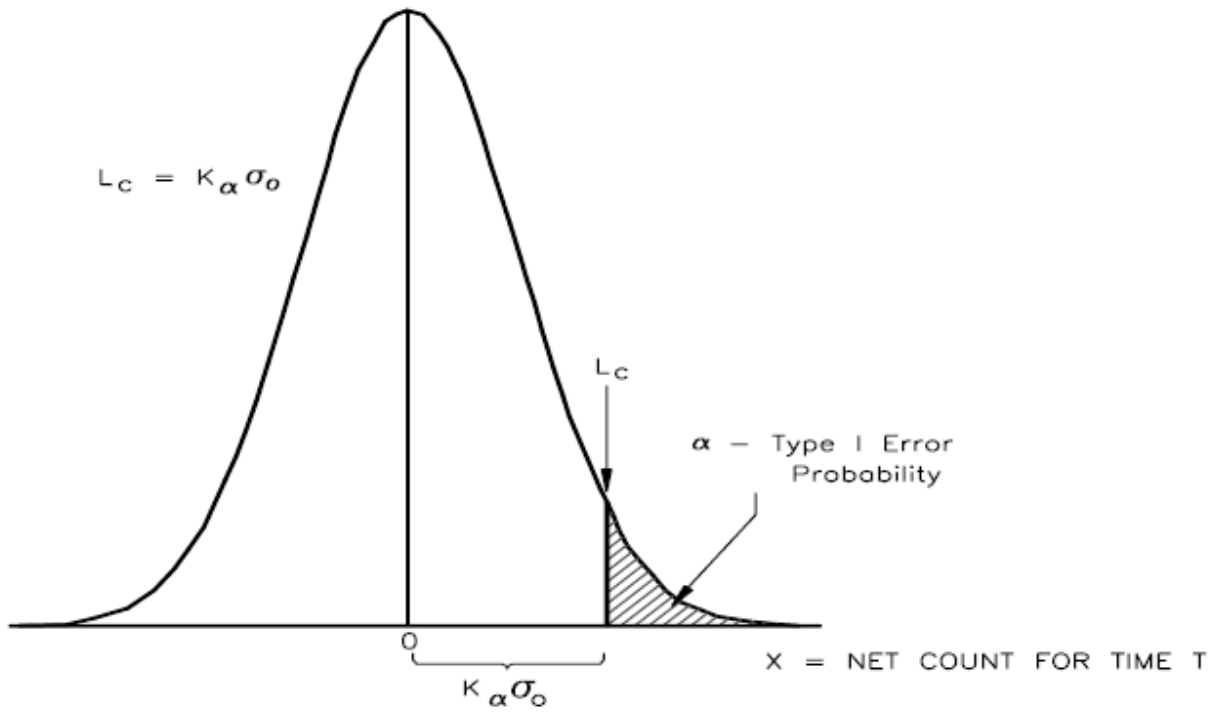


Figure 3-1 Critical Level,  $L_c$

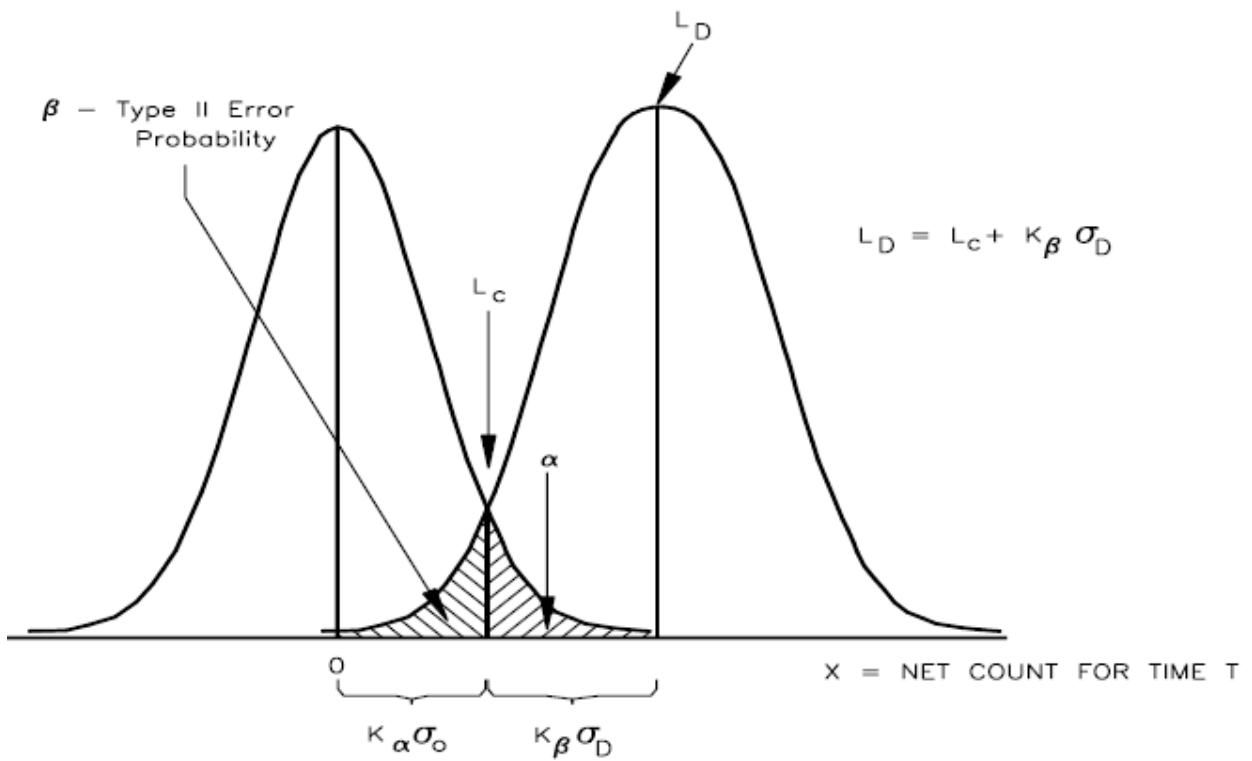


Figure 3-2 Detection Limit,  $L_D$



## 4 VARIABLES AFFECTING INSTRUMENT MINIMUM DETECTABLE CONCENTRATIONS

Before the MDC for a particular instrument and survey procedure can be determined, it is necessary to introduce the expression for total alpha or beta surface activity per unit area. ISO 7503-1:1988 recommends that the total surface activity,  $A_s$ , be calculated similarly to the following:

$$A_s = \frac{R_{S+B} - R_B}{\epsilon_i W \epsilon_s} \quad (\text{Eq. 4.1})$$

where,

$R_{S+B}$  is the gross count rate of the measurement in counts per minute (cpm)

$R_B$  is the background count rate in cpm

$\epsilon_i$  is the instrument or detector efficiency (unitless)

$\epsilon_s$  is the efficiency of the potential contamination source (unitless)

$W$  is the area of the detector window ( $\text{cm}^2$ )

(For instances in which  $W$  does not equal  $100 \text{ cm}^2$ , probe area corrections are necessary to convert the detector response to units of dpm per  $100 \text{ cm}^2$ .)

This expression clearly distinguishes between instrument (detector) efficiency and source (surface) efficiency. The product of the instrument and source efficiency yields the total efficiency ( $\epsilon_{\text{tot}}$ ). Currently, surface contamination is assessed by converting the instrument response to surface activity using one overall total efficiency. This usage of total efficiency is not a problem, provided that the calibration source exhibits characteristics similar to the surface contamination (including radiation energy, backscatter effects, source geometry, and self-absorption). In practice, this is hardly the case; more likely, total efficiencies are determined with a clean, stainless steel source, and then those efficiencies are used to measure, for example, contamination on a dust-covered concrete surface. By separating the efficiency into two components, the surveyor is better able to consider the actual characteristics of the surface contamination.

The instrument efficiency is defined as the ratio between the net count rate of the instrument and the surface emission rate of a source for a specified geometry. The surface emission rate ( $q_{2\pi}$ ) is defined as the "number of particles of a given type above a given energy emerging from the front face of the source per unit time" (ISO 7503-1:1988). The surface emission rate is the  $2\pi$  particle fluence that embodies both the absorption and scattering processes that affect the radiation emitted from the source. Thus, the instrument efficiency is determined by the following:

$$\epsilon_i = \frac{R_{S+B} - R_B}{q_{2\pi}} \quad (\text{Eq. 4.2})$$

The instrument efficiency is determined during calibration by obtaining a static count with the detector over a calibration source that has a traceable activity or surface emission rate or both. In many cases, it is the source surface emission rate that is measured by the manufacturer and certified as NIST-traceable. The source activity is then calculated from the surface emission rate based on assumed backscatter and self-absorption properties of the source. The theoretical maximum value of instrument efficiency is 1.

The calculation must also account for, if applicable, the relative sizes of the probe and source. ISO-8769, “Reference Sources—Calibration of Surface Contamination Monitors—Alpha-, Beta-, and Photon Emitters,” issued 2016, recommends use of a calibration source with an area of at least 100 cm<sup>2</sup>. For many applications, a calibration source of 150 cm<sup>2</sup> is used because it has an area larger than many probe areas. Instrument efficiencies must therefore account only for the fraction of the surface emissions that are subtended by the physical probe area. For example, a gas proportional detector with the surface area of 126 cm<sup>2</sup> is calibrated using a 150-cm<sup>2</sup> source with a 2π emission rate of 54,401 cpm. In this case, 84 percent (126 divided by 150) of the 2π surface emissions would be used in the calculation of ε<sub>i</sub>. If the background count value is established at 345 cpm and a 1-minute source check produces 9,171 cpm, the instrument efficiency is estimated as follows:

$$\epsilon_i = \frac{9,171 - 345}{54,401 \times (126/150)} = 0.2 \quad (\text{Eq. 4.3})$$

Adjustments (e.g., the 126/150 term in Equation 4.3) are not required when the probe area is larger than the source area. That is, the fraction of the surface emissions that are subtended by the physical probe area is 1.0 (100 percent) when the source area is smaller than the probe area.

The source efficiency (ε<sub>s</sub>) is defined as the ratio between the number of particles of a given type above a given energy emerging from the front face of a source or its window per unit time (surface emission rate) and the number of particles of the same type created or released within the source (for a thin source) or its saturation layer thickness (for a thick source) per unit time (ISO 7503-1:1988). The source (or surface) efficiency takes into account the increased particle emission resulting from backscatter effects, as well as the decreased particle emission because of self-absorption losses. For an ideal source (no backscatter or self-absorption), the value of ε<sub>s</sub> is 0.5. Many real sources will exhibit values of ε<sub>s</sub> that are less than 0.5, although values greater than 0.5 are possible, depending on the relative importance of the absorption and backscatter processes. Source efficiencies may be either determined experimentally or simply selected from the guidance in ISO 7503 (refer to Section 5.3.2) (1988 and 2016).

It is important to note that the preceding discussion on source efficiency is based on guidance in ISO 7503-1:1988. Since the ISO 7503 series was updated prior to Revision 1 of this NUREG report, a comparison of the 1988 and 2016 versions of ISO 7503 was performed in order to understand any differences in approach to surface or source efficiency, and to determine if the methodology/terminology in this NUREG report should be updated. Detailed reiterations of methods and equations from the ISO 7503 series are not presented in this NUREG report, as ISO standards are subject to copyright. For additional details, the reader should refer directly to the ISO 7503 standards.

To begin at a fundamental level, the term “source efficiency” was compared between the 1988 and 2016 ISO 7503 series. In ISO 7503-1:1988, efficiency of a source is defined as the “ratio between the number of particles of a given type above a given energy emerging from the front face of a source or its window per unit time (surface emission rate) and the number of particles of the same type created or released within the source (for a thin source) or its saturation layer thickness (for a thick source) per unit time [ISO 7503-1:1988), pg. 2].”

ISO 7503-3:2016 defines source efficiency, very similarly, as the “ratio of the number of particles of a given type above a given energy or of photons emerging from the front face of a source or its window per unit time (surface emission rate) and the number of particles of the

same type or of photons created or released within the source (for a thin source) or its saturation layer thickness (for a thick source) per unit time [ISO 7503-3:2016, pg. 2].”

The concept of an “ideal” source was then compared between the 1988 and 2016 ISO 7503 series. ISO 7503-1:1988 notes that “for this procedure to yield a unique calibration factor, the sources are required to be ideal thin sources, i.e. sources with no self-absorption and no back-scatter,” and that “however, in practice, the sources can be far from ideal, especially when alpha-emitters and low energy beta-emitters (maximum beta energy lower than approximately 0.4 MeV) are concerned [ISO 7503-1:1988, pg. 6].” ISO 7503-1:1988 notes later in the document that “for an ideal source (no self-absorption, no back-scatter), the value of  $\epsilon_s$  is 0.5,” and that “for a real source, the value of  $\epsilon_s$  is usually less than 0.5, but may also be greater than 0.5 depending on the relative importance of self-absorption and back-scatter processes [ISO 7503-1:1988, pg. 7].”

For comparison, ISO 7503-3:2016 describes an “ideal situation” which “assumes contamination is in an infinitely thin layer and there is no scattering,” and that “for these assumptions, exactly half of the emissions resulting from a radioactive disintegration will emerge and have the potential to enter the detector.” ISO 7503-3:2016 also introduces a “*P*-Factor” term and indicates that “for those cases where there is only one emission per decay, the *P*-Factor has a value of 2 and the activity per unit area is twice the emission rate per unit area provided by the detector response [ISO 7503-3:2016, pg. 7].” The *P*-Factor is described in ISO 7503-3:2016 as a factor “to convert a measurement of emission rate from a monoenergetic conform calibration source (ISO 8769) into a measure of activity,” and ISO 7503-3:2016 further notes that “because such calibration sources are single radionuclides with essentially a single emission which has a 100 % emission probability, the *P*-Factor could be used very simply to achieve this conversion [ISO 7503-3:2016 pg. 6].”

The comparison of “source efficiency” terminology from the 1988 and 2016 ISO 7503 series shows that the definitions exist in both series, and they are essentially the same. By comparing the *P*-Factor concept from the 2016 ISO series to the 1988 series, the *P*-Factor could be viewed as the reciprocal of the “efficiency of a source ( $\epsilon_s$ ).” As such, ISO 7503-1:1988 describes the source efficiency of an ideal source in terms of an  $\epsilon_s$  of 0.5, while ISO 7503-3:2016 discusses the reciprocal as a *P*-Factor of 2.

A comparison of the 1988 and 2016 ISO 7503 equations to evaluate contamination measurement data, and the associated usage of  $\epsilon_s$  and the *P*-Factor was performed. ISO 7503-1:1988 Equation 1 describes the beta- or alpha-activity per unit area ( $A_s$ ) of fixed and removable contamination on the surface being checked (in Bq/cm<sup>2</sup>) in relation to the measured count rate, similar to Equation 4.1 in this NUREG report. ISO 7503-1:2016 Equation 8 provides a similar approach but utilizes the *P*-Factor in lieu of a source efficiency term. ISO 7503-1:2016 describes this approach as applicable to evaluate radioactive contamination per unit area “where only one radionuclide is known to be responsible for the contamination and the nature of the contaminated surface is well-characterized.” A comparison of the 1988 and 2016 equations to assess contamination measurement data shows that the equations are essentially the same, while different terminology has been used.

ISO 7503-3:2016 notes that the “original” definition of the *P*-Factor (i.e., the ratio between the activity per unit area of a source and its surface emission rate per unit area) “was correct, but only for the single emission ISO 8769 calibration sources [ISO 7503-3:2016 pg. 6].” Because of this, ISO 7503-3:2016 introduces the concept of the “emergence factor” which “characterizes the ratio of the generation of individual emissions to the fraction of those emissions which

emerge from the surface,” and defines this factor as  $E_{ij}$  for the relevant energy  $i$  and for emission of alpha-, beta- or gamma- radiation  $j$ .” ISO 7503-3:2016 further notes that “each emission can then be taken in turn, the appropriate value for  $E_{ij}$  estimated, this combined with the emission probability per decay and then the effects combined of all emissions in the decay taking into account the potential for coincident detections.” [ISO 7503-3:2016, pp. 7-8]

The specific definition of “emergence factor of a source” is provided in ISO 7503-3:2016 as the “ratio of the number of particles of a given type or of photons created or released within the source (for a thin source) or its saturation layer thickness (for a thick source) per unit time and the number of particles of the same type above a given energy or of photons emerging from the front face of a source or its window per unit time (surface emission rate) [ISO 7503-3:2016, pg. 2].” Note that while the “emergence factor” term allows for a consideration of relevant energies and emission intensities, the fundamental definition could be viewed as the reciprocal of “source efficiency,” as it was defined in both the 1988 and 2016 ISO 7503 series.

Since both Revision 0 of this NUREG and MARSSIM, Revision 1 provided default source efficiencies based upon ISO 7503-1:1988, a comparison of default values in ISO 7503-1:1988 and ISO 7503-3:2016 was performed. In both the 1988 and 2016 standards, default values were derived assuming only self-absorption (and no back-scattering) in the source and considering the following types of contamination sources:

- thin layers of beta-emitters covered by about 2.5 mg/cm<sup>2</sup> of inactive material;
- homogeneous beta sources of the thickness of a wipe test filter paper (~10 mg/cm<sup>2</sup>).

ISO 7503-1:1988 indicates that “plausible and conservative assumptions” were utilized to provide default  $\epsilon_s$  values for use “in the absence of more precisely known values.” Those values are presented as:

$$\begin{aligned}\epsilon_s &= 0.5 \text{ for beta-emitters } (E_{\beta\text{max}} > 0.4 \text{ MeV}) \\ \epsilon_s &= 0.25 \text{ for beta-emitters } (0.15 \text{ MeV} < E_{\beta\text{max}} < 0.4 \text{ MeV}) \text{ and alpha-emitters} \\ &[\text{ISO 7503-1:1988, pg. 3 and pg. 9/Table-2}]\end{aligned}$$

ISO 7503-3:2016 similarly discusses a “conservative approach” to using emergence factors and notes that those factors “should be used only with great precaution, if no or insufficient information is available concerning the nature, specific properties, and condition of a contaminated surface.” Those factors are presented as:

$$\begin{aligned}E &= 2 \text{ for beta emitters with } E_{\beta\text{max}} \geq 0.4 \text{ MeV} \\ E &= 4 \text{ for beta emitters with } 0.15 \text{ MeV} < E_{\beta\text{max}} < 0.4 \text{ MeV} \text{ and alpha emitters} \\ &[\text{ISO 7503-3:2016, pg. 20}]\end{aligned}$$

It is evident from the comparison that these emergence factors are the reciprocal of the “recommended values for  $\epsilon_s$ ” from ISO 7503-1:1988 – or in other words, an  $E$  of 2 equates to an  $\epsilon_s$  of 0.5, and an  $E$  of 4 equates to an  $\epsilon_s$  of 0.25.

ISO 7503-3:2016 acknowledges that complex decay schemes are more likely to be encountered in practice, and indicates that “the majority of radionuclides do not exhibit simple decay schemes and may have multiple branches from the parent to the ground state, including the emission of photon(s), conversion electrons and secondary emissions such as X-rays and Auger electrons,” and that “for any single decay event, it is possible also that more than one



emission may be produced, for example, a beta particle followed by a gamma ray [ISO 7503-3:2016, pg. 7].” ISO 7503-3:2016 further notes that an “instrument may detect any or all of the emissions arising from a single decay but only one event is registered as the emissions occur at the same time,” and concludes that “interpreting readings from surface contamination instruments is complex, as it means that it is incorrect to sum the detection probabilities for all the emissions without correction for the summation.” ISO 7503-3:2016 addresses this cascade effect by combining the emergence factor with the emission probability per decay, where the probability of not detecting any of the emissions is considered.

The cascade effect calculation methods described in ISO 7503-3:2016 are complex, and they require an understanding of the behavior of radionuclides under various circumstances in order to accurately assess *E*-Factors for multiple decay paths. ISO 7503-3:2016 acknowledges this complexity and presents a “simplified calibration method” in Annex A of ISO 7503-3:2016, which is based on the classification of particle and/or photon emission intensity data for the radionuclide of interest into specific emission energy regions. The “simplified calibration method” is based only on the radionuclide emission intensity data and does not utilize decay path abundance. The methodology also uses the “conservative approach” to consider source efficiency (as discussed previously), which uses the default values of *E* (i.e., *E* = 2 for beta emitters with  $E_{\beta\max} \geq 0.4$  MeV, *E* = 4 for beta-emitters with  $0.15 \text{ MeV} < E_{\beta\max} < 0.4$  MeV, and *E* = 4 for alpha emitters). Examples within ISO 7503-3:2016 Annex A also evaluated the consequences of the coincidence summing effect when multiple emissions are registered as a single detector response. This assessment was performed by comparing the relative effect between summation of detection efficiencies versus a product and was performed for 158 different radionuclides. ISO 7503-3:2016 concludes that “the analysis of the extent of the coincidence summing effect on the detection efficiency shows, that this effect does not exceed 7% [ISO 7503-3:2016, pg. 21].”

Annex B of ISO 7503-3:2016 presents multiple calibration examples (4 of which include summation correction, and 1 that utilizes the “simplified” approach). Detection efficiencies for the simplified approaches are calculated in terms of instrument efficiency ( $\epsilon_i$ ), emergence factor ( $E_{i,j}^{-1}$ ), and the summarized emission intensity ( $n_{i,j}$ ) for a given energy region *i* and for the radiation type *j* (alpha or beta or photon radiation). As would be expected, the summation correction examples are more complicated and can involve many more steps depending on the complexity of the decay scheme.

The evaluation and comparison of the 1988 and 2016 ISO 7503 series, as described in the preceding paragraphs, was performed to assess the need for updates to instrument calibration and measurement methodologies in Revision 1 of this NUREG report. The ISO 7503-1:1988 standard was integral to the scan MDC methods which were developed in Revision 0 of this NUREG report and which are also used in the MARSSIM guidance. As such, those methods have been broadly accepted and used by decommissioning professionals for a number of years. With this in mind, the goal of this comparison was to compare the fundamental principles of surface contamination measurement from the 1988 and 2016 series, and to ensure that Revision 1 of this NUREG report represents acceptable practices which are also easily implementable by decommissioning professionals. To that end, the following observations and conclusions were generated:

- The fundamental principles of surface efficiency appear to be the same between the 1988 and 2016 standards, while new terminology (such as the *P*- and *E*-Factor) have been presented in 2016.
- The “default” values which are recommended for  $\epsilon_s$  (per the 1988 standard) and for *E* (per the 2016 standard) appear to be the same (acknowledging that one is essentially presented as a reciprocal of the other).
- The determination of detection efficiencies for multiple radionuclide decay paths/emissions, as presented in 2016, is a useful concept for decommissioning surveys.
- The 2016 summation correction methods are perhaps a more accurate methodology, but they require more effort and knowledge by the implementer. Evaluations in ISO 7503-3:2016 with respect to the consequences of the coincidence summing effect indicate that the extent of the coincidence summing effect on detection efficiency was not relatively large (i.e., the effect did not exceed 7 percent).
- The “simplified” approach presented in 2016 is more easily implementable by decommissioning professionals.

Based upon the ISO 7503 series comparison, it was concluded that there was no compelling reason to update the usage of the “surface efficiency” concept and terminology for Revision 1 of this NUREG. The continued usage of the “recommended values for  $\epsilon_s$ ,” as presented in Table 2 of ISO 7503-1:1988, are considered acceptable and valid as defaults. The comparison between the 1988 default surface efficiencies and the default emergence factors from the “simplified” 2016 approach indicates that the same fundamental principles and the same assumptions on self-absorption/back-scattering were utilized for both the 1988 and 2016 recommendations. However, there is still an understanding that site/radionuclide specific surface efficiencies could also be experimentally determined.

Based upon the ISO 7503 series comparison, it was also concluded that methodology presented in ISO 7503-3:2016 to address the cascade effect and coincident detection (i.e., where only one pulse is registered on an instrument during a cascade of multiple radiation emissions) provides a more accurate calibration approach than simplified methods which do not account for coincident detection. Such methodology would be acceptable and may be useful for complex calibrations. However, based upon the evaluation performed in ISO 7503-3:2016 on the extent of the coincidence summing effect (which concludes that “the analysis of the extent of the coincidence summing effect on the detection efficiency shows, that this effect does not exceed 7%”), consideration of coincident detection is not viewed as necessary for the purpose of calibrations of field instruments for decommissioning use. As such, the consideration of coincident detection is not further evaluated in this NUREG report.

Finally, it was concluded from the ISO 7503 comparison that there is a need for the determination of detection efficiencies for use with multiple radionuclides or with complex decay series. ISO 7503-3:2016 Annex A presents a method which utilizes instrument efficiency, the emergence factor, and the radiation emission intensity, and ISO 7503-3:2016 Annexes C and D describe considerations for mixtures of radionuclides. Revision 1 to this NUREG report similarly presents “weighted efficiency” calculations that utilize the concepts of instrument efficiency, source efficiency, and emission intensity, while also considering the relative fraction of radionuclides and branching ratios. The weighted efficiency concept is introduced below, and is further expanded upon in Appendix A.

The following discussion considers some of the factors that affect the instrument efficiency ( $\epsilon_i$ ). These detector-related factors include detector size (probe surface area), window density thickness, geometry, instrument response time, and ambient conditions, such as temperature, pressure, and humidity. The instrument efficiency also depends on the radionuclide source used for calibration and the solid angle effects, which include source-to-detector distance and source geometry. Finally, instrument efficiency is dependent on the energy of the radiation type. That is, the instrument efficiency for technetium (Tc)-99 (maximum beta energy of 294 keV) will not be the same as the efficiency for SrY-90 (maximum beta energy of 1,413 keV) given  $\epsilon_i$  increases with increasing energy. Appendix A presents detailed examples for estimating  $\epsilon_i$  when the source contains multiple radiological contaminants emitting a range of radiation energies. As Appendix A implies, the calculation of  $\epsilon_i$  follows these basic rules:

- Rule 1: If possible, select a source with the same radiation type and energy distribution as the contaminant.
- Rule 2: If a source that matches the contaminant energy is not available, select a source with a lesser average energy. This will underestimate the efficiency, which is preferred to overestimation when making decommissioning decisions.
- Rule 3: If there is a mixture of contaminants, calculate a weighted efficiency (for both  $\epsilon_i$  and  $\epsilon_s$ ), when possible, based on the relative fraction of radiological contaminants.

As an example, cobalt (Co)-60 and SrY-90 are the site contaminants, and preliminary data suggest activity fractions of 0.4 and 0.6, respectively. An SrY-90 check source is available. A Co-60 check source is not available, but a Tc-99 source is available. Tc-99 is a suitable proxy for Co-60, as the maximum Co-60 beta energy is 318 keV (with an emission intensity of 99.9 percent), and the maximum Tc-99 beta energy is 294 keV. A weighted efficiency is calculated by summing the products of the radionuclide-specific efficiencies and relative fractions:

$$\epsilon_i \text{ (weighted)} = (\epsilon_i \times RF)_{\text{Co-60}} + (\epsilon_i \times RF)_{\text{SrY-90}} \quad (\text{Eq. 4.4})$$

where  $RF$  is the relative fraction. If the instrument efficiencies for Tc-99 (the Co-60 proxy) and SrY-90 are 0.30 and 0.55, respectively, the weighted instrument efficiency is calculated as follows:

$$\epsilon_i \text{ (weighted)} = (0.30 \times 0.4) + (0.55 \times 0.6) = 0.45 \quad (\text{Eq. 4.5})$$

Section 5 covers some of the factors that affect the source efficiency ( $\epsilon_s$ ). Among these source-related factors are the type of radiation and its energy, source uniformity, surface roughness and coverings, and surface composition (e.g., wood, metal, concrete).

#### **4.1 Radionuclide Sources for Calibration**

For accurate measurements of total surface activity, field instruments must be calibrated appropriately. The MDC of an instrument depends on a variety of parameters, one of which involves the selection of calibration sources. Calibration sources should be selected that emit alpha or beta radiation with energies similar to those expected of the contaminant in the field. ISO 8769 recommends calibration source characteristics. As discussed in Section 5.5, the most representative calibration source would be one prepared from the radioactive material being assessed in the field. For example, both the uranium and thorium series emit a complex decay scheme of alpha, beta, and gamma radiations. Calibration to a single radionuclide must be

carefully assessed to ensure that it is representative of the detector's response to these decay series.

An instrument's MDC depends on the type and energy of radiation. The radionuclides selected for this study were chosen to represent the types or the range, or both, of energies commonly encountered in decommissioned facilities. These radionuclides are carbon (C)-14, nickel (Ni)-63, SrY-90, Tc-99, and thallium (Tl)-204 for beta measurements, and thorium (Th)-230 and plutonium (Pu)-239 for alpha measurements (uranium [U]-238 and americium [Am]-241 are also used in Appendix A case studies). The calibration sources used in the studies are traceable to NIST standards. Generally, the sources are of three geometric shapes: "button" sources (simulating a point source) of approximately 5 cm<sup>2</sup>, disc sources covering a standard area of approximately 15 cm<sup>2</sup>, or distributed sources that typically range from 126 to 150 cm<sup>2</sup>. Table 4-1 summarizes the calibration sources used.

The efficiencies determined in this section are for ideal laboratory conditions, which include the use of smooth, clean calibration source surfaces. Table 4-2 presents the average total efficiencies for the gas proportional, GM, and ZnS detectors compiled from historical calibration data at ORAU. Table 4-3 shows MDCs calculated for the gas proportional detector ( $\alpha + \beta$  mode) and the GM detector using the ambient background count rates given in Table 5-1 and the total efficiencies in Table 4-2. As expected, the MDCs decrease with increasing beta energy. Figures 4-1 and 4-2 show this graphically for the gas proportional and GM detectors, respectively. For beta energies (beta endpoint energies are used here) ranging from 300 to 1,400 keV, the calculated MDCs are generally constant. However, the MDCs increase rapidly with decreasing beta energies below 300 keV.

The determination of source efficiencies in Section 5 required the assessment of instrument efficiencies under specific experimental conditions. Among these conditions are active area of source, detector specifications, and a source-to-detector geometry that included two sheets of Mylar. Table 4-4 shows instrument efficiencies determined under these conditions.

## **4.2 Source-to-Detector Distance**

The distance between a source and the detector is another factor that may affect the instrument efficiency and, thus, the MDC. In this study, instrument MDC was evaluated as a function of distance from the source. The range of distances was selected to be appropriate for the type of radiation being measured, with consideration of the typical detector-to-surface distances encountered in performing surveys in support of decommissioning. Counts of 1 minute in duration were made with the detector at various distances above the source.

The source-to-detector distance was evaluated using a Ludlum model 43-68 gas proportional detector with a 0.8 mg/cm<sup>2</sup> window for beta-emitters, including C-14, Ni-63, SrY-90, Tc-99 (two source geometries were used), and Tl-204, and for Pu-239 and Th-230 (two source geometries were used). Five 1-minute measurements were made at contact and at distances of 0.5, 1, and 2 centimeters. The distances were obtained by cutting out the specified thicknesses of plastic and using them to maintain the desired source-to-detector spacing. Tables 4-5 and 4-6 show the results of an increasing source-to-detector distance on instrument response. Specifically, the net count rate obtained at each distance was normalized to the net count rate obtained in contact with the source. These results demonstrate the significant reduction in instrument response that can occur when source-to-detector distance is increased by less than 1 centimeter.

As expected, the greatest reduction in detector response per increased distance from the source was obtained for the alpha and low-energy beta-emitters (i.e., Ni-63 and C-14). The modest reduction in instrument response for the alpha-emitting Pu-239 and Th-230 sources, from being in contact with the source to 1 cm, was somewhat unexpected. Compared to the alpha-emitters, C-14 and Ni-63 exhibited equal or greater reductions in instrument response over this range. Somewhat more expected was the dramatic reduction in instrument response from 1 to 2 centimeters for the Pu-239 and Th-230 sources. The instrument response to the Th-230 disc source at 2 centimeters was only 4 percent of the response obtained in contact with the source. The Th-230 response was contrasted to the Pu-239 disc source that exhibited 20 percent of the response at 2 centimeters relative to the contact measurement. The greater instrument response of Pu-239 at 2 centimeters compared to Th-230 at the same distance was likely the result of the higher energy of the Pu-239 alpha emission (i.e., 5.1 megaelectron volts (MeV) for Pu-239 versus 4.7 MeV for Th-230).

The data presented in Tables 4-5 and 4-6 were used to determine total efficiencies as a function of detector-to-source distance. Although total efficiencies were determined and reported at each distance, the detector-to-source distance influences the instrument efficiency ( $\epsilon_i$ ) (as opposed to  $\epsilon_s$ ). These total efficiencies were used to calculate the MDCs presented in Tables 4-7 and 4-8. Figures 4-3 and 4-4 illustrate the effects of source-to-detector distance on the MDC for the beta-emitters. These figures show that the source-to-detector distance effect on MDCs was relatively minor for the higher energy beta-emitters (e.g., SrY-90 and TI-204), but considerable for the low- to mid-energy beta-emitters. Figure 4-5 shows the effects of source-to-detector distance on the MDC for alpha-emitters. For alpha-emitters, the MDCs gradually increased as the detector-to-source spacing increased from contact to 1 centimeter. At a distance of 2 centimeters, consistent with the substantial reduction in total efficiency, the MDCs increased significantly. The MDC determined for Ni-63 at a detector-to-source distance of 2 centimeters was  $52,000 \pm 56,000$  dpm/100 cm<sup>2</sup>, with the relatively large uncertainty attributed to the error in the total efficiency determination. This magnitude of uncertainty in the MDC term suggests that the detection capability for the measurement process (i.e., detecting Ni-63 with a gas proportional detector 2 centimeters from the surface) is likely overestimated. This particular example illustrates the need to adjust the MDC to account for uncertainties in the calibration factors (refer to Section 3.1 for a discussion of MDC adjustment factors).

The practicality of these results is evident by the deviation in instrument response that results when the source-to-detector distance during calibration is only slightly different (i.e., less than 1 centimeter for some radionuclides) from the detector-to-surface spacing maintained during field measurements of surface activity. That is, small changes in detector-to-surface distance produce significant changes in detector response, especially for alpha and low-energy beta radiation (1 to 2-centimeter spacing is not unusual for a roughly scabbled concrete surface). The effects of distance on TI-204 and SrY-90, although less than those on lower energy beta-emitters, were still appreciable.

To minimize the effects of source-to-detector distance on MDCs, it is recommended that the detector be calibrated at a source-to-detector distance that is similar to the expected detector-to-surface spacing in the field.

### **4.3 Window Density Thickness**

The detector-related factors that may change the instrument MDC are detector size (probe surface area), window density thickness, geotropism, instrument response time, and ambient conditions such as temperature, pressure, and humidity. Often, this information is already

available. For example, the effects of ambient conditions and geotropism are usually tested by users concerned about the instrument or detector performance (Swinth & Kenoyer, 1984; Los Alamos National Laboratory, 1986).

One detector-related factor evaluated in this report was the effect of window density thickness on instrument response (using the Ludlum model 43-68) for C-14, Ni-63, Sr-90, Tc-99 (two source geometries were used for Tc-99), and Tl-204. Window density thickness for gas proportional detectors may be varied to provide a mechanism to control instrument response to various surface activity conditions. For example, in the assessment of low-energy beta-emitters, a relatively thin window (e.g., 0.4 mg/cm<sup>2</sup>) provides greater sensitivity. Similarly, when beta radiation in the presence of alpha radiation must be assessed, it is possible to selectively discriminate out the alpha radiation using an alpha shield (i.e., using 3.8-mg/cm<sup>2</sup> window density thickness).

Measurements were made for window density thicknesses of 0.3, 0.4, 0.8, and 3.8 mg/cm<sup>2</sup>. In addition, measurements at window density thicknesses of 1.3, 1.8, 2.3, 2.8, and 3.3 mg/cm<sup>2</sup> were taken for the two Tc-99 source geometries. Window density thicknesses were varied by adding sheets of 0.5-mg/cm<sup>2</sup> Mylar between the source and the detector. Table 4-9 gives the results of these measurements. Figures 4-6 and 4-7 illustrate the effects of window density thickness on the total efficiency. The total efficiency was reduced more significantly for the lower energy beta-emitters as the window density thickness was increased.

The total efficiencies presented in Table 4-9 were used to calculate the MDCs as a function of window density thickness (Table 4-10). Figures 4-8 and 4-9 illustrate the effects of window density thickness on the MDC for the beta-emitters. These figures show, as did the source-to-detector distance evaluation, that the window density thickness over the range of 0.3 to 3.8 mg/cm<sup>2</sup> has a moderate effect (less than a 30-percent increase) on MDCs for the higher energy beta-emitters (e.g., SrY-90 and Tl-204), but the effect was considerable for the low- to mid-energy beta-emitters. These figures illustrate how the window density thickness significantly affects the detector MDC calibrated to lower energy beta-emitters. As with source-to-detector distance on MDCs, it is essential that the detector be calibrated with the same window density thickness that will be used for survey measurements in the field. This concern may arise if the window is replaced in the field with one of a different thickness and returned to service without recalibration.

#### **4.4 Source Geometry Factors**

The source geometry must be considered in determining the instrument MDC. The contaminant's distribution on the surface being assessed may influence the detector's response. For example, if the contamination is characterized by relatively large, uniform areas of activity, then the detector should be calibrated to a distributed or extended source. Similarly, if the surface is characterized by localized spots of surface contamination that may be approximated by a point source, then the calibration source should be similar to a point source geometry.

The study evaluated the source geometry effect on detector response by determining the instrument efficiencies ( $\epsilon_i$ ) for gas proportional, GM, and ZnS detectors placed in contact with both distributed and disc sources. The radionuclide sources used in this evaluation were Tc-99 and Th-230. Table 4-11 shows the instrument efficiencies determined for each detector and geometry configuration. The instrument efficiencies determined with the disc sources were 6 to 42 percent greater than those obtained with the distributed sources. These results were expected because of the solid angle of the measurement geometry. That is, for the smaller disc

source, a larger fraction of the radiation particles ( $\alpha$  and  $\beta$ ) emitted from the source intersect the detector probe area. Walker (1994) provides more information on the effects of source-to-detector geometry.

During the performance of field survey measurements, it would be time consuming to select the most appropriate instrument efficiency for determining the contaminant geometry at each measurement location. The benefits of a better defined contaminant geometry should be weighed against the increased labor expended in characterizing the contamination. It may be appropriate (conservative) to use the instrument efficiency obtained from a distributed source geometry for all surface activity measurement locations, except for those locations of elevated direct radiation. In fact, many facilities perform calibrations during decommissioning that include efficiencies determined from both large-area and small disc calibration sources. Then, the contaminant geometry is characterized only for locations of elevated direct radiation so as to select the most appropriate instrument efficiency. This effort is usually made when a cost/benefit analysis demonstrates that the less conservative disc (i.e., hotspot) efficiency is warranted. Additionally, ISO-8769:2016 recommends that the calibration source dimensions be sufficient to provide an area of at least 100 cm<sup>2</sup>—certainly a distributed source.

#### **4.5 Ambient Background Count Rate**

The study evaluated the effects of ambient background (in particular, relatively high ambient background) on the calculated MDC and measured activity concentration of a radioactive source using a GM detector. The procedure included collecting five 1-minute measurements of the ambient background, followed by five 1-minute measurements of a NIST-traceable Tc-99 disc source (activity concentration was 1,500 dpm within a 5-cm<sup>2</sup> active area). A jig was used to ensure that a reproducible geometry was maintained for each measurement. The ambient background was increased by placing cesium (Cs)-137 sources at various distances from the GM detector. The ambient background levels ranged from approximately 50 to 1,500 cpm. This procedure allowed a comparison of the *a priori* MDC and the measured activity concentration of the Tc-99 source. The measured activity concentration was calculated using a total efficiency of 0.17 c/dis (from Table 4-2); no probe area correction was made since it was known that the source activity was limited to a 5-cm<sup>2</sup> area. Table 4-12 presents the tabulated results.

As expected from the MDC equation, the calculated detection sensitivity (or MDC) of the GM detector increased directly with the square root of the ambient background level (Figure 4-10). For ambient background levels ranging from 50 to 145 cpm (consistent with background levels typically encountered during final status surveys), the measured activity of the Tc-99 was very similar to the stated activity of the source. As the ambient background levels were increased to 1,000 cpm, the measured activity was, with one exception, consistently lower than the certified source activity. As the ambient background was further increased to 1,500 cpm, the measured activity was less than 60 percent of the certified source activity, with significant uncertainty at the 95-percent confidence level.

In general, as the ambient background increases, and the ratio of the calculated MDC to the actual activity concentration present approaches unity, the uncertainty in the measured activity increases. However, only when the calculated MDC was approximately 70 percent of the actual activity concentration (MDC equal to 1,070 dpm per 5 cm<sup>2</sup>) was there significant uncertainty and inaccuracy in the measured activity. For the case in which the MDC is a small fraction of the guideline value, significant uncertainty in the value is acceptable (e.g.,  $\pm 100\%$  uncertainty in a value that is 20 percent of the guideline gives adequate assurance of compliance with the

guideline). If this is not the case, caution must be used when making measurements that are close to the MDC, because they may have substantial uncertainties.

**Table 4-1 Characteristics of Radionuclide Sources Used for Calibration and Static Measurements**

| Radionuclide | Active Area (cm <sup>2</sup> ) | Activity (Emission Rate) | Source Backing Material | Surface Coating                         |
|--------------|--------------------------------|--------------------------|-------------------------|---|
| C-14         | 13                             | 12,860 cpm               | Stainless steel (S.S.)  | 0.9 mg/cm <sup>2</sup> aluminized Mylar |
| C-14         | 13                             | 959,000 cpm              | S.S.                    | 0.9 mg/cm <sup>2</sup> aluminized Mylar |
| Ni-63        | 15                             | 16,600 cpm               | Ni                      | NA                                      |
| SrY-90       | 15                             | 36,800 cpm               | S.S./Kapton/Al          | NA                                      |
| SrY-90       | 13                             | 8,080 cpm                | Ni                      | NA                                      |
| Tc-99        | 4.9                            | 940 cpm                  | S.S.                    | NA                                      |
| Tc-99        | 4.9                            | 83,400 cpm               | S.S.                    | NA                                      |
| Tc-99        | 126                            | 26,300 cpm               | S.S./Al                 | NA                                      |
| Tc-99        | 150                            | 14,400 cpm               | S.S.                    | NA                                      |
| Tl-204       | 15                             | 6,920 cpm                | S.S.                    | NA                                      |
| Th-230       | 150                            | 25,100 cpm               | S.S.                    | NA                                      |
| Th-230       | 126                            | 28,200 cpm               | S.S./Al                 | NA                                      |
| Th-230       | 5.1                            | 52,700 cpm               | Ni                      | NA                                      |
| Pu-239       | 5.1                            | 46,300 cpm               | Ni                      | NA                                      |

**Table 4-2 Average Total Efficiencies for Various Detectors and Radionuclides**

| Radionuclide<br>(Maximum $\beta$ Energy) | Total Efficiency (c/dis) <sup>a</sup> |                   |                                      |        |      |
|--|---------------------------------------|-------------------|--------------------------------------|--------|------|
|  | Gas Proportional                      |                   |                                      | GM     | ZnS  |
|  | $\alpha$ Only                         | $\beta$ Only      | $\alpha+\beta$                       |        |      |
| <b>Beta</b>                              |                                       |                   |                                      |        |      |
| Ni-63 (67 keV)                           | — <sup>b</sup>                        | —                 | 0.08, <sup>c</sup> 0.06 <sup>d</sup> | 0.0025 | —    |
| C-14 (156 keV)                           | —                                     | 0.04 <sup>e</sup> | 0.11 <sup>d</sup>                    | 0.05   | —    |
| Tc-99 (294 keV)                          | —                                     | 0.16 <sup>e</sup> | 0.22 <sup>d</sup>                    | 0.17   | —    |
| Tl-204 (764 keV)                         | —                                     | 0.29 <sup>e</sup> | 0.35 <sup>d</sup>                    | 0.26   | —    |
| SrY-90 (1,413 keV)                       | —                                     | 0.36 <sup>e</sup> | 0.42 <sup>d</sup>                    | 0.32   | —    |
| Ru-106/Rh-106<br>(1,410 keV)             | —                                     | 0.55 <sup>e</sup> | 0.57 <sup>c</sup>                    | 0.56   | —    |
| <b>Alpha</b>                             |                                       |                   |                                      |        |      |
| Th-230                                   | 0.19 <sup>d</sup>                     | —                 | —                                    | —      | 0.18 |
| Pu-239                                   | —                                     | —                 | —                                    | —      | 0.19 |

<sup>a</sup>The total efficiencies represent average values compiled from historical instrument calibration data. These values should be considered as the ideal efficiencies obtained under laboratory conditions. Calibration sources were typically on stainless steel or nickel backing material.

<sup>b</sup>Data not obtained.

<sup>c</sup>For window density thickness of 0.4 mg/cm<sup>2</sup>.

<sup>d</sup>For window density thickness of 0.8 mg/cm<sup>2</sup>.

<sup>e</sup>For window density thickness of 3.8 mg/cm<sup>2</sup>.



**Table 4-3 MDCs for Various Detectors and Radionuclides**

| Radionuclide<br>(Endpoint $\beta$ Energy) | Minimum Detectable Concentration (dpm/100 cm <sup>2</sup> ) <sup>a</sup> |        |
|---|--|--------|
|   | Gas Proportional ( $\alpha+\beta$ )                                      | GM     |
| Ni-63 (66 keV)                            | 1,160 <sup>b</sup>   | 70,000 |
| C-14 (156 keV)                            | 630  | 3,500  |
| Tc-99 (294 keV)                           | 320  | 1,000  |
| Tl-204 (763 keV)                          | 200  | 670    |
| SrY-90 (1,415 keV)                        | 170  | 550    |

<sup>a</sup>MDCs were calculated on the basis of the ambient background count rates presented in Table 5-1 for the gas proportional detector ( $\alpha+\beta$  mode) and the GM detector and the total efficiencies in Table 4-2. Probe area corrections of 126 and 20 cm<sup>2</sup>, respectively, were made for the gas proportional and GM detectors. The following MDC equation was used for 1-minute counts:

$$MDC = \frac{3 + 4.65\sqrt{C_B}}{KT}$$

<sup>b</sup>MDC was calculated using total efficiency for window density thickness of 0.8 mg/cm<sup>2</sup> (0.06 c/dis).

**Table 4-4 Instrument Efficiencies**

| Radionuclide | Instrument Efficiency <sup>a</sup> |  |               |               |                |               |
|--------------|------------------------------------|--|---------------|---------------|----------------|---------------|
|              | $\alpha + \beta$                   | Active Area of Source (cm <sup>2</sup> ) | $\beta$ only  | GM            | $\alpha$ only  | ZnS           |
| C-14         | 0.254 ± 0.006 <sup>b</sup>         | 13                                       | 0.081 ± 0.002 | 0.099 ± 0.002 | — <sup>c</sup> | —             |
| Tc-99        | 0.364 ± 0.029                      | 126                                      | 0.191 ± 0.016 | 0.193 ± 0.021 | —              | —             |
| Tl-204       | 0.450 ± 0.025                      | 15                                       | 0.355 ± 0.021 | 0.278 ± 0.017 | —              | —             |
| SrY-90       | 0.537 ± 0.027                      | 13                                       | 0.465 ± 0.024 | 0.388 ± 0.020 | —              | —             |
| Th-230       | —                                  | 126                                      | —             | —             | 0.349 ± 0.015  | 0.259 ± 0.013 |

<sup>a</sup>The instrument efficiency was determined with the detector at contact with the source, separated by two sheets of Mylar (0.22 mg/cm<sup>2</sup> per sheet). The instrument efficiency was calculated by dividing the net count rate by the 2 $\pi$  emission rate of the source.

<sup>b</sup>Uncertainties represent the 95-percent confidence interval, based on propagating the errors in the calibration source emission rate and in counting statistics.

<sup>c</sup>Measurement not made.

**Table 4-5 Source-to-Detector Distance Effects for Beta-Emitters**

| Distance from Source (cm) | Normalized Net Count Rate <sup>a, b</sup> |               |                 |                     |               |                 |
|---------------------------|---|---------------|-----------------|---------------------|---------------|-----------------|
|                           | Ni-63 (Disc)                              | C-14 (Disc)   | Tc-99 (Disc)    | Tc-99 (Distributed) | Tl-204 (Disc) | SrY-90 (Disc)   |
| Contact                   | 1   | 1             | 1               | 1                   | 1             | 1               |
| 0.5                       | 0.381 ± 0.064 <sup>c</sup>                | 0.786 ± 0.047 | 0.864 ± 0.016   | 0.803 ± 0.015       | 0.910 ± 0.024 | 0.9189 ± 0.0065 |
| 1                         | 0.196 ± 0.053                             | 0.648 ± 0.048 | 0.7779 ± 0.0085 | 0.701 ± 0.023       | 0.836 ± 0.026 | 0.8534 ± 0.0088 |
| 2                         | 0.038 ± 0.041                             | 0.431 ± 0.034 | 0.5920 ± 0.0090 | 0.503 ± 0.014       | 0.645 ± 0.033 | 0.6995 ± 0.0063 |

<sup>a</sup>Normalized net count rate determined by dividing the net count rate at each distance by the net count rate at contact with the source.

<sup>b</sup>Gas proportional detector operated in the  $\alpha + \beta$  mode was used for all measurements.

<sup>c</sup>Uncertainties represent the 95-percent confidence interval, based on propagating the counting errors in each measurement.

**Table 4-6 Source-to-Detector Distance Effects for Beta-Emitters**

| Distance from Source (cm) | Normalized Net Count Rate <sup>a, b</sup> |                 |                      |
|---------------------------|---|-----------------|----------------------|
|                           | Pu-239 (Disc)                             | Th-230 (Disc)   | Th-230 (Distributed) |
| Contact                   | 1   | 1               | 1                    |
| 0.5                       | 0.808 ± 0.013 <sup>c</sup>                | 0.812 ± 0.010   | 0.761 ± 0.026        |
| 1                         | 0.656 ± 0.015                             | 0.606 ± 0.012   | 0.579 ± 0.021        |
| 2                         | 0.1974 ± 0.0046                           | 0.0423 ± 0.0027 | 0.0990 ± 0.0093      |

<sup>a</sup>Normalized net count rate determined by dividing the net count rate at each distance by the net count rate at contact with the source.

<sup>b</sup>Gas proportional detectors operated in the α mode were used for all measurements.

<sup>c</sup>Uncertainties represent the 95-percent confidence interval, based on propagating the counting errors in each measurement.

**Table 4-7 MDCs for Various Source-to-Detector Distances for Beta-Emitters**

| Distance from Source (cm) | Total Efficiency (c/dis) and MDC (dpm/100 cm <sup>2</sup> ) <sup>a, b</sup> |                 |                 |             |                 |          |                     |          |               |          |               |             |
|---------------------------|---|-----------------|-----------------|-------------|-----------------|----------|---------------------|----------|---------------|----------|---------------|-------------|
|                           | Ni-63   |                 | C-14            |             | Tc-99 (Disc)    |          | Tc-99 (Distributed) |          | TI-204        |          | SrY-90        |             |
|                           | EFF   | MDC             | EFF             | MDC         | EFF             | MDC      | EFF                 | MDC      | EFF           | MDC      | EFF           | MDC         |
| Contact                   | 0.0360 ± 0.0041 <sup>c</sup>  | 2,000 ± 250     | 0.1006 ± 0.0051 | 715 ± 51    | 0.250 ± 0.010   | 287 ± 19 | 0.207 ± 0.016       | 347 ± 32 | 0.338 ± 0.015 | 213 ± 14 | 0.464 ± 0.016 | 154.9 ± 9.5 |
| 0.5                       | 0.0137 ± 0.0019   | 5,250 ± 760     | 0.0790 ± 0.0034 | 910 ± 61    | 0.2164 ± 0.0090 | 332 ± 22 | 0.166 ± 0.013       | 433 ± 41 | 0.308 ± 0.013 | 234 ± 16 | 0.427 ± 0.014 | 169 ± 10    |
| 1                         | 0.0071 ± 0.0018   | 10,200 ± 2,600  | 0.0652 ± 0.0040 | 1,103 ± 88  | 0.1947 ± 0.0076 | 369 ± 24 | 0.145 ± 0.012       | 496 ± 49 | 0.282 ± 0.013 | 255 ± 18 | 0.396 ± 0.014 | 181 ± 11    |
| 2                         | 0.0014 ± 0.0015   | 52,000 ± 56,000 | 0.0434 ± 0.0029 | 1,660 ± 140 | 0.1482 ± 0.0060 | 485 ± 32 | 0.1042 ± 0.0086     | 690 ± 67 | 0.218 ± 0.014 | 330 ± 27 | 0.325 ± 0.011 | 221 ± 14    |

<sup>a</sup>Measurements were made with a gas proportional detector operated in the α + β mode with an 0.8-mg/cm<sup>2</sup> window density thickness.

<sup>b</sup>The instrument background was 355 counts, and probe area corrections of 126 cm<sup>2</sup> were made for the gas proportional detectors. The following MDC equation was used for 1-minute counts:

$$MDC = \frac{3 + 4.65 \sqrt{C}}{KT} B$$

<sup>c</sup>Uncertainties represent the 95-percent confidence interval, based on propagating the errors in the calibration source activity and in counting statistics.

**Table 4-8 MDCs for Various Source-to-Detector Distances for Alpha-Emitters**

| Distance from Source (cm) | Total Efficiency (c/dis) and MDC (dpm/100 cm <sup>2</sup> ) <sup>a, b</sup> |          |                   |           |                      |           |
|---------------------------|---|----------|-------------------|-----------|----------------------|-----------|
|                           | Pu-239 (Disc)   |          | Th-230 (Disc)     |           | Th-230 (Distributed) |           |
|                           | EFF   | MDC      | EFF               | MDC       | EFF                  | MDC       |
| Contact                   | 0.2549 ± 0.0053 <sup>c</sup>  | 24 ± 14  | 0.2495 ± 0.0044   | 24 ± 15   | 0.2002 ± 0.0097      | 30 ± 18   |
| 0.5                       | 0.2061 ± 0.0036   | 29 ± 18  | 0.1910 ± 0.0034   | 32 ± 19   | 0.1524 ± 0.0067      | 40 ± 24   |
| 1                         | 0.1672 ± 0.0040   | 36 ± 22  | 0.1426 ± 0.0034   | 43 ± 26   | 0.1160 ± 0.0052      | 52 ± 32   |
| 2                         | 0.0503 ± 0.0012   | 121 ± 73 | 0.00994 ± 0.00069 | 610 ± 370 | 0.0198 ± 0.0019      | 310 ± 190 |

<sup>a</sup>Measurements were made with a gas proportional detector operated in the α mode with a 0.8 mg/cm<sup>2</sup> window density thickness.

<sup>b</sup>The instrument background was 1 count, and probe area corrections of 126 cm<sup>2</sup> were made for the gas proportional detectors. The following MDC equation was used for 1-minute counts:

$$MDC = \frac{3 + 4.65 \sqrt{C}}{KT} B$$

<sup>c</sup>Uncertainties represent the 95-percent confidence interval, based on propagating the errors in the calibration source activity and in counting statistics.

**Table 4-9 Window Density Thickness Effects for Beta-Emitters**

| Window Density Thickness (mg/cm <sup>2</sup> ) | Total Efficiency (C/dis) <sup>a</sup> |                 |                 |                     |               |               |
|--|---------------------------------------|-----------------|-----------------|---------------------|---------------|---------------|
|  | Ni-63 (Disc)                          | C-14 (Disc)     | Tc-99 (Disc)    | Tc-99 (Distributed) | Tl-204 (Disc) | SrY-90 (Disc) |
| 0.3  | 0.0695 ± 0.0041 <sup>b</sup>          | 0.1273 ± 0.0032 | 0.288 ± 0.011   | 0.227 ± 0.018       | 0.354 ± 0.018 | 0.477 ± 0.017 |
| 0.4  | 0.0699 ± 0.0032                       | 0.1302 ± 0.0039 | 0.291 ± 0.011   | 0.224 ± 0.018       | 0.359 ± 0.015 | 0.482 ± 0.019 |
| 0.8  | 0.0409 ± 0.0020                       | 0.1096 ± 0.0032 | 0.266 ± 0.011   | 0.209 ± 0.017       | 0.342 ± 0.015 | 0.474 ± 0.017 |
| 1.3  | — <sup>c</sup>                        | —               | 0.247 ± 0.010   | 0.196 ± 0.016       | —             | —             |
| 1.8  | —                                     | —               | 0.2268 ± 0.0092 | 0.183 ± 0.015       | —             | —             |
| 2.3  | —                                     | —               | 0.2117 ± 0.0090 | 0.170 ± 0.013       | —             | —             |
| 2.8  | —                                     | —               | 0.1980 ± 0.0085 | 0.157 ± 0.012       | —             | —             |
| 3.3  | —                                     | —               | 0.1848 ± 0.0074 | 0.149 ± 0.012       | —             | —             |
| 3.8  | 0.0005 ± 0.0011                       | 0.0383 ± 0.0018 | 0.1638 ± 0.0064 | 0.129 ± 0.010       | 0.275 ± 0.012 | 0.429 ± 0.015 |

<sup>a</sup>Gas proportional detectors operated in the α + β mode were used for all measurements.

<sup>b</sup>Uncertainties represent the 95-percent confidence interval, based on propagating the errors in the calibration source activity and in counting statistics.

<sup>c</sup>Measurement not made.

**Table 4-10 Window Density Thickness Effects for Beta-Emitters**

| Window Density Thickness (mg/cm <sup>2</sup> ) | MDC (dpm/100 cm <sup>2</sup> ) <sup>a, b</sup> |             |              |                     |               |               |
|--|--|-------------|--------------|---------------------|---------------|---------------|
|  | Ni-63 (Disc)                                   | C-14 (Disc) | Tc-99 (Disc) | Tc-99 (Distributed) | Tl-204 (Disc) | SrY-90 (Disc) |
| 0.3  | 1,014 ± 80 <sup>c</sup>                        | 554 ± 32    | 245 ± 16     | 311 ± 30            | 199 ± 14      | 147.9 ± 9.4   |
| 0.4  | 1,016 ± 71                                     | 546 ± 33    | 244 ± 16     | 317 ± 30            | 198 ± 13      | 147.3 ± 9.6   |
| 0.8  | 1,760 ± 120                                    | 656 ± 39    | 270 ± 18     | 344 ± 32            | 210 ± 14      | 151.8 ± 9.6   |
| 1.3  | — <sup>d</sup>                                 | —           | 291 ± 19     | 367 ± 34            | —             | —             |
| 1.8  | —  | —           | 317 ± 21     | 392 ± 38            | —             | —             |
| 2.3  | —  | —           | 340 ± 23     | 423 ± 40            | —             | —             |
| 2.8  | —  | —           | 363 ± 24     | 457 ± 43            | —             | —             |
| 3.3  | —  | —           | 389 ± 25     | 482 ± 46            | —             | —             |
| 3.8  | 130,000 ± 290,000                              | 1,860 ± 130 | 435 ± 28     | 555 ± 52            | 259 ± 18      | 166 ± 10      |

<sup>a</sup>Gas proportional detectors operated in the α + β mode were used for all measurements.

<sup>b</sup>Background levels were determined for each window density thickness, and efficiencies were used from Table 4-9. Probe area corrections of 126 cm<sup>2</sup> were made for the gas proportional detectors. The following MDC equation was used for 1-minute counts:

$$MDC = \frac{3 + 4.65 \sqrt{C_B}}{KT}$$

<sup>c</sup>Uncertainties represent the 95-percent confidence interval, based on propagating the errors in the calibration source activity and in counting statistics.

<sup>d</sup>Measurement not made.

**Table 4-11 Source Geometry Effects on Instrument Efficiency**

| Source Geometry                      | Instrument Efficiency <sup>a</sup> |               |               |                 |                 |  |
|--------------------------------------|------------------------------------|---------------|---------------|-----------------|-----------------|--|
|                                      | Tc-99                              |               |               | Th-230          |                 |  |
|                                      | $\alpha + \beta$                   | $\beta$ only  | GM            | $\alpha$ only   | ZnS             |  |
| Point (Disc) Source <sup>b</sup>     | 0.445 ± 0.017 <sup>c</sup>         | 0.253 ± 0.010 | 0.278 ± 0.012 | 0.4979 ± 0.0089 | 0.3304 ± 0.0068 |  |
| Distributed Source <sup>d</sup>      | 0.382 ± 0.030                      | 0.199 ± 0.016 | 0.195 ± 0.023 | 0.397 ± 0.020   | 0.313 ± 0.016   |  |
| Ratio of Point-to-Distributed Source | 1.16                               | 1.27          | 1.42          | 1.25            | 1.06            |  |

<sup>a</sup>The instrument efficiency was determined by dividing the net count rate by the  $2\pi$  emission rate of the source.

<sup>b</sup>The point (disc) source area for both Tc-99 and Th-230 was 5 cm<sup>2</sup>.

<sup>c</sup>Uncertainties represent the 95-percent confidence interval, based on propagating the errors in the calibration source emission rate and in counting statistics.

<sup>d</sup>The distributed source area for both Tc-99 and Th-230 was 126 cm<sup>2</sup>.

**Table 4-12 Ambient Background Effects**

| <b>Background<sup>a</sup> (cpm)</b> | <b>Gross Counts (cpm)</b> | <b>Measured Activity<sup>b</sup> (dpm)</b> | <b>MDC<sup>c</sup> (dpm)</b> |
|-------------------------------------|---------------------------|--|------------------------------|
| 53.0 ± 9.2 <sup>d</sup>             | 295 ± 32                  | 1,420 ± 190                                | 220                          |
| 117 ± 22                            | 375 ± 26                  | 1,520 ± 200                                | 310                          |
| 145 ± 20                            | 413 ± 56                  | 1,580 ± 350                                | 350                          |
| 192 ± 26                            | 399 ± 38                  | 1,220 ± 270                                | 400                          |
| 223 ± 26                            | 458 ± 35                  | 1,380 ± 280                                | 430                          |
| 291 ± 44                            | 538 ± 54                  | 1,450 ± 410                                | 480                          |
| 445 ± 46                            | 725 ± 66                  | 1,650 ± 480                                | 590                          |
| 594 ± 42                            | 815 ± 38                  | 1,300 ± 330                                | 680                          |
| 1,021 ± 38                          | 1,223 ± 55                | 1,190 ± 390                                | 890                          |
| 1,490 ± 100                         | 1,642 ± 91                | 880 ± 800                                  | 1,070                        |

<sup>a</sup>Measurements were made with an Eberline model HP-260 GM detector.

<sup>b</sup>Measured activity was calculated by subtracting the background from the gross counts and dividing by a total efficiency of 0.17 c/dis. Gross counts were determined by the average of five 1-minute measurements of a Tc-99 source.

<sup>c</sup>The following MDC equation was used for 1-minute counts and an assumed efficiency of 0.17 c/dis:

$$MDC = \frac{3 + 4.65\sqrt{C_B}}{KT}$$

<sup>d</sup>Uncertainties represent the 95-percent confidence interval, based on propagating the counting errors in each measurement

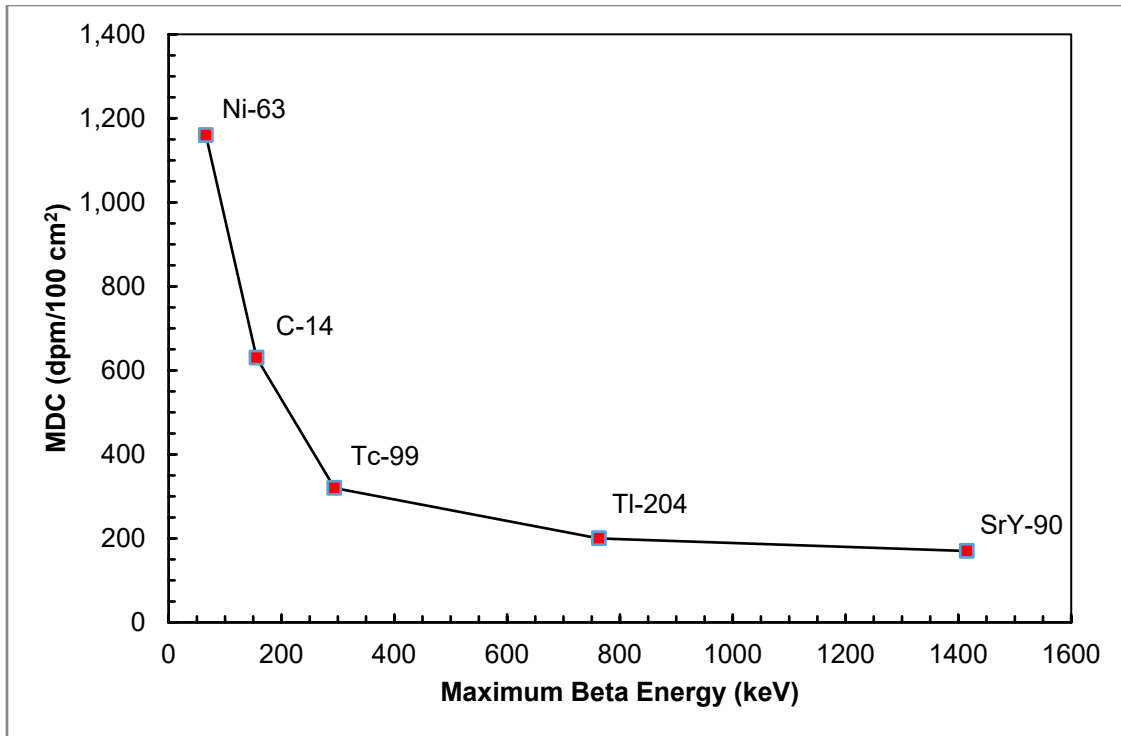


Figure 4-1 MDCs for Gas Proportional Detector ( $\alpha+\beta$ ) Mode for Various Radionuclides

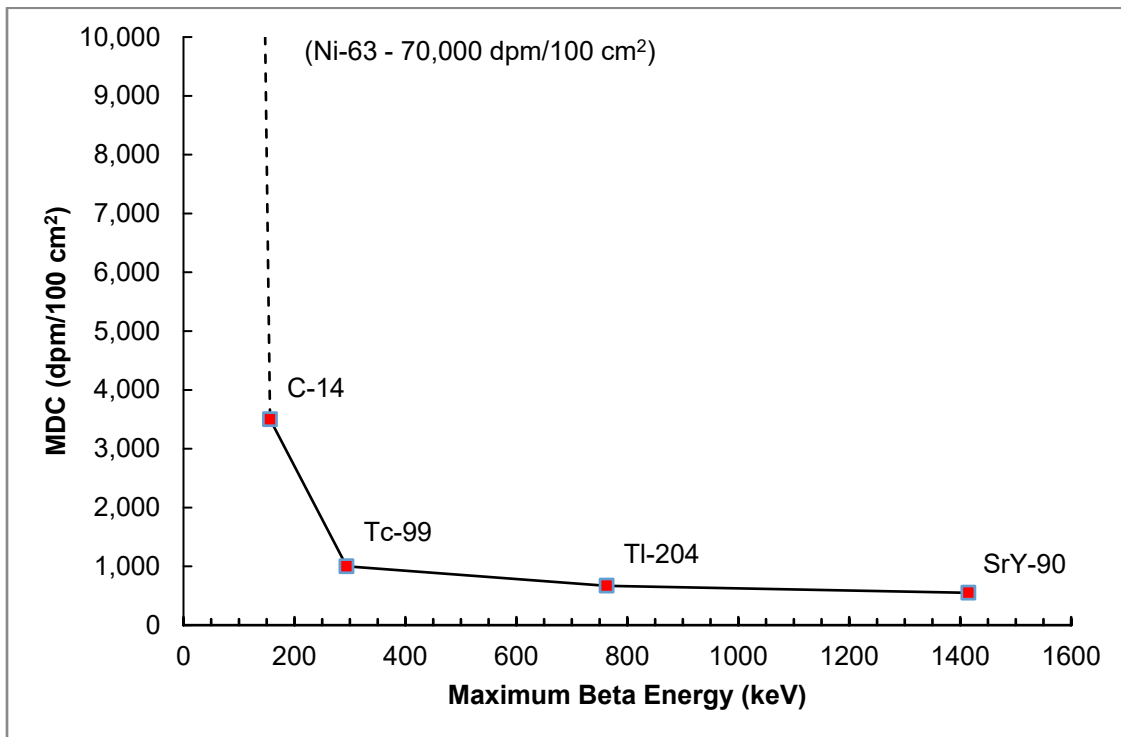


Figure 4-2 MDCs for GM Detector for Various Radionuclides



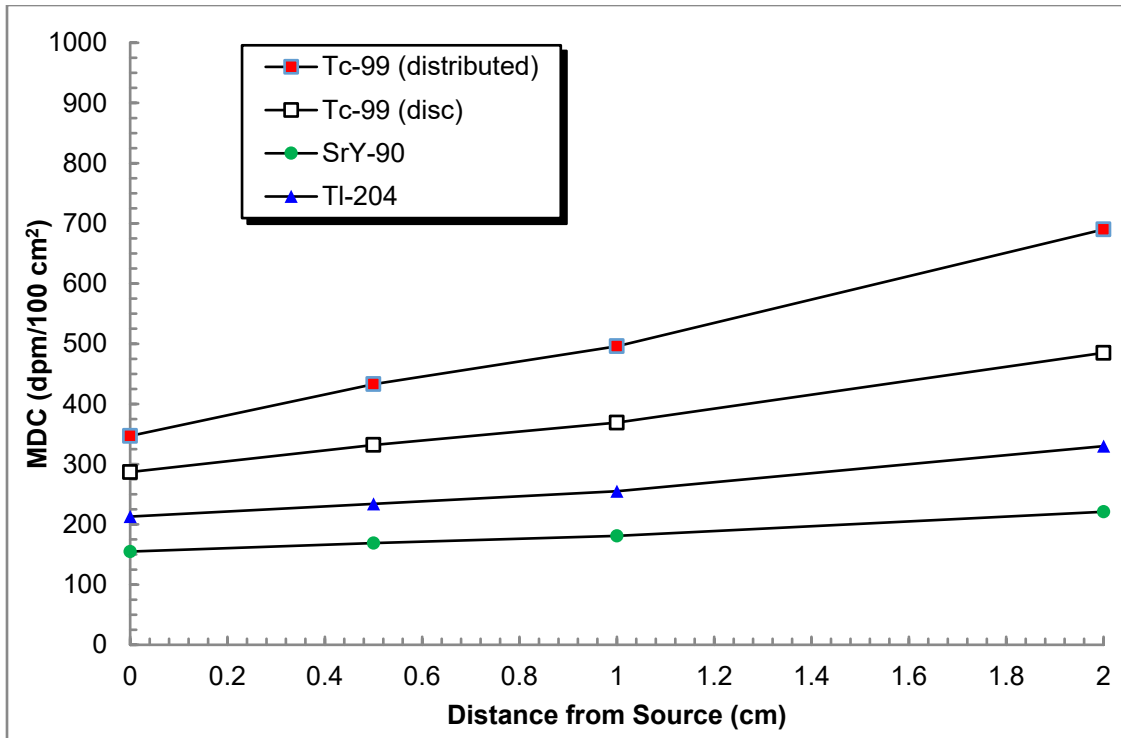


Figure 4-3 Source-to-Detector Distance Effects on MDC for Higher Energy Beta Emitters

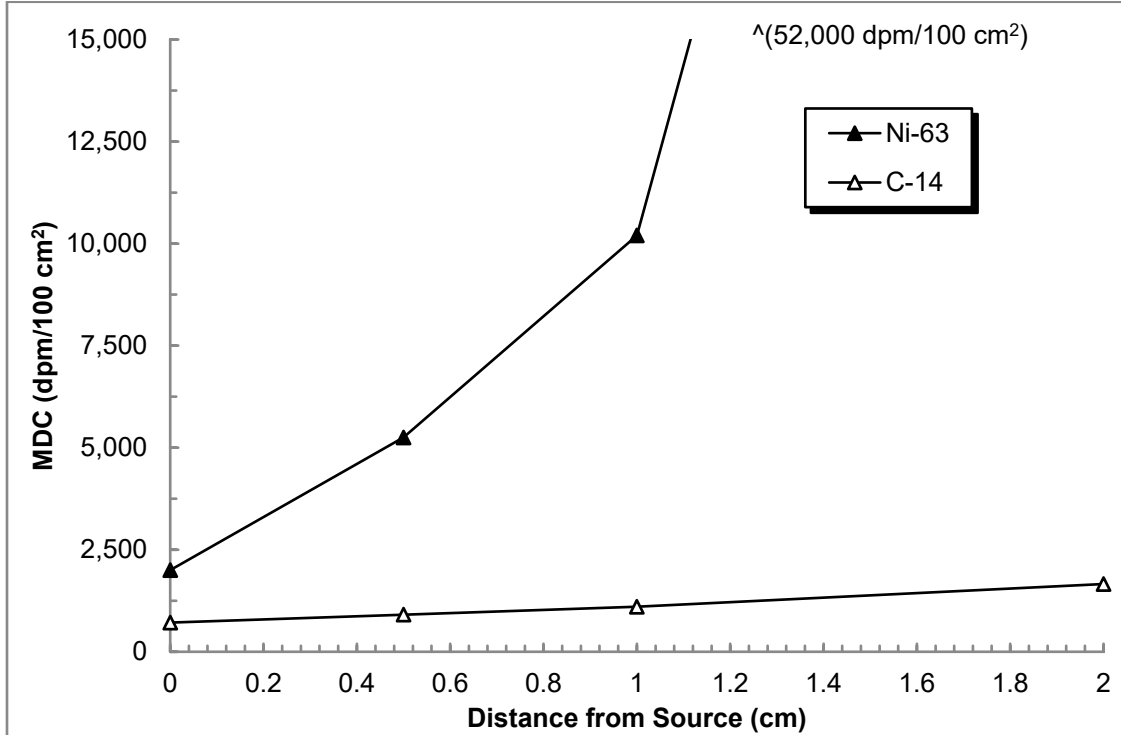


Figure 4-4 Source-to-Detector Distance Effects on MDC for Lower Energy Beta Emitters

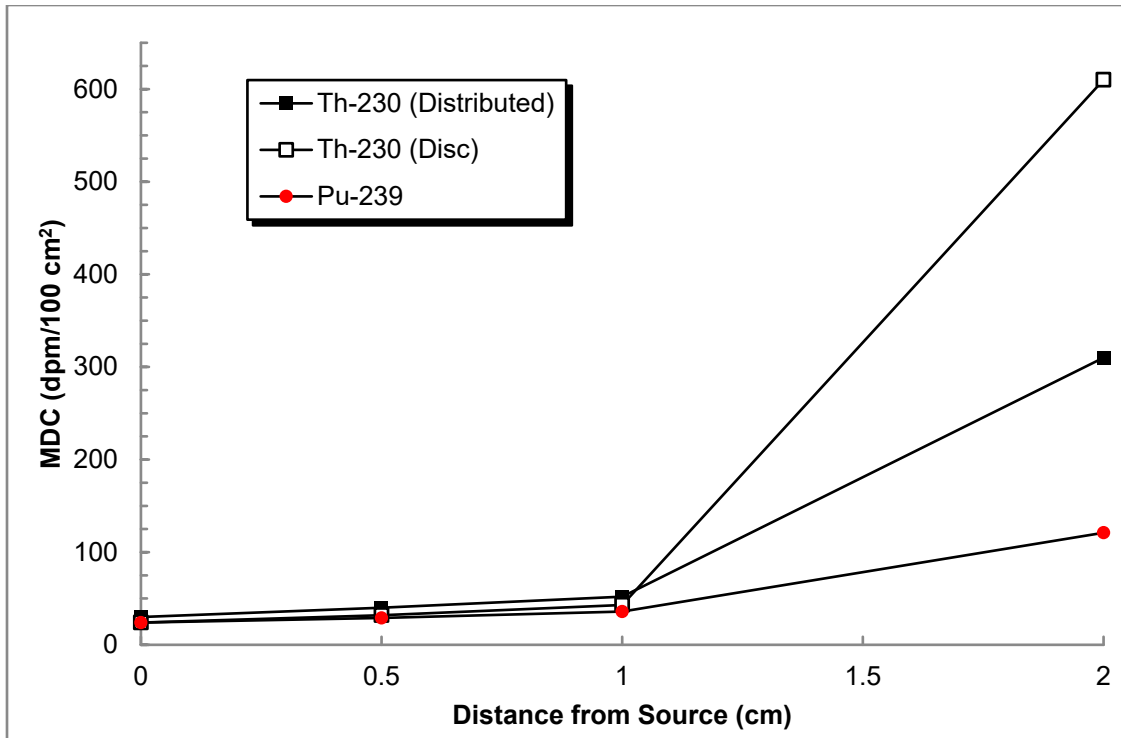


Figure 4-5 Source-to-Detector Distance Effects on MDC for Alpha-Emitters

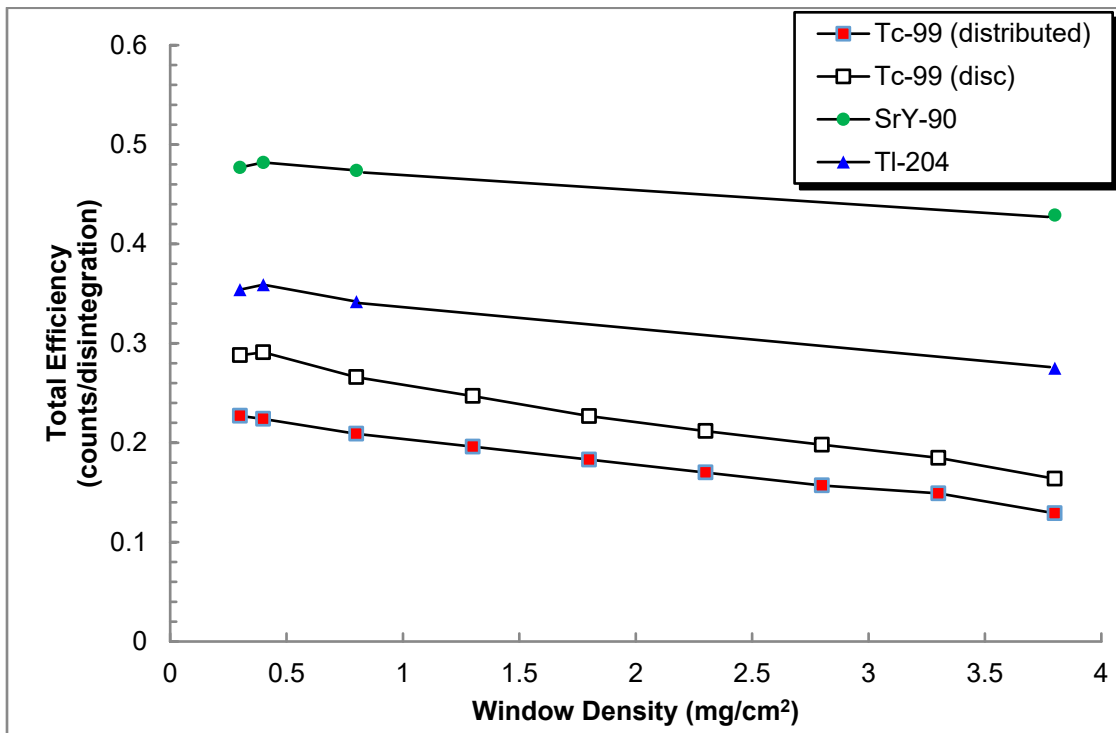
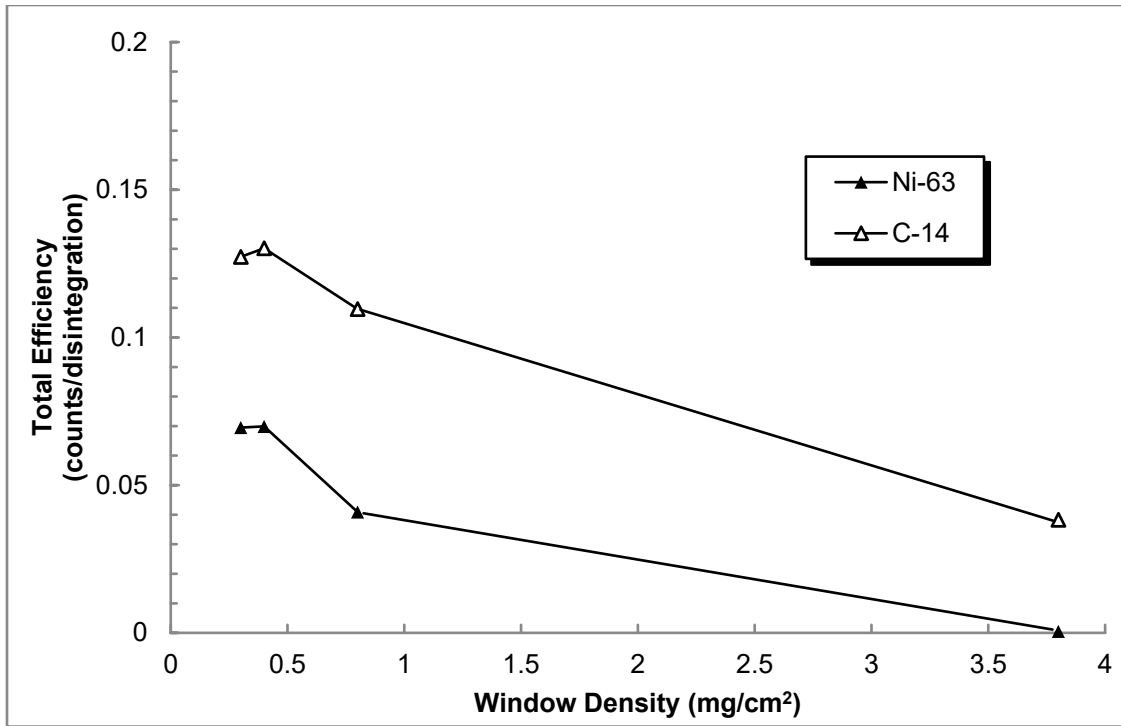
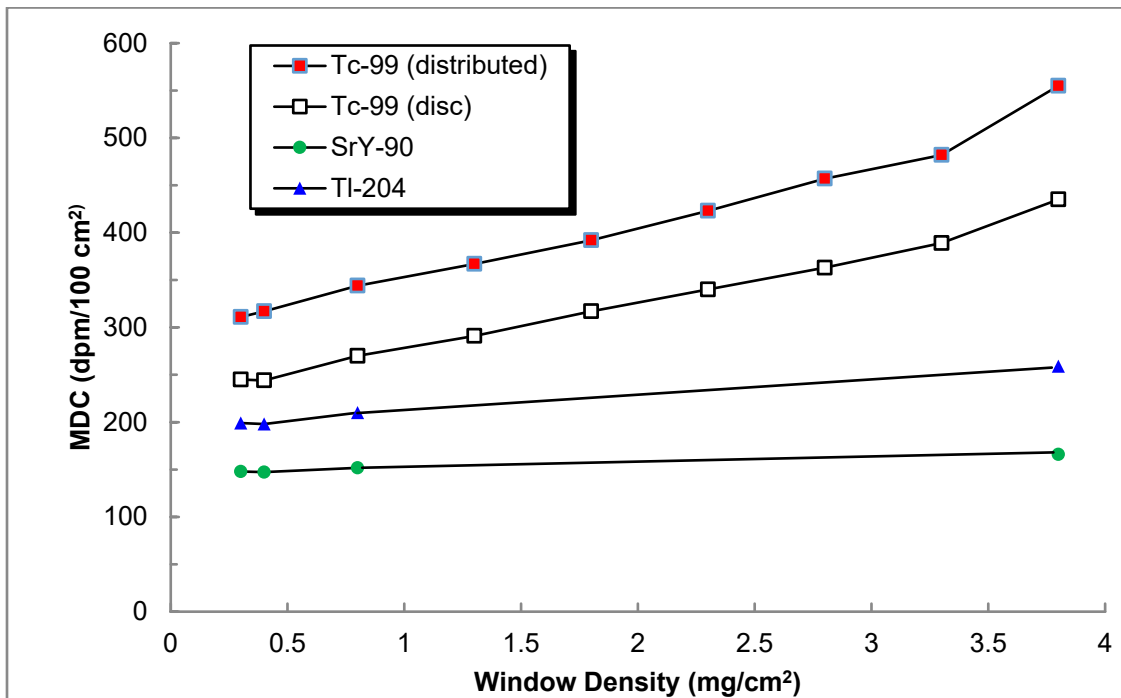


Figure 4-6 Effects of Window Density Thickness on Total Efficiency for Higher Energy Beta-Emitters



**Figure 4-7 Effects of Window Density Thickness on Total Efficiency for Lower Energy Beta Emitters**



**Figure 4-8 Effects of Window Density Thickness on MDC for Higher Energy Beta Emitters**

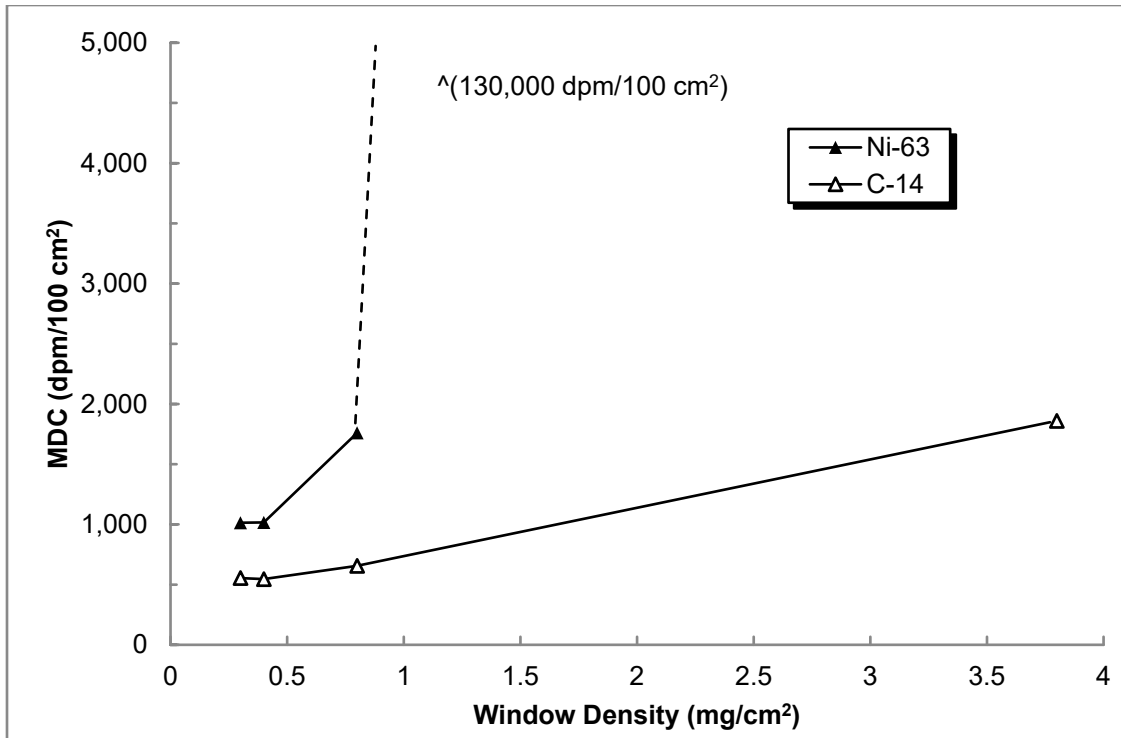


Figure 4-9 Effects of Window Density Thickness on MDC for Lower Energy Beta Emitters

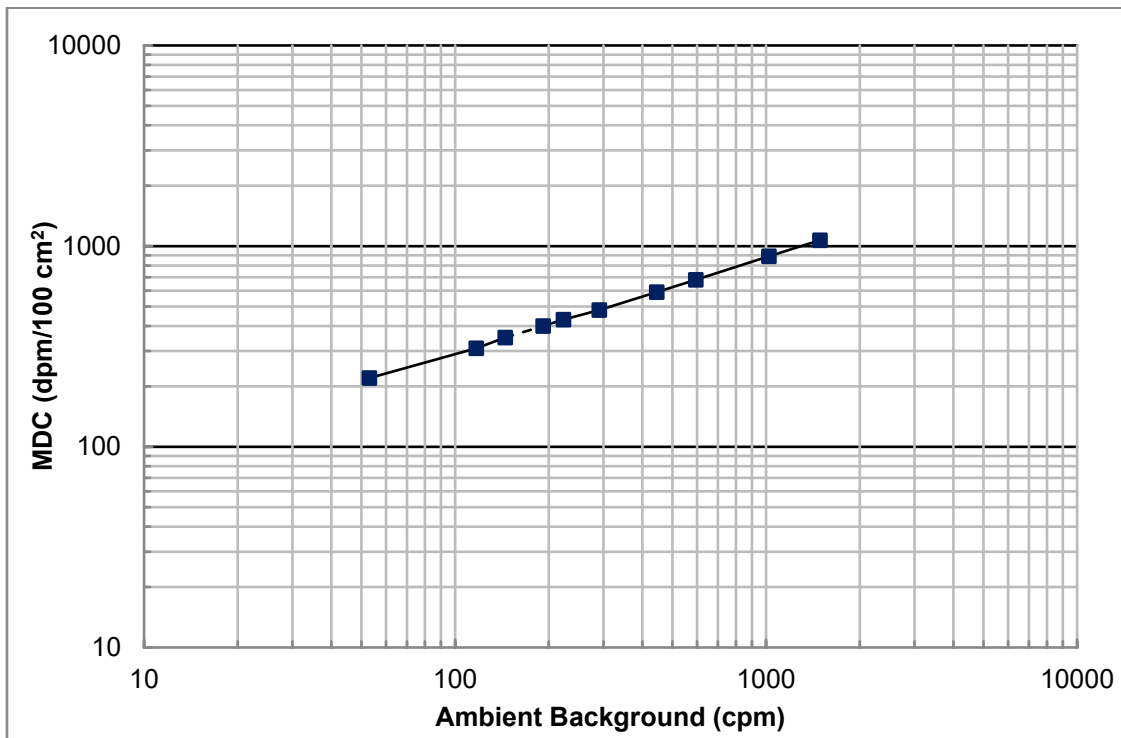


Figure 4-10 Effects of Ambient Background on MDC Calculation

## 5 VARIABLES AFFECTING MINIMUM DETECTABLE CONCENTRATIONS IN THE FIELD

Surface activity levels are assessed by converting detector response, through the use of a calibration factor, to radioactivity. Once the detector has been calibrated and an instrument efficiency ( $\epsilon_i$ ) established, several factors still affect use of that instrument in the field. These factors involve the background count rate for the particular surface and the surface efficiency ( $\epsilon_s$ ), which addresses the physical composition of the surface and any surface coatings. Ideally, the surveyor should use experimentally determined surface efficiencies for the anticipated field conditions. The surveyor needs to know how and to what degree these different field conditions can affect the sensitivity of the instrument. A particular field condition may significantly affect the usefulness of a particular instrument (e.g., wet surfaces for alpha measurements or scabbled surfaces for low energy beta measurements).

One of the more significant implicit assumptions commonly made during instrument calibration and subsequent use of the instrument in the field is that the composition and geometry of contamination in the field are the same as that of the calibration source. This assumption may not be the case, considering that many calibration sources are fabricated from materials different from those that make up the surfaces of interest in the field (e.g., activity plated on a metallic disc (Walker, 1994). This difference usually manifests itself in the varying backscatter characteristics of the calibration and field surface materials.

Generally, it will not be necessary to recalculate the instrument MDC to adjust for the field conditions. For most of the items discussed below, the detection limit (in net counts or net count rate) remains the same, but the MDC may be different (because of the varying  $\epsilon_s$ ). This study quantitatively evaluated the effects of typically encountered surface types and field conditions, as discussed in the following sections.

### 5.1 Background Count Rates for Various Materials

Several different types of surface materials may be encountered in a facility undergoing decommissioning. The typical surface materials evaluated in this study include brick, ceramic block, ceramic tile, concrete block, unpainted drywall, vinyl floor tile, linoleum, steel, wood pine treated with a commercially available water sealant product, and untreated pine. The main difference considered was the background activity associated with each of these types of surface materials. In most cases, the background count rate for the type of surface needs to be determined and a new MDC established, unless the initial evaluation of the instrument's MDC considered the specific surface type.

Ambient background count rates were initially determined for gas proportional, ZnS scintillation, GM, and NaI scintillation detectors. Three variations were used for the gas proportional detectors: (1) detection of alpha radiation only (using a high-voltage setting that discriminated all beta pulses), (2) detection of beta radiation only (using sufficient window density thickness to block alpha radiation), and (3) detection of alpha-plus-beta radiation. Table 5-1 presents the results of ambient background counts. Because the ambient backgrounds were determined at the same location for all the tested surface materials, the ambient background was sometimes greater than a particular surface material background. This result was considered acceptable because a primary study objective was to evaluate detector responses in common field conditions.

Background count rates were obtained for 10 surface materials using the same instrument/detector combinations that determined the ambient background. In general, background count rates were lowest for the linoleum, carbon steel, and wood and highest for the brick and ceramic materials (Table 5-1). These background count rates will vary depending on the local area background radiation levels; however, the data do show the relative backgrounds in common construction materials.

MDCs for the gas proportional detectors operated in both the alpha-only and beta-only modes were calculated for each of the surface materials assuming a total efficiency ( $\epsilon_{\text{tot}}$ ) of 0.20 and 0.25 c/dis for alpha and beta, respectively (Table 5-2). The MDCs were calculated from Equation 3.10, using the background count rates presented in Table 5-1. The MDCs in the alpha-only mode ranged from 28 to 83 dpm/100 cm<sup>2</sup>, while the MDCs in the beta-only mode ranged from 268 to 425 dpm/100 cm<sup>2</sup>. Since the detector MDC varies directly with the background count rate, the lowest MDCs were obtained for linoleum, carbon steel and wood, and concrete block and drywall, while the highest MDCs were for brick and ceramic materials. Figures 5-1 and 5-2 illustrate the effect of surface material background count rates on detector MDC for the gas proportional detectors operated in both the alpha-only and beta-only modes, respectively. These figures demonstrate the importance of carefully assessing the alpha background for various surface materials because of the wide range of MDC values. This is in contrast to the beta MDCs, which are fairly consistent for all materials examined, with the notable exception of brick and ceramics. In application, it is important that the surveyor establish specific material backgrounds that are representative of the surface types and field conditions.

NUREG-1501, "Background as a Residual Radioactivity Criterion for Decommissioning," issued August 1994, presents additional information on background radionuclide concentrations.

## **5.2 Backscatter Effects**

An experiment was performed to evaluate the backscatter characteristics of surfaces commonly encountered when performing decommissioning surveys and to address their effect on surface activity assessments. A thin sheet of Mylar (0.22 mg/cm<sup>2</sup>) was stretched across a metal frame with an area of approximately 126 cm<sup>2</sup>. Two milliliters of a liquid SrY-90 radionuclide standard was deposited on the Mylar and allowed to air dry; about 4,100 dpm was deposited on the Mylar sheet. Various surfaces with the same activity-spiked Mylar sheet positioned between the surface of interest and the gas flow proportional detector were then measured. In this experimental setup, any differences in the detector response are solely attributable to the differences resulting from backscatter radiation. Gas flow proportional detectors were used to make surface activity measurements with both 0.4 and 3.8 mg/cm<sup>2</sup> window thicknesses. Table 5-3 depicts the different total efficiencies—determined by dividing the net count rate by deposited activity—obtained for the various surfaces used in this experiment. The efficiency data were normalized to the efficiency in air, which was assumed to produce negligible backscatter radiation. The backscatter factor, calculated by dividing the particular surface material efficiency by the efficiency in air, ranged from 1.20 to 1.43 for the detector with 0.4-mg/cm<sup>2</sup> window thickness and from 1.11 to 1.37 for the detector with 3.8-mg/cm<sup>2</sup> window thickness. Of particular interest is the backscatter factor for stainless steel—which is often the substrate material for calibration sources—as compared to the other surfaces. For the detector with 0.4-mg/cm<sup>2</sup> window thickness, the backscatter factor for stainless steel was 1.43, compared to 1.20 for wood, 1.24 for drywall, 1.25 for a tile floor, and 1.30 for a sealed concrete floor. Thus, efficiencies for surfaces other than stainless steel may be overestimated by 10 to 20 percent because of the backscatter effect alone (the efficiency overestimation for the 3.8-mg/cm<sup>2</sup> window thickness ranged from 11 to 24 percent). The relatively high efficiency

obtained with stainless steel calibration sources may result in the surface activity for materials like wood, drywall and concrete being underestimated by 10 to 20 percent. Furthermore, the total efficiency for SrY-90 on stainless steel versus concrete surfaces exhibits similar differences (about 10 percent) when the SrY-90 source was deposited on each of these surfaces (discussed in Section 5.5 and shown in Table 5-29).

### **5.3 Effects of Surface Condition on Detection Sensitivity**

The conversion of the surface emission rate to the activity of the contamination source is often a complicated task that may result in significant uncertainty if there are deviations from the assumed source geometry. For example, consider the measurement error associated with an alpha surface activity measurement on a rough surface, such as scabbled concrete, where substantial attenuation reduces the count rate as compared to the calibration performed on the smooth surface of a NIST-traceable source.

This study evaluated the effects of surface condition on detection sensitivity for surfaces commonly encountered during decommissioning surveys. The surfaces studied were abraded (scabbled) concrete, finished (sealed) concrete, carbon steel, stainless steel, and wood. The results provide a quantitative range of how various surface conditions may affect the detectability of various contaminants.

#### **5.3.1 Surface Preparation**

For this study, known quantities of NIST-traceable Tc-99 and Th-230 standard sources in aqueous solutions were dispensed on each of the surfaces. The preparation of the reference sources from the traceable solution involved measurement uncertainties (e.g., pipetting errors, volumetric determinations) that were propagated into the overall statement of uncertainty.

Background count rates were obtained for instrument and surface combinations that were used to determine the surface activity measurements so that the proper background could be subtracted from the gross counts. For the surface materials studied, the Tc-99 and Th-230 were dispensed to simulate both a point source and distributed source geometry. (The Tc-99 and Th-230 were not mixed but were dispensed on separate areas of each surface.) The areal extent of the point source activity ranged from approximately 4 to 10 m<sup>2</sup>, while the distributed source geometry was fabricated by uniformly depositing droplets of the Tc-99 and Th-230 activity over a larger area (126 cm<sup>2</sup>). The total Tc-99 activity dispensed in the point source geometry was 2,828 ± 91 dpm (5,660 ± 110 dpm for the sealed concrete), while 4,595 ± 79 dpm of Th-230 was dispensed in a point source geometry. The Tc-99 and Th-230 activity dispensed in the distributed source geometry was 2,830 ± 100 dpm and 4,600 ± 170 dpm, respectively. Once dispensed, the radioactive material was allowed to dry overnight in a ventilated hood.

Uniformity measurements with a GM detector for distributed sources were made to evaluate how well the activity was spread over the surfaces (refer to Section 5.4.1 for a detailed description of uniformity measurements). It was important that the activity was precisely distributed in the same way for each of the materials. Because the instrument response depends on the source geometry (Section 4.4), the instrument efficiencies ( $\epsilon_i$ ) determined by placing the detectors in contact with the NIST-traceable plate sources were applicable to the measurements performed on the ORAU fabricated sources in cases where the activity was uniformly deposited over the same active area (126 cm<sup>2</sup>) as the NIST-traceable source. Note that the preparation of a scabbled surface source by deposition on a “pre-scabbled” surface may not be representative of the actual field surface condition. That is, on a real scabbled

surface, the activity will likely be concentrated in the “peaks” or undisturbed surface and will be absent in the “valleys.”

### 5.3.2 Measurement Results for Various Surface Types

Beta measurements were made with gas proportional and GM detectors. Two variations were used for the gas proportional detectors: detection of beta radiation only (using 3.8-mg/cm<sup>2</sup> window density thickness to block alpha radiation) and detection of alpha-plus-beta radiation. Five 1-minute measurements were made for each combination of material, geometry, and surface material. Table 5-4 presents the results. Table 5-5 presents the results of alpha measurements made with gas proportional ( $\alpha$ -only mode) and ZnS detectors. Both alpha and beta measurements were taken at contact with the sources. The total efficiency for the point source geometry was determined by simply dividing the average net count rate by the total activity dispensed. No correction for the decay of Tc-99 or Th-230 was necessary because of their long half-lives. The following equation determined the total efficiency for the distributed source:

$$\text{Total Efficiency} = \frac{\text{Net Count Rate}}{\left( \frac{\text{Total Activity}}{126 \text{ cm}^2} \right) \text{ Probe Area}} \quad (\text{Eq. 5.1})$$

The total efficiencies determined for the distributed activity on surfaces should use the active or physical probe area, as opposed to the effective probe area, in converting instrument response to surface activity. During instrument calibration, the total efficiency is determined by placing the probe in contact with the calibration source and recording the net counts and then dividing by the activity of the source. No correction is made for the probe’s protective screen; the total efficiency and instrument efficiency allow for part of the active area of the probe being covered and possibly insensitive to incident radiation. Thus, surface activity measurements in the field should be corrected for the physical area of the probe, with no corrections made for the protective screen, to be consistent with the manner in which the instrument was calibrated. (Refer to Section 2 for the comparison of the physical probe area and the effective probe area for each of the detectors studied.)

The source efficiencies ( $\epsilon_s$ ) were calculated by dividing the total efficiency by the instrument efficiency. The instrument efficiencies were determined for each detector and geometry using appropriate NIST-traceable sources. As discussed in Section 4, following the guidance of ISO-7503-1:1988 for surface activity measurements requires knowledge of both the instrument and source efficiencies. The instrument efficiency ( $\epsilon_i$ ) is determined during calibration using the stated  $2\pi$  emission rate of the source. Source efficiencies must be experimentally determined for a given surface type and coating. Tables 5-4 and 5-5 present experimental data on source efficiencies for several common surface types. The data indicate that the source efficiency varies widely depending on the amount of self-absorption and backscatter provided by the surface. The total efficiencies may be determined from Tables 5-4 and 5-5 by simply taking the product of  $\epsilon_i$  and  $\epsilon_s$ .

The total efficiencies for Tc-99 and Th-230 on various surfaces determined from this experiment can be compared to the average detector efficiencies (historical calibration data from ORAU) in Table 4-2. The average Tc-99 total efficiency for a gas proportional detector operated in an alpha-plus-beta mode was 0.22 c/dis (on a NIST-traceable source). This study indicates that this is an appropriate total efficiency to use for untreated wood in a point source geometry (for  $\alpha + \beta$  on treated wood,  $\epsilon_i$  multiplied by  $\epsilon_s$  equals 0.23), but it may be overly conservative for



stainless steel surfaces and for sealed concrete. Similarly, for Th-230, the average total efficiencies during calibration were 0.18 and 0.19 c/dis, respectively, for the ZnS and gas proportional (alpha-only mode) detectors. This study indicates that for a point source geometry on untreated wood, the total efficiency is less than 50 percent of the historical average alpha total efficiency (0.097 and 0.061, respectively, for  $\alpha$ -only and ZnS detectors). For scabbled concrete, the alpha total efficiency is approximately 50 to 75 percent of the total efficiency obtained from historic ORAU calibration data. The effect of reduced total efficiency in the field is an increase in the survey instrumentation MDCs. Table 5-6 gives information on the MDCs for these surface types.

The MDCs shown in Table 5-6 reflect the differences in the source efficiency for each surface. That is, the background, counting time, and instrument efficiency were constant for each given detector and geometry. The large variations in MDC for the surface types studied should be noted. For example, using an  $\alpha + \beta$  gas proportional detector to measure Tc-99 distributed over a 126-cm<sup>2</sup> area has an MDC range of 260 to 950 dpm/100 cm<sup>2</sup>, depending on the surface type. However, it is the lower bound value that is typically calculated and used as the MDC (because the calibration is performed on a clean, high-backscatter reference source, with no consideration given to the actual surface measured). Furthermore, if the uncertainty in the total efficiency is incorporated into the MDC equation (Equation 3.12), the MDC for finished concrete is 2,300 dpm/100 cm<sup>2</sup> (compared to 950 dpm/100 cm<sup>2</sup>).

Energy response to the source, backscatter from media, and self-absorption of radiation in the surface can all affect instrument response. Possibly, the relatively low efficiency obtained for some of the concrete surfaces was the result of penetration of the reference material into the surface and the resultant self-absorption. This porosity effect was also evident for the untreated wood (Table 5-5). The high source efficiencies obtained on the stainless steel surface resulted in part from backscattered particles entering the detector. The backscatter contribution measured was approximately 50 percent for Tc-99 on stainless steel, somewhat higher than anticipated. NCRP 112, "Calibration of Survey Instruments Used in Radiation Protection for the Assessment of Ionizing Radiation Fields and Radioactive Surface Contamination," dated December 31, 1991, estimated the backscatter contribution from Tc-99 on a stainless steel surface as 22 percent.

The ISO recommends the use of factors to correct for alpha and beta self-absorption losses when determining the surface activity. Specifically, the ISO recommends using a source efficiency of 0.5 for maximum beta energies exceeding 0.4 MeV and using a source efficiency of 0.25 for maximum beta energies between 0.15 and 0.4 MeV and for alpha-emitters; these values "should be used in the absence of more precisely known values" (ISO 7503-1:1988, pg. 3). Although this guidance provides a starting point for selecting source efficiencies, the data in Tables 5-4 and 5-5 illustrate the need for experimentally determined source efficiencies.

In summary, both backscatter and self-absorption effects may produce considerable error in the reported surface activity levels if the field surface is composed of material significantly different in atomic number from the calibration source. Therefore, it is important to consider the effects that result when the calibration source has backscatter and self-absorption characteristics different from the field surface to be measured. When making measurements on concrete surfaces and using the conventional total efficiency to convert count data to surface activity (i.e., source efficiencies are not considered separately), it is good practice to use a calibration source that is mounted on an aluminum disc, since the backscatter characteristics for concrete and aluminum are similar (NCRP 112).

## **5.4 Attenuation Effects of Overlaying Material (Self-Absorption)**

Calibration sources invariably consist of a clean, smooth surface and thus do not reproduce the self-absorption characteristics of surfaces in the field. Thus, the surface condition can affect the detection sensitivity of an instrument significantly, depending on the radionuclide of concern. For example, paint has a smaller impact on detection of Co-60 (beta radiation) than it does for Am-241 (alpha radiation). The effects that various surface conditions have on detection sensitivities were evaluated by depositing varying amounts of the material (i.e., water, dust, oil, paint) between the detector and the radioactive source.

### **5.4.1 Methodology**

The effects of dusty, wet, oily, and painted surface conditions were evaluated quantitatively. To allow comparison of the results from this study, it was necessary to reproducibly simulate known thicknesses of materials such as dust, water, or paint on surfaces. Therefore, known quantities of soil (dust), water, oil, and paint were evenly spread over a surface with standard (known) dimensions to produce the desired thickness of material on the surface.

The material to be evaluated (e.g., water, dust, oil, paint) was uniformly deposited between two Mylar sheets, within the area of the Plexiglas jig. The net weight of the material was obtained, and the density thickness of the material (in mg/cm<sup>2</sup>) was calculated by dividing the weight by the area over which the material was deposited (typically 126 cm<sup>2</sup>). It was necessary to ensure that the material was evenly spread over the active area of the Plexiglas. The following text describes how the surface coatings were prepared. (Section 5.4.2 discusses oil.)

#### *5.4.1.1 Paint*

The Mylar was attached tightly to the Plexiglas jig and weighed for initial weight. A 126-cm<sup>2</sup> hole was cut in a piece of cardboard to match the exact active area of the Ludlum model 43-68 detector. The Mylar was placed beneath the cardboard jig. The paint was sprayed lightly over the surface of the Mylar at a distance that varied from 15 to 30 centimeters. After the paint had dried, a new weight was obtained and subtracted from the initial weight. This yielded the test weight. After measurements were completed and the Mylar was checked for tears, the next quantity of paint was applied.

#### *5.4.1.2 Water*

A piece of Kimwipe was cut exactly to fit the active area of a Ludlum model 43-68 detector (126 cm<sup>2</sup>) and placed on a new piece of Mylar. In this case, the Mylar was not stretched or attached tightly across the Mylar jig. The initial weights for the Kimwipe and Mylar sheets were then determined. A known quantity of water was then pipetted onto the Kimwipe as evenly as possible. The water was uniformly absorbed over the Kimwipe. After measurements had been made, the Kimwipe and Mylar were folded and reweighed to measure the amount of evaporation and to determine the next test weight. Evaporation was very rapid in most cases, and weight determinations had to be made following each instrument measurement series.

#### *5.4.1.3 Dust*

Dust was made by grinding potting soil and sieving it through 250-mesh screen. An empty plastic dish was weighed, and dust was added to the dish until the desired weight was reached. Dust was then poured onto the Mylar that was tightly stretched across the Plexiglas jig. The dish

was then reweighed to obtain the exact amount of dust applied to the Mylar. The dust was spread across the Mylar over 126 cm<sup>2</sup>. This was done by using a small (approximately 0.6 centimeter [1/4-inch]-wide), very fine bristle brush. The brush was first weighed. The dust was so fine that it could not be brushed or swept; instead it was blotted until it appeared evenly distributed and within the 126-cm<sup>2</sup> active area of the probe. Another sheet of Mylar was placed over the dust. After the dust was distributed, the brush was again weighed to determine if any dust remained in the brush and to obtain the final test weight. This process was repeated for each test weight.

#### 5.4.1.4 Uniformity Measurements

The uniformity of the material deposition between the Mylar sheets was evaluated by measuring the attenuation produced by the two Mylar sheets and material at five locations within the active area of the Plexiglas. Specifically, at each location, the GM detector (20-cm<sup>2</sup> probe area) and radioactive disc source (a low-energy beta or alpha source was used to ensure that the source was being attenuated by the material) were placed on opposite sides of the Mylar sheets. Five 1-minute measurements were taken at each location. The measurements were averaged, and the standard error in the mean was calculated at each location. Uniformity of the material was assumed to be sufficient if the relative standard error in the mean of 25 measurements (5 measurements at each location) was less than 15 percent. The evaluation showed that exact uniformity was not practical, or even desirable, since one objective of the study was to reproduce realistic field conditions.

If the uniformity test failed, efforts continued to distribute the material more evenly. Once the desired level of uniformity had been achieved, measurements were made using the necessary detectors and calibration sources. The instrument background was determined by a series of five 1-minute counts. For each data point (i.e., combination of material, thickness, detector, and source) evaluated, five 1-minute measurements were collected. (In general, the radioactive sources used in this study possessed sufficient activity to ensure that the uncertainty from counting statistics alone was less than 5 percent.) Each data point was statistically evaluated by calculating the mean of the gross counts and standard error in this mean. The background was subtracted from the mean of the gross counts, and the detector efficiency was calculated by dividing by the activity of the calibration source. The pressure and temperature in the measurement hood were recorded.

### 5.4.2 Measurement of Various Surface Coatings

Initially, this study was limited to measuring MDCs with a gas proportional detector (Ludlum model 43-68) with oil deposited between the Mylar sheets. The radioactive sources used in the pilot study were C-14, Tc-99, and SrY-90. The Tc-99 source used was a 100-cm<sup>2</sup> plate source; the C-14 and SrY-90 sources had disc-shaped geometries with a 32-millimeter diameter. The detector background for 1 minute was 326 counts. Table 5-7 presents the results of MDC measurements for each source under the following conditions:

- detector face alone (0.4-mg/cm<sup>2</sup> window)
- detector face and two sheets of Mylar (0.8-mg/cm<sup>2</sup>, total density thickness)
- plus 1.5 mg/cm<sup>2</sup> of 20W-50 motor oil (2.3-mg/cm<sup>2</sup>, total density thickness)
- plus 2.9 mg/cm<sup>2</sup> of 20W-50 motor oil (3.7-mg/cm<sup>2</sup>, total density thickness)
- plus 4.5 mg/cm<sup>2</sup> of 20W-50 motor oil (5.3-mg/cm<sup>2</sup>, total density thickness)

Figure 5-3 shows the effects of oil density thickness on the source efficiency. The first data point for each source (at 0.4 mg/cm<sup>2</sup>, not shown in figure) in Table 5-7 may be considered to yield the total efficiency under optimum laboratory conditions (smooth, clean surface). As various density thicknesses of oil were added, the source efficiency was decreased as the result of absorption losses. The source efficiency appeared to be reduced more significantly for the lower energy beta-emitters as the density thickness of oil on the surface was increased. Figure 5-4 illustrates the effects of oil density thickness on the detector MDC (which is a function of source efficiency). The first data point for each source may be considered as the theoretical detector MDC under optimum laboratory conditions. This figure illustrates how the oil density thickness on the surface significantly affected the detector MDC, calibrated to lower energy beta-emitters.

This portion of the study continued with the evaluation of various thicknesses of paint, dust, and water deposited between the detector and the source. Measurements were made with gas proportional, GM, and ZnS detectors. Three variations were used for the gas proportional detectors: (1) detection of alpha radiation only, (2) detection of beta radiation only (using 3.8-mg/cm<sup>2</sup> window density thickness to block alpha radiation), and (3) detection of alpha-plus-beta radiation. The radioactive sources used in the pilot study were C-14, Tc-99, Tl-204, and SrY-90 for beta measurements and Th-230 for alpha measurements. When measurements were taken over large area sources (i.e., 126 or 150 cm<sup>2</sup>), the source activity within the physical area of the detector was determined. This corrected activity was used to determine total efficiencies:

$$\text{Corrected Activity} = \frac{\text{Source Activity} \times \text{Probe Area}}{\text{Active Area of Source}} \quad (\text{Eq. 5.2})$$

Tables 5-8 through 5-28 present the results of material density thicknesses for paint, dust, and water versus source efficiency for all of the detector types evaluated. These results are consistent with the results obtained with the oil deposition. As before, the source efficiency appeared to be reduced more significantly for the lower energy beta-emitters as the density thickness of the material on the surface was increased. The instrument efficiency was determined with the Mylar in place above the source for the paint and dust studies and with the Mylar and Kimwipe sheet for the water attenuation studies. The total efficiency may be calculated for any evaluated surface coating by multiplying the instrument efficiency by the source efficiency. Figures 5-5 through 5-19 illustrate the effects of material density thicknesses on source efficiency. Each figure shows the measured data and the best-fit exponential curve. Figures 5-20 to 5-23 illustrate the effects of increasing dust density thickness on the MDC calculation.

The measured source efficiency versus density thickness was fit to an exponential curve. Tables 5-8 through 5-28 present the results of this regression fit. The data associated with the source efficiency and density thickness were examined for the best way to present the error associated with the given measurements. Regression techniques proved to be the best approach to describing the data, as well as to providing the average source efficiency and 95-percent confidence interval at each density thickness. The density thickness was assumed to be known without error. This is undoubtedly incorrect, but it does not affect the results significantly because the error associated in the weight measurements is small compared with the error associated with the count measurements used to determine the source efficiency. NUREG/CR-4604, "Statistical Methods for Nuclear Material Management," issued December 1988, discusses this practice, which is common in most regression situations. The regression was used to determine the intercept and slope of the line—transformed by taking the natural logarithm—using a least squares fit. The regression also outputs the residual mean square, which is an unbiased estimator of the variance associated with the source efficiency

values. The predicted values associated with the density thickness measurements were determined using the slope and intercept. A confidence interval was also determined using the following equation (Walpole & Myers, 1985):

$$Y_0 - t_{\alpha/2} s \left( \frac{1}{n} + \frac{(x_0 - \bar{x})^2}{S_x} \right)^{1/2} < Y < Y_0 + t_{\alpha/2} s \left( \frac{1}{n} + \frac{(x_0 - \bar{x})^2}{S_x} \right)^{1/2} \quad (\text{Eq. 5.3})$$

where:

|                |                                       |           |                                 |
|----------------|---------------------------------------|-----------|---------------------------------|
| $Y_0$          | = predicted source efficiency         | $x_0$     | = density thickness of interest |
| $t_{\alpha/2}$ | = test statistic for desired accuracy | $\bar{x}$ | = average density thickness     |
| $s$            | = square root of residual mean square | $S_x$     | = $\sum (x_i - \bar{x})^2$      |
| $n$            | = number of points in regression      | $Y$       | = measured source efficiency    |

One interesting finding was that the alpha and beta attenuations for a given radionuclide were similar, regardless of the specific material responsible for the attenuation. Figure 5-24 illustrates that the source efficiencies versus density thickness for SrY-90, Tl-204, Tc-99, and C-14 decrease fairly consistently for each of the materials tested and may be considered independent of material type (i.e., the source efficiency decreases with increasing density thickness in the same manner for water, dust, and paint).

The exponential term in each regression fit is a measure of the alpha or beta attenuation. That is, the exponential terms were consistent for each radionuclide. The terms ranged as follows:

- C-14—0.211 to 0.291
- Tc-99—0.086 to 0.110
- Tl-204—0.031 to 0.046
- SrY-90—0.016 to 0.028
- Th-230—0.331 to 0.906

The alpha radiation experienced the greatest variability in attenuation with different materials.

When using the fitted source efficiency data in Tables 5-8 to 5-28, it is important to note that the exponential reduction resulting from a given density thickness is obtained from the exponential term alone. As an example to clarify the use of these data, a GM detector is calibrated to a Tc-99 point source, resulting in an  $\epsilon_i$  equal to 0.278. It is determined that surface activity measurements will be made on a concrete surface (refer to Table 5-4 to obtain  $\epsilon_s$  equal to 0.630). Therefore, the total efficiency is calculated by multiplying  $\epsilon_i$  by  $\epsilon_s$  (equals 0.175). Now assume that there is a coating of dust 2 mg/cm<sup>2</sup> thick on the concrete surface, and the surface efficiency ( $\epsilon_s$ ) must be corrected for this dust layer. Table 5-16 provides the regression equation for Tc-99 with a GM detector:

$$\epsilon_s = 0.669 e^{-0.093 x} \quad (\text{Eq. 5.4})$$

To correct the surface efficiency (0.630) for the dust layer, multiply  $\epsilon_s$  by the exponential term, substituting the density thickness for  $x$ :

$$\epsilon_s (\text{for } 2 \text{ mg/cm}^2 \text{ dust}) = (0.630) \times e^{-0.093 (2)} = 0.523 \quad (\text{Eq. 5.5})$$

Now the total efficiency for this condition becomes

$$\epsilon_{tot} = \epsilon_j \times \epsilon_s = (0.278) (0.523) = 0.145 \quad (\text{Eq. 5.6})$$

as compared to 0.175 without consideration of the dust layer.

## **5.5 Use of Alpha and/or Beta Measurements to Assess Surface Activity**

The uranium and thorium decay series emit both alpha and beta radiation. A common practice has been to use beta measurements to demonstrate compliance with surface activity guidelines expressed as alpha activity. In the case of uranium, the current surface activity guidelines are specified in alpha dpm (e.g., 5,000  $\alpha$  dpm/100 cm<sup>2</sup>). When applying beta measurements to assess compliance with uranium and thorium surface activity guidelines, the radionuclide (specifically, the energy of the radionuclide) used to calibrate the detector should be considered. For example, SrY-90, a high-energy beta-emitter, is often used to calibrate a detector for surface activity measurements of uranium. That is, an SrY-90 calibration source is assumed to be sufficiently representative of the beta emissions from the uranium surface contamination, and therefore, it is assumed that the total efficiency using an SrY-90 source will adequately represent the uranium contamination. An experiment was designed to evaluate the agreement between total efficiencies obtained from an SrY-90 source and processed uranium contamination. Additionally, an experiment was performed with 3-percent enriched uranium (3 percent of U-235 by weight) to assess the applicability of calculating the total efficiency for uranium by considering the detector's response to each of the alpha and beta emissions in the decay series.

For these experiments, known quantities of NIST-traceable SrY-90, ruthenium (Ru)-106 (rhodium [Rh]-106), processed uranium, and 3-percent enriched uranium (in aqueous solutions), were dispensed on various surface materials (i.e., stainless steel, concrete, wood, and drywall). Processed uranium includes U-238 that is in equilibrium with U-234, but with the remaining decay series radionuclides removed, and U-235 is present at the natural isotopic ratio (0.7 percent of U-235 by weight). The 3-percent enriched uranium exhibited a U-234 to U-235 ratio of 24 and had the following alpha activity fractions: 0.167, U-238; 0.033, U-235; and 0.799, U-234. For each surface material, SrY-90, Ru-106 (Rh-106), and uranium were dispensed to simulate a small disc-source geometry. The areal extent of the source activity was less than 20 cm<sup>2</sup>. The total SrY-90 activity dispensed was 5,229 dpm and approximately 4,200 dpm for the Ru-106 (Rh-106). The total processed uranium activity was 7,840 alpha dpm, composed of about 3,900 dpm U-238, 3,760 dpm U-234, and 180 dpm U-235. The amount of enriched uranium dispensed was 4,520 dpm (uranium isotopic fractions can be calculated using the alpha activity fractions provided above). Once dispensed, the radioactivity was allowed to dry overnight in a ventilated hood.

Background count rates were obtained for instrument/surface combinations that were used to measure the surface activity of the deposited activity. Beta measurements were made with gas proportional and GM detectors. As before, two variations were used for the gas proportional detectors, including detection of beta radiation only (using 3.8 mg/cm<sup>2</sup> window density thickness to absorb alpha radiation) and detection of alpha-plus-beta radiation. Alpha measurements were taken with gas proportional (alpha-only mode) and ZnS detectors. Five 1-minute measurements were made for each source and surface material combination. Total efficiencies were calculated by dividing the net count rate by the activity dispensed on the particular surface. For uranium, the total alpha activity was used to determine the total efficiencies. Table 5-29 presents the results.

The first observation from this experiment is that the alpha efficiencies for the alpha-only gas proportional and ZnS detectors are low compared to the historical efficiencies obtained from ORAU electroplated calibration sources (refer to Table 4-2). One possible reason for this reduction in alpha efficiency is that the liquid sources were allowed to air dry, and thus, the resulting source deposition did not constitute a “weightless” source (i.e., a source with virtually no self-absorption). That is, the uranium source deposition was probably responsible for measurable self-absorption of the alpha radiation. While experimental controls could have been exercised to make the uranium source deposition approximately “weightless,” the actual source deposition used is likely a more realistic representation of the uranium contamination measured in the field.

The second observation was that the SrY-90 source deposited on stainless steel and concrete surfaces exhibited total efficiencies for the alpha-plus-beta gas proportional and GM detectors very similar to those of processed uranium. The total efficiency for SrY-90 with the beta-only gas proportional detector was about 50 percent higher than the processed uranium total efficiency (i.e., 0.38 c/dis versus 0.24 c/dis on stainless steel). Therefore, the assessment of uranium contamination using a beta-only gas proportional detector calibrated to SrY-90 would result in an underestimate of the surface activity. An explanation for the difference is provided. The alpha-plus-beta gas proportional and GM detectors’ response to processed uranium includes a measurable component from the alpha radiation. Specifically, the detector is responding to a variety of radiations from the processed uranium—including alpha radiation from the three isotopes of uranium and beta radiations from the progeny of U-238 and U-235—and the total efficiency is related only to the total alpha activity of the uranium. Therefore, the total efficiency based on the alpha activity of processed uranium is similar to the efficiency of these detectors (alpha-plus-beta gas proportional and GM) calibrated to SrY-90. In the case of the beta-only gas proportional detector, the response to alpha radiation has been nearly eliminated through the use of the 3.8 mg/cm<sup>2</sup> window. The resulting detector response to the beta component of processed uranium is much less than that of SrY-90 (a subsequent example will illustrate the components of the detector response to uranium). However, consistent with the scope of this document, the total efficiency for processed uranium should be considered under field conditions. That is, while there is agreement between the total efficiencies for SrY-90 and the processed uranium under ideal laboratory conditions, field conditions may affect the detectors’ response to these materials to varying degrees.

To evaluate the potential effect of overlaying material in the field, thin sheets of Mylar were placed over the processed uranium deposited on stainless steel. Five 1-minute measurements were made for each Mylar thickness and detector combination. The total efficiencies were calculated by dividing the net count rate by the activity dispensed on the particular surface, and the results were normalized to the total efficiency obtained with no Mylar. Table 5-30 presents the results. As expected, the total efficiency for the alpha detectors showed a significant reduction for the range of Mylar thicknesses evaluated (0.22 to 3.30 mg/cm<sup>2</sup>). Conversely, the detectors that respond primarily to beta radiation experienced only a modest reduction in total efficiency. Because a large fraction of the detector’s response to processed uranium results from the high-energy protactinium (Pa)-234m beta radiation, the addition of absorber sheets serves to primarily attenuate the lower energy beta radiation and alpha radiation associated with uranium. For comparison, the attenuation effects of overlaying material over this thickness range for SrY-90, discussed in Section 5.4 and illustrated in the corresponding tables, shows a normalized total efficiency of approximately 0.90 for 3.30 mg/cm<sup>2</sup> of Mylar (compared to 0.76 and 0.80 for the alpha-plus-beta gas proportional and GM detectors, respectively, for processed uranium). Therefore, depending on the expected field conditions, the use of an SrY-90 calibration source for processed uranium may slightly underestimate the surface activity using

alpha-plus-beta gas proportional and GM detectors. Only a minor correction (reduction in SrY-90 determined efficiency) would likely be necessary for field conditions because most of the response is from the high-energy beta.

As discussed previously, using the beta-only gas proportional detector calibrated to SrY-90 would underestimate the processed uranium surface activity, because of the comparison of total efficiencies (i.e., 0.38 c/dis for SrY-90 versus 0.24 c/dis for processed uranium). However, as Table 5-30 indicates, the total efficiency for the beta-only gas proportional detector is largely insensitive to the range of absorber thicknesses used to assess detector responses under field conditions. Therefore, it may be desirable to use this detector for the assessment of processed uranium contamination with the detector calibrated to an appropriate beta energy (to yield about 24-percent total efficiency). Table 4-2 indicates that an appropriate beta energy source may be Tl-204, or a radionuclide with a slightly less maximum beta energy.

The total efficiencies for the 3-percent enriched uranium were less than those for processed uranium, because of the increased alpha activity fraction from U-234 (Table 5-29). The determination of an appropriate beta calibration energy is more difficult than for processed uranium because of the increase in alpha activity. The most representative calibration source would be one prepared from the radioactive material (e.g., uranium or thorium) that is being measured in the field. Because many detectors used for surface activity assessment can respond to alpha and beta radiations to varying degrees, using a single radionuclide (or even one in equilibrium with another radionuclide [SrY-90]) for calibration may not be representative of the complex decay scheme of the uranium and thorium decay series. In this situation, determining the total efficiency by considering the detector's response to each of the alpha and beta emissions in the decay series may be more appropriate. An example of this approach is presented for 3-percent enriched uranium on stainless steel.

To evaluate the detector's response to each of the alpha and beta emissions in the decay of low-enriched uranium, the decay scheme of the contamination must be completely understood in terms of radiation type, energy, and abundance. Table 5-31 illustrates the total efficiency calculation for 3-percent low-enriched uranium, as measured by a 126-cm<sup>2</sup> alpha-plus-beta gas proportional detector. The alpha fractions of U-238, U-235, and U-234 were determined for 3-percent enriched uranium, and the detector's total efficiency ( $4\pi$ ) for each radiation emission was determined by experiment and/or empirical relationship. For example, the detector's response to the alpha emissions of U-238, U-235, and U-234 were assessed experimentally with Th-230 and Pu-239 calibration sources, and the Th-231 beta energies from the U-235 series were determined using a Tc-99 calibration source. Beta energies that could not be determined via experiment because of the lack of an appropriate beta calibration standard were calculated empirically. In this regard, the beta efficiency for Ru-106 (Rh-106) was determined to assist with the appropriate efficiency for Pa-234m. As Table 4-2 shows, the total efficiency for SrY-90 (maximum beta energy of 1,413 keV) is about 0.42, while the total efficiency for Ru-106 (maximum beta from Rh-106 is 3,541 keV) on stainless steel is 0.57; therefore, it was possible to determine the total efficiency for Pa-234m (2,240 keV maximum beta energy) using these data. The total weighted efficiency for 3-percent enriched uranium was 0.257, which compares favorably to the measured total efficiency of 0.23.

Using this approach, it is possible to assess the fractional detector response from each radionuclide in the decay series. In this example, about 33 percent of the gas proportional detector's response comes from the high-energy beta of Pa-234m, while nearly 60 percent is from the alpha activity. Therefore, the 25.7-percent total efficiency calculated should be considered as the ideal laboratory efficiency and should be corrected for expected field



conditions. For example, each of the individual radionuclide total efficiencies could be corrected for field conditions using the exponential reduction discussed in Section 5.4.

Alternatively, the same approach illustrated in Table 5-31 could be used for the beta-only detector, which has the advantage of not being as sensitive to field conditions as are the detectors that respond to alpha radiation. With this approach, the resulting total efficiency was 0.096 (Table 5-32). The measured total efficiency of 0.09 compared favorably. Most of the response (about 80 percent) is from the high-energy beta of Pa-234m, which is not likely to be attenuated significantly. This calculation technique is detector dependent (i.e., the specific detector's response to various radiations must be carefully assessed).

## **5.6 The Effects of Radon Progeny and Beryllium-7 on Detection Sensitivity**

### **5.6.1 Interferences from Radon Decay Products**

Radon (Rn) is a radioactive noble gas produced by the decay of radium (Ra). Three isotopes occur in nature including Rn-219 (actinon), Rn-220 (thoron), and Rn-222. Actinon has a half-life of 4 seconds, is produced from the decay of Ra-223 in the actinium (U-235) decay series, and is typically present at negligible concentrations because of its short half-life. Thoron has a half-life of 56 seconds, is produced from the decay of Ra-224 in the thorium (Th-232) decay series, and is most relevant when addressing thorium ores or associated waste. Rn-222, the focus of this discussion, has a half-life of 3.8 days, is produced from the decay of Ra-226 in the uranium (U-238) decay series, and is the isotope most commonly referred to as "radon."

Its 3.8-day half-life and chemical inertness allow radon to reach the environment (i.e., air) once produced either in building materials or in the top few feet of soil. The nuclide will then follow a series of radiological decays to include the following short-lived decay products:

| <b>Nuclide</b> | <b>Half-Life</b> | <b>Alpha Energy</b> | <b>Max Beta Energy</b> | <b>Gamma Energy (yield)</b>              |
|----------------|------------------|---------------------|------------------------|--|
| Rn-222         | 3.82 days        | 5.5 MeV             | ---                    | Negligible                               |
| Po-218         | 3.11 min         | 6.0 MeV             | ---                    | Negligible                               |
| Pb-214         | 26.8 min         | ---                 | 0.72 MeV               | 0.295 MeV (19%), 0.352 MeV (37%), others |
| Bi-214         | 19.9 min         | ---                 | 1.8 MeV                | 0.609 MeV (46%), 1.12 MeV (15%), others  |
| Po-214         | 164 µsec         | 7.7 MeV             | ---                    | Negligible                               |

Unlike radon, the short-lived decay products are chemically active and carry an ionic charge that may result in the nuclide "sticking" to a particle of dust or a surface.

Because radium is naturally abundant in soil, rock, and common building materials (e.g., brick and concrete), there is a continuous source of radon and decay products unassociated with site operations and sources of contamination. Once a radon atom is formed, it is subject to the general flow of soil gas (e.g., through fissures or interstitial spaces), air-handling systems, wind, and other factors and will eventually decay into the short-lived decay products according to standard rules. Factors that impact this general "air" flow include pressure, moisture, temperature, and other conditions that can vary by season, time of day, atmospheric conditions, thermostat adjustments, and other variables. The combinations of variables are endless and extraordinarily difficult to predict in the short term. The primary problem considered here is that some combination of these factors may, in a few moments, produce a significant amount of radon decay products in soils or on building surfaces that are subject to a radiological survey.

The existence of naturally occurring radionuclides is not the issue, as background measurements account for detector responses to materials or radiation sources (e.g., cosmic) *not* associated with contamination. The complication here is that radiation produced by radon decay products can vary greatly over short periods of time. For example, small changes in the barometric pressure can result in large changes in radon concentrations in soil. Soil moisture also affects the radon emanation rate. These factors can result in a buildup of short-lived radon decay products. This variability inevitably leads to false positive errors (i.e., the conclusion that an unacceptable level of contamination is present when it is not).

For example, a team has produced a plan to characterize a facility with potential soil and structural contamination. The contaminants are Cs-137 and SrY-90. Scan and static MDCs were calculated using methods described in this report. Multiple crews have been concurrently performing soil and structural surveys and, so far, have encountered no contamination. However, surveyors are now reporting significantly elevated radiation levels both in surface soils (from gamma) and on structural surfaces (from beta). It just rained, which will need to be considered as the team asks the following questions. Are the elevated readings the result of contamination, radon, or a combination of both? Should the surveyors collect samples, wait for some period of time and resurvey, or ignore the elevated readings?

Additionally, the team must consider that lead (Pb)-210 is a long-lived (22-year half-life) radon decay product that can complicate the interpretation of surface measurement data. Lead is easily oxidized and can become fixed to a surface through corrosion processes. Rust and oxide films can, therefore, produce elevated alpha and beta radiation readings from the buildup of bismuth (Bi)-210 and polonium (Po)-210, as seen below:

| <b>Nuclide</b> | <b>Half-Life</b> | <b>Alpha Energy</b> | <b>Max Beta Energy</b> | <b>Gamma Energy (yield)</b> |
|----------------|------------------|---------------------|------------------------|-----------------------------|
| Pb-210         | 22.3 yr          | ---                 | 0.024 MeV              | Negligible                  |
| Bi-210         | 5.0 days         | ---                 | 1.16 MeV               | Negligible                  |
| Po-210         | 138 days         | 5.3 MeV             | ---                    | Negligible                  |

Rain scavenges radon progeny from the air, so areas where rain collects can show elevated concentrations of Pb-210 and associated decay products. Gamma emissions from Pb-210 and decay products are negligible, so interferences (i.e., false positive detections) are most likely encountered while measuring alpha and beta radiation levels.

So many factors can contribute to variability in radon concentrations that no method of accounting for radon progeny interferences will apply in all survey situations. In this example scenario, the problem is related to short-term radon progeny buildup. Resurveying a selection of exact locations that had previously been found contamination free will roughly indicate the magnitude of radon daughter interference. A common method to address potential false positives from recent radon depositions is to simply wait. The effective half-life of short-term radon progeny is 30 minutes. Pb-210, with a half-life of over 22 years, decays by low-energy beta emission and will not contribute to a short-term measurement. An elevated measurement suspected to be caused by short-term buildup from radon can be repeated after a few hours. Contamination levels of longer lived radionuclides will not change, while radon levels will drop by roughly 75 percent per hour. Provided the surface being measured is not the source of the radon, the area of interest may be covered during this waiting period to preclude additional buildup via aerial deposition. Additionally, both alpha and beta radiation are attributed to radon decay products. Therefore, measurement of both elevated alpha and elevated beta radiation on

a surface could indicate the presence of radon decay products when, for example, beta-only activity is associated with the contaminant.

Sampling, whether by the collection of a smear sample or a volumetric sample, can also be used to deal with interference from the short-lived radon progeny. For smears, the 75 percent per hour rule of thumb that applies to the total measurement (fixed plus removable) also applies to the removable fraction on the smear. Alternatively, a scraping of rust or small sample of soil can be analyzed via gamma spectroscopy for Po-210, though close coordination with the laboratory may be required to ensure that sufficient sample mass is available to produce reliable results. Appendix A presents a case study that explores in greater detail the methods for better planning and awareness of radon-related interferences.

### **5.6.2 Interferences from Beryllium-7**

Beryllium (Be)-7 is produced from the interaction of nitrogen or oxygen with cosmic radiation in the upper atmosphere. With a half-life of 53.3 days, Be-7 has time to reach the lower atmosphere where, like radon decay products, it can be scavenged by rain and deposited on open surfaces. Be-7 produces a 0.477-MeV gamma that can be measured during a gamma radiation survey. Additionally, at the onset of a rain event, an almost instantaneous increase will often occur in the background gamma count rate, adversely affecting the assumed *a priori* scan MDC, which may have been based on a lower ambient background count rate. In addition to the increase of the detector background response, Be-7 will often accumulate in natural terrain ponding areas or minor depressions on outdoor pavement. Unless surveyors account for the possibility of Be-7 interferences, these accumulation points may appear as an anomaly that could lead to false positive decisions.

### **5.7 Potential Impacts of Signal Degradation**

A key input to the discussion in Section 6 of gamma radiation scan MDC calculation is a variable, often provided by the detector vendor as a sensitivity, and defined here as the “count-rate-to-exposure-rate ratio” (CPMR) in units of cpm/ $\mu$ R/h. This variable represents the energy-dependent detector response or signal (in cpm) to a known gamma radiation field (in  $\mu$ R/h). For example, Ludlum provides a CPMR of 900 cpm/ $\mu$ R/h for exposure to Cs-137 (662-keV gamma) for the model 44-10. As NaI detectors are often used to perform gamma radiation surveys, some components may incur normal wear or degradation that can lower the detector’s sensitivity. This sensitivity loss means the CPMR may be overestimated, and the actual scan MDC may be higher than originally calculated when using the manufacturer-provided data. If the scan MDC is higher than calculated, operators may not identify contamination when the contamination is actually present (a false negative decision error). As noted, normal wear and detector degradation can lower a detector’s energy-dependent scan sensitivity, though operators can most likely compensate for any signal loss and avoid these false negative decision errors. This evaluation includes the collection of count rate data in cpm from a large population of 2"  $\times$  2" NaI detectors all of the same make and model, but representing a wide range of use histories and detector ages.

### 5.7.1 Signal Degradation Investigation Design

Three subpopulations (SPs) of detectors were evaluated:

- (1) 19 new detectors manufactured in 2012 and 2013 (SP1)
- (2) 11 detectors manufactured from 2010 to 2012 and used to perform routine radiological surveys across the continental United States (SP2)
- (3) 12 detectors manufactured about 1995 and used for decades for training (SP3)

SP1 detectors are new, and SP2 detectors have been managed, maintained, and used by trained health physics professionals. The operational history of SP3 detectors is not well known. Users had a wide range of experiences, and it can be assumed that some, if not all, detectors were inadvertently dropped, kicked, dragged, or otherwise mishandled.

Investigators adjusted measurement distances to ensure that responses from exposure to all sources were on the same order of magnitude. This resulted in the following source-and-distance relationships: Am-241, 10 centimeters; Cs-137, 20 centimeters; and Co-60, 5 centimeters. Figure 5-25 presents the apparatus used to control detector-to-source distances. Results at these distances also produced net signals greater than 10,000 cpm for counting statistics, achieving at least 1-percent measurement precision.

Two sets of results were collected for each detector. One set was the source-specific detector cpm responses at peak voltages as determined by the manufacturer's peak signal procedure (Ludlum, 2013). This procedure determines the optimum voltage to bracket the energy-dependent gamma peak and calibrates the threshold and window display values against this peak. The second set includes the same count data but with a constant 900-volt setting for each measurement, per the detector's general procedure (Ludlum, 2014).

Differences in cpm response to each of the three sources between the three subpopulations were tested using statistical procedures of analysis of variance (ANOVA) for parametric data and Kruskal Wallis for nonparametric data. Setting the Type I (alpha) error to 0.05, the position that age and wear have no impact on detector signal is rejected if the ANOVA p-value is less than 0.05.

### 5.7.2 Plateauing Overview

The purpose of this investigation was to describe how diminished scan sensitivity may culminate in an increased scan MDC and subsequent increase in false negative decisions. Figure 5-26 illustrates a generic detector response curve with a voltage plateau. To generate the curve, an operator records the detector signal in counts for each increasing voltage setting. As shown, the curve "plateaus" over a range of voltages; thus, before conducting surveys, the operator will set the detector's high voltage to a value in the plateau region. For example, Ludlum suggests a high-voltage setting of 900 volts, on the low end of this plateau curve, while the procedures adapted for this study require that instrument voltages be set to about two-thirds higher than the "knee" of the curve. Figure 5-27 illustrates how the signal may degrade over time (i.e., how the signal decreases for any single voltage setting). In this example, the signal at 900 volts is on the knee, meaning the detector may under-respond (have a lower sensitivity) to a low-energy gamma-emitter; thus, the detector's operational high-voltage setting should be increased. The plateauing procedure should optimize the detector's response across the gamma energy range

and adjust for loss of detection efficiency at the lower energies. Finally, Figure 5-28 presents a possible response curve for a detector with a damaged NaI crystal. In this case, there is no plateau, and small adjustments in the high voltage at any magnitude will significantly alter the resulting signal. The signal from this detector may be unreliable, increasing the likelihood of decision errors.

### 5.7.3 Signal Degradation Investigation Results—Peak Voltage

Table 5-33 presents raw data collected using the peak signal procedure. Data are organized by subpopulation and age in ascending order (i.e., with newer detectors first). Figure 5-29 is a strip chart that presents the same voltage data. In the figure, each subpopulation of detectors is segregated with detector age increasing from left to right. Figure 5-29 illustrates a clear difference across subpopulations with very little variability in SP1 results, moderate variability in SP2 results, and relatively large variability in SP3 results. SP1 results are very well-behaved (small variance) and form the baseline for comparison. SP2 results show a mixture of peak voltages that sometimes fall within the baseline range and are sometimes well above the maximum SP1 value. This suggests that degradation may occur soon after a detector is subject to routine operational use. Results for two detectors in SP3 specifically stand out (see the values on the far right in Figure 5-29) requiring over 100 volts above the recommended setting of 900 volts to achieve the peak signal. Even when disregarding these two data points, almost the entire SP3 subpopulation requires higher voltages to achieve the peak signal.

Table 5-34 presents summary statistics including ANOVA output for each subpopulation, and Figure 5-30 illustrates these results using a box-and-whisker plot. The plot presents average values as a small diamond, median values as a horizontal line within each box, and outliers (if present) as a small circle. Boxes represent quantiles above and below the median values, and the vertical bar plus terminal lines (i.e., the “whiskers”) represent the outer two quantiles. The ANOVA, with a p-value less than 0.05, shows that at least one subpopulation is significantly different and results in rejection of the null hypothesis. In this case, that subpopulation is SP1, which has a standard error ( $\sigma/\sqrt{N}$ ) an order of magnitude less than that of the other subpopulations. These results lead to the same general conclusion that peak signals generally require higher voltages over time, implying that detector (and signal) degradation begins to occur within a few years of routine use.

### 5.7.4 Signal Degradation Investigation Results—900 Volts

Table 5-35 presents raw data after setting the voltage of all detectors at a constant 900 volts, per the manufacturer’s setup procedure. As with the peak signal investigation, data are organized by subpopulation and age in ascending order. Figures 5-31, 5-32, and 5-33 are strip charts that present cpm results by subpopulation from exposure to Am-241, Cs-137, and Co-60 sources, respectively. As before, SP1 results are very well-behaved (small variances) and are used here as the baseline for comparison. Overall data trends are consistent with the peak signal experiment: signal degrades with age, and obvious degradation can appear soon after the detector is used for routine surveys.

Most notable is the relationship between signal and radiation energy. The signal variability is most pronounced for low gamma energies, while there is less variability across all subpopulations for high gamma energies (noting three SP3 exceptions). This suggests that low-energy gamma-emitters will experience the most detector response variability. For low gamma energies (e.g., from Am-241 or U-238), there is clear potential for a reduction in detection efficiency and signal loss when the high-voltage setting is less than optimal. This

under-response may be attributed to degradation in the crystalline structure of the NaI scintillator or in the photo-multiplier tube (PMT), moisture leaks, and/or prolonged exposure to high levels of radiation. Additionally, the sensitivity of a PMT tends to decrease when operated in harsh conditions for lifetimes exceeding several thousand hours (Hamamatsu, 2007). The ratemeter threshold could be lowered to help compensate, but doing so also increases the noise and may not offer an effective solution to signal degradation problems.

Tables 5-36, 5-37, and 5-38 present summary statistics including ANOVA output for each subpopulation when exposed to Am-241, Cs-137, and Co-60, respectively. Figures 5-34, 5-35, and 5-36 are the corresponding box-and-whisker plots. The ANOVA, with a p-value less than 0.05, shows that at least one subpopulation is significantly different than the others and results in rejection of the null hypothesis. In this case, that subpopulation is SP1, which has a standard error an order of magnitude less than SP2 and SP3. These results lead to the same general conclusion that signal loss is most pronounced for low gamma energies in older detectors.

### **5.7.5 Results Using Peak Voltage for Detector Setup**

Table 5-33 includes raw data for Cs-137 after setting the voltage to bracket the Cs-137 peak, per the manufacturer's manual. Figure 5-37 is a strip chart that presents these cpm results, and Figure 5-38 is the corresponding box-and-whisker plot. For this method, the results for the three subpopulations are well aligned with little apparent variability.

Count results taken after applying the peak voltage setup method do not show the same age-dependent trends as described using the constant (900 volts) approach. Table 5-39 presents summary statistics including ANOVA output for these data. Contrary to the other cases, the rejection of the null hypothesis is not warranted, as the p-value is greater than 0.05; it is not proven that the three populations differ.

Count results for Co-60 and for Am-241 using voltages set for the Cs-137 peak also showed less variability, as shown in Figures 5-39 and 5-40. Table 5-33 also presents the raw data for Co-60 and Am-241. The relatively large spread in Am-241 results in all subpopulations is most likely the result of the easily attenuated 59-keV gamma and the small signal it produces within the detector.

One detector in the SP3 population appears as an outlier in Figures 5-39 and 5-40. This same detector, measurement number 40 on the x-axis, is also the greatest outlier in other plots. The study did not investigate the underlying cause of the nonconformance of this particular NaI probe.

### **5.7.6 Discussion of Detector Signal Loss**

Two general observations are immediately evident from these results. First, it is clear that the risk of detector degradation and diminished scan sensitivity increases with age and use. This is observed even with relatively new and moderately used detectors, such as the one illustrated in Figure 5-41, and signal loss is most diminished for gammas in the low-energy range (roughly from 50 to 200 keV). Second, detector-specific peak voltages should be established and adjusted, as required, to optimize the detection sensitivity. These adjustments will help minimize the risk of underestimating the scan MDC and false negative decision errors. For further technical discussions on the causes of signal loss, the reader is directed to Hamamatsu (2007) and Knoll (2010).

### 5.7.7 Conclusions and Recommendations

Degradation in the form of diminished scan sensitivity increases the detection thresholds and appears well before total failure of the device. The typical user neither has nor needs access to interior probe components to assess the degree of loss. The NaI probe is treated as a “black box,” with any symptoms of degradation, whether mechanically or electronically caused, apparent in the output. This output in the form of counting results should be monitored. Calibration results should be maintained and examined for changes indicating any loss of scan sensitivity. This investigation leads to the following recommendations:

- “Plateau” detectors before operation using a standard source with known energies. This is the process of establishing an acceptable operating voltage (i.e., within the plateau) by plotting the detector response as a function of high voltage. Best practice is to set the operating voltage at approximately two-thirds above the first knee of the plateau curve. By setting the operating voltage well above the knee, some degradation will not dramatically lower the signal and thus will lower the possibility of significant loss in scan sensitivity.
- Maintain a control chart of peak response and operating voltage records. A decline in the peak response may indicate that some detector degradation is occurring and an increase in the high-voltage setting is warranted. An under-responding detector may culminate in an underestimated scan MDC or false negative decisions during a survey. ANSI Standard N323AB-2013, “American National Standard for Radiation Protection Instrumentation Test and Calibration, Portable Survey Instruments,” suggests yearly detector calibrations (plateauing in this case), though some operators may calibrate more often.
- Maintain a control chart of detection efficiencies. Though operating voltage and detection efficiency are linked, shifts in the sensitivity may also indicate signal loss because of detector degradation. By tracking sensitivities, licensees will be able to track changes in the manufacturer’s stated sensitivity and thus the state of detector health.
- Remove detectors from service if and when the detector cannot be plateaued, which suggests the NaI crystal is significantly damaged.

By plateauing detectors before use and selecting an operating voltage accordingly and by maintaining detector control charts to assess detector health, operators should be able to achieve relatively consistent NaI detector responses. These actions should help limit the loss of scan sensitivity and thus help lower the frequency of false negative decision errors.

**Table 5-1 Background Count Rate for Various Materials**

| Surface Material     | Background Count Rate (cpm) <sup>a</sup> |              |                  |             |             |            |
|----------------------|--|--------------|------------------|-------------|-------------|------------|
|                      | Gas Proportional                         |              |                  | GM          | ZnS         | NaI        |
|                      | $\alpha$ Only                            | $\beta$ Only | $\alpha + \beta$ |             |             |            |
| Ambient <sup>b</sup> | 1.00 ± 0.45 <sup>c</sup>                 | 349 ± 12     | 331.6 ± 6.0      | 47.6 ± 2.6  | 1.00 ± 0.32 | 4,702 ± 16 |
| Brick                | 6.00 ± 0.84                              | 567.2 ± 7.0  | 573.2 ± 6.4      | 81.8 ± 2.3  | 1.80 ± 0.73 | 5,167 ± 23 |
| Ceramic block        | 15.0 ± 1.1                               | 792 ± 11     | 770.2 ± 6.4      | 107.6 ± 3.8 | 8.0 ± 1.1   | 5,657 ± 38 |
| Ceramic tile         | 12.6 ± 0.24                              | 647 ± 14     | 648 ± 16         | 100.8 ± 2.7 | 7.20 ± 0.66 | 4,649 ± 37 |
| Concrete block       | 2.60 ± 0.81                              | 344.0 ± 6.2  | 325.0 ± 6.0      | 52.0 ± 2.5  | 1.80 ± 0.49 | 4,733 ± 27 |
| Drywall              | 2.60 ± 0.75                              | 325.2 ± 8.0  | 301.8 ± 7.0      | 40.4 ± 3.0  | 2.40 ± 0.24 | 4,436 ± 38 |
| Floor tile           | 4.00 ± 0.71                              | 308.4 ± 6.2  | 296.6 ± 6.4      | 43.2 ± 3.6  | 2.20 ± 0.58 | 4,710 ± 13 |
| Linoleum             | 2.60 ± 0.98                              | 346.0 ± 8.3  | 335.4 ± 7.5      | 51.2 ± 2.8  | 1.00 ± 0.45 | 4,751 ± 27 |
| Carbon steel         | 2.40 ± 0.68                              | 322.6 ± 8.7  | 303.4 ± 3.4      | 47.2 ± 3.3  | 1.00 ± 0.54 | 4,248 ± 38 |
| Treated wood         | 0.80 ± 0.37                              | 319.4 ± 8.7  | 295.2 ± 7.9      | 37.6 ± 1.7  | 1.20 ± 0.20 | 4,714 ± 40 |
| Untreated wood       | 1.20 ± 0.37                              | 338.6 ± 9.4  | 279.0 ± 5.7      | 44.6 ± 2.9  | 1.40 ± 0.51 | 4,623 ± 34 |

<sup>a</sup>Background count rates determined from the mean of five 1-minute counts.

<sup>b</sup>Ambient background determined at the same location as for all measurements, but without the surface material present.

<sup>c</sup>Uncertainties represent the standard error in the mean count rate, based only on counting statistics.



**Table 5-2 MDCs for Various Materials**

| Surface Material | MDC<br>(dpm/100 cpm <sup>2</sup> ) <sup>a</sup> |        |
|------------------|---|--------|
|                  | Gas Proportional                                |        |
|                  | α Only  | β Only |
| Ambient          | 30  | 285    |
| Brick            | 57  | 361    |
| Ceramic block    | 83  | 425    |
| Ceramic tile     | 78  | 385    |
| Concrete block   | 41  | 283    |
| Drywall          | 41  | 275    |
| Floor tile       | 49  | 268    |
| Linoleum         | 41  | 284    |
| Steel            | 40  | 275    |
| Treated wood     | 28  | 273    |
| Untreated wood   | 32  | 281    |

<sup>a</sup>MDCs were calculated based on the background count rates presented in Table 5-1 for the gas proportional detector. The alpha-only and beta-only efficiencies were assumed to be 0.20 and 0.25 c/dis, respectively. Probe area corrections of 126 cm<sup>2</sup> were made for the gas proportional detectors. The following MDC equation was used for 1-minute counts:

$$MDC = \frac{3 + 4.65\sqrt{C_B}}{KT}$$

**Table 5-3 Efficiencies and Backscatter Factors for SrY-90**

| Surface Material | Gas Proportional Detector with<br>0.4-mg/cm <sup>2</sup> Window |                                    | Gas Proportional Detector with<br>3.8-mg/cm <sup>2</sup> Window |                       |
|------------------|---|------------------------------------|---|-----------------------|
|                  | Total Efficiency <sup>a</sup><br>(c/dis)                        | Backscatter<br>Factor <sup>b</sup> | Total Efficiency<br>(c/dis)                                     | Backscatter<br>Factor |
| Air              | 0.28  | 1.00                               | 0.25  | 1.00                  |
| Wood             | 0.34  | 1.20                               | 0.29  | 1.14                  |
| Stainless steel  | 0.40  | 1.43                               | 0.35  | 1.37                  |
| Drywall          | 0.35  | 1.24                               | 0.28  | 1.11                  |
| Carbon steel     | 0.40  | 1.42                               | 0.33  | 1.32                  |
| Floor tile       | 0.35  | 1.25                               | 0.31  | 1.23                  |
| Sealed concrete  | 0.37  | 1.30                               | 0.31  | 1.22                  |
| Concrete block   | 0.35  | 1.25                               | 0.31  | 1.22                  |

<sup>a</sup>Total efficiency was determined by dividing the instrument net counts by the deposited SrY-90 activity.

<sup>b</sup>The backscatter factor was calculated by dividing the particular surface material efficiency by the efficiency in the air.

**Table 5-4 Surface Material Effects on Source Efficiency for Tc-99 Distributed on Various Surfaces**

| Surface Material                      | Source Efficiency <sup>a, b</sup> |                   |                   |
|---------------------------------------|-----------------------------------|-------------------|-------------------|
|                                       | Gas Proportional                  |                   | GM                |
|                                       | $\beta$ Only                      | $\alpha + \beta$  |                   |
| <b>Point Source<sup>c</sup></b>       |                                   |                   |                   |
| Sealed concrete <sup>d</sup>          | $0.703 \pm 0.079^e$               | $0.694 \pm 0.063$ | $0.630 \pm 0.076$ |
| Stainless steel                       | $0.755 \pm 0.096$                 | $0.761 \pm 0.076$ | $0.773 \pm 0.091$ |
| Untreated wood                        | $0.53 \pm 0.11$                   | $0.504 \pm 0.053$ | $0.512 \pm 0.061$ |
| <b>Distributed Source<sup>f</sup></b> |                                   |                   |                   |
| Sealed concrete                       | $0.299 \pm 0.096$                 | $0.20 \pm 0.12$   | $0.19 \pm 0.18$   |
| Stainless steel                       | $0.81 \pm 0.13$                   | $0.73 \pm 0.11$   | — <sup>g</sup>    |
| Treated wood                          | $0.66 \pm 0.11$                   | $0.551 \pm 0.088$ | $0.61 \pm 0.52$   |

<sup>a</sup>Source efficiency determined by dividing the total efficiency by the instrument efficiency.

<sup>b</sup>The instrument efficiencies for the point source geometry were 0.25, 0.45, and 0.28, respectively, for the  $\beta$  only,  $\alpha + \beta$ , and GM detectors. Instrument efficiencies for the distributed source geometry were 0.20, 0.38, and 0.20, respectively, for the  $\beta$  only,  $\alpha + \beta$ , and GM detectors.

<sup>c</sup>The Tc-99 activity ( $2,828 \pm 91$  dpm) was dispensed in an area less than  $5 \text{ cm}^2$ .

<sup>d</sup>For sealed concrete, the Tc-99 activity ( $5,660 \pm 110$  dpm) was dispensed over an area of approximately  $4 \text{ cm}^2$ .

<sup>e</sup>Uncertainties represent the 95-percent confidence interval, based on propagating the errors in pipetting, volumetric measurements, calibration source activity, and counting statistics.

<sup>f</sup>The Tc-99 activity ( $2,830 \pm 100$  dpm) was evenly distributed over an area of  $126 \text{ cm}^2$ .

<sup>g</sup>Measurement not taken.

**Table 5-5 Surface Material Effects on Source Efficiency for Th-230 Distributed on Various Surfaces**

| Surface Material                      | Source Efficiency <sup>a, b</sup> |                   |
|---------------------------------------|-----------------------------------|-------------------|
|                                       | Gas Proportional ( $\alpha$ only) | ZnS               |
| <b>Point Source<sup>c</sup></b>       |                                   |                   |
| Scabbled concrete                     | 0.276 $\pm$ 0.013 <sup>d</sup>    | 0.288 $\pm$ 0.026 |
| Stainless steel                       | 0.499 $\pm$ 0.028                 | 0.555 $\pm$ 0.043 |
| Untreated wood                        | 0.194 $\pm$ 0.023                 | 0.185 $\pm$ 0.025 |
| <b>Distributed Source<sup>e</sup></b> |                                   |                   |
| Sealed concrete                       | 0.473 $\pm$ 0.053                 | 0.428 $\pm$ 0.054 |
| Carbon steel                          | 0.250 $\pm$ 0.042                 | 0.216 $\pm$ 0.031 |
| Treated wood                          | 0.527 $\pm$ 0.057                 | 0.539 $\pm$ 0.065 |

<sup>a</sup>Source efficiency was determined by dividing the total efficiency by the instrument efficiency.

<sup>b</sup>The instrument efficiencies for the point source geometry were 0.50 and 0.33, respectively, for the  $\alpha$ -only and ZnS detectors. Instrument efficiencies for the distributed source geometry were 0.40 and 0.31, respectively, for the  $\alpha$ -only and ZnS detectors.

<sup>c</sup>The Th-230 activity (4,595  $\pm$  79 dpm) was dispensed in an area less than 10 cm<sup>2</sup>.

<sup>d</sup>Uncertainties represent the 95-percent confidence interval, based on propagating the errors in pipetting, volumetric measurements, calibration source activity, and counting statistics.

<sup>e</sup>The Th-230 activity (4,600  $\pm$  170 dpm) was evenly distributed over an area of 126 cm<sup>2</sup>.

**Table 5-6 Surface Material Effects on MDC for Tc-99 and Th-230 Distributed on Various Surfaces**

| Surface Material                      | MDC <sup>a</sup> (dpm/100 cm <sup>2</sup> ) |              |               |               |           |
|---------------------------------------|---|--------------|---------------|---------------|-----------|
|                                       | Tc-99                                       |              |               | Th-230        |           |
|                                       | $\alpha + \beta$                            | $\beta$ only | GM            | $\alpha$ only | ZnS       |
| <b>Point Source<sup>b</sup></b>       |   |              |               |               |           |
| Sealed concrete                       | 242 ± 13 <sup>c</sup>                       | 396 ± 46     | 1,090 ± 180   | —             | —         |
| Scabbled concrete                     | —   | —            | —             | 88 ± 16       | 131 ± 89  |
| Stainless steel                       | 192 ± 19                                    | 359 ± 47     | 850 ± 130     | 32 ± 13       | 68 ± 28   |
| Untreated wood                        | 285 ± 31                                    | 520 ± 110    | 1,200 ± 150   | 67 ± 30       | 190 ± 100 |
| <b>Distributed Source<sup>d</sup></b> |   |              |               |               |           |
| Sealed concrete                       | 950 ± 560                                   | 1,220 ± 380  | 5,100 ± 4,800 | 37 ± 23       | 84 ± 40   |
| Stainless steel                       | 260 ± 34                                    | 446 ± 64     | —             | —             | —         |
| Treated wood                          | 312 ± 44                                    | 523 ± 79     | 1,500 ± 1,300 | 27 ± 8        | 65 ± 9.8  |
| Carbon steel                          | —   | —            | —             | 81 ± 21       | 153 ± 54  |

<sup>a</sup>The MDC was calculated using 1-minute counts and total efficiencies determined on the basis of the known amount of activity deposited.

<sup>b</sup>The point (disc) source areas for Tc-99 and Th-230 were approximately 5 and 10 cm<sup>2</sup>, respectively.

<sup>c</sup>Uncertainties represent the 95-percent confidence interval, based on propagating the errors in pipetting, volumetric measurements, calibration source activity, and counting statistics.

<sup>d</sup>The distributed source area for both Tc-99 and Th-230 was 126 cm<sup>2</sup>.

**Table 5-7 Effects of Oil Density Thickness on Source Efficiency and MDC (Gas Proportional— $\alpha + \beta$ )**

| Surface Material                                    | Density Thickness (mg/cm <sup>2</sup> ) | C-14 (0.254) <sup>a</sup>      |   | Tc-99 (0.364)     |                                | SrY-90 (0.536)    |                                |
|---|---|--------------------------------|---|-------------------|--------------------------------|-------------------|--------------------------------|
|   |   | Source Efficiency <sup>b</sup> | MDC <sup>c</sup> (dpm/100 cm <sup>2</sup> ) | Source Efficiency | MDC (dpm/100 cm <sup>2</sup> ) | Source Efficiency | MDC (dpm/100 cm <sup>2</sup> ) |
| Detector face <sup>d</sup>                          | 0.4                                     | NA                             | 605   | NA                | 304                            | NA                | 164                            |
| Detector face <sup>e</sup> plus two sheets of Mylar | 0.8                                     | 0.386                          | 703   | 0.596             | 317                            | 0.772             | 167                            |
| Plus 1.5 mg/cm <sup>2</sup> oil <sup>f</sup>        | 2.3                                     | 0.236                          | 1,148                                       | 0.467             | 406                            | 0.744             | 173                            |
| Plus 2.9 mg/cm <sup>2</sup> oil                     | 3.7                                     | 0.193                          | 1,406                                       | 0.401             | 472                            | 0.700             | 184                            |
| Plus 4.5 mg/cm <sup>2</sup> oil                     | 5.3                                     | 0.102                          | 2,651                                       | 0.349             | 543                            | 0.677             | 190                            |

<sup>a</sup>Instrument efficiency appears in parentheses.

<sup>b</sup>Source efficiency was determined by dividing the total efficiency by the instrument efficiency.

<sup>c</sup>Probe area corrections of 126 cm<sup>2</sup> were made for the gas proportional detectors. The following MDC equation was used for 1-minute counts and a background of 326 cpm:

$$MDC = \frac{3 + 4.65 \sqrt{C_B}}{KT}$$

<sup>d</sup>Measurements were made with a Ludlum model 43-68 gas proportional detector with a standard 0.4-mg/cm<sup>2</sup> window.

<sup>e</sup>Each sheet of Mylar has a density thickness of 0.22 mg/cm<sup>2</sup>.

<sup>f</sup>20W-50 motor oil was used for the study.

**Table 5-8 Effects of Paint Density Thickness on Source Efficiency and MDC (Gas Proportional— $\alpha + \beta$ )**

| Surface Material                                       | Density Thickness (mg/cm <sup>2</sup> ) | C-14 (0.254 ± 0.006) <sup>a</sup> |   |        | Tc-99 (0.364 ± 0.029)             |               |       | Tl-204 (0.450 ± 0.025)            |               |     | SrY-90 (0.537 ± 0.027)            |               |     |
|--|---|-----------------------------------|---|--------|-----------------------------------|---------------|-------|-----------------------------------|---------------|-----|-----------------------------------|---------------|-----|
|  |   | Source Efficiency                 | MDC <sup>d</sup> (dpm/100 cm <sup>2</sup> ) | MDC    | Source Efficiency                 | MDC           | MDC   | Source Efficiency                 | MDC           | MDC | Source Efficiency                 | MDC           | MDC |
|  |   | Meas <sup>b</sup>                 | Fit <sup>c</sup>                            |        | Meas                              | Fit           |       | Meas                              | Fit           |     | Meas                              | Fit           |     |
| Detector face <sup>e</sup>                             | 0.4                                     | NA                                | NA  | 510    | NA                                | NA            | 278   | NA                                | NA            | 202 | NA                                | NA            | 177 |
| Detector face <sup>f</sup><br>plus two sheets of Mylar | 0.84                                    | 0.437                             | 0.426 ± 0.065                               | 600    | 0.626                             | 0.572 ± 0.100 | 291   | 0.716                             | 0.675 ± 0.079 | 206 | 0.697                             | 0.643 ± 0.103 | 178 |
| Plus 1.93 mg/cm <sup>2</sup> paint <sup>g</sup>        | 2.77                                    | 0.252                             | 0.243 ± 0.030                               | 1,037  | 0.427                             | 0.463 ± 0.066 | 427   | 0.596                             | 0.622 ± 0.060 | 247 | 0.584                             | 0.615 ± 0.080 | 212 |
| Plus 2.48 mg/cm <sup>2</sup> paint                     | 3.32                                    | 0.215                             | 0.207 ± 0.024                               | 1,215  | — <sup>h</sup>                    | —             | —     | —                                 | —             | —   | —                                 | —             | —   |
| Plus 5.54 mg/cm <sup>2</sup> paint                     | 6.38                                    | 0.074                             | 0.085 ± 0.008                               | 3,542  | 0.300                             | 0.311 ± 0.034 | 608   | 0.515                             | 0.535 ± 0.039 | 286 | 0.530                             | 0.565 ± 0.056 | 233 |
| Plus 9.48 mg/cm <sup>2</sup> paint                     | 10.32                                   | 0.026                             | 0.027 ± 0.004                               | 9,955  | 0.201                             | 0.202 ± 0.027 | 907   | 0.449                             | 0.454 ± 0.042 | 329 | 0.513                             | 0.515 ± 0.064 | 241 |
| Plus 12.63 mg/cm <sup>2</sup> paint                    | 13.47                                   | 0.012                             | 0.011 ± 0.002                               | 22,593 | 0.147                             | 0.143 ± 0.027 | 1,238 | 0.410                             | 0.398 ± 0.051 | 360 | 0.498                             | 0.479 ± 0.083 | 249 |
| Regression equation                                    |   | $\epsilon_s = 0.544 e^{-0.291 x}$ |   |        | $\epsilon_s = 0.628 e^{-0.110 x}$ |               |       | $\epsilon_s = 0.699 e^{-0.042 x}$ |               |     | $\epsilon_s = 0.656 e^{-0.023 x}$ |               |     |

<sup>a</sup>Instrument efficiency appears in parentheses; uncertainties represent the 95-percent confidence interval.

<sup>b</sup>Source efficiency was determined by dividing the total efficiency by the instrument efficiency.

<sup>c</sup>The measured source efficiency versus density thickness was fit to an exponential curve; uncertainties represent the 95-percent confidence interval.

<sup>d</sup>Probe area corrections of 126 cm<sup>2</sup> were made for the gas proportional detectors. The following MDC equation was used for 1-minute counts and a background of 301 cpm:

$$MDC = \frac{3 + 4.65\sqrt{C_B}}{KT}$$

<sup>e</sup>Measurements were made with a Ludlum model 43-68 gas proportional detector with a standard 0.4-mg/cm<sup>2</sup> window.

<sup>f</sup>Each sheet of Mylar has a density thickness of 0.22 mg/cm<sup>2</sup>.

<sup>g</sup>Orange fluorescent water-based paint was used.

<sup>h</sup>Measurement was not made.

**Table 5-9 Effects of Paint Density Thickness on Source Efficiency and MDC**

| Surface Material                                    | Density Thickness (mg/cm <sup>2</sup> ) | Th-230 (0.349 ± 0.015) <sup>a</sup> |                  |   |
|---|---|-------------------------------------|------------------|---|
|   |   | Source Efficiency                   |                  | MDC <sup>d</sup> (dpm/100 cm <sup>2</sup> ) |
|   |   | Meas <sup>b</sup>                   | Fit <sup>c</sup> |   |
| Detector face <sup>e</sup>                          | 0.4                                     | NA                                  | NA               | 30  |
| Detector face <sup>f</sup> plus two sheets of Mylar | 0.84                                    | 0.509                               | 0.513 ± 0.085    | 34  |
| Plus 1.93 mg/cm <sup>2</sup> paint <sup>g</sup>     | 2.77                                    | 0.129                               | 0.123 ± 0.013    | 135   |
| Plus 2.48 mg/cm <sup>2</sup> paint                  | 3.32                                    | 0.078                               | 0.082 ± 0.009    | 223   |
| Plus 5.54 mg/cm <sup>2</sup> paint                  | 6.38                                    | 0.008                               | 0.008 ± 0.002    | 2,060                                       |
| Plus 9.48 mg/cm <sup>2</sup> paint                  | 10.32 <sup>h</sup>                      | 0.001                               | NA               | 17,369                                      |
| Regression equation                                 |   | $\epsilon_s = 0.956 e^{-0.741 x}$   |                  |   |

<sup>a</sup>Instrument efficiency appears in parentheses; uncertainties represent the 95-percent confidence interval.

<sup>b</sup>Source efficiency was determined by dividing the total efficiency by the instrument efficiency.

<sup>c</sup>The measured source efficiency versus density thickness was fit to an exponential curve; uncertainties represent the 95-percent confidence interval.

<sup>d</sup>Probe area corrections of 126 cm<sup>2</sup> were made for the gas proportional detectors. The following MDC equation was used for 1-minute counts and a background of 1 cpm:

$$MDC = \frac{3 + 4.65\sqrt{C_B}}{KT}$$

<sup>e</sup>Measurements were made with a Ludlum model 43-68 gas proportional detector with a standard 0.4-mg/cm<sup>2</sup> window.

<sup>f</sup>Each sheet of Mylar has a density thickness of 0.22 mg/cm<sup>2</sup>.

<sup>g</sup>Orange fluorescent water-based paint was used.

<sup>h</sup>Data point was not used in regression fit because of limited alpha range.

**Table 5-10 Effects of Paint Density Thickness on Source Efficiency and MDC (Gas Proportional—β Only)**

| Surface Material                                       | Density Thickness (mg/cm <sup>2</sup> ) | C-14 (0.081 ± 0.002) <sup>a</sup> |                                  |   | Tc-99 (0.191 ± 0.016) |                                   |                                | Tl-204 (0.355 ± 0.021) |                                   |                                | SrY-90 (0.465 ± 0.024) |                                   |                                |
|--|---|-----------------------------------|----------------------------------|---|-----------------------|-----------------------------------|--------------------------------|------------------------|-----------------------------------|--------------------------------|------------------------|-----------------------------------|--------------------------------|
|  |   | Source Efficiency                 |                                  | MDC <sup>d</sup> (dpm/100 cm <sup>2</sup> ) | Source Efficiency     |                                   | MDC (dpm/100 cm <sup>2</sup> ) | Source Efficiency      |                                   | MDC (dpm/100 cm <sup>2</sup> ) | Source Efficiency      |                                   | MDC (dpm/100 cm <sup>2</sup> ) |
|  |   | Meas <sup>b</sup>                 | Fit <sup>c</sup>                 |   | Meas                  | Fit                               |                                | Meas                   | Fit                               |                                | Meas                   | Fit                               |                                |
| Detector face <sup>e</sup>                             | 3.8                                     | NA                                | NA                               | 1,823                                       | NA                    | NA                                | 577                            | NA                     | N/A                               | 280                            | NA                     | NA                                | 222                            |
| Detector face <sup>f</sup><br>plus two sheets of Mylar | 4.24                                    | 0.435                             | 0.445 ± 0.055                    | 2,039                                       | 0.628                 | 0.625 ± 0.008                     | 599                            | 0.715                  | 0.707 ± 0.040                     | 283                            | 0.696                  | 0.691 ± 0.021                     | 222                            |
| Plus 1.93 mg/cm <sup>2</sup> paint <sup>g</sup>        | 6.17                                    | 0.269                             | 0.255 ± 0.026                    | 3,296                                       | 0.521                 | 0.522 ± 0.005                     | 722                            | 0.657                  | 0.663 ± 0.030                     | 308                            | 0.669                  | 0.669 ± 0.017                     | 231                            |
| Plus 2.48 mg/cm <sup>2</sup> paint                     | 6.72                                    | 0.228                             | 0.217 ± 0.021                    | 3,882                                       | — <sup>h</sup>        | —                                 | —                              | —                      | —                                 | —                              | —                      | —                                 | —                              |
| Plus 5.54 mg/cm <sup>2</sup> paint                     | 9.78                                    | 0.081                             | 0.090 ± 0.007                    | 10,893                                      | 0.370                 | 0.373 ± 0.003                     | 1,105                          | 0.592                  | 0.588 ± 0.021                     | 342                            | 0.627                  | 0.631 ± 0.012                     | 246                            |
| Plus 9.48 mg/cm <sup>2</sup> paint                     | 13.72                                   | 0.028                             | 0.029 ± 0.003                    | 31,920                                      | 0.259                 | 0.258 ± 0.002                     | 1,450                          | 0.499                  | 0.516 ± 0.023                     | 405                            | 0.583                  | 0.592 ± 0.014                     | 265                            |
| Plus 12.63 mg/cm <sup>2</sup> paint                    | 16.87                                   | 0.012                             | 0.012 ± 0.002                    | 72,542                                      | 0.192                 | 0.192 ± 0.003                     | 1,958                          | 0.475                  | 0.465 ± 0.028                     | 426                            | 0.570                  | 0.562 ± 0.019                     | 271                            |
| Regression equation                                    |   |                                   | $\epsilon_s = 1.51 e^{-0.289 x}$ |   |                       | $\epsilon_s = 0.929 e^{-0.093 x}$ |                                |                        | $\epsilon_s = 0.813 e^{-0.033 x}$ |                                |                        | $\epsilon_s = 0.740 e^{-0.016 x}$ |                                |

<sup>a</sup>Instrument efficiency appears in parentheses; uncertainties represent the 95-percent confidence interval.

<sup>b</sup>Source efficiency was determined by dividing the total efficiency by the instrument efficiency.

<sup>c</sup>The measured source efficiency versus density thickness was fit to an exponential curve; uncertainties represent the 95-percent confidence interval.

<sup>d</sup>Probe area corrections of 126 cm<sup>2</sup> were made for the gas proportional detectors. The following MDC equation was used for 1-minute counts and a background of 354 cpm:

$$MDC = \frac{3 + 4.65\sqrt{CB}}{KT}$$

<sup>e</sup>Measurements were made with a Ludlum model 43-68 gas proportional detector with a standard alpha-blocking 3.8-mg/cm<sup>2</sup> window.

<sup>f</sup>Each sheet of Mylar has a density thickness of 0.22 mg/cm<sup>2</sup>.

<sup>g</sup>Orange fluorescent water-based paint was used.

<sup>h</sup>Measurement was not made.



**Table 5-11 Effects of Paint Density Thickness on Source Efficiency and MDC (GM Detector)**

| Surface Material                                    | Density Thickness (mg/cm <sup>2</sup> ) | C-14 (0.099 ± 0.002) <sup>a</sup>   |                  | Tc-99 (0.193 ± 0.021)                       |                        | Tl-204 (0.278 ± 0.017)            |                                | SrY-90 (0.388 ± 0.020)            |       | MDC (dpm/100 cm <sup>2</sup> ) |
|---|---|-------------------------------------|------------------|---|------------------------|-----------------------------------|--------------------------------|-----------------------------------|-------|--------------------------------|
|   |   | Source Efficiency Meas <sup>b</sup> | Fit <sup>c</sup> | MDC <sup>d</sup> (dpm/100 cm <sup>2</sup> ) | Source Efficiency Meas | Fit                               | MDC (dpm/100 cm <sup>2</sup> ) | Source Efficiency Meas            | Fit   |                                |
| Detector face <sup>e</sup>                          | — <sup>f</sup>                          | NA                                  | NA               | 3,757                                       | NA                     | 1,454                             | NA                             | 888                               | NA    | 648                            |
| Detector face <sup>g</sup> plus two sheets of Mylar | 0.44                                    | 0.436                               | 0.465 ± 0.050    | 4,098                                       | 0.627                  | 1,468                             | 0.716 ± 0.028                  | 894                               | 0.697 | 657                            |
| Plus 1.93 mg/cm <sup>2</sup> paint <sup>h</sup>     | 2.37                                    | 0.284                               | 0.266 ± 0.023    | 6,294                                       | 0.527                  | 1,748                             | 0.670 ± 0.021                  | 952                               | 0.666 | 688                            |
| Plus 2.48 mg/cm <sup>2</sup> paint                  | 2.92                                    | 0.239                               | 0.227 ± 0.019    | 7,485                                       | —                      | —                                 | —                              | —                                 | —     | —                              |
| Plus 5.54 mg/cm <sup>2</sup> paint                  | 5.98                                    | 0.089                               | 0.094 ± 0.007    | 20,012                                      | 0.388                  | 2,373                             | 0.599 ± 0.015                  | 1,068                             | 0.594 | 771                            |
| Plus 9.48 mg/cm <sup>2</sup> paint                  | 9.92                                    | 0.029                               | 0.030 ± 0.003    | 61,664                                      | 0.245                  | 3,767                             | 0.529 ± 0.016                  | 1,238                             | 0.575 | 797                            |
| Plus 12.63 mg/cm <sup>2</sup> paint                 | 13.07                                   | 0.012                               | 0.012 ± 0.002    | 145,037                                     | 0.172                  | 5,362                             | 0.479 ± 0.020                  | 1,312                             | 0.571 | 802                            |
| Regression equation                                 |   | $\epsilon_s = 0.528 e^{-0.289 x}$   |                  | $\epsilon_s = 0.676 e^{-0.103 x}$           |                        | $\epsilon_s = 0.722 e^{-0.031 x}$ |                                | $\epsilon_s = 0.686 e^{-0.016 x}$ |       |                                |

<sup>a</sup>Instrument efficiency appears in parentheses; uncertainties represent the 95-percent confidence interval.

<sup>b</sup>Source efficiency was determined by dividing the total efficiency by the instrument efficiency.

<sup>c</sup>The measured source efficiency versus density thickness was fit to an exponential curve; uncertainties represent the 95-percent confidence interval.

<sup>d</sup>The following MDC equation was used for 1-minute counts, with a background of 49 cpm and a probe area of 20 cm<sup>2</sup>.

$$MDC = \frac{3 + 4.65\sqrt{C_B}}{KT}$$

<sup>e</sup>Measurements were made with an Eberline model HP-260 GM detector with a standard mica window (typical thickness 1.4 to 2.0 mg/cm<sup>2</sup>).

<sup>f</sup>Detector face is a fixed part of the detector and not removable.

<sup>g</sup>Each sheet of Mylar has a density thickness of 0.22 mg/cm<sup>2</sup>.

<sup>h</sup>Orange fluorescent water-based paint was used.

<sup>i</sup>Measurement was not made.

**Table 5-12 Effects of Paint Density Thickness on Source Efficiency and MDC**

| Surface Material                                    | Density Thickness (mg/cm <sup>2</sup> ) | Th-230 (0.259 ± 0.013) <sup>a</sup> |                  |   |
|---|---|-------------------------------------|------------------|---|
|   |   | Source Efficiency                   |                  | MDC <sup>d</sup> (dpm/100 cm <sup>2</sup> ) |
|   |   | Meas <sup>b</sup>                   | Fit <sup>c</sup> |   |
| Detector face <sup>e</sup>                          | — <sup>f</sup>                          | NA                                  | NA               | 65  |
| Detector face <sup>g</sup> plus two sheets of Mylar | 0.44                                    | 0.509                               | 0.523 ± 0.125    | 294   |
| Plus 1.93 mg/cm <sup>2</sup> paint <sup>h</sup>     | 2.37                                    | 0.099                               | 0.091 ± 0.014    | 404   |
| Plus 2.48 mg/cm <sup>2</sup> paint                  | 2.92                                    | 0.053                               | 0.055 ± 0.008    | 756   |
| Plus 5.54 mg/cm <sup>2</sup> paint                  | 5.98                                    | 0.003                               | 0.004 ± 0.001    | 11,619                                      |
| Plus 9.48 mg/cm <sup>2</sup> paint                  | 9.92 <sup>i</sup>                       | 0.001                               | NA               | 67,400                                      |
| Regression equation                                 |   | $\epsilon_s = 0.779 e^{-0.906 x}$   |                  |   |

<sup>a</sup>Instrument efficiency appears in parentheses; uncertainties represent the 95-percent confidence interval.

<sup>b</sup>Source efficiency was determined by dividing the total efficiency by the instrument efficiency.

<sup>c</sup>The measured source efficiency versus density thickness was fit to an exponential curve; uncertainties represent the 95-percent confidence interval.

<sup>d</sup>The following MDC equation was used for 1-minute counts, with a background of 1 cpm and a probe area of 74 cm<sup>2</sup>:

$$MDC = \frac{3 + 4.65\sqrt{C_B}}{KT}$$

<sup>e</sup>Measurements were made with an Eberline model AC3-7 ZnS scintillation detector with a standard 1.5-mg/cm<sup>2</sup> window.

<sup>f</sup>Detector face is a fixed part of the detector and not removable.

<sup>g</sup>Each sheet of Mylar has a density thickness of 0.22 mg/cm<sup>2</sup>.

<sup>h</sup>Orange fluorescent water-based paint was used.

<sup>i</sup>Data point is not used in regression fit because of limited alpha range.

**Table 5-13 Effects of Dust Density Thickness on Source Efficiency and MDC (Gas Proportional— $\alpha + \beta$ )**

| Surface Material                                    | Density Thickness (mg/cm <sup>2</sup> ) | C-14 (0.254 ± 0.006) <sup>a</sup>   |                                    |   | Tc-99 (0.364 ± 0.029)  |                                  |                                | Tl-204 (0.450 ± 0.025) |                                  |                                | SrY-90 (0.537 ± 0.027) |                                  |                                |
|---|---|-------------------------------------|------------------------------------|---|------------------------|----------------------------------|--------------------------------|------------------------|----------------------------------|--------------------------------|------------------------|----------------------------------|--------------------------------|
|   |   | Source Efficiency Meas <sup>b</sup> | Source Efficiency Fit <sup>c</sup> | MDC <sup>d</sup> (dpm/100 cm <sup>2</sup> ) | Source Efficiency Meas | Source Efficiency Fit            | MDC (dpm/100 cm <sup>2</sup> ) | Source Efficiency Meas | Source Efficiency Fit            | MDC (dpm/100 cm <sup>2</sup> ) | Source Efficiency Meas | Source Efficiency Fit            | MDC (dpm/100 cm <sup>2</sup> ) |
| Detector face <sup>e</sup>                          | 0.4                                     | NA                                  | NA                                 | 510   | NA                     | NA                               | 278                            | NA                     | NA                               | 202                            | NA                     | NA                               | 177                            |
| Detector face <sup>f</sup> plus two sheets of Mylar | 0.84                                    | 0.437                               | 0.432 ± 0.148                      | 599   | 0.626                  | 0.592 ± 0.086                    | 292                            | 0.716                  | 0.706 ± 0.037                    | 206                            | 0.697                  | 0.691 ± 0.031                    | 178                            |
| Plus 2.28 mg/cm <sup>2</sup> dust <sup>g</sup>      | 3.12                                    | 0.218                               | 0.265 ± 0.064                      | 1,201                                       | 0.425                  | 0.465 ± 0.045                    | 430                            | 0.620                  | 0.636 ± 0.024                    | 238                            | 0.642                  | 0.649 ± 0.021                    | 193                            |
| Plus 4.11 mg/cm <sup>2</sup> dust                   | 4.95                                    | 0.205                               | 0.179 ± 0.035                      | 1,276                                       | 0.407                  | 0.383 ± 0.032                    | 449                            | 0.595                  | 0.585 ± 0.018                    | 248                            | 0.616                  | 0.617 ± 0.016                    | 201                            |
| Plus 6.10 mg/cm <sup>2</sup> dust                   | 6.94                                    | 0.142                               | 0.116 ± 0.023                      | 1,847                                       | 0.297                  | 0.310 ± 0.026                    | 614                            | 0.536                  | 0.534 ± 0.016                    | 275                            | 0.594                  | 0.583 ± 0.015                    | 208                            |
| Plus 7.99 mg/cm <sup>2</sup> dust                   | 8.83                                    | 0.071                               | 0.078 ± 0.019                      | 3,675                                       | 0.245                  | 0.253 ± 0.027                    | 745                            | 0.474                  | 0.490 ± 0.019                    | 311                            | 0.536                  | 0.553 ± 0.018                    | 231                            |
| Plus 9.99 mg/cm <sup>2</sup> dust                   | 10.83                                   | 0.047                               | 0.050 ± 0.017                      | 5,534                                       | 0.215                  | 0.205 ± 0.029                    | 848                            | 0.456                  | 0.447 ± 0.023                    | 323                            | 0.532                  | 0.523 ± 0.023                    | 233                            |
| Regression equation                                 |   |                                     | $\epsilon_s = 0.518 e^{-0.215x}$   |   |                        | $\epsilon_s = 0.647 e^{-0.106x}$ |                                |                        | $\epsilon_s = 0.733 e^{-0.046x}$ |                                |                        | $\epsilon_s = 0.708 e^{-0.028x}$ |                                |

<sup>a</sup>Instrument efficiency appears in parentheses; uncertainties represent the 95-percent confidence interval.

<sup>b</sup>Source efficiency was determined by dividing the total efficiency by the instrument efficiency.

<sup>c</sup>The measured source efficiency versus density thickness was fit to an exponential curve; uncertainties represent the 95-percent confidence interval.

<sup>d</sup>Probe area corrections of 126 cm<sup>2</sup> were made for the gas proportional detectors. The following MDC equation was used for 1-minute counts and a background of 301 cpm:

$$MDC = \frac{4.65\sqrt{CB}}{KT}$$

<sup>e</sup>Measurements were made with a Ludlum model 43-68 gas proportional detector with a standard 0.4-mg/cm<sup>2</sup> window.

<sup>f</sup>Each sheet of Mylar has a density thickness of 0.22 mg/cm<sup>2</sup>.

<sup>g</sup>Dust was obtained by grinding potting soil and sieving through 250-mesh screen.

**Table 5-14 Effects of Dust Density Thickness on Source Efficiency and MDC (Gas Proportional—α-Only)**

| Surface Material                                    | Density Thickness (mg/cm <sup>2</sup> ) | Th-230 (0.349 ± 0.015) <sup>a</sup> |                  |   |
|---|---|-------------------------------------|------------------|---|
|   |   | Source Efficiency                   |                  | MDC <sup>d</sup> (dpm/100 cm <sup>2</sup> ) |
|   |   | Meas <sup>b</sup>                   | Fit <sup>c</sup> |   |
| Detector face <sup>e</sup>                          | 0.4                                     | NA                                  | NA               | 30  |
| Detector face <sup>f</sup> plus two sheets of Mylar | 0.84                                    | 0.509                               | 0.428 ± 0.215    | 34  |
| Plus 2.28 mg/cm <sup>2</sup> dust <sup>g</sup>      | 3.12                                    | 0.145                               | 0.201 ± 0.071    | 120   |
| Plus 4.11 mg/cm <sup>2</sup> dust                   | 4.95                                    | 0.134                               | 0.110 ± 0.031    | 130   |
| Plus 6.10 mg/cm <sup>2</sup> dust                   | 6.94                                    | 0.056                               | 0.057 ± 0.016    | 310   |
| Plus 7.99 mg/cm <sup>2</sup> dust                   | 8.83                                    | 0.026                               | 0.030 ± 0.011    | 674   |
| Plus 9.99 mg/cm <sup>2</sup> dust                   | 10.83                                   | 0.018                               | 0.016 ± 0.008    | 974   |
| Regression equation                                 |   |                                     |                  | $\epsilon_s = 0.565 e^{-0.331x}$            |

<sup>a</sup>Instrument efficiency appears in parentheses; uncertainties represent the 95-percent confidence interval.

<sup>b</sup>Source efficiency was determined by dividing the total efficiency by the instrumental efficiency.

<sup>c</sup>The measured source efficiency versus density thickness was fit to an exponential curve; uncertainties represent the 95-percent confidence interval.

<sup>d</sup>Probe area corrections of 126 cm<sup>2</sup> were made for the gas proportional detectors. The following MDC equation was used for 1-minute counts and a background of 1 cpm:

$$MDC = \frac{KT}{3 + 4.65\sqrt{CB}}$$

<sup>e</sup>Measurements were made with a Ludlum model 43-68 gas proportional detector with a standard 0.4-mg/cm<sup>2</sup> window.

<sup>f</sup>Each sheet of Mylar has a density thickness of 0.22 mg/cm<sup>2</sup>.

<sup>g</sup>Dust was obtained by grinding potting soil and sieving through 250-mesh screen.

**Table 5-15 Effects of Dust Density Thickness on Source Efficiency and MDC (Gas Proportional—β-Only)**

| Surface Material                                    | Density Thickness (mg/cm <sup>2</sup> ) | C-14 (0.081 ± 0.002) <sup>a</sup> |   |                   | Tc-99 (0.191 ± 0.016)            |                   |                                | Tl-204 (0.355 ± 0.021)           |                                |                   | SrY-90 (0.465 ± 0.024)           |  |  |
|---|---|-----------------------------------|---|-------------------|----------------------------------|-------------------|--------------------------------|----------------------------------|--------------------------------|-------------------|----------------------------------|--|--|
|   |   | Source Efficiency                 | MDC <sup>d</sup> (dpm/100 cm <sup>2</sup> ) | Source Efficiency | MDC (dpm/100 cm <sup>2</sup> )   | Source Efficiency | MDC (dpm/100 cm <sup>2</sup> ) | Source Efficiency                | MDC (dpm/100 cm <sup>2</sup> ) | Source Efficiency | MDC (dpm/100 cm <sup>2</sup> )   |  |  |
|   |   | Meas <sup>b</sup>                 | Fit <sup>c</sup>                            | Meas              | Fit                              | Meas              | Fit                            | Meas                             | Fit                            | Meas              | Fit                              |  |  |
| Detector face <sup>e</sup>                          | 3.8                                     | NA                                | NA  | 1,823             | NA                               | NA                | NA                             | NA                               | NA                             | NA                | NA                               |  |  |
| Detector face <sup>f</sup> plus two sheets of Mylar | 4.24                                    | 0.435                             | 0.448 ± 0.136                               | 2,039             | 0.628                            | 0.632 ± 0.061     | 599                            | 0.715                            | 0.715 ± 0.031                  | 0.696             | 0.696 ± 0.028                    |  |  |
| Plus 2.28 mg/cm <sup>2</sup> dust <sup>g</sup>      | 6.52                                    | 0.242                             | 0.278 ± 0.060                               | 3,659             | 0.501                            | 0.519 ± 0.036     | 751                            | 0.648                            | 0.660 ± 0.020                  | 0.649             | 0.665 ± 0.019                    |  |  |
| Plus 4.11 mg/cm <sup>2</sup> dust                   | 8.35                                    | 0.218                             | 0.189 ± 0.033                               | 4,074             | 0.479                            | 0.443 ± 0.025     | 785                            | 0.626                            | 0.619 ± 0.015                  | 0.655             | 0.641 ± 0.015                    |  |  |
| Plus 6.10 mg/cm <sup>2</sup> dust                   | 10.34                                   | 0.149                             | 0.124 ± 0.022                               | 5,957             | 0.371                            | 0.373 ± 0.021     | 1,013                          | 0.594                            | 0.577 ± 0.014                  | 0.627             | 0.617 ± 0.014                    |  |  |
| Plus 7.99 mg/cm <sup>2</sup> dust                   | 12.23                                   | 0.076                             | 0.083 ± 0.018                               | 11,680            | 0.305                            | 0.317 ± 0.022     | 1,233                          | 0.529                            | 0.540 ± 0.017                  | 0.593             | 0.594 ± 0.017                    |  |  |
| Plus 9.99 mg/cm <sup>2</sup> dust                   | 14.23                                   | 0.051                             | 0.055 ± 0.016                               | 17,243            | 0.270                            | 0.267 ± 0.025     | 1,395                          | 0.502                            | 0.504 ± 0.021                  | 0.564             | 0.571 ± 0.022                    |  |  |
| Regression equation                                 |   | $\epsilon_s = 1.10 e^{-0.211x}$   |   |                   | $\epsilon_s = 0.912 e^{-0.086x}$ |                   |                                | $\epsilon_s = 0.830 e^{-0.035x}$ |                                |                   | $\epsilon_s = 0.757 e^{-0.020x}$ |  |  |

<sup>a</sup>Instrument efficiency appears in parentheses; uncertainties represent the 95-percent confidence interval.

<sup>b</sup>Source efficiency was determined by dividing the total efficiency by the instrumental efficiency.

<sup>c</sup>The measured source efficiency versus density thickness was fit to an exponential curve; uncertainties represent the 95-percent confidence interval.

<sup>d</sup>Probe area corrections of 126 cm<sup>2</sup> were made for the gas proportional detectors. The following MDC equation was used for 1-minute counts and a background of 354 cpm:

$$MDC = \frac{3 + 4.65\sqrt{CB}}{KT}$$

<sup>e</sup>Measurements were made with a Ludlum model 43-68 gas proportional with a standard alpha-blocking 3.8-mg/cm<sup>2</sup> window.

<sup>f</sup>Each sheet of Mylar has a density thickness of 0.22 mg/cm<sup>2</sup>.

<sup>g</sup>Dust was obtained by grinding potting soil and sieving through 250-mesh screen.

**Table 5-16 Effects of Dust Density Thickness on Source Efficiency and MDC (GM Detector)**

| Surface Material                                    | Density Thickness (mg/cm <sup>2</sup> ) | C-14 (0.099 ± 0.002) <sup>a</sup> |   |                   | Tc-99 (0.193 ± 0.021)            |                   |                                | TI-204 (0.278 ± 0.017)           |                                |                   | SrY-90 (0.388 ± 0.020)           |     |  |
|---|---|-----------------------------------|---|-------------------|----------------------------------|-------------------|--------------------------------|----------------------------------|--------------------------------|-------------------|----------------------------------|-----|--|
|   |   | Measured Source Efficiency        | MDC <sup>d</sup> (dpm/100 cm <sup>2</sup> ) | Source Efficiency | MDC (dpm/100 cm <sup>2</sup> )   | Source Efficiency | MDC (dpm/100 cm <sup>2</sup> ) | Source Efficiency                | MDC (dpm/100 cm <sup>2</sup> ) | Source Efficiency | MDC (dpm/100 cm <sup>2</sup> )   |     |  |
|   |   | Meas <sup>b</sup>                 | Fit <sup>c</sup>                            | Meas              | Fit                              | Meas              | Fit                            | Meas                             | Fit                            | Meas              | Fit                              |     |  |
| Detector face <sup>e</sup>                          | -f                                      | NA                                | NA  | NA                | NA                               | 1,454             | NA                             | NA                               | NA                             | NA                | NA                               | 648 |  |
| Detector face <sup>g</sup> plus two sheets of Mylar | 0.44                                    | 0.436                             | 0.474 ± 0.176                               | 0.627             | 0.642 ± 0.087                    | 1,469             | 0.716                          | 0.715 ± 0.015                    | 894                            | 0.697             | 0.706 ± 0.031                    | 657 |  |
| Plus 2.28 mg/cm <sup>2</sup> dust <sup>h</sup>      | 2.72                                    | 0.257                             | 0.291 ± 0.077                               | 0.490             | 0.520 ± 0.050                    | 1,877             | 0.658                          | 0.661 ± 0.010                    | 973                            | 0.668             | 0.670 ± 0.021                    | 686 |  |
| Plus 4.11 mg/cm <sup>2</sup> dust                   | 4.55                                    | 0.234                             | 0.196 ± 0.041                               | 0.473             | 0.439 ± 0.034                    | 1,949             | 0.617                          | 0.621 ± 0.007                    | 1,036                          | 0.645             | 0.642 ± 0.016                    | 710 |  |
| Plus 6.10 mg/cm <sup>2</sup> dust                   | 6.54                                    | 0.160                             | 0.128 ± 0.027                               | 0.392             | 0.365 ± 0.028                    | 2,345             | 0.590                          | 0.580 ± 0.007                    | 1,084                          | 0.632             | 0.613 ± 0.015                    | 725 |  |
| Plus 7.99 mg/cm <sup>2</sup> dust                   | 8.43                                    | 0.080                             | 0.085 ± 0.023                               | 0.300             | 0.306 ± 0.030                    | 3,067             | 0.543                          | 0.543 ± 0.008                    | 1,178                          | 0.591             | 0.587 ± 0.019                    | 776 |  |
| Plus 9.99 mg/cm <sup>2</sup> dust                   | 10.43                                   | 0.049                             | 0.056 ± 0.020                               | 0.243             | 0.255 ± 0.034                    | 3,789             | 0.504                          | 0.507 ± 0.010                    | 1,270                          | 0.547             | 0.560 ± 0.024                    | 838 |  |
| Regression equation                                 |   | $\epsilon_s = 0.521 e^{-0.215x}$  |   |                   | $\epsilon_a = 0.669 e^{-0.093x}$ |                   |                                | $\epsilon_s = 0.726 e^{-0.084x}$ |                                |                   | $\epsilon_s = 0.713 e^{-0.023x}$ |     |  |

<sup>a</sup>Instrument efficiency appears in parentheses; uncertainties represent the 95-percent confidence interval.

<sup>b</sup>Source efficiency was determined by dividing the total efficiency by the instrument efficiency.

<sup>c</sup>The measured source efficiency versus density thickness was fit to an exponential curve; uncertainties represent the 95-percent confidence interval.

<sup>d</sup>The following equation was used for 1-minute counts, with a background of 49 cpm and a probe area of 20 cm<sup>2</sup>:

$$MDC = \frac{3 + 4.65\sqrt{CB}}{KT}$$

<sup>e</sup>Measurements were made with an Eberline model HP-260 GM detector with a standard mica window having a typical thickness of 1.4 to 2.0 mg/cm<sup>2</sup>.

<sup>f</sup>Detector face is a fixed part of the detector and not removable.

<sup>g</sup>Each sheet of Mylar has a density thickness of 0.22 mg/cm<sup>2</sup>.

<sup>h</sup>Dust was obtained by grinding potting soil and sieving through 250-mesh screen.

**Table 5-17 Effects of Dust Density Thickness on Source Efficiency and MDC (ZnS Scintillation Detector)**

| Surface Material                                    | Density Thickness (mg/cm <sup>2</sup> ) | Th-230 (0.259 ± 0.013) <sup>a</sup> |                  |   |
|---|---|-------------------------------------|------------------|---|
|   |   | Source Efficiency                   |                  | MDC <sup>d</sup> (dpm/100 cm <sup>2</sup> ) |
|   |   | Meas <sup>b</sup>                   | Fit <sup>c</sup> |   |
| Detector face <sup>e</sup>                          | — <sup>f</sup>                          | NA                                  | NA               | 65  |
| Detector face <sup>g</sup> plus two sheets of Mylar | 0.44                                    | 0.509                               | 0.410 ± 0.327    | 78  |
| Plus 2.28 mg/cm <sup>2</sup> dust <sup>h</sup>      | 2.72                                    | 0.118                               | 0.179 ± 0.092    | 340   |
| Plus 4.11 mg/cm <sup>2</sup> dust                   | 4.55                                    | 0.109                               | 0.092 ± 0.039    | 367   |
| Plus 6.10 mg/cm <sup>2</sup> dust                   | 6.54                                    | 0.045                               | 0.045 ± 0.024    | 885   |
| Plus 7.99 mg/cm <sup>2</sup> dust                   | 8.43                                    | 0.023                               | 0.022 ± 0.017    | 1,735                                       |
| Plus 9.99 mg/cm <sup>2</sup> dust                   | 10.43                                   | 0.017 <sup>i</sup>                  | NA               | 2,390                                       |
| Regression equation                                 |   | $\epsilon_s = 0.481 e^{-0.364 x}$   |                  |   |

<sup>a</sup>Instrument efficiency appears in parentheses; uncertainties represent the 95-percent confidence interval.

<sup>b</sup>Source efficiency was determined by dividing the total efficiency by the instrument efficiency.

<sup>c</sup>The measured source efficiency versus density thickness was fit to an exponential curve; uncertainties represent the 95-percent confidence interval.

<sup>d</sup>The following MDC equation was used for 1-minute counts, with a background of 1 cpm and a probe area of 74 cm<sup>2</sup>:

$$MDC = \frac{3 + 4.65\sqrt{C_B}}{KT}$$

<sup>e</sup>Measurements were made with an Eberline model AC3-7 ZnS scintillation detector with a standard 1.5-mg/cm<sup>2</sup> window.

<sup>f</sup>Detector face is a fixed part of detector and not removable.

<sup>g</sup>Each sheet of Mylar has a density thickness of 0.22 mg/cm<sup>2</sup>.

<sup>h</sup>Dust was obtained by grinding potting soil and sieving through 250-mesh screen.

<sup>i</sup>Data point is not used in regression fit because of limited alpha range.

**Table 5-18 Effects of Water Density Thickness on Source Efficiency and MDC  
(Gas Proportional— $\alpha+\beta/C-14$ )**

| Surface Material  | Density Thickness (mg/cm <sup>2</sup> ) | C-14 (0.139 ± 0.003) <sup>a</sup> |                  |   |
|---|---|-----------------------------------|------------------|---|
|   |   | Source Efficiency                 |                  | MDC <sup>d</sup> (dpm/100 cm <sup>2</sup> ) |
|   |   | Meas <sup>b</sup>                 | Fit <sup>c</sup> |   |
| Detector face <sup>e</sup>  | 0.4                                     | NA                                | NA               | 629   |
| Detector face plus two Mylar sheets with one Kimwipe <sup>f</sup> | 2.70                                    | 0.436                             | 0.442 ± 0.042    | 1,249                                       |
| Plus 0.44 mg/cm <sup>2</sup> water <sup>g</sup>                   | 3.14                                    | 0.362                             | 0.397 ± 0.035    | 1,502                                       |
| Plus 0.62 mg/cm <sup>2</sup> water                                | 3.32                                    | 0.360                             | 0.380 ± 0.032    | 1,513                                       |
| Plus 0.78 mg/cm <sup>2</sup> water                                | 3.48                                    | 0.349                             | 0.365 ± 0.030    | 1,558                                       |
| Plus 1.23 mg/cm <sup>2</sup> water                                | 3.93                                    | 0.333                             | 0.327 ± 0.025    | 1,637                                       |
| Plus 2.29 mg/cm <sup>2</sup> water                                | 4.99                                    | 0.284                             | 0.252 ± 0.017    | 1,920                                       |
| Plus 3.04 mg/cm <sup>2</sup> water                                | 5.74                                    | 0.237                             | 0.210 ± 0.014    | 2,297                                       |
| Plus 5.14 mg/cm <sup>2</sup> water                                | 7.84                                    | 0.138                             | 0.125 ± 0.011    | 3,940                                       |
| Plus 6.49 mg/cm <sup>2</sup> water                                | 9.19                                    | 0.083                             | 0.090 ± 0.010    | 6,533                                       |
| Plus 7.62 mg/cm <sup>2</sup> water                                | 10.32                                   | 0.063                             | 0.068 ± 0.009    | 8,599                                       |
| Regression equation   |   | $\epsilon_s = 0.858 e^{-0.245 x}$ |                  |   |

<sup>a</sup>Instrument efficiency appears in parentheses; uncertainties represent the 95-percent confidence interval.

<sup>b</sup>Source efficiency was determined by dividing the total efficiency by the instrument efficiency.

<sup>c</sup>The measured source efficiency versus density thickness was fit to an exponential curve; uncertainties represent the 95-percent confidence interval.

<sup>d</sup>Probe area corrections of 126 cm<sup>2</sup> were made for the gas proportional detectors. The following MDC equation was used for 1-minute counts and a background of 396 cpm:

$$MDC = \frac{3 + 4.65\sqrt{C_B}}{KT}$$

<sup>e</sup>Measurements were made with a Ludlum model 43-68 gas proportional detector with a standard 0.4-mg/cm<sup>2</sup> window.

<sup>f</sup>Each sheet of Mylar has a density thickness of 0.22 mg/cm<sup>2</sup>, and one Kimwipe has a density thickness of 1.86 mg/cm<sup>2</sup>.

<sup>g</sup>Reagent water from the radiochemistry laboratory was used in analytical procedures.



**Table 5-19 Effects of Water Density Thickness on Source Efficiency and MDC  
(Gas Proportional— $\alpha+\beta$ /Tc-99)**

| Surface Material  | Density Thickness (mg/cm <sup>2</sup> ) | Tc-99 (0.239 ± 0.020) <sup>a</sup> |                  |  |
|---|---|------------------------------------|------------------|--|
|   |   | Source Efficiency                  |                  | MDC <sup>d</sup><br>(dpm/100 cm <sup>2</sup> ) |
|   |   | Meas <sup>b</sup>                  | Fit <sup>c</sup> |  |
| Detector face <sup>e</sup>  | 0.4                                     | NA                                 | NA               | 368  |
| Detector face plus two Mylar sheets with one Kimwipe <sup>f</sup> | 2.70                                    | 0.626                              | 0.642 ± 0.020    | 506  |
| Plus 0.19 mg/cm <sup>2</sup> water <sup>g</sup>                   | 2.89                                    | 0.628                              | 0.630 ± 0.019    | 505  |
| Plus 0.76 mg/cm <sup>2</sup> water                                | 3.46                                    | 0.595                              | 0.596 ± 0.016    | 533  |
| Plus 2.85 mg/cm <sup>2</sup> water                                | 5.55                                    | 0.501                              | 0.487 ± 0.010    | 633  |
| Plus 3.97 mg/cm <sup>2</sup> water                                | 6.67                                    | 0.443                              | 0.436 ± 0.009    | 716  |
| Plus 5.49 mg/cm <sup>2</sup> water                                | 8.19                                    | 0.386                              | 0.377 ± 0.009    | 822  |
| Plus 6.67 mg/cm <sup>2</sup> water                                | 9.37                                    | 0.327                              | 0.336 ± 0.010    | 969  |
| Plus 8.17 mg/cm <sup>2</sup> water                                | 10.87                                   | 0.287                              | 0.290 ± 0.011    | 1,104  |
| Regression equation   |   | $\epsilon_s = 0.834 e^{-0.097 x}$  |                  |  |

<sup>a</sup>Instrument efficiency appears in parentheses; uncertainties represent the 95-percent confidence interval.

<sup>b</sup>Source efficiency was determined by dividing the total efficiency by the instrument efficiency.

<sup>c</sup>The measured source efficiency versus density thickness was fit to an exponential curve; uncertainties represent the 95-percent confidence interval.

<sup>d</sup>Probe area corrections of 126 cm<sup>2</sup> were made for the gas proportional detectors. The following MDC equation was used for 1-minute counts and a background of 396 cpm:

$$MDC = \frac{3 + 4.65\sqrt{C_B}}{KT}$$

<sup>e</sup>Measurements were made with a Ludlum model 43-68 gas proportional detector with a standard 0.4-mg/cm<sup>2</sup> window.

<sup>f</sup>Each sheet of Mylar has a density thickness of 0.22 mg/cm<sup>2</sup>, and one Kimwipe has a density thickness of 1.86 mg/cm<sup>2</sup>.

<sup>g</sup>Reagent water from the radiochemistry laboratory was used in analytical procedures.

**Table 5-20 Effects of Water Density Thickness on Source Efficiency and MDC  
(Gas Proportional— $\alpha+\beta$ /SrY-90)**

| Surface Material  | Density Thickness (mg/cm <sup>2</sup> ) | SrY-90 (0.484 ± 0.025) <sup>a</sup> |                  |  |
|---|---|-------------------------------------|------------------|--|
|   |   | Source Efficiency                   |                  | MDC <sup>d</sup><br>(dpm/100 cm <sup>2</sup> ) |
|   |   | Meas <sup>b</sup>                   | Fit <sup>c</sup> |  |
| Detector face <sup>e</sup>  | 0.4                                     | NA                                  | NA               | 207  |
| Detector face plus two Mylar sheets with one Kimwipe <sup>f</sup> | 2.70                                    | 0.697                               | 0.705 ± 0.018    | 225  |
| Plus 2.56 mg/cm <sup>2</sup> water <sup>g</sup>                   | 5.26                                    | 0.666                               | 0.664 ± 0.010    | 235  |
| Plus 3.25 mg/cm <sup>2</sup> water                                | 5.95                                    | 0.666                               | 0.653 ± 0.009    | 235  |
| Plus 4.81 mg/cm <sup>2</sup> water                                | 7.51                                    | 0.627                               | 0.630 ± 0.009    | 250  |
| Plus 6.28 mg/cm <sup>2</sup> water                                | 8.98                                    | 0.608                               | 0.608 ± 0.011    | 258  |
| Plus 7.88 mg/cm <sup>2</sup> water                                | 10.58                                   | 0.582                               | 0.586 ± 0.014    | 269  |
| Regression equation   |   | $\epsilon_s = 0.751 e^{-0.023 x}$   |                  |  |

<sup>a</sup>Instrument efficiency appears in parentheses; uncertainties represent the 95-percent confidence interval.

<sup>b</sup>Source efficiency was determined by dividing the total efficiency by the instrument efficiency.

<sup>c</sup>The measured source efficiency versus density thickness was fit to an exponential curve; uncertainties represent the 95-percent confidence interval.

<sup>d</sup>Probe area corrections of 126 cm<sup>2</sup> were made for the gas proportional detectors. The following MDC equation was used for 1-minute counts and a background of 396 cpm:

$$MDC = \frac{3 + 4.65\sqrt{C_B}}{KT}$$

<sup>e</sup>Measurements were made with a Ludlum model 43-68 gas proportional detector with a standard 0.4-mg/cm<sup>2</sup> window.

<sup>f</sup>Each sheet of Mylar has a density thickness of 0.22 mg/cm<sup>2</sup>, and one Kimwipe has a density thickness of 1.86 mg/cm<sup>2</sup>.

<sup>g</sup>Reagent water from the radiochemistry laboratory was used in analytical procedures.

**Table 5-21 Effects of Water Density Thickness on Source Efficiency and MDC (Gas Proportional— $\alpha$  Only)**

| Surface Material  | Density Thickness (mg/cm <sup>2</sup> ) | Th-230 (0.085 ± 0.005) <sup>a</sup> |                  |   |
|---|---|-------------------------------------|------------------|---|
|   |   | Source Efficiency                   |                  | MDC <sup>d</sup> (dpm/100 cm <sup>2</sup> ) |
|   |   | Meas <sup>b</sup>                   | Fit <sup>c</sup> |   |
| Detector face <sup>e</sup>  | 0.4                                     | NA                                  | NA               | 30  |
| Detector face plus two Mylar sheets with one Kimwipe <sup>f</sup> | 2.70                                    | 0.508                               | 0.516 ± 0.071    | 140   |
| Plus 0.11 mg/cm <sup>2</sup> water <sup>g</sup>                   | 2.81                                    | 0.469                               | 0.485 ± 0.065    | 151   |
| Plus 0.25 mg/cm <sup>2</sup> water                                | 2.95                                    | 0.441                               | 0.448 ± 0.058    | 161   |
| Plus 0.48 mg/cm <sup>2</sup> water                                | 3.18                                    | 0.372                               | 0.393 ± 0.048    | 191   |
| Plus 1.23 mg/cm <sup>2</sup> water                                | 3.93                                    | 0.274                               | 0.257 ± 0.027    | 259   |
| Plus 2.03 mg/cm <sup>2</sup> water                                | 4.73                                    | 0.168                               | 0.163 ± 0.016    | 423   |
| Plus 3.51 mg/cm <sup>2</sup> water                                | 6.21                                    | 0.090                               | 0.071 ± 0.009    | 787   |
| Plus 4.23 mg/cm <sup>2</sup> water                                | 6.93                                    | 0.039                               | 0.047 ± 0.007    | 1,827                                       |
| Plus 5.88 mg/cm <sup>2</sup> water                                | 8.58                                    | 0.018                               | 0.018 ± 0.004    | 3,983                                       |
| Regression equation   |   | $\epsilon_s = 2.39 e^{-0.567 x}$    |                  |   |

<sup>a</sup>Instrument efficiency appears in parentheses; uncertainties represent the 95-percent confidence interval.

<sup>b</sup>Source efficiency was determined by dividing the total efficiency by the instrument efficiency.

<sup>c</sup>The measured source efficiency versus density thickness was fit to an exponential curve; uncertainties represent the 95-percent confidence interval.

<sup>d</sup>Probe area corrections of 126 cm<sup>2</sup> were made for the gas proportional detectors. The following MDC equation was used for 1-minute counts and a background of 1 cpm:

$$MDC = \frac{3 + 4.65\sqrt{C_B}}{KT}$$

<sup>e</sup>Measurements were made with a Ludlum model 43-68 gas proportional detector with a standard 0.4-mg/cm<sup>2</sup> window.

<sup>f</sup>Each sheet of Mylar has a density thickness of 0.22 mg/cm<sup>2</sup>, and one Kimwipe has a density thickness of 1.86 mg/cm<sup>2</sup>.

<sup>g</sup>Reagent water from the radiochemistry laboratory was used in analytical procedures.

**Table 5-22 Effects of Water Density Thickness on Source Efficiency and MDC (Gas Proportional— $\beta$  Only/C-14)**

| Surface Material  | Density Thickness (mg/cm <sup>2</sup> ) | C-14 (0.046 ± 0.001) <sup>a</sup> |                  |   |
|---|---|-----------------------------------|------------------|---|
|   |   | Source Efficiency                 |                  | MDC <sup>d</sup> (dpm/100 cm <sup>2</sup> ) |
|   |   | Meas <sup>b</sup>                 | Fit <sup>c</sup> |   |
| Detector face <sup>e</sup>  | 3.8                                     | NA                                | NA               | 1,869                                       |
| Detector face plus two Mylar sheets with one Kimwipe <sup>f</sup> | 6.10                                    | 0.436                             | 0.445 ± 0.041    | 3,544                                       |
| Plus 0.44 mg/cm <sup>2</sup> water <sup>g</sup>                   | 6.54                                    | 0.367                             | 0.399 ± 0.034    | 4,209                                       |
| Plus 0.62 mg/cm <sup>2</sup> water                                | 6.72                                    | 0.358                             | 0.382 ± 0.031    | 4,317                                       |
| Plus 0.78 mg/cm <sup>2</sup> water                                | 6.88                                    | 0.354                             | 0.367 ± 0.029    | 4,363                                       |
| Plus 1.23 mg/cm <sup>2</sup> water                                | 7.33                                    | 0.338                             | 0.329 ± 0.024    | 4,576                                       |
| Plus 2.29 mg/cm <sup>2</sup> water                                | 8.39                                    | 0.282                             | 0.253 ± 0.016    | 5,480                                       |
| Plus 3.04 mg/cm <sup>2</sup> water                                | 9.14                                    | 0.239                             | 0.210 ± 0.013    | 6,457                                       |
| Plus 5.14 mg/cm <sup>2</sup> water                                | 11.24                                   | 0.136                             | 0.125 ± 0.011    | 11,359                                      |
| Plus 6.49 mg/cm <sup>2</sup> water                                | 12.59                                   | 0.084                             | 0.090 ± 0.010    | 18,320                                      |
| Plus 7.62 mg/cm <sup>2</sup> water                                | 13.72                                   | 0.063                             | 0.068 ± 0.009    | 24,606                                      |
| Regression equation   |   | $\epsilon_s = 2.01 e^{-0.247 x}$  |                  |   |

<sup>a</sup>Instrument efficiency appears in parentheses; uncertainties represent the 95-percent confidence interval.

<sup>b</sup>Source efficiency was determined by dividing the total efficiency by the instrument efficiency.

<sup>c</sup>The measured source efficiency versus density thickness was fit to an exponential curve; uncertainties represent the 95-percent confidence interval.

<sup>d</sup>Probe area corrections of 126 cm<sup>2</sup> were made for the gas proportional detectors. The following MDC equation was used for 1-minute counts and a background of 354 cpm:

$$MDC = \frac{3 + 4.65\sqrt{C_B}}{KT}$$

<sup>e</sup>Measurements were made with a Ludlum model 43-68 gas proportional detector with a standard alpha-blocking 3.8-mg/cm<sup>2</sup> window.

<sup>f</sup>Each sheet of Mylar has a density thickness of 0.22 mg/cm<sup>2</sup>, and one Kimwipe has a density thickness of 1.86 mg/cm<sup>2</sup>.

<sup>g</sup>Reagent water from the radiochemistry laboratory was used in analytical procedures.

**Table 5-23 Effects of Water Density Thickness on Source Efficiency and MDC (Gas Proportional—β Only/Tc-99)**

| Surface Material  | Density Thickness (mg/cm <sup>2</sup> ) | Tc-99 (0.148 ± 0.013) <sup>a</sup> |                  |   |
|---|---|------------------------------------|------------------|---|
|   |   | Source Efficiency                  |                  | MDC <sup>d</sup> (dpm/100 cm <sup>2</sup> ) |
|   |   | Meas <sup>b</sup>                  | Fit <sup>c</sup> |   |
| Detector face <sup>e</sup>  | 3.8                                     | NA                                 | NA               | 620   |
| Detector face plus two Mylar sheets with one Kimwipe <sup>f</sup> | 6.10                                    | 0.626                              | 0.643 ± 0.026    | 773   |
| Plus 0.19 mg/cm <sup>2</sup> water <sup>g</sup>                   | 6.29                                    | 0.630                              | 0.632 ± 0.025    | 769   |
| Plus 0.74 mg/cm <sup>2</sup> water                                | 6.84                                    | 0.590                              | 0.602 ± 0.022    | 821   |
| Plus 2.85 mg/cm <sup>2</sup> water                                | 8.95                                    | 0.518                              | 0.500 ± 0.013    | 934   |
| Plus 3.97 mg/cm <sup>2</sup> water                                | 10.07                                   | 0.469                              | 0.452 ± 0.012    | 1,033                                       |
| Plus 5.49 mg/cm <sup>2</sup> water                                | 11.59                                   | 0.402                              | 0.396 ± 0.012    | 1,206                                       |
| Plus 6.67 mg/cm <sup>2</sup> water                                | 12.77                                   | 0.357                              | 0.356 ± 0.014    | 1,356                                       |
| Plus 8.17 mg/cm <sup>2</sup> water                                | 14.27                                   | 0.300                              | 0.312 ± 0.015    | 1,614                                       |
| Regression equation   |   | $\epsilon_s = 1.10 e^{-0.088 x}$   |                  |   |

<sup>a</sup>Instrument efficiency appears in parentheses; uncertainties represent the 95-percent confidence interval.

<sup>b</sup>Source efficiency was determined by dividing the total efficiency by the instrument efficiency.

<sup>c</sup>The measured source efficiency versus density thickness was fit to an exponential curve; uncertainties represent the 95-percent confidence interval.

<sup>d</sup>Probe area corrections of 126 cm<sup>2</sup> were made for the gas proportional detectors. The following MDC equation was used for 1-minute counts and a background of 354 cpm:

$$MDC = \frac{3 + 4.65\sqrt{C_B}}{KT}$$

<sup>e</sup>Measurements were made with a Ludlum model 43-68 gas proportional detector with a standard alpha-blocking 3.8-mg/cm<sup>2</sup> window.

<sup>f</sup>Each sheet of Mylar has a density thickness of 0.22 mg/cm<sup>2</sup>, and one Kimwipe has a density thickness of 1.86 mg/cm<sup>2</sup>.

<sup>g</sup>Reagent water from the radiochemistry laboratory was used in analytical procedures.

**Table 5-24 Effects of Water Density Thickness on Source Efficiency and MDC (Gas Proportional—β Only/SrY-90)**

| Surface Material  | Density Thickness (mg/cm <sup>2</sup> ) | SrY-90 (0.429 ± 0.023) <sup>a</sup> |                  |   |
|---|---|-------------------------------------|------------------|---|
|   |   | Source Efficiency                   |                  | MDC <sup>d</sup> (dpm/100 cm <sup>2</sup> ) |
|   |   | Meas <sup>b</sup>                   | Fit <sup>c</sup> |   |
| Detector face <sup>e</sup>  | 3.8                                     | NA                                  | NA               | 222   |
| Detector face plus two Mylar sheets with one Kimwipe <sup>f</sup> | 6.10                                    | 0.697                               | 0.700 ± 0.021    | 241   |
| Plus 2.56 mg/cm <sup>2</sup> water <sup>g</sup>                   | 8.66                                    | 0.665                               | 0.666 ± 0.013    | 252   |
| Plus 3.25 mg/cm <sup>2</sup> water                                | 9.35                                    | 0.661                               | 0.657 ± 0.011    | 253   |
| Plus 4.81 mg/cm <sup>2</sup> water                                | 10.91                                   | 0.635                               | 0.637 ± 0.011    | 264   |
| Plus 6.28 mg/cm <sup>2</sup> water                                | 12.38                                   | 0.632                               | 0.619 ± 0.013    | 265   |
| Plus 7.88 mg/cm <sup>2</sup> water                                | 13.98                                   | 0.590                               | 0.600 ± 0.017    | 284   |
| Regression equation   |   | $\epsilon_s = 0.790 e^{-0.020 x}$   |                  |   |

<sup>a</sup>Instrument efficiency appears in parentheses; uncertainties represent the 95-percent confidence interval.

<sup>b</sup>Source efficiency was determined by dividing the total efficiency by the instrument efficiency.

<sup>c</sup>The measured source efficiency versus density thickness was fit to an exponential curve; uncertainties represent the 95-percent confidence interval.

<sup>d</sup>Probe area corrections of 126 cm<sup>2</sup> were made for the gas proportional detectors. The following MDC equation was used for 1-minute counts and a background of 354 cpm:

$$MDC = \frac{3 + 4.65\sqrt{C_B}}{KT}$$

<sup>e</sup>Measurements were made with a Ludlum model 43-68 gas proportional detector with a standard alpha-blocking 3.8-mg/cm<sup>2</sup> window.

<sup>f</sup>Each sheet of Mylar has a density thickness of 0.22 mg/cm<sup>2</sup>, and one Kimwipe has a density thickness of 1.86 mg/cm<sup>2</sup>.

<sup>g</sup>Reagent water from the radiochemistry laboratory was used in analytical procedures.

**Table 5-25 Effects of Water Density Thickness on Source Efficiency and MDC (GM Detector/C-14)**

| Surface Material  | Density Thickness (mg/cm <sup>2</sup> ) | C-14 (0.056 ± 0.001) <sup>a</sup> |                  |   |
|---|---|-----------------------------------|------------------|---|
|   |   | Source Efficiency                 |                  | MDC <sup>d</sup> (dpm/100 cm <sup>2</sup> ) |
|   |   | Meas <sup>b</sup>                 | Fit <sup>c</sup> |   |
| Detector face <sup>e</sup>  | — <sup>f</sup>                          | NA                                | NA               | 3,758                                       |
| Detector face plus two Mylar sheets with one Kimwipe <sup>g</sup> | 2.30                                    | 0.436                             | 0.494 ± 0.053    | 7,294                                       |
| Plus 0.44 mg/cm <sup>2</sup> water <sup>h</sup>                   | 2.74                                    | 0.422                             | 0.445 ± 0.044    | 7,526                                       |
| Plus 0.62 mg/cm <sup>2</sup> water                                | 2.92                                    | 0.412                             | 0.427 ± 0.041    | 7,716                                       |
| Plus 0.78 mg/cm <sup>2</sup> water                                | 3.08                                    | 0.405                             | 0.411 ± 0.038    | 7,847                                       |
| Plus 1.23 mg/cm <sup>2</sup> water                                | 3.53                                    | 0.382                             | 0.369 ± 0.032    | 8,320                                       |
| Plus 2.29 mg/cm <sup>2</sup> water                                | 4.59                                    | 0.320                             | 0.287 ± 0.021    | 9,925                                       |
| Plus 3.04 mg/cm <sup>2</sup> water                                | 5.34                                    | 0.277                             | 0.241 ± 0.018    | 11,481                                      |
| Plus 5.14 mg/cm <sup>2</sup> water                                | 7.44                                    | 0.162                             | 0.146 ± 0.015    | 19,622                                      |
| Plus 6.49 mg/cm <sup>2</sup> water                                | 8.79                                    | 0.104                             | 0.106 ± 0.014    | 30,496                                      |
| Plus 7.62 mg/cm <sup>2</sup> water                                | 9.92                                    | 0.071                             | 0.082 ± 0.013    | 44,680                                      |
| Regression equation   |   | $\epsilon_s = 0.851 e^{-0.236 x}$ |                  |   |

<sup>a</sup>Instrument efficiency appears in parentheses; uncertainties represent the 95-percent confidence interval.

<sup>b</sup>Source efficiency was determined by dividing the total efficiency by the instrument efficiency.

<sup>c</sup>The measured source efficiency versus density thickness was fit to an exponential curve; uncertainties represent the 95-percent confidence interval.

<sup>d</sup>The following MDC equation was used for 1-minute counts, with a background of 49 cpm and probe area of 20 cm<sup>2</sup>:

$$MDC = \frac{3 + 4.65\sqrt{C_B}}{KT}$$

<sup>e</sup>Measurements were made with an Eberline model HP-260 GM detector with a standard mica window (typical thickness of 1.4 to 2.0 mg/cm<sup>2</sup>).

<sup>f</sup>Detector face is a fixed part of the detector and not removable.

<sup>g</sup>Each sheet of Mylar has a density thickness of 0.22 mg/cm<sup>2</sup>, and one Kimwipe has a density thickness of 1.86 mg/cm<sup>2</sup>.

<sup>h</sup>Reagent water from the radiochemistry laboratory was used in analytical procedures.

**Table 5-26 Effects of Water Density Thickness on Source Efficiency and MDC (GM Detector/Tc-99)**

| Surface Material  | Density Thickness (mg/cm <sup>2</sup> ) | Tc-99 (0.161 ± 0.018) <sup>a</sup> |                  |   |
|---|---|------------------------------------|------------------|---|
|   |   | Source Efficiency                  |                  | MDC <sup>d</sup> (dpm/100 cm <sup>2</sup> ) |
|   |   | Meas <sup>b</sup>                  | Fit <sup>c</sup> |   |
| Detector face <sup>e</sup>  | — <sup>f</sup>                          | NA                                 | NA               | 1,454                                       |
| Detector face plus two Mylar sheets with one Kimwipe <sup>g</sup> | 2.30                                    | 0.627                              | 0.631 ± 0.022    | 1,762                                       |
| Plus 0.19 mg/cm <sup>2</sup> water <sup>h</sup>                   | 2.49                                    | 0.611                              | 0.621 ± 0.021    | 1,805                                       |
| Plus 0.76 mg/cm <sup>2</sup> water                                | 3.06                                    | 0.580                              | 0.590 ± 0.018    | 1,902                                       |
| Plus 2.85 mg/cm <sup>2</sup> water                                | 5.15                                    | 0.501                              | 0.490 ± 0.011    | 2,204                                       |
| Plus 3.97 mg/cm <sup>2</sup> water                                | 6.27                                    | 0.463                              | 0.444 ± 0.010    | 2,383                                       |
| Plus 5.49 mg/cm <sup>2</sup> water                                | 7.79                                    | 0.392                              | 0.387 ± 0.010    | 2,814                                       |
| Plus 6.67 mg/cm <sup>2</sup> water                                | 8.97                                    | 0.347                              | 0.349 ± 0.012    | 3,179                                       |
| Plus 8.17 mg/cm <sup>2</sup> water                                | 10.47                                   | 0.296                              | 0.305 ± 0.013    | 3,731                                       |
| Regression equation   |   | $\epsilon_s = 0.775 e^{-0.089 x}$  |                  |   |

<sup>a</sup>Instrument efficiency appears in parentheses; uncertainties represent the 95-percent confidence interval.

<sup>b</sup>Source efficiency was determined by dividing the total efficiency by the instrument efficiency.

<sup>c</sup>The measured source efficiency versus density thickness was fit to an exponential curve; uncertainties represent the 95-percent confidence interval.

<sup>d</sup>The following MDC equation was used for 1-minute counts, with a background of 49 cpm and probe area of 20 cm<sup>2</sup>:

$$MDC = \frac{3 + 4.65\sqrt{C_B}}{KT}$$

<sup>e</sup>Measurements were made with an Eberline model HP-260 GM detector with a standard mica window (typical thickness of 1.4 to 2.0 mg/cm<sup>2</sup>).

<sup>f</sup>Detector face is a fixed part of the detector and not removable.

<sup>g</sup>Each sheet of Mylar has a density thickness of 0.22 mg/cm<sup>2</sup>, and one Kimwipe has a density thickness of 1.86 mg/cm<sup>2</sup>.

<sup>h</sup>Reagent water from the radiochemistry laboratory was used in analytical procedures.



**Table 5-27 Effects of Water Density Thickness on Source Efficiency and MDC (GM Detector/SrY-90)**

| Surface Material  | Density Thickness (mg/cm <sup>2</sup> ) | SrY-90 (0.373 ± 0.020) <sup>a</sup> |                  |   |
|---|---|-------------------------------------|------------------|---|
|   |   | Source Efficiency                   |                  | MDC <sup>d</sup> (dpm/100 cm <sup>2</sup> ) |
|   |   | Meas <sup>b</sup>                   | Fit <sup>c</sup> |   |
| Detector face <sup>e</sup>  | — <sup>f</sup>                          | NA                                  | NA               | 648   |
| Detector face plus two Mylar sheets with one Kimwipe <sup>g</sup> | 2.30                                    | 0.697                               | 0.708 ± 0.029    | 684   |
| Plus 2.56 mg/cm <sup>2</sup> water <sup>h</sup>                   | 4.86                                    | 0.678                               | 0.676 ± 0.017    | 703   |
| Plus 3.25 mg/cm <sup>2</sup> water                                | 5.55                                    | 0.678                               | 0.668 ± 0.015    | 703   |
| Plus 4.81 mg/cm <sup>2</sup> water                                | 7.11                                    | 0.665                               | 0.649 ± 0.015    | 717   |
| Plus 6.28 mg/cm <sup>2</sup> water                                | 8.58                                    | 0.620                               | 0.632 ± 0.018    | 768   |
| Plus 7.88 mg/cm <sup>2</sup> water                                | 10.18                                   | 0.608                               | 0.613 ± 0.024    | 783   |
| Regression equation   |   | $\epsilon_s = 0.739 e^{-0.018 x}$   |                  |   |

<sup>a</sup>Instrument efficiency appears in parentheses; uncertainties represent the 95-percent confidence interval.

<sup>b</sup>Source efficiency was determined by dividing the total efficiency by the instrument efficiency.

<sup>c</sup>The measured source efficiency versus density thickness was fit to an exponential curve; uncertainties represent the 95-percent confidence interval.

<sup>d</sup>The following MDC equation was used for 1-minute counts, with a background of 49 cpm and probe area of 20 cm<sup>2</sup>:

$$MDC = \frac{3 + 4.65\sqrt{C_B}}{KT}$$

<sup>e</sup>Measurements were made with an Eberline model HP-260 GM detector with a standard mica window (typical thickness of 1.4 to 2.0 mg/cm<sup>2</sup>).

<sup>f</sup>Detector face is a fixed part of the detector and not removable.

<sup>g</sup>Each sheet of Mylar has a density thickness of 0.22 mg/cm<sup>2</sup>, and one Kimwipe has a density thickness of 1.86 mg/cm<sup>2</sup>.

<sup>h</sup>Reagent water from the radiochemistry laboratory was used in analytical procedures.

**Table 5-28 Effects of Water Density Thickness on Source Efficiency and MDC (ZnS Scintillation Detector)**

| Surface Material  | Density Thickness (mg/cm <sup>2</sup> ) | Th-230 (0.069 ± 0.005) <sup>a</sup> |                  |   |
|---|---|-------------------------------------|------------------|---|
|   |   | Source Efficiency                   |                  | MDC <sup>d</sup> (dpm/100 cm <sup>2</sup> ) |
|   |   | Meas <sup>b</sup>                   | Fit <sup>c</sup> |   |
| Detector face <sup>e</sup>  | — <sup>f</sup>                          | NA                                  | NA               | 65  |
| Detector face plus two Mylar sheets with one Kimwipe <sup>g</sup> | 2.30                                    | 0.508                               | 0.453 ± 0.060    | 294   |
| Plus 0.11 mg/cm <sup>2</sup> water <sup>h</sup>                   | 2.41                                    | 0.433                               | 0.423 ± 0.054    | 345   |
| Plus 0.25 mg/cm <sup>2</sup> water                                | 2.55                                    | 0.366                               | 0.389 ± 0.048    | 407   |
| Plus 0.48 mg/cm <sup>2</sup> water                                | 2.78                                    | 0.296                               | 0.338 ± 0.040    | 504   |
| Plus 1.23 mg/cm <sup>2</sup> water                                | 3.53                                    | 0.232                               | 0.214 ± 0.021    | 645   |
| Plus 2.03 mg/cm <sup>2</sup> water                                | 4.33                                    | 0.145                               | 0.131 ± 0.012    | 1,030                                       |
| Plus 3.51 mg/cm <sup>2</sup> water                                | 5.81                                    | 0.046                               | 0.053 ± 0.006    | 3,265                                       |
| Plus 4.23 mg/cm <sup>2</sup> water                                | 6.53                                    | 0.031                               | 0.034 ± 0.005    | 4,814                                       |
| Plus 5.88 mg/cm <sup>2</sup> water                                | 8.18                                    | 0.014                               | 0.012 ± 0.003    | 10,465                                      |
| Regression equation   |   | $\epsilon_s = 1.84 e^{-0.610 x}$    |                  |   |

<sup>a</sup>Instrument efficiency appears in parentheses; uncertainties represent the 95-percent confidence interval.

<sup>b</sup>Source efficiency was determined by dividing the total efficiency by the instrument efficiency.

<sup>c</sup>The measured source efficiency versus density thickness was fit to an exponential curve; uncertainties represent the 95-percent confidence interval.

<sup>d</sup>The following MDC equation was used for 1-minute counts, with a background of 1 cpm and probe area of 74 cm<sup>2</sup>:

$$MDC = \frac{3 + 4.65\sqrt{C_B}}{KT}$$

<sup>e</sup>Measurements were made with an Eberline model AC3-7 ZnS scintillation detector with a standard 1.5-mg/cm<sup>2</sup> window.

<sup>f</sup>Detector face is a fixed part of the detector and not removable.

<sup>g</sup>Each sheet of Mylar has a density thickness of 0.22 mg/cm<sup>2</sup>, and one Kimwipe has a density thickness of 1.86 mg/cm<sup>2</sup>.

<sup>h</sup>Reagent water from the radiochemistry laboratory was used in analytical procedures.

**Table 5-29 Total Efficiencies for Detectors Used To Assess Uranium Surface Activity**

| Radioactive Material<br>(Surface Type) | Total Efficiency (c/dis) <sup>a</sup> |                           |                               |      |      |
|--|---------------------------------------|---------------------------|-------------------------------|------|------|
|  | Gas Proportional                      |                           |                               | GM   | ZnS  |
|  | $\alpha$ Only <sup>b</sup>            | $\beta$ Only <sup>c</sup> | $\alpha + \beta$ <sup>b</sup> |      |      |
| <b>Processed Uranium<sup>d</sup></b>   |                                       |                           |                               |      |      |
| Stainless steel                        | 0.13                                  | 0.24                      | 0.45                          | 0.28 | 0.08 |
| Concrete                               | 0.10                                  | 0.22                      | 0.44                          | 0.19 | 0.06 |
| Wood                                   | 0.04                                  | 0.21                      | 0.32                          | 0.22 | 0.02 |
| Drywall                                | 0.10                                  | 0.23                      | 0.43                          | 0.27 | 0.06 |
| <b>Enriched Uranium (3%)</b>           |                                       |                           |                               |      |      |
| Stainless steel                        | 0.10                                  | 0.09                      | 0.23                          | 0.12 | 0.06 |
| Concrete                               | 0.07                                  | 0.07                      | 0.18                          | 0.10 | 0.05 |
| Wood                                   | 0.06                                  | 0.08                      | 0.17                          | 0.10 | 0.03 |
| Drywall                                | 0.07                                  | 0.07                      | 0.18                          | 0.10 | 0.04 |
| <b>Ru-106 (Rh-106)</b>                 |                                       |                           |                               |      |      |
| Stainless steel                        | — <sup>e</sup>                        | 0.55                      | 0.57                          | 0.56 | —    |
| Concrete                               | —                                     | 0.50                      | 0.51                          | 0.47 | —    |
| Wood                                   | —                                     | 0.46                      | 0.46                          | 0.45 | —    |
| Drywall                                | —                                     | 0.35                      | 0.34                          | 0.30 | —    |
| <b>SrY-90</b>                          |                                       |                           |                               |      |      |
| Stainless steel                        | —                                     | 0.38                      | 0.43                          | 0.27 | —    |
| Concrete                               | —                                     | 0.34                      | 0.38                          | 0.23 | —    |

<sup>a</sup>The total efficiencies were calculated by dividing net detector counts by radioactivity dispensed on the particular surface. All measurements were at contact with surface. For uranium, the alpha radioactivity (U-238, U-235, and U-234) was used. Activity was distributed over a 20-cm<sup>2</sup> area.

<sup>b</sup>Using window density thickness of 0.4 mg/cm<sup>2</sup>.

<sup>c</sup>Using window density thickness of 3.8 mg/cm<sup>2</sup>.

<sup>d</sup>Processed uranium includes U-238 in equilibrium with U-234, and U-235 present at natural isotopic ratios; the only other radionuclides present include the immediate progeny of U-238 and U-235.

<sup>e</sup>Data not obtained.

**Table 5-30 Normalized Total Efficiencies for Processed Uranium with Various Absorber Thicknesses**

| Processed Uranium <sup>a</sup> on Stainless Steel with Mylar Absorber Thicknesses | Normalized Total Efficiency <sup>b</sup> |                           |                               |      |      |
|---|--|---------------------------|-------------------------------|------|------|
|   | Gas Proportional                         |                           |                               | GM   | ZnS  |
|   | $\alpha$ Only <sup>c</sup>               | $\beta$ Only <sup>d</sup> | $\alpha + \beta$ <sup>c</sup> |      |      |
| No Mylar (at contact)   | 1.0                                      | 1.0                       | 1.0                           | 1.0  | 1.0  |
| 0.22 mg/cm <sup>2</sup> Mylar   | 0.85                                     | 1.0                       | 0.96                          | 1.0  | 0.69 |
| 0.44 mg/cm <sup>2</sup> Mylar   | 0.72                                     | 1.0                       | 0.93                          | 0.99 | 0.58 |
| 0.88 mg/cm <sup>2</sup> Mylar   | 0.53                                     | 1.0                       | 0.90                          | 0.97 | 0.33 |
| 1.32 mg/cm <sup>2</sup> Mylar   | 0.32                                     | 1.0                       | 0.84                          | 0.94 | 0.17 |
| 2.20 mg/cm <sup>2</sup> Mylar   | 0.05                                     | 0.98                      | 0.77                          | 0.90 | 0.03 |
| 3.30 mg/cm <sup>2</sup> Mylar   | 0.02                                     | 0.97                      | 0.76                          | 0.80 | 0.01 |

<sup>a</sup>Processed uranium includes U-238 in equilibrium with U-234, and U-235 present at natural isotopic ratios; the only other radionuclides present include the immediate progeny of U-238 and U-235.

<sup>b</sup>The total efficiencies were calculated by dividing net detector counts by radioactivity dispensed on the particular surface. Total efficiencies were then normalized to the total efficiency obtained with no Mylar. The alpha radioactivity (U-238, U-235, and U-234) was distributed over a 20-cm<sup>2</sup> area.

<sup>c</sup>Using window density thickness of 0.4 mg/cm<sup>2</sup>.

<sup>d</sup>Using window density thickness of 3.8 mg/cm<sup>2</sup>.

**Table 5-31 Detector Efficiency for Low-Enriched Uranium (3 Percent) Using a 126-cm<sup>2</sup> Proportional Detector with a 0.4-mg/cm<sup>2</sup> Window (Gas Proportional— $\alpha + \beta$ )**

| Radionuclide                     | Radiation/Average Energy (MeV) | Alpha Fraction | Radiation Yield | Detection Efficiency | Weighted Efficiency   |
|----------------------------------|--------------------------------|----------------|-----------------|----------------------|-----------------------|
| U-238                            | Alpha/4.2                      | 0.167          | 100%            | 0.15                 | 2.51×10 <sup>-2</sup> |
| Th-234                           | Beta/0.0435                    | 0.167          | 100%            | 0.11                 | 1.84×10 <sup>-2</sup> |
| Pa-234m                          | Beta/0.819                     | 0.167          | 100%            | 0.49                 | 8.17×10 <sup>-2</sup> |
| U-234                            | Alpha/4.7                      | 0.799          | 100%            | 0.15                 | 1.20×10 <sup>-1</sup> |
| U-235                            | Alpha/4.4                      | 0.033          | 100%            | 0.15                 | 5.00×10 <sup>-3</sup> |
| Th-231                           | Beta/0.0764                    | 0.033          | 100%            | 0.22                 | 7.27×10 <sup>-3</sup> |
| <b>Total Weighted Efficiency</b> |                                |                |                 |                      | <b>0.257</b>          |

**Table 5-32 Detector Efficiency for Low-Enriched Uranium (3 Percent) Using a 126-cm<sup>2</sup> Proportional Detector with a 3.8-mg/cm<sup>2</sup> Window (Gas Proportional— $\beta$  only)**

| Radionuclide                     | Radiation/Average Energy (MeV) | Alpha Fraction | Radiation Yield | Detection Efficiency | Weighted Efficiency   |
|----------------------------------|--------------------------------|----------------|-----------------|----------------------|-----------------------|
| U-238                            | Alpha/4.2                      | 0.167          | 100%            | 0.01                 | 1.67×10 <sup>-3</sup> |
| Th-234                           | Beta/0.0435                    | 0.167          | 100%            | 0.038                | 6.36×10 <sup>-3</sup> |
| Pa-234m                          | Beta/0.819                     | 0.167          | 100%            | 0.453                | 7.58×10 <sup>-2</sup> |
| U-234                            | Alpha/4.7                      | 0.799          | 100%            | 0.01                 | 7.99×10 <sup>-3</sup> |
| U-235                            | Alpha/4.4                      | 0.033          | 100%            | 0.01                 | 3.33×10 <sup>-4</sup> |
| Th-231                           | Beta/0.0764                    | 0.033          | 100%            | 0.118                | 3.93×10 <sup>-3</sup> |
| <b>Total Weighted Efficiency</b> |                                |                |                 |                      | <b>0.096</b>          |

**Table 5-33 Raw Voltages Producing the Peak Response by Subpopulation**

| SP No. | Nal Serial No. | Manufacture Year | Background (cpm) | Am-241 @ 10 cm(cpm) | Cs-137@ 20 cm(cpm) | Co-60@ 5 cm(cpm) | Volts |
|--------|----------------|------------------|------------------|---------------------|--------------------|------------------|-------|
| SP1    | PR329958       | 2013             | 15030            | 35815               | 66493              | 48897            | 692   |
|        | PR329940       | 2013             | 15046            | 35209               | 66051              | 48898            | 719   |
|        | PR329933       | 2013             | 14050            | 31421               | 60214              | 46700            | 682   |
|        | PR329950       | 2013             | 15121            | 36655               | 66418              | 48574            | 671   |
|        | PR325118       | 2013             | 15123            | 32249               | 65575              | 46342            | 675   |
|        | PR329957       | 2013             | 15438            | 35626               | 66128              | 47235            | 679   |
|        | PR329947       | 2013             | 15248            | 32708               | 65824              | 49440            | 701   |
|        | PR329956       | 2013             | 14978            | 34025               | 67557              | 51008            | 674   |
|        | PR329929       | 2013             | 14668            | 34338               | 67099              | 48417            | 679   |
|        | PR329937       | 2013             | 15309            | 34976               | 66639              | 49664            | 679   |
|        | PR325120       | 2013             | 15259            | 34906               | 66140              | 49344            | 707   |
|        | PR329945       | 2013             | 14977            | 33302               | 65302              | 47247            | 687   |
|        | PR329936       | 2013             | 15436            | 34656               | 66515              | 47241            | 693   |
|        | PR325145       | 2013             | 14631            | 34728               | 66000              | 48591            | 696   |
|        | PR329939       | 2013             | 15480            | 32637               | 65860              | 48919            | 667   |
|        | PR329948       | 2013             | 15084            | 33217               | 66030              | 48293            | 691   |
|        | PR329949       | 2013             | 15461            | 33644               | 66914              | 48313            | 675   |
|        | PR329927       | 2012             | 14907            | 32365               | 65315              | 46985            | 674   |
|        | PR329932       | 2012             | 15740            | 35197               | 66239              | 48319            | 679   |
| SP2    | PR320638       | 2012             | 15953            | 33105               | 65051              | 47962            | 720   |
|        | PR320642       | 2012             | 14826            | 33835               | 63816              | 45770            | 725   |
|        | PR315778       | 2012             | 15285            | 34615               | 67107              | 48879            | 799   |
|        | PR288435       | 2012             | 14802            | 29437               | 64128              | 47042            | 851   |
|        | PR320650       | 2012             | 15217            | 33806               | 66964              | 49757            | 751   |
|        | PR320633       | 2012             | 14777            | 31709               | 65206              | 46998            | 681   |
|        | PR288433       | 2010             | 14804            | 31980               | 67530              | 50179            | 723   |
|        | PR288444       | 2010             | 15342            | 31108               | 64054              | 46600            | 687   |
|        | PR288442       | 2010             | 15254            | 30415               | 64236              | 46524            | 857   |
|        | PR288425       | 2010             | 15178            | 32706               | 63189              | 48944            | 827   |
|        | PR288421       | 2010             | 14907            | 32308               | 65969              | 47908            | 746   |
| SP3    | PR119802       | 1995             | 16008            | 35691               | 67022              | 48766            | 843   |
|        | PR119663       | 1995             | 16108            | 35096               | 66493              | 46965            | 738   |
|        | PR119743       | 1995             | 16458            | 33329               | 66114              | 49341            | 761   |
|        | PR123446       | 1995             | 16481            | 34097               | 66476              | 47085            | 753   |
|        | PR121045       | 1995             | 15477            | 34086               | 66700              | 47779            | 774   |
|        | PR123350       | 1995             | 16124            | 32080               | 66472              | 49066            | 860   |
|        | PR121035       | 1995             | 15863            | 33082               | 66901              | 47943            | 908   |
|        | PR122641       | 1995             | 16053            | 33568               | 65792              | 48183            | 843   |
|        | PR119751       | 1995             | 16357            | 34418               | 67147              | 50721            | 647   |
|        | PR123445       | 1995             | 27244            | 44849               | 80052              | 64536            | 1093  |
|        | PR121028       | 1995             | 16468            | 32859               | 64743              | 44842            | 929   |
|        | PR123443       | 1995             | 15527            | 33221               | 65601              | 47493            | 1020  |

**Table 5-34 Statistical Analysis for Peak Response Investigation**

| SP No.   | N  | Mean           | Std Error   | 95% CL         | Median | Min | Max  |
|--|----|----------------|-------------|----------------|--------|-----|------|
| SP1  | 19 | 685.26         | 3.10        | 678.75, 691.77 | 679    | 667 | 719  |
| SP2  | 11 | 760.64         | 19.01       | 718.29, 802.99 | 746    | 681 | 857  |
| SP3  | 12 | 847.42         | 36.36       | 767.38, 927.45 | 843    | 647 | 1093 |
| ANOVA—Comparison of Mean Voltage (across Sources) between Subpopulations |    |                |             |                |        |     |      |
| Source   | DF | Sum of Squares | Mean Square | F Value        | P > F  |     |      |
| Among  | 2  | 194676.187002  | 97338.09350 | 17.4496        | <.0001 |     |      |
| Within   | 39 | 217551.146332  | 5578.23452  |                |        |     |      |

**Table 5-35 Raw Results for 900-Volt Default Setting**

| SP No. | Nal Serial No. | Manufacture Year | Background (cpm) | Am-241 @ 10 cm(cpm) | Cs-137@ 20 cm(cpm) | Co-60@ 5 cm(cpm) | Volts |
|--------|----------------|------------------|------------------|---------------------|--------------------|------------------|-------|
| SP1    | PR329958       | 2013             | 13997            | 32009               | 65355              | 45962            | 900   |
|        | PR329940       | 2013             | 14040            | 31922               | 65261              | 46956            | 900   |
|        | PR329933       | 2013             | 14504            | 32914               | 67797              | 46782            | 900   |
|        | PR329950       | 2013             | 13893            | 33084               | 66163              | 46525            | 900   |
|        | PR325118       | 2013             | 14746            | 32580               | 64064              | 43080            | 900   |
|        | PR329957       | 2013             | 14491            | 31584               | 66807              | 47953            | 900   |
|        | PR329947       | 2013             | 14588            | 30952               | 65320              | 47136            | 900   |
|        | PR329956       | 2013             | 14352            | 32112               | 66521              | 48720            | 900   |
|        | PR329929       | 2013             | 14661            | 32123               | 65100              | 47408            | 900   |
|        | PR329937       | 2013             | 14201            | 32519               | 66549              | 48781            | 900   |
|        | PR325120       | 2013             | 14340            | 32697               | 65503              | 46293            | 900   |
|        | PR329945       | 2013             | 14111            | 33378               | 66080              | 47653            | 900   |
|        | PR329936       | 2013             | 14928            | 32783               | 66028              | 47928            | 900   |
|        | PR325145       | 2013             | 14904            | 32080               | 66043              | 46495            | 900   |
|        | PR329939       | 2013             | 14138            | 32992               | 66042              | 47942            | 900   |
|        | PR329948       | 2013             | 14562            | 33340               | 67613              | 46525            | 900   |
|        | PR329949       | 2013             | 14173            | 33547               | 65635              | 46734            | 900   |
|        | PR329927       | 2012             | 14821            | 32940               | 66000              | 46862            | 900   |
|        | PR329932       | 2012             | 14853            | 32193               | 66452              | 49158            | 900   |
| SP2    | PR320638       | 2012             | 14379            | 32968               | 63582              | 45387            | 900   |
|        | PR320642       | 2012             | 14194            | 30810               | 62665              | 45638            | 900   |
|        | PR315778       | 2012             | 13674            | 31276               | 60734              | 47206            | 900   |
|        | PR288435       | 2012             | 13297            | 17909               | 58091              | 42117            | 900   |
|        | PR320650       | 2012             | 14064            | 31562               | 64839              | 47734            | 900   |
|        | PR320633       | 2012             | 14798            | 31741               | 63728              | 44895            | 900   |
|        | PR288433       | 2010             | 13956            | 30679               | 63428              | 45275            | 900   |
|        | PR288444       | 2010             | 15155            | 29826               | 63383              | 45950            | 900   |
|        | PR288442       | 2010             | 13047            | 14444               | 56498              | 41724            | 900   |

| SP No. | Nal Serial No. | Manufacture Year | Background (cpm) | Am-241 @ 10 cm(cpm) | Cs-137@ 20 cm(cpm) | Co-60@ 5 cm(cpm) | Volts |
|--------|----------------|------------------|------------------|---------------------|--------------------|------------------|-------|
|        | PR288425       | 2010             | 13449            | 23885               | 59011              | 44377            | 900   |
|        | PR288421       | 2010             | 13805            | 29273               | 62747              | 45583            | 900   |
| SP3    | PR119802       | 1995             | 14099            | 25986               | 61045              | 46439            | 900   |
|        | PR119663       | 1995             | 14587            | 32482               | 64259              | 45080            | 900   |
|        | PR119743       | 1995             | 14429            | 29913               | 63540              | 48358            | 900   |
|        | PR123446       | 1995             | 14417            | 33157               | 63123              | 45976            | 900   |
|        | PR121045       | 1995             | 14778            | 30451               | 63069              | 47081            | 900   |
|        | PR123350       | 1995             | 13042            | 20852               | 58473              | 42762            | 900   |
|        | PR121035       | 1995             | 11578            | 11630               | 55692              | 44222            | 900   |
|        | PR122641       | 1995             | 13743            | 22236               | 60135              | 43845            | 900   |
|        | PR119751       | 1995             | 15256            | 34498               | 67056              | 46210            | 900   |
|        | PR123445       | 1995             | 3674             | 3528                | 28288              | 24732            | 900   |
|        | PR121028       | 1995             | 11081            | 11017               | 51699              | 36743            | 900   |
|        | PR123443       | 1995             | 6082             | 6524                | 40112              | 31211            | 900   |

**Table 5-36 Statistical Analysis for 900-Volt Default Investigation—Am-241 Source**

| SP No.   | N  | Mean           | Std Error   | 95% CL       | Min    | Median | Max   |
|--|----|----------------|-------------|--------------|--------|--------|-------|
| <b>SP1</b>   | 19 | 32513.11       | 153.11      | 32191, 32835 | 30952  | 32580  | 33547 |
| <b>SP2</b>   | 11 | 27670.27       | 1867.07     | 23510, 31830 | 14444  | 30679  | 32968 |
| <b>SP3</b>   | 12 | 21856.17       | 3198.58     | 14816, 29996 | 3528   | 24111  | 34498 |
| ANOVA—Comparison of Mean Counts between Subpopulations |    |                |             |              |        |        |       |
| Source   | DF | Sum of Squares | Mean Square | F Value      | P > F  |        |       |
| <b>Among</b>   | 2  | 839472039.981  | 419736020.0 | 9.3973       | 0.0005 |        |       |
| <b>Within</b>  | 39 | 1741955879.638 | 44665535.4  |              |        |        |       |

**Table 5-37 Statistical Analysis for 900-Volt Default Investigation—Cs-137 Source**

| SP No.  | N  | Mean           | Std Error   | 95% CL       | Min    | Median | Max   |
|---|----|----------------|-------------|--------------|--------|--------|-------|
| SP1   | 19 | 66017.53       | 199.81      | 65598, 66437 | 64064  | 66042  | 67797 |
| SP2   | 11 | 61700.55       | 818.00      | 59877, 63523 | 56498  | 62747  | 64839 |
| SP3   | 12 | 56374.25       | 3295.97     | 49120, 53629 | 28288  | 60590  | 67056 |
| ANOVA—Comparison of Mean cpm between Subpopulations |    |                |             |              |        |        |       |
| Source  | DF | Sum of Squares | Mean Square | F Value      | P > F  |        |       |
| Among   | 2  | 686716879.619  | 343358439.8 | 8.8028       | 0.0007 |        |       |
| Within  | 39 | 1521225155.714 | 39005773.2  |              |        |        |       |

**Table 5-38 Statistical Analysis for 900-Volt Default Investigation—Co-60 Source**

| SP No.  | N  | Mean           | Std Error   | 95% CL       | Min    | Median | Max   |
|---|----|----------------|-------------|--------------|--------|--------|-------|
| SP1   | 19 | 47099.63       | 304.24      | 46560, 47739 | 43080  | 46956  | 49158 |
| SP2   | 11 | 45080.55       | 552.58      | 43849, 46312 | 41724  | 45387  | 47734 |
| SP3   | 12 | 41888.25       | 2096.10     | 37274, 46502 | 24732  | 44651  | 48358 |
| ANOVA—Comparison of Mean cpm between Subpopulations |    |                |             |              |        |        |       |
| Source  | DF | Sum of Squares | Mean Square | F Value      | P > F  |        |       |
| Among   | 2  | 199746397.7445 | 99873198.87 | 6.0369       | 0.0052 |        |       |
| Within  | 39 | 645202763.3983 | 16543660.60 |              |        |        |       |

**Table 5-39 Statistical Analysis for Peak Voltage Investigation—Cs-137 Source**

| SP No.  | N  | Mean           | Std Error   | 95% CL       | Min    | Median  | Max   |
|---|----|----------------|-------------|--------------|--------|---------|-------|
| SP1   | 19 | 65911.21       | 342.72      | 65191, 66321 | 60214  | 33128   | 67557 |
| SP2   | 11 | 65204.55       | 448.65      | 64205, 66204 | 63189  | 65051   | 67530 |
| SP3   | 12 | 67459          | 1161.41     | 64903, 70016 | 64743  | 66484.5 | 80052 |
| ANOVA—Comparison of Mean cpm between Subpopulations |    |                |             |              |        |         |       |
| Source  | DF | Sum of Squares | Mean Square | F Value      | P > F  |         |       |
| Among   | 2  | 31476641.6744  | 15738320.84 | 2.5536       | 0.0907 |         |       |
| Within  | 39 | 240362750.8018 | 6163147.46  |              |        |         |       |



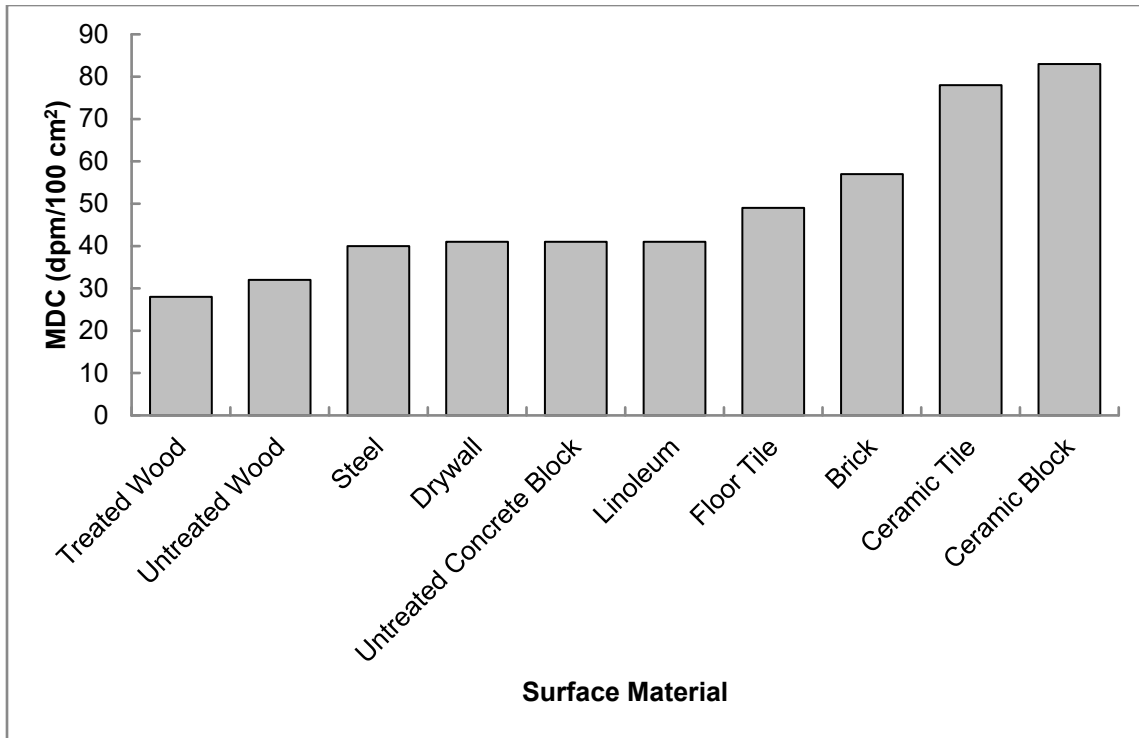


**Figure 5-1 Effect of Surface Material on Gas Proportional Detector ( $\alpha$  Only) MDC**

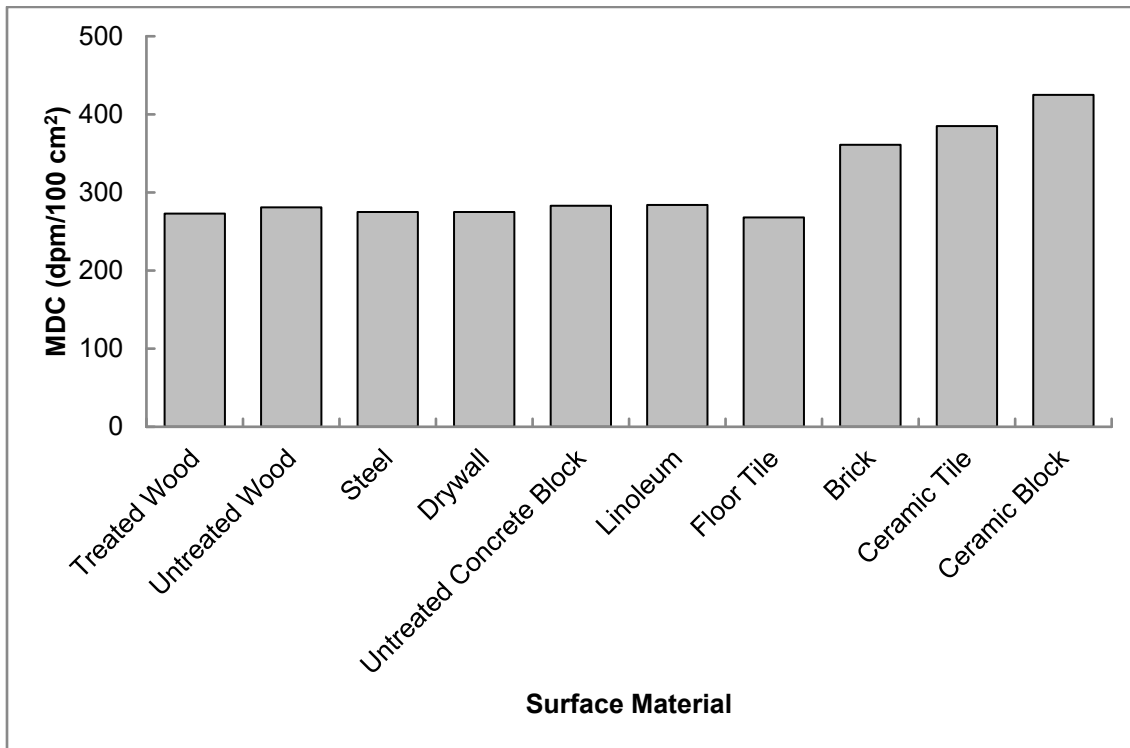


**Figure 5-2 Effect of Surface Material on Gas Proportional Detector ( $\beta$  Only) MDC**

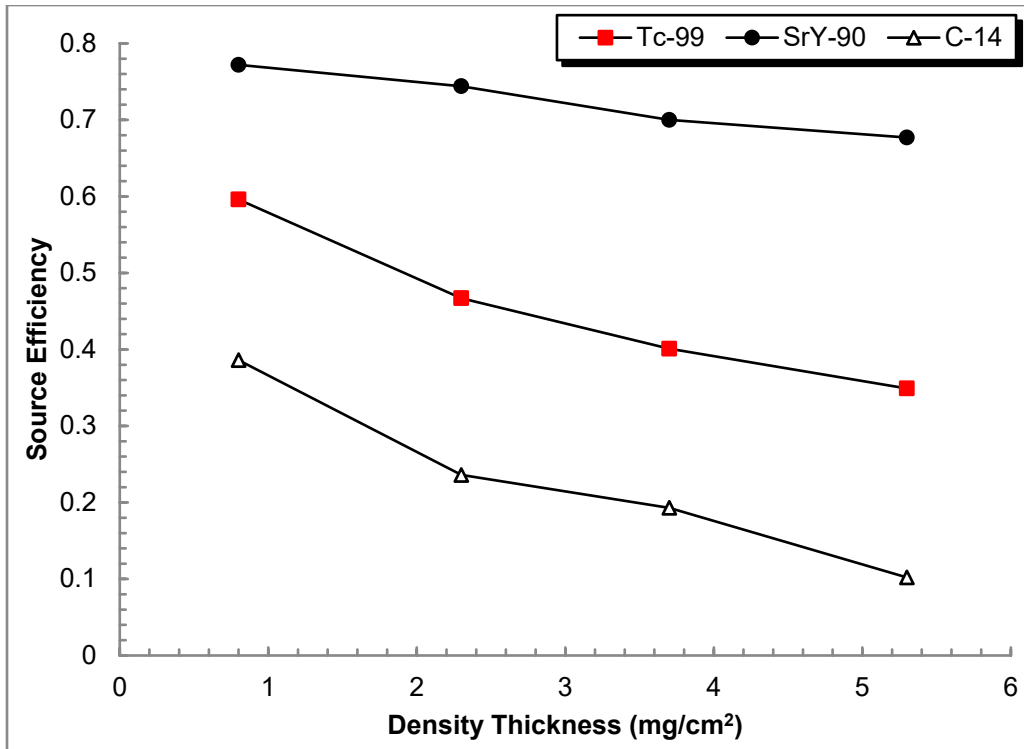


**Figure 5-3 Effects of Oil Density Thickness on Source Efficiency for Various Sources**

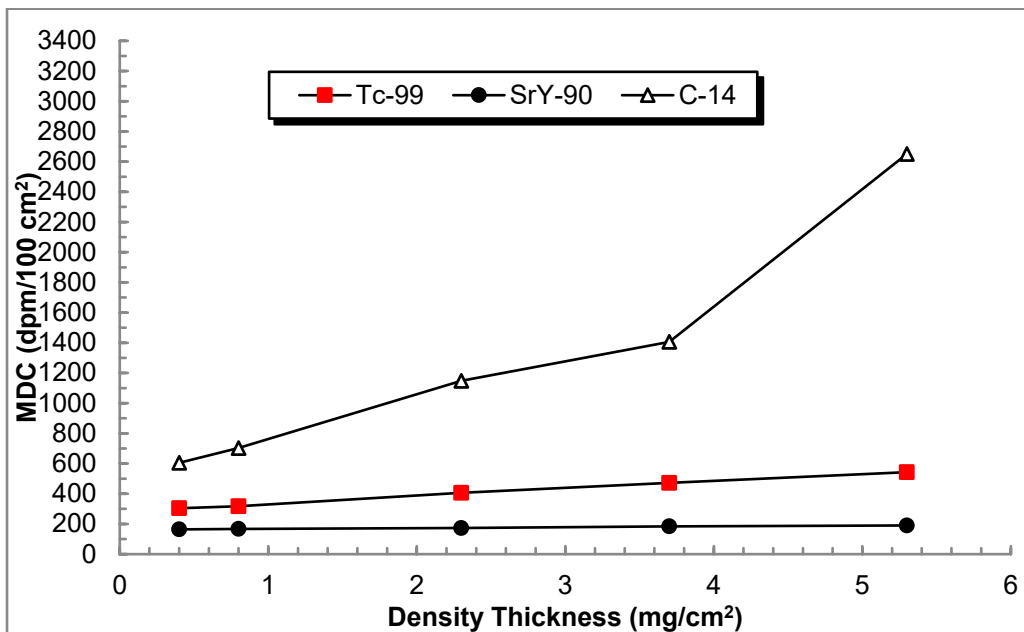


**Figure 5-4 Effects of Oil Density Thickness on MDC**

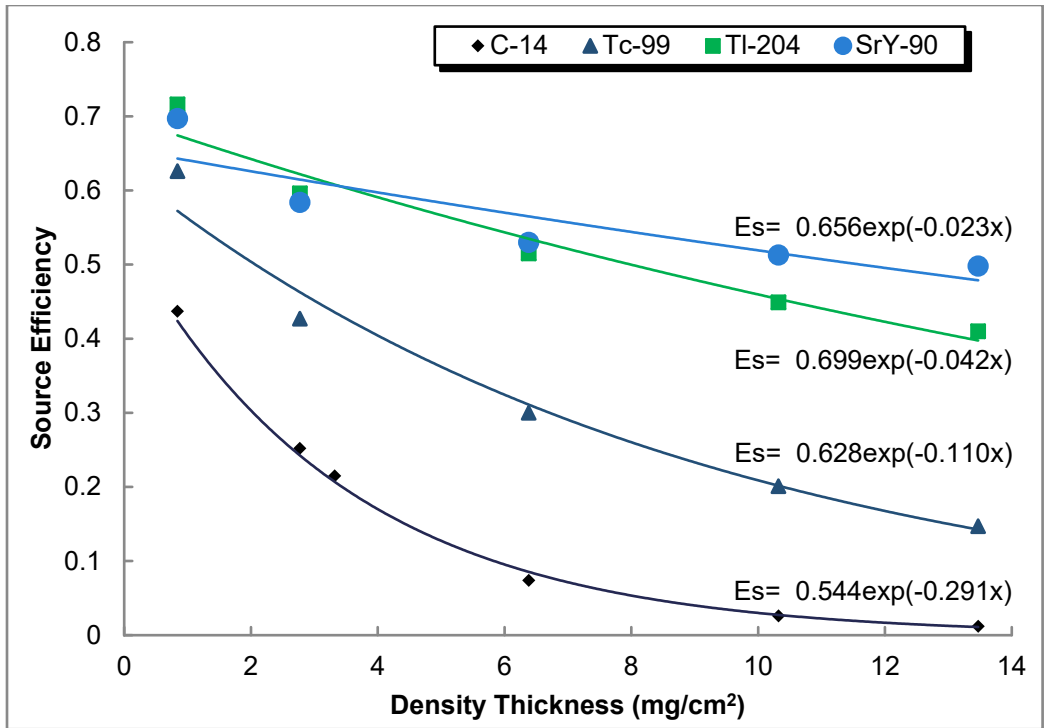


**Figure 5-5 Effects of Paint Density Thickness on Source Efficiency (Gas Proportional— $\alpha+\beta$ )**

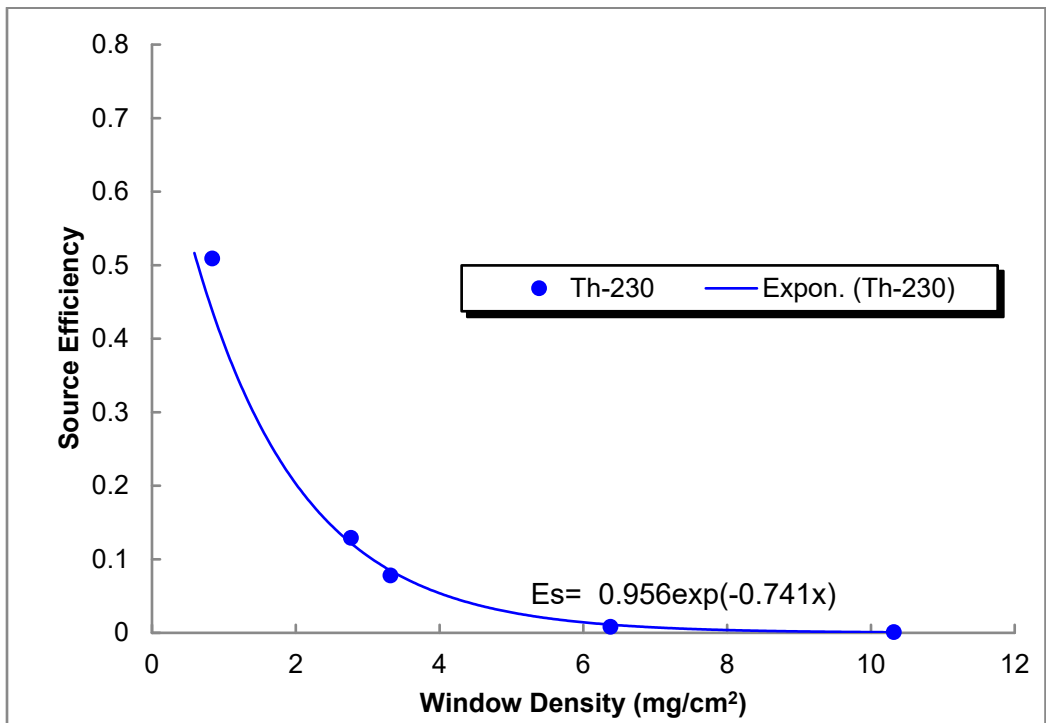


**Figure 5-6 Effects of Paint Density Thickness on Source Efficiency (Gas Proportional— $\alpha$ -only)**

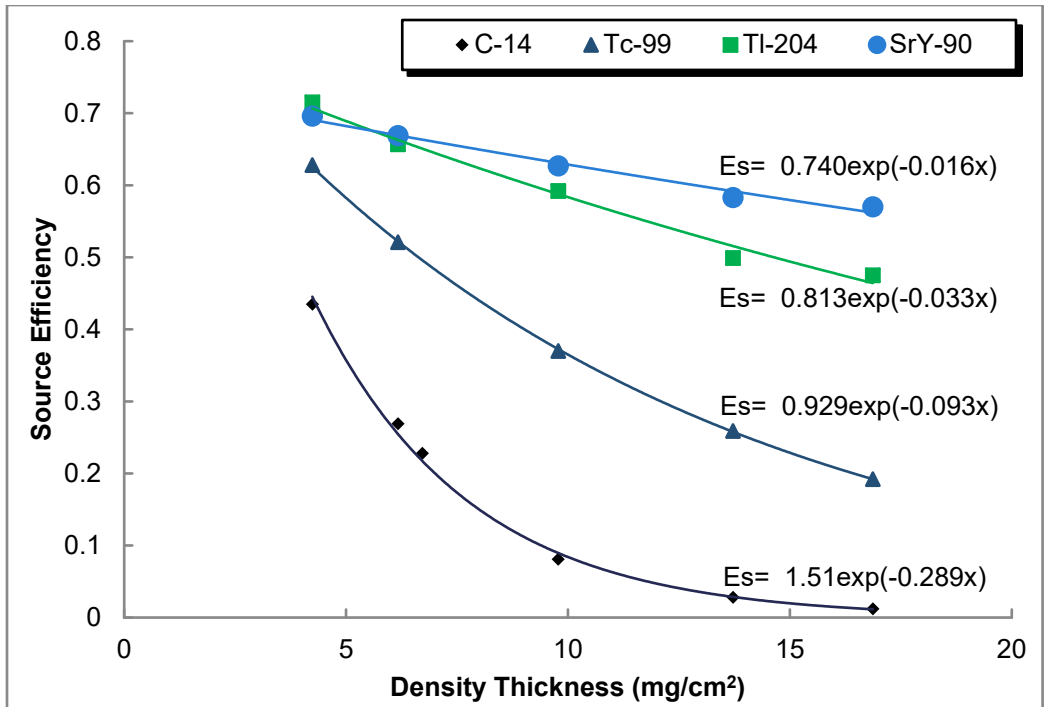


Figure 5-7 Effects of Paint Density Thickness on Source Efficiency (Gas Proportional—β-Only)

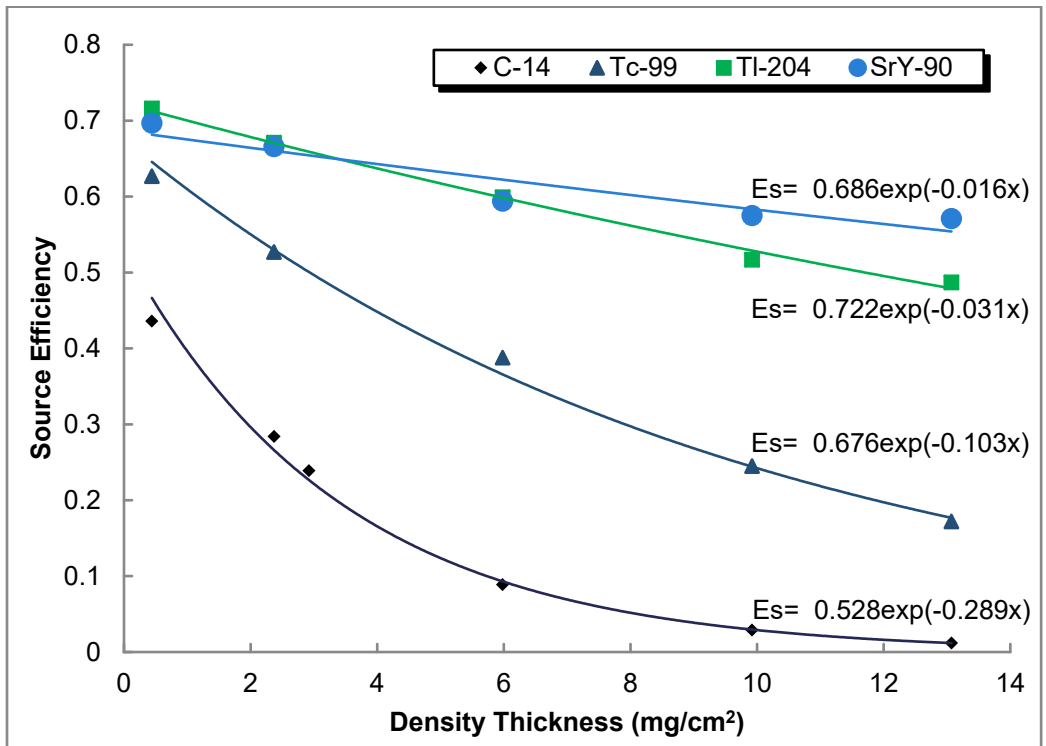


Figure 5-8 Effects of Paint Density Thickness on Source Efficiency (GM Detector)

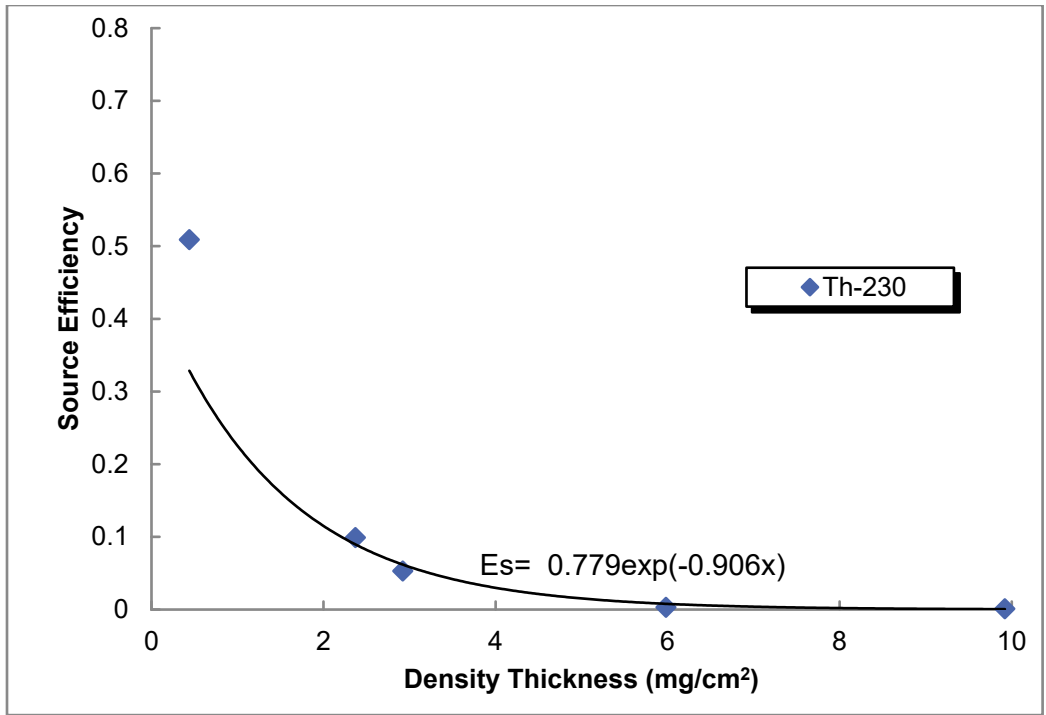


Figure 5-9 Effects of Paint Density Thickness on Source Efficiency (ZnS Scintillation Detector)

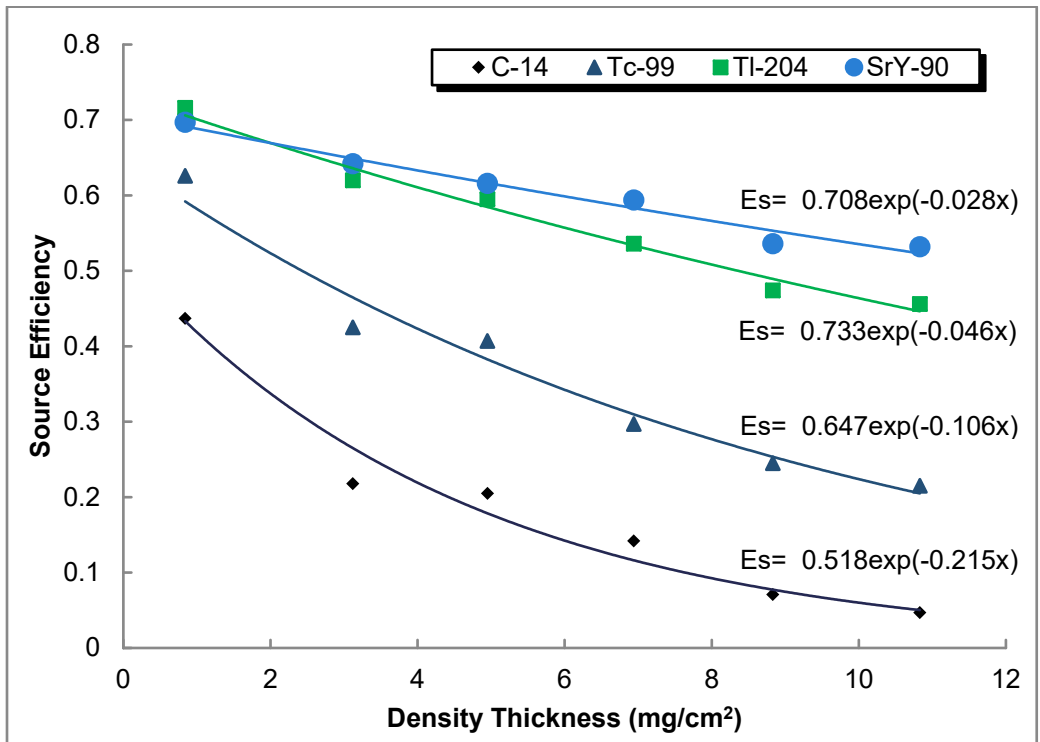
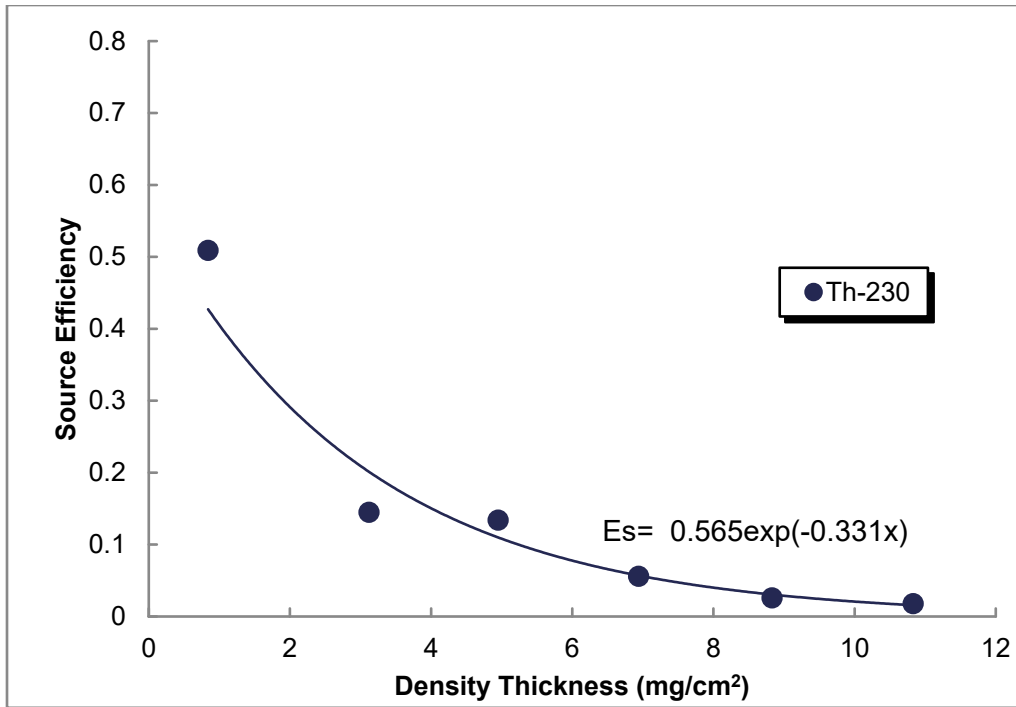
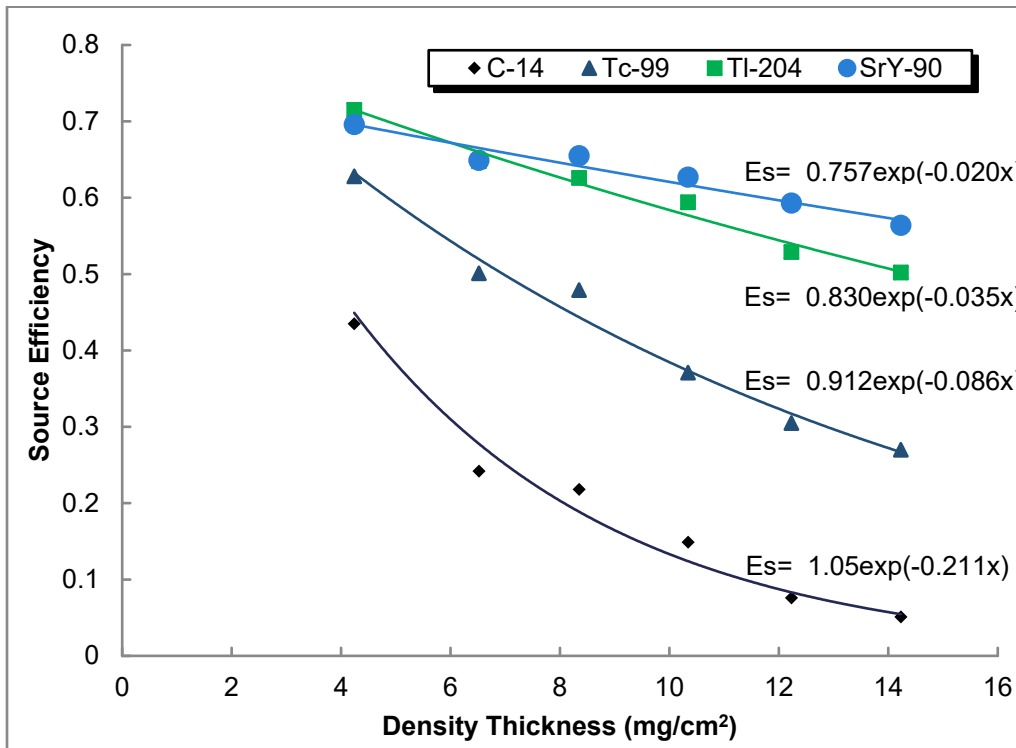


Figure 5-10 Effects of Dust Density Thickness on Source Efficiency (Gas Proportional— $\alpha + \beta$ )



**Figure 5-11 Effects of Dust Density Thickness on Source Efficiency (Gas Proportional— $\alpha$ -only)**



**Figure 5-12 Effects of Dust Density Thickness on Source Efficiency (Gas Proportional— $\beta$ -Only)**

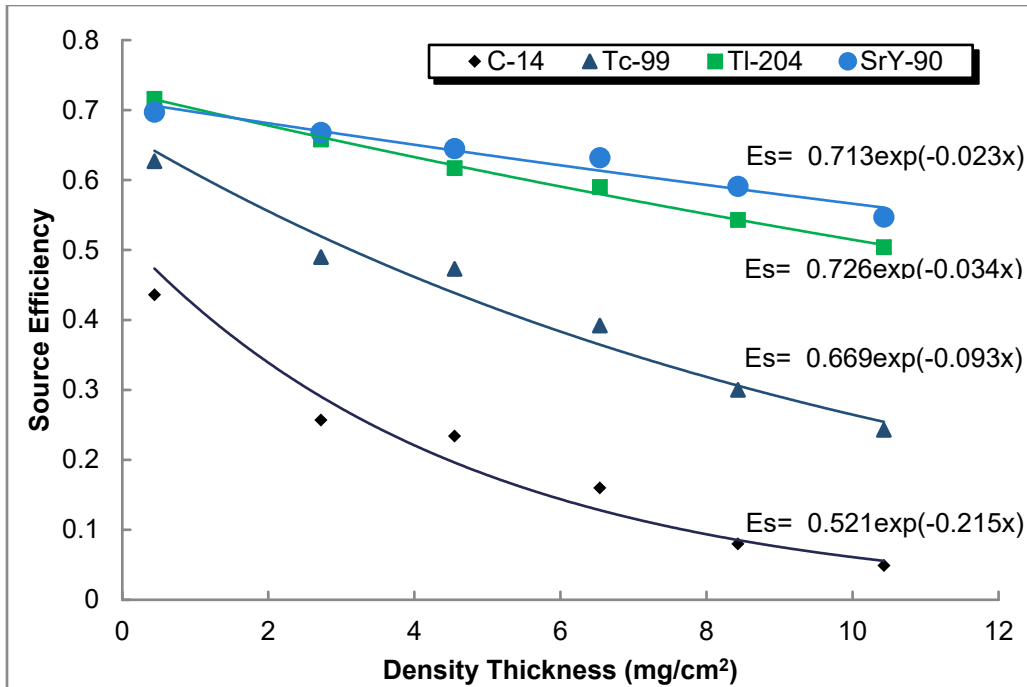


**Figure 5-13 Effects of Dust Density Thickness on Source Efficiency (GM Detector)**

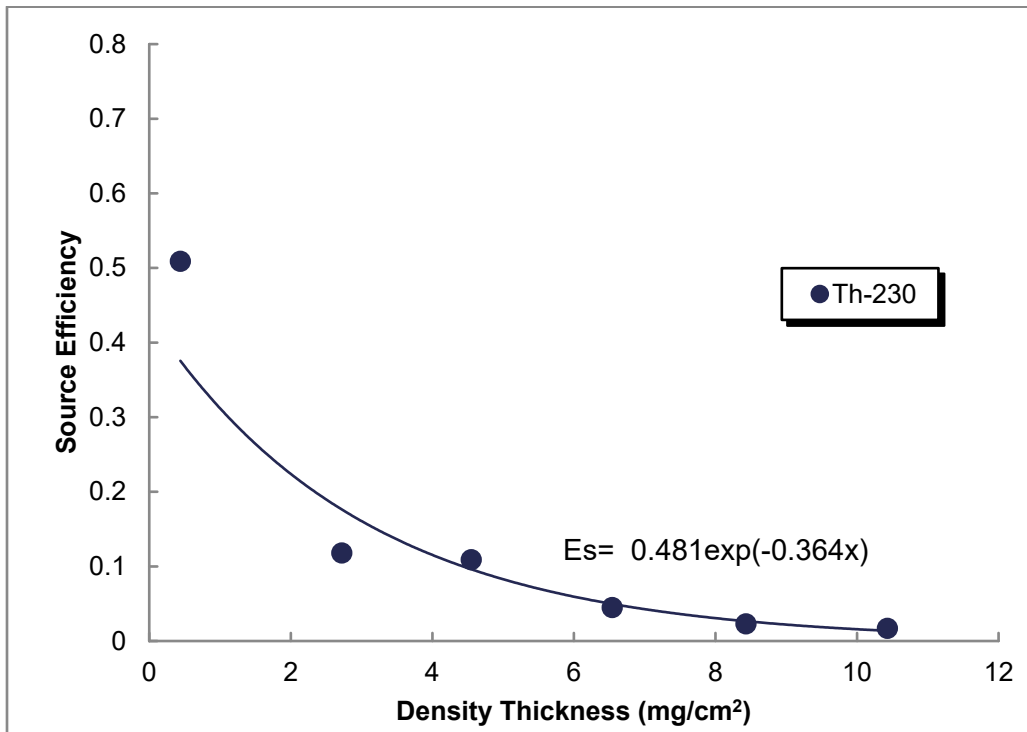


**Figure 5-14 Effects of Dust Density Thickness on Source Efficiency (ZnS Scintillation Detector)**

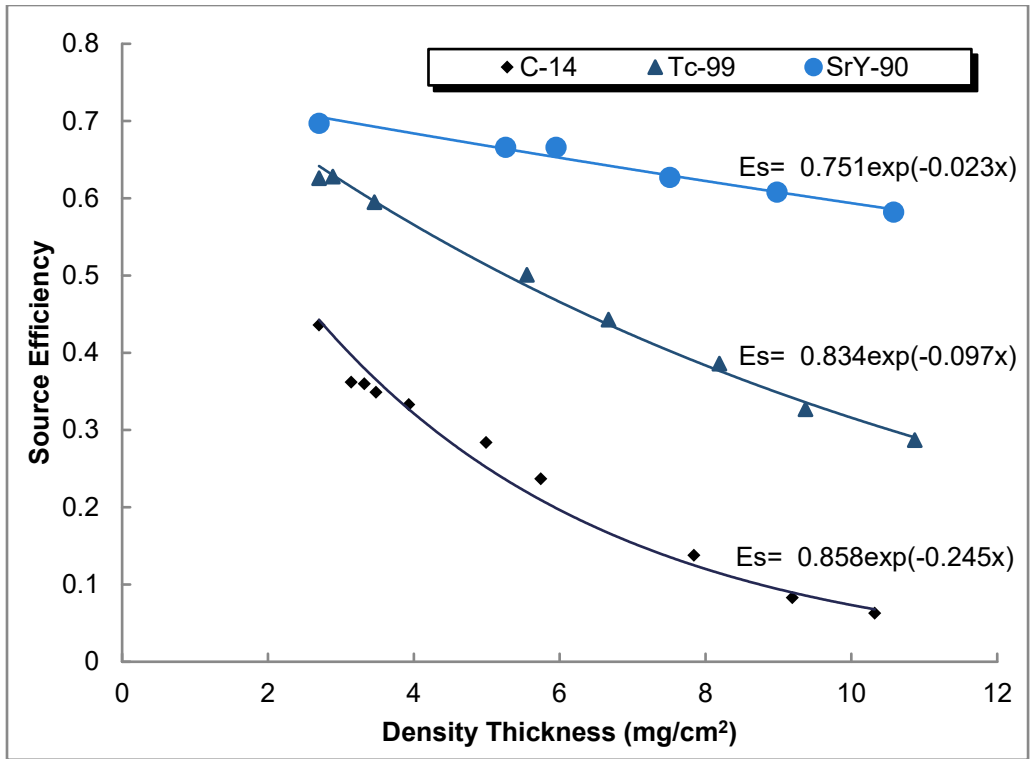


Figure 5-15 Effects of Water Density Thickness on Source Efficiency (Gas Proportional— $\alpha + \beta$ )

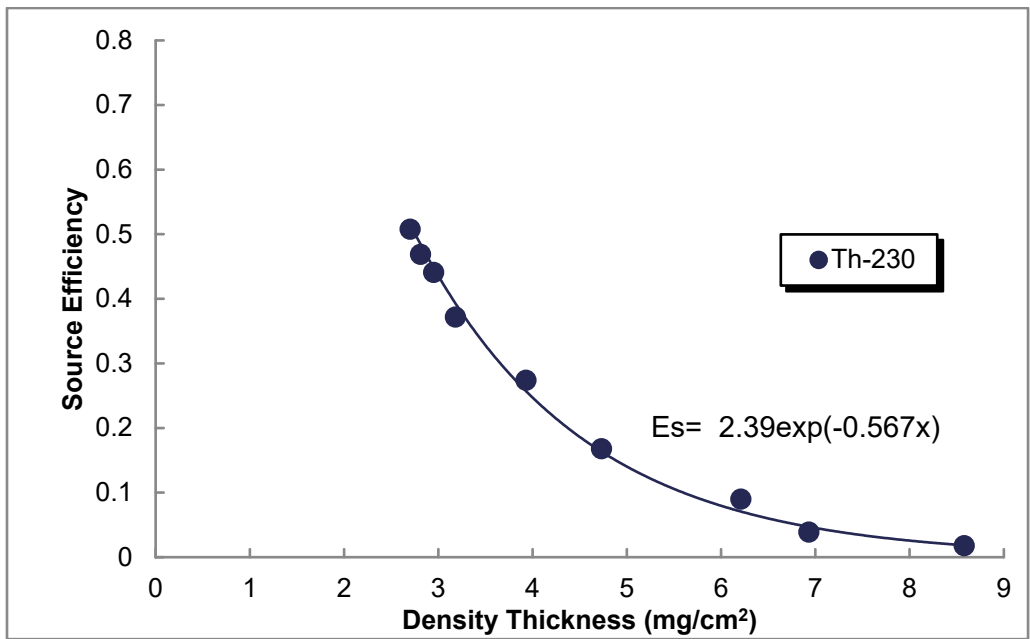
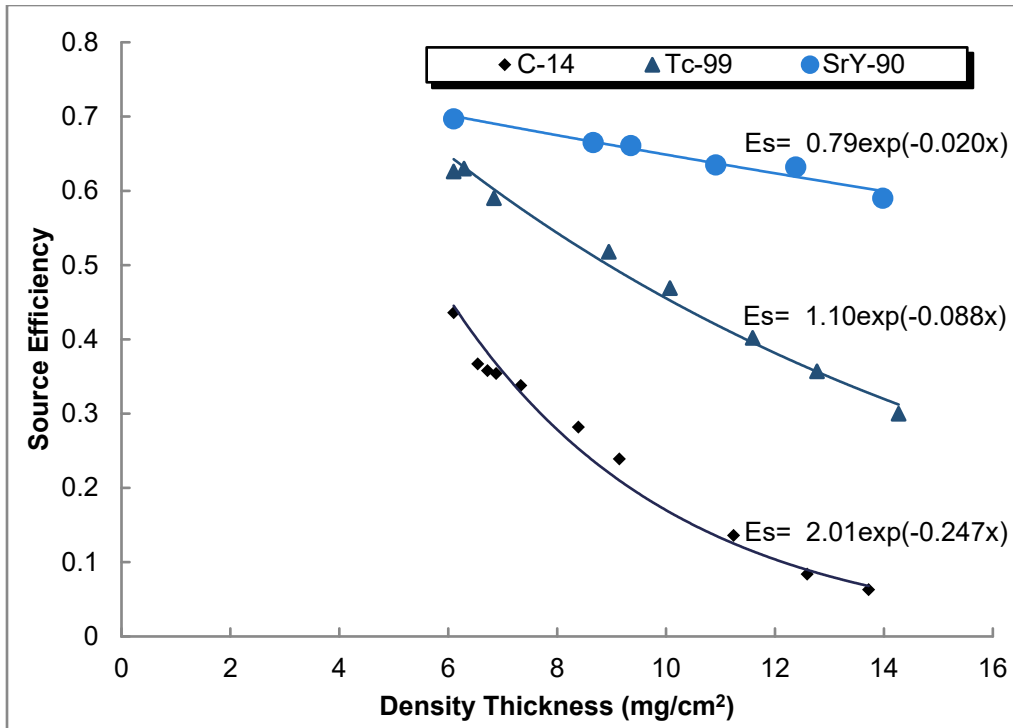
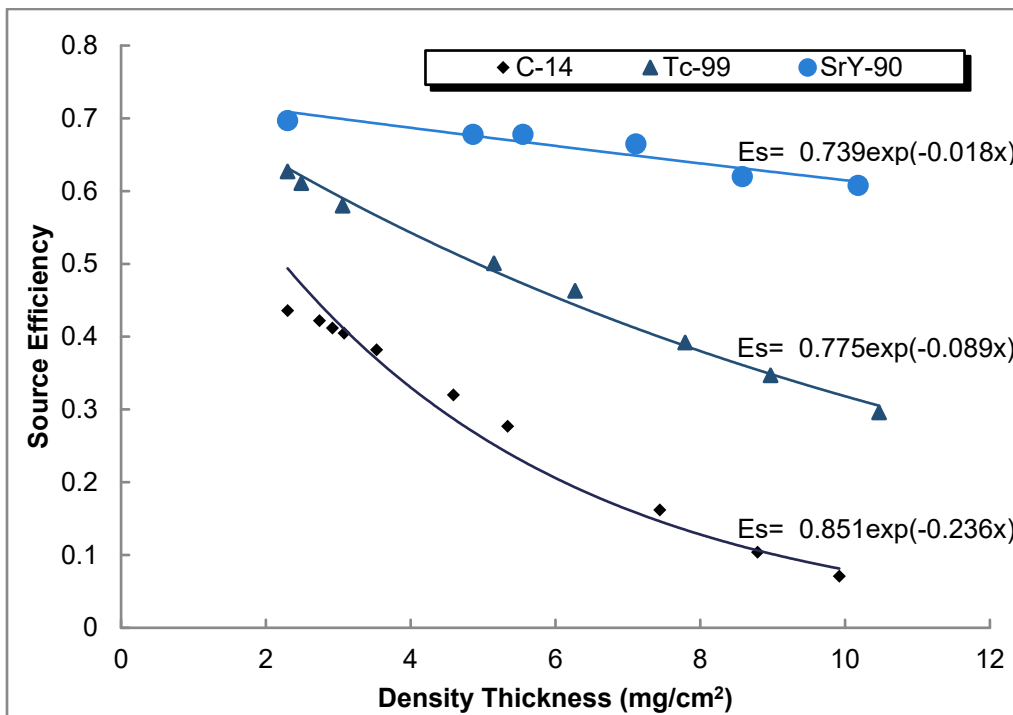


Figure 5-16 Effects of Water Density Thickness on Source Efficiency (Gas Proportional— $\alpha$ -only)





**Figure 5-17** Effects of Water Density Thickness on Source Efficiency (Gas Proportional—β only)



**Figure 5-18** Effects of Water Density Thickness on Source Efficiency (GM Detector)

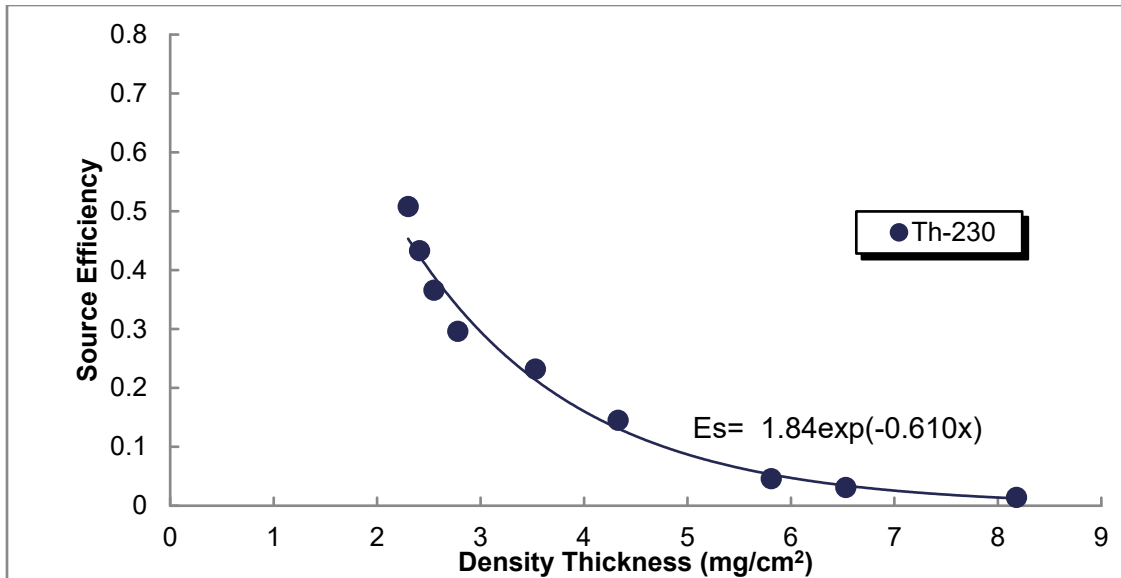


**Figure 5-19** Effects of Water Density Thickness on Source Efficiency (ZnS Scintillation Detector)

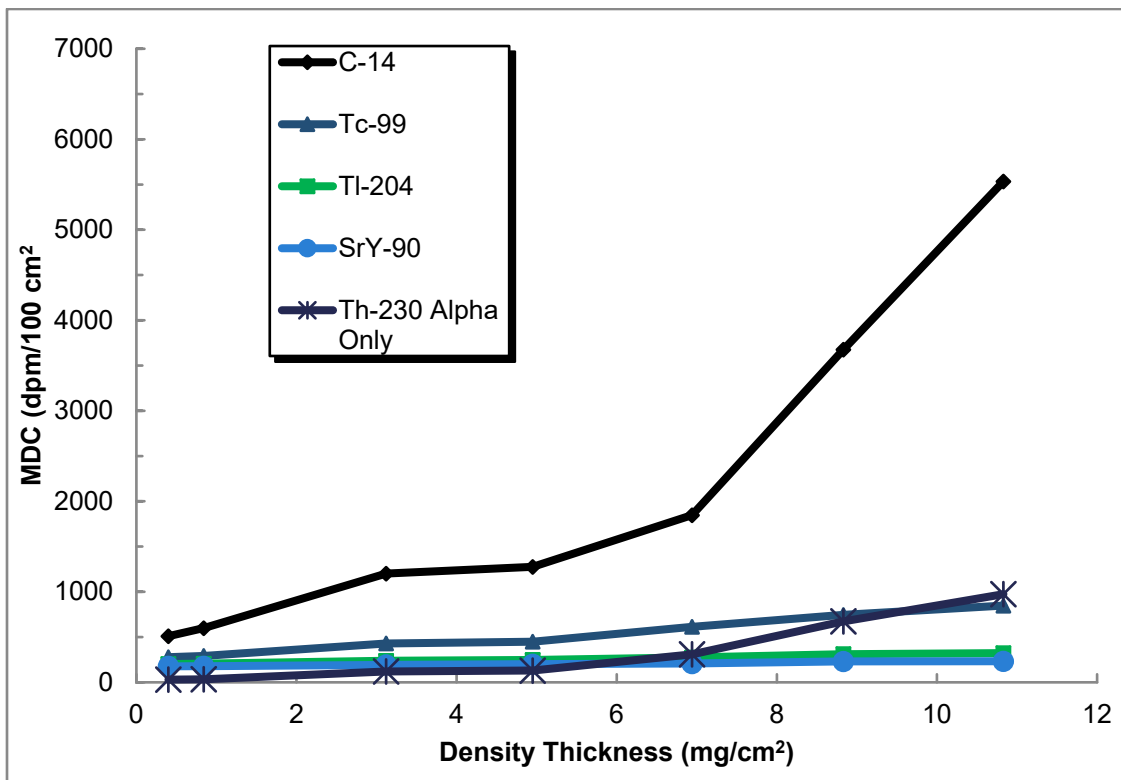


**Figure 5-20** Effects of Dust Density Thickness on MDC for Various Sources Using the Gas Proportional Detector in  $\alpha + \beta$  and  $\alpha$ -Only Modes

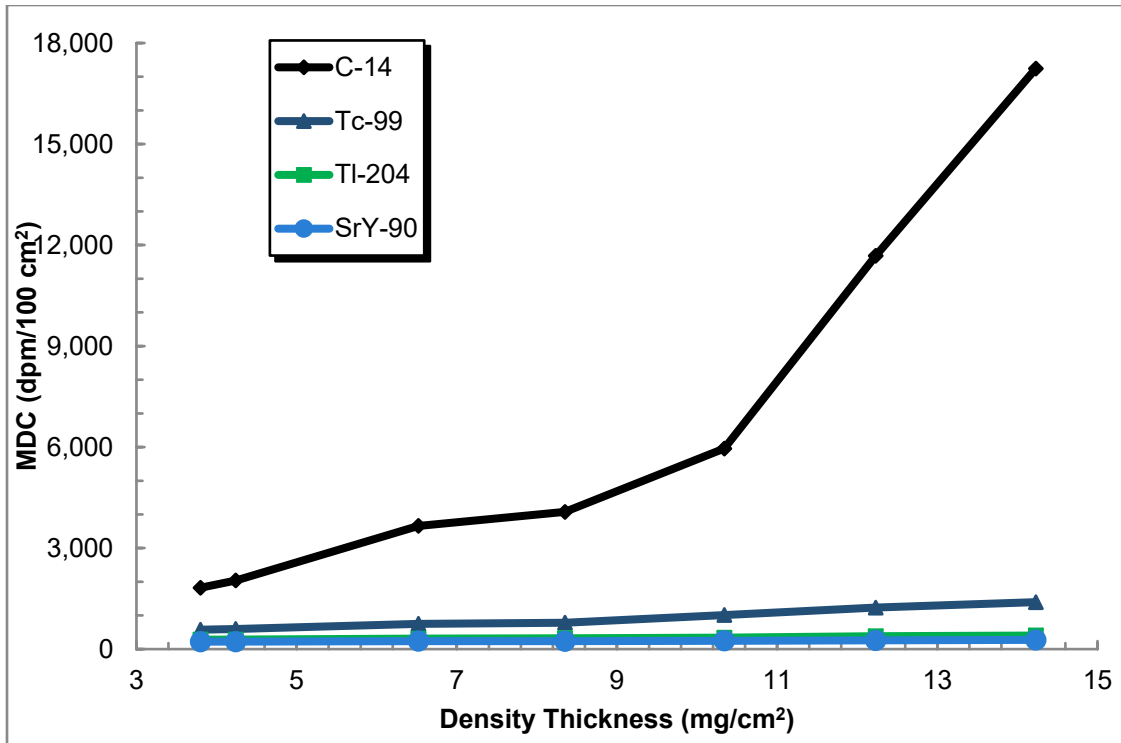


**Figure 5-21 Effects of Dust Density Thickness on MDC for Various Sources Using the Gas Proportional Detector in  $\beta$ -Only Mode**

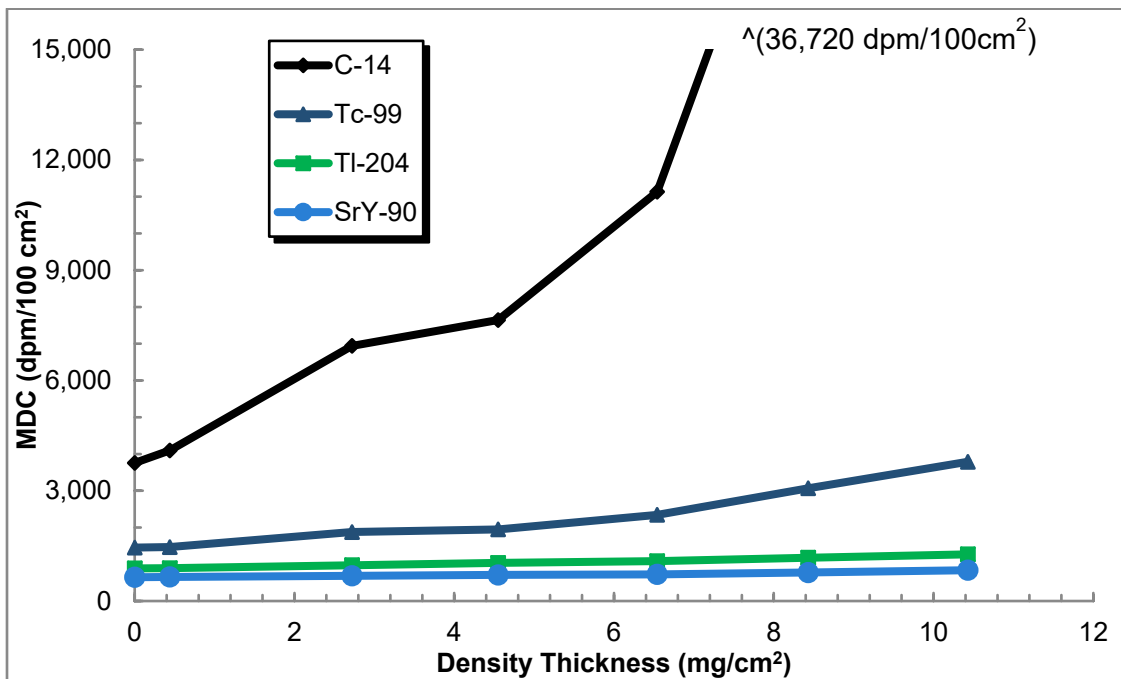


**Figure 5-22 Effects of Dust Density Thickness on MDC for Various Sources Using the GM Detector**

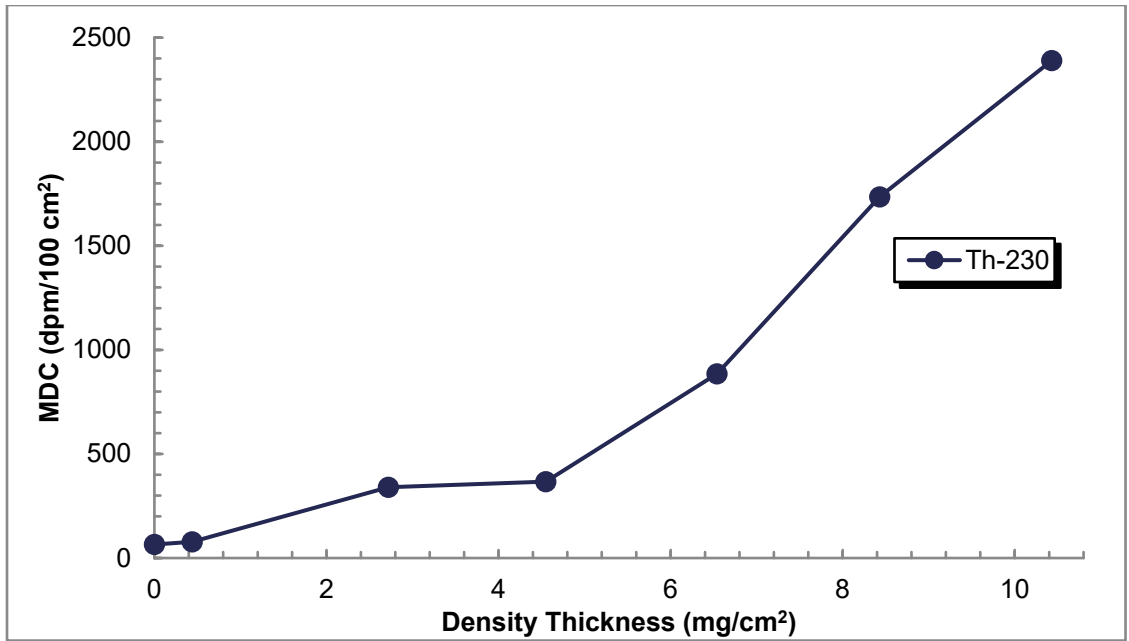


**Figure 5-23 Effects of Dust Density Thickness on MDC for an Alpha Source Using the ZnS Scintillation Detector**

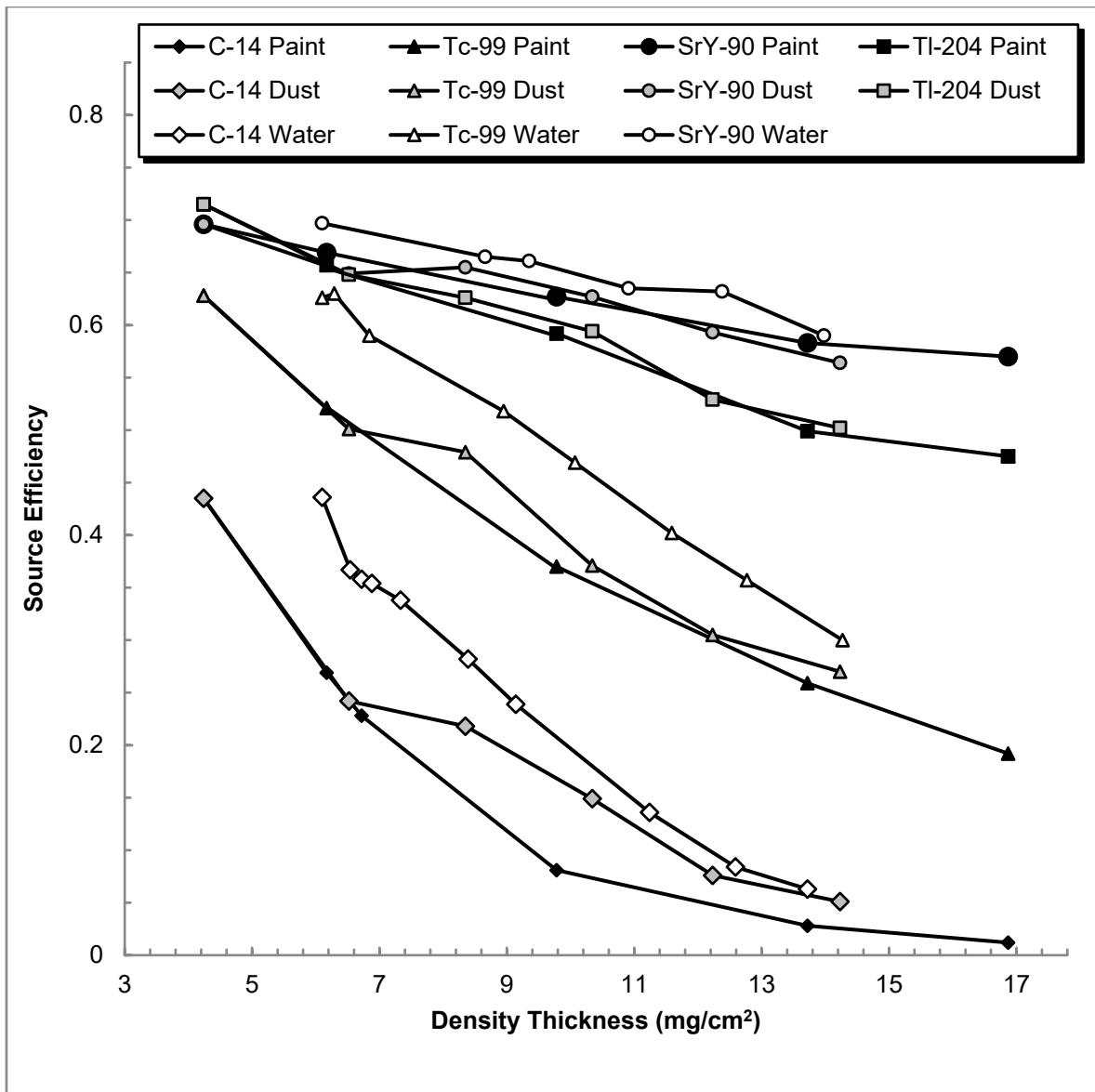


**Figure 5-24 Overall Effects of Paint, Dust, and Water Density Thickness on Source Efficiency for Various Sources Using the Gas Proportional Detector in  $\beta$ -Only Mode**

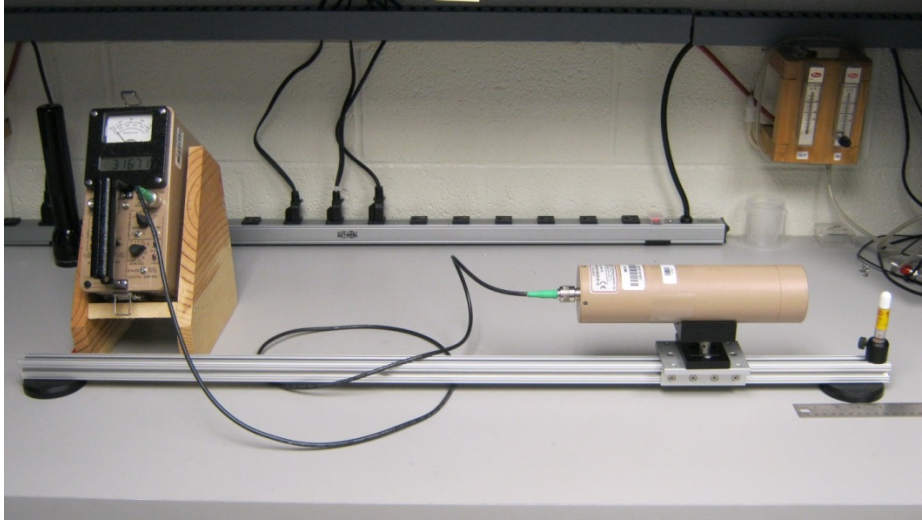


**Figure 5-25** Apparatus for Controlling Detector-to-Source Distances

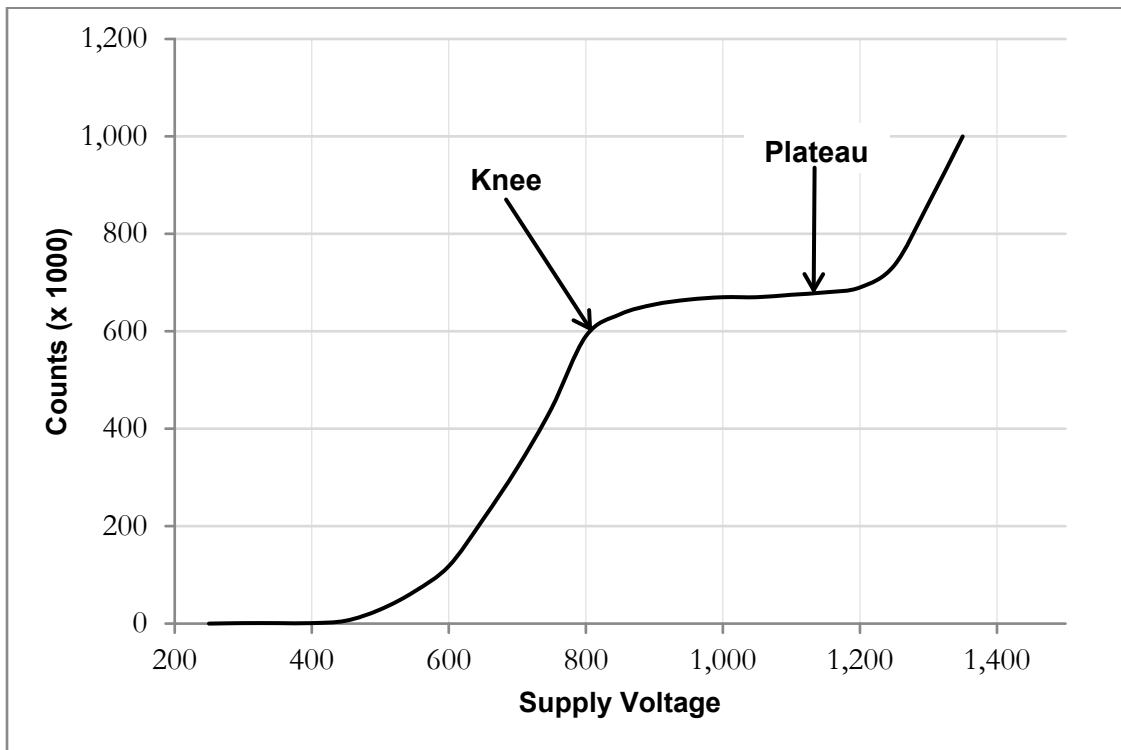


**Figure 5-26** Example Voltage Plateau for a New Detector

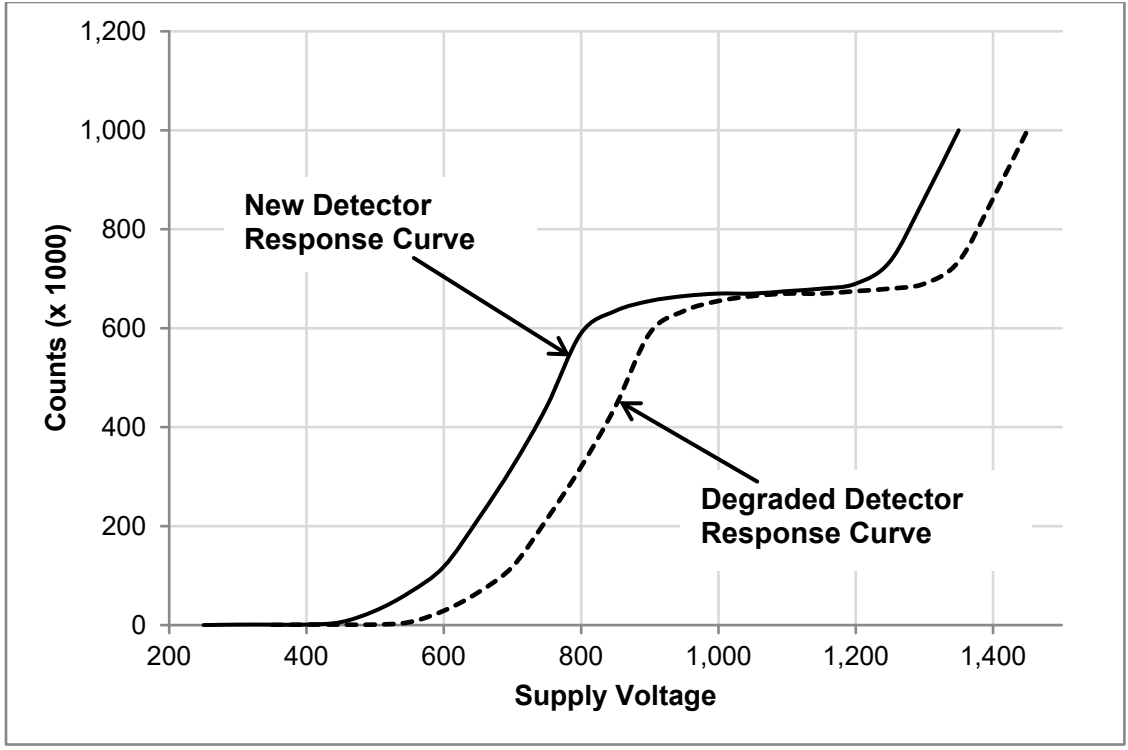


Figure 5-27 Example Voltage Plateau for a New Detector with a Degraded Signal

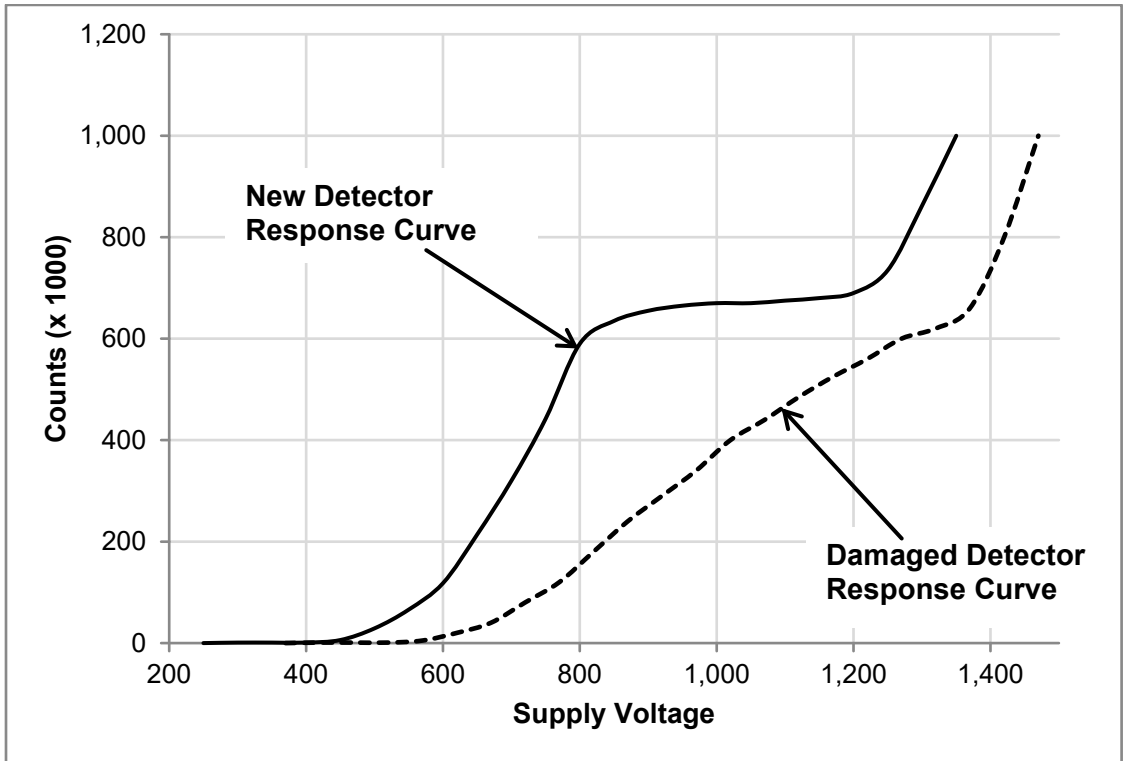


Figure 5-28 Example Voltage Plateau for a Detector with a Damaged Crystal

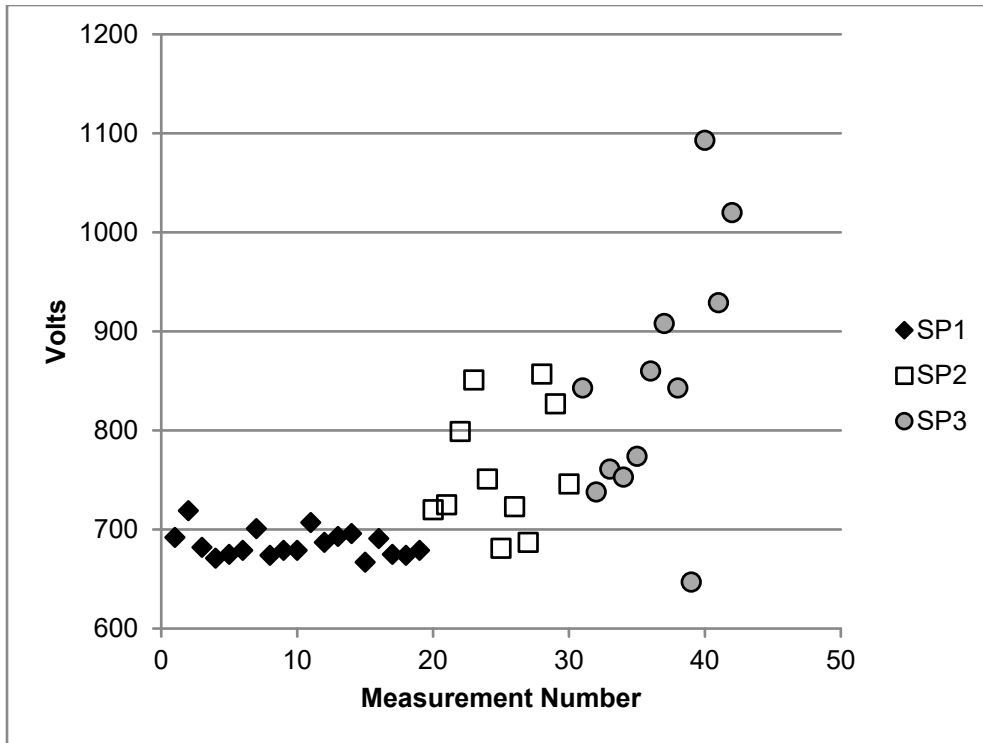


Figure 5-29 Peak Voltages by Subpopulation

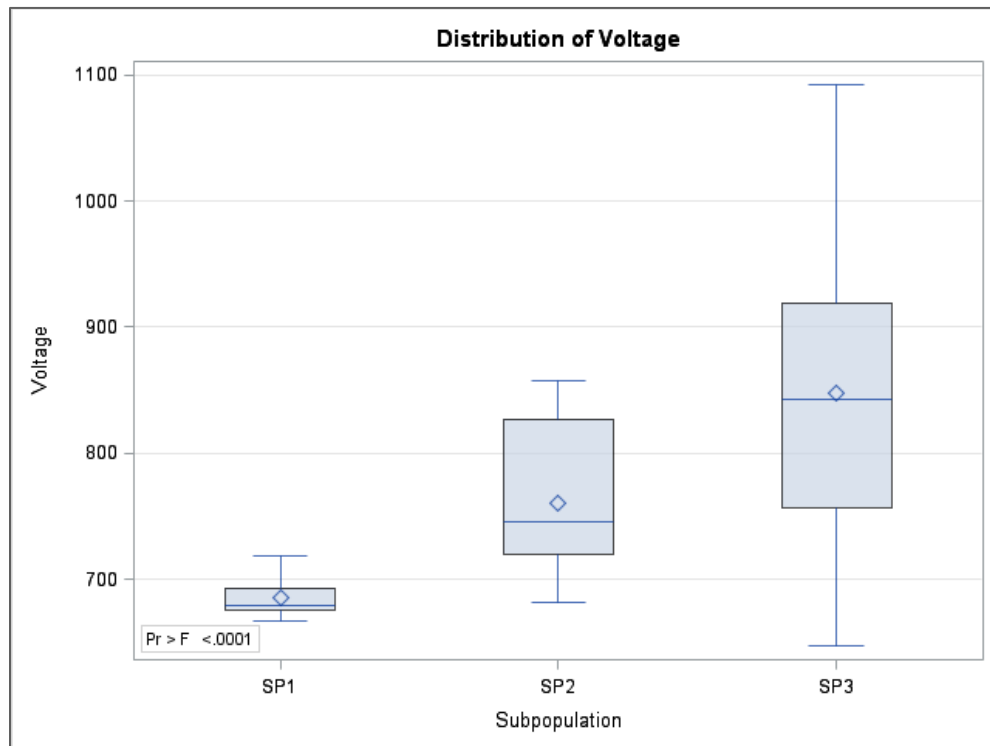


Figure 5-30 Quartile Plot of Voltages Producing Peak Detector Responses



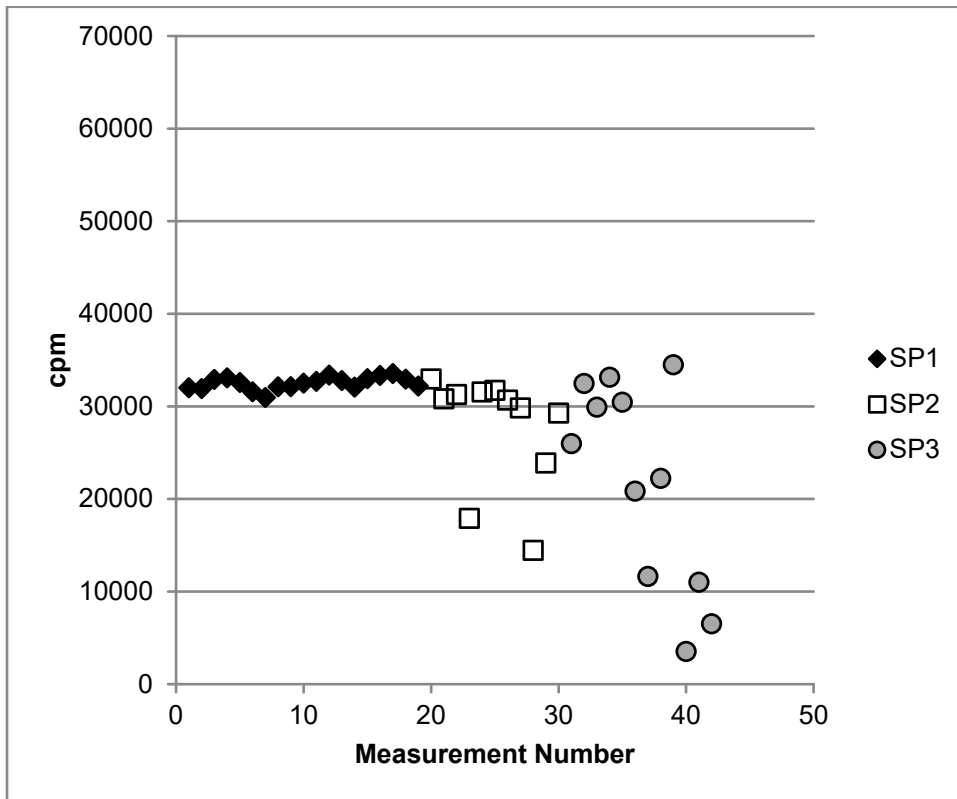


Figure 5-31 Counts per Minute for Am-241 by Subpopulation at 900 Volts

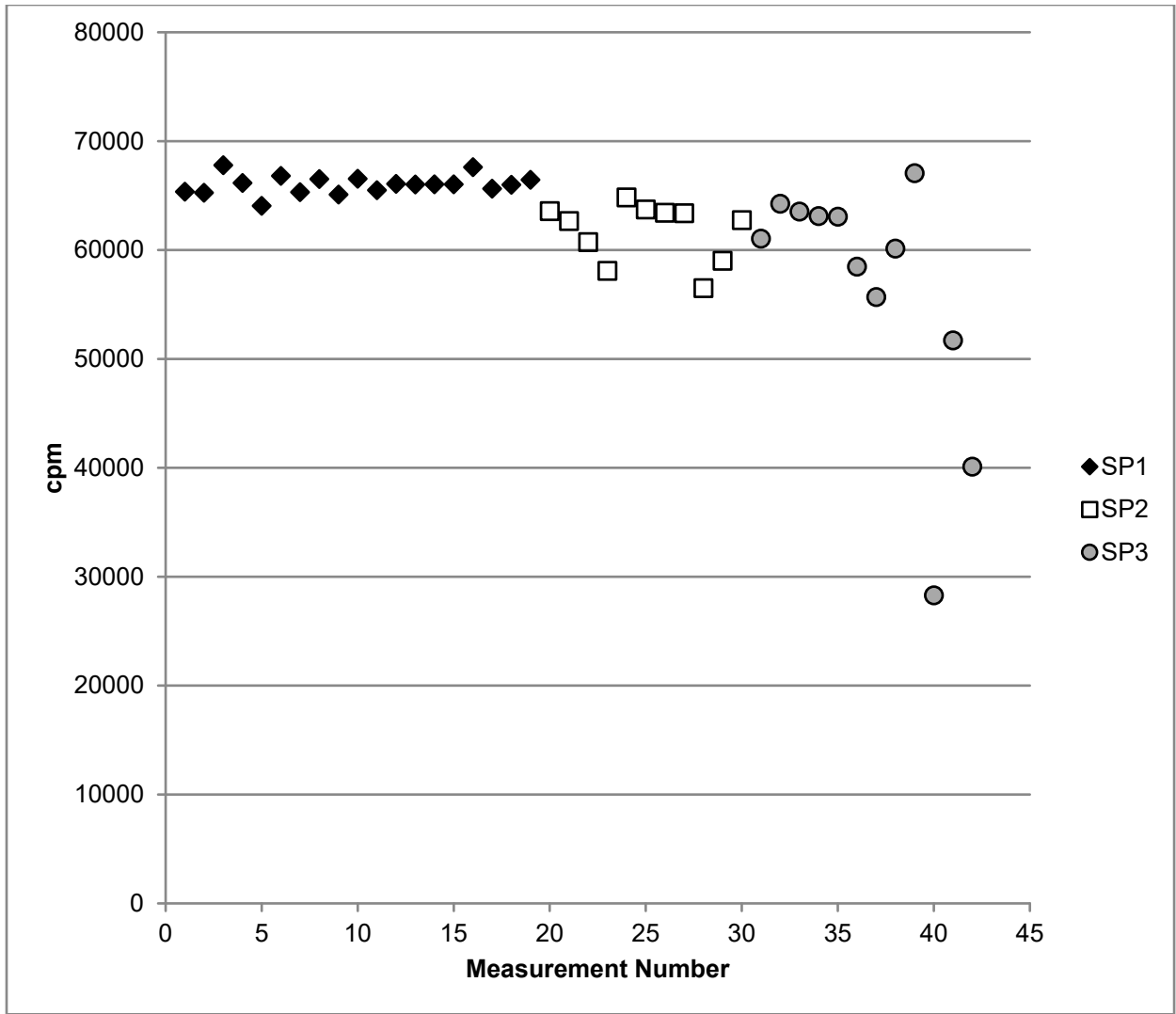
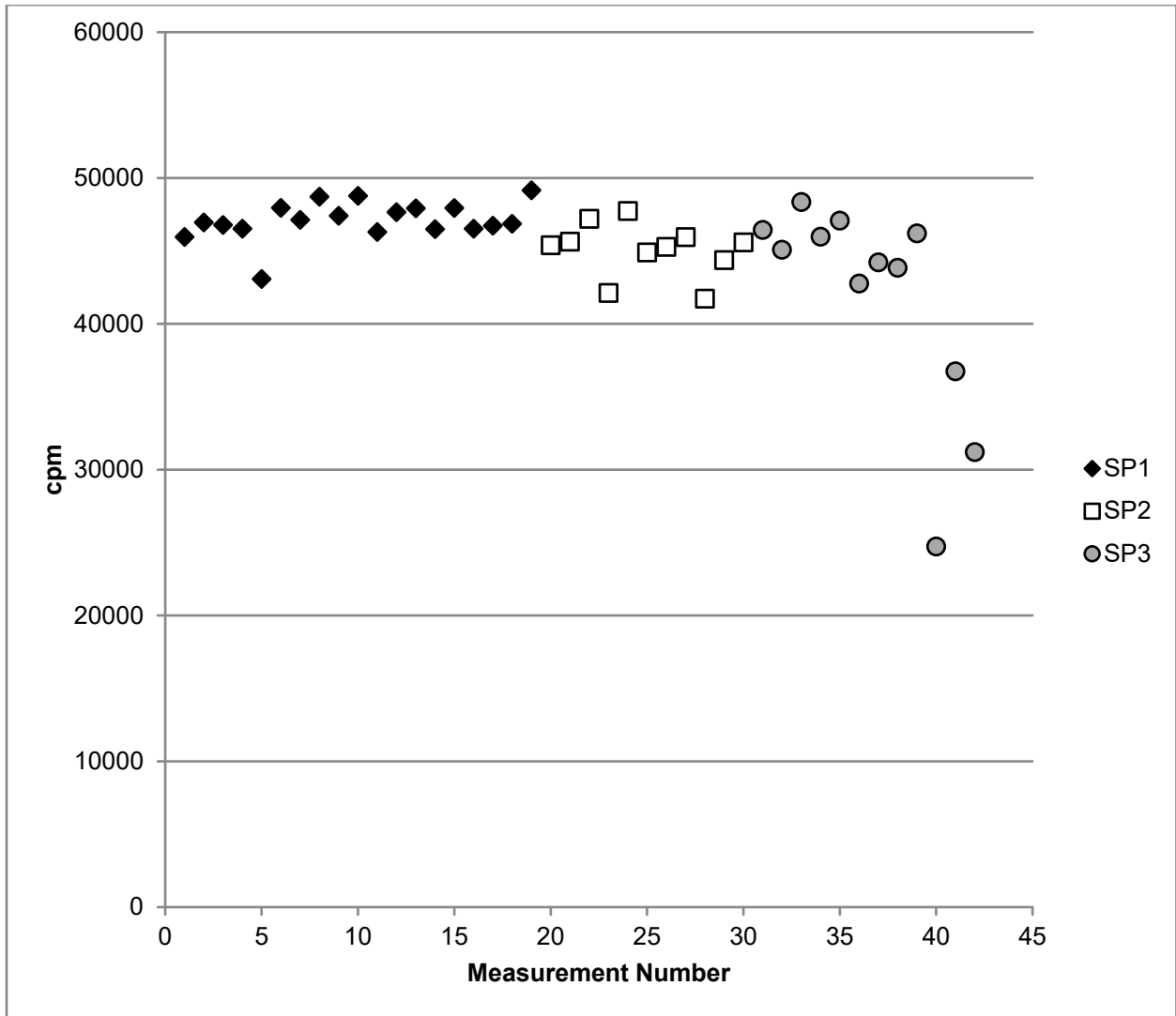


Figure 5-32 Counts per Minute for Cs-137 by Subpopulation at 900 Volts



**Figure 5-33 Counts per Minute for Co-60 by Subpopulation at 900 Volts**

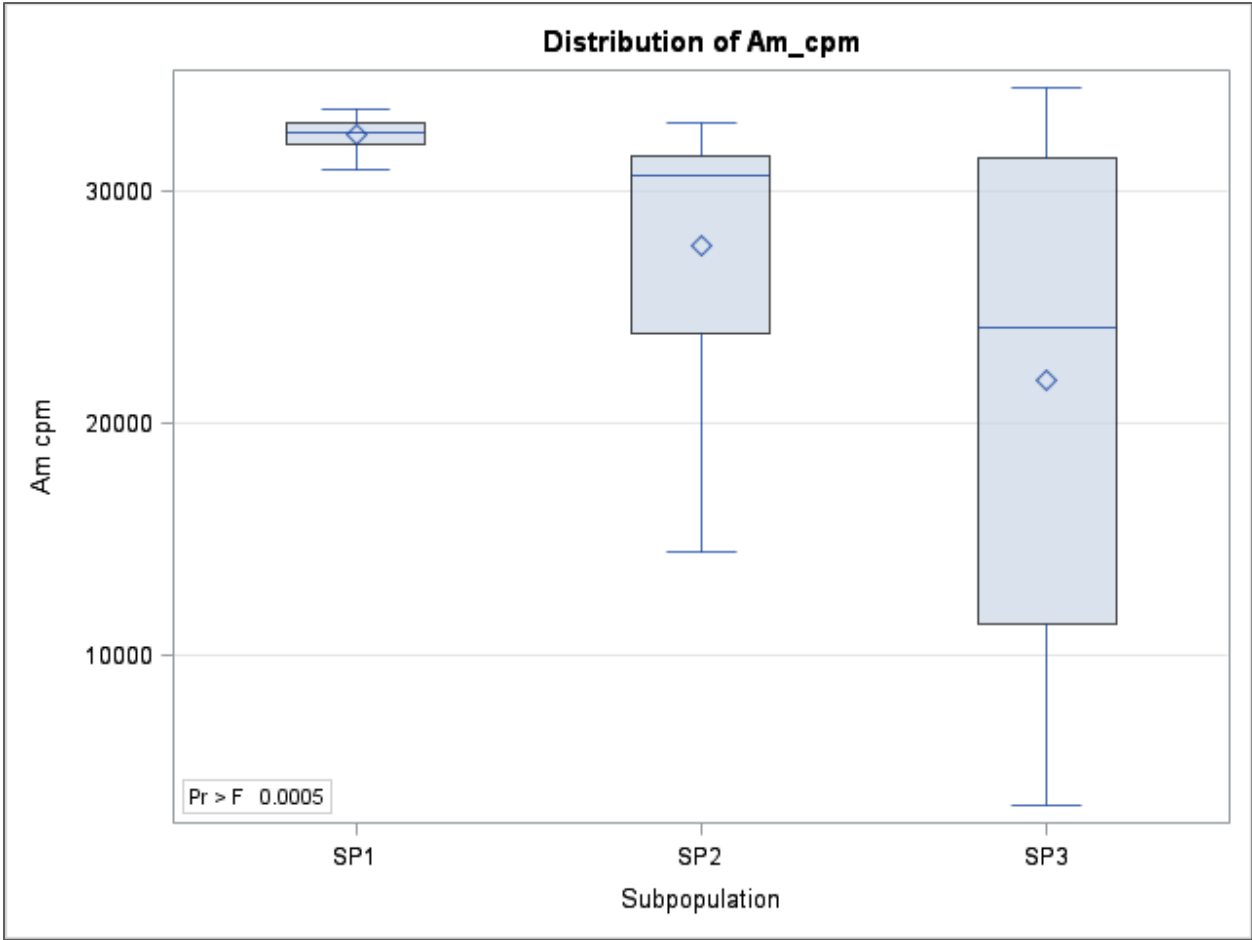
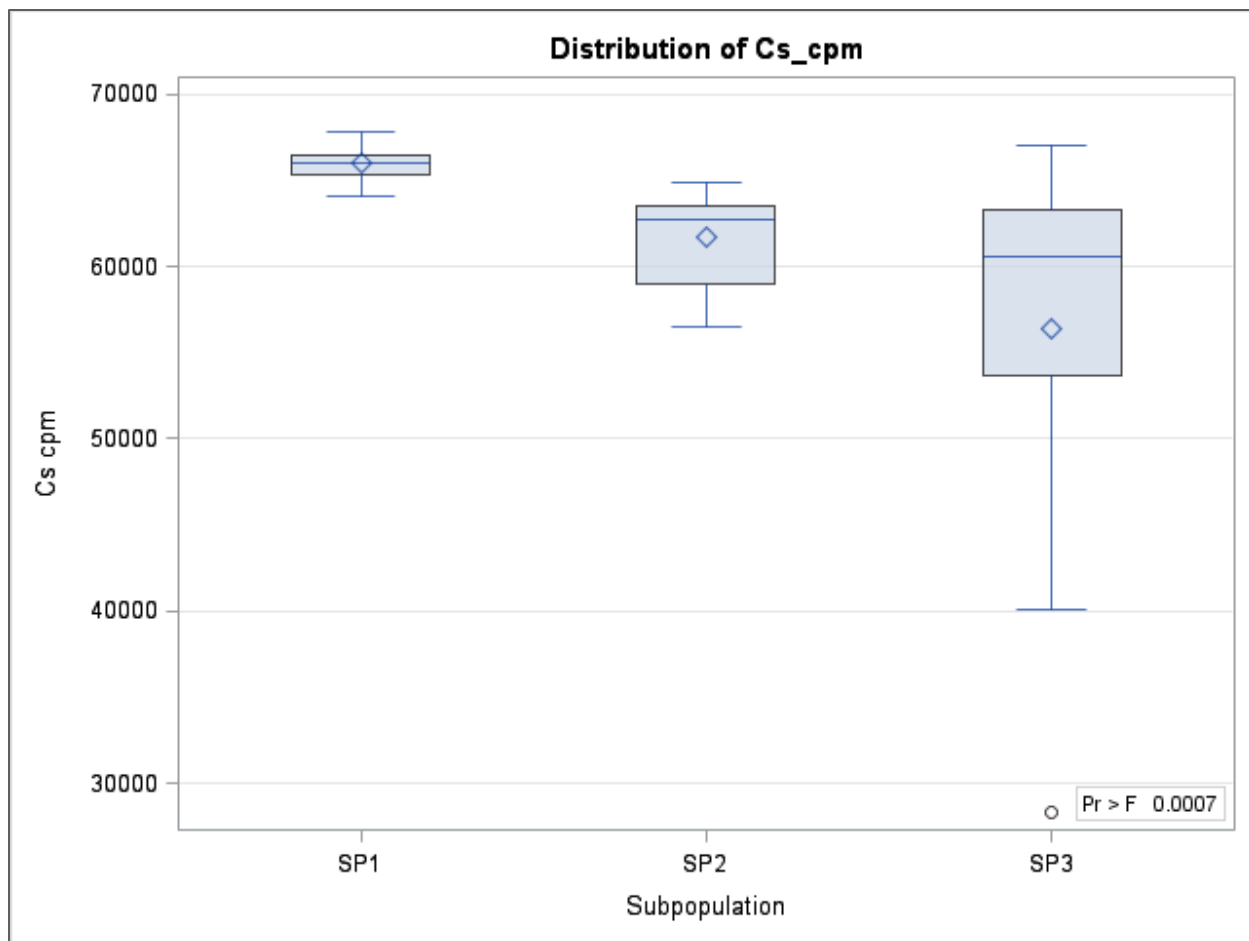


Figure 5-34 Quartile Plot of Response for Am-241 at 900 Volts



**Figure 5-35** Quartile Plot of Response for Cs-137 at 900 Volts

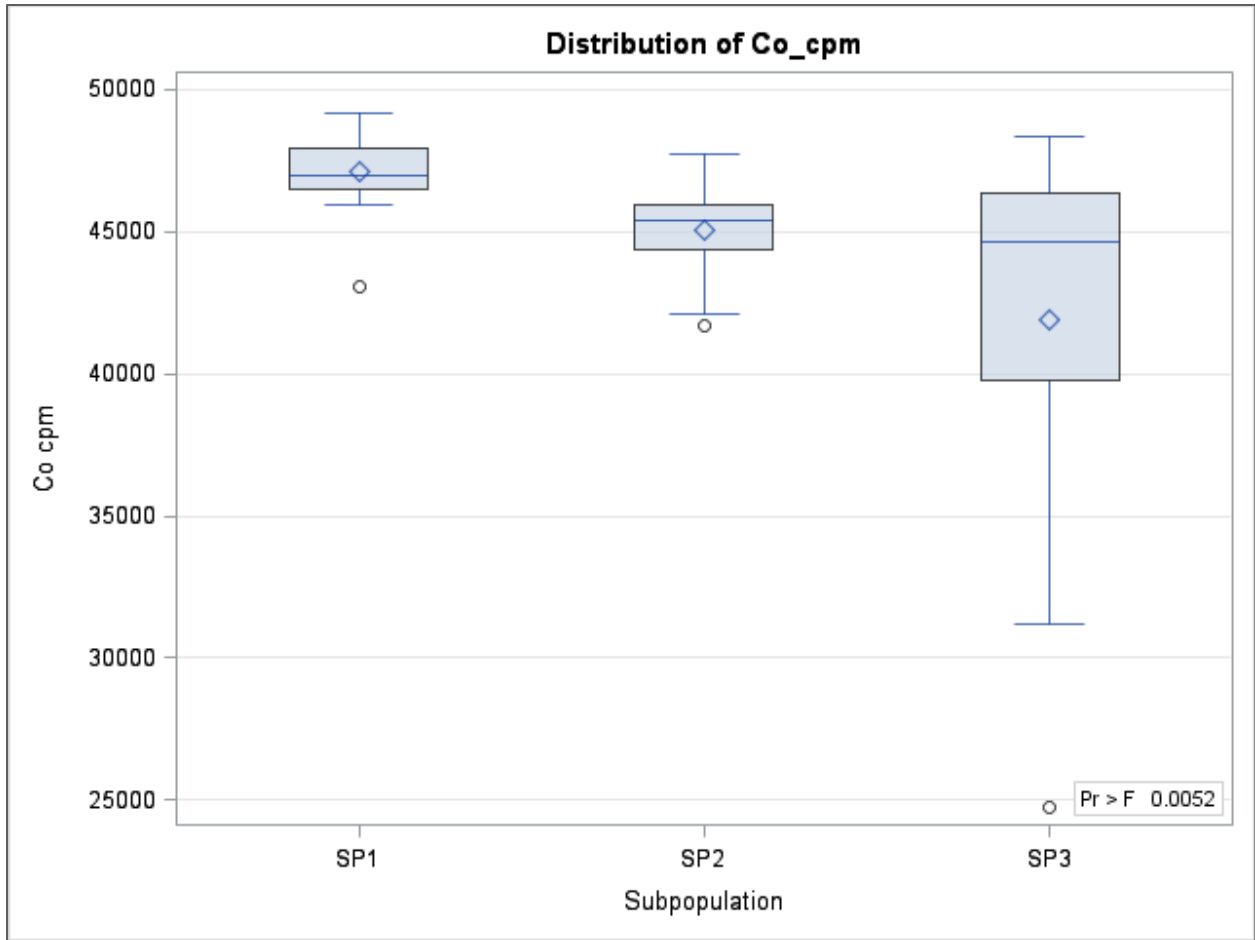
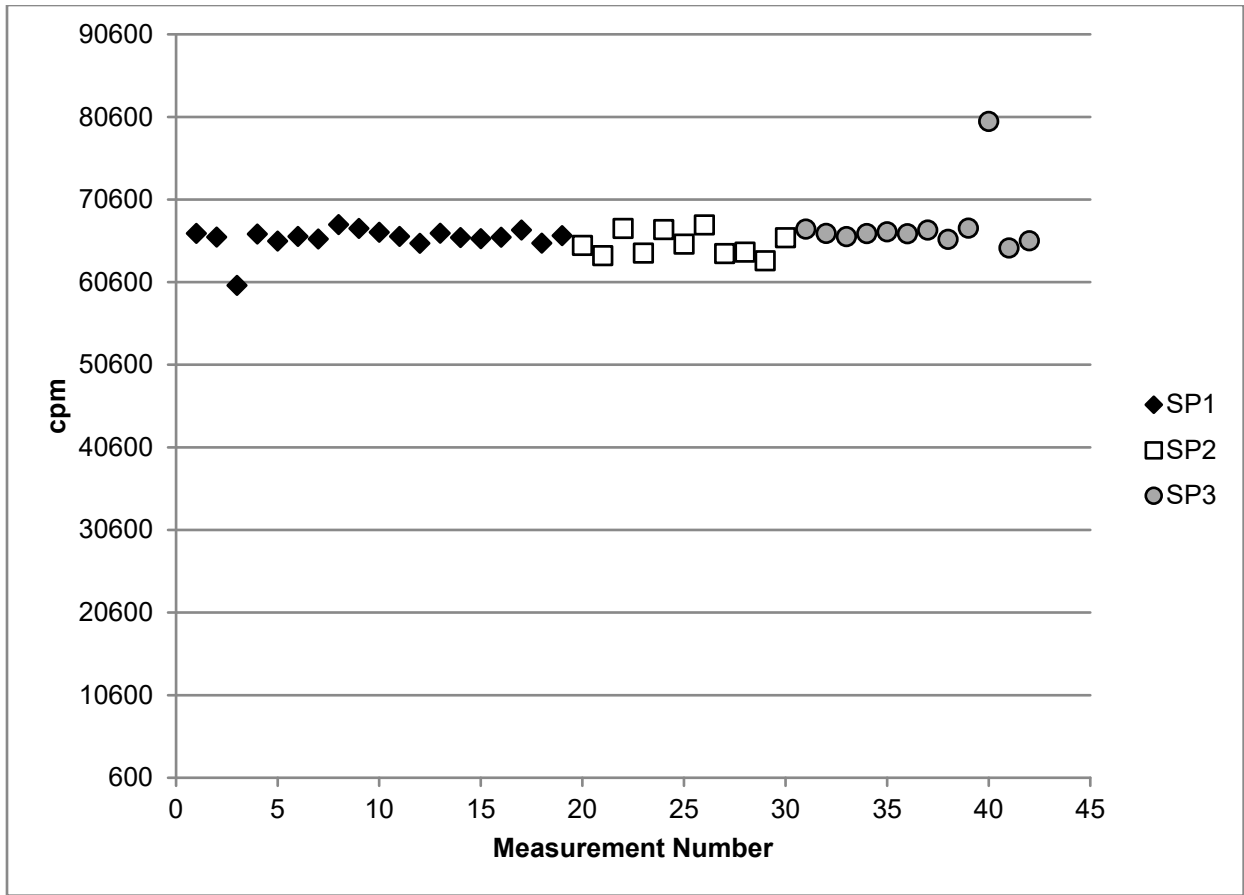


Figure 5-36 Quartile Plot of Response for Co-60 at 900 Volts



**Figure 5-37 Counts Obtained at Peak Voltage, Cs-137 Source**

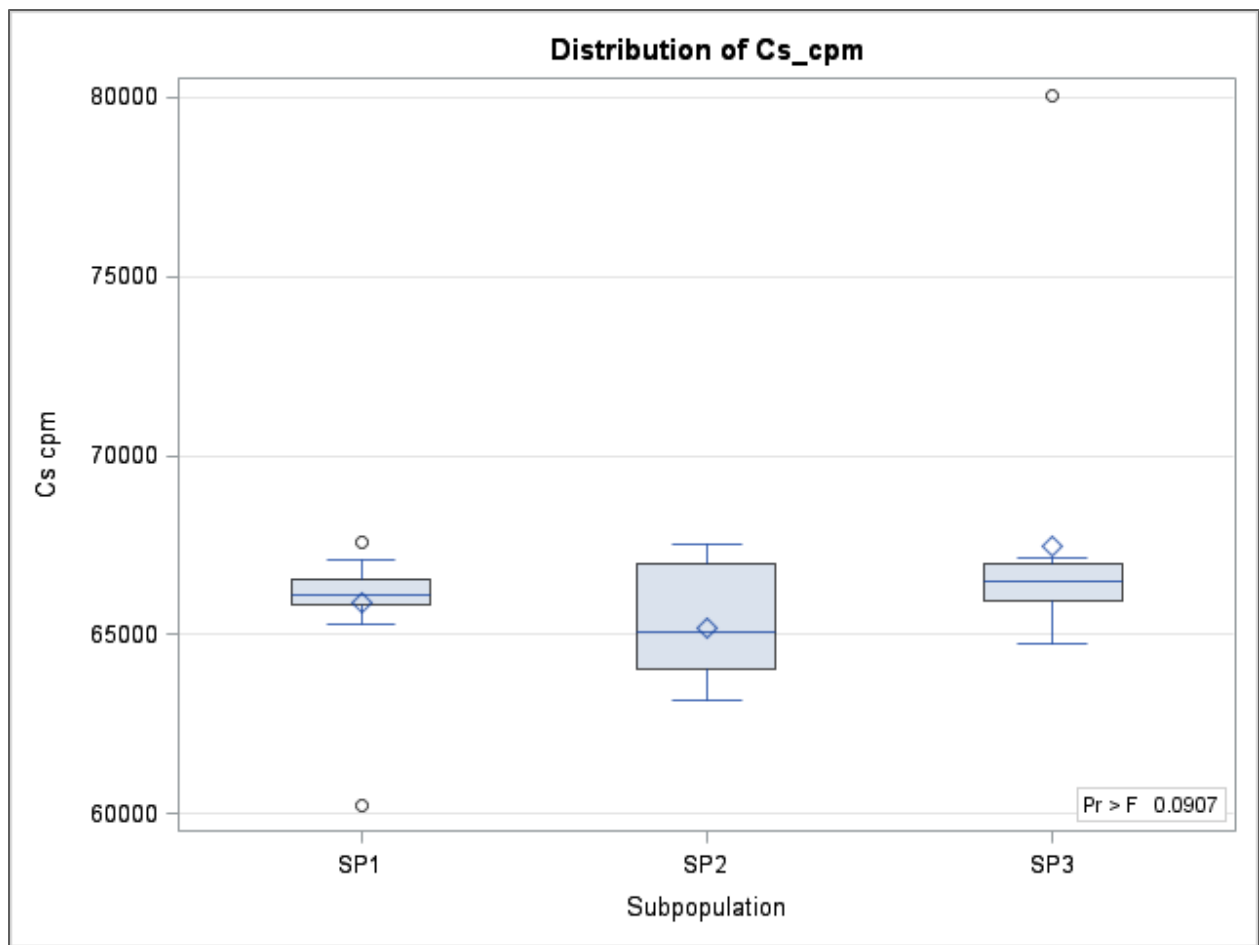


Figure 5-38 Quartile Plot of Response for Cs-137 at Peak Voltage



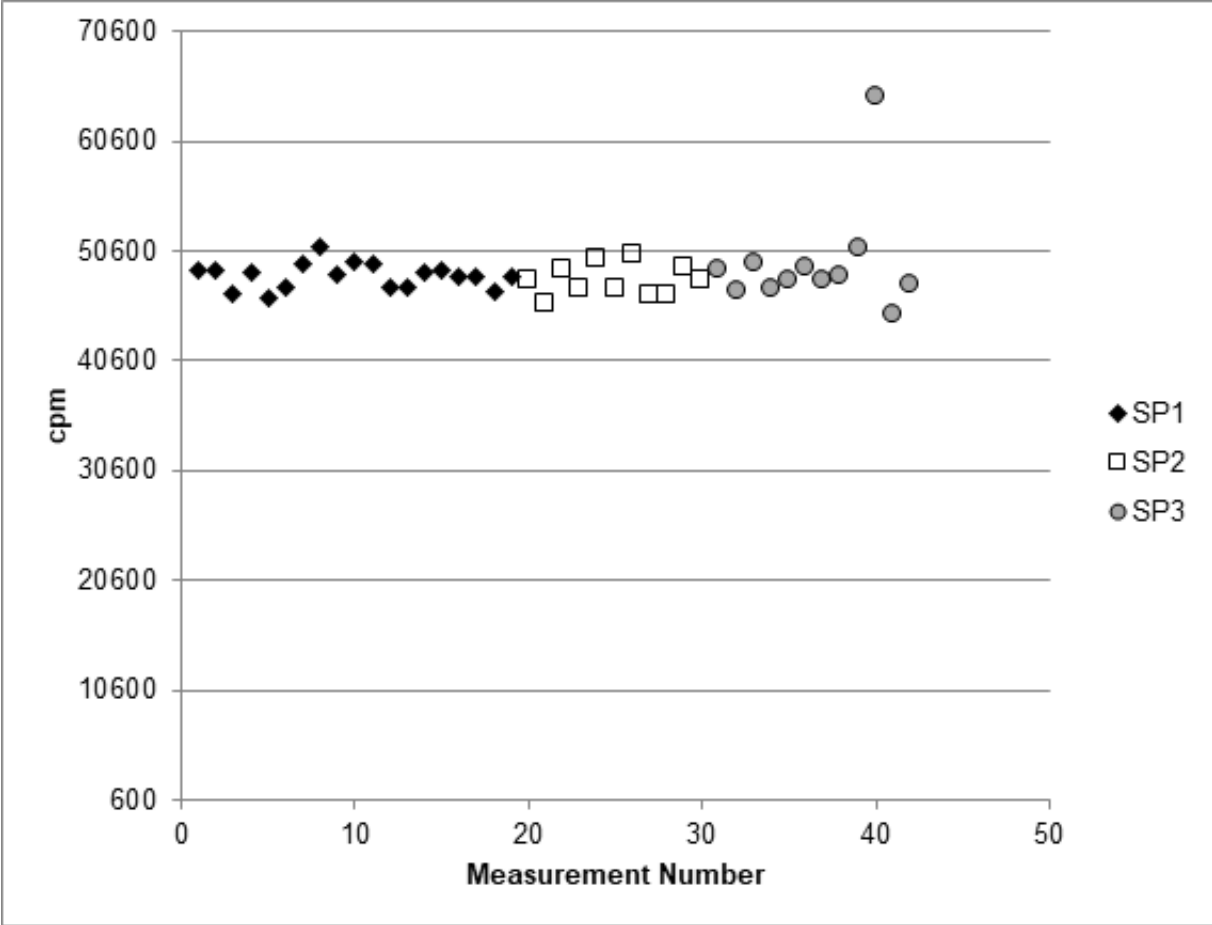


Figure 5-39 Counts Obtained at Cs-137 Peak Voltage, Co-60 Source

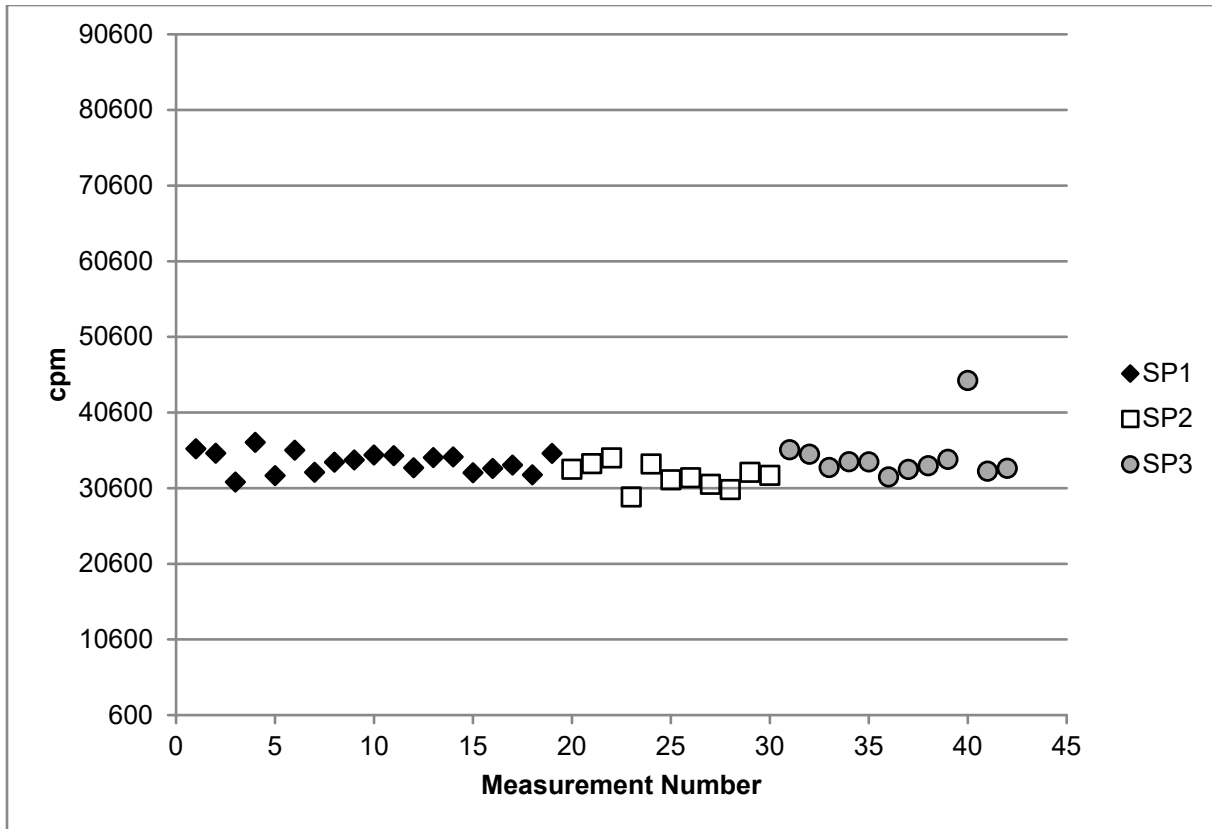


Figure 5-40 Counts Obtained at Cs-137 Peak Voltage, Am-241 Source

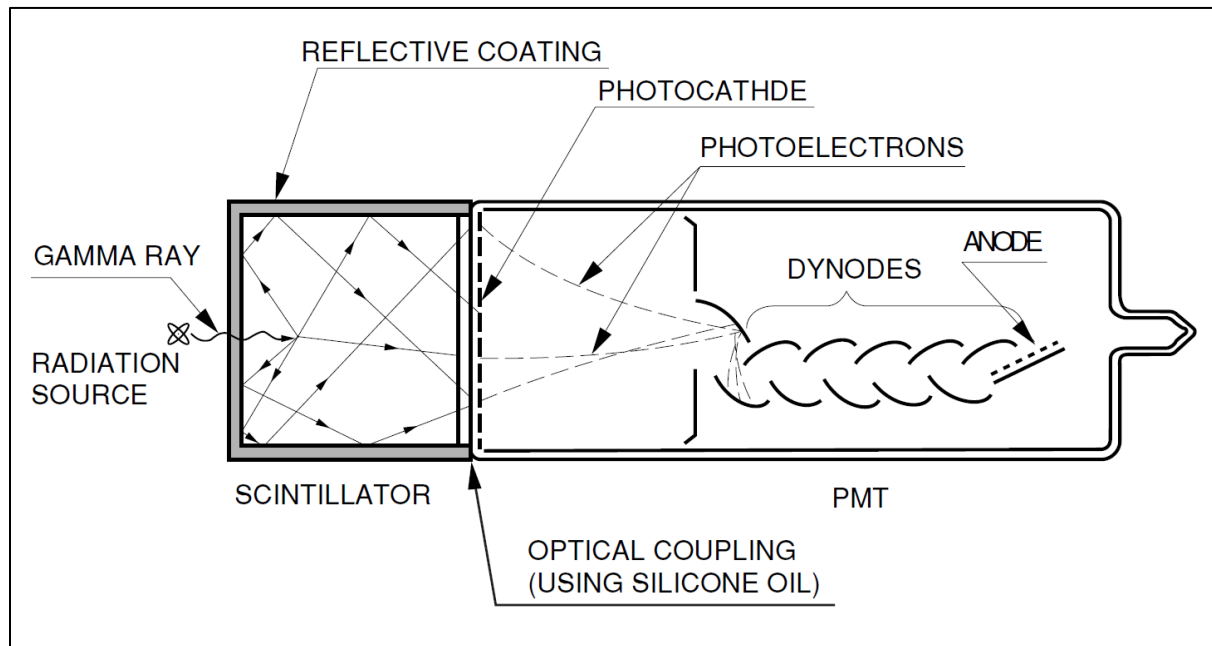


Figure 5-41 Gamma Detection Using an NaI Scintillator and a PMT (Hamamatsu, 2007)

## 6 SCANNING SENSITIVITY

### 6.1 Introduction

Scanning is performed during radiological surveys in support of decommissioning to identify locations of elevated direct radiation that require further investigation. The minimum detectable concentration of a scan survey (scan MDC) depends on the characteristics of the detector (such as efficiency and window area), the nature (type and energy of emissions) and relative distribution of the potential contamination (point versus distributed source and depth of contamination), and other factors related to the physical survey environment. The scan MDC also depends on the surveyor's technique (e.g., scan rate) and ability to decide whether the signal represents only the background count response, or more generally, whether detector response in cpm represents residual contamination in excess of noise (i.e., the background detector response).

The following sections consider surveyor technique and ability, using the traditional approach for estimating the scan MDC during the planning phase of a decommissioning project (*a priori*), when surveyors make contamination detection decisions based on the radiation detector's audible output. Three variables, or human factors, are specifically used to describe the surveyor's decisionmaking abilities: the index of sensitivity ( $d'$ ), the surveyor efficiency ( $p$ ), and the residence time ( $i$ ). Section 6.2 describes the *a priori* scan MDC determination using these human factors.

Advances in data storage and mapping technology have, however, partially or completely separated the surveyor from the decisionmaking process. That is, some surveyors are instructed simply to collect the data without listening to the audible detector response. Contamination detection decisions under this scenario are made during the assessment phase of a decommissioning project (*a posteriori*). In this scenario,  $d'$  is not relevant for making assessment phase decisions. Section 6.3 describes methods for estimating an investigation level based on the *a posteriori* (assessment phase) approach, when data analysts, not surveyors, make contamination detection decisions based on a review of digitally collected and processed survey data.

Decommissioning planners can estimate the *a priori* scan MDC using the methods described in Section 6.2, or they can set an *a posteriori* action level using the methods described in Section 6.3. Section 6.4 presents an example of data quality objectives for two parallel decommissioning projects, one that relies on surveyors to locate hotspots and make judgmental sampling decisions and one that relies on GIS technicians to locate hotspots and make judgmental sampling decisions. Section 6.5 contains conclusions and recommendations intended to harmonize *a priori* and *a posteriori* decisionmaking processes.

Underlying this entire discussion is the assumption that decommissioning projects will compare scan MDCs against established cleanup goals. As in the MARSSIM approach, these cleanup goals, or DCGLs, will be developed using project-specific DQOs that address some of the inputs used to calculate investigation levels (either *a priori* or *a posteriori*). In other words, the examples provided here should not be accepted without considering the specific requirements of projects, sites, and stakeholders.

## 6.2 Human Factors and *A Priori* Scan MDC Calculations

The *a priori* scan MDC is determined by (1) estimating the net minimum detectable count rate (MDCR) that a surveyor can distinguish from the background detector response, and (2) applying efficiency factors that relate to the surveyor, instrumentation, and source of radiation. Generically, these factors may be mathematically described as follows:

$$\text{Scan MDC} = \frac{\text{MDCR}}{(\text{Surveyor Eff.}) \times (\text{Instrument Effs.}) \times (\text{Source Effs.})} \quad (\text{Eq. 6.1})$$

where efficiencies (“Effs.”) are used to convert MDCR in cpm to a quantity that is directly comparable to a cleanup goal (e.g., dpm/100 cm<sup>2</sup> for surfaces or pCi/g for soil). Of the Equation 6.1 terms, the instrument efficiency is either known (e.g., from the literature) or calculated. The source efficiency may be determined by modeling the radionuclide contamination in a specific geometry and includes considerations of material density and contaminant depth distribution. However, the MDCR and surveyor efficiency are estimated considering human factors that can be challenging to quantify or justify; these two inputs are addressed first because they are produced using the same approach no matter the target medium (i.e., building or structure surfaces, land areas, or other volumetric sources).

NUREG/CR-6364, “Human Performance in Radiological Survey Scanning,” published March 1998, discusses in detail the human factors as they relate to surveyor performance during scan surveys. During the planning phase of a decommissioning project, these human factors are used to predict a surveyor’s ability to identify contamination in the environment using a detector’s audio response (i.e., audible “clicks”). Some factors that may affect the surveyor’s performance include the costs associated with various outcomes (e.g., the cost of missed contamination versus the cost of incorrectly identifying areas as being contaminated) and the surveyor’s *a priori* expectation of the likelihood of contamination present. For example, if the surveyor believes that the potential for contamination is very low, as in a presumably unaffected area, a relatively large signal may be required for the surveyor to conclude that contamination is present.

Signal detection theory provides a framework for deciding whether the audible output of the survey meter during scanning resulted from background or signal plus background levels. An index of sensitivity ( $d'$ ) that represents the distance between the means of the background and background plus signal, in units of their common standard deviation, can be calculated for various decision errors—Type I error ( $\alpha$ ), and Type II error ( $\beta$ ). As an example, for a correct detection or true positive rate of 95 percent ( $1-\beta$ ) and a false positive rate ( $\alpha$ ) of 5 percent,  $d'$  is 3.29 (similar to the static MDC in Section 3 for the same decision error rates). The index of sensitivity is independent of human factors, and therefore, the ability of an ideal observer (a theoretical construct) may be used to determine the minimum  $d'$  that can be achieved for particular decision errors. The ideal observer makes optimal use of the available information to maximize the percentage of correct responses, providing an effective upper bound for comparisons with actual surveyors. The resulting expression for the ideal observer’s MDCR, in cpm, can be written as the following:

$$\text{MDCR} = s_i \times (60/i) = d' \times \sqrt{b_i} \times (60/i) \quad (\text{Eq. 6.2})$$

where:

*MDCR* = minimum detectable (net) count rate for the ideal observer in cpm

$s_i$  = minimum detectable number of net source counts in the observation interval

$d'$  = the index of sensitivity

$b_i$  = background counts in the observation interval

$i$  = observational interval (in seconds), based on the scan speed and areal extent of the contamination

Table 6-2 presents example MDCR values for a wide range of background levels. For the less-than-ideal (i.e., human) observer, the surveyor efficiency ( $p$ ) is applied to the minimum detectable number of net source counts ( $s_i$ ) and, therefore, the MDCR. This term accounts for the real-world condition that the surveyor will perform less efficiently than the ideal observer:

$$\text{MDCR}_{\text{surveyor}} = \frac{s_i \times (60/i)}{\sqrt{p}} = \frac{d' \times \sqrt{b_i} \times (60/i)}{\sqrt{p}} \quad (\text{Eq. 6.3})$$

The generic scan MDC equation may now be rewritten as follows:

$$\text{Scan MDC} = \frac{d' \times \sqrt{b_i} \times (60/i)}{\sqrt{p} \times (\text{Instrument Eff.}) \times (\text{Source Eff.})} \quad (\text{Eq. 6.4})$$

The following subsections describe and give the rationale for selecting the human factor input  $d'$ ,  $p$ , and  $i$ .

### 6.2.1 Index of Sensitivity

The audible detector response available to the surveyor can arise from either noise alone or from signal-plus-noise and can be represented by two (typically overlapping) probability density distributions (Figure 6-1). The task of the surveyor is to indicate whether an increase in survey instrument output arose from a “noise alone” or a “noise plus signal” event. To make this decision, a criterion must be established at some point along the continuum (e.g., once the criterion point is set, any measurement greater (to the right) than the criterion will be interpreted as contamination). If the underlying distributions can be assumed to be normal and of equal variance, an index of sensitivity ( $d'$ ) can be calculated that represents the distance between the means of the distributions in units of their common standard deviations. The index is calculated by transforming the true positive and false positive rates to standard deviation units (i.e., z-scores) (Egan, 1975, p. 61) and taking the difference:

$$d' = z (\text{false positive}) - z (\text{true positive}) \quad (\text{Eq. 6.5})$$

Table 6-1 shows values of  $d'$  associated with various true positive and false positive rates. The  $d'$  measure is independent of the criterion adopted by the surveyor, thus allowing meaningful comparisons of sensitivity under conditions in which surveyors' criteria may be different. It is conventional in signal detection theory analysis to describe performance in terms of the true positive rate ( $1-\beta$ ) and the false positive rate ( $\alpha$ ). True and false positive rates can be established on program-, site-, project-, or survey-specific bases and documented, for example, as part of DQO development in the decommissioning plan.

As an example, a decommissioning project receives approval for a 5-percent probability of concluding that radiation levels are below the scan MDC when, in fact, radiation levels above

the scan MDC are present. This Type I error presumes that the ideal observer will identify contamination above the scan MDC 95 percent of the time. The decommissioning contractor must also accept some probability that the surveyor will identify contamination when none is actually present. This Type II error may result in additional measurements, samples, or cleanup (cost to the project) when none was actually required. The contractor has accepted a false positive rate of 25 percent, meaning there is a 25-percent probability the ideal observer will incorrectly conclude that radiation levels are present above the scan MDC when they are not. With a true positive rate of 95 percent and the false positive rate of 25 percent, the project-specific  $d'$  value is 2.32.

## 6.2.2 Surveyor Efficiency

It was assumed that a surveyor's performance can be related to that expected of an ideal observer by an efficiency factor ( $p$ ), which represents the probability that an audible detector response above the scan MDC will be identified. This value is used to consider the efficiency of the surveyor relative to an ideal observer, which is a minimum increment in counting rate that could be detected based on the desired true-positive rate, false positive limit, and observation interval. NUREG/CR-6364 describes experiments demonstrating that (1) even under ideal circumstances (i.e., with defined observation intervals) humans do not perform at 100-percent efficiency (i.e., they are less efficient than the ideal observer) and (2) in scanning, where actual observation intervals may vary considerably without mechanical assistance, the efficiency of the surveyor (relative to the ideal observer) declines further. The factors that affect an individual's performance include, but are not limited to, survey technique, experience, the cost of false positive and false negative decision errors, and the *a priori* expectation of the likelihood that contamination will be identified. The results of an experiment on defined-interval confidence rating indicate that  $p$ , as a general rule, is no greater than 0.75, but an efficiency value of 0.5 may be the more appropriate default for estimating field performance during the planning phase of a decommissioning project (see NUREG/CR-6364 for details).

To adjust an estimated MDCR as calculated previously to reflect an assumed efficiency, the counting rate is divided by the square root of the efficiency to provide a surveyor-specific MDCR ( $MDCR_{surveyor}$ ), as follows (also see Equation 6.3):

$$MDCR_{surveyor} = \frac{MDCR}{\sqrt{p}} \quad (\text{Eq. 6.6})$$

Some controls can be implemented during project planning to optimize the surveyor efficiency. For example, individual surveyors can be blind tested to demonstrate their proficiency in conducting surveys according to procedure and in identifying hidden radiation sources at or just above the MDCR during, for example, qualifications testing. Scan coverage may also be optimized using actual or virtual grid lines that help keep surveyors within desired survey lanes. Like the index of sensitivity,  $p$  can be established on program-, site-, project-, or survey-specific bases and documented, for example, as part of DQO development in the decommissioning plan.

As an example, a decommissioning project will conduct a 100-percent survey of a land area suspected of containing moderately elevated concentrations of Cs-137. The survey team includes highly experienced technicians who have demonstrated proficiency in identifying small areas of elevated activity. The decommissioning plan also specifies that 1.5-meter survey lanes will be established over the survey area, giving surveyors visual lane references. Based on

empirical data and established controls, project planners believe that the survey team is able to perform at a level closer to the ideal observer; thus, selecting a  $p$  of 0.75 is considered justified.

### 6.2.3 Observation Interval

The observation interval during scanning is the actual time that the detector can respond to the contamination source. It depends on the scan speed, detector orientation, and size of the hotspot. In this context, the size of the hotspot relates to the area of detection defined by the detector-to-source geometry (for instance, a point source of 2 square millimeters may produce an effective hotspot area of over 100 cm<sup>2</sup>). Therefore, the greater the contamination source effective area and the slower the scan rate, the greater the observation interval.

In practice, surveyors do not make detection decisions on the basis of a single indication. Rather, upon noting an increased number of counts, the surveyor will pause briefly and then decide whether to move on or take further measurements. Thus, scanning consists of two components: continuous monitoring and stationary sampling. In the first component, characterized by continuous movement of the probe, the surveyor may have only a brief “look” at potential sources, determined by the scan speed and the size of the hotspot. The surveyor’s willingness to decide that a signal is present at this stage is likely to be liberal, in that the surveyor should respond positively on scant evidence, because the only “cost” of a false positive is a little time. The second component occurs only after a positive response was made at the first stage. The surveyor marks it, interrupting his scanning and holding the probe stationary over the “source” for a period of time while comparing the instrument output signal during that time to the background count rate.

Because scanning can be divided into two stages, the surveyor’s scan sensitivity must be considered for each of the stages. Typically, the MDCR associated with the first scanning stage will be greater because of the brief observation intervals of continuous monitoring, provided that the length of the pause during the second stage is significantly longer. Typically, observation intervals during the first stage are on the order of 1 or 2 seconds, while the second-stage pause may be several seconds long.

The greater value of MDCR from each of the scan stages is used to determine the scan sensitivity for the surveyor, as the following example shows.

A site planner is tasked with estimating the MDCR for a gas proportional detector with an established background count rate of 350 cpm and a project-approved  $d'$  of 1.96. Preliminary data suggest there are small areas of elevated activity on the order of 100 cm<sup>2</sup> and smaller. Some members of the survey team lack experience, so site planners have selected a conservative surveyor efficiency of 0.5. A surveyor moving a detector at one detector width per second across the center of a hypothetical 100-cm<sup>2</sup> hotspot will have an observation interval of about 1 second (assuming a nonvarying cross-section), so the MDCR and the MDCR<sub>surveyor</sub> are as follows:

$$(1) \quad b_i = (350 \text{ cpm}) \times (1 \text{ sec}) \times (1 \text{ min}/60 \text{ sec}) = 5.8 \text{ counts}$$

$$(2) \quad \text{MDCR} = (1.96) \times \left( \sqrt{\left( \frac{350 \text{ cpm}}{60 \text{ sec}} \right)} \right) \times (60 \text{ sec}/1 \text{ min}) = 284 \text{ cpm}$$

$$(3) \quad \text{MDCR}_{\text{surveyor}} = \frac{\text{MDCR}}{\sqrt{p}} = \frac{284}{\sqrt{0.5}}, \text{ or alternatively:}$$

$$MDCR_{\text{surveyor}} = 1.96 \times \sqrt{\frac{350 \text{ cpm}}{0.5} \times \frac{1 \text{ min}}{60 \text{ sec}} \times \frac{1 \text{ sec}}{\text{interval}}} \times \left(\frac{60 \text{ sec}}{1 \text{ sec}}\right) = 402 \text{ cpm}$$

Therefore, if the surveyors do not pause or pause only briefly, a gross response of 350 + 402 = 752 cpm (more than twice background) is the estimated *a priori* minimum detectable gross response that would warrant additional investigations. Based on this result, the project instructs the surveyors to slow the pace to 0.5 detector widths per second to increase the observation interval and therefore the probability of identifying contamination. The  $MDCR_{\text{surveyor}}$  is, therefore, adjusted for a 2-second observational interval as follows:

$$MDCR_{\text{surveyor}} = 1.96 \times \sqrt{\frac{350 \text{ cpm}}{0.5} \times \frac{1 \text{ min}}{60 \text{ sec}} \times \frac{2 \text{ sec}}{\text{interval}}} \times \left(\frac{60 \text{ sec}}{2 \text{ sec}}\right) = 284 \text{ cpm}$$

The gross response that would warrant a followup investigation is now 350 + 284 = 634 cpm. The project accepted this value and added it to the decommissioning plan.

The next two sections discuss the methods for estimating *a priori* scan MDCs for building and structure surfaces (Section 6.2.4) and land areas (Section 6.2.5).

## 6.2.4 A Priori Scan MDCs for Building and Structure Surfaces

To select instrumentation, the survey design for determining the number of data points for areas of elevated activity (as in the MARSSIM guidance) depends on the scan MDC. In general, alpha or beta scans are performed on structure surfaces to satisfy the survey design for elevated activity measurements, while gamma scans are used for land areas. Because of their low background levels, the determination of scan MDCs for alpha-only emitting contaminants must be considered separately from beta-emitters (or alpha-plus-beta emitters in a mixed source). Therefore, Section 6.2.4.1 addresses the scan MDC for beta-emitters, and Section 6.2.4.2 addresses this topic for alpha-emitters.

### 6.2.4.1 A Priori Scan MDCs for Beta-Emitters

The *a priori* scan MDC for building and structure surfaces is determined from the MDCR by applying conversion factors that account for surveyor, detector, and source efficiencies. The MDCR and surveyor efficiency are described above. The detector and source efficiencies are applied to the scan MDC calculation for building and structural surfaces as follows:

$$\text{Scan MDC} = \frac{MDCR}{\sqrt{p} \times (\text{Instrument Effs.}) \times (\text{Source Effs.})} = \frac{d' \times \sqrt{b_i} \times (60/i)}{\sqrt{p} \epsilon_i \epsilon_s \frac{\text{probe area}}{100}} \quad (\text{Eq. 6.7})$$

where:

$\epsilon_i$  is the instrument efficiency (see Section 4)

$\epsilon_s$  is the surface efficiency (see Section 5)

*probe area* is the physical probe area of the radiation detector (cm<sup>2</sup>)

Note that the probe area is divided by 100 to obtain the Scan MDC in units of dpm/100 cm<sup>2</sup>.

For example, the scan MDC (in dpm/100 cm<sup>2</sup>) for Tc-99 on a target material may be determined for a background level of 200 cpm and a 1-second observation interval using a hand-held gas proportional detector (126-cm<sup>2</sup> probe area). For a specified level of performance at the first scanning stage of 95-percent true positive rate and 25-percent false positive rate,  $d'$  equals 2.32 (Table 6-1). The approved site-specific DCGL<sub>EMC</sub> is 2,000 dpm/100 cm<sup>2</sup> (over a 100-cm<sup>2</sup> area),



and a project objective calls for the use of scan MDCs no larger than the hotspot limit, if reasonably achievable. Project procedures indicate a survey rate of no more than one detector width per second. For a hypothetical hotspot of about 100 cm<sup>2</sup>, this gives an observation interval of about 1 second. Using a surveyor efficiency of 0.5, and assuming instrument and surface efficiencies of 0.44 and 0.25, respectively, the scan MDC is calculated as follows:

(1)  $b_i = (200 \text{ cpm}) \times (1 \text{ sec}) \times (1 \text{ min}/60 \text{ sec}) = 3.3 \text{ counts}$

(2)  $MDCR = (2.32) \times \left( \sqrt{\left( \frac{200 \text{ cpm}}{60 \text{ sec}} \right)} \right) \times (60 \text{ sec}/1 \text{ sec}) = 254.1 \text{ cpm}$

(3) Calculate scan MDC:

$$\text{Scan MDC} = \frac{254.1}{\sqrt{0.5 (0.44)(0.25)(1.26)}} = 2,593 \text{ dpm}/100 \text{ cm}^2$$

This scan MDC is more than the 2,000 dpm/100 cm<sup>2</sup> hotspot DCGL<sub>EMC</sub>. Project planners, therefore, determine that a new scan MDC must be calculated. Efficiencies in this case cannot be improved, so surveyors are instructed to slow the scan rate to half of the detector width per second to produce an observation interval of 2 seconds:

(1)  $b_i = (200 \text{ cpm}) \times (2 \text{ sec}) \times (1 \text{ min}/60 \text{ sec}) = 6.7 \text{ counts}$

(2)  $MDCR = (2.32) \times (\sqrt{6.7}) \times (60 \text{ sec}/2 \text{ sec}) = 179.7 \text{ cpm}$

(3) Calculate scan MDC:

$$\text{Scan MDC} = \frac{179.7}{\sqrt{0.5 (0.44)(0.25)(1.26)}} = 1,834 \text{ dpm}/100 \text{ cm}^2$$

This value is below the 2,000 dpm/100 cm<sup>2</sup> DCGL<sub>EMC</sub>, so site planners conclude that this scan MDC is acceptable for this material. However, there are two target materials, and the second material considered has an average background of 300 cpm. Assuming other parameters remain constant, the calculation steps are as follows:

(1)  $b_i = (300 \text{ cpm}) \times (2 \text{ sec}) \times (1 \text{ min}/60 \text{ sec}) = 10 \text{ counts}$

(2)  $MDCR = (2.32) \times (\sqrt{10}) \times (60 \text{ sec}/2 \text{ sec}) = 220 \text{ cpm}$

(3) Calculate scan MDC:

$$\text{Scan MDC} = \frac{220}{\sqrt{0.5 (0.44)(0.25)(1.26)}} = 2,245 \text{ dpm}/100 \text{ cm}^2$$

This value is more than the DCGL<sub>EMC</sub>, so site planners consider other methods to lower the scan MDC. As a final consideration, planners retain the 95-percent true positive proportion but now accept a 35-percent false positive proportion ( $d' = 2.02$ ). Revisiting the above equations, the final scan MDCs accepted by the project are about 1,597 and about 1,955 dpm/100 cm<sup>2</sup> for the two materials, respectively. Both values are below the DCGL<sub>EMC</sub> and are incorporated into the decommissioning plan. The surveyors are instructed to survey at a rate of about half of the

detector face per second. The surveyor efficiency could also have been adjusted, if justified by empirical data, to lower the scan MDC.

Some of the survey technicians prefer using GM detectors even though they are less sensitive than the gas proportional detector. This is because the GMs are simpler to use and operate and will also fit into tight spaces that would be inaccessible to the gas proportional detector. In response to this preference, the scan MDC is calculated using the same set of  $d'$  and surveyor efficiency requirements. Assuming an average background (for either material) of 60 cpm, a probe area of 20 cm<sup>2</sup>, and instrument and surface efficiencies of 0.18 and 0.25, respectively, the scan MDC is calculated as follows:

- (1)  $b_i = (60 \text{ cpm}) \times (3 \text{ sec}) \times (1 \text{ min}/60 \text{ sec}) = 3 \text{ counts}$
- (2)  $MDCR = (2.02) \times (\sqrt{3}) \times (60 \text{ sec}/3 \text{ sec}) = 70 \text{ cpm}$
- (3) Calculate scan MDC:

$$\text{Scan MDC} = \frac{70}{\sqrt{0.5} (0.18)(0.25)(0.20)} = 10,995.5 \text{ dpm}/100 \text{ cm}^2$$

A 3-second observation interval is used because it will take longer for the detector face to travel over the same area. Even with the longer observation interval, this scan MDC is several times higher than the DCGL<sub>EMC</sub>; thus, it is concluded that the GM is not a suitable detector for this project, and surveyors must use gas proportional detectors.

Finally, a separate example is given for an *a priori* scan MDC for a floor monitor. The scan MDC for a large-area (573-cm<sup>2</sup>) gas proportional floor monitor may be calculated once a hotspot area has been postulated. The postulated hotspot area is necessary not only to determine the observation interval, but also to calculate an appropriate probe area correction. It is typical for the postulated hotspot size to be less than the floor monitor probe area. As described in Section 4, when combined with the small distance between the detector and the postulated hotspot, this large detector surface relative to the hotspot area effectively produces a  $2\pi$  geometric efficiency. Therefore, applying the standard probe area correction of 573 cm<sup>2</sup>/100 cm<sup>2</sup> (5.73) is likely not appropriate. For example, assume that the floor monitor is used to scan a concrete floor for SrY-90 contamination, and the postulated hotspot area is 100 cm<sup>2</sup> (the probe correction factor is unity). Detector parameters include a background level of 1,200 cpm, instrument and surface efficiencies of 0.58 and 0.65, respectively, and a scan rate that yields a 1-second observation interval. The scan MDC is determined for the same level of performance ( $d'$  equals 2.32):

- (1)  $b_i = (1,200 \text{ cpm}) \times (1 \text{ sec}) \times (1 \text{ min}/60 \text{ sec}) = 20 \text{ counts}$
- (2)  $MDCR = (2.32) \times (\sqrt{20}) \times (60 \text{ sec}/1 \text{ sec}) = 623 \text{ cpm}$
- (3) Calculate scan MDC:

$$\text{Scan MDC} = \frac{623}{\sqrt{0.5} (0.58)(0.65)(1)} \approx 2,335 \text{ dpm}/100 \text{ cm}^2$$

In summary, these examples provide decommissioning planners with the calculational methods for estimating *a priori* scan MDCs for building and structure surfaces. The examples also

demonstrate how planners may justify human factor and instrument selection decisions to satisfy DQO and DCGL requirements. A similar approach is used to estimate the *a priori* scan MDC for land areas, as discussed in Section 6.2.5.

#### 6.2.4.2 Scanning MDC for Alpha-Emitters

Scanning for alpha-only emitters differs significantly from scanning for beta (or alpha-plus-beta) emitters in that the expected background detector response (cpm) of most alpha detectors is very close to zero. MARSSIM (NRC, 2000, pg. 6-46) addresses the issues as follows:

Since the time a contaminated area is under the probe varies and the background count rate of some alpha instruments is less than 1 cpm, it is not practical to determine a fixed MDC for scanning. Instead, it is more useful to determine the probability of detecting an area of contamination at a predetermined DCGL for given scan rates.

For alpha survey instrumentation with backgrounds ranging from greater than 1 to 3 cpm, a single count gives a surveyor sufficient cause to stop and investigate further. Assuming this to be true, the probability of detecting given levels of alpha surface contamination can be calculated by use of Poisson summation statistics. The Poisson probability of observing one or more counts based on the contamination activity, efficiencies, and the observation interval is given by the following:

$$P(n \geq 1) = 1 - e^{-\frac{G\varepsilon_i\varepsilon_s i}{60}} \quad (\text{Eq. 6.8})$$

where:

$P(n \geq 1)$  = Poisson probability of observing a single count

$G$  = contamination activity (dpm)

$\varepsilon_i$  = the instrument efficiency (unitless)

$\varepsilon_s$  = the surface efficiency (unitless)

$i$  = the observation interval(s)

Appendix J to MARSSIM presents the complete derivation of the alpha scanning equations used to estimate the probability of detecting a single count while passing an alpha radiation detector over a contaminated area, so the derivation is not repeated here. However, Abelquist (2014) extends the MARSSIM presentation by calculating the probability of detecting given levels of alpha contamination using Poisson summation statistics. Specifically, by defining the alpha scan MDC at a certain Poisson probability of being detected, the alpha scan MDC may be estimated by first solving Equation 6.8 for  $G$ :

$$G = \frac{[-\ln(1-P(n \geq 1))] \times (60/i)}{\varepsilon_i \varepsilon_s} \quad (\text{Eq. 6.9})$$

Finally, the scan MDC calculation must account for the probe area to produce results in proper dpm/100-cm<sup>2</sup> units. With the addition of probe area terms, Equation 6.9 is restated as an MDC as follows:

$$\text{Alpha Scan MDC} = \frac{[-\ln(1-P(n \geq 1))] \times (60/i)}{\varepsilon_i \times \varepsilon_s \times \frac{\text{probe area}}{100}} \quad (\text{Eq. 6.10})$$

Thus, the beta (or alpha plus beta) and alpha-only surface scan MDC calculations assume the same general form:

Beta or Alpha-Plus-Beta Scan MDC

$$\frac{MDCR}{\sqrt{p} \times (\text{Instrument Effs.}) \times (\text{Source Effs.})}$$

$$MDCR = d' \times \sqrt{b_i} \times (60/i)$$

$$\frac{d' \times \sqrt{b_i} \times (60/i)}{\sqrt{p} \times \varepsilon_i \times \varepsilon_s \times \frac{\text{probe area}}{100}}$$

Alpha-Only Scan MDC

$$\frac{MDCR}{(\text{Instrument Effs.}) \times (\text{Source Effs.})}$$

$$MDCR = [-\ln(1 - P(n \geq 1))] \times (60/i)$$

$$\frac{[-\ln(1 - P(n \geq 1))] \times (60/i)}{\varepsilon_i \times \varepsilon_s \times \frac{\text{probe area}}{100}}$$

Note the absence of the surveyor efficiency ( $p$ ) in the alpha scan MDC equation. When applicable, the term is intended to quantify the likelihood that a surveyor will pause once a count is registered, and then make a decision if there are additional counts in that interval. NUREG/CR-6364 does not evaluate very low background conditions, and in either case, it is presumed that a surveyor will always recognize additional counts when the background count rate is close to zero. Therefore,  $p = 1.0$  in the alpha scan MDC equation and thus is omitted.

Decommissioning planners must still define the probability of detecting a count (or counts). Abelquist (2014) again addresses practical limitations in Equation 6.10 inputs, including the probability term. For example, this approach may lead to a high incidence of false positives when background count rates are significantly greater than zero. For this discussion, however, decommissioning planners should address the probability term during DQO development in a manner similar to that for  $d'$ . If, for example, planners would select a  $d'$  value based on a true positive proportion of 0.90, then a 90-percent probability of detecting an alpha particle may also be selected.

As an example, a decommissioning project is tasked with surveying a surface potentially contaminated with recently processed uranium (i.e., before ingrowth of the short-lived beta-emitters). The site applies a 5,000 dpm/100 cm<sup>2</sup> action level for equipment release surveys and has set a DQO that requires a scan MDC of no more than 10 percent of the action level. Planners postulate a typical hotspot size of 200 cm<sup>2</sup>, and surveyors are using 100-cm<sup>2</sup> alpha scintillation detectors. Procedure dictates a scan speed of about one-half of the detector face per second. The instrument efficiency has been estimated at 0.48, and the surface efficiency of 0.25 is assigned for alpha radiation. The scan MDC based on a 90-percent probability of detecting a single count is calculated as follows:

$$\text{Alpha Scan MDC} = \frac{-\ln(1-0.9) \times (60/4)}{0.48 \times 0.25 \times (100/100)} = 288 \text{ dpm}/100 \text{ cm}^2$$

This scan MDC is less than 10 percent of the 5,000 dpm/100 cm<sup>2</sup> DCGL and thus satisfies the DQO.

In this example, assuming the surveyor pauses or scans over the contaminated area for 4 seconds, this alpha scintillation detector should produce more than two alpha counts:

$$(288 \text{ dpm}/100 \text{ cm}^2) \times (0.48) \times (0.25) \times (4/60) = 2.3 \text{ counts}$$

The surveyor who observes two counts in this example will pause over the area. If the surveyor observes no additional counts, the initial count is either at background levels or less than the scan MDC (Abelquist, 2014). Alternately, if additional counts are observed the surveyor could delineate the area of elevated activity, collect a static measurement, or complete other actions as required by the decommissioning project. Though not repeated here, MARSSIM addresses scenarios where the background count rate may be more than a few cpm (e.g., 5 to 10 cpm). For these scenarios, the probability of detecting two or more counts is calculated, and this is further described in MARSSIM (2000) Section 6.7.2.2.

### 6.2.5 *A Priori* Scan MDCs for Land Areas

Recalling the form of the generic *a priori* scan MDC from Equation 6.1, the same MDCR and surveyor efficiency ( $p$ ) discussed for building and structure surfaces also apply here. However, methods for estimating the instrument and source efficiencies are significantly different when estimating *a priori* scan MDCs (in pCi/g) for land areas. These efficiencies relate to the areal extent and depth of the source, the source radionuclide or radionuclides (i.e., energy and yield of gamma emissions), and the energy-dependent detector response to gamma radiation. The instrument efficiency is defined here as the CPMR in units of cpm per  $\mu\text{R/h}$ . Manufacturers may provide this value, or it may be taken from the literature. For example, Ludlum lists a value of 900 cpm/ $\mu\text{R/h}$  for the model 44-10 2"  $\times$  2" NaI scintillation detector from exposure to a 0.662-MeV gamma (Cs-137). The CPMR is energy dependent, so must be derived when the value is not known or if there is a mixture of radionuclides and gamma energies. The source efficiency is defined as the exposure-rate-to-concentration ratio (ERC) in units of  $\mu\text{R/h}$  per pCi/g, which is the measured or estimated exposure rate at some distance from a source with a well-defined geometry (i.e., areal extent and depth). The following discussion describes these efficiencies in more detail and explains their use in the *a priori* scan MDC calculation for land areas:

$$\text{Scan MDC} = \frac{MDCR}{\sqrt{p} \times CPMR \times ERC} \quad (\text{Eq. 6.11})$$

**Count-rate-to-exposure-rate ratio.** It is generally assumed that NaI scintillation detectors are used for scanning land areas. Figure 6-2 presents an example of an energy dependence curve that illustrates how a 2"  $\times$  2" NaI scintillation detector responds (in cpm per  $\mu\text{R/h}$ ) depending on the incident gamma energy. For very low energies (e.g., about 10 keV and less), the gamma may not penetrate the detector's metal housing. However, as the energies increase, the gamma is more likely to deposit all of its energy in the crystal, via the photoelectric effect, and create a pulse that the detector registers as a count. The detector reaches a maximum efficiency when the gamma energies are in the 60 to 80 keV. With still increasing gamma energies, interactions within the crystal are dominated by Compton scattering. These higher energy gammas may deposit only a fraction of their energy or may pass completely through the crystal without interaction; therefore, Figure 6-2 shows a lower efficiency. To calculate the CPMR term, a decommissioning project must define the relationship between the detector response and incident gamma energy. The values illustrated in Figure 6-2 and listed in Table 6-3 are examples prepared for this NUREG.

Manufacturers typically provide a single value on this curve for a given detector (e.g., 900 cpm/ $\mu\text{R/h}$  for a 2"  $\times$  2" NaI). In most cases, however, the CPMR is unknown and must be estimated. For example, the source may contain both Cs-137 and Co-60, or may include natural uranium in equilibrium with associated decay products. The following describes a method for estimating the CPMR for any combination of gamma-emitting radionuclides, starting with a simple hypothetical source that emits mono-energetic gamma radiation.

The CPMR for a single gamma energy may be determined in four steps. These steps are described below for a 2" × 2" NaI detector and a 400-keV gamma. Step 1 is to estimate the fluence rate for the specific energy of interest:

$$\text{Fluence Rate} = \frac{1 \mu\text{R/h}}{(E_\gamma)(\mu_{en}/\rho)_{air}} = \frac{1}{(400)(0.02949)} = 0.08477 \quad (\text{Eq. 6.12})$$

where  $(\mu_{en}/\rho)$  is the mass energy absorption coefficient for air and the value used is for 400 keV (Shleien, 1992).

Step 2 is to estimate the probability of interaction within the detector's NaI crystal, assuming that the primary gamma interaction producing the detector response occurs through the end of the detector, as opposed to the sides:

$$P = 1 - e^{-(\mu/\rho)_{NaI}(x)(\rho_{NaI})} = 1 - e^{-(0.110)(5.08)(3.67)} = 0.871 \quad (\text{Eq. 6.13})$$

where:

$(\mu/\rho)_{NaI}$  is the mass absorption coefficient for NaI (0.110 cm<sup>2</sup>/g at 400 keV) (Shleien et al., 1998)

x is the thickness of the NaI (5.08 centimeters)

$\rho_{NaI}$  is the density of NaI (3.67 g/cm<sup>3</sup>)

Step 3 is to estimate the relative detector response, which is the product of the fluence rate and probability of interaction:

$$\text{Relative Response} = \text{Fluence Rate} \times P = 0.08477 \times 0.871 = 0.0739 \quad (\text{Eq. 6.14})$$

Steps 1, 2, and 3 are repeated for the energy with the known CPMR value (in this case, 662 keV with a CPMR of 900 cpm/μR/h). The CPMR for a 662-keV gamma is estimated to be 0.0388.

Finally, Step 4 is to estimate the energy-specific CPMR (for 400 keV) by adjusting the known CPMR (for 662 keV) using calculated relative responses:

$$\text{CPMR}_{400} = \text{CPMR}_{662} \times \frac{\text{Relative Response}_{400}}{\text{Relative Response}_{662}} = 900 \times \frac{0.0739}{0.0388} \approx 1,700 \text{ cpm}/\mu\text{R/h} \quad (\text{Eq. 6.15})$$

This is the simplest case, with just one gamma energy to consider. A weighted CPMR is required for mixed gamma fields, and this weighting involves using the ERC efficiency factor. Therefore, this section presents the weighted CPMR for mixed sources after describing the ERC term.

**Exposure-rate-to-concentration ratio.** The ERC is traditionally generated by estimating the exposure rate in μR/h at some distance from a source with a well-defined geometry and concentration. For this discussion, Microshield™ is used to estimate the exposure rate at a position 10 centimeters above 1 pCi/g of Cs-137 in a 0.25-m<sup>2</sup>, 15-centimeter-thick cylindrical hotspot in a soil-like medium. This position (10 centimeters) is selected because it relates to the assumed average height of the NaI scintillation detector above the source (i.e., the ground) during scanning. The factors considered in the modeling include:

- energy emissions from the radionuclide of interest (e.g., 662 keV for Cs-137)
- concentration of the radionuclide of interest (e.g., 1 pCi/g)

- areal dimensions of hotspot (e.g., 0.25 m<sup>2</sup>)
- depth of hotspot (e.g., 15 centimeters)
- location of dose point (e.g., 10 centimeters above the center)
- density of soil (e.g., concrete at 1.6 g/cm<sup>3</sup> assumed as a close approximation)

Both Cs-137 and its short-lived progeny, barium (Ba)-137m, were chosen from the Microshield™ library. The source activity was selected based on unit concentration of 1 pCi/g and converted to the appropriate units required by the code:

$$(1 \text{ pCi/g}) \times (1.6 \text{ g/cm}^3) \times (1 \text{ } \mu\text{Ci}/10^6 \text{ pCi}) = 1.6\text{E-}6 \text{ } \mu\text{Ci/cm}^3$$

The modeling code performed the appropriate calculations and estimated an exposure rate of 0.247  $\mu\text{R/h}$  (accounting for buildup) 10 centimeters from the 0.25-m<sup>2</sup> source. Because unit concentrations were used, the ERC is 0.247  $\mu\text{R/h}$  per pCi/g. Although the resulting gamma energy spectrum incident on the NaI detector (both primary and scattered gamma radiation) must be accounted for, the Microshield™ modeling code considered only primary gamma energies when evaluating the buildup from scattered photons. The NaI detector response will be greater than the calculated detector response during field applications, because the detector is more efficient at detecting lower energy scattered photons. This situation is expected to yield a conservative determination of the detector response and resulting scan MDC estimate.

The *a priori* scan MDC may now be calculated for given values of the MDCR and the efficiency terms *p*, *CPMR*, and *ERC*.

**Land area *a priori* scan MDC example—single gamma energy.** The following example demonstrates the relatively straightforward method for estimating the *a priori* scan MDC for land areas. The example considers the same potential 0.25-m<sup>2</sup>, 15-centimeter-thick hotspot contaminated with Cs-137. Surveyors will scan the area using 2" × 2" NaI scintillation detectors with an established average background count rate of 9,750 cpm. An observation interval of 2 seconds is assumed. Approved DQOs include 95-percent true positive and 25-percent false positive proportions (*d'* is 2.32), and a conservative surveyor efficiency of 0.5 is assumed. Finally, the project-specific DCGL<sub>EMC</sub> for Cs-137 is 20 pCi/g. The *a priori* scan MDC is estimated as follows:

$$\text{Scan MDC (Cs-137)} = \frac{\text{MDCR}}{\sqrt{p} \times \text{CPMR} \times \text{ERC}} = \frac{d' \times \sqrt{b_i} \times (60/i)}{\sqrt{p} \times \text{CPMR} \times \text{ERC}} = \frac{2.32 \times \sqrt{9750 \times 2/60} \times (60/2)}{\sqrt{0.5} \times 900 \times 0.247} = 8.0 \text{ pCi/g}$$

This scan MDC is well below the DCGL<sub>EMC</sub>, so site planners accept the result and incorporate it into the decommissioning plan.

**Land area *a priori* scan MDC example—mixed gamma sources.** Determining the *a priori* scan MDC for more complex radioactive materials, such as uranium and thorium, must consider the gamma radiation emitted from the entire decay series. The following example considers the scan MDC for 3-percent enriched uranium using a 3" × 3" NaI scintillation detector with a background count rate of 23,000 cpm. The project has determined that 90-percent correct detections and a 25-percent false positive rate are acceptable (*d'* = 1.96) and has committed to remediating any residual contamination above 100 pCi/g of total uranium. Finally, the project

has empirical data documenting the survey team's high level of performance, justifying a  $p$  of 0.75.

Because the source produces a mixed gamma (and x-ray) radiation field, the CPMR and ERC are evaluated concurrently. Specifically, Microshield™ dictates (i.e., bins) the energies that will be considered, and the ERC values (Microshield™ output) will be used to weight the energy-specific CPMR values. First, however, the Microshield™ inputs must be determined.

The first step is to determine the source term for 3-percent enriched uranium. Table 6-4 presents activity fraction estimates based on the alpha activity equation in EGG-2350/UC-41, "Health Physics Manual of Good Practices for Uranium Facilities" (Idaho National Engineering Laboratory, 1998). The activity fractions of 3-percent enriched uranium are 0.2057, 0.0409, and 0.7535, respectively, for U-238, U-235, and U-234. The short-lived progeny of U-238, Th-234, and Pa-234m will also be present at the same activity fraction as U-238 (0.2057). Th-231, the progeny of U-235, will also be present at an activity concentration of 0.0409. There are no short-lived progeny in the decay series immediately following U-234. The source activity was selected based on a unit concentration of 1 pCi/g for total uranium, divided between the uranium isotopes according to their activity fractions, and converted to appropriate units accepted by the code. Therefore, the source term entered from the Microshield™ library is as follows:

- U-238            3.29x10<sup>-7</sup> μCi/cm<sup>3</sup>
- Th-234        3.29x10<sup>-7</sup> μCi/cm<sup>3</sup>
- Pa-234m      3.29x10<sup>-7</sup> μCi/cm<sup>3</sup>
- U-234        1.21x10<sup>-6</sup> μCi/cm<sup>3</sup>
- U-235        6.54x10<sup>-8</sup> μCi/cm<sup>3</sup>
- Th-231       6.54x10<sup>-8</sup> μCi/cm<sup>3</sup>

The modeling code performed the appropriate calculations and determined the total exposure rate, with buildup, of 4.293E-3 μR/h. Therefore, the ERC for the total uranium source is 4.293E-3 μR/h per pCi. Additionally, Microshield™ provided the exposure rates for a specific number of gamma energies associated with the assigned source term. The project uses Equations 6.12 through 6.15 to estimate the CPMR at each energy line (or bin), and then the energy-specific ERC values are used to weight the energy-specific CPMR values. The total ERC and the total weighted CPMR are then compiled as follows:

| <u>Energy (keV)</u><br><u>(from Microshield™)</u> | <u>ERC<sub>j</sub> (μR/h/pCi/g)</u><br><u>(from Microshield™)</u> | <u>CPMR<sub>j</sub> (cpm/μR/h)</u><br><u>(from Table 6-3)</u> | <u>Weighted CPMR<sub>j</sub> (cpm/μR/h)</u><br><u>(see Equation 6.16)</u> |
|---|---|---|---|
| 15  | 3.109x10 <sup>-04</sup>   | 2,540   | 184   |
| 30  | 2.238x10 <sup>-05</sup>   | 11,030  | 57.5  |
| 50  | 6.366x10 <sup>-06</sup>   | 24,820  | 36.8  |
| 60  | 8.345x10 <sup>-05</sup>   | 27,870  | 542   |
| 80  | 8.972x10 <sup>-05</sup>   | 26,410  | 552   |
| 100   | 4.588x10 <sup>-04</sup>   | 21,870  | 2338  |
| 150   | 3.374x10 <sup>-04</sup>   | 13,580  | 1068  |
| 200   | 2.005x10 <sup>-03</sup>   | 9,510   | 4443  |
| 800   | 1.466x10 <sup>-04</sup>   | 1,850   | 63.3  |
| 1,000   | 8.325x10 <sup>-04</sup>   | 1,460   | 283   |
| <b>Totals</b>                                     | <b>4.293E-03</b>  |   | <b>9,567</b>  |



Each energy-specific weighted  $CPMR$  ( $CPMR_j$ ) is calculated as follows:

$$\text{Weighted } CPMR_j \text{ (cpm}/\mu\text{R/h)} = \frac{ERC_j \times CPMR_j}{\sum ERC_j} \quad (\text{Eq. 6.16})$$

The total weighted  $CPMR$  is estimated to be 9,567 cpm/ $\mu$ R/h; therefore, the scan MDC for 3-percent enriched uranium can now be calculated. Assuming a surveyor observation interval of 1 second, the scan MDC is as follows:

$$\begin{aligned} \text{Scan MDC (3\% EU)} &= \frac{MDCR}{\sqrt{p} \times CPMR \times ERC} = \frac{d' \times \sqrt{b_i} \times (60/i)}{\sqrt{p} \times CPMR \times ERC} \\ &= \frac{1.96 \times \sqrt{23,000 \times 1/60} \times (60/1)}{\sqrt{0.75} \times 9,567 \times 4.293E-03} \approx 65 \text{ pCi/g} \end{aligned}$$

This value is below the 100 pCi/g commitment, so site planners accept the 65 pCi/g scan MDC, and surveyors are instructed to scan at a rate of no more than 1 meter per second. Planners could also account for the 3"  $\times$  3" NaI scintillation detector's relatively high sensitivity to increase the observation interval without slowing the survey pace (i.e., the detector will respond to a hotspot a little before and a little after its location is traversed). This assumption could be applied during DQO development or as data are collected to prove that the default survey rate is sufficient.

Table 6-5 provides scan MDCs for common radionuclides and radioactive mixtures in soil. To generate Table 6-5, all inputs not specifically associated with the listed NaI detector were held constant. That is, each scan MDC is calculated for  $p = 0.5$ ,  $d' = 2.32$ , and  $i = 2$  seconds and for 0.25-m<sup>2</sup>  $\times$  15-cm cylindrical soil-like source with a detector-to-source distance of 10 centimeters. Changes in any of these values, or the stated detector-specific background count rates, would result in different scan MDC estimates. These values are examples that each decommissioning project should consider and modify according to site-specific conditions and project-specific DQOs. To illustrate changes that may result based on site-specific conditions, Table 6-6 presents relatively low *a priori* scan MDCs for inputs  $p = 0.75$ ,  $d' = 1.96$ , and  $i = 2$  seconds, and Table 6-7 presents relatively high *a priori* scan MDCs for inputs  $p = 0.5$ ,  $d' = 2.92$ , and  $i = 1$  second. Depending on which DQOs are selected, the *a priori* scan MDC for Cs-137 in these examples ranges from 5.5 pCi/g to 14 pCi/g. This example of a two-fold range of detectable activity illustrates the need for each project to specifically assess its instrumentation procedures and personnel as they apply to the input parameters in the development of realistic and achievable *a priori* scan MDCs.

Finally, Table 6-8 presents for completeness the  $ERC$  and weighted  $CPMR$  values for the suite of contaminants considered in Tables 6-5 through 6-7. These values are inserted into Equation 6.11 with the  $MDCR_{\text{surveyor}}$  to calculate the *a priori* scan MDC. As the following section will show, the product of the  $ERC$  and weighted  $CPMR$ , in units of cpm per pCi/g, can also be used to estimate the net concentration associated with a given detector response. This allows decommissioning projects to easily relate detector responses to net soil concentration, assuming the source material is similar to that described in Section 6.2.5 (0.25 m<sup>2</sup>, 15 centimeters thick, etc.). For example, if a decommissioning project is required to estimate the net 2"  $\times$  2" detector response assuming the DCGL is 5 pCi/g of Ra-226 in equilibrium with decay products, the calculation is performed as follows:

$$\left(5 \frac{\text{pCi}}{\text{g}}\right) \times \left(0.71 \frac{\mu\text{R}}{\text{pCi}}\right) \times \left(841 \frac{\text{cpm}}{\mu\text{R}}\right) = \left(5 \frac{\text{pCi}}{\text{g}}\right) \times \left(597 \frac{\text{cpm}}{\frac{\text{pCi}}{\text{g}}}\right) = \sim 3,000 \text{ cpm}$$

This does not consider surveyor efficiencies, the survey method, or other factors. The 3,000 cpm value is simply interpreted as a gross estimate of the 2" × 2" detector response that may be achieved from a 0.25-m<sup>2</sup>, 15-centimeter-thick source containing a net concentration of 5 pCi/g of Ra-226 in equilibrium with its short-lived decay products.

### 6.3 A Posteriori Decisions Using an Investigation Level

The preceding section described methods for estimating scan MDCs during the planning phase of a project. These *a priori* values are used to predict how effectively surveyors can locate hotspots and assume that surveyors will listen to the audible detector output. That is, if a surveyor notices a significant increase in the number of “clicks,” that increase will presumably represent the signal (over noise) associated with a radiological contaminant.

However, some decommissioning projects do not rely on the surveyors’ decisionmaking abilities. These projects may rely on geospatial data logging and instruct surveyors to perform surveys without listening to the audio output of the detector. Rather than the identification of anomalous locations in real-time based on audio response during the first and second stages of scanning described for the *a priori* methodology, data capture technologies are used to record detector response, the date and time of measurements, and the location (i.e., coordinates) of each measurement. Captured data are processed, binned, and mapped, and followup investigation decisions are made *a posteriori* based on post-processed data by, for example, a GIS technician who likely did not perform the survey.

This does not mean that either an *a priori* scan MDC or an *a posteriori* investigation level for post-processed data (IL<sub>PP</sub>) is superior or even preferred (either method can be valid), and integrating the methods provides synergistic advantages over the individual methods. (Section 6.4 demonstrates how projects may develop DQOs using either an *a priori* scan MDC or an *a posteriori* IL<sub>PP</sub>.) Ultimately, a project should select the method that will satisfy DQOs and, just as important, correspond to the measurement process and then apply that method through the project lifecycle.

The following discussion addresses an approach to establish an *a posteriori* IL<sub>PP</sub> based on a statistical background threshold value (BTV). The BTV determination examples provided here are based on the concepts and the statistical approaches examined extensively in EPA/600/R-07/041, “ProUCL Version 5.0.00 Technical Guide, Statistical Software for Environmental Applications for Data Sets with and without Nondetect Observations,” issued September 2013.

Before addressing the *a posteriori* IL<sub>PP</sub>, the statistical paradigm shift that occurs when moving from a *a priori* to a *a posteriori* decisionmaking should be considered. For the *a priori* decision process, Section 3 of this NUREG describes methods for calculating the critical level ( $L_C$ ) and MDC ( $L_D$ ) using Poisson statistics. In the *a priori* scenario, it is reasonable to assume for surveyor decisions that the distribution of a background measurement is comparable to the distribution of a background plus signal measurement. For example, normality is expected if a blank measurement is repeated numerous times (i.e., at any given background location).

Normality is also expected if identical measurements are repeated, but this time including background plus signal. Finally, it is reasonable to assume that if the standard deviations of two populations are comparable—standard normal statistics apply and background/signal measurements are pairwise comparable.

This is not the case when considering only *a posteriori* datasets without human factor involvement and second-stage scanning implementation during the data collection phase. That is, if the surveyor is not listening, the *a priori* MDCR inputs  $d'$ ,  $i$ , and  $p$ , defined during the planning phase of a project, are no longer valid. Furthermore, without pausing, the electronically captured count rate data may not accurately reflect the peak count rate at a given location as the ratemeter may not reach full scale if the observation interval over an area of elevated direct radiation is less than 2 to 4 seconds, equivalent to an area of 3 to 12 m<sup>2</sup> at a scan speed of 1 meter per second.

The *a posteriori* datasets can contain hundreds or thousands of independent, short count time (e.g., 1- to 2-second) measurements across an area, and these datasets, whether representative of background or background plus signal, may or may not be normally distributed. In addition, the standard deviation of the counts within the distributions of background and background plus signal populations cannot be assumed to be equivalent. That is, the statistical paradigm changes for projects where the surveyors do not listen to the audio output and pause to investigate potential anomalies (second-stage scanning). Rather, anomalies must be identified based on evaluations of the processed data. The techniques used may consist of visual color-coded data mapping, population outlier tests, count-rate-to-concentration correlation/threshold studies, an upper confidence/tolerance limit of background data, or other methods. Unfortunately, a single, practical method for calculating an *a posteriori*  $IL_{PP}$ , which could serve as an analog to  $L_C$  and  $L_D$  as described in Section 3, requires additional research. Until the development of further, consistent guidance, decommissioning projects should follow the DQO process and consider stakeholder requirements and resources to establish an acceptable  $IL_{PP}$  that balances an acceptable false positive probability with control of false negative decisions and thus provides confidence that the selected  $IL_{PP}$  will satisfy detection sensitivity at the  $DCGL_W$ ,  $DCGL_{EMC}$ , or other project-specific concentration-based limit.

To meet the  $IL_{PP}$  detection objective, a defensible *a posteriori* scan sensitivity methodology must be developed and vetted. The proposed methods used to develop the  $IL_{PP}$  may be statistically and/or empirically based and may employ commercially available statistical software for evaluating data and setting an  $IL_{PP}$  relative to representative background populations. Common statistical  $IL_{PP}$  values, above which anomaly investigations are performed, include z-scores (normality assumed) or various background threshold value calculations, such as an upper tolerance level (UTL), upper simultaneous limit (USL), or other statistic when the underlying data distribution is unknown or otherwise does not exhibit the characteristics of a normal distribution.

The following *a posteriori* planning examples for an exterior soil area illustrate a sequential method that a decommissioning project might use to calculate the  $IL_{PP}$  and then demonstrate that the  $IL_{PP}$  is acceptable in terms of both false negative and false positive decision probabilities. Although other processes may be used based on project-specific resources and requirements, the example applies the MARSSIM framework in determining if the initial sample density in a Class 1 survey area can be maintained or must be increased if the required sensitivity of the data evaluation process is unable to satisfy requirements for detecting, at a given confidence level, i.e., potential contamination at the  $DCGL_{EMC}$  (NUREG-1757). Essentially, the process would be comparable to the evaluation of a required scan MDC for

planning and assessing radiological surveys. The goal of this approach is the development of a defensible background threshold value as the  $IL_{PP}$ . Several tools are available to facilitate both the relationship in the concentration to detector response and comparing that response, whether modeled or empirically determined, to a required performance criterion that includes controls of false negative and false positive decision errors.

The sequence begins with estimating the relative operating characteristic for the scan measurement system and the probability of correct decision to that of the false positive probability in relationship to candidate  $IL_{PP}$  values. The efficiency terms described in Section 6.2 of this NUREG are used to estimate the cpm value that equates to the  $DCGL_W$  or  $DCGL_{EMC}$  value. The value is determined based on Microshield™ modeling to get the cpm/uR/h (CPMR) response. For example, a project may assume that the Section 6.2 source configuration applies (i.e., a 0.25-m<sup>2</sup>, 15-centimeter-thick cylindrical hotspot in a soil-like medium); in this case, a given net cpm value can be converted to pCi/g using the following equation:

$$\text{cpm-to-concentration ratio} = \frac{\text{net cpm}}{CPMR \times ERC} \quad (\text{Eq. 6.17})$$

The Section 6.2 calculated results will serve as the initial example data. Assume that the required detection sensitivity is 5 pCi/g and the cpm-to-concentration ratio for the detector response is about 3,000 cpm. Additionally, the example will be expanded to demonstrate the impact on the  $IL_{PP}$  decision if the required detection sensitivity had been determined to be lower (2,000 cpm will be used) or higher (5,000 cpm), perhaps because of a change in the DCGL or use of a less or more sensitive detector.

Next, the actual detection sensitivity analog, the  $IL_{PP}$ , is developed by first examining a suitable background reference area *a priori*, using the same electronic data capture and radiation detection equipment that will be used during the radiological site investigation process. The background population characteristics include basic statistical parameters (e.g., mean, median, standard deviation, range) and tests of normality. The planning team uses the test of normality to decide whether the  $IL_{PP}$  will be based on parametric or nonparametric statistics. EPA/600/R-07/041 pp. 16-17 provides additional guidance for selecting the background areas as follows:

Based upon the conceptual site model (CSM), the project team familiar with the site selects background or reference areas. Depending upon the site activities and the pollutants, the background area can be site-specific or a general reference area. An appropriate random sample of independent observations (e.g., independently and identically distributed) should be collected from the background area. A defensible background data set represents a “single” population possibly without any outliers. In a background data set, in addition to reporting and/or laboratory errors, statistical outliers may also be present. A few elevated statistical outliers present in a background data set may actually represent potentially contaminated locations belonging to an impacted site area and/or possibly from other polluted site(s); those elevated outliers may not be coming from the main dominant background population under evaluation. Since the presence of outliers in a data set tends to yield distorted (incorrect and misleading) values of the decision making statistics...elevated outliers should not be included in background data sets and estimation of BTVs (background threshold values). The objective here is to compute background statistics based upon the majority of the data set representing the main dominant background population, and not to accommodate a few low probability high outliers (e.g.,

coming from extreme tails of the data distribution) that may also be present in the background data set. The occurrence of elevated outliers is common when background samples are collected from various onsite areas (e.g., large Federal Facilities). The proper disposition of outliers, to include or not include them in statistical computations, should be decided by the project team. The project team may want to compute decision statistics with and without the outliers to evaluate the influence of outliers on the decision making statistics.

In continuing the example, a suitable background area is identified, and a gamma radiation walk-over survey performed using an NaI/ratemeter combination coupled to a GPS unit. The gamma radiation data were captured at 1-second intervals (in units of cpm based on firmware conversions) together with the georeferenced coordinate. The data were downloaded and processed using available commercial software (such as SAS and Minitab 16) or freeware statistical software(s) with appropriate design functionality for environmental data assessment, such as ProUCL. The data for this example were analyzed using ProUCL.

| <b>General Statistics</b>     |        |                                  |        |
|-------------------------------|--------|----------------------------------|--------|
| Total Number of Observations: | 13,601 | Number of Distinct Observations: | 3,206  |
| Minimum:                      | 7,513  | First Quartile:                  | 9,131  |
| Second Largest:               | 11,696 | Median:                          | 9,608  |
| Maximum:                      | 11,699 | Third Quartile:                  | 10,097 |
| Mean:                         | 9,623  | SD:                              | 725.9  |
| Coefficient of Variation:     | 0.0754 | Skewness:                        | 0.0787 |
| Mean of Logged Data:          | 9.169  | SD of Logged Data:               | 0.0757 |

The data were examined graphically via a histogram and Q-Q plot shown to identify the presence of bi- or multi-modal distributions that would affect the condition that the background represented a single population or potential outliers that influence the ordered statistics (percentiles). As Figures 6-3 and 6-4 show, both conditions were satisfied. If the analysis had identified a bi- or multi-modal population, the background would be further examined to determine if the variable results were the result of spatial considerations such as different geologic conditions or material types (including soil, gravel, or asphalt) were represented in the distributions. If so, further evaluations are conducted, potentially resulting in the application of several, distinct background populations to be used in establishing  $IL_{PP}$  values for site data comparisons. The requirement for multiple  $IL_{PP}$  values ultimately depends on the detection sensitivity needed to identify anomalous areas corresponding to the applicable DCGL, as will be shown. A second Q-Q plot (Figure 6-5) illustrates two distinct background populations that would necessitate independent assessment.

Next, the software analysis performed the test of normality and concluded that this background population did not exhibit a normal distribution at the 5-percent significance level. The software also returned multiple values, both parametric and nonparametric, for the planning team to consider as potential background threshold values. These are the UTL, upper prediction limit (UPL), and USL:

- UTL: A confidence limit on a percentile of the population rather than a confidence limit on the mean. For example, a 95-percent one-sided UTL for 95-percent coverage represents the value below which 95 percent of the population values are expected to fall with 95-percent confidence. In other words, a 95-percent UTL with a coverage coefficient of 95 percent represents a 95-percent UCL for the 95th percentile. Reduced confidence or coverage percentages will return lower UTL values.

- UPL: The upper boundary of a prediction interval for an independently obtained observation (or an independent future observation).
- USL: The upper boundary of the largest value.

Both the parametric (normal, gamma, and lognormal distribution) and nonparametric thresholds (in units of cpm) are shown below.

| <b>IL<sub>PP</sub> Assuming Normal Population</b>      |        |  |        |
|--|--------|--|--------|
| 95% UTL with 95% Coverage                              | 10,833 | 90% Percentile (z)   | 10,553 |
| 95% UPL (t)  | 10,817 | 95% Percentile (z)   | 10,817 |
| 95% USL  | 12,876 | 99% Percentile (z)   | 11,312 |
| <b>IL<sub>PP</sub> Assuming Gamma Distribution</b>     |        |  |        |
| 95% Wilson Hilferty (WH) Approx. Gamma UPL             | 10,849 | 90% Percentile   | 10,566 |
| 95% Hawkins Wixley (HW) Approx. Gamma UPL              | 10,854 | 95% Percentile   | 10,849 |
| 95% WH Approx. Gamma UTL with 95% Coverage             | 10,866 | 99% Percentile   | 11,395 |
| 95% HW Approx. Gamma UTL with 95% Coverage             | 10,871 | --   | --     |
| 95% WH USL   | 13,241 | 95% HW USL   | 13,295 |
| <b>IL<sub>PP</sub> Assuming Lognormal Distribution</b> |        |  |        |
| 95% UTL with 95% Coverage                              | 10,886 | 90% Percentile (z)   | 10,573 |
| 95% UPL (t)  | 10,868 | 95% Percentile (z)   | 10,868 |
| 95% USL  | 13,473 | 99% Percentile (z)   | 11,444 |
| <b>Nonparametric Upper Limits for IL<sub>PP</sub></b>  |        |  |        |
| 95% Percentile Bootstrap UTL with 95% Coverage         | 10,896 | 95% bias-corrected accelerated Bootstrap UTL with 95% Coverage | 10,893 |
| 95% UPL  | 10,866 | 90% Percentile   | 10,576 |
| 90% Chebyshev UPL                                      | 11,801 | 95% Percentile   | 10,865 |
| 95% Chebyshev UPL                                      | 12,787 | 99% Percentile   | 11,388 |
| 95% USL  | 11,699 | --   | --     |

Because a scan survey captures thousands of data points, in some scenarios, there could be many comparisons to an IL<sub>PP</sub>, simply because of probability. Consider a sample case where 1,000 data points are captured and compared to the upper 95<sup>th</sup> percentile of background population. From a probability standpoint, 5 percent or 50 individual data points can be expected to exceed that threshold simply due to background variability. This scenario is also likely if the parametric UPL is selected as the IL<sub>PP</sub> and is therefore not recommended because of the overly burdensome high false positive error probability. Conversely, the use of a nonparametric UPL, based on the Chebyshev inequality, tends to result in higher estimates for an IL<sub>PP</sub> and could potentially lead to an unacceptable false negative probability. Therefore, the remainder of this example will examine only the selection of an appropriate IL<sub>PP</sub> that is based on either a parametric or nonparametric UTL or USL and conditions, cautions, and false positive or false negative considerations.

False positives can be minimized by selecting the USL; however, as the above results show, the USL returned the highest potential  $IL_{PP}$  in each case, as the USL represents an upper limit of the largest value observed in the background dataset. Therefore, because of the potentially unacceptable false negative decision probability, the USL is considered as an  $IL_{PP}$  only when:

- The background dataset is free of outliers.
- The background data represent a single distribution.
- The evaluation of the scanning equipment detection capability—including any uncertainty in the detector source response modeling or empirical study correlation, as well as peak count rate response time error and procedural systematic error—confidently concludes that the cpm-to-concentration ratio is well outside this uppermost percentile of the background distribution.

Furthermore, as the USL is based on the largest value, it will not be “adjustable” in a way that can be used to control decision errors, in particular false negatives, during the post-processing data assessment phase. A UTL-based  $IL_{PP}$  can be chosen such that decision errors are controlled by adjusting the coverage on the upper percentile. As the upper percentile coverage is decreased, the false negative decision error probability can be maintained so as not to exceed 0.05, although there will be a corresponding increase in false positive probability. On the other hand, increasing the percentile coverage can reduce the false positive probability but at the expense of increased false negative occurrences. The following data illustrate the change in coverage effect on the UTL-based  $IL_{PP}$ .

**Nonparametric UTL-Based  $IL_{PP}$  (shown as cpm)**

|  |        |
|--|--------|
| 95% Percentile Bootstrap UTL with 99% Coverage (95/99) | 11,413 |
| 95% Percentile Bootstrap UTL with 95% Coverage (95/95) | 10,896 |
| 95% Percentile Bootstrap UTL with 90% Coverage (95/90) | 10,593 |
| 95% Percentile Bootstrap UTL with 85% Coverage (95/85) | 10,590 |
| 95% Percentile Bootstrap UTL with 80% Coverage (95/80) | 10,245 |

Ultimately, regardless of the case for USL or the UTL together with corresponding coverage, the planning team should receive concurrence from the cognizant regulatory authority for the proposed  $IL_{PP}$  and include the available supporting empirical information in a technical basis document.

Based on the previously discussed normality test result, the remainder of the example assumes the  $IL_{PP}$  will be determined from either the nonparametric USL or UTL background threshold value and ultimately selected in conjunction with the detection sensitivity determined using Equation 6.17, which by itself does not have statistical significance, does not account for surveyor efficiency or variation across detectors, survey procedures, or other conditions, and presumes nothing about background or contaminant distributions.

To establish significance, the background population is graphically represented by Figure 6-6. The frequency bins in Figure 6-7 were selected as the 1<sup>st</sup>, 2<sup>nd</sup>, and 3<sup>rd</sup> quartiles, representing the 25<sup>th</sup>, 50<sup>th</sup>, and 75<sup>th</sup> data percentiles, and also the lower and upper tail quantiles at the <1, 2.5<sup>th</sup>, and 97.5<sup>th</sup> percentiles, and greater than USL. Figure 6-6 also shows the cumulative percentile.

The simulated background plus signal continuum is then plotted with the background population dataset to establish detection performance and the false negative and false positive probabilities. Three illustrations of the process are shown. The first (Figure 6-7) represents the

background and background plus signal at the initial 3,000 cpm-to-concentration ratio, the second (Figure 6-8) shows an example where the ratio has increased to 5,000 cpm, and the third (Figure 6-9) assumes that the ratio is 2,000 cpm perhaps because of the use of a less sensitive detector or a reduction in the applicable DCGL. The vertical lines represent several candidate  $IL_{PP}$  values and the corresponding associated count rates. The illustrated  $IL_{PP}$  values shown are the nonparametric USL, 95/95 UTL, 95/90 UTL, or 95/80 UTL. The intersections of the  $IL_{PP}$  values with the distributions provide the points at which the various false negative and false positive decision errors are estimated. Figure 6-7 also provides a potential color coding for the binning scheme that may be used for the data mapping.

The various percentiles, upon which the error probabilities are estimated at the intersections of the  $IL_{PP}$ s with the distribution, can be calculated using the linear interpolation of the nearest rank method in accordance with Equation 6.18:

$$p_n = \frac{100}{N} \left( n - \frac{1}{2} \right) \quad (\text{Eq. 6.18})$$

where:

$P_n$  is the percentile to be estimated of the distributions to estimate the errors

$N$  is the number of observations, which is 13,601 cpm for the example background dataset

$n$  is the  $n^{\text{th}}$  observation of the ranked ordered statistics that correspond to the candidate  $IL_{PPS}$

Based on the large sample sizes, Equation 6.18 may be reduced and simplified as follows:

$$p_n = \frac{100 \times n}{N} \quad (\text{Eq. 6.19})$$

Example calculations for Figure 6-7 to estimate the false negative (F-) and false positive (F+) probabilities are as follows for the 95-percent USL of 11,699 cpm. F- is estimated by finding in the ranked order statistics of the background plus signal (B+S) continuum the observation number where 11,699 cpm is located, which is the 1,375<sup>th</sup> value of the 13,601 ranked observations. Therefore, the applicable percentile =  $\frac{100 \times 1,375}{13,601} = 10.1$ . The same calculation is performed to determine F+ using the background (B or Bkg) ranked order statistics. As 11,699 is the highest value, the percentile is simply 100.

The various false positive and false negative values, as applicable, for Figures 6-7 and 6-9 were calculated from the respective distribution percentile and are summarized as follows:

### Distribution Percentiles for Figure 6-7

| Candidate $IL_{PP}$ /cpm | $p_n (B+S) / p_n (B)^a$ | F-    | F+   |
|--------------------------|-------------------------|-------|------|
| 95% USL/11,699           | 10.1/~100               | 0.1   | ~0   |
| 95/95 UTL/10,896         | 0.83/95.3               | <0.01 | 0.05 |
| 95/90 UTL/10,593         | 0.007/90.4              | <0.01 | 0.1  |

<sup>a</sup> B+S = background plus signal and B = background (or Bkg)



## Distribution Percentiles for Figure 6-9

| Candidate IL <sub>PP</sub> /cpm | $p_n(B+S)/p_n(B)^a$ | F-   | F+   |
|---------------------------------|---------------------|------|------|
| 95% USL/11,699                  | 55.3/~100           | 0.55 | ~0   |
| 95/95 UTL/10,896                | 15.7/95.3           | 0.16 | 0.05 |
| 95/80 UTL/10,245                | 2.6/80.6            | 0.03 | 0.19 |

For Figure 6-7, the results show a very favorable F+ probability, with very little chance of incorrectly concluding that contamination is present when only background conditions exist. However, the F- is not adequate to ensure that residual contamination will be identified with an acceptable confidence. The 95/95 UTL would provide a less than 1 percent probability of concluding that contamination is not present when it is, while maintaining a reasonable false positive probability of 5 percent or less.

The summarized results for Figure 6-9 show the impact to the F- and F+ probabilities in the presence of a lower cpm-to-concentration ratio (required detection sensitivity). The UTL under these conditions would produce no more than a 5-percent false negative probability, which lies between the 95/80 and 95/85 UTLs, and results in upwards of approximately 20 percent false positive potential. If this number of investigations could not be tolerated, then the required detection sensitivity would have to be increased, which in a Class 1 survey unit requires a higher sampling density.

Finally, it is presumed that GIS technicians will present survey data by binning data according to project-specific criteria. For example, a different color, such as shown in Figure 6-7, may be used for each standard deviation away from the mean response value, or for various quantiles, or for some other criterion. Conceivably, a contaminant could be present in an area that produces a low local background response (e.g., 7,000 to 8,000 cpm compared to an overall background range of 7,000 to 12,000 cpm) such as that used in the IL<sub>PP</sub> example datasets. If the contaminant is located in a low background area, resulting in a 3,000-count jump in the response, the surveyor will notice (if listening), but the GIS technician may recognize only responses that fall within the range of background. In such cases, the hotspot may be identified if (1) the location happens to be selected for sampling, (2) the surveyor reports the anomaly, or (3) the GIS technician notes the localized color change suggesting the presence of contamination. This problem arises because the surveyor can recognize slight, localized anomalies (the basis of the *a priori* scan MDC), but the GIS technician cannot recognize these unless binning is sufficiently granular and visual inspection is used to identify localized anomalies. If the project limits investigations to an IL<sub>PP</sub> based on some value near the upper end of the background distribution, contamination in areas with a relatively low background may be missed. Projects that make *a posteriori* decisions should, therefore, consider where the investigation may fall, taking into account the entire range of background.

Another approach, an empirical study, requires more time and resources but may be necessary when the concentration-based limit is indistinguishable from background. An example study could include the collection of soil samples at locations representing a range of detector responses. The range may span, for example, from the investigation level to multiples of mean background value. Linear correlation methods may then be used to plot pCi/g versus cpm data to generate a pCi/g-per-cpm relationship, which can be applied in a manner similar to that using Equation 6.17. A project-specific DQO will establish whether the relationship is based on tolerance levels (e.g., the 95-percent low tolerance level), best-fit relationships, or other

statistics. The objective is for the project to demonstrate that, when the contaminant is difficult to detect, the investigation level selected will not lead to an unacceptable rate of false negative decisions.

### 6.3.1 *A Posteriori* Investigation Levels

Data capture tools coupled to, for example, GPS equipment can record the detector response in cpm, plus the collection date and time and the x-y coordinates of each measurement. GIS technicians can map captured data by using, for example, binning and color-coded isopleths to show locations of radiological contamination. As mentioned, GIS technicians can also statistically analyze the data to determine the investigation level for which followup measurements are advisable. Decommissioning projects should select an *a posteriori*  $IL_{PP}$  that best satisfies site-specific requirements (such as DQOs and regulatory approvals). An example of a simple approach to develop an  $IL_{PP}$  is provided below which utilizes a z-score to establish acceptable false positive decision errors. In this case the background population is assumed to be normally distributed. The z-score is calculated as follows:

$$z = \frac{(X - \mu)}{\sigma} \quad (\text{Eq. 6.20})$$

where:

X is the data point value

$\mu$  is the background population mean

$\sigma$  is the background population standard deviation

In this context:

- A z-score equal to 0 represents a measurement equal to the mean cpm response.
- A z-score equal to +1 represents a measurement that is one standard deviation above the mean cpm response.
- A z-score equal to +2 represents a measurement two standard deviations above the mean response and so on.

Specifically, a decommissioning project can establish DQOs that define an  $IL_{PP}$  based on a number of standard deviations (z-score) above the mean background response:

$$\text{Investigation Level (cpm)} = \mu + (z \times \sigma) \quad (\text{Eq. 6.21})$$

The following five examples show how a project may establish an investigation level or levels under a range of conditions. All sites involve surface soils that are surveyed using 2" x 2" NaI detectors connected to GPS equipment, and data are logged for post-processing. Data presented for these examples are from surveys of real sites, though sometimes the datasets are amended or shifted to support the objective of the example. These data and associated results should not be used to establish  $IL_{PP}$  values for any purpose other than to illustrate the method.

The Example 1 project is set at a former clock factory that used luminous radium paint in the 1930s and 1940s. The factory was demolished in the 1970s, but the potential for residual contamination remains. The DCGL of 5 pCi/g above background has been established, and DQOs produce a preliminary  $IL_{PP}$  at  $z = +3$ . The project has identified a suitable offsite reference area, and surveyors have collected a background dataset ahead of site characterization. The

GIS technician processes the reference area survey data, verifies normality, and calculates the population mean of 9,060 cpm and standard deviation of 580 cpm. The preliminary  $IL_{PP}$  is, therefore, calculated using Equation 6.21, as follows:

$$IL_{PP} \text{ (cpm)} = 9,060 \text{ cpm} + (3 \times 580 \text{ cpm}) = 10,800 \text{ cpm}$$

Using Equation 6.17 and inputs from Table 6-8, the associated concentration is calculated as follows:

$$IL_{PP} \text{ (pCi/g)} = (3 \times 580 \text{ cpm}) / (597 \text{ cpm/pCi/g}) = 2.9 \text{ pCi/g}$$

Figure 6-10 shows the location of the  $IL_{PP}$  relative to the background dataset. For planning purposes, the project also estimates the net 2" × 2" NaI response that would be expected from a 0.25-m<sup>2</sup>, 0.15-m-thick hotspot in surface soils. This value is estimated as 5 pCi/g × 597 cpm/pCi/g = 2,985 cpm, or approximately 3,000 cpm. These results show that the  $IL_{PP}$  is well below the DCGL (when compared to the average background response) and meets project requirements—the project has accepted 10,800 cpm as the final  $IL_{PP}$ . To limit false negative decisions in low background areas, surveyors are instructed to listen and document anomalies in real time, and the GIS technician is instructed to review survey maps and identify localized anomalies that may require a followup investigation. The project concludes that there is a high probability of identifying concentrations above the DCGL by considering both surveyor and GIS technician input.

The Example 2 project is also at a site with radium contamination and a DCGL of 5 pCi/g above background. However, the project has not identified a suitable offsite reference area, so must estimate background using a subset of the onsite data population (i.e., from an area that produced detector responses that are characteristic of a background distribution without outliers that could be attributed to contamination). As in Example 1, the 5 pCi/g DCGL is distinguishable from background, and the project commits to an  $IL_{PP}$  at  $z = +3$ . The GIS technician initially processes all onsite survey data together and calculates a mean of 8,606 cpm and a standard deviation of 864 cpm. The initial preliminary  $IL_{PP}$  is calculated as follows:

$$IL_{PP} \text{ (cpm)} = 8,606 \text{ cpm} + (3 \times 864 \text{ cpm}) = 11,198 \text{ cpm, or } \sim 11,200 \text{ cpm}$$

However, the data are bimodal (i.e., they contain two easily distinguishable modes) and are not normally distributed because surveyors collected data over both surface soils and roadways. Detector responses are relatively low in the roadway. The GIS technician isolates roadway data from soil data and calculates a  $z = +3$   $IL_{PP}$  from each medium, assuming contamination has not been identified (i.e., there is no obvious evidence of contamination upon first review):

$$IL_{PP} \text{ for soil (cpm)} = 9,060 \text{ cpm} + (3 \times 578 \text{ cpm}) = 10,794 \text{ cpm, or } \sim 10,800 \text{ cpm,}$$

and

$$IL_{PP} \text{ for roadways (cpm)} = 7,649 \text{ cpm} + (3 \times 517 \text{ cpm}) = 9,200 \text{ cpm.}$$

Figure 6-11 presents the two detector response populations, the preliminary  $IL_{PP}$  (on the far right), and medium-specific  $IL_{PP}$  values. The relatively large standard deviation for the combined dataset produces a preliminary  $IL_{PP}$  that is too high for either medium. Additionally, the soil-specific  $IL_{PP}$  is not suitable for the roadway dataset, and tests confirm that the roadway dataset is not normally distributed. In fact, these results indicate a potential hotspot in the roadway that

may not have been identified without separating the survey results into medium-specific populations. Based on these results, the GIS technician identifies a small number of locations in the soil above the 10,800-cpm investigation level (as expected), plus potential anomalies in the roadway. Because anomalies have been identified in the roadway, the associated dataset is likely not representative of background conditions. A new area must be selected for defining the roadway background, and a new investigation level must be calculated.

The Example 2 project could have instructed surveyors to conduct medium-specific surveys. That is, surveyors would not cross from one medium to the next during a single survey event, or within a single data file so that each data file transferred to the GIS technician would be for a single medium. The GIS technician would then have processed soil data only or roadway data only, and the anomalies in the roadway results (for this example) would have been obvious at the onset. While medium-specific surveys are not always practical, decisions to segregate data at the surveyor level should be considered during DQO development.

The Example 3 project is set at a uranium recovery facility with a surface-soil processed natural uranium DCGL of 200 pCi/g. The project has identified a suitable offsite reference area, and surveyors collect a background dataset for processing by the GIS technician. The GIS technician processes the reference area survey data and calculates the population mean of 9,060 cpm and standard deviation of 578 cpm. Using Table 6-8, the project has demonstrated that 200 pCi/g in surface soil should be easily distinguishable from (about 3,700 cpm above) the background mean, producing a response above  $z = +5$ . The project would like to minimize the false positive investigations that would be associated with the  $z = +3$  action level. Because  $z = +5$  corresponds to the DCGL, the project selects an investigation level at  $z = +4$ :

Investigation Level (cpm) =  $9,060 \text{ cpm} + (4 \times 578 \text{ cpm}) = 11,372 \text{ cpm}$ , or  $\sim 11,400 \text{ cpm}$ ,

which corresponds to a net concentration of about 130 pCi/g (or about 65 percent of the DCGL).

Therefore, the GIS technician will identify any detector response above 11,400 cpm for followup investigation, possibly including the collection of judgmental samples. Figure 6-12 shows the investigation level (at  $z = +4$ ) relative to the background population. The figure also presents responses that correspond to  $z = +3$  and  $z = +5$  for reference.

The Example 4 project is set at a uranium recovery facility with a surface-soil processed natural uranium DCGL of 200 pCi/g. The project has not, however, identified a suitable offsite reference area, so it must estimate background using onsite data. The project has demonstrated that 200 pCi/g in surface soil is easily distinguishable from background and sets the  $IL_{PP}$  at  $z = +4$ . The GIS technician initially processes all onsite survey data together and calculates the population mean of 9,103 cpm and standard deviation of 661 cpm. The initial investigation level is calculated as follows:

$IL_{PP} \text{ (cpm)} = 9,103 \text{ cpm} + (4 \times 661 \text{ cpm}) = 11,747 \text{ cpm}$ , or  $\sim 11,700 \text{ cpm}$

However, the data include a small subset of elevated results that could be from uranium contamination. The GIS technician isolates data from an onsite area that is not linked to site operations and has shown no evidence of contamination. The associated data are used as the proxy background dataset. The GIS technician processes this proxy dataset and calculates a mean of 9,049 cpm and a standard deviation of 517 cpm, resulting in a  $z = +4$   $IL_{PP}$  of:

$IL_{PP} \text{ (cpm)} = 9,049 \text{ cpm} + (4 \times 517 \text{ cpm}) = 11,117 \text{ cpm}$ , or  $\sim 11,100 \text{ cpm}$ ,

which corresponds to a net concentration of about 110 pCi/g (or about 55 percent of the DCGL).

Therefore, the GIS technician identifies detector responses above 11,100 cpm for followup investigation, including potential anomalies. Figure 6-13 shows the entire dataset, the smaller subset used as a proxy for background, and the associated  $IL_{PP}$  values.

Example 4 demonstrates how the GIS technician may introduce the potential for false negative decisions by failing to set the  $IL_{PP}$  based on background data. That is, if the standard deviation is estimated using the data population that includes detector responses from hotspots (or gross contamination), the  $IL_{PP}$  can be overestimated. Figure 6-14 presents gamma walkover survey data from a staged survey performed in Oak Ridge, TN. Several Cs-137 button sources were hidden from view, a survey was performed, and the data were delivered to a GIS technician for processing. The GIS technician was instructed to set a z-score = +3 as the  $IL_{PP}$  using the background dataset (from an area with no radiation sources), and to set a different z-score = +3 as the  $IL_{PP}$  using the data that included responses from the hidden sources. The figure on the left shows that, if the  $IL_{PP}$  was set using background data, the GIS technician would have identified all 10 hidden sources (note the two false positive results near the upper right corner—a few false positives are expected in a large dataset given that there is a statistical probability that 0.13 percent of the results would be expected to exceed the  $z = 3$  value). However, the figure on the right shows that when the  $IL_{PP}$  is set using site data that include responses resulting from the sources, the GIS technician would have identified only 5 of 10 hidden sources.

Finally, the Example 5 project is set at a uranium recovery facility with surface soil contaminated with processed natural uranium. A  $DCGL_W$  of 20 pCi/g above background and a  $DCGL_{EMC}$  of 200 pCi/g above background have been established, and DQOs produce a preliminary  $IL_{PP}$  at  $z = +3$ . The project has identified a suitable offsite reference area, and surveyors have collected a background dataset ahead of site characterization. The GIS technician processes the reference area survey data, verifies normality, and calculates the population mean of 9,060 cpm and standard deviation of 580 cpm. The preliminary  $IL_{PP}$  is, therefore, calculated using Equation 6.21, as follows:

$$IL_{PP} \text{ (cpm)} = 9,060 \text{ cpm} + (3 \times 580 \text{ cpm}) = 10,800 \text{ cpm}$$

Using Equation 6.17 and Table 6-8 inputs, the associated concentration is calculated as follows:

$$IL_{PP} \text{ (pCi/g)} = (3 \times 580 \text{ cpm}) / (18.3 \text{ cpm/pCi/g}) = 95 \text{ pCi/g}$$

For planning purposes, the project also estimates the net 2" × 2" NaI response that would be expected from a 0.25-m<sup>2</sup>, 0.15-m-thick hotspot in surface soils. This value is estimated as 20 pCi/g × 18.3 cpm/pCi/g = 366 cpm. Therefore, the  $IL_{PP}$  corresponds to a concentration several times the  $DCGL_W$ , and a modeled response from a hotspot at the  $DCGL_W$  is less than one standard deviation above the mean background response. However, both the surveyor (if listening) and the GIS technician should be able to detect the expected response at the  $DCGL_{EMC}$  (200 pCi/g × 18.3 cpm/pCi/g = 3,660 cpm) from background. The concentration detectable by either the surveyor or the GIS technician is somewhere below the  $DCGL_{EMC}$ . The project decides to accept a higher false positive error, adjusts the  $IL_{PP}$  to  $z = +2$  (10,220 cpm), and then commits to collecting soil samples at locations that produce responses between the corresponding revised  $IL_{PP}$  and  $DCGL_{EMC}$  values. The project can then use the scanning data and soil sample analytical results to determine if a cpm-to-concentration correlation can support project decisions. The results can also be used to support the conclusion that the project can

effectively demonstrate that scan sensitivity is adequate to detect residual concentrations. In the MARSSIM framework, the project that cannot meet scan sensitivity requirements would need to increase the sample density to compensate.

### 6.3.2 *A Priori* MDCRs Versus *A Posteriori* Investigation Levels Using Radiation Survey Data

Early in the planning process, projects will determine whether surveyors, GIS technicians, or both will conduct followup investigations (e.g., judgmental sampling). The following discussion presents several hypothetical scenarios to evaluate how *a priori* MDCRs and *a posteriori*  $IL_{PP}$  values might compare when considering actual survey data. The data used to generate these scenarios are raw results from verified clean or reference area sites in California, Maryland, Tennessee, and Washington State.

Because the MDCR is dependent on three inputs that predict future outcomes (specifically,  $i$ ,  $p$ , and  $d'$ ), the comparison is limited to an observation interval of 1 or 2 seconds, a surveyor efficiency of 0.5 or 0.75, and indexes of sensitivity of 1.38, 1.96, 2.32, and 2.56. Gross MDCR results (MDCR plus mean background) are compared to potential  $IL_{PP}$  values set at  $z = +2$ ,  $+3$ ,  $+4$ , and  $+5$ . This discussion presumes that radionuclide concentrations at the DCGL are difficult to detect using standard survey equipment; therefore, projects will set the *a posteriori*  $IL_{PP}$  at  $z = +3$ .

Figure 6-15 presents site-specific results for  $i = 1$  second and  $p = 0.5$ . For a given survey speed, a short observation interval and low surveyor efficiency imply that small hotspots are expected (e.g., the 0.25-m<sup>2</sup> areas considered in the Section 6.2 scan MDC calculations) and that surveyors are less experienced or otherwise efficient at identifying anomalies. If the contaminant is difficult to detect at the DCGL, then these results suggest that a  $d'$  between 1.38 and 1.96 would have generated *a priori* a gross MDCR similar to the *a posteriori*  $z = +3$   $IL_{PP}$ . Larger  $d'$  values may be selected *a priori* if the contaminant is easily distinguishable from background, or the project wants to limit false positive decision errors.

Figure 6-16 presents site-specific results for  $i = 1$  second and  $p = 0.75$ , so all conditions are the same as in Figure 6-15 except the surveyors are more experienced and efficient at identifying anomalies. These results show that, in three of the four cases, the gross MDCR for  $d' = 1.38$  is the same as the  $z = +2$   $IL_{PP}$ , which would be expected to result in a high incidence of false positive decisions. In these cases, the gross MDCR for a  $d'$  of 1.96 to 2.32 would be more comparable to a  $z = +3$   $IL_{PP}$  and result in fewer false positives.

Figure 6-17 presents site-specific results for  $i = 2$  seconds and  $p = 0.5$ . The longer observation interval and low surveyor efficiency imply that larger hotspots are expected and surveyors are less experienced. These data suggest that selecting a small  $d'$  will result in a high incidence of false positive decision errors (sometimes within two standard deviations from the mean) and a  $d'$  of 1.96 to 2.32 is more comparable to a  $z = +3$   $IL_{PP}$ .

Figure 6-18 presents site-specific results for  $i = 2$  seconds and  $p = 0.75$ . For a given survey speed, the longer observation interval and higher surveyor efficiency imply that larger hotspots are anticipated and surveyors are experienced or efficient in identifying anomalies. These data suggest that all gross MDCRs fall within range of the reference dataset population, smaller  $d'$  selections imply a very high tolerance for false positive decisions, and a  $d'$  of 2.56 (or higher) would be more comparable to a  $z = +3$   $IL_{PP}$ .

Finally, the following presents average z-scores calculated for gross MDCR values plotted in Figures 6-15 through 6-18. That is,  $X$  in Equation 6.20 was replaced with the gross MDCR for each dataset (for a given  $i$ ,  $p$ , and  $d'$ ), and the values were averaged. These results show what z-score, on average, would be comparable to the *a priori* gross MDCR for given values of  $i$ ,  $p$ , and  $d'$ :

| $i =$ | 1 sec           | 2 sec | 1 sec | 2 sec |
|-------|-----------------|-------|-------|-------|
| $p =$ | 0.50            | 0.50  | 0.75  | 0.75  |
| $d'$  | Average z-score |       |       |       |
| 1.38  | 2.66            | 1.91  | 2.16  | 1.56  |
| 1.96  | 3.77            | 2.72  | 3.12  | 2.16  |
| 2.32  | 4.52            | 3.22  | 3.73  | 2.61  |
| 2.56  | 4.98            | 3.52  | 4.07  | 2.86  |

This comparison is for information purposes only, and the decommissioning project should not presume that an *a priori* MDCR will necessarily align with an *a posteriori*  $IL_{PP}$ . Reasons they may not align include the use of different calculation methods, the MDCR's failure to account for the variability in background, and the use of different DQOs to apply methods (see Section 6.4). However, *a priori* inputs may result in a planned MDCR well within (e.g., z-score of about 1.6) or well outside of (e.g., z-score of about 5) the background distribution. The point is that the selection of  $i$ ,  $p$ , and  $d'$  should not be completely separated from the expectation that surveyors will implement the survey as planned. Planners should, for example, consider whether it is reasonable to expect surveyors to investigate signals less than two standard deviations from the mean of background, or whether it is tolerable to set an investigation level well outside of the distribution of background.

### 6.3.3 A Posteriori Assessment of Surveyor Efficiency

A series of trial surveys were performed over a land area, using a 2" x 2" NaI detector, and over block walls using a gas proportional detector. The primary objectives for these trials were to determine if headphones improved a surveyor's ability to locate radiation sources and whether a GIS technician was better at locating radiation sources using post-processed data compared to the surveyor in real time. Radiation sources of various strengths and sizes were hidden from view in each area. Surveyors were instructed to complete a 100-percent survey of each area and to identify any locations that produced detector responses above background.

Each surveyor completed independent blind surveys with and without headphones to see if headphone use affected the surveyor's ability to detect hotspots. All locations indicated by the surveyor as a hotspot were recorded on survey forms (both true and false positives). Count rate data, survey durations, and position data were also electronically captured for mapping and analysis by a GIS technician. Surveyors' decisions were then tabulated, and the GIS technician then processed captured survey data. The GIS technician calculated the *a posteriori*  $IL_{PP}$  (at  $z = +3$ ) based on actual surveyor results from the same areas but before source placement. Decisions made by each surveyor could then be compared to decisions made at the *a posteriori*  $IL_{PP}$ . Surveyor results were also evaluated based on the percent coverage and percent of the hidden sources located (i.e., true positives).

**Statistical Analytical Methods.** Surveyor efficiency, or the true positive percentage, was calculated for each experiment as the number of sources found, divided by the total number of

sources in the experiment. Within each experiment, two methods were used for determining the number of sources found: the number per surveyor and the number per GIS technician. Thus, three null hypotheses were tested for both the outdoor and indoor experiment conditions:

- $H_0$ : Percent of the hidden sources found by the surveyor when wearing headphones is less than or equal to the percent found without headphones (one-sided/one-tail probability student's t-test).
- When the surveyor is wearing headphones,  $H_0$ : Percent of the hidden sources found by the surveyor equals the percent found during post-processing (two-sided/two-tail probability student's t-test).
- When the surveyor was not wearing headphones,  $H_0$ : Percent of the hidden sources found by the surveyor equals the percent found calculated in post-processing (two-sided/two-tail probability student's t-test).

The first hypothesis is evaluated using a one-sided test, as it is expected that wearing headphones should improve surveyor efficiency. The second and third hypotheses are evaluated using two-sided tests as there was no *a priori* expectation that one method of determining the number of sources (and hence calculation of percent found) would be better or worse than the other. However, the purpose was to determine whether the methods differ.

As each surveyor and each hidden source present an opportunity, or trial, in which a correct decision can be made, 95-percent confidence intervals of the percent found and the significance for the difference in percent found between experimental conditions were calculated based on the normal approximation to the binomial distribution, with continuity correction (as described in Kuzma & Bohlenblust, 2004).

Additional data collected included the survey duration (minutes) and percent coverage. These variables were described and tested for correlation with percent found (two-sided test), where the correlation coefficient ( $r$ ) has the following characteristics:

- 0 indicates no linear relationship.
- +1 indicates a perfect positive linear relationship: As one variable increases in its values, the other variable also increases in its values in the same proportion for each unit.
- -1 indicates a perfect negative linear relationship: As one variable increases in its values, the other variable decreases in its values in the same proportion for each unit.
- Values between 0 and 0.3 (0 and -0.3) indicate a weak positive (negative) linear relationship.
- Values between 0.3 and 0.7 (-0.3 and -0.7) indicate a moderate positive (negative) linear relationship.
- Values between 0.7 and 1.0 (-0.7 and -1.0) indicate a strong positive (negative) linear relationship.



For correlation analyses, there is no *a priori* hypothesis about the relationship between variables. The objective here is to estimate the strength (or weakness) of the relationship that may lead to procedural guidelines that optimize true positive decisionmaking. Data analyses were conducted in Excel and SAS 9.3 (SAS Institute, Inc., Cary, NC). For all t-tests and tests for correlation, the significance level was 0.05, such that p-values less than 0.05 indicate a statistically significant test or difference (see NUREG-1475, "Applying Statistics," issued March 2011, for discussions of inference, hypothesis testing, and correlations).

**Statistical Analytical Results.** Table 6-9 presents summary results for land area surveys performed without headphones, and Table 6-10 presents summary results for a separate land area survey performed with headphones. Table 6-11 presents summary results for wall surveys performed without headphones, and Table 6-12 presents summary results for a separate wall survey performed with headphones. These tables present the time each surveyor took to complete each survey, an estimate of the percent coverage, and the number of true and false positive decisions made by both the surveyor and the GIS technician. Table 6-13 presents results for trials designed to determine whether headphones improved the percentage of sources found as determined by the surveyor and GIS technician. Table 6-14 presents correlation results for survey time and percent coverage, survey time and the number of sources found, and survey coverage and the number of sources found. It also shows how results compare between surveyors with and without headphones.

Table 6-13 shows that for outdoor land area tests, the percent found improved significantly from 84 to 92 percent with the addition of headphones (p-value of 0.041). Similarly, for the indoor wall survey tests, the percent found improved significantly from 71 to 79 percent with the addition of headphones (p-value of 0.046). These results strongly suggest that the use of headphones improves a surveyor's ability to identify sources, thus lowering false negative decision errors. When comparing the surveyor decisions to GIS technician decisions for results where headphones were not used, there is no statistically significant difference for outdoor surveys (p-value of 0.207), but for indoor surveys where no headphones were used the surveyor found 71 percent of the sources, significantly better than the GIS technician, who found only 58 percent (p-value of 0.022). When headphones are used, the percentages found by the surveyors and the GIS technician are not significantly different for either the outdoor or indoor tests. These results suggest that surveyors and GIS technicians perform at about the same level overall (three out of four tests), though for indoor surveys, surveyors who use headphones may have fewer false negative decision errors than GIS technicians.

Table 6-14 shows that survey time and percent coverage are moderately correlated with significance when surveyors wear headphones during both outdoor surveys (r of 0.69, p-value of 0.028) and indoor surveys (r of 0.67, p-value of 0.013). When headphones are not used, the correlations are less but still moderate, although not statistically significant. These results suggest that survey time and percent coverage are correlated in general, but when headphones are used, surveyors are more focused and perform a more thorough survey.

In comparisons of survey time and the number of sources found in Table 6-14, all findings are moderately correlated, though the only statistically significant correlations are for the surveyor indoors without headphones (r of 0.57, p-value of 0.039) and with headphones (r of 0.56, p-value of 0.045). These results suggest that survey time and the percent of the sources found are moderately correlated, but indoor surveyors were more successful when they spent more time to complete surveys.

In comparisons of survey coverage and the number of sources found in Table 6-14, correlations ranged dramatically. Statistically significant results include strong correlations for outdoor surveys without headphones by both the surveyors (r of 0.80, p-value of 0.006) and the GIS technician (r of 0.75, p-value of 0.013), and only a strong correlation was observed when the GIS technician processed results where a surveyor used headphones (r of 0.71, p-value of 0.011). For surveyors using headphones, the percent coverage and number of sources found are moderately correlated but not with statistical significance (r of 0.51, p-value of 0.135). These results suggest that, in general for outdoor surveys (three of the four tests), there is a strong correlation between the percent coverage and the number of sources found. One reason for this relationship may be that sources used outdoors were relatively strong, so the surveys were likely to correctly identify the source location if the path crossed over or very near the source. This finding is countered by results for indoor surveys, which show no statistical significance for any result, no correlation (r of -0.01) when headphones are used, and only weak or moderate correlations with no headphones (r of 0.25 to 0.36). Source strengths used during indoor surveys were more variable and more difficult to detect when compared to those used for outdoor surveys. The results may be interpreted to mean that, when sources are close to detection limits, coverage alone is less important than survey time (or speed of the survey), regardless of whether headphones are used. That is, especially for weaker sources, emphasis on increased coverage is less important than an increased observation interval.

The most obvious conclusion from these tests is that surveyors improved performance when they slowed down and wore headphones. Slower survey times may translate to higher observation intervals, and headphones appear to focus the surveyor and result in fewer false negative decision errors. In general, the surveyor and GIS technician produced comparable results—the surveyor is more successful in some tests, and the GIS technician is more successful in others. However, if the surveyor listens with headphones, and both the surveyor and GIS technician contribute to the decisionmaking process, projects should anticipate fewer false negative decisions. For example, if by wearing headphones, the surveyor is more likely to pause over a hotspot, the resulting detector response is more likely to reach full scale and hence result in a higher probability of true positive decisions by both the surveyor (in real time) and the GIS technician (during post-processing).

#### **6.4 Decommissioning Planning and Data Quality Objectives**

Decommissioning planners may estimate the *a priori* scan MDC by predicting contaminant conditions (e.g., hot-spot size, source efficiencies) using the methods described in Section 6.2, or they may set an *a posteriori*  $IL_{PP}$  based on the data collected at the site using the methods described in Section 6.3. Planners should not, however, plan a survey by estimating an *a priori* scan MDC, ignoring surveyor input, and then make decisions based on an *a posteriori*  $IL_{PP}$ . For example, with the widespread use of GPS and GIS equipment, planners may inappropriately (1) demonstrate via an *a priori* scan MDC calculation that surveyors can detect the contaminant at an acceptable level, (2) instruct surveys to collect data *without listening to audible output*, and (3) allow GIS technicians to make judgmental sample location decisions based on an *a posteriori* z-score. If the surveyors are not listening, the *a priori* scan MDC is invalidated, and the decommissioning plan is suspect at best.

Table 6-15 presents examples of DQOs for hypothetical sites potentially contaminated with Ra-226 and associated decay products. Parallel decommissioning projects are preparing plans to survey surface soils using 2" × 2" NaI detectors. Project 1 will use a traditional approach by estimating an *a priori* scan MDC and allowing surveyors to make real-time judgmental sample location decisions. Project 2 will allow a GIS technician, not the surveyor, to identify judgmental

sample locations based on an *a posteriori*  $IL_{PP}$ . For the purpose of this comparison, Project 1 does not necessarily use GPS/GIS technology or any form of electronic data collection—surveyors make all the judgmental sampling decisions.

As seen in Table 6-15, DQOs Step 1 (State the Problem) and Step 2 (Identify the Decision) are identical at both sites. Both must demonstrate that surface soils are (or are not) below a DCGL of 5.0 pCi/g. Project DQOs deviate under Step 3 (Identify the Inputs to the Decision) because Project 1 allows surveyors to select judgmental sample locations, while Project 2 relies on GIS technicians to select these locations. Step 4 (Define the Boundaries of the Study) is identical for these hypothetical sites. Step 5 (Develop a Decision Rule) shows that both projects will collect reference area survey and soil data. Project 1, however, will use the reference area survey data as an input to the *a priori* scan MDC calculation. Alternatively, Project 2 will use the reference area survey data to set the z-score  $IL_{PP}$ .

(Note that if a suitable reference area is not available, Project 1 could assume an average background response based on the literature or on experience, and Project 2 could instruct the GIS technician to establish the z-score  $IL_{PP}$  based on actual site survey data. These decisions should be addressed during DQO development, starting no later than Step 4.)

DQOs under Step 6 (Specify Limits on Decision Errors) are dramatically different. The Project 1 DQO is qualitative, establishing decision errors and an *a priori* scan MDC calculation that is used to demonstrate contaminant detectability. The Project 2 DQO is semiquantitative and does not directly relate a detector response to a soil concentration. Project 2 could, in this or other DQO steps, specify how survey data will be binned or otherwise processed to support judgmental sample decisions. For example, it may be prudent to test the data for normality and plan for associated consequences. As presented, however, Project 1 predicts surveyors will be able to locate contamination below the DCGL, and Project 2 predicts the GIS technician will locate potential contamination outside of the range of background.

Finally, both projects describe in DQO Step 7 (Optimize the Design for Collecting Data) procedures for collecting survey data and making judgmental sample decisions. The notable difference is the description of how the surveyor or the GIS technician selects a location.

These seven DQO steps are streamlined, and an actual decommissioning project may include many more details to ensure that data are of sufficient quality and quantity for decisionmaking. However, Table 6-15 shows that decommissioning projects should, during the planning stage of the project life cycle, consider how survey data will be collected and interpreted. Additionally, it should be obvious that a decommissioning plan should not use *a priori* (*d'*) DQO Steps 1 through 6 and then jump to an *a posteriori* (z-score) DQO Step 7 at the end of the process.

## **6.5 Conclusions and Recommendations**

Based on the information in this section, conclusions and best practice recommendations include the following:

- Projects should identify a reference area or areas that have physical, chemical, radiological, and biological characteristics similar to those of the site area or areas being investigated, but that have not been impacted by site activities. Survey data from these areas should be evaluated by examining the summary statistics and the underlying population distribution for normality or multimodality and by ensuring the dataset is free of outliers that may indicate site impact. These evaluations are

necessary to ensure that an appropriate and defensible decision statistic is determined, such as the *a posteriori*  $IL_{PP}$  calculation. If available during the planning phase of a project, reference area data should also be used to estimate the mean detector response in the *a priori* scan MDC calculation. Reference areas can be located off site when they are available and meet the above criteria, or they can be separated out from the site data by using population partitioning and extraction techniques if suitable offsite areas are not available. In either case, *a priori* scan MDCs and *a posteriori*  $IL_{PP}$  values should be calculated using detector responses from areas that have not been contaminated by site activities.

- Examples of acceptable methods may include the *a priori* scan MDC using the MDCR, a statistically based *a posteriori*  $IL_{PP}$ , or an empirically determined method demonstrated to be capable of minimizing false negative decisions in locating anomalous radiation levels measured during a radiation survey. Whichever method is selected, projects should develop DQOs that describe the rationale for associated inputs and then execute surveys according to that plan.
- Several examples are presented to establish an *a posteriori*  $IL_{PP}$ , though other methods may be suitable. Planners should consider which method for calculating the  $IL_{PP}$  best suits the project based on site-specific requirements (such as DQOs or regulations) and is acceptable to the regulator.
- A project that develops DQOs that include an *a priori* MDCR should allow the surveyor to listen to the detector's audible response and identify anomalies in real time. Alternatively, if a project instructs surveyors not to listen or not to respond to anomalous detector responses, and a GIS technician or other independent observer makes the decisions, then an *a priori* scan MDCR calculation should not be used for planning purposes.
- For planning, projects should ensure that detection sensitivities and investigation levels are adequate to sufficiently respond to and investigate contaminated areas. Accordingly, the input parameters chosen for *a priori* strategies (i.e., *i*, *p*, and *d'*) or the  $IL_{PP}$  chosen for *a posteriori* strategies should be appropriate for the survey conditions, and planners should ensure that detection sensitivities and investigation levels are adequate relative to the DCGL. MARSSIM and NUREG-1757 guidance provide additional information on setting MDCs and investigation levels.
- The use of headphones for listening to the audio output enhances the surveyor's ability to distinguish signal from noise and, therefore, helps decrease the incidence of false negative decisions.
- Slower systematic surveys, with increased observation intervals, enhance the project's ability to distinguish signal from noise and, therefore, help decrease the incidence of false negative decisions.

**Table 6-1 Values of d' for Selected True Positive and False Positive Proportions**

| False Positive Proportion | True Positive Proportion |      |      |      |      |      |      |      |
|---------------------------|--------------------------|------|------|------|------|------|------|------|
|                           | 0.60                     | 0.65 | 0.70 | 0.75 | 0.80 | 0.85 | 0.90 | 0.95 |
| 0.05                      | 1.90                     | 2.02 | 2.16 | 2.32 | 2.48 | 2.68 | 2.92 | 3.28 |
| 0.10                      | 1.54                     | 1.66 | 1.80 | 1.96 | 2.12 | 2.32 | 2.56 | 2.92 |
| 0.15                      | 1.30                     | 1.42 | 1.56 | 1.72 | 1.88 | 2.08 | 2.32 | 2.68 |
| 0.20                      | 1.10                     | 1.22 | 1.36 | 1.52 | 1.68 | 1.88 | 2.12 | 2.48 |
| 0.25                      | 0.93                     | 1.06 | 1.20 | 1.35 | 1.52 | 1.72 | 1.96 | 2.32 |
| 0.30                      | 0.78                     | 0.91 | 1.05 | 1.20 | 1.36 | 1.56 | 1.80 | 2.16 |
| 0.35                      | 0.64                     | 0.77 | 0.91 | 1.06 | 1.22 | 1.42 | 1.66 | 2.02 |
| 0.40                      | 0.51                     | 0.64 | 0.78 | 0.93 | 1.10 | 1.30 | 1.54 | 1.90 |
| 0.45                      | 0.38                     | 0.52 | 0.66 | 0.80 | 0.97 | 1.17 | 1.41 | 1.77 |
| 0.50                      | 0.26                     | 0.38 | 0.52 | 0.68 | 0.84 | 1.04 | 1.28 | 1.64 |
| 0.55                      | 0.12                     | 0.26 | 0.40 | 0.54 | 0.71 | 0.91 | 1.15 | 1.51 |
| 0.60                      | 0.00                     | 0.13 | 0.27 | 0.42 | 0.58 | 0.82 | 1.02 | 1.38 |

**Table 6-2 Scanning Sensitivity (MDCR) of the Ideal Observer for Various Background Levels<sup>a</sup>**

| Background (cpm) | MDCR (net cpm) | Scan Sensitivity (gross cpm) |
|------------------|----------------|------------------------------|
| 45               | 51             | 96                           |
| 60               | 59             | 120                          |
| 260              | 120            | 380                          |
| 300              | 130            | 430                          |
| 350              | 140            | 490                          |
| 400              | 150            | 550                          |
| 1,000            | 240            | 1,240                        |
| 2,000            | 340            | 2,340                        |
| 4,000            | 480            | 4,480                        |
| 6,000            | 590            | 6,590                        |
| 8,000            | 680            | 8,680                        |
| 10,000           | 760            | 10,760                       |
| 12,000           | 830            | 12,830                       |
| 15,000           | 930            | 15,930                       |
| 20,000           | 1,100          | 21,100                       |
| 25,000           | 1,200          | 26,200                       |
| 30,000           | 1,300          | 31,300                       |

<sup>a</sup>The sensitivity of the ideal observer during the first scanning stage is based on an index of sensitivity ( $d'$ ) of 2.32 and a 2-second observation interval.

**Table 6-3 NaI Scintillation Detector Count Rate versus Exposure Rate (cpm per  $\mu\text{R/h}$ )**

| Gamma Energy (keV) | cpm per $\mu\text{R/h}$ <sup>a</sup> |                                   |                                   |                     |
|--------------------|--------------------------------------|-----------------------------------|-----------------------------------|---------------------|
|                    | 1" x 1" NaI Detector <sup>b</sup>    | 2" x 2" NaI Detector <sup>c</sup> | 3" x 3" NaI Detector <sup>d</sup> | FIDLER <sup>e</sup> |
| 15                 | 340                                  | 1,160                             | 2,540                             | 5,500               |
| 20                 | 630                                  | 2,150                             | 4,720                             | 10,220              |
| 30                 | 1,460                                | 5,030                             | 11,030                            | 23,480              |
| 40                 | 2,470                                | 8,480                             | 18,610                            | 40,290              |
| 50                 | 3,300                                | 11,300                            | 24,820                            | 53,640              |
| 60                 | 3,700                                | 12,700                            | 27,870                            | 59,000              |
| 80                 | 3,510                                | 12,000                            | 26,410                            | 47,180              |
| 100                | 2,900                                | 9,970                             | 21,870                            | 29,280              |
| 150                | 1,790                                | 6,190                             | 13,580                            | 8,580               |
| 200                | 1,190                                | 4,320                             | 9,510                             | 3,460               |
| 300                | 600                                  | 2,540                             | 5,820                             | 1,140               |
| 400                | 370                                  | 1,710                             | 4,110                             | 610                 |
| 500                | 260                                  | 1,270                             | 3,160                             | 400                 |
| 600                | 200                                  | 1,010                             | 2,560                             | 290                 |
| 662                | 180                                  | 900                               | 2,300                             | 250                 |
| 800                | 130                                  | 710                               | 1,850                             | 190                 |
| 1,000              | 100                                  | 550                               | 1,460                             | 140                 |
| 1,500              | 62                                   | 350                               | 970                               | 80                  |
| 2,000              | 46                                   | 270                               | 740                               | 58                  |
| 3,000              | 32                                   | 190                               | 530                               | 39                  |

<sup>a</sup>Based on normalizing detector response to the cpm per  $\mu\text{R/h}$  value provided by manufacturer for Cs-137. The text describes the calculation approach in Section 6.2.5.

<sup>b</sup>Detector used was Ludlum model 44-2; manufacturer provided 175 cpm per  $\mu\text{R/h}$  for Cs-137 (662 keV).

<sup>c</sup>Detector used was Ludlum model 44-10; manufacturer provided 900 cpm per  $\mu\text{R/h}$  for Cs-137 (662 keV).

<sup>d</sup>Detector used was Ludlum model 44-20; manufacturer provided 2,300 cpm per  $\mu\text{R/h}$  for Cs-137 (662 keV).

<sup>e</sup>Detector used was Thermo Scientific model G5; modeled value of 59,000 cpm per  $\mu\text{R/h}$  for Am-241 (60 keV) using the MCNP computer code.

**Table 6-4 Activity Fraction Estimates for Various Enrichments of Uranium**

| Uranium Enrichment | Uranium Isotope | Specific Activity <sup>a</sup> (Ci/g) | Mass Fraction <sup>b</sup> | Activity <sup>c</sup> (Ci) | Activity Fraction <sup>d</sup> |
|--------------------|-----------------|---------------------------------------|----------------------------|----------------------------|--------------------------------|
| Depleted           | U-234           | 6.19E-03                              | —                          | 1.90E-07                   | 0.3596                         |
|                    | U-235           | 2.14E-06                              | 0.0034                     | 7.28E-09                   | 0.0137                         |
|                    | U-238           | 3.33E-07                              | 0.9966                     | 3.32E-07                   | 0.6266                         |
|                    | U-Total         |                                       |                            |                            | 5.30E-07                       |
| Natural            | U-234           | 6.19E-03                              | —                          | 3.29E-07                   | 0.4877                         |
|                    | U-235           | 2.14E-06                              | 0.0072                     | 1.54E-08                   | 0.0228                         |
|                    | U-238           | 3.33E-07                              | 0.9928                     | 3.31E-07                   | 0.4895                         |
|                    | U-Total         |                                       |                            |                            | 6.75E-07                       |
| 3%                 | U-234           | 6.19E-03                              | —                          | 1.18E-06                   | 0.7535                         |
|                    | U-235           | 2.14E-06                              | 0.03                       | 6.42E-08                   | 0.0409                         |
|                    | U-238           | 3.33E-07                              | 0.97                       | 3.23E-07                   | 0.2057                         |
|                    | U-Total         |                                       |                            |                            | 1.57E-06                       |
| 20%                | U-234           | 6.19E-03                              | —                          | 8.67E-06                   | 0.9258                         |
|                    | U-235           | 2.14E-06                              | 0.2                        | 4.28E-07                   | 0.0457                         |
|                    | U-238           | 3.33E-07                              | 0.8                        | 2.66E-07                   | 0.0285                         |
|                    | U-Total         |                                       |                            |                            | 9.36E-06                       |
| 50%                | U-234           | 6.19E-03                              | —                          | 2.67E-05                   | 0.9557                         |
|                    | U-235           | 2.14E-06                              | 0.5                        | 1.07E-06                   | 0.0384                         |
|                    | U-238           | 3.33E-07                              | 0.5                        | 1.67E-07                   | 0.0060                         |
|                    | U-Total         |                                       |                            |                            | 2.79E-05                       |
| 75%                | U-234           | 6.19E-03                              | —                          | 4.63E-05                   | 0.9648                         |
|                    | U-235           | 2.14E-06                              | 0.75                       | 1.61E-06                   | 0.0334                         |
|                    | U-238           | 3.33E-07                              | 0.25                       | 8.33E-08                   | 0.0017                         |
|                    | U-Total         |                                       |                            |                            | 4.80E-05                       |

<sup>a</sup>Specific activities from *Decommissioning Health Physics—A Handbook for MARSSIM Users* (Abelquist, 2014).

<sup>b</sup>Mass fraction of 1 gram of uranium assuming the relative fraction of U-234 is approximately 0.

<sup>c</sup>Derived from EGG-2350/UC-41 (Idaho National Engineering Laboratory, 1988):

Activity U-Total = Mass U-Total × (0.4 + 0.38 × [Mass Fraction U-235 × 100] + 0.0034 × [Mass Fraction U-235 × 100]<sup>2</sup>) × 1E-6

Activity U-235 = (Specific Activity U-235) × (Mass Fraction U-235)

Activity U-238 = (Specific Activity U-238) × (Mass Fraction U-238)

Activity U-234 = (Activity U-Total) – (Activity U-235) – (Activity U-238)

<sup>d</sup>Normalized activity fraction.

**Table 6-5 NaI Scintillation Detector Scan MDCs for Common Radiological Contaminants—Example 1<sup>a</sup>**

| Radionuclide/Radioactive Material    | 1" x 1" NaI Detector |                         | 2" x 2" NaI Detector |                         | 3" x 3" NaI Detector |                         | FIDLER           |                         |
|--------------------------------------|----------------------|-------------------------|----------------------|-------------------------|----------------------|-------------------------|------------------|-------------------------|
|                                      | Scan MDC (pCi/g)     | Weighted cpm/ $\mu$ R/h | Scan MDC (pCi/g)     | Weighted cpm/ $\mu$ R/h | Scan MDC (pCi/g)     | Weighted cpm/ $\mu$ R/h | Scan MDC (pCi/g) | Weighted cpm/ $\mu$ R/h |
| Am-241                               | 57                   | 3,701                   | 39                   | 12,710                  | 27                   | 27,870                  | 5.6              | 47,540                  |
| Co-60                                | 10                   | 77                      | 4.1                  | 429                     | 2.3                  | 1,165                   | 12               | 102                     |
| Cs-137                               | 18                   | 175                     | 8.0                  | 900                     | 4.8                  | 2,300                   | 19               | 253                     |
| Th-230                               | 3,200                | 2,633                   | 2,100                | 9,082                   | 1,500                | 19,920                  | 420              | 31,860                  |
| Ra-226+C in equilibrium              | 6.0                  | 179                     | 3.0                  | 841                     | 1.8                  | 2,087                   | 2.9              | 582                     |
| Th-232+C in equilibrium              | 4.0                  | 191                     | 2.1                  | 840                     | 1.3                  | 2,048                   | 1.6              | 753                     |
| 0.034% Depleted Uranium <sup>b</sup> | 140                  | 1,072                   | 90                   | 3,836                   | 62                   | 8,570                   | 22               | 9,841                   |
| 0.072% Natural Uranium <sup>b</sup>  | 140                  | 1,130                   | 92                   | 3,836                   | 63                   | 8,996                   | 25               | 9,379                   |
| 3% Enriched Uranium <sup>b</sup>     | 150                  | 1,212                   | 96                   | 4,328                   | 66                   | 9,567                   | 34               | 8,186                   |
| 20% Enriched Uranium <sup>b</sup>    | 180                  | 1,408                   | 110                  | 5,027                   | 80                   | 11,060                  | 49               | 7,218                   |
| 50% Enriched Uranium <sup>b</sup>    | 220                  | 1,431                   | 140                  | 5,106                   | 98                   | 11,230                  | 62               | 7,085                   |
| 75% Enriched Uranium <sup>b</sup>    | 250                  | 1,437                   | 160                  | 5,129                   | 110                  | 11,270                  | 71               | 7,067                   |

<sup>a</sup>+C<sup>+</sup> indicates the associated decay chain that ultimately results from the decay of the listed parent radionuclide.

<sup>b</sup>Refer to Section 6.2.5 of the text for complete explanation of factors used to calculate scan MDCs. For these examples, the following inputs were used:

Background levels = 1,800 cpm for the 1" x 1"; 9,750 for the 2" x 2"; 23,000 for the 3" x 3"; and 4,500 for the FIDLER

Observation interval (*t*) = 2 seconds

Index of sensitivity (*c*<sup>+</sup>) = 2.32 for 0.95 true positive proportion and 0.25 false positive proportion (see Table 6-1)

Surveyor efficiency (*p*) = 0.5

<sup>c</sup>Scan MDC for uranium includes sum of U-238, U-235, and U-234.



**Table 6-6 NaI Scintillation Detector Scan MDCs for Common Radiological Contaminants—Example 2<sup>a</sup>**

| Radionuclide/Radioactive Material    | 1" x 1" NaI Detector |                    | 2" x 2" NaI Detector |                   | 3" x 3" NaI Detector |                   | FIDLER           |                   |
|--------------------------------------|----------------------|--------------------|----------------------|-------------------|----------------------|-------------------|------------------|-------------------|
|                                      | Scan MDC (pCi/g)     | Weighted cpm/uR/hr | Scan MDC (pCi/g)     | Weighted cpm/uR/h | Scan MDC (pCi/g)     | Weighted cpm/uR/h | Scan MDC (pCi/g) | Weighted cpm/uR/h |
| Am-241                               | 40                   | 3,701              | 27                   | 12,710            | 19                   | 27,870            | 3.8              | 47,540            |
| Co-60                                | 7                    | 77                 | 2.8                  | 429               | 1.6                  | 1,165             | 8                | 102               |
| Cs-137                               | 12                   | 175                | 5.5                  | 900               | 3.3                  | 2,300             | 13               | 253               |
| Th-230                               | 2,200                | 2,633              | 1,500                | 9,082             | 1,000                | 19,920            | 290              | 31,860            |
| Ra-226+C in equilibrium              | 4.1                  | 179                | 2.1                  | 841               | 1.3                  | 2,087             | 2.0              | 582               |
| Th-232+C in equilibrium              | 2.8                  | 191                | 1.5                  | 840               | 0.9                  | 2,048             | 1.1              | 753               |
| 0.034% Depleted Uranium <sup>b</sup> | 96                   | 1,072              | 62                   | 3,836             | 43                   | 8,570             | 15               | 9,841             |
| 0.072% Natural Uranium <sup>b</sup>  | 97                   | 1,130              | 63                   | 3,836             | 44                   | 8,996             | 17               | 9,379             |
| 3% Enriched Uranium <sup>b</sup>     | 100                  | 1,212              | 66                   | 4,328             | 46                   | 9,567             | 24               | 8,186             |
| 20% Enriched Uranium <sup>b</sup>    | 120                  | 1,408              | 79                   | 5,027             | 55                   | 11,060            | 34               | 7,218             |
| 50% Enriched Uranium <sup>b</sup>    | 150                  | 1,431              | 97                   | 5,106             | 68                   | 11,230            | 43               | 7,085             |
| 75% Enriched Uranium <sup>b</sup>    | 170                  | 1,437              | 110                  | 5,129             | 78                   | 11,270            | 49               | 7,067             |

<sup>a</sup>“+C” indicates the associated decay chain that ultimately results from the decay of the listed parent radionuclide.

<sup>b</sup>Refer to Section 6.2.5 of the text for complete explanation of factors used to calculate scan MDCs. For these examples, the following inputs were used:

Background levels = 1,800 cpm for the 1" x 1"; 9,750 for the 2" x 2"; 23,000 for the 3" x 3"; and 4,500 for the FIDLER

Observation interval (t) = 2 seconds

Index of sensitivity (c<sup>2</sup>) = 1.96 for 0.90 true positive proportion and 0.25 false positive proportion (see Table 6-1)

Surveyor efficiency (β) = 0.75.

<sup>c</sup>Scan MDC for uranium includes sum of U-238, U-235, and U-234.

**Table 6-7 NaI Scintillation Detector Scan MDCs for Common Radiological Contaminants—Example 3<sup>a</sup>**

| Radionuclide/Radioactive Material    | 1" x 1" NaI Detector |                   | 2" x 2" NaI Detector |                   | 3" x 3" NaI Detector |                   | FIDLER           |                   |
|--------------------------------------|----------------------|-------------------|----------------------|-------------------|----------------------|-------------------|------------------|-------------------|
|                                      | Scan MDC (pCi/g)     | Weighted cpm/μR/h | Scan MDC (pCi/g)     | Weighted cpm/μR/h | Scan MDC (pCi/g)     | Weighted cpm/μR/h | Scan MDC (pCi/g) | Weighted cpm/μR/h |
| Am-241                               | 100                  | 3,701             | 69                   | 12,710            | 49                   | 27,870            | 9.9              | 47,540            |
| Co-60                                | 17                   | 77                | 7.3                  | 429               | 4.1                  | 1,165             | 21               | 102               |
| Cs-137                               | 31                   | 175               | 14                   | 900               | 8.5                  | 2,300             | 34               | 253               |
| Th-230                               | 5,700                | 2,633             | 3,800                | 9,082             | 2,700                | 19,920            | 740              | 31,860            |
| Ra-226+C in equilibrium              | 11.0                 | 179               | 5.3                  | 841               | 3.3                  | 2,087             | 5.2              | 582               |
| Th-232+C in equilibrium              | 7.1                  | 191               | 3.8                  | 840               | 2.4                  | 2,048             | 2.9              | 753               |
| 0.034% Depleted Uranium <sup>b</sup> | 250                  | 1,072             | 160                  | 3,836             | 110                  | 8,570             | 40               | 9,841             |
| 0.072% Natural Uranium <sup>b</sup>  | 250                  | 1,130             | 160                  | 3,836             | 110                  | 8,996             | 45               | 9,379             |
| 3% Enriched Uranium <sup>b</sup>     | 260                  | 1,212             | 170                  | 4,328             | 120                  | 9,567             | 61               | 8,186             |
| 20% Enriched Uranium <sup>b</sup>    | 310                  | 1,408             | 200                  | 5,027             | 140                  | 11,060            | 88               | 7,218             |
| 50% Enriched Uranium <sup>b</sup>    | 380                  | 1,431             | 250                  | 5,106             | 180                  | 11,230            | 110              | 7,085             |
| 75% Enriched Uranium <sup>b</sup>    | 440                  | 1,437             | 290                  | 5,129             | 200                  | 11,270            | 130              | 7,067             |

<sup>a</sup>“+C” indicates the associated decay chain that ultimately results from the decay of the listed parent radionuclide.

<sup>b</sup>Refer to Section 6.2.5 of the text for complete explanation of factors used to calculate scan MDCs. For these examples, the following inputs were used:

Background levels = 1,800 cpm for the 1" x 1"; 9,750 for the 2" x 2"; 23,000 for the 3" x 3"; and 4,500 for the FIDLER

Observation interval (t) = 1 seconds

Index of sensitivity (c<sup>2</sup>) = 2.92 for 0.95 true positive proportion and 0.10 false positive proportion (see Table 6-1)

Surveyor efficiency (β) = 0.5

<sup>c</sup>Scan MDC for uranium includes sum of U-238, U-235, and U-234.

**Table 6-8 NaI Scintillation Detector Scan MDCs ERC and CPMR Input Values**

| Radionuclide/Radioactive Material    | ERC <sup>a</sup><br>μR/h/<br>pCi/g | 1" x 1" NaI Detector              |                               | 2" x 2" NaI Detector              |                               | 3" x 3" NaI Detector              |                               | FIDLER NaI Detector               |                               |
|--------------------------------------|------------------------------------|-----------------------------------|-------------------------------|-----------------------------------|-------------------------------|-----------------------------------|-------------------------------|-----------------------------------|-------------------------------|
|                                      |                                    | CPMR <sup>b</sup><br>cpm/<br>μR/h | CPMR<br>xERC<br>cpm/<br>pCi/g | CPMR <sup>a</sup><br>cpm/<br>μR/h | CPMR<br>xERC<br>cpm/<br>pCi/g | CPMR <sup>a</sup><br>cpm/<br>μR/h | CPMR<br>xERC<br>cpm/<br>pCi/g | CPMR <sup>a</sup><br>cpm/<br>μR/h | CPMR<br>xERC<br>cpm/<br>pCi/g |
| Am-241                               | 3.58E-03                           | 3,701                             | 13.3                          | 12,710                            | 45.6                          | 27,870                            | 99.9                          | 47,540                            | 170                           |
| Co-60                                | 1.01E+00                           | 77.1                              | 78.1                          | 429                               | 435                           | 1,165                             | 1,180                         | 102                               | 103                           |
| Cs-137                               | 2.47E-01                           | 175                               | 43.2                          | 900                               | 222                           | 2,300                             | 568                           | 253                               | 62.6                          |
| Th-230                               | 9.10E-05                           | 2,633                             | 0.239                         | 9,082                             | 0.826                         | 19,920                            | 1.81                          | 31,860                            | 2.90                          |
| Ra-226+C in equilibrium              | 7.10E-01                           | 179                               | 127                           | 841                               | 597                           | 2,087                             | 1,480                         | 582                               | 413                           |
| Th-232+C in equilibrium              | 9.96E-01                           | 191                               | 190                           | 840                               | 836                           | 2,048                             | 2,040                         | 753                               | 750                           |
| 0.034% Depleted Uranium <sup>c</sup> | 5.13E-03                           | 1,072                             | 5.50                          | 3,836                             | 19.7                          | 8,570                             | 43.9                          | 9,841                             | 50.5                          |
| 0.072% Natural Uranium <sup>c</sup>  | 4.78E-03                           | 1,130                             | 5.40                          | 3,836                             | 18.3                          | 8,996                             | 43.0                          | 9,379                             | 44.8                          |
| 3% Enriched Uranium <sup>c</sup>     | 4.29E-03                           | 1,212                             | 5.20                          | 4,328                             | 18.6                          | 9,567                             | 41.1                          | 8,186                             | 35.1                          |
| 20% Enriched Uranium <sup>c</sup>    | 3.08E-03                           | 1,408                             | 4.34                          | 5,027                             | 15.5                          | 11,060                            | 34.1                          | 7,218                             | 22.3                          |
| 50% Enriched Uranium <sup>c</sup>    | 2.47E-03                           | 1,431                             | 3.53                          | 5,106                             | 12.6                          | 11,230                            | 27.7                          | 7,085                             | 17.5                          |
| 75% Enriched Uranium <sup>c</sup>    | 2.13E-03                           | 1,437                             | 3.06                          | 5,129                             | 10.9                          | 11,270                            | 24.0                          | 7,067                             | 15.1                          |

<sup>a</sup>Assumes 0.25-m<sup>2</sup>, 15-centimeter-thick "soil" source uniformly contaminated with radionuclides. Measurement distance is 10 centimeters above the source.

<sup>b</sup>Weighted values as described in Section 6.2.5.

<sup>c</sup>Scan MDC for uranium includes sum of U-238, U-235, and U-234.

**Table 6-9 Land Surveys without Headphones**

| Surveyor No.     | Survey Duration (min) | Percent <sup>a</sup> Coverage | Per Surveyor |            |                 | Per GIS Technician |            |                 |
|------------------|-----------------------|-------------------------------|--------------|------------|-----------------|--------------------|------------|-----------------|
|                  |                       |                               | No. Misses   | No. Found  | False Positives | No. Misses         | No. Found  | False Positives |
| 1                | 23                    | 78                            | 2            | 8          | 0               | 2                  | 8          | 0               |
| 2                | 22                    | 72                            | 3            | 7          | 0               | 0                  | 10         | 0               |
| 3                | 42                    | 89                            | 0            | 10         | 0               | 0                  | 10         | 0               |
| 4                | 33                    | 72                            | 0            | 10         | 0               | 0                  | 10         | 0               |
| 5                | 16                    | 61                            | 4            | 6          | 0               | 4                  | 6          | 0               |
| 6                | 20                    | 83                            | 0            | 10         | 0               | 0                  | 10         | 0               |
| 7                | 30                    | 61                            | 3            | 7          | 0               | 2                  | 8          | 0               |
| 8                | 20                    | 67                            | 3            | 7          | 0               | 2                  | 8          | 0               |
| 9                | 20                    | 83                            | 0            | 10         | 1               | 0                  | 10         | 0               |
| 10               | 32                    | 89                            | 1            | 9          | 0               | 0                  | 10         | 1               |
| <b>Sums:</b>     | <b>NA</b>             | <b>NA</b>                     | <b>16</b>    | <b>84</b>  | <b>1</b>        | <b>10</b>          | <b>90</b>  | <b>1</b>        |
| <b>Averages:</b> | <b>26</b>             | <b>76</b>                     | <b>1.6</b>   | <b>8.4</b> | <b>0.1</b>      | <b>1.0</b>         | <b>9.0</b> | <b>0.1</b>      |

<sup>a</sup>Percent coverage is generally based on the number of parallel survey lanes completed, divided by the ideal number of lanes (18) in the test land area; judgment was used when surveyors strayed from parallel.

**Table 6-10 Land Surveys with Headphones**

| Surveyor No.     | Survey Duration (min) | Percent <sup>a</sup> Coverage | Per Surveyor |            |                 | Per GIS Technician |            |                 |
|------------------|-----------------------|-------------------------------|--------------|------------|-----------------|--------------------|------------|-----------------|
|                  |                       |                               | No. Misses   | No. Found  | False Positives | No. Misses         | No. Found  | False Positives |
| 1                | 21                    | 83                            | 1            | 9          | 0               | 1                  | 9          | 0               |
| 2                | 12                    | 56                            | 1            | 9          | 0               | 1                  | 9          | 0               |
| 3                | 35                    | 83                            | 0            | 10         | 0               | 0                  | 10         | 1               |
| 4                | 31                    | 83                            | 0            | 10         | 0               | 0                  | 10         | 0               |
| 5                | 20                    | 89                            | 1            | 9          | 0               | 0                  | 10         | 3               |
| 6                | 18                    | 67                            | 2            | 8          | 0               | 2                  | 8          | 1               |
| 7                | 26                    | 72                            | 2            | 8          | 0               | 2                  | 8          | 0               |
| 8                | 35                    | 94                            | 1            | 9          | 0               | 0                  | 10         | 0               |
| 9                | 22                    | 83                            | 0            | 10         | 0               | 0                  | 10         | 1               |
| 10               | 28                    | 94                            | 0            | 10         | 0               | 0                  | 10         | 0               |
| <b>Sums:</b>     | <b>NA</b>             | <b>NA</b>                     | <b>8</b>     | <b>92</b>  | <b>0</b>        | <b>6</b>           | <b>94</b>  | <b>6</b>        |
| <b>Averages:</b> | <b>25</b>             | <b>81</b>                     | <b>0.8</b>   | <b>9.2</b> | <b>0</b>        | <b>0.6</b>         | <b>9.4</b> | <b>0.6</b>      |

<sup>a</sup>Percent coverage is generally based on the number of parallel survey lanes completed, divided by the ideal number of lanes (18) in the test land area; judgment was used when surveyors strayed from parallel.

**Table 6-11 Wall Surveys without Headphones**

| Surveyor No.     | Survey Duration (min) | Percent <sup>a</sup> Coverage | Per Surveyor |            |                 | Per GIS Technician |            |                 |
|------------------|-----------------------|-------------------------------|--------------|------------|-----------------|--------------------|------------|-----------------|
|                  |                       |                               | No. Misses   | No. Found  | False Positives | No. Misses         | No. Found  | False Positives |
| 1                | 14                    | 58                            | 5            | 7          | 1               | 7                  | 5          | 0               |
| 2                | 32                    | 83                            | 3            | 9          | 0               | 3                  | 9          | 0               |
| 3                | 24                    | 50                            | 2            | 10         | 9               | 4                  | 8          | 1               |
| 4                | 27                    | —                             | 3            | 9          | 1               | —                  | —          | —               |
| 5                | 25                    | 71                            | 6            | 6          | 1               | 7                  | 5          | 1               |
| 6                | 13                    | 54                            | 8            | 4          | 1               | 8                  | 4          | 2               |
| 7                | 28                    | 75                            | 5            | 7          | 5               | 6                  | 6          | 0               |
| 8                | 68                    | 67                            | 1            | 11         | 2               | 4                  | 8          | 0               |
| 9                | 29                    | 92                            | 2            | 10         | 1               | 3                  | 9          | 0               |
| 10               | 24                    | —                             | 3            | 9          | 0               | —                  | —          | —               |
| 11               | 39                    | 75                            | 2            | 10         | 0               | 4                  | 8          | 0               |
| 12               | 11                    | 50                            | 4            | 8          | 7               | 3                  | 9          | 0               |
| 13               | 18                    | 58                            | 2            | 10         | 19              | 7                  | 5          | 0               |
| <b>Sums:</b>     | <b>NA</b>             | <b>NA</b>                     | <b>46</b>    | <b>110</b> | <b>47</b>       | <b>56</b>          | <b>76</b>  | <b>4</b>        |
| <b>Averages:</b> | <b>27</b>             | <b>67</b>                     | <b>3.5</b>   | <b>8.5</b> | <b>3.6</b>      | <b>5.1</b>         | <b>6.9</b> | <b>0.4</b>      |

<sup>a</sup>Percent coverage is generally based on the number of parallel survey lanes completed, divided by the ideal number of lanes (12) in the test wall area; judgment was used when surveyors strayed from parallel.

**Table 6-12 Wall Surveys with Headphones**

| Surveyor No.     | Survey Duration (min) | Percent <sup>a</sup> Coverage | Per Surveyor |            |                 | Per GIS Technician |            |                 |
|------------------|-----------------------|-------------------------------|--------------|------------|-----------------|--------------------|------------|-----------------|
|                  |                       |                               | No. Misses   | No. Found  | False Positives | No. Misses         | No. Found  | False Positives |
| 1                | 15                    | 67                            | 4            | 6          | 3               | 4                  | 6          | 2               |
| 2                | 48                    | 92                            | 1            | 9          | 7               | 0                  | 10         | 4               |
| 3                | 23                    | 58                            | 0            | 10         | 6               | 4                  | 6          | 1               |
| 4                | 34                    | —                             | 2            | 8          | 4               | —                  | —          | —               |
| 5                | 26                    | 58                            | 0            | 10         | 16              | 4                  | 6          | 1               |
| 6                | 15                    | 67                            | 4            | 6          | 5               | 5                  | 5          | 3               |
| 7                | 26                    | 83                            | 2            | 8          | 9               | 5                  | 5          | 3               |
| 8                | 40                    | 75                            | 1            | 9          | 2               | 2                  | 8          | 1               |
| 9                | 20                    | 83                            | 6            | 4          | 2               | 5                  | 5          | 1               |
| 10               | 20                    | —                             | 1            | 9          | 1               | —                  | —          | —               |
| 11               | 36                    | 75                            | 0            | 10         | 2               | 1                  | 9          | 3               |
| 12               | 11                    | 50                            | 5            | 5          | 6               | 1                  | 9          | 3               |
| 13               | 19                    | 58                            | 1            | 9          | 21              | 1                  | 9          | 3               |
| <b>Sums:</b>     | <b>NA</b>             | <b>NA</b>                     | <b>27</b>    | <b>103</b> | <b>84</b>       | <b>32</b>          | <b>78</b>  | <b>25</b>       |
| <b>Averages:</b> | <b>26</b>             | <b>70</b>                     | <b>2.1</b>   | <b>7.9</b> | <b>6.5</b>      | <b>2.9</b>         | <b>7.1</b> | <b>2.3</b>      |

<sup>a</sup>Percent coverage is generally based on the number of parallel survey lanes completed, divided by the ideal number of lanes (12) in the test wall area; judgment was used when surveyors strayed from parallel.

**Table 6-13 Test Results for Headphones versus No Headphones**

| Trial                            | Percent Found (%) | p-value <sup>a</sup> by Test and Trial |                                   |
|----------------------------------|-------------------|--|-----------------------------------|
|                                  |                   | Two-Tail Probability <sup>b</sup>      | One-Tail Probability <sup>c</sup> |
| Outdoor, No Headphones, Surveyor | 84                | NA                                     | <b>0.041</b>                      |
| Outdoor, Headphones, Surveyor    | 92                |  |                                   |
| Outdoor, No Headphones, Surveyor | 84                | 0.207                                  | NA                                |
| Outdoor, No Headphones, z-score  | 90                |  |                                   |
| Outdoor, Headphones, Surveyor    | 92                | 0.58                                   | NA                                |
| Outdoor, Headphones, z-score     | 94                |  |                                   |
| Indoor, No Headphones, Surveyor  | 71                | NA                                     | <b>0.046</b>                      |
| Indoor, Headphones, Surveyor     | 79                |  |                                   |
| Indoor, No Headphones, Surveyor  | 71                | <b>0.022</b>                           | NA                                |
| Indoor, No Headphones, z-score   | 58                |  |                                   |
| Indoor, Headphones, Surveyor     | 79                | 0.136                                  | NA                                |
| Indoor, Headphones, z-score      | 71                |  |                                   |

NA = not applicable for the indicated test

<sup>a</sup>A p-value less than 0.05 (highlighted) indicates a statistically significant test or difference.

<sup>b</sup>Two-sided/two-tail probability student's t-test

<sup>c</sup>One-sided/one-tail probability student's t-test

**Table 6-14 Correlations Comparing Time, Coverage, and Percent Found**

| <b>Trial</b>  | <b>r</b> | <b>p-value<sup>a</sup></b> |
|---|----------|----------------------------|
| <b>Correlation of Time with Percent Coverage</b>            |          |                            |
| Outdoor, No Headphones                                      | 0.42     | 0.226                      |
| Outdoor, Headphones   | 0.69     | 0.028                      |
| Indoor, No Headphones                                       | 0.41     | 0.163                      |
| Indoor, Headphones  | 0.67     | 0.013                      |
| <b>Correlation of Time with Number of Sources Found</b>     |          |                            |
| Outdoor, No Headphones, Surveyor                            | 0.48     | 0.164                      |
| Outdoor, No Headphones, z-score                             | 0.47     | 0.175                      |
| Outdoor, Headphones, Surveyor                               | 0.42     | 0.230                      |
| Outdoor, Headphones, z-score                                | 0.48     | 0.156                      |
| Indoor, No Headphones, Surveyor                             | 0.57     | 0.039                      |
| Indoor, No Headphones, z-score                              | 0.61     | 0.158                      |
| Indoor, Headphones, Surveyor                                | 0.56     | 0.045                      |
| Indoor, Headphones, z-score                                 | 0.35     | 0.290                      |
| <b>Correlation of Coverage with Number of Sources Found</b> |          |                            |
| Outdoor, No Headphones, Surveyor                            | 0.80     | 0.006                      |
| Outdoor, No Headphones, z-score                             | 0.75     | 0.013                      |
| Outdoor, Headphones, Surveyor                               | 0.51     | 0.135                      |
| Outdoor, Headphones, z-score                                | 0.71     | 0.011                      |
| Indoor, No Headphones, Surveyor                             | 0.25     | 0.455                      |
| Indoor, No Headphones, z-score                              | 0.36     | 0.275                      |
| Indoor, Headphones, Surveyor                                | -0.01    | 0.980                      |
| Indoor, Headphones, z-score                                 | -0.01    | 0.980                      |

<sup>a</sup>Two-tailed probability; a p-value less than 0.05 indicates a statistically significant test or difference.



**Table 6-15 Parallel DQOs for Hypothetical Radium Sites**

|  |  |
|--|--|
| <b>DQO Step 1—State the Problem: Define the problem that necessitates the study</b>  |  |
| <b>Both <i>A Priori (d')</i> and <i>A Posteriori (IL<sub>PP</sub>)</i></b>   |  |
| A decommissioning project must demonstrate that Ra-226 concentrations in surface soils are less than the DCGL of 5 pCi/g (above background).   |  |
| <b>DQO Step 2—Identify the Decision: Identify the principal study question, alternate actions and the decision statement</b>   |  |
| <b>Both <i>A Priori (d')</i> and <i>A Posteriori (IL<sub>PP</sub>)</i></b>   |  |
| Principal Study Question: Will surveys demonstrate that Ra-226 concentrations in soils are less than the 5 pCi/g DCGL?   | Alternate Action(Yes): Surface soils satisfy decommissioning criteria—no further action is required.<br>Alternate Action (No): Surface soils do not satisfy decommissioning criteria—further action is required.   |
| Decision Statement: The decommissioning survey (does or does not) demonstrate that Ra-226 concentrations in soil satisfy the 5 pCi/g (above background) DCGL.  |  |
| <b>DQO Step 3—Identify the Inputs to the Decision: Identify both the information needed and the sources for this information, determine the basis for action levels, and identify sampling and analytical methods that will meet data requirements</b>   |  |
| <b><i>A Priori (d')</i></b>  | <b><i>A Posteriori (IL<sub>PP</sub>)</i></b>   |
| 2" × 2" NaI detectors and ratemeter/scalers, pin flags, logbook and site maps for recording results, soil-sampling equipment, gamma walkover survey and soil-sampling procedures, reference area for establishing background Ra-226 concentrations and 2" × 2" detector responses, and an analytical laboratory statement of work<br><br>Survey unit soil samples will be selected from locations the surveyors identify as producing a signal above the MDCR. | 2" × 2" NaI detectors and ratemeter/scalers, GIS equipment with data logger, GPS/GIS data processing equipment and procedures, soil-sampling equipment, gamma walkover survey and soil-sampling procedures, reference area for establishing background Ra-226 concentrations and 2" × 2" detector responses, and an analytical laboratory statement of work<br><br>Survey unit soil samples will be selected from locations the GIS technicians identify as producing a signal above the project-specific threshold above the background distribution. |
| <b>DQO Step 4—Define the Boundaries of the Study: Define target populations and spatial, temporal, and practical boundaries and define the smallest subpopulations for which separate decisions must be made.</b>  |  |
| <b>Both <i>A Priori (d')</i> and <i>A Posteriori (IL<sub>PP</sub>)</i></b>   |  |
| Physical boundaries include surface soils within safely accessible portions of the facility; temporal boundaries are specified by the decommissioning project schedule. The budget allows for the collection and analysis of 20 judgmental soil samples. The project has conservatively committed to removing any soils with concentrations above the DCGL.  |  |

| <b>DQO Step 5—Develop a Decision Rule: Specify appropriate population parameters (i.e., background conditions) and develop an if...then... decision rule statement.</b>   |   |
|---|---|
| <b><i>A Priori</i> (<i>d'</i>)</b>  | <b><i>A Posteriori</i> (<i>IL<sub>PP</sub></i>)</b>   |
| <p>Surveyors will survey and sample the reference area to estimate the average background detector response and soil concentrations. The survey data will be used to estimate the <i>a priori</i> scan MDC, and the soil concentrations will be used to compare laboratory data to the DCGL.</p> <p>If surveyors locate elevated gamma responses in a survey unit and collect soil samples with Ra-226 concentrations above the DCGL, then the decommissioning project will remediate the area.</p>   | <p>Surveyors will survey and sample the reference area to define the distribution of background responses and average soil concentrations. The survey data will be used to estimate the <i>a posteriori</i> <i>IL<sub>PP</sub></i>, and the soil concentrations will be used to compare laboratory data to the DCGL.</p> <p>If the GIS technician locates elevated gamma responses in a survey unit and subsequent judgmental soil samples contain Ra-226 concentrations above the DCGL, then the decommissioning project will remediate the area.</p>  |
| <b>DQO Step 6—Specify Limits on Decision Errors: Specify the limits on decision errors, which are then used to establish performance goals for the survey.</b>  |   |
| <b><i>A Priori</i> (<i>d'</i>)</b>  | <b><i>A Posteriori</i> (<i>IL<sub>PP</sub></i>)</b>   |
| <p>The decommissioning project accepts a false negative (alpha) error of 10% and a false negative (beta) error of 25%, so a <i>d'</i> of 1.96 is selected. Surveyors are experienced and well trained, so a surveyor efficiency of 75% is assigned. For planning purposes, the presumed average background response is 9,750 cpm, the observation interval is 1 second, and the average Ra-226 concentration is 1 pCi/g. Using techniques described in NUREG-1507, Section 6.2.5, with a count-rate-to-exposure-rate ratio of 179 (cpm/μR/h) and an energy-dependent detector efficiency of 0.71 μR/h, the <i>a priori</i> scan MDC is calculated as follows:</p> $\text{Scan MDC (Ra-226)} = \frac{d' \times \sqrt{b_i} \times (60/i)}{\sqrt{p} \times \text{CPMR} \times \text{ERC}} =$ $\frac{1.96 \times \sqrt{9,750 \times 1/60} \times (60/1)}{\sqrt{0.75} \times 179 \times 0.71} = 2.9 \text{ pCi/g}$ <p>The scan MDC of 2.9 pCi/g (3.9 pCi/g gross) is directly comparable to the 5 pCi/g (6 pCi/g gross) DCGL and the analytical detection limit of 0.5 pCi/g. The decommissioning project accepts a field screening method at about 60% of the DCGL and an analytical method at 10% of the DCGL.</p> | <p>Any location with a detector signal greater than three standard deviations from the mean background response (z-score = 3) will be targeted for sampling and laboratory analysis. Responses above a z-score = 3 are above 99.9% of the background results (one-sided confidence interval, normal distribution assumed) and represent the most likely location of Ra-226 contamination. The analytical detection limit is 0.5 pCi/g. The decommissioning project accepts a field screening threshold at a level that represents the 99.9<sup>th</sup> percentile and an analytical method at 10% of the DCGL.</p> |

**DQO Step 7—Optimize the Design for Collecting Data: Develop data collection design alternatives, formulate mathematical expressions for each design, select the sample size to satisfy DQOs, decide on the most resource-effective design of agreed alternatives, and document requisite details.**

| <b><i>A Priori (d')</i></b>   | <b><i>A Posteriori (IL<sub>PP</sub>)</i></b>  |
|---|---|
| <p>Surveyors will traverse the survey unit at a pace of about 0.5 m/sec in parallel paths spaced about 1.5 meters (5 feet) apart, swinging the detectors in a serpentine pattern about 10 centimeters (4 inches) above the ground surface, and will collect a static 1-minute measurement above the point of the highest scanning response in each area that is distinguishable from background. These locations will be considered for volumetric sampling (up to 20 judgmental samples are planned). Samples will be collected per procedure and submitted to the analytical laboratory for analysis.</p> | <p>Surveyors will traverse the survey unit at a pace of about 0.5 m/sec in parallel paths spaced about 1.5 meters (5 feet) apart, swinging the detectors in a serpentine pattern about 10 centimeters (4 inches) above the ground surface. Survey data and GPS coordinates will be logged, and a GIS map will be generated. The GIS technician will direct surveyors to collect samples at locations above the <i>a posteriori</i> IL<sub>PP</sub> (i.e., above z-score = 3)—these locations will be considered for volumetric sampling (up to 20 judgmental samples are planned). Samples will be collected per procedure and submitted to the analytical laboratory for analysis.</p> |

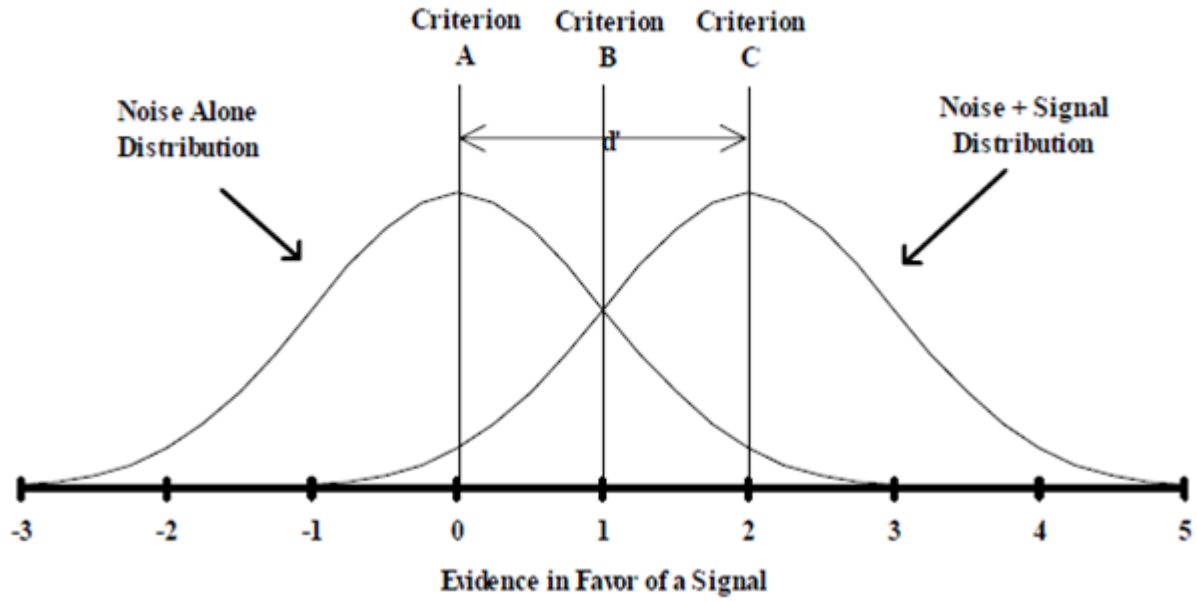


Figure 6-1 Signal Detection Theory Measures of Sensitivity ( $d'$ ) and Criterion Shown Relative to Assumed Underlying Distributions

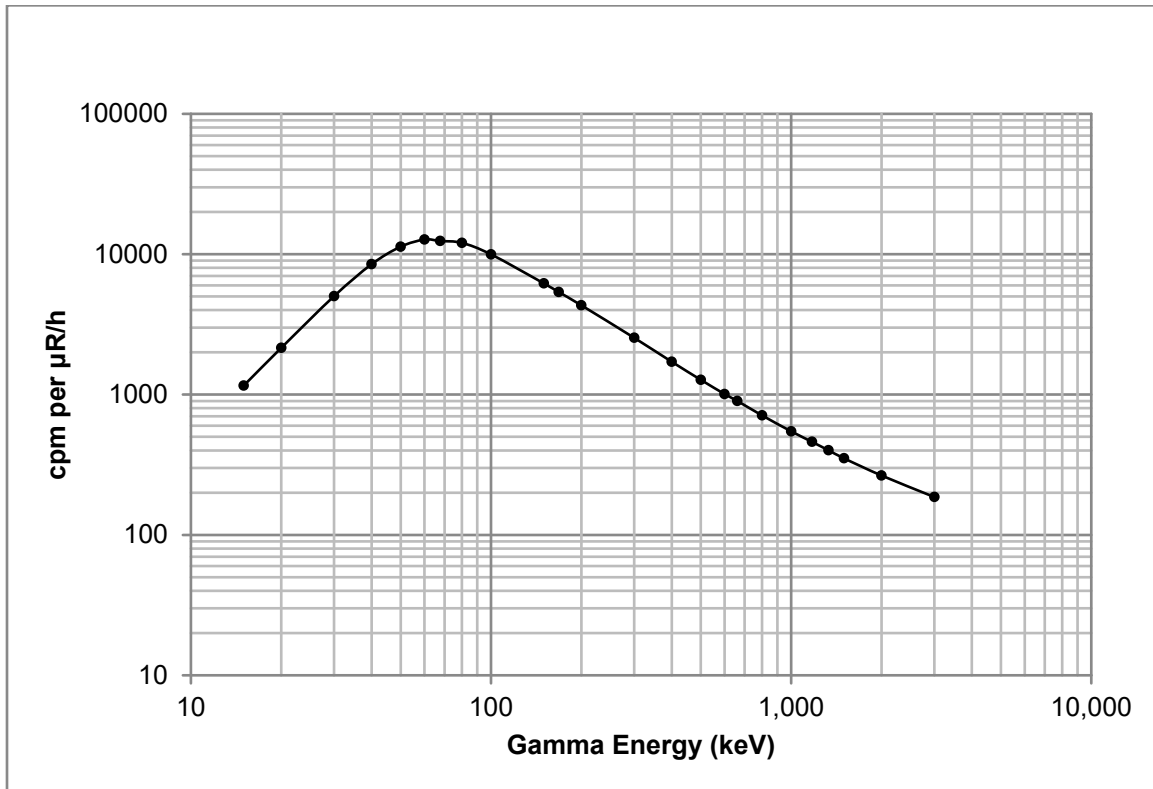
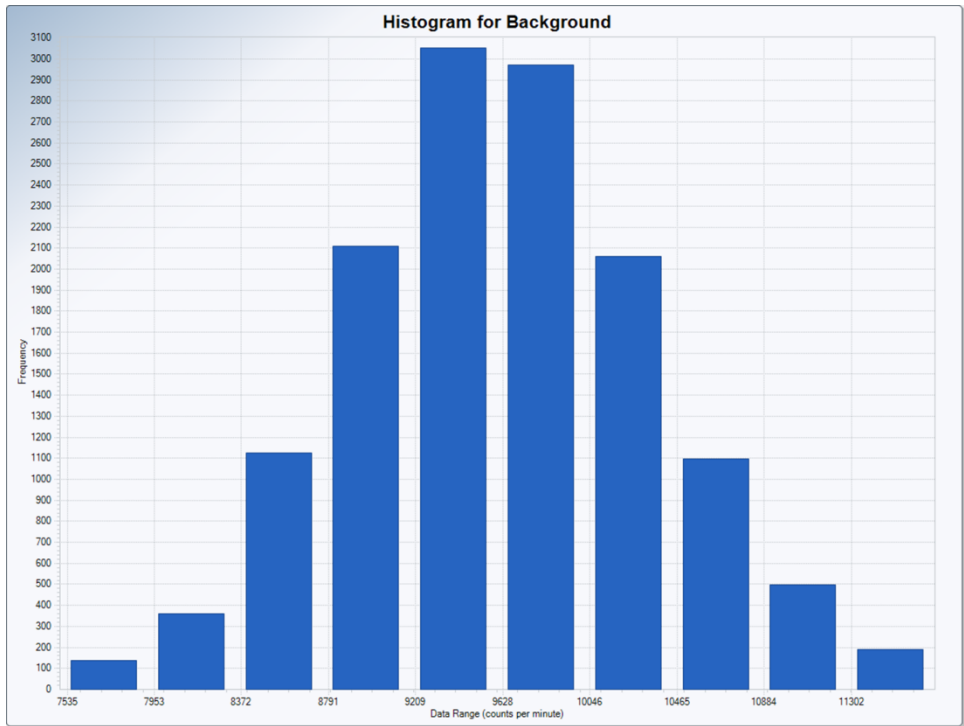
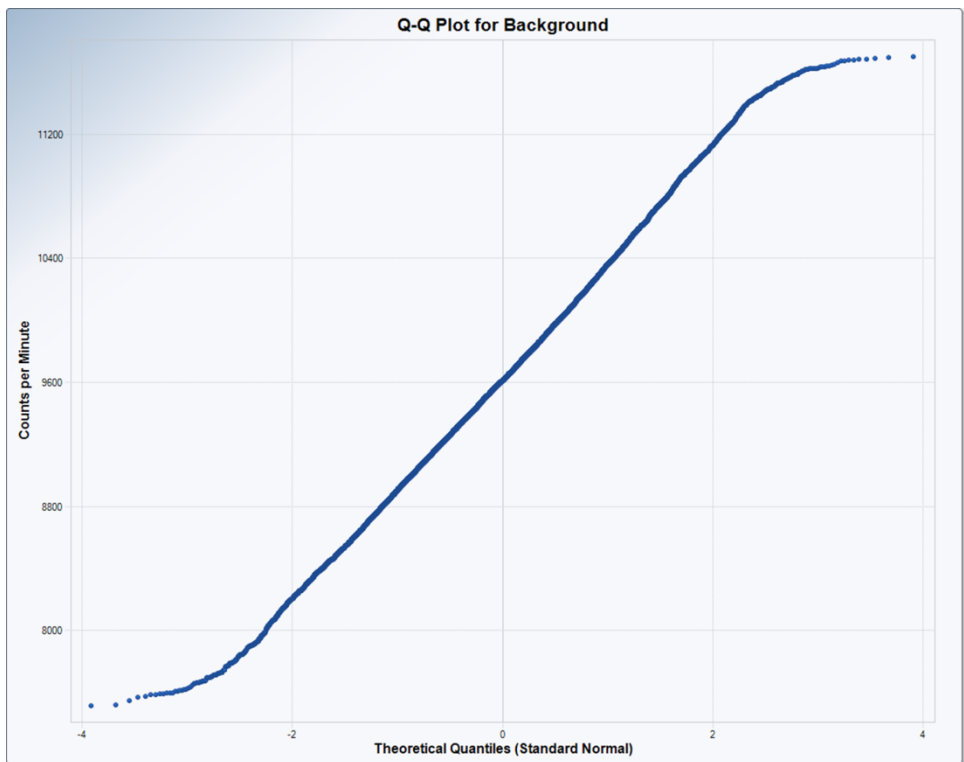


Figure 6-2 Example NaI Scintillation Detector Response as a Function of Gamma Energy



**Figure 6-3 Example Histogram of Normally Distributed Background Dataset**



**Figure 6-4 Example Q-Q Plot of Normally Distributed Background Dataset**

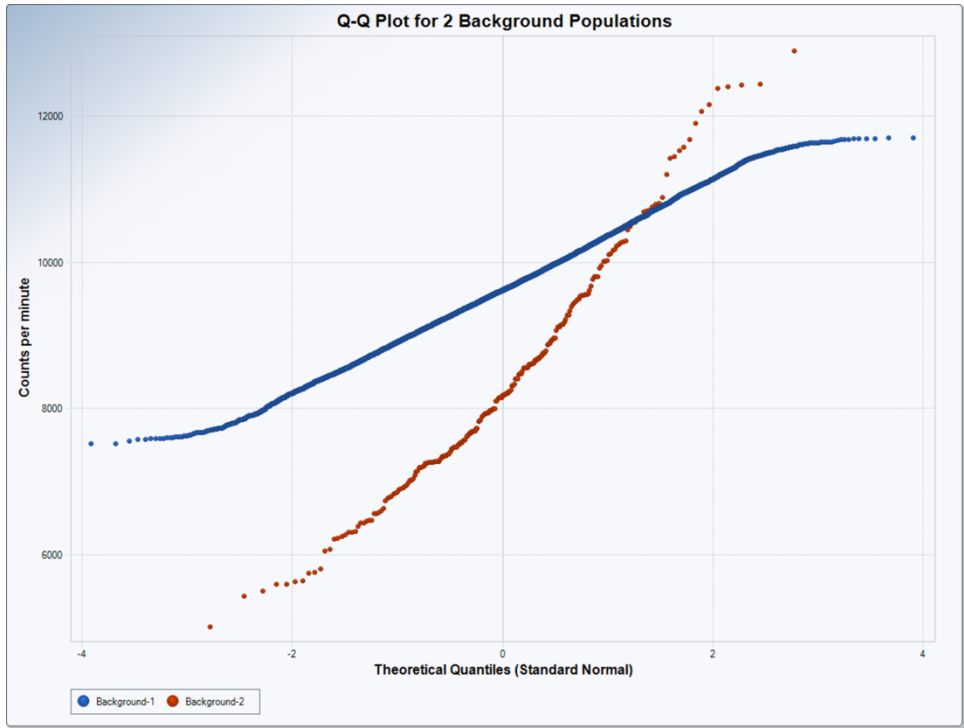


**Figure 6-5 Example Q-Q Plot of Bimodal Distributed Background Dataset**

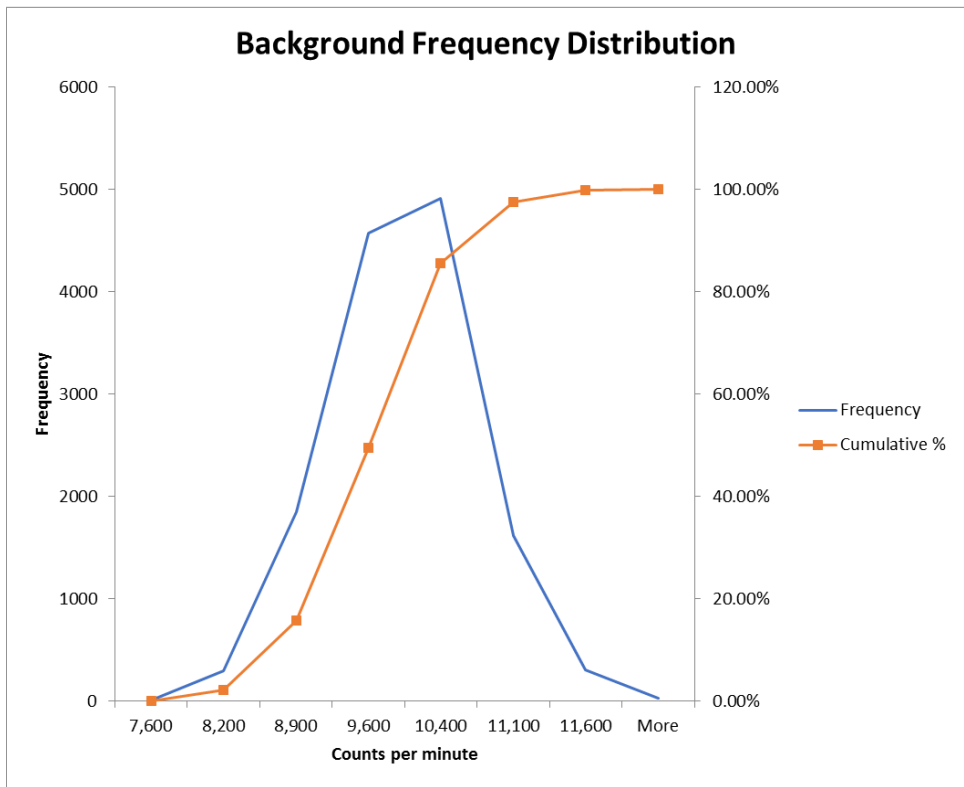


**Figure 6-6 Example Background Frequency Distribution**

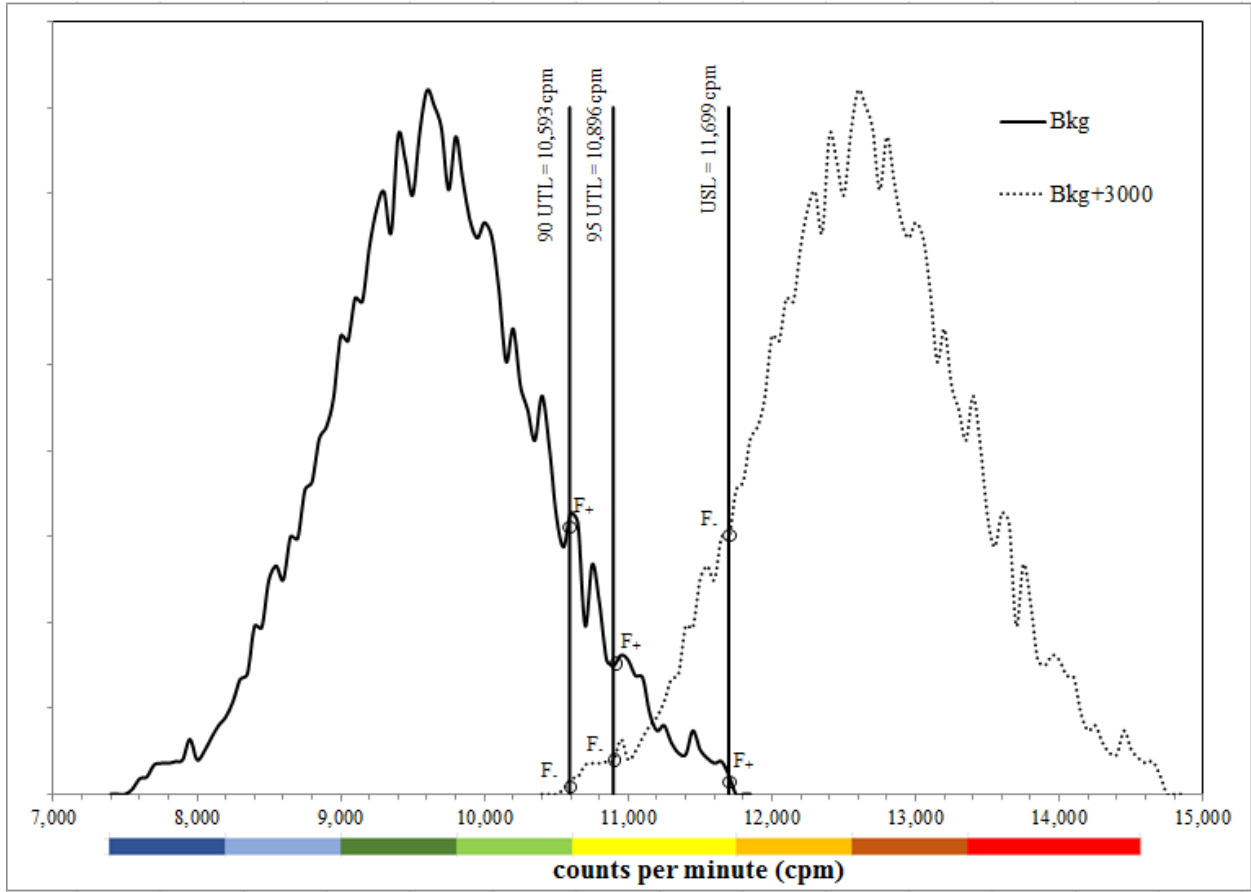


**Figure 6-7 Example Background and Background Plus Signal at the Initial 3,000 cpm-to-Concentration Ratio**

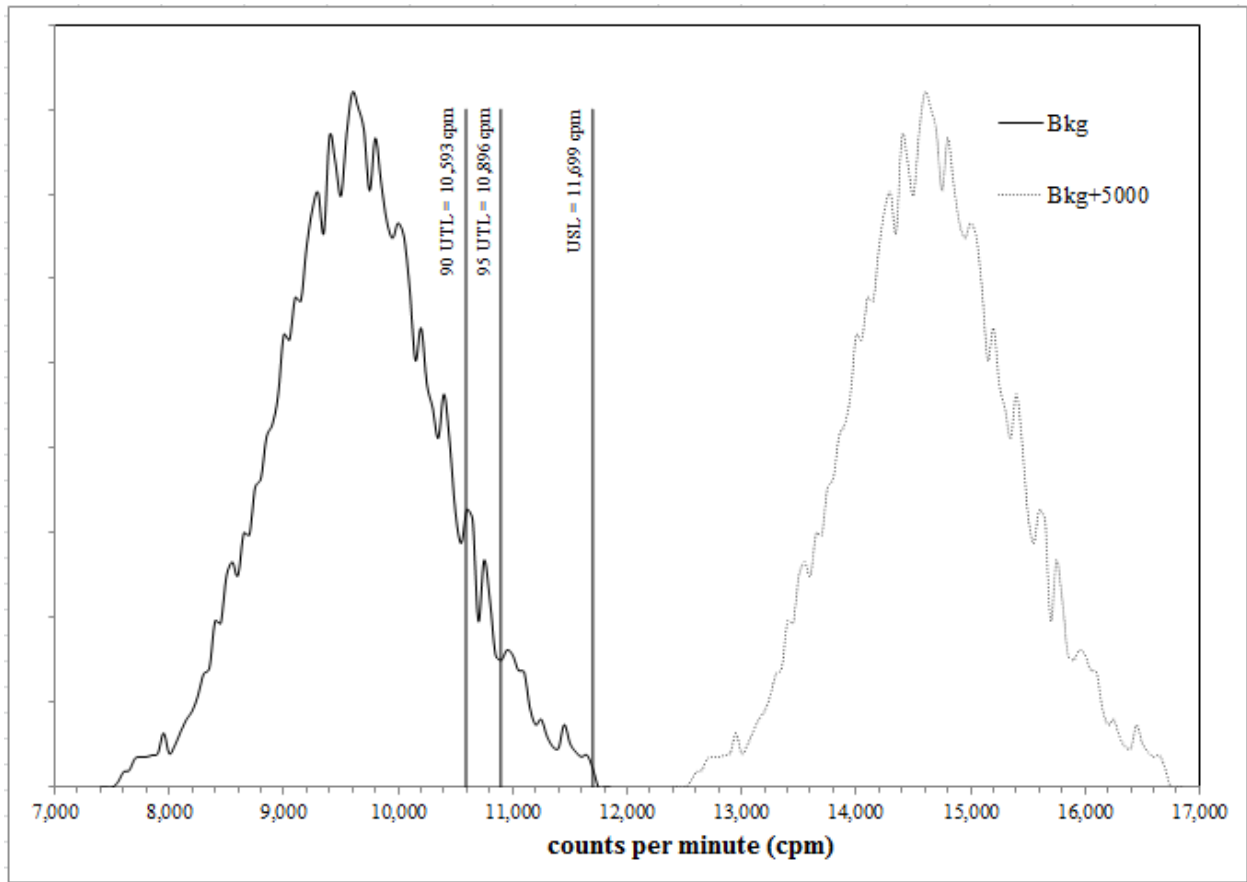


**Figure 6-8 Example Background and Background Plus Signal at the Initial 5,000 cpm-to-Concentration Ratio**



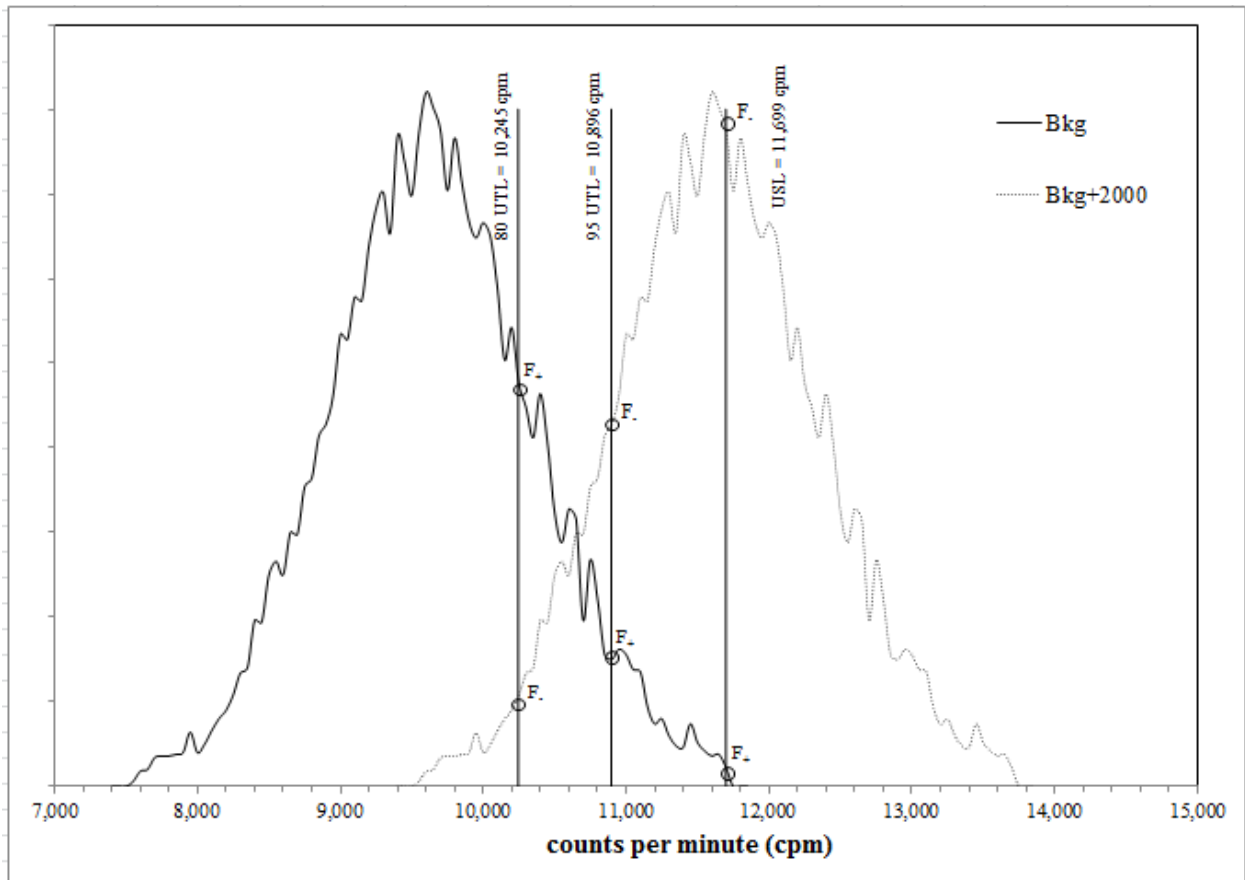


**Figure 6-9 Example Background and Background Plus Signal at the Initial 2,000 cpm-to-Concentration Ratio**

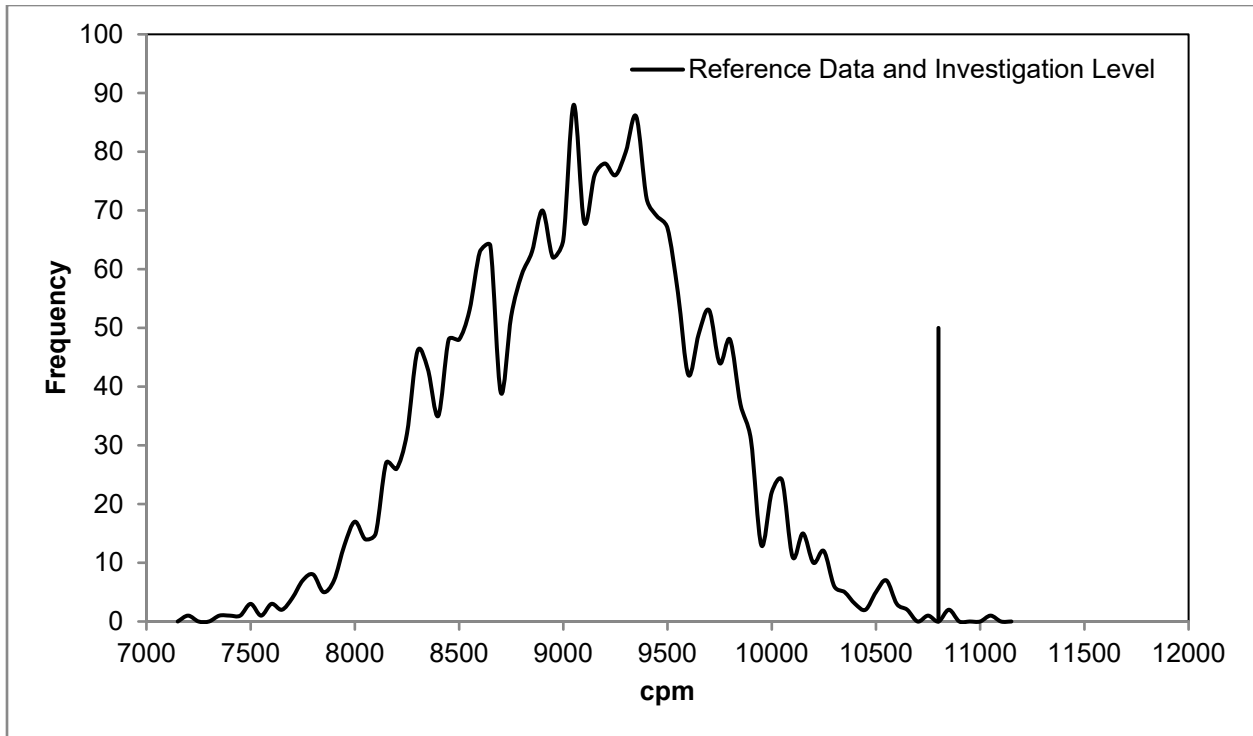


**Figure 6-10 Example 1 Background Population and Investigation Level**

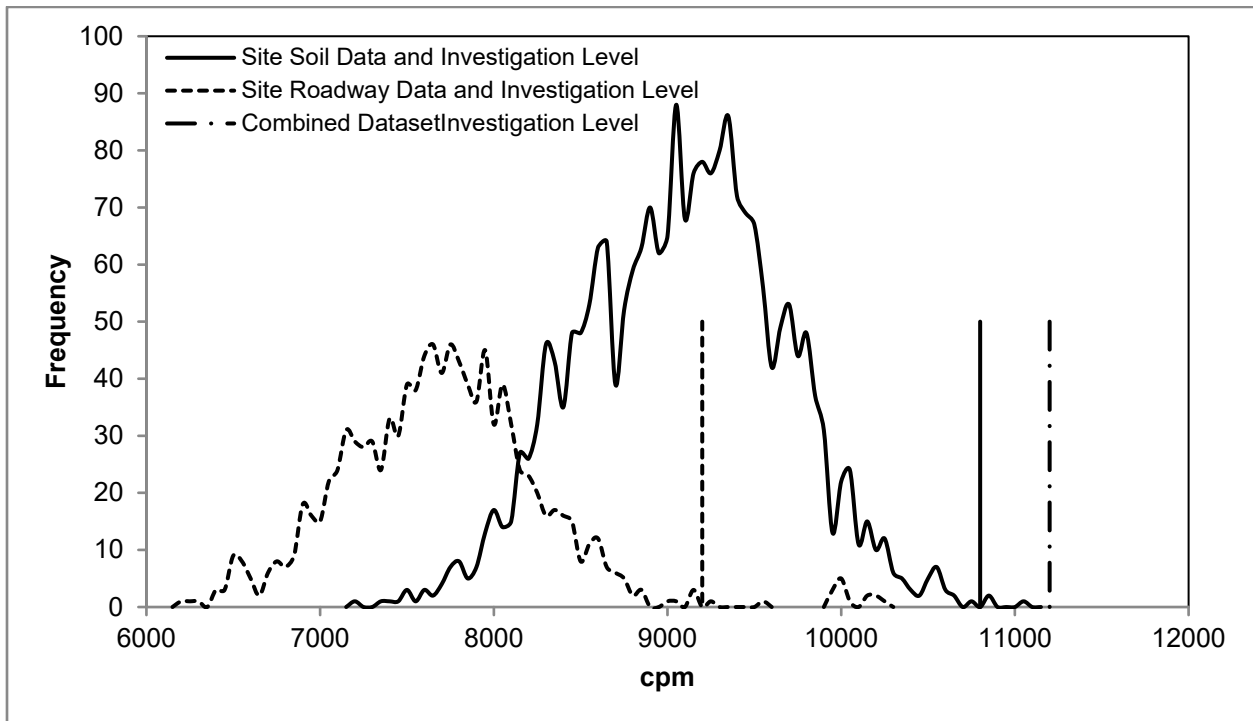


**Figure 6-11 Example 2 Medium-Specific Populations and Investigation Levels**

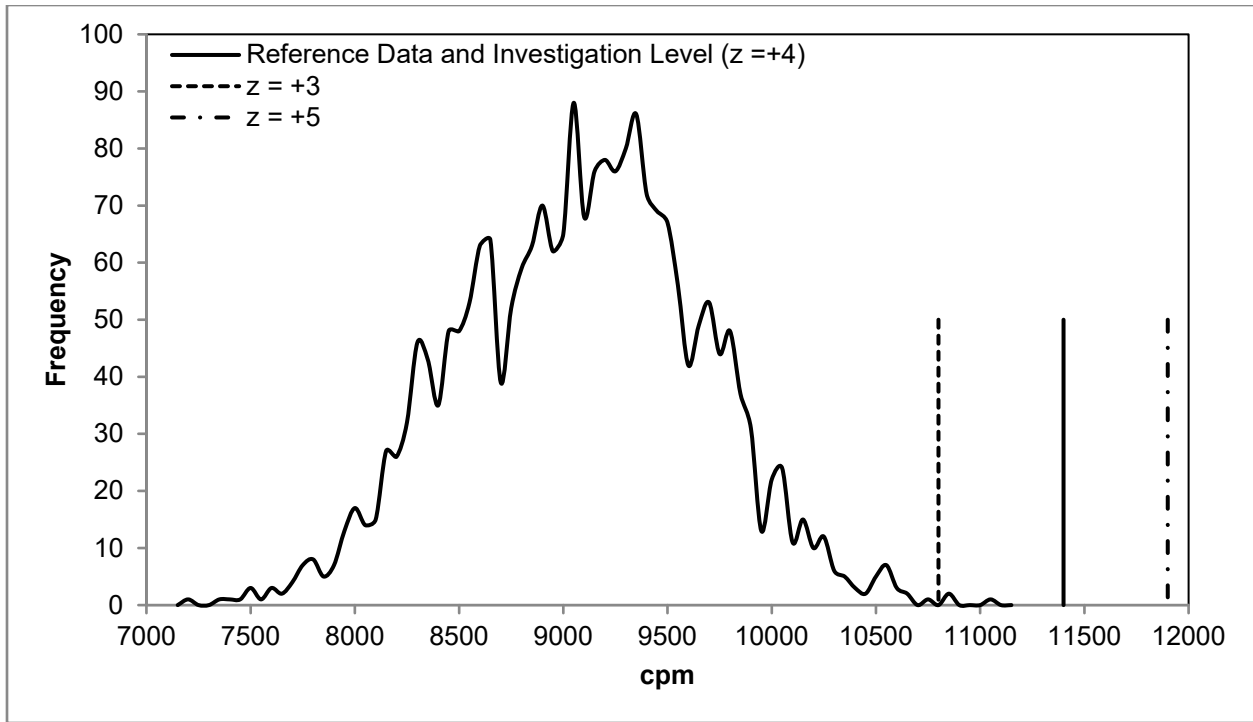


**Figure 6-12 Example 3 Background Population and Investigation Level**

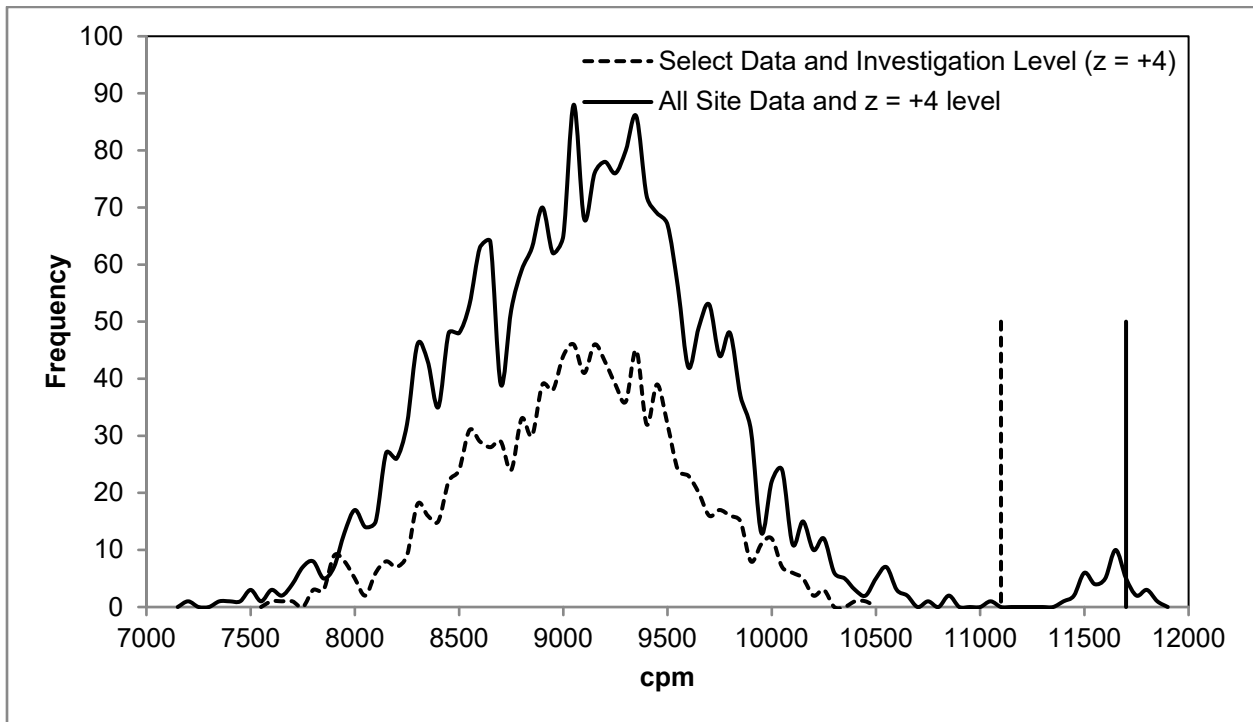


**Figure 6-13 Example 4 Site Data Populations and Associated Investigation Levels**

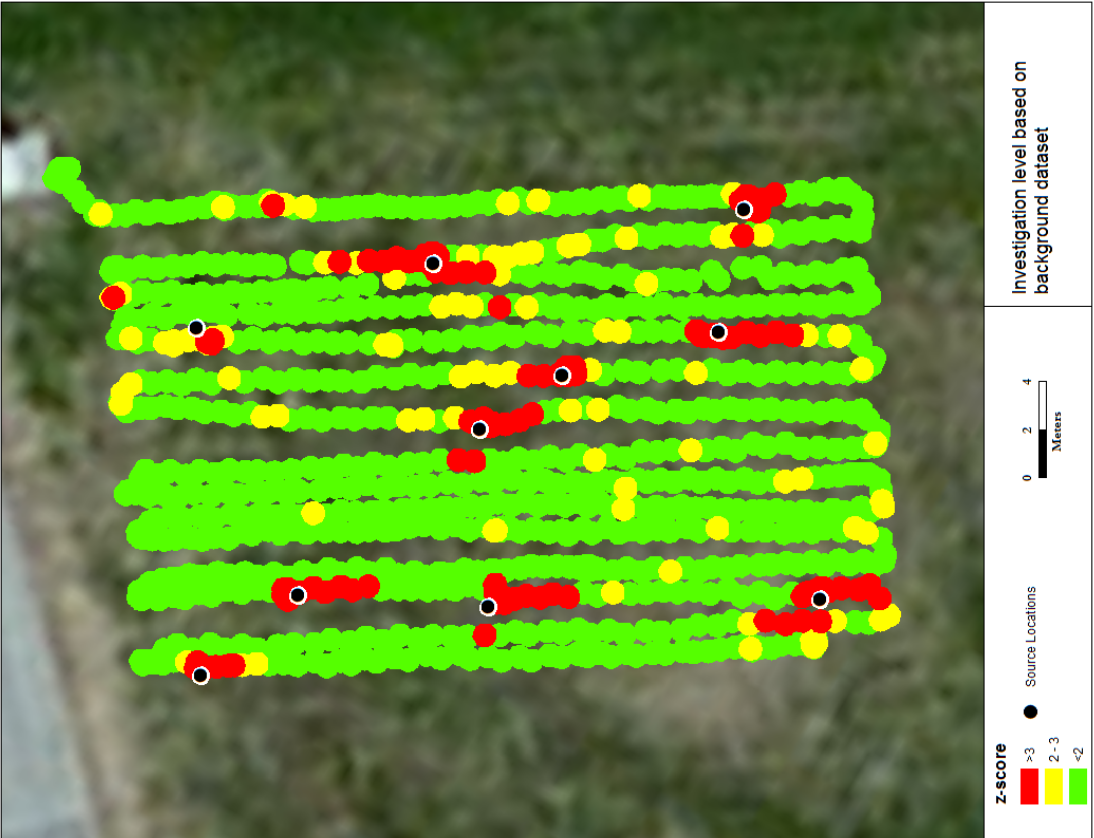
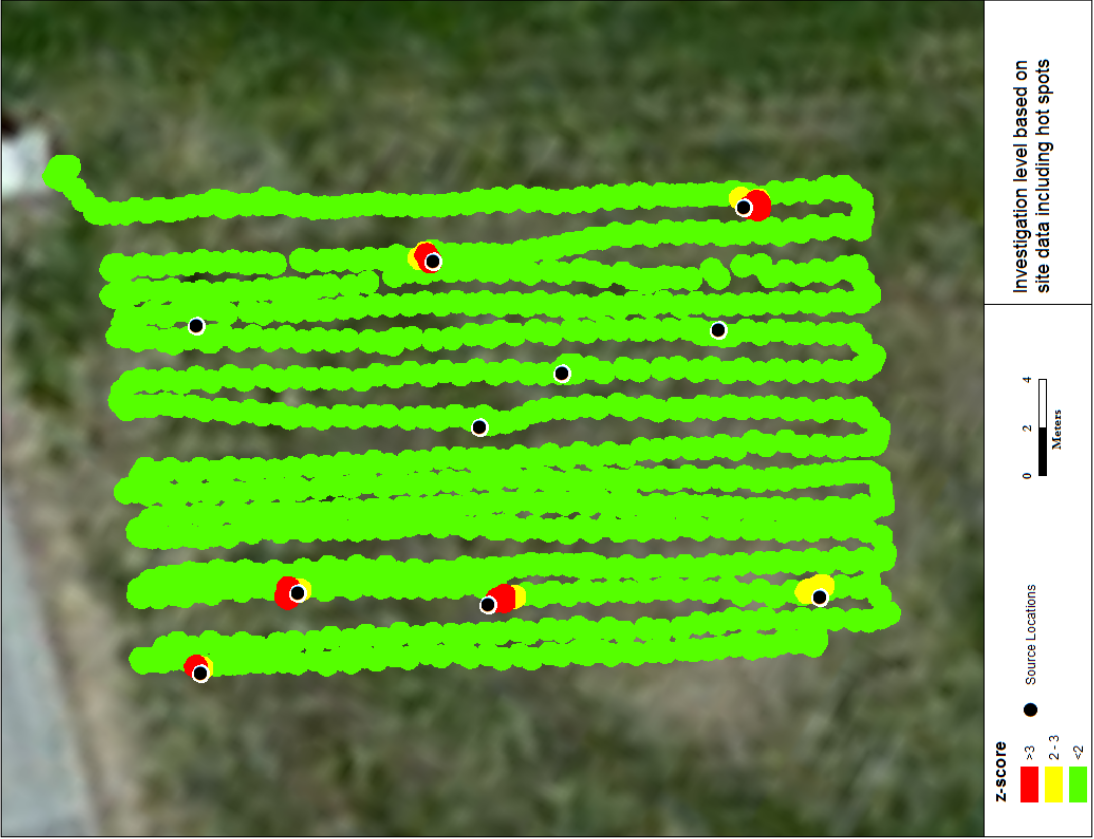
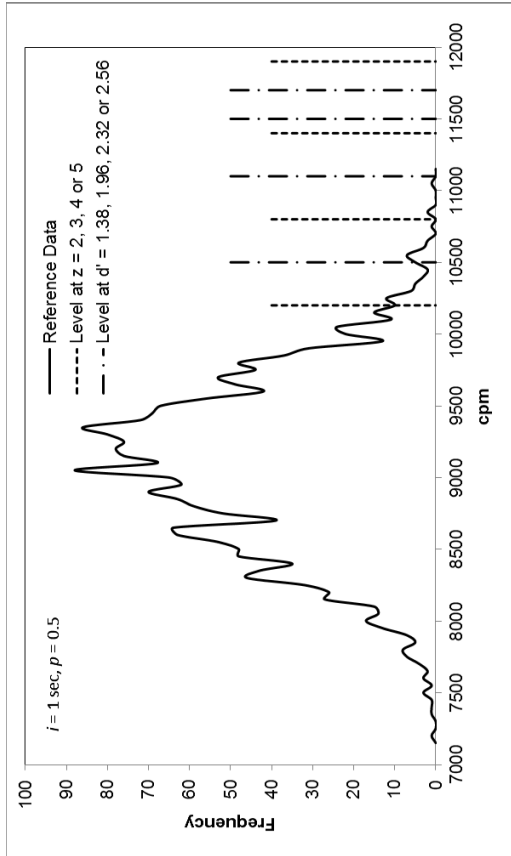
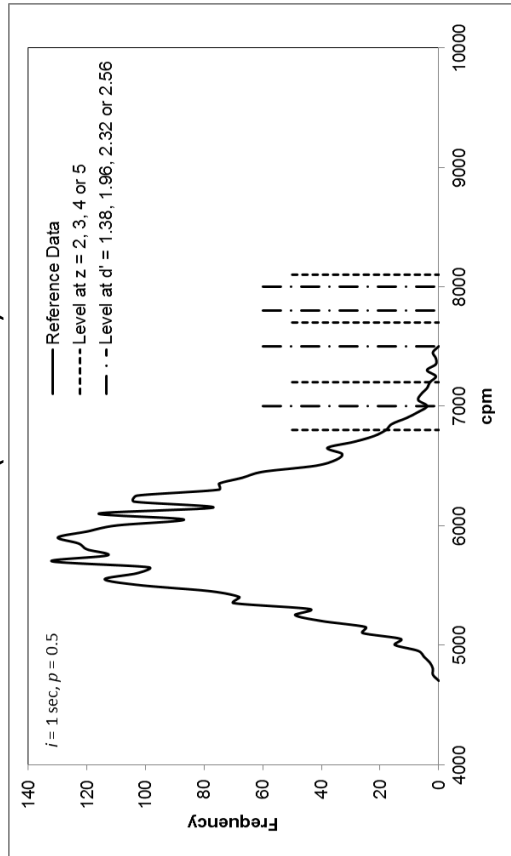


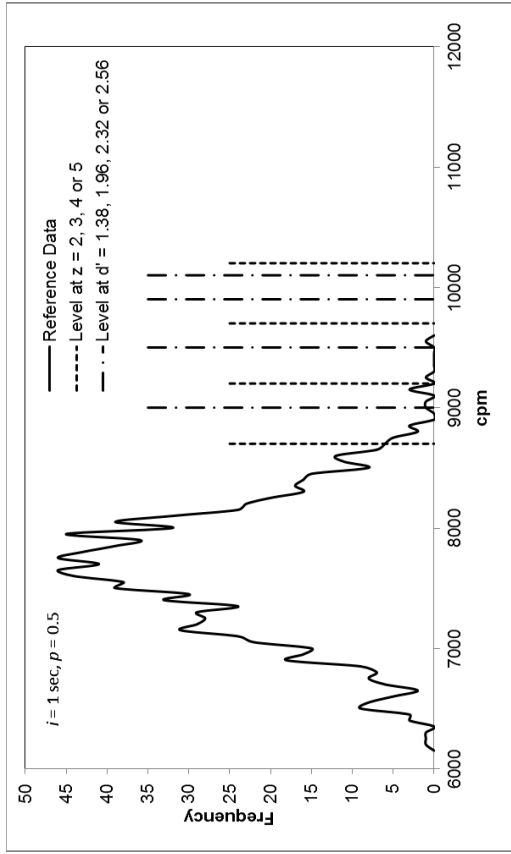
**Figure 6-14 Hidden Source Identified Using Background or Site Data To Establish Investigation Levels**



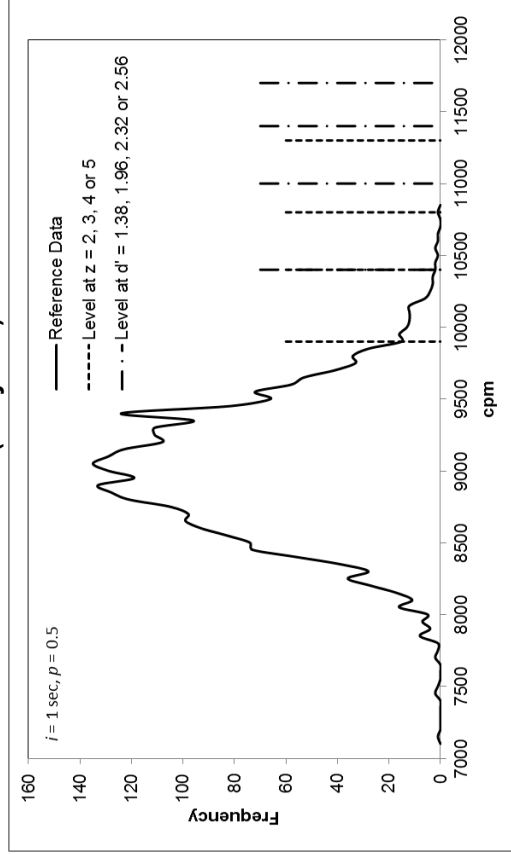
Site 1 (Tennessee)



Site 3 (California)

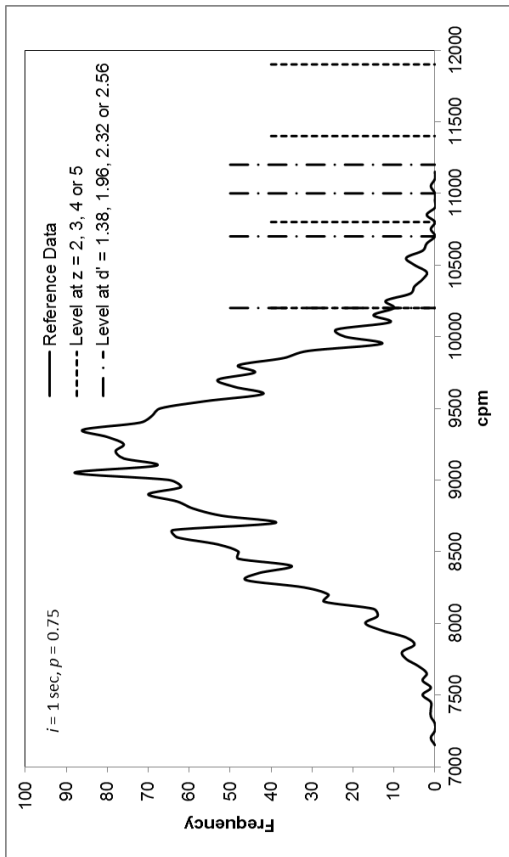


Site 2 (Maryland)

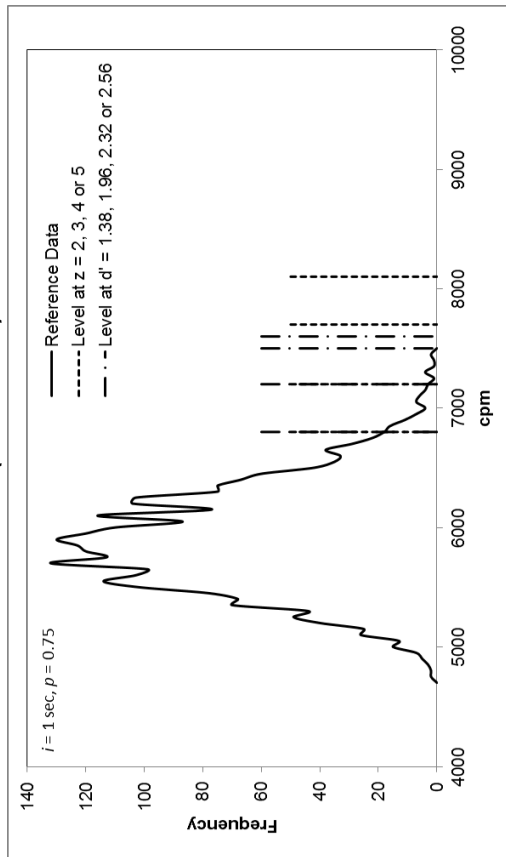


Site 4 (Washington)

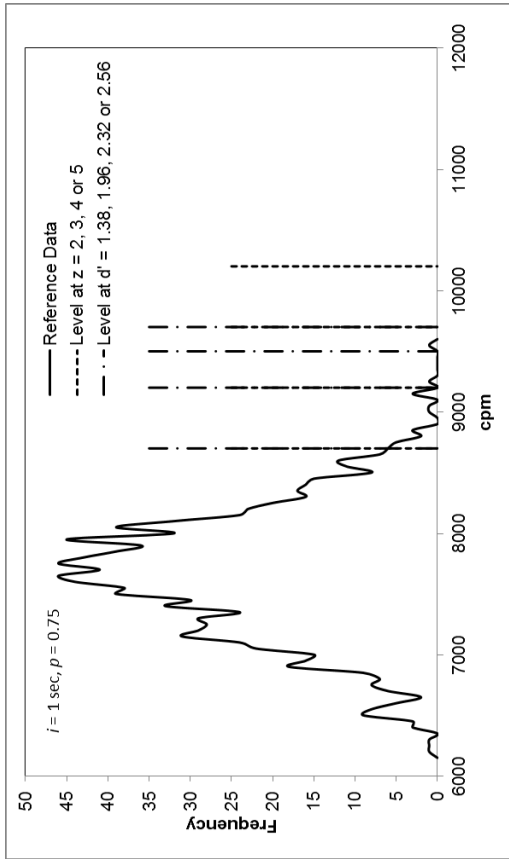
Figure 6-15 Gross MDCRs and Investigation Levels for  $i = 1$  and  $p = 0.5$



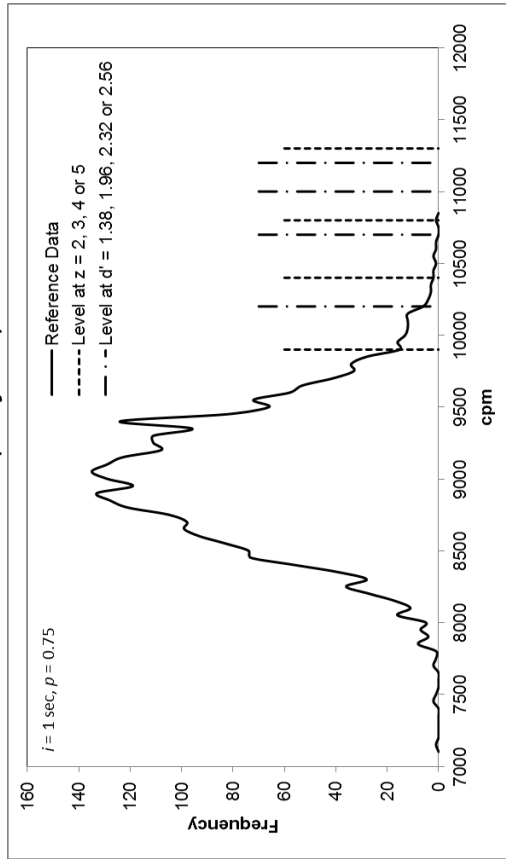
Site 1 (Tennessee)



Site 3 (California)



Site 2 (Maryland)



Site 4 (Washington)

Figure 6-16 Gross MDCRs and Investigation Levels for  $i = 1$  and  $p = 0.75$

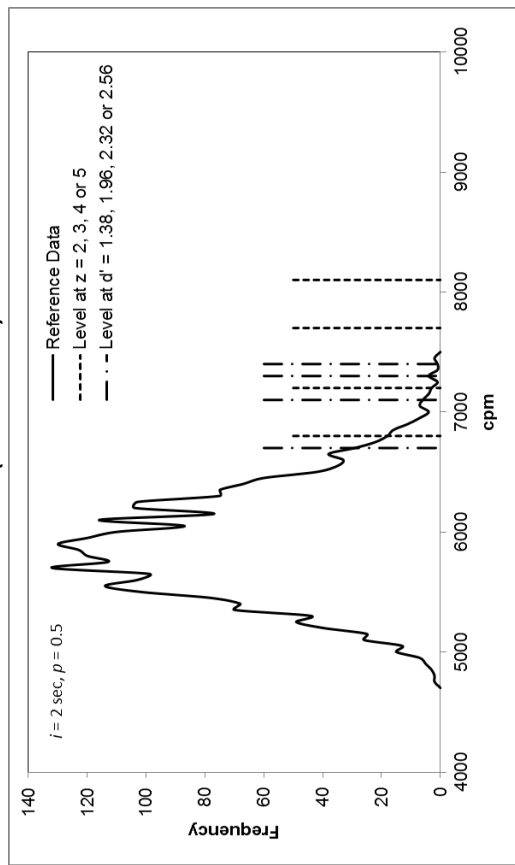
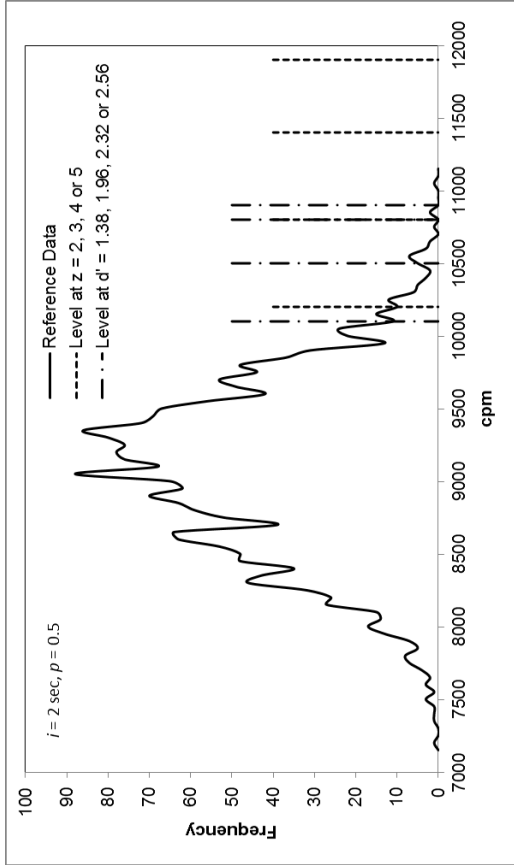
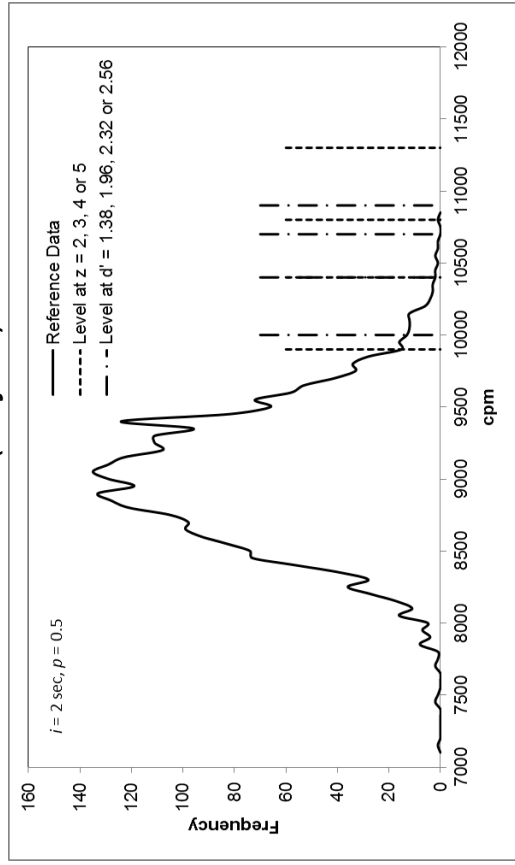
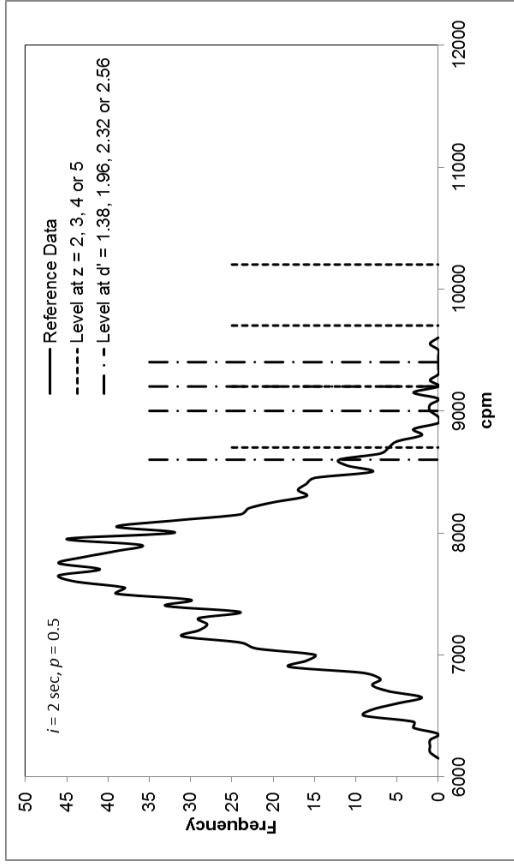


**Figure 6-17 Gross MDCRs and Investigation Levels for  $i = 2$  and  $p = 0.5$**

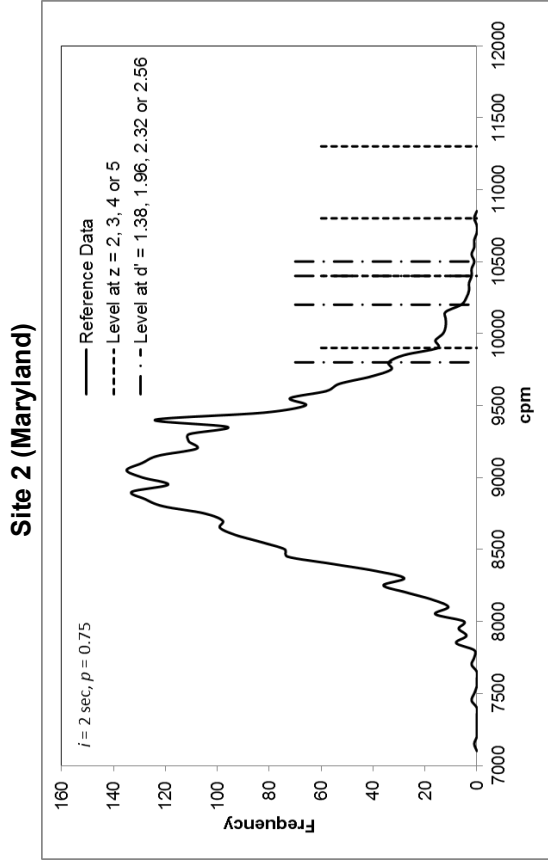
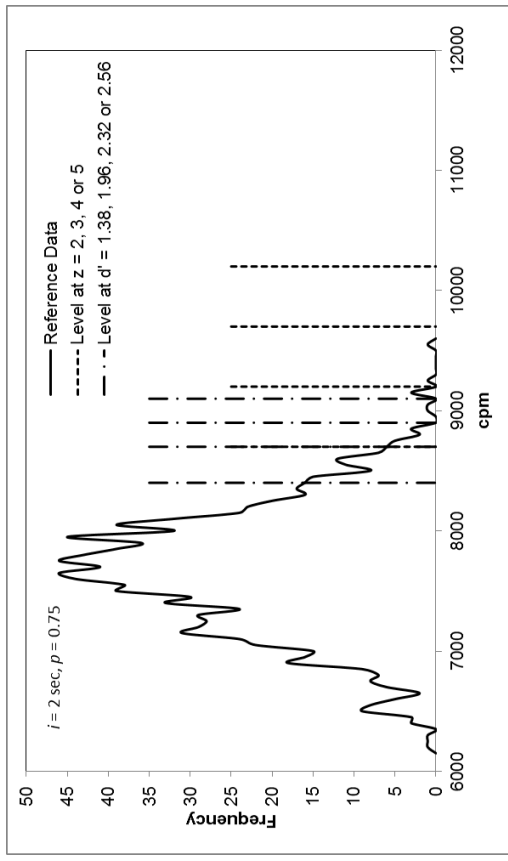
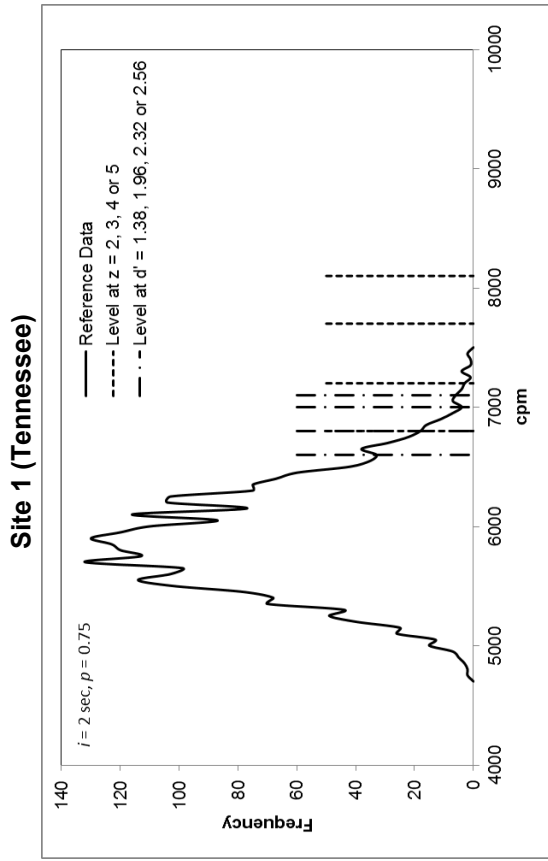
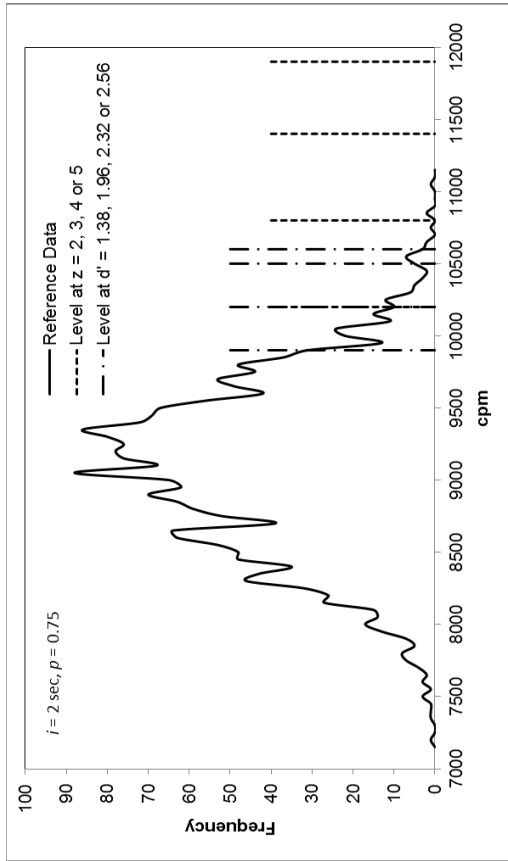


**Figure 6-18 Gross MDCRs and Investigation Levels for  $i = 2$  and  $p = 0.75$**



## 7 IN SITU GAMMA SPECTROMETRY AND EXPOSURE RATE MEASUREMENTS

The use of spectrometric techniques to assess radioactivity may produce a significant increase in sensitivity compared to radiation measurements that rely on gross instrument counts. Spectrometry allows a specific radionuclide to be measured by relying on characteristic energies of the radionuclide of concern to discriminate it from all sources present. In situ gamma spectrometry (ISGS) refers to the assessment of the ambient gamma ray flux that is collected in the field and analyzed to identify and quantify the radionuclides present. Current in situ technology can detect very low concentrations of radionuclides below a nominal hotspot concentration (i.e., MARSSIM's  $DCGL_{EMC}$ ) and, for many isotopes, below a nominal  $DCGL_W$ . However, when using ISGS, the identification of spatially dependent radioisotopic distribution is lost, and analytical results are averaged over the volume defined by the field of view (FOV) and the model assumption for contaminant depth (Chapman et al., 2006). Table 7-1 summarizes important parameters to consider when making ISGS measurements.

### 7.1 Detection Technologies

As the name "in situ gamma spectrometry" implies, the detection system must have a way to determine photon energy per detection event. Most in situ systems use a high-resolution gamma spectrometry system such as high-purity germanium (HPGe). This technology has drawbacks, such as the need for a liquid nitrogen supply and cost. The advent of electric cooling systems has helped remove the requirement for a liquid nitrogen supply. The advantage of high-resolution gamma spectrometry is the ability to discern between photopeaks from the radionuclide of interest and photopeaks from naturally occurring radioactive material and other contaminants.

Lower resolution detectors include scintillation technology such as sodium iodide (NaI) and lanthanum bromide ( $LaBr_3$ ). These detectors do not require cryogenic cooling and are generally less expensive than HPGe systems for the same efficiency. NaI crystals can be made extremely large for high-sensitivity detectors at the cost of low-energy resolution.

Many in situ detection systems come prepackaged from the manufacturer, meaning the detector, collimator, cart, and software are available as a complete package. In their most basic form, they are a detection, collimation, and mounting system. Radioanalytical laboratories have been using high-resolution, gamma-ray spectrometric methods since the 1970s, first with the introduction of solid-state lithium-drifted germanium or "GeLi" (pronounced jelly) detectors, and then by the late 1990s, HPGe detectors. These detectors revolutionized the performance of pulse height analysis, thereby significantly increasing the selectivity and identification of all gamma-emitting radionuclides. The early systems, including both the detector (germanium crystal, cryostat, and field-effect transistor) and the electronics (amplifier, analog to digital converter, and multichannel analyzer), were rarely deployed in the field. HPGe-based systems were analytical, laboratory-grade instruments. With advances in personal-computing technology and significant technological advances in detector fabrication, mounting, cryostat design, and digital electronics, manufacturers made significant progress in miniaturizing these systems and making them more rugged (Chapman et al., 2006).

ISGS semiconductor systems require calibration for their intended use. While ISGS semiconductor systems can be calibrated using traditional prepared radioactive sources, some ISGS systems have software that enables the user to calculate efficiencies by entering

parameters such as elemental composition, density, standoff distance, and physical dimensions. Supplied geometry templates assist in generating calibration curves that can be applied to multiple collected spectra. The high resolution of these systems, coupled with advanced electronic controls for system parameters, allows them to overcome issues related to source-to-detector geometry and produce quantitative concentrations of multiple radionuclides in a variety of media (e.g., soil, water, air filters). Because ISGS systems integrate all radioactivity within their FOV, lead shielding and collimation may be required to “focus” the FOV on a specified target for some applications.

## **7.2 Collimation**

To increase the sensitivity of a detection system to a particular radionuclide, it is common practice to shield unwanted radiation from sources within the environment. These sources are not only from the earth, but are in building materials, radioactive material storage, and any process that uses radionuclides. Collimation effectively limits the response of the detector to an FOV that can be controlled by adding or removing shielding. A collimated ISGS measures a disc source with radius ( $r$ ) and thickness ( $z$ ). The thickness ( $z$ ) that can be detected is limited by the energy-dependent attenuation coefficient that describes the scattering and absorption properties of the medium as a function of gamma-ray energy. The deeper the source is located in soil, the less likely it will be detected. Under normal measurement circumstances with ISGS, a single small source (of 1  $\mu\text{Ci}$ ) buried any deeper than 50 centimeters will remain undetected. In many cases, however, ISGS can be set up on contact with uncontaminated soil and used to acquire the spectrum for longer periods of time to detect deeply buried sources (of significant activity) at depths of up to 5 meters.

When a 90-degree collimator is selected for use, the radius of the disc source is equivalent to the height of the detector. For example, with a detector height ( $h$ ) equal to 100 centimeters, the radius for the field of view is also 100 centimeters. The FOV described by the radius ( $r$ ) is not perfect: there are minor edge effects in establishing the detector response function at this boundary. However, these radial edge effects are relatively small when compared to the vertical profile of the source term. As alluded to earlier, the most important parameters to describe in the model are based on the depth of the source term and any stratification or heterogeneities in the depth or areal distribution.

## **7.3 Efficiency Software**

There are two goals in gamma spectrometry: identification and quantification. In general, identification of nuclides is far less complex than their quantification. Each gamma radioisotope will have a nearly unique emission spectrum of energy lines that can be identified via analysis sequence in the spectroscopy software or manually with lookup references. Though the sample matrix may shield some low-energy lines, the target radionuclide or a radionuclide in series may emit additional energy lines. Enough information is usually available from other radionuclides to make a highly confident identification.

Each in situ measurement scenario may have a completely different geometry, especially if many different shaped items must be measured. Because of this, the detection efficiency will vary. The in situ calibration software will often have multiple templates, which approximate the shape and composition of many different simplified geometry items, such as barrels, ducts, and pipes. The measurements of the real-world item are entered into the program template, and a detection efficiency is generated for that item. Detection efficiency is specific to photon energy, and the efficiency curve depends on the probabilities of interactions within the sample, shielding

material, and the detector. Efficiency curves generated from a simulation also must account for self-absorption of photons within the sample. Measurement inputs for the simulation include physical dimensions, density, and chemical content. The detector dimensions and other input parameters must also be included, but ordinarily this information is preloaded in the vendor software application. The users must ensure that they state the correct assumptions for the sample, the detector, and the measurement geometry.

Large errors are possible when using this method. Unknown sample matrix composition, container thicknesses, and nonhomogeneous distribution of the radioactive material strongly affect the efficiency. Measuring these attributes and accounting for them can reduce some of this error. In some cases, physical and chemical matrix parameters are available in historical documents or may be available from other references. As an example, detailed information and maps on soils are available from the U.S. Department of Agriculture's Natural Resources Conservation Service. To evaluate measurement system and operator performance, it is common practice to prepare mockups of items that will be measured that contain known activity sources.

Multiple factors affect the uncertainty of the total result. Sample matrix, thickness and composition of attenuating material, physical measurement errors, and positioning errors are examples of contributors to total measurement uncertainty. The impact of these factors can be quantified by taking measurements on real-world mockups or running simulations while varying each parameter through an expected range of values.

#### **7.4 Sensitivity Measurements for ISGS Systems**

Detection sensitivity, measured as an MDC, largely depends on the instrument background. The background value is used to calculate uncertainty as a standard deviation. Spectrometric background measurements differ from those used in single-channel counting systems. In contrast with other measurement techniques, spectrometers categorize individual electronic pulses generated during the detection event according to pulse height. The size of the pulse, in volts, is proportional to the energy deposited in the detector.

As detection events are logged in the detector memory system, individual pulses are sorted into different channels. Gamma spectrometry systems have a set number of channels (i.e., a distinct number of size categories) depending on the resolution capabilities of the system. Low-resolution scintillators typically use a 2048-channel conversion gain, while HPGe systems have channel conversion gains of 4096, 8192, or 16384.

As photons deposit energy in the detector, peaks form on the spectrum in the channels associated with that photon energy. The computer or human analyst selects a region of interest (ROI) encompassing those channels associated with the peak. Peaks on the spectrum ride on top of a background continuum, and the continuum generally increases in size from the high-energy to the low-energy end of the spectrum. In other words, the background will be different for photons of different energy, and background will be higher for low-energy photons than for high-energy photons. Each peak will have a unique background. The ROI contains the gross counts measured in the selected energy range, and the computer must distinguish sample counts from background counts.

Background for a given peak is established by measuring background continuum channels to the left and right of the peak. The number of channels used for background determinations can depend on software settings, peak width, and how close the peak of interest is to other peaks.

Since the number of ROI and background channels may differ, some allowance may be necessary to address the discrepancy. Various sources (e.g., ANSI N42.14, "Calibration and Use of Germanium Spectrometers for the Measurement of Gamma Ray Emission Rates of Radionuclides," issued in 1999) may provide different methods to calculate uncertainty for a gamma spectroscopy system. One method uses the ratio between peak channel numbers and background channel numbers (Gilmore, 2008). The Section 3 uncertainty Equation 3.1 may be modified for a gamma spectrometer to include information about the difference between ROI and background channel numbers:

$$\sigma_0 = \sqrt{\sigma_B^2 + C_B \left(\frac{n}{2m}\right)} \quad (\text{Eq. 7.1})$$

where  $n$  is the number of channels in the peak ROI and  $m$  is the number of channels to the left and to the right of the ROI used to establish the average background per channel. If the number of peak channels ( $n$ ) equals the number of background channels ( $2m$ ), the equation simplifies to Equation 3.1. If fewer channels were used to establish the average background, then the variance for the nonradioactive sample would be larger than expected by Equation 3.1.

Under normal circumstances, vendor software would calculate uncertainty terms and the associated critical levels and MDCs. The human analyst may be required to perform manual calculations as a part of a verification program and should be aware that manual calculations could produce a different result from a computer-calculated MDC. If the number of ROI and background channels is different, the critical level Equation 3.3 may be rearranged as follows:

$$L_C = 1.645 \sqrt{C_B \left(1 + \frac{n}{2m}\right)} \quad (\text{Eq. 7.2})$$

The detection limit Equation 3.8 may be modified to the following:

$$L_D = 3 + 3.29 \sqrt{C_B \left(1 + \frac{n}{2m}\right)} \quad (\text{Eq. 7.3})$$

The MDC Equation 3.10 may be modified as follows:

$$\text{MDC} = \frac{3 + 3.29 \sqrt{C_B \left(1 + \frac{n}{2m}\right)}}{KT} \quad (\text{Eq. 7.4})$$

## **7.5 Geometric Issues for ISGS Measurements**

The most important disadvantage of ISGS is that the accuracy of the analysis depends on a separate knowledge of the radioactivity distribution across and within soil depth and, to a lesser extent, knowledge of the soil density, moisture content, and chemical composition. Different source geometries cause different angular distributions of the primary photon fluence. Usually, the efficiency of a detector is measured for a selected reference direction of primary photons. However, the appropriate use of collimation can mitigate angular effects in uniformly distributed large fields.

### 7.5.1 Depth Distribution

Determining the radionuclide depth in soil and concrete using ISGS has previously been studied based on various principles (Whetstone et al., 2011). Methods include the following:

- different, specially designed multiple collimators and/or shields (Whetstone et al., 2011; Benke & Kearfott, 2002; Benke & Kearfott, 2001; Van Riper et al., 2002)
- the peak-to-valley ratio method (Zombori et al., 1992; Tyler, 1999)
- the multiple photopeak method (Sowa et al., 1989; Beck et al., 1972; Karlberg, 1990) or the primary photopeak and x-ray lines (Rybacek et al., 1992)

By placing a lead plate in front of an in situ detector, it has been shown that the response of the detector above the ground is dependent on the plate to detector distance. The unattenuated gamma rays incident on the detector at large angles, measured from the axis of the cylindrical detector crystal, originate predominately from shallower layers of soil. By attenuating the gamma rays emitted directly beneath the detector with a lead plate, the detector responds primarily to the gamma emissions from the shallower layers of soil. The main advantage of the lead plate method is its applicability to radionuclides, which emit gamma rays at a single energy (Korun et al., 1994). Zombori et al. (1992) developed a method based on the ratio of count rates between the 662-keV photopeak and 631–649 keV valley region, between the Compton edge and Cs-137 photopeak. This photopeak-to-valley method applies to single gamma-ray emitters. However, the method's effectiveness depends on the intensity of gamma emissions. Therefore, it can be adversely affected by interfering gamma-ray emissions at energies close to the photopeak or valley region. The multiple photopeak method requires *a priori* knowledge of the depth distribution and cannot yield any depth distribution information for radionuclides that emit fewer than two significant gamma-ray energies.

Each of these methods has its particular advantages and disadvantages. According to Whetstone et al. (2011), the first method seems to deliver the most accurate results. However, one drawback of this method is that the activity distribution in the horizontal direction is usually considered to be relatively homogeneous which is not always the case (e.g., when hotspots are present). Moreover, multiple measurements on one spot are required to determine the radionuclide contamination depth. Each method requires *a priori* assumptions of the depth distribution function. In addition to usually assuming a uniform soil density with depth, all three approaches for determining depth distributions also assume a spatially uniform radionuclide distribution (Benke & Kearfott, 2001). Currently, the determination of depth distribution is based on prior experimental core sampling results at similar locations, any known site history, or radionuclide transport models. A method developed by Dewey et al. (2011) uses multiple in situ measurements at a single site to determine the analytical form that best represents the true depth distribution.

### 7.5.2 Discrete Particles

An ORAU study assessed the in situ gamma spectrometer response for a “discrete particle” (or hotspot) (Chapman et al., 2006). One of the assumptions the efficiency generating software makes during geometry modeling is that the radioactive material is homogeneously distributed within the FOV of the detector. The efficiency of a collimated detector is highest at the center of its FOV and lowest at its edges. When a hotspot of radioactive material is present at the edge of the FOV of the detector, its activity will be underestimated. The objective of the research was to

determine what level of radioactivity in a discrete particle will trigger a positive measurement result (and investigation) distinguishable from the background. Or, more simply, what is the discrete particle detectability using an in situ gamma spectrometer? Discrete particles were defined as a small localized volume of soil containing one or several particles of radioactivity that is significantly more radioactive than the average low-level concentration of the surrounding soil.

ORAU made ISGS measurements with reference source materials of Cs-137, Co-60, and natural thorium. A 38-percent efficient HPGe detector was positioned at heights of 1 and 2 meters above the ground; sources were placed on the surface and subsurface at 7.5 and 15 centimeters, and in addition, at radii of 0 (on axis), 1 and 2 meters. The amount of activity selected for each source was calculated to be somewhat less than the equivalent volumetric average concentrations associated with nominal DCGLs.

The primary goal of this study was to calculate the discrete particle activity located at various radial and depth locations that would result in further investigation. This discrete particle activity represents the “hotspot MDA” for the specified test conditions. Two pieces of information are required to calculate the hotspot MDA as defined in this study: (1) the minimum detectable (MD) counts in the photopeak region from background spectra, and (2) the hotspot efficiency for a specific source geometry. Hotspot MDAs were then calculated by dividing the MD counts obtained from the background spectra by the efficiency of the particular detector. For example, with no source present, the MD counts at the 1-meter detector height for the Co-60 1,173-keV gamma line were 32.2 counts based on the nuclide MDA report, which provided 0.1467  $\mu\text{Ci}/\text{unit}$  in the photopeak region. This value was multiplied by the efficiency ( $6.6 \times 10^{-6}$ ), conversion factor ( $2.22 \times 10^6 \text{ dpm}/\mu\text{Ci}$ ), and 15-minute live time. For the 1-meter detector height, a Co-60 test source (1.2  $\mu\text{Ci}$ ) was positioned at a 1-meter radial location and surface position (zero depth). The Co-60 source produced a net count in the photopeak region (1,173 keV) of 117 counts. The following gives the detector efficiency for this particular discrete particle geometry:

$$\text{Detector efficiency} = \frac{117 \text{ counts}}{1.2 \mu\text{Ci}} = 97.5 \text{ counts}/\mu\text{Ci}$$

The hotspot MDA is then calculated by dividing the MD counts by the detector efficiency:

$$\text{Hot spot MDA} = \frac{32.2 \text{ counts}}{97.5 \text{ counts}/\mu\text{Ci}} = 0.33 \mu\text{Ci}$$

Tables 7-2 and 7-3 provide hotspot MDAs for 1- and 2-meter detector heights for the various experimental configurations of the discrete source activity (Chapman et al., 2006). The results indicate that when the discrete source is directly beneath the detector at 1-meter height, it is possible to detect 0.02–0.04  $\mu\text{Ci}$  of Co-60 or Cs-137. When the detector height is increased to 2 meters, the hotspot MDA for each radionuclide increases to 0.08–0.16  $\mu\text{Ci}$ . This is because of the detector’s greater FOV at the 2-meter height and the corresponding  $1/r^2$  decrease in geometric efficiency. Furthermore, as the discrete source is moved from directly beneath the detector’s 1-meter radius, the hotspot MDAs increase by a factor of 5–8 for both Co-60 and Cs-137. Finally, the increasing depth of the discrete source burial from the surface to

15 centimeters has less of an impact on the hotspot MDA than moving it to the 1-meter radial location.

Because of the higher MDA experienced when a hotspot is at the edge of the FOV, the center-to-center spacing of multiple in situ measurements is decreased to the point where there is sufficient overlap between the multiple measurements, and the chance of completely missing a hotspot is alleviated. As seen in Figure 7-1, hexagonal circle packing provides the densest possible arrangement of multiple FOVs and can be adjusted further by decreasing the center-to-center spacing of the circular FOVs to the point where three adjacent FOVs overlap.

## **7.6 ISGS Measurements in Outdoor Test Area**

The U.S. Department of Energy's Environmental Measurements Laboratory has performed detailed and quantitative evaluations of portable gamma spectrometry systems. NUREG-1506, "Measurement Methods for Radiological Surveys in Support of New Decommissioning Criteria (Draft Report for Comment)," issued August 1995, gives detailed guidance on how to use ISGS during survey activities. That report gives examples of MDCs using a typical 25-percent relative efficiency p-type germanium detector and a 10-minute count time at typical background radiation levels. Using these assumptions, the MDCs for Co-60, Cs-137, europium (Eu)-152, Ra-226 (based on measurement of progeny), and actinium (Ac)-228 (to infer Th-232) are all approximately 0.05 pCi/g. A more efficient detector, such as a 75-percent relative efficiency n-type germanium detector, is needed to measure the radionuclides that are more difficult to detect. For example, using the 75-percent relative efficiency n-type germanium detector for a 10-minute count time results in an MDC of 0.5 pCi/g for Am-241 and 2 pCi/g for U-238 (based on measurement of short-lived Th-234 progeny) and Ra-226 (based on measurement of the 186-keV gamma energy line). These typical MDCs scale as the square root of the count time; that is, quadrupling the count time results in a factor of 2 increase in the sensitivity of the in situ measurement.

ISGS measurements were performed within the outdoor test area (this same area was also used to evaluate the scan sensitivity of surveyors) to determine the spectrometer's ability to identify and locate the sources. This particular exercise was intended to evaluate the scanning capabilities of the in situ gamma spectrometer, not its ability to determine radionuclide concentrations in soil, which requires detailed detector calibration and modeling of the contaminant distribution in the soil.

ORAU buried 25 gamma-emitting sources in the test area, including 12 Co-60 sources and 5 Cs-137 sources. Measurements were made at nine grid locations in the test area, at both 0.5 and 1 meter above the ground (Figure 7-2). A background measurement was made at 1 meter above the ground in an adjacent area unaffected by the test area sources. ORAU used a 13-percent relative efficiency p-type germanium detector and a 30-minute count time at each measurement location. Table 7-4 gives the net counts collected in both the Co-60 and Cs-137 peak regions. Figure 7-2 presents the Co-60 data to allow a visual correlation between the detector response and the Co-60 source location. The Cs-137 data were not evaluated in this manner because levels of Cs-137 exceeded background in only a few locations.

The results indicated that the portable gamma spectrometry system was able to identify the presence of Cs-137 and Co-60 contamination in the test area. This elementary finding should not be dismissed without considering its implications for the use of ISGS as a scanning tool. Recognizing that ISGS is able to detect relatively low levels of gamma-emitting radionuclides is of particular value when the detector is used to verify the absence of contamination in an area.

That is, if the detector's MDC can be demonstrated to be sufficiently below the contamination guidelines, then ISGS measurements may be used to demonstrate that additional survey efforts in an area are not warranted. Furthermore, using ISGS to determine that residual radioactivity is below a specified concentration has an additional benefit in the improved documentation of the scan survey. Records of ISGS measurements are generally more objective and less likely to be influenced by human factors than the conventional scan survey records obtained with NaI scintillation detectors or other portable field instrumentation, which require the surveyor's subjective interpretation of the detector response.

For the present experiment, the in situ gamma spectrometer did identify the presence of Co-60 and Cs-137 contamination and, therefore, the data were analyzed to locate the contamination. Figure 7-2 shows the net counts in the Co-60 peak region at both 1 and 0.5 meters above the surface at each grid coordinate (the top number is the 1-meter value, and the bottom number is the 0.5-meter value). In the case of uniform contamination and a detector height of 1 meter, approximately 80 percent of the detector's response would be from a 5-meter radius (NUREG-1506, "Measurement Methods for Radiological Surveys in Support of New Decommissioning Criteria (Draft for Comment)"). Because detector height above the surface affects the amount of ground being viewed, moving the detector closer to the ground results in a smaller area being viewed.

The greatest quantity of Co-60 activity was identified at grid location 15N,5W. The increase in the net counts for Co-60 as the detector was moved closer to the ground indicates that the source is relatively close to the sampled grid coordinate. Also, because the Co-60 result at coordinate 10N,5W has significantly less Co-60 activity than at 15N,5W, it is likely that the source is not south of grid coordinate 15N,5W.

The Co-60 results for grid coordinates 5N,5W and 15N,10W (both have 1-meter readings greater than the 0.5-meter readings) indicate that Co-60 contamination is nearby, but not necessarily in the immediate vicinity of the sampled grid coordinate. Although this analysis does not direct the surveyor to the exact location of the contamination, it does provide a focused plan for subsequent NaI scintillation scan surveys.

## **7.7 Exposure Rate Measurements in Outdoor Test Area**

Exposure rate measurements using a PIC were performed within the outdoor test area to evaluate the PIC's sensitivity in measuring exposure rate. Measurements were taken at six grid coordinate locations, each reading at 1 meter above the surface (Figure 7-3). The background exposure rate (10.3  $\mu\text{R/h}$ ) was determined in an area adjacent to the test area, but unaffected by the test area sources.

The sensitivity of the PIC is directly proportional to the standard deviation of the background exposure rate. Therefore, areas exhibiting only minor background exposure rate variations will have the lowest minimum detectable exposure rates. The exposure rate measurements in the test area ranged from 10.2 to 11.1  $\mu\text{R/h}$  (Table 7-5). Figure 7-3 illustrates the correlation between the exposure rate measurements and the source locations. The larger exposure rates correspond to the larger gamma radiation levels that were obtained during characterization of the test area (refer to grid locations 15N,15W and 15N,5W). These results indicate that the PIC response was affected by the gamma-emitting sources. The minimum detectable exposure rate obtained with the PIC can be expected to be approximately 1  $\mu\text{R/h}$  above background levels, depending on the background variability.



## 7.8 ISGS Measurement of Scrap Metal

ORAU performed an experiment to determine the magnitude of the ISGS detection capabilities for a release of scrap metal from a nuclear facility (NUREG-1761, "Radiological Surveys for Controlling Release of Solid Materials," issued July 2002). In this case, 1 metric ton of 12.7-centimeter (5-inch) diameter steel conduit was selected. To determine how much radioactivity was required for the experiment, the mass-based, critical-group dose factors reported in draft NUREG-1640, "Radiological Assessments for Clearance of Materials from Nuclear Facilities," issued June 2003, were used. For comparison with draft NUREG-1640, the calculations assumed a normalized unit dose factor of 10 microsieverts per year ( $\mu\text{Sv}/\text{yr}$ ) (1 mrem/yr). As the following example calculation shows, 38 kilobecquerels (kBq) (1  $\mu\text{Ci}$ ) of Cs-137 on steel would produce approximately 10  $\mu\text{Sv}/\text{yr}$  (1 mrem/yr) to the critical member of the group:

$$\frac{10 \mu\text{Sv}/\text{y}}{260 \left( \frac{\mu\text{Sv}}{\text{y}} \right) \left( \frac{\text{g}}{\text{Bq}} \right)} \times (10^6 \text{g}) \times \frac{\text{kBq}}{1000 \text{Bq}} = 38 \text{kBq}$$

Therefore, if the ISGS system can demonstrate a sensitivity less than 38 kBq (1  $\mu\text{Ci}$ ), this is a reasonable technique. Table 7-6 summarizes the total activity calculations for steel.

For this experiment, 20 sources each of Cs-137 and Co-60 were fabricated; each source was approximately 1/20th of 38 kBq (1  $\mu\text{Ci}$ ). The Cs-137 sources were randomly placed inside the steel conduit interiors. A measurement was taken at the midpoint of each side of the pallet on which the conduit was resting for 10 minutes, for a total of 40 minutes of count time. The process was repeated for nine additional measurement sets with the Cs-137 sources placed randomly each time. The Co-60 measurements were independently made in the same manner. No shielding or collimation was used, and the detector was placed 1-meter (vertically) from the floor and generally as close as possible to the pallet of steel conduit.

The efficiency for the ROI corresponding to the appropriate total absorption peak for Co-60 or Cs-137 was calculated. First, the net counts in the ROI were calculated by subtracting the Compton continuum counts in the ROI from the gross counts in the total absorption peak ROI. Next, the net counts for the total absorption peak ROI were divided by the total activity of the particular source and the count time in minutes to determine efficiency in net cpm per kBq. The MDA, in kBq, for the total absorption peak ROI was calculated by the equation below, using the experimentally determined efficiency, where the background values, or continuum counts, were determined by the gross peak counts minus the net peak counts:

$$MDA[\text{kBq}] = \frac{3+4.65\sqrt{C_B}}{T[\text{min}] \times \epsilon \times [\text{net peak counts per minute per Bq}]} \quad (\text{Eq. 7.5})$$

Table 7-6 summarizes the ISGS measurements of the steel conduit pallet.

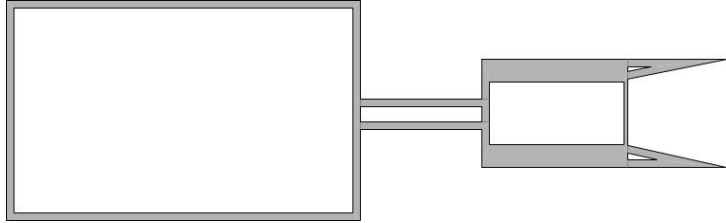
Multiple sets of measurements with randomly placed sources (in a nonuniform geometry) were made to calculate an unbiased range of efficiencies for this particular geometry. Using the lower 5-percent confidence interval on the 2-sigma range of the efficiency from Table 7-7 allows the MDA to be conservatively reported for comparison to potential dose limits. Table 7-7 indicates that, at an alternative dose criterion of 10  $\mu\text{Sv}/\text{yr}$  (1 mrem/yr), ISGS is a viable technology for determining the appropriateness of releasing 1 metric ton of 12.7-centimeter(5-inch)-diameter steel conduit from a nuclear facility. The upper range MDA for Cs-137 at 19 kBq (0.5  $\mu\text{Ci}$ ) is below the total activity of 38 kBq (1.0  $\mu\text{Ci}$ ) required to produce 10  $\mu\text{Sv}/\text{yr}$  (1 mrem/yr). The upper

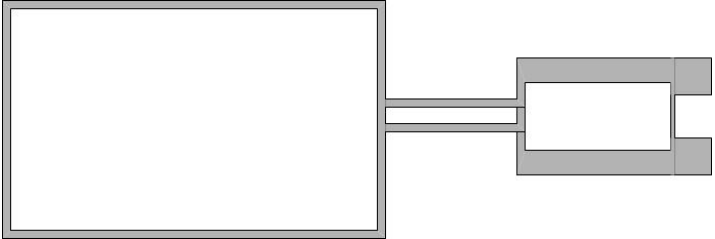
range MDA for Co-60 at 22 kBq (0.6  $\mu$ Ci) is below the total activity of 40 kBq (1.1  $\mu$ Ci) required to produce 10  $\mu$ Sv/yr (1 mrem/yr). However, if the more restrictive dose limit of 1  $\mu$ Sv/yr (0.1 mrem/yr) is assumed, ISGS would lack the necessary sensitivity to detect 3.8 kBq (0.1  $\mu$ Ci) of either Co-60 or Cs-137.

Using the same Cs-137 and Co-60 sources with the steel conduit experiment, a second experimental configuration consisting of a pallet of 148 insulated copper wires with a total weight of 490 kilograms (1,080 pounds) was set up. The only difference between the steel and copper experiment was that the count time was increased from 10 to 30 minutes per measurement to allow for the increased attenuation of the gamma rays by the copper. Table 7-8 shows the dose calculation results.

Table 7-9 shows that for an alternative dose criterion of 10  $\mu$ Sv/yr (1 mrem/yr) and for the given experimental conditions, ISGS may not be a viable technology for a typical volume of copper released from a nuclear facility. The upper range MDA for Cs-137 at 89 kBq (2.4  $\mu$ Ci) is above the total activity of 78 kBq (2.1  $\mu$ Ci) required to produce 10  $\mu$ Sv/yr (1 mrem/yr). The upper range MDA for Co-60 at 59 kBq (1.6  $\mu$ Ci) is above the total activity of 19 kBq (0.5  $\mu$ Ci) required to produce 10  $\mu$ Sv/yr (1 mrem/yr). However, if the less restrictive dose limit of 100  $\mu$ Sv/yr (10 mrem/yr) were adopted, ISGS would have the necessary sensitivity to detect 780 kBq (21  $\mu$ Ci) of Cs-137 or 190 kBq (5  $\mu$ Ci) of Co-60 in this copper matrix.

**Table 7-1 Important Parameters for ISGS Measurements**

| Subsystem                                       | Parameter                 | Discussion/Options   |
|---|---------------------------|--|
| Solid-State, High-Resolution Gamma-Ray Detector | Type of HPGe detector     | Planar (GeLi); coaxial-> n-type (or reverse electrode germanium, REGe), p-type (HPGe), or broad-energy germanium (BEGe). Unless the radionuclide is very low energy (<50 keV) and "surface only," planar detectors are not applicable. Most ISGS measurements are performed with coaxial detectors (REGe, HPGe, BEGe).   |
|   | Efficiency                | Most vendors provide this single performance value under the ANSI/IEEE Std 325-1996 definition. For ISGS, it is most important to understand the complete <u>efficiency function</u> over the energy range of interest. For many applications (e.g., Cs-137), a 60% detector is not twice as "good" as a 30% detector. Quality ISGS measurements have been made with detectors from 20 to 150% efficient.          |
|   | End- or Window-Cap        | When the radionuclide of interest emits low-energy photons, window properties are important. If the radionuclide is "at or near infinite depth," then window material and thickness are less important: the photon does not survive the collisions in the soil. For low-energy analysis, use C or Be end-caps.   |
|   | Detector Characterization | Manufacturer's engineering evaluation/calibration of the detector. This is a response function normalization of mathematically computed efficiency versus direct measurement of point source (e.g., Eu-155 and Na-22). All mathematical models developed for the in situ analysis then use the normalized/calibrated efficiency characteristics. Not all vendors perform this characterization/calibration record. |
|   | Resolution                | For most deployed systems, expect a nominal resolution of 2 keV at 1,333 keV and 600 eV at 122 keV. In most cases, existing systems easily meet this requirement; however, it is important that the analyst calibrate the detector for it.   |
| Collimator                                      | Tapered                   | <p>The collimator angle of view from the detector is tapered.</p>    |

| Subsystem                 | Parameter  | Discussion/Options   |
|---------------------------|--|--|
|                           | Nontapered   | <p>The collimator is not tapered.</p>    |
|                           | Angular FOV  | <p>Various collimator sets are available to measure small pipes (small solid angle subtended by the source at the detector). Most in situ soil measurements use a 90-degree collimator, though some have used 180-degree collimators. This parameter is very important when defining the measurement capability and whether the DQOs can be met.</p>   |
|                           | Offset (or recess of the detector)   | <p>Offset refers to how far back into the collimator the detector is located. This is another technique to change the FOV.</p>   |
|                           | Back-shield  | <p>Back-shield reduces background flux impinging from the rear of the detector (opposite the measurement sample). A back-shield should be used to reduce background.</p>   |
| Counting Geometry         | Standoff (or detector height)  | <p>The further from the ground the detector is placed, the larger the “sampling area” and the smaller the MDC (pCi/g) because more soil is being measured (denominator), and the angular sensitivity to incoming photons is increased (numerator). The further the standoff (or the higher the detector is positioned), the greater the “average areal/volumetric” response. It is the standoff, coupled with the FOV, that permits very low MDCs to be achieved using ISGS.</p> |
| Data Acquisition Settings | Gain   | <p>The gain of the amplifier needs to be adjusted to ensure that all photons of interest are detected and registered by the multichannel analyzer.</p>   |
|                           | Count Time (Live Time)   | <p>The theoretical MDC decreases as <math>1/\sqrt{t}</math>. A factor of 4 increase in count time decreases the MDC by a factor of 2. This is the only measurement setting that can be expressed as an absolute performance measurement parameter.</p>   |
| Analysis Model Parameters | Depth of Contaminant   | <p>Most analyses for a final status survey use a contaminant depth of 15 centimeters. (Section 3.6.3.1 of MARSSIM). Because photon scattering and absorption in soil are exponential functions (Beer’s Law), contaminant depth must be properly understood in order to yield accurate analysis results.</p>  |
|                           | Contaminant Function of Depth Distribution (e.g., as uniform, exponential) | <p>The contaminant is normally either uniform or exponentially distributed. This parameter is important if the contaminant is believed to exist at depth or the contaminant emits low-energy photons (less than 150 keV).</p>  |

| Subsystem                                | Parameter                                   | Discussion/Options  |
|--|---|---|
|  | Contaminant Profile (stratification, lumps) | Efficiency models available commercially can account for stratification in the source term, nonuniformities in the source, and, to some degree, "lumps." This effort lends itself to uncertainty bounding in the model results.   |
|  | Matrix Properties                           | Chemical properties of the local soil include moisture density and igneous rock stratifications in the measurement sample.  |
|  | Application of Most Accurate Model          | The model should account for all available process knowledge about the actual site contaminant profile. All parameters discussed above should be represented properly, including description of the detector, collimator, field of view, contaminant profile, and geologic setting. |
|  | Multienergy Model Correction                | Some information about the contaminant profile can be accounted for by direct measurement, when multiple photon energies are emitted from the same radionuclide.  |
|  | MDC   | The minimum detectable concentration (MDC) is one of the most misunderstood terms in ISGS. It is important to review the methodology and the assumptions used to describe "the source term" for which the MDC is calculated.  |
| Analysis of the High-Resolution Spectrum | Background Subtraction                      | When the radiocontaminant of interest is naturally occurring, then active background subtraction is necessary (spectral stripping). When the radiocontaminant does not exist in the natural spectrum, then standard photopeak area integration methods are sufficient.              |
|  | Multiplet Deconvolution                     | Multiplet deconvolution is normally not required for fission products. For source materials (uranium and thorium) and special nuclear materials (plutonium), multiplet deconvolution is necessary and can significantly impact the measurement results.                             |

**Table 7-2 Discrete Source MDAs at 1-Meter Detector Height**

| <b>Co-60 (1.2 µCi) (MD Counts 33.4)</b>   |                   |                      |                          |
|---|-------------------|----------------------|--------------------------|
| <b>Radius (m)</b>                         | <b>Depth (cm)</b> | <b>Net Peak Area</b> | <b>Hotspot MDA (µCi)</b> |
| 0   | 0                 | 1,070                | 0.037                    |
| 1   | 0                 | 137                  | 0.292                    |
| 0   | 7.5               | 467                  | 0.086                    |
| 1   | 7.5               | 76.3                 | 0.525                    |
| 0   | 15                | 253                  | 0.158                    |
| 1   | 15                | 103                  | 0.389                    |
| <b>Cs-137 (4.2 µCi) (MD Counts 28.5)</b>  |                   |                      |                          |
| <b>Radius (m)</b>                         | <b>Depth (cm)</b> | <b>Net Peak Area</b> | <b>Hotspot MDA (µCi)</b> |
| 0   | 0                 | 6,480                | 0.018                    |
| 1   | 0                 | 905                  | 0.132                    |
| 0   | 7.5               | 2,280                | 0.053                    |
| 1   | 7.5               | 388                  | 0.309                    |
| 0   | 15                | 1260                 | 0.095                    |
| 1   | 15                | 415                  | 0.289                    |
| <b>Th-232 (0.32 µCi) (MD Counts 28.5)</b> |                   |                      |                          |
| <b>Radius (m)</b>                         | <b>Depth (cm)</b> | <b>Net Peak Area</b> | <b>Hotspot MDA (µCi)</b> |
| 0   | 0                 | 141                  | 0.143                    |
| 1   | 0                 | 86                   | - <sup>a</sup>           |
| 0   | 7.5               | 107                  | 0.302                    |
| 1   | 7.5               | 104                  | 0.305                    |
| 0   | 15                | 69.5                 | - <sup>a</sup>           |
| 1   | 15                | 72.6                 | - <sup>a</sup>           |

<sup>a</sup>Indistinguishable from background. Th-232 (Ac-228, 911-keV) background net peak area is 76.5 counts.

**Table 7-3 Discrete Source MDAs at 2-Meter Detector Height**

| <b>Co-60 (1.2 <math>\mu</math>Ci) (MD Counts 33.4)</b>      |                   |                      |   |
|---|-------------------|----------------------|---|
| <b>Radius (m)</b>   | <b>Depth (cm)</b> | <b>Net Peak Area</b> | <b>Hotspot MDA (<math>\mu</math>Ci)</b> |
| 0   | 0                 | 251                  | 0.159                                   |
| 1   | 0                 | 34                   | 1.173                                   |
| 0   | 7.5               | 83.7                 | 0.477                                   |
| 1   | 7.5               | 60.4                 | 0.660                                   |
| 0   | 15                | 70.8                 | 0.563                                   |
| 1   | 15                | 30                   | 1.329                                   |
| <b>Cs-137 (4.2 <math>\mu</math>Ci) (MD Counts 28.5)</b>     |                   |                      |   |
| <b>Radius (m)</b>   | <b>Depth (cm)</b> | <b>Net Peak Area</b> | <b>Hotspot MDA (<math>\mu</math>Ci)</b> |
| 0   | 0                 | 1,460                | 0.082                                   |
| 1   | 0                 | 277                  | 0.432                                   |
| 2   | 0                 | 64.5                 | 1.855                                   |
| 0   | 7.5               | 499                  | 0.240                                   |
| 1   | 7.5               | 315                  | 0.380                                   |
| 2   | 7.5               | 104                  | 1.150                                   |
| 0   | 15                | 423                  | 0.283                                   |
| 1   | 15                | 257                  | 0.465                                   |
| 2   | 15                | 82.8                 | 1.455                                   |
| <b>Th-232 (0.32 <math>\mu</math>Ci) (MD 423Counts 28.5)</b> |                   |                      |   |
| <b>Radius (m)</b>   | <b>Depth (cm)</b> | <b>Net Peak Area</b> | <b>Hotspot MDA (<math>\mu</math>Ci)</b> |
| 0   | 0                 | 81.7                 | - <sup>a</sup>                          |
| 1   | 0                 | 39.6                 | - <sup>a</sup>                          |
| 0   | 7.5               | 105                  | 0.356                                   |
| 1   | 7.5               | 58.9                 | - <sup>a</sup>                          |
| 0   | 15                | 84.3                 | - <sup>a</sup>                          |
| 1   | 15                | 51                   | - <sup>a</sup>                          |

<sup>a</sup>Indistinguishable from background. Th-232 (Ac-228, 911 keV) background net peak area is 76.5 counts.

**Table 7-4 ISGS Data from Outdoor Test Area**

| Measurement Location <sup>a</sup> |                  | Net Count in Peak Region |   |    |                   |   |    |
|-----------------------------------|------------------|--------------------------|---|----|-------------------|---|----|
|                                   |                  | Cs-137 (662 keV)         |   |    | Co-60 (1,332 keV) |   |    |
| Background                        | 1 m <sup>b</sup> | -4                       | ± | 8  | 6                 | ± | 14 |
| 5N, 5W                            | 1 m              | -18                      | ± | 10 | 30                | ± | 10 |
| 5N, 5W                            | 0.5 m            | -4                       | ± | 8  | 5                 | ± | 16 |
| 10N, 5W                           | 1 m              | 5                        | ± | 7  | 27                | ± | 13 |
| 10N, 5W                           | 0.5 m            | 15                       | ± | 7  | 26                | ± | 12 |
| 15N, 5W                           | 1 m              | 11                       | ± | 8  | 163               | ± | 18 |
| 15N, 5W                           | 0.5 m            | -2                       | ± | 7  | 234               | ± | 25 |
| 5N, 15W                           | 1 m              | -1                       | ± | 8  | 38                | ± | 7  |
| 5N, 15W                           | 0.5 m            | 4                        | ± | 8  | 40                | ± | 13 |
| 10N, 15W                          | 1 m              | 7                        | ± | 9  | 9                 | ± | 17 |
| 10N, 15W                          | 0.5 m            | 8                        | ± | 9  | 36                | ± | 15 |
| 15N, 15W                          | 1 m              | 7                        | ± | 8  | 40                | ± | 12 |
| 15N, 15W                          | 0.5 m            | -11                      | ± | 9  | 18                | ± | 16 |
| 5N, 25W                           | 1 m              | 7                        | ± | 8  | 20                | ± | 18 |
| 5N, 25W                           | 0.5 m            | 19                       | ± | 9  | 23                | ± | 17 |
| 10N, 25W                          | 1 m              | 3                        | ± | 8  | 4                 | ± | 17 |
| 10N, 25W                          | 0.5 m            | 17                       | ± | 8  | 36                | ± | 13 |
| 15N, 25W                          | 1 m              | -6                       | ± | 8  | 8                 | ± | 15 |
| 15N, 25W                          | 0.5 m            | 10                       | ± | 8  | 25                | ± | 11 |

<sup>a</sup> Refer to Figure 7-2.

<sup>b</sup> Distance refers to detector height above the surface.

**Table 7-5 Exposure Rate Measurements from Outdoor Test Area**

| Measurement Location <sup>a</sup> | Exposure Rate <sup>b</sup> (μR/h) |
|-----------------------------------|-----------------------------------|
| Background                        | 10.3                              |
| 5N, 5W                            | 10.8                              |
| 5N, 15W                           | 10.2                              |
| 5N, 25W                           | 10.9                              |
| 15N, 5W                           | 11.1                              |
| 15N, 15W                          | 11.0                              |
| 15N, 25W                          | 11.0                              |

<sup>a</sup> Refer to Figure 7-3.

<sup>b</sup> Measurements made 1 meter above the surface.



**Table 7-6 Calculated Total Activity for Selected Radionuclides Using Mass-Based, Critical Group Dose Factors for Steel (106 grams)**

| Radionuclide (keV)   | Mean Dose Factor ( $\mu\text{Sv/yr} \times \text{g/Bq}$ ) | Mean Dose Factor ( $\text{mrem/yr} \times \text{g/pCi}$ ) | Total Activity for $10 \mu\text{Sv/yr}$ (kBq) | Total Activity for $10 \mu\text{Sv/yr}$ ( $\mu\text{Ci}$ ) |
|----------------------|---|---|---|--|
| Cs-137 (662)         | 260   | 0.962   | 38  | 1.027  |
| Co-60 (1,173, 1,332) | 250   | 0.925   | 40  | 1.081  |

**Table 7-7 Efficiency and MDA Summary for ISGS Measurements of Scrap Steel Pallet with a 10-Minute Count Time**

| Radionuclide (keV) | Efficiency (Standard Deviation) (net cpm per kBq) | 2-Sigma Efficiency Range (net cpm per kBq) | MDA (kBq) | MDA ( $\mu\text{Ci}$ ) |
|--------------------|---|--|-----------|------------------------|
| Cs-137 (662)       | 0.41 (0.09)                                       | 0.23–0.59                                  | 11        | 0.297                  |
| Co-60 (1,173)      | 0.33 (0.07)                                       | 0.19–0.47                                  | 11        | 0.297                  |
| Co-60 (1,332)      | 0.30 (0.06)                                       | 0.18–0.42                                  | 11        | 0.297                  |

**Table 7-8 Calculated Total Activity for Selected Radionuclides Using Mass-Based, Critical Group Dose Factors for Copper (106 grams)**

| Radionuclide (keV)   | Mean Dose Factor ( $\mu\text{Sv/yr} \times \text{g/Bq}$ ) | Mean Dose Factor ( $\text{mrem/yr} \times \text{g/pCi}$ ) | Total Activity for $10 \mu\text{Sv/yr}$ (kBq) | Total Activity for $10 \mu\text{Sv/yr}$ ( $\mu\text{Ci}$ ) |
|----------------------|---|---|---|--|
| Cs-137 (662)         | 62  | 0.229   | 78  | 2.108  |
| Co-60 (1,173, 1,332) | 250   | 0.925   | 19  | 0.514  |

**Table 7-9 Efficiency and MDA Summary for ISGS Measurements of Scrap Copper Pallet with a 30-Minute Count Time**

| Radionuclide (keV) | Efficiency (Standard Deviation) (net cpm per kBq) | 2-Sigma Efficiency Range (net cpm per kBq) | MDA (kBq) | MDA ( $\mu\text{Ci}$ ) |
|--------------------|---|--|-----------|------------------------|
| Cs-137 (662)       | 0.13 (0.04)                                       | 0.05–0.21                                  | 33        | 0.892                  |
| Co-60 (1,173)      | 0.11 (0.03)                                       | 0.05–0.17                                  | 37        | 1.000                  |
| Co-60 (1,332)      | 0.09 (0.02)                                       | 0.05–0.13                                  | 30        | 0.811                  |

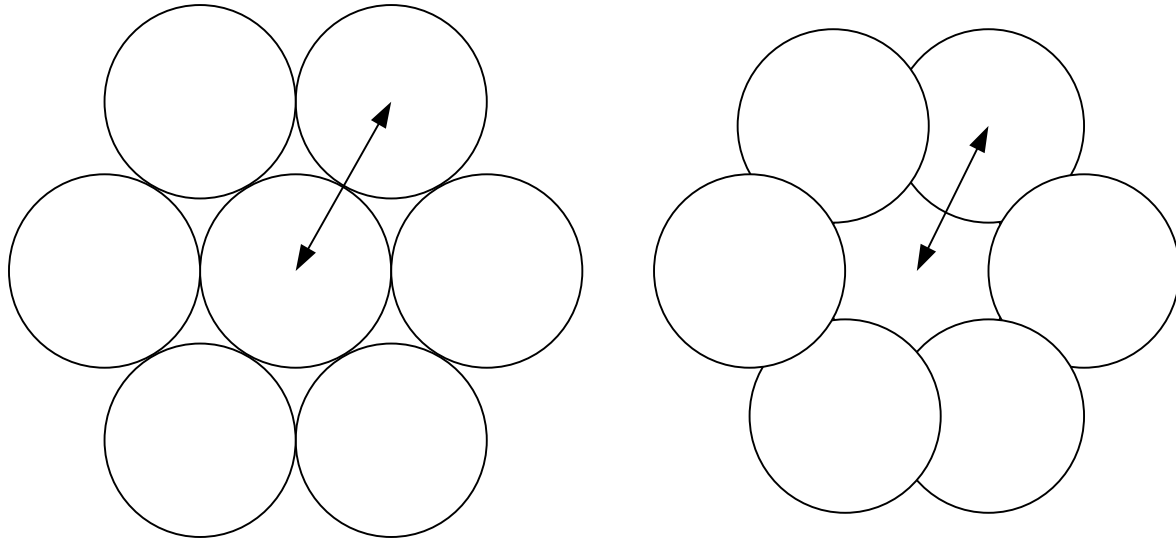


**Figure 7-1 Hexagonal Circle Packing and Reduced Center-to-Center Distances to Increase Overlap of FOVs**

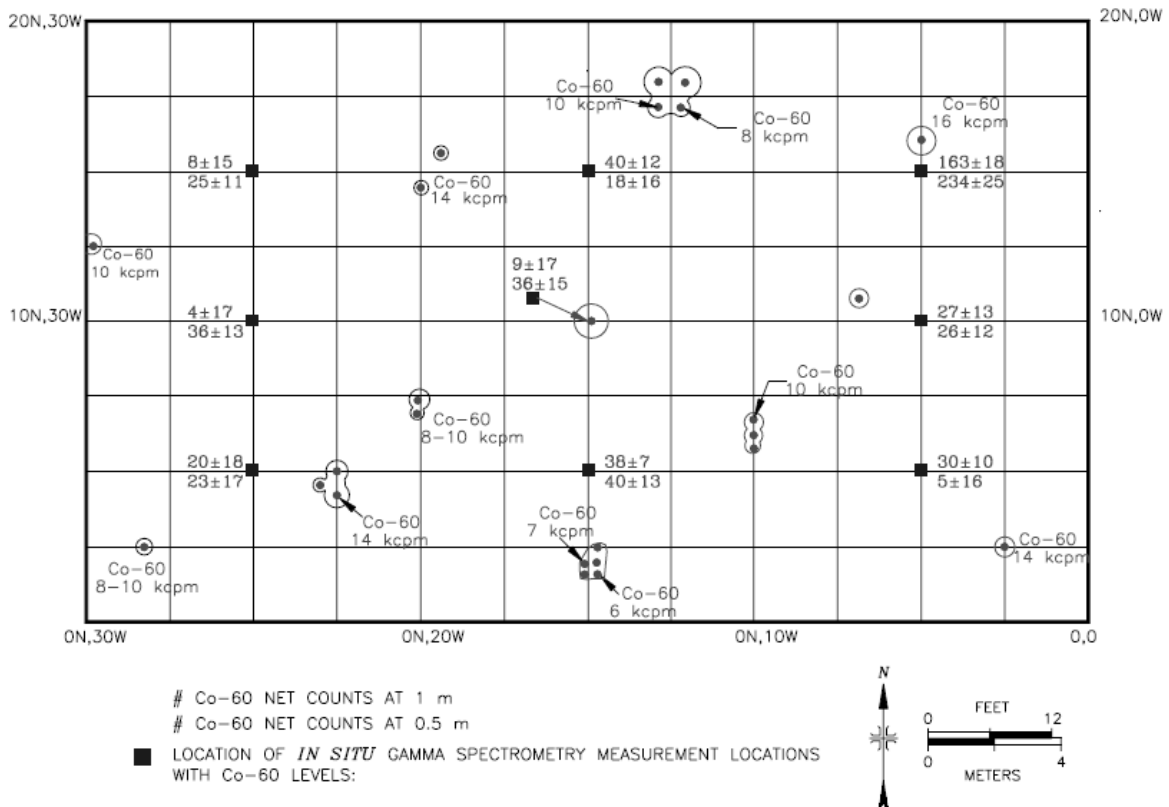


**Figure 7-2 Co-60 ISGS Results in Outdoor Test Area**

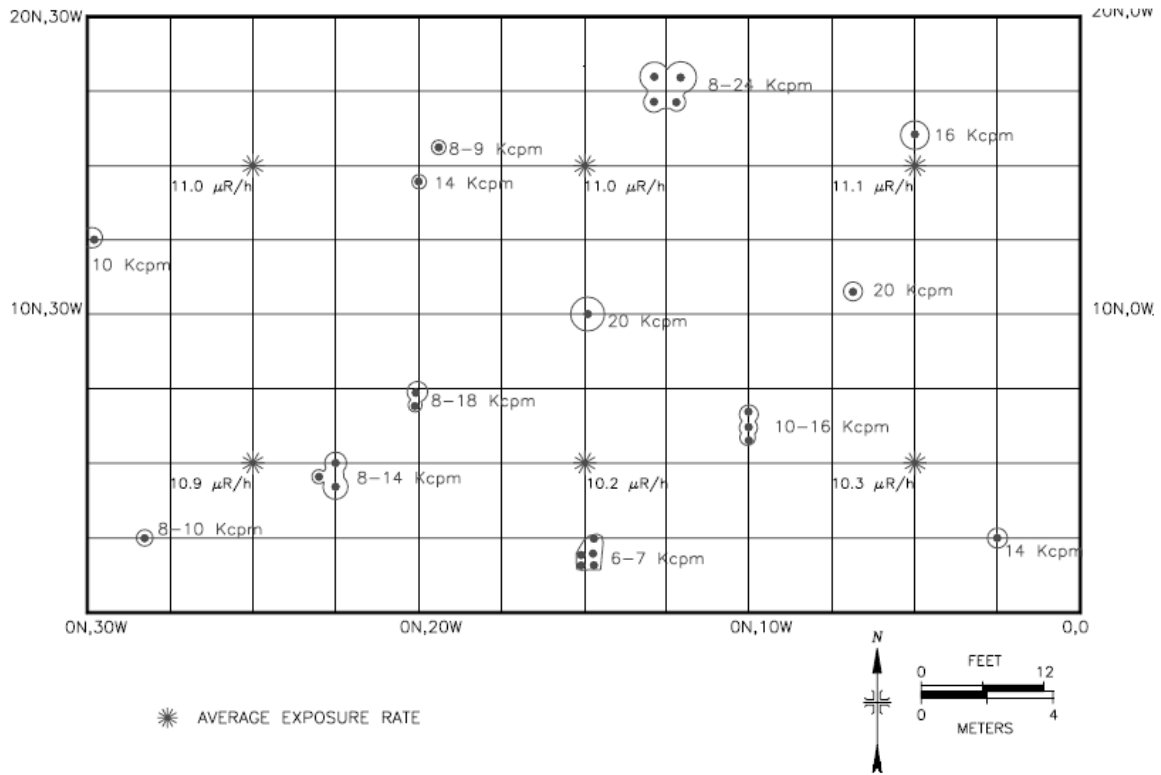


**Figure 7-3 Exposure Rate Measurements in the Outdoor Test Area**



## 8 LABORATORY INSTRUMENTATION DETECTION LIMITS

Frequently during surveys in support of decommissioning, it is not feasible, or even possible, to detect the contaminants with portable field instrumentation; thus, laboratory analysis of media samples is needed. This is especially true for media samples such as soil, which result in significant self-absorption of the radiation from the residual radioactivity. Another common situation that necessitates the use of laboratory analysis occurs when the contaminants are difficult to detect even under ideal conditions. This includes residual radioactivity that emits only low-energy beta radiation (e.g., tritium and Ni-63) or x-ray radiation (e.g., iron (Fe)-55).

Laboratory analyses for radionuclide identification, using spectrometric techniques, are often performed during scoping or characterization surveys. In these surveys, the principal objective is simply to determine the specific radionuclides present, without necessarily having to assess the quantity of contamination. Once the radioactive contaminants have been identified, sufficiently sensitive field survey instrumentation and techniques are selected to demonstrate compliance with the DCGLs.

### 8.1 Review of Analytical MDCs

In 1993, M.H. Chew and Associates prepared a database that contains a list of MDCs for various radionuclides, sample sizes, count times, instrument efficiencies, and background count rates. This information was compiled by surveying several government and commercial laboratories which provided their "best estimates" in response to the survey. The instrumentation used, instrument efficiencies, and sample geometries varied among laboratories and, for the same laboratory, varied from one radionuclide to the other. These variations are given as ranges. In short, the report constitutes a survey, not a controlled study.

The list prepared by Chew and Associates is helpful in identifying approximate MDCs to be expected for detection of specific radionuclides. However, on the basis of that information, it is not possible to predict accurately how the MDC will be affected quantitatively by changes in sample density, sample background activity, the mixture of radionuclides, or chemical composition of soil samples. These can be very significant factors in determining the MDC. For example, in some geographic locations, there may be increased concentrations of aluminum in the soil. These interfere with the nitric acid leaching procedure in radiochemical analysis for thorium or uranium; increased levels of calcium or potassium interfere with radiochemical analysis for Sr-90; and increased levels of iron interfere with several radiochemical analysis procedures. Other field conditions may affect the detectability of contaminants. The effects of these conditions were quantitatively evaluated for various types of radionuclides.

### 8.2 Background Activities for Various Soil Types

Radionuclide concentrations in background soil samples vary for many reasons, such as the soil type and density, geology, geographic location, and radioactive fallout patterns. NUREG-1501 provides an indepth study of the factors responsible for variations in the background radioactivity in soil.

During the performance of environmental assessments of background radioactivity throughout the United States, ORAU stated that background radionuclide concentrations vary both regionally (e.g., western United States, southeastern United States, coastal areas) and within a particular region. Table 8-1 gives typical U-238, Th-232, and Cs-137 concentrations found in

background soil samples in the United States. These data were compiled from historical databases on background soil concentrations and are intended to give information on the variations both among and within various regions. For many locations, the soil samples represent different soil types, such as silty loam, sandy loam, and clay. The radionuclide analyses performed on these samples used both alpha and gamma spectrometry.

The fallout radioactivity, Cs-137, was determined to have the greatest variability within a particular region compared to the terrestrial radionuclides from the uranium and thorium decay series. The large variation in fallout radioactivity may be the result of the specific soil sample locations. Wooded areas tend to exhibit higher concentrations of fallout radioactivity than open field areas, likely because of the increased foliar interception in forested areas.

### **8.3 Effects of Soil Condition on MDC**

The density and chemical composition of the soil can affect the detection sensitivity of survey instruments. Soil density and composition can also affect the MDC of laboratory instrumentation and procedures. For example, higher densities may result in an underestimation of gamma activity, particularly for low-energy gamma-emitters.

Within each category of soil, detection sensitivity of the instruments may be affected by variations in moisture content and soil density, and the presence of high-Z (atomic number) materials in the sample. One part of this study involved the evaluation of the effects of soil density and composition, moisture content, and presence of high-Z material on the gamma spectrometry analysis. It was necessary to prepare soil standards for this evaluation.

Each germanium detector was calibrated for each counting geometry using a NIST-traceable standard (typically mixed gamma-emitting activity in liquid form). Vendors that supplied the standards can demonstrate traceability to NIST.

The ORAU counting room presently prepares two standards for the 0.5-liter Marinelli soil geometry. One standard is prepared from top soil and weighs between 700 and 800 grams. This standard was used to quantify soil samples that weigh in the range of 450–850 grams. The second Marinelli standard was prepared using sand; it weighs approximately 1,000 grams. This standard was used to quantify soil samples that weigh between 850 and 1,150 grams.

For the smaller aluminum-can geometries (approximately 120-gram capacity), a comparison of the counting efficiencies obtained from both the top soil and sand standards resulted in the counting efficiencies being equal within the statistical limits. For this reason, only one counting efficiency curve was used for the aluminum-can geometry.

The soil calibration standard, consisting of Am-241, Ce-139, Cs-137, and Co-60, was prepared by weighing a known quantity of the liquid standard and adding this quantity to either the top soil or sand matrix. To ensure that the soil standard had been adequately mixed, equal aliquots (soil fractions) were placed in the aluminum-can geometry and analyzed with the germanium detector. The radionuclide concentration of each soil fraction was determined. The radionuclide concentrations of the soil fractions were evaluated to determine if they were statistically equal and, thus, to conclude that the soil standard was homogeneous. Once homogeneity was demonstrated, the standard was used to calibrate the germanium detectors for the various soil-counting geometries.

### **8.3.1 Effects of Soil Moisture on MDC**

The moisture content of the soil can vary significantly, depending on geographic location, time after rainfall, and other factors and can have a major impact on the detection of radionuclides with beta and low-energy gamma emissions. Therefore, this study examined a relatively wide range of moisture contents.

Water content can be measured accurately in the laboratory and can be changed by homogenizing known quantities of water in the soil. A calibrated counting geometry with a known weight was obtained. The initial weight was 112.9 grams. At first, 5.9-percent moisture was added to the initial weight. This amount of water was not great enough to evenly disburse throughout the soil. To evenly disburse the water, 95-percent ethyl alcohol was used. A visual check was used to determine if the soil was saturated. The soil was allowed to air dry to the desired weight of 119 grams. Among the problems discovered while working with lower moisture contents were soil loss by airflow because of the small particle size and not being able to return all of the soil to the container after the water was added. These soil loss problems were controlled by increasing the amount of water added and then allowing the soil to dry to the next desired weight. At this point, 20-percent moisture was added for a test weight of 125.6 grams. Because of the increased volume of water added, 8.7 grams of dry soil could not be returned to the container. The moisture added was sufficient to saturate the soil thoroughly. After the addition of water, the soil was allowed to absorb the moisture for approximately 1 hour. The next percent moisture was obtained by simply allowing the soil to air dry. The subsequent moisture percentage to be tested was 15 percent at a weight of 118.3 grams. The 10.5-percent moisture was obtained in the same manner as above for a test weight of 112.25 grams. At this point, it was necessary to increase the moisture content. A moisture content of 35.5 percent was obtained for a total weight of 152.70 grams. This amount was then allowed to air dry to 31-percent moisture for a total weight of 145.03 grams. At this moisture content, the soil was barely able to absorb all the water added. Finally, water was added to the point of total saturation. The maximum amount of water that could be added to the container geometry was 38.5 percent, for a final weight of 162.7 grams.

Because the addition of water to the soil standard diluted the radionuclide concentration, it was necessary to account for the dilution factor. This was done by increasing the measured concentration by a degree equal to the weight percent of the water added to the standard. This concentration corrected for dilution and was compared to the measured concentration (Table 8-2).

The results indicate that lower concentrations obtained from the increasing moisture content are largely the result of the dilution effect. That is, the radionuclide concentration in soil is lower as a result of the contaminated soil being replaced by water.

### **8.3.2 Effects of Soil Density on MDC**

As stated previously, soil density can affect the MDC of laboratory instrumentation and procedures. Higher density samples, relative to the calibration soil standard, can result in an underestimation of gamma activity, particularly for low-energy gamma-emitters.

The gamma efficiency for a particular geometry is decreased as the soil density is increased. Figure 8-1 illustrates this effect for three soil calibration geometries with densities of 1.1, 1.54, and 2.02 grams per milliliter. The greatest gamma efficiency deviation in the three samples occurs in the low-energy range.

### 8.3.3 Effects of High-Z Materials on MDC

Gamma spectrometry analyses to determine the radionuclide concentration in soil samples commonly involves the use of a calibration standard traceable to NIST. The calibration standards used for the analysis of soils should consist of a material similar in composition to that of soil (e.g., a silica-based material). Efficiencies at each gamma energy are then established for each radionuclide energy in the calibration standard. An efficiency versus energy curve is generated from each of the individual efficiency data points. This efficiency curve is then used to assess the radionuclide concentrations in media considered similar in composition to soil.

A potential deviation from the calibrated geometry described above occurs when a sample contains a measurable quantity of high-Z material, such as metals. The presence of high-Z materials produces attenuation of the gamma radiation (especially the low-energy gamma emissions) in the sample that may not be accounted for in the calibration standard. If no correction is made to account for the absorption of the gamma radiation, use of the standard efficiency curve will underestimate the true radionuclide concentration in the sample. The magnitude of these effects was evaluated by mixing in measurable quantities of metal fines and powder. Specifically, the metals studied were iron, lead, and zirconium, which were mixed in the calibration standards at 1, 5, and 10 weight percent. Table 8-3 presents the results of this experiment. Because the addition of material (i.e., high-Z material) to the soil standard dilutes radionuclide concentration, it is necessary to account for the dilution factor. This was done by increasing the measured concentration by a degree equal to the weight percent of material added to the standard. For example, the measured radionuclide concentration for the sample containing 5 percent lead was increased proportionately. The results indicate that, in general, the high-Z material effects are most pronounced at the lower gamma energies. Zirconium produces the most significant attenuation losses, followed by lead and then iron.

In summary, using a typical low-Z soil calibration standard to assay a high-Z material sample will likely result in an underestimation of the radionuclide concentration in that sample. This is because low-energy gamma radiation is attenuated more in the high-Z material sample than it is in the calibration standard. Application of the direct ratio method of gamma radiation counting may address sample attenuation concerns. The direct ratio method works by comparing the gamma photopeak energy of interest in the sample to the gamma photopeak in a suitable calibration standard, with both photopeaks corrected for the relative amount of attenuation present in the sample and calibration standard. Additional details on applying this technique appear in Abelquist et al. (1996).



**Table 8-1 Typical Radionuclide Concentrations Found in Background Soil Samples in the United States**

| Location         | Radionuclide Concentration (pCi/g) |             |                |
|------------------|------------------------------------|-------------|----------------|
|                  | U-238                              | Th-232      | Cs-137         |
| Boston, MA       | 0.7 to 1.3                         | <0.2 to 1.5 | — <sup>a</sup> |
| Cambridge, MA    | 0.4 to 1.2                         | —           | 0.1 to 0.7     |
| Cincinnati, OH   | <0.4 to 2.5                        | 0.3 to 1.5  | 0.2 to 1.5     |
| Jacksonville, FL | 0.4 to 1.0                         | 0.5 to 1.0  | <0.1 to 0.5    |
| Kingsport, TN    | <0.5 to 2.2                        | 0.8 to 1.8  | —              |
| Platteville, CO  | 0.9 to 2.1                         | 1.5 to 2.2  | <0.1 to 0.2    |
| San Diego, CA    | 1.0 to 1.6                         | 0.7 to 1.6  | <0.1 to 0.4    |

<sup>a</sup>Measurement not taken.

**Table 8-2 Effects of Moisture Content on Gamma Spectrometry Analyses**

| % Moisture <sup>a</sup> | Radionuclide Concentration (pCi/g) |                   |                    |                   |                   |                    |                   |                   |                    |                   |                   |                    |
|-------------------------|------------------------------------|-------------------|--------------------|-------------------|-------------------|--------------------|-------------------|-------------------|--------------------|-------------------|-------------------|--------------------|
|                         | Am-241                             |                   |                    | Ce-139            |                   |                    | Cs-137            |                   |                    | Co-60             |                   |                    |
|                         | Meas <sup>b</sup>                  | Corr <sup>c</sup> | %Diff <sup>d</sup> | Meas <sup>b</sup> | Corr <sup>c</sup> | %Diff <sup>d</sup> | Meas <sup>b</sup> | Corr <sup>c</sup> | %Diff <sup>d</sup> | Meas <sup>b</sup> | Corr <sup>c</sup> | %Diff <sup>d</sup> |
| Dry                     | 125.1                              | —                 | —                  | 7.7               | —                 | —                  | 117.3             | —                 | —                  | 133.4             | —                 | —                  |
| 5%                      | 108.4                              | 115.2             | 7.92               | 15.5              | 16.4              | 7.39               | 102.3             | 108.7             | 7.32               | 116.1             | 123.4             | 7.51               |
| 10%                     | 108.5                              | 121.2             | 3.09               | 14.8              | 16.6              | 6.53               | 102.1             | 114.1             | 2.75               | 114.3             | 127.7             | 4.27               |
| 15%                     | 103.2                              | 121.6             | 2.83               | 14.5              | 17.1              | 3.59               | 96.5              | 113.7             | 3.07               | 110.2             | 129.8             | 2.70               |
| 20%                     | 95.8                               | 119.8             | 4.25               | 13.2              | 16.6              | 6.71               | 89.6              | 112.0             | 4.51               | 98.8              | 123.5             | 7.42               |
| 31%                     | 83.1                               | 120.5             | 3.68               | 11.2              | 16.2              | 8.75               | 83.6              | 121.1             | -3.28              | 93.5              | 135.6             | -1.62              |
| 35%                     | 79.5                               | 123.3             | 1.46               | 10.7              | 16.6              | 6.66               | 79.4              | 123.1             | -4.93              | 90.4              | 140.1             | -5.05              |
| 38%                     | 73.5                               | 119.5             | 4.47               | 9.2               | 15.0              | 15.64              | 69.7              | 113.3             | 3.42               | 79.5              | 129.3             | 3.07               |

<sup>a</sup>Moisture content calculated by the following:

$$\text{Moisture Content} = \frac{\text{Wet Weight} - \text{Dry Weight}}{\text{Wet Weight}}$$

<sup>b</sup>Measured radionuclide concentration.

<sup>c</sup>Radionuclide concentration corrected for dilution by dividing the measured concentration by 1 minus the moisture content.

<sup>d</sup>Percent difference between the measured and calculated concentrations.

**Table 8-3 Effects of High-Z Content on Gamma Spectrometry Analyses**

| High-Z Material (%) | Radionuclide Concentration (pCi/g) |                   |                    |                   |                   |                    |                   |                   |                    |                   |                   |                    |
|---------------------|------------------------------------|-------------------|--------------------|-------------------|-------------------|--------------------|-------------------|-------------------|--------------------|-------------------|-------------------|--------------------|
|                     | Am-241                             |                   |                    | Ce-139            |                   |                    | Cs-137            |                   |                    | Co-60             |                   |                    |
|                     | Meas <sup>a</sup>                  | Corr <sup>b</sup> | %Diff <sup>c</sup> | Meas <sup>a</sup> | Corr <sup>b</sup> | %Diff <sup>c</sup> | Meas <sup>a</sup> | Corr <sup>b</sup> | %Diff <sup>c</sup> | Meas <sup>a</sup> | Corr <sup>b</sup> | %Diff <sup>c</sup> |
| <b>Lead</b>         |                                    |                   |                    |                   |                   |                    |                   |                   |                    |                   |                   |                    |
| No Z Material       | 109.8                              | —                 | —                  | 14.6              | —                 | —                  | 112.8             | —                 | —                  | 115.8             | —                 | —                  |
| 1                   | 108.2                              | 109.3             | 0.45               | 13.8              | 14.0              | 4.0                | 109.4             | 110.5             | 2.0                | 111.2             | 112.3             | 3.0                |
| 5                   | 92.9                               | 97.8              | 10.9               | 12.6              | 13.2              | 9.2                | 105.9             | 111.5             | 1.2                | 110.0             | 115.8             | 0.01               |
| 10                  | 79.7                               | 88.9              | 19.0               | 11.3              | 12.6              | 13.9               | 101.5             | 113.2             | -0.4               | 104.6             | 116.7             | -0.8               |
| <b>Iron</b>         |                                    |                   |                    |                   |                   |                    |                   |                   |                    |                   |                   |                    |
| No Z Material       | 111.3                              | —                 | —                  | 13.6              | —                 | —                  | 108.0             | —                 | —                  | 113.4             | —                 | —                  |
| 1                   | 113.1                              | 114.2             | -2.6               | 13.5              | 13.6              | -0.4               | 107.6             | 108.7             | -0.6               | 110.3             | 111.4             | 1.8                |
| 5                   | 97.0                               | 102.1             | 8.3                | 13.0              | 13.7              | -0.8               | 102.4             | 107.8             | 0.2                | 106.9             | 112.5             | 0.8                |
| 10                  | 98.4                               | 109.5             | 1.6                | 13.5              | 15.0              | -10.4              | 102.7             | 114.4             | -5.9               | 104.6             | 116.5             | -2.7               |
| <b>Zirconium</b>    |                                    |                   |                    |                   |                   |                    |                   |                   |                    |                   |                   |                    |
| No Z Material       | 121.0                              | —                 | —                  | 14.7              | —                 | —                  | 113.4             | —                 | —                  | 115.2             | —                 | —                  |
| 1                   | 98.8                               | 99.8              | 17.5               | 14.3              | 14.4              | 1.5                | 110.2             | 111.3             | 1.8                | 112.2             | 113.3             | 0.05               |
| 5                   | 80.9                               | 85.2              | 29.6               | 13.7              | 14.4              | 1.6                | 109.1             | 114.8             | -1.3               | 107.7             | 113.4             | 0.03               |
| 10                  | 62.7                               | 69.6              | 42.5               | 12.3              | 13.7              | 6.5                | 100.4             | 111.6             | 1.6                | 100.2             | 111.3             | 1.8                |

<sup>a</sup>Measured radionuclide concentration.

<sup>b</sup>Radionuclide concentration corrected for dilution by dividing the measured concentration by 1 minus the high-Z material content.

<sup>c</sup>Percent difference between the measured (no Z material) and calculated concentrations.

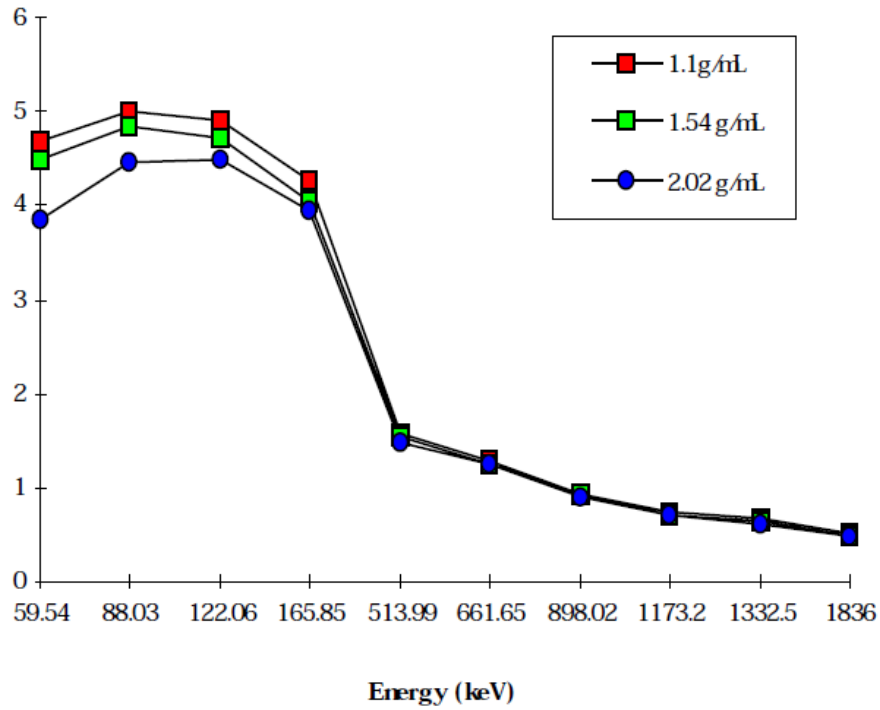


**Figure 8-1 Efficiency versus Energy for Various Densities**



## 9 REFERENCES

- Abelquist, E.W., *Decommissioning Health Physics—A Handbook for MARSSIM Users*, Second Edition, Taylor and Francis, Boca Raton, FL, 2014.
- Abelquist, E.W., R.D. Condra, and M.J. Laudeman, "Determination of Uranium and Thorium Concentrations in High Z Material Samples Using Direct Counting Method of Gamma Spectroscopy," *Radiation Protection Management* 13:42-49, 1996.
- American National Standards Institute, ANSI N42.14, "Calibration and Use of Germanium Spectrometers for the Measurement of Gamma Ray Emission Rates of Radionuclides," New York, NY, 1999.
- American National Standards Institute, ANSI N42.33, "American National Standard for Portable Radiation Detection Instrumentation for Homeland Security," New York, NY, 2007. American National Standards Institute, ANSI N13.30, "Performance Criteria for Radiobioassay," New York, NY, 2011.
- American National Standards Institute, ANSI N323AB-2013, "American National Standard for Radiation Protection Instrumentation Test and Calibration, Portable Survey Instruments," New York, NY, 2013.
- Beck, H.L., J. DeCampo, and C. Gogolak, "In situ Ge(Li) and NaI(Tl) Gamma-ray Spectrometry," Report HASL-258, U.S. Atomic Energy Commission, New York, NY, 1972.
- Benke, R.R., and K.J. Kearfott, "An Improved in Situ Method for Determining Depth Distributions of Gamma-Ray Emitting Radionuclides," *Nuclear Instruments and Methods in Physics Research*, A 463: 393–412, 2001.
- Benke, R.R., and K.J. Kearfott, "Demonstration of a Collimated in Situ Method for Determining Depth Distributions Using Gamma-Ray Spectrometry," *Nuclear Instruments and Methods in Physics Research*, A 482: 814–831, 2002.
- Brodsky, A. "Exact Calculation of Probabilities of False Positives and False Negatives for Low Background Counting," *Health Physics* 63(2):198–204, August 1992.
- Brodsky, A., and R.G. Gallagher, "Statistical Considerations in Practical Contamination Monitoring," *Radiation Protection Management* 8(4):64–78, July/August 1991.
- Chapman, J.A., A.J. Boerner, and E.W. Abelquist, "Spatially-Dependent Measurements of Surface and Near-Surface Radioactive Material Using in Situ Gamma Ray Spectrometry (ISGRS) for Final Status Surveys," ORAU, Oak Ridge, TN, November 2006.
- Chapman, J.A., B.A. Watson, A.J. Boerner, and E.W. Abelquist, "Spatially-Dependent Measurements of Surface and Near-Surface Radioactive Material Using In situ Gamma Ray Spectrometry (ISGRS) for Final Status Surveys," Oak Ridge Associated Universities, U.S. Nuclear Regulatory Commission, Presented at 52nd Annual Meeting of the Health Physics Society, Portland, Oregon, July 8-12, 2007.

- Chew and Associates, Inc., "Summary of Current Capabilities with Regards to Detection of Radioactivity: A Survey of Commercial Radiochemistry Laboratories and Instrument Suppliers (Interim Report)," Washington, DC, August 1993.
- Currie, L.A., "Limits for Qualitative Detection and Quantitative Determination," *Analytical Chemistry* 40(3):586–593, 1968.
- Dewey, S.C., Z.D. Whetstone, and K.J. Kearfott, "A Method for Determining the Analytical Form of a Radionuclide Depth Distribution using Multiple Gamma Spectrometry Measurements," *Journal of Environmental Radioactivity*, 102: 581–588, 2011.
- Egan, J.P., *Signal Detection Theory and ROC Analysis*, Academic Press, New York, NY, 1975.
- Gilmore, G., *Practical Gamma-ray Spectrometry*, Second Edition, John Wiley & Sons, Inc., New York, NY, 2008.
- Hamamatsu, *Photomultiplier Tubes, Basics and Applications*, Third Edition (Edition 3a), Hamamatsu Photonics K.K., August 2007.
- Idaho National Engineering Laboratory, "Health Physics Manual of Good Practices for Uranium Facilities," EGG-2350/UC-41, Idaho Falls, ID, June 1988.
- Institute of Electrical and Electronics Engineers, "IEEE Standard Test Procedures for Germanium Gamma-Ray Detectors," IEEE Std 325-1996, New York, New York, 1997.
- International Organization for Standardization, ISO 7503-1, "Evaluation of Surface Contamination—Part 1: Beta Emitters and Alpha Emitters," First Edition, Geneva, Switzerland, 1988.
- International Organization for Standardization, ISO 7503-3:2016, "Measurement of Radioactivity—Measurement and Valuation of Surface Contamination—Part 3: Apparatus Calibration," Geneva, Switzerland, 2016.
- International Organization for Standardization, ISO 8769, "Reference Sources—Calibration of Surface Contamination Monitors—Alpha-, Beta-, and Photon Emitters," Third Edition, Geneva, Switzerland, 2016.
- Karlberg, O., "In Situ Gamma Ray Spectrometry of the Chernobyl Fallout on Urban and Rural Surfaces," Report Studsvik/NP-89/109, Studsvik Nuclear, Nyköping, Sweden, 1990.
- Knoll, G.F., *Radiation Detection and Measurement*, 4th Edition, John Wiley & Sons, Inc., New York, NY, 2010.
- Korun, M., A. Likar, M. Lipoglavšek, R. Martincič, and B. Pucelj, B., "In Situ Measurement of Cs Distribution in the Soil," *Nuclear Instruments and Methods in Physics Research*, B 93, 485–491, 1994.
- Kuzma, J.W., and S. Bohlenblust, *Basic Statistics for Health Sciences*, Fifth Edition. McGraw Hill, New York, NY, 2004.

- Los Alamos National Laboratory, "Alpha RADIAC Evaluation Project," LA-10729, Los Alamos, NM, June 1986.
- Ludlum Measurements, Inc., *Ludlum Model 2221 Portable Scaler Ratemeter Manual*, instrument manual for Serial Number 161568 and Succeeding Serial Numbers, Sweetwater, TX, November 2013.
- Ludlum Measurements, Inc., *Ludlum Model 44-10 Gamma Scintillation Manual*, instrument manual for Serial Number PR107232 and Succeeding Serial Numbers, Sweetwater, TX, September 2014.
- National Council on Radiation Protection and Measurements, "A Handbook of Radioactivity Measurements Procedures," NCRP 58, Bethesda, MD, February 1, 1985.
- National Council on Radiation Protection and Measurements, "Calibration of Survey Instruments Used in Radiation Protection for the Assessment of Ionizing Radiation Fields and Radioactive Surface Contamination," NCRP 112, Bethesda, MD, December 31, 1991.
- Rybacek, K., P. Jacop, and R. Meckbach, "In situ Determination of Deposited Radionuclide Activities: Improved Method Using Derived Depth Distributions from the Measured Photon Spectra," *Health Physics* 62(6): 519–528, 1992.
- Shleien, B., *Handbook of Health Physics and Radiological Health*, Williams and Wilkins, Baltimore, MD, 1992.
- Shleien, B., L.A. Slaback, and B.K. Birkey, *Handbook of Health Physics and Radiological Health*, Williams and Wilkins, Baltimore, MD, 1998.
- Sowa, W., E.K. Martini, K. Gehrcke, P. Marschner, and M.J. Naziry, "Uncertainties of in Situ Gamma Spectrometry for Environmental Monitoring," *Radiation Protection Dosimetry*, 27:93–101, 1989.
- Strom, D.J., and P.S. Stansbury, "Minimum Detectable Activity When Background Is Counted Longer than the Sample," *Health Physics* 63(3):360–361, September 1992.
- Swinth, K.L., and J.L. Kenoyer, "Evaluation of Draft ANSI Standard N42. 17 by Testing," Pacific Northwest Laboratory, Richland, WA, November 1985.
- Tyler, A.N., "Monitoring Anthropogenic Radioactivity in Salt Marsh Environments through in Situ Gamma-ray Spectrometry," *Journal of Environmental Radioactivity* 45(3):235–252, 1999.
- U.S. Environmental Protection Agency, "Upgrading Environmental Radiation Data," Health Physics Society Committee Report HPSR-1, Office of Radiation Protection, Washington, DC, August 1980.
- U.S. Environmental Protection Agency, "ProUCL Version 5.0.00 Technical Guide, Statistical Software for Environmental Applications for Data Sets with and without Nondetect Observations," EPA/600/R-07/041, Washington, DC, September 2013.

- U.S. Nuclear Regulatory Commission, Title 10 of the Code of Federal Regulations (10 CFR) Part 20, "Standards for Protection against Radiation."
- U.S. Nuclear Regulatory Commission, "Applying Statistics," NUREG-1475, ML11102A076, March 2011.
- U.S. Nuclear Regulatory Commission, "Background as a Residual Radioactivity Criterion for Decommissioning" (Draft Report for Comment), NUREG-1501, ML003675949, August 1994.
- U.S. Nuclear Regulatory Commission, "Measurement Methods for Radiological Surveys in Support of New Decommissioning Criteria" (Draft Report for Comment), NUREG-1506, August 1995.
- U.S. Nuclear Regulatory Commission, "Multiagency Radiation Survey and Site Investigation Manual (MARSSIM)," NUREG-1575, Rev. 1, ML082470583, August 2000.
- U.S. Nuclear Regulatory Commission, "Radiological Assessments for Clearance of Materials from Nuclear Facilities," NUREG-1640, ML031700258, June 2003.
- U.S. Nuclear Regulatory Commission, "Consolidated Decommissioning Guidance—Decommissioning Process for Materials Licensees," NUREG-1757, Vol. 1 (Rev. 2), ML063000243, and Vol. 2 (Rev. 1), ML063000252, Office of Nuclear Material Safety and Safeguards, September 2006.
- U.S. Nuclear Regulatory Commission, "Radiological Surveys for Controlling Release of Solid Materials," NUREG-1761, ML022320121, July 2002.
- U.S. Nuclear Regulatory Commission, "Lower Limit of Detection: Definition and Elaboration of a Proposed Position for Radiological Effluent and Environmental Measurements," NUREG/CR-4007, ML16152A647, September 1984.
- U.S. Nuclear Regulatory Commission, "Statistical Methods for Nuclear Material Management," NUREG/CR-4604, ML103430339, December 1988.
- U.S. Nuclear Regulatory Commission, "Performance of Portable Radiation Survey Instruments," NUREG/CR-6062, December 1993.
- U.S. Nuclear Regulatory Commission, "Human Performance in Radiological Survey Scanning," NUREG/CR-6364, ML15141A071, March 1998.
- Van Riper, K.A., R.L. Metzger, and K.J. Kearfott, "Radionuclide Depth Distribution by Collimated Spectroscopy," Proceedings of the Topical Meeting on Radiation Serving Society, Santa Fe, NM, 2002.
- Walker, E., "Proper Selection and Application of Portable Survey Instruments for Unrestricted Release Surveys," Bechtel Environmental, Inc., Presented at 1994 International Symposium on D&D, Knoxville, TN, April 24–29, 1994.
- Walpole, R.E., and R.H. Myers, *Probability and Statistics for Engineers and Scientists*, MacMillan Publishing Company, New York, NY, 1985.



Whetstone Z.D., S.C. Dewey, and K.J. Kearfott, "Simulation of a Method for Determining One-Dimensional Cs-137 Distribution using Multiple Gamma Spectroscopic Measurements with an Adjustable Cylindrical Collimator and Center Shield," *Applied Radiation and Isotopes* 69:790–802, 2011.

Zombori P., A. Andrasi, I. Nemeth. "A New Method for the Determination of Radionuclide Distribution in the Soil by Gamma-Ray Spectroscopy," KFKI-1992-20/K, Central Research Institute for Physics, Institute for Atomic Energy Research, Budapest, Hungary, 1992.



## 10 GLOSSARY

*A Posteriori.* Relating to what can be known by observation rather than through an understanding of how certain things work.

*A Priori.* Relating to what can be known through an understanding of how certain things work rather than by observation.

*Action Level.* The numerical value that will cause the decisionmaker to choose one of the alternative actions (e.g., to remediate or not remediate). It may be a regulatory threshold standard (e.g., maximum contaminant level for drinking water), a dose- or risk-based concentration level (e.g., *derived concentration guideline level [DCGL]*), or a reference-based standard.

*Activity.* The rate of disintegration (transformation) or decay of radioactive material. The units of activity are the curie (Ci) and the becquerel (Bq).

*Alpha Particle.* A positively charged particle emitted by some radioactive materials undergoing *radioactive decay*.

*Alternative Hypothesis ( $H_a$ ).* See *hypothesis*.

*Analysis of Variance (ANOVA).* A collection of statistical models used to analyze the differences among group means and their procedures.

*Area.* A general term referring to any portion of a *site*, up to and including the entire *site*.

*Area of Elevated Activity.* An *area* over which *residual radioactivity* exceeds a specified value  $DCGL_{EMC}$ .

*Background Radiation.* Radiation from cosmic sources, naturally occurring radioactive material including radon (except as a decay product of source or special nuclear material), and global fallout as it exists in the environment from the testing of nuclear explosive devices or from past nuclear accidents such as Chernobyl that contribute to background radiation and are not under the control of the licensee.

*Beta ( $\beta$ ).* The probability of a *Type II error* (i.e., the probability of accepting the null hypothesis when it is false). The complement of *beta* ( $1 - \beta$ ) is referred to as the power of the test.

*Beta Particle.* An electron emitted from the nucleus during radioactive decay.

*Calibration.* Comparison of a measurement standard, instrument, or item with a standard or instrument of higher accuracy to detect and quantify inaccuracies and to report or eliminate those inaccuracies by adjustments.

*Cleanup.* See *decontamination*.

*Confidence Interval.* A range of values for which there is a specified probability (e.g., 80, 90, or 95 percent) that this set contains the true value of an estimated parameter.

*Contamination.* The presence of *residual radioactivity* in excess of levels that are acceptable for release of a *site* or facility for unrestricted use.

*Control Chart.* A graphic representation of a process, showing plotted values of some statistic gathered from that characteristic and one or two control limits. It has two basic uses: (1) as a judgment to determine if a process was in control and (2) as an aid in achieving and maintaining statistical control.

*Count-Rate-to-Exposure-Rate Ratio (CPMR).* The energy-dependent detector response or signal (in counts per minute) to a known gamma radiation field (in microrentgens per hour [ $\mu\text{R/h}$ ]).

*Critical Group.* The group of individuals reasonably expected to receive the greatest exposure to residual radioactivity for any applicable set of circumstances.

*Critical Level ( $L_c$ ).* A fixed value of the *test statistic* corresponding to a given probability level, as determined from the sampling distribution of the *test statistic*.  $L_c$  is the level at which there is a statistical probability (with a predetermined confidence) of correctly identifying a background value as “greater than background.”

*Data Quality Objectives (DQOs).* Qualitative and quantitative statements derived from the DQO process that clarify study technical and quality objectives, define the appropriate type of data, and specify tolerable levels of potential decision errors that will be used as the basis for establishing the quality and quantity of data needed to support decisions.

*Data Quality Objective (DQO) Process.* A systematic strategic planning tool based on the scientific method that identifies and defines the type, quality, and quantity of data needed to satisfy a specified use. The key elements of the process include the following:

- concisely defining the problem
- identifying the decision to be made
- identifying the inputs to that decision
- defining the boundaries of the study
- developing the decision rule
- specifying tolerable limits on potential decision errors
- selecting the most resource-efficient data collection design

DQOs are the qualitative and quantitative outputs from the DQO process. The U.S. Environmental Protection Agency originally developed the DQO process, but other organizations have adapted it to meet their specific planning requirements.

*Decay.* See *radioactive decay*.

*Decision Rule.* A statement that describes a logical basis for choosing among alternative actions.

*Decommission.* To remove a facility or site safely from service and reduce residual radioactivity to a level that permits (1) release of the property for unrestricted use and termination of the license or (2) release of the property under restricted conditions and termination of the license.

*Decommissioning.* The process of removing a facility or *site* from operation, followed by *decontamination*, and license termination (or termination of authorization for operation) if appropriate. The objective of *decommissioning* is to reduce the *residual radioactivity* in structures, materials, soils, ground water, and other media at the *site* so that the concentration of each radionuclide contaminant that contributes to *residual radioactivity* is indistinguishable from the *background radiation* concentration for that radionuclide.

*Decommissioning Plan.* A detailed description of the activities that the licensee intends to use to assess the radiological status of its facility, to remove radioactivity attributable to licensed operations at its facility to levels that permit release of the site in accordance with the U.S. Nuclear Regulatory Commission's (NRC's) regulations and termination of the license, and to demonstrate that the facility meets the NRC's requirements for release. A decommissioning plan typically consists of several interrelated components, including (1) site characterization information, (2) a remediation plan that has several components, including a description of remediation tasks, a health and safety plan, and a quality assurance plan, (3) site-specific cost estimates for the decommissioning, and (4) a final status survey plan.

*Decontamination.* The removal of undesired residual radioactivity from facilities, soils, or equipment before the release of a site or facility and termination of a license. Also known as remediation, remedial action, and cleanup.

*Derived Concentration Guideline Level (DCGL).* A derived, radionuclide-specific activity concentration within a survey unit corresponding to the release criterion. The DCGL is based on the spatial distribution of the contaminant and thus is derived differently for the nonparametric statistical test (DCGL<sub>W</sub>) and the *Elevated Measurement Comparison* (DCGL<sub>EMC</sub>). DCGLs are derived from activity/dose relationships through various exposure pathway scenarios.

*Detection Limit.* The net response level that can be expected to be seen with a detector with a fixed level of certainty.

*Detection Sensitivity.* The minimum level of ability to identify the presence of radiation or radioactivity.

*Direct Measurement.* Radioactivity measurement obtained by placing the detector near the surface or media being surveyed. An indication of the resulting radioactivity level is read out directly.

*Disintegration per Minute (dpm).* Measurement of ionizing radiation, which is sometimes expressed as a rate of counts per unit of time, as registered by a monitoring instrument.

*Dose (or Radiation Dose).* A generic term that means absorbed dose, dose equivalent, effective dose equivalent, committed dose equivalent, committed effective dose equivalent, or total effective dose equivalent.

*Effective Probe Area.* The *physical probe area* corrected for the amount of the probe area covered by a protective screen.

*Elevated Measurement Comparison (EMC).* This comparison is used in conjunction with the Wilcoxon test to determine if any measurements exceed a specified value of DCGL<sub>EMC</sub>.

*Empirical.* Based on testing or experience.

*Exposure-Rate-to-Concentration Ratio (ERC).* The exposure rate in  $\mu\text{R/h}$  at some distance from a defined gamma radiation source.

*False Negative Decision Error.* The error that occurs when the null hypothesis ( $H_0$ ) is not rejected when it is false. For example, the false negative decision error occurs when the decisionmaker concludes that the waste is hazardous when it truly is not hazardous. A statistician usually refers to a false negative error as a *Type II decision error*. The measure of the size of this error is called *beta* and is also known as the complement of the power of a hypothesis test.

*False Positive Decision Error.* A false positive decision error occurs when the null hypothesis ( $H_0$ ) is rejected when it is true. For example, the decisionmaker presumes that a certain waste is hazardous (i.e., the null hypothesis or baseline condition is “the waste is hazardous”). If the decisionmaker concludes that there is insufficient evidence to classify the waste as hazardous when it truly is hazardous, this is a false positive decision error. A statistician usually refers to the false positive error as a *Type I decision error*. The measure of the size of this error is called alpha, the level of significance, or the size of the critical region.

*Fluence Rate.* A fundamental parameter for assessing the level of radiation at a measurement site. In the case of in situ spectrometric measurements, a calibrated detector provides a measure of the *fluence rate* of primary photons at specific energies that are characteristic of a particular radionuclide.

*Gamma Radiation.* Penetrating high-energy, short-wavelength electromagnetic radiation (similar to x-rays) emitted during *radioactive decay*. Gamma rays are very penetrating and require dense materials (such as lead or steel) for shielding.

*Half-Life.* The time required for one-half of the atoms of a particular radionuclide present to disintegrate.

*Hotspot.* See *area of elevated activity*.

*Hypothesis.* An assumption about a property or characteristic of a set of data under study. The goal of statistical inference is to decide which of two complementary hypotheses is likely to be true. The *null hypothesis* ( $H_0$ ) describes what is assumed to be the true state of nature, and the *alternative hypothesis* ( $H_a$ ) describes the opposite situation.

*Index of Sensitivity ( $d'$ ).* Represents the distance between the means of the background detector response and background plus signal, in units of their common standard deviation. The index can be calculated for various decision errors (Type I error [ $\alpha$ ] and Type II error [ $\beta$ ]).

*Indistinguishable from Background.* Refers to the detectable concentration distribution of a radionuclide that is not statistically different from the background concentration distribution of that radionuclide in the vicinity of the site or, in the case of structures, in similar materials using adequate measurement technology, survey, and statistical techniques.

*Instrument Efficiency ( $\epsilon_i$ ).* The ratio between the net count rate of the instrument and the surface emission rate of a source for a specified geometry.

*Investigation Level.* A derived media-specific, radionuclide-specific concentration of activity that (1) is based on the release criterion and (2) triggers a response, such as further investigation or cleanup, if exceeded.

*Isopleth.* A line drawn through points on a graph or plot at which a given quantity has the same numerical value or occurs with the same frequency.

*Licensee.* A person who possesses a license, or a person who possesses licensable material, whom the NRC could require to obtain a license.

*Measurement.* For the purpose of *MARSSIM*, used interchangeably to mean (1) the act of using a detector to determine the level or quantity of radioactivity on a surface or in a sample of material removed from a media being evaluated or (2) the quantity obtained by the act of measuring.

*millirem per year (mrem/yr).* One one-thousandth (0.001) of a *rem* per year.

*Minimum Detectable Concentration (MDC).* The *a priori* activity level that a specific instrument and technique can be expected to detect 95 percent of the time. In statements of the detection capability of an instrument, this value should be used. The *MDC* is the detection limit,  $L_D$ , multiplied by an appropriate conversion factor to give units of activity.

*Minimum Detectable Count Rate (MDCR).* The net minimum detectable count rate that an ideal observer is expected to distinguish from the background detector response.

*Monitoring.* Monitoring (radiation monitoring, radiation protection monitoring) is the measurement of radiation levels, concentrations, surface area concentrations, or quantities of radioactive material and the use of the results of these measurements to evaluate potential exposures and doses.

*Multi-Agency Radiation Site Survey and Investigation Manual (MARSSIM) (NUREG-1575).* Multi-agency consensus manual that provides information on planning, conducting, evaluating, and documenting building surface and surface soil final status radiological surveys for demonstrating compliance with dose- or risk-based regulations or standards.

*Normal (Gaussian) Distribution.* A family of bell-shaped distributions described by the mean and variance.

*Null Hypothesis ( $H_0$ ).* See *hypothesis*.

*Observation Interval ( $i$ ).* The time that the detector can respond to the contamination source; dependent on the scan speed, detector orientation, and geometry of the source.

*Outlier.* Measurement that is unusually large or small relative to other measurements and therefore is suspected of misrepresenting the population from which it was collected.

*Physical Probe Area.* The physical surface area assessed by a detector. The physical probe area is used to make probe area corrections in the activity calculations.

*Radiation Survey (or Radiological Survey).* Measurements of radiation levels and radioactivity associated with a *site*, along with appropriate documentation and data evaluation.

**Radioactive Decay.** The spontaneous transformation of an unstable atom into one or more different nuclides accompanied by either the emission of energy and/or particles from the nucleus, nuclear capture or ejection of orbital electrons, or fission. Unstable atoms decay into a more stable state, eventually reaching a form that does not decay further or has a very long *half-life*.

**Radioactivity.** The mean number of nuclear transformations occurring in a given quantity of radioactive material per unit time. The International System unit of radioactivity is the becquerel (Bq). The customary unit is the curie (Ci).

**Radionuclide.** An unstable nuclide that undergoes *radioactive decay*.

**Reference Area.** Geographic area from which representative reference measurements are taken for comparison with measurements made in specific *survey units* at remediation sites. A site radiological *reference area* (background area) is an area that has physical, chemical, radiological, and biological characteristics similar to those of the site area being remediated but has not been contaminated by site activities. The distribution and concentration of *background radiation* in the *reference area* should be the same as that expected on the *site* if that *site* had never been contaminated. More than one *reference area* may be necessary for valid comparisons if a *site* exhibits considerable physical, chemical, radiological, or biological variability.

**Release Criterion.** A regulatory limit expressed in terms of dose or risk.

**rem.** The special unit of any of the quantities expressed as dose equivalent. The dose equivalent in rem is equal to the absorbed dose in rad multiplied by the quality factor (1 rem = 0.01 sievert).

**Remediation.** See *decontamination*.

**Removable Activity.** Surface activity that is readily removable by wiping the surface with moderate pressure and that can be assessed with standard radiation detectors. It is usually expressed in units of disintegrations per minute per 100 centimeters squared (dpm/100 cm<sup>2</sup>).

**Residual Radioactivity.** Radioactivity in structures, materials, soils, ground water, and other media at a site resulting from activities under the licensee's control. This includes radioactivity from all licensed and unlicensed sources used by the licensee but excludes background radiation. It also includes radioactive materials remaining at the site as a result of routine or accidental releases of radioactive material at the site and previous burials at the site.

**Scanning.** An evaluation technique performed by moving a detection device over a surface at a specified speed and distance above the surface to detect radiation.

**Site.** Any installation, facility, or discrete, physically separate parcel of land, or any building or structure or portion thereof that is being considered for survey and investigation.

**Smear.** A radiation survey technique used to determine levels of removable surface contamination. A medium (typically filter paper) is rubbed over a surface (typically an area of 100 cm<sup>2</sup>), followed by a quantification of the activity on the medium. Also known as a swipe.

**Source Term.** A conceptual representation of the residual radioactivity at a site or facility.



*Surface Contamination.* Residual radioactivity found on building or equipment surfaces and expressed in units of activity per surface area (Bq/m<sup>2</sup> or dpm/100 cm<sup>2</sup>).

*Surface Efficiency ( $\epsilon_s$ ).* The ratio between the number of radiation particles emerging from a surface and the total number of particles released within the source.

*Survey.* An evaluation of the radiological conditions and potential hazards incident to the production, use, transfer, release, disposal, or presence of radioactive material or other sources of radiation. When appropriate, such an evaluation includes a physical survey of the location of radioactive material and measurements or calculations of levels of radiation, or concentrations or quantities of radioactive material present.

*Survey Unit.* A geographic *area* consisting of structures or land areas of specified size and shape at a *site* for which a separate decision will be made as to whether the unit attains the site-specific reference-based cleanup standard for the designated pollution parameter. Survey units are generally formed by grouping contiguous site areas with similar use histories and having the same contamination potential (classification). Survey units are established to facilitate the survey process and the statistical analysis of survey data.

*Surveyor Efficiency ( $p$ ).* The probability that a surveyor will identify an audible detector response above the scan MDC.

*Type I Error.* A decision error that occurs when the *null hypothesis* is rejected when it is true. The probability of making a *Type I decision error* is called *alpha* ( $\alpha$ ).

*Type II Error.* A decision error that occurs when the *null hypothesis* is accepted when it is false. The probability of making a *Type II decision error* is called *beta* ( $\beta$ ).

*z-score.* The number of standard deviations an observation of datum is above the mean.



# APPENDIX A

## CASE STUDY—DETECTOR CALIBRATIONS FOR MIXED SOURCE/COMPLEX DECAY SERIES CONTAMINATION FIELDS, METHODS, AND EXAMPLES

### A.1 Introduction

When establishing data and measurement quality objectives (DQOs and MQOs) for the assessment of residual surface contamination during both scanning and direct measurement surveys, many sites will need to address radiological mixtures or individual radionuclides with complex decay series in order to achieve the regulatory goals for decommissioning. Examples of mixed sources and complex decay series include mixed fission and activation products from reactor operations and the thorium and uranium series. A critical consideration of the DQOs and associated MQOs is the assurance that the radiation detectors selected and the calibration procedures accurately represent the mixture of the radionuclides of concern (ROCs) and produce defensible data for the intended end use. In many cases, these data form the basis of the decision process and respective contamination thresholds for the release of materials, equipment, personal property, and/or site property from radiological controls or license termination. To ensure that the scanning and measurement sensitivities meet detection requirements and that the calculated surface activity levels accurately represent residual surface contamination, detector efficiencies must represent the site-specific radiological mixtures. For example, consider the complexity of establishing instrument performance specifications at a conventional uranium recovery facility where the radionuclides of concern may include those associated with raw ore, fresh or aged yellowcake, and tailings. Each scenario involves a different mix of the uranium and progeny affecting the determination of efficiency and detection capability.

This appendix explains various considerations for radiation detection efficiency determinations that are ultimately used to calculate the minimum detectable concentration (MDC) and the surface activity levels that are then compared with the project MQO requirements and investigation or action (I/A) levels. The applicable MQOs and I/A levels may be in terms of nonspecific gross activity or may be for a specific radionuclide within a mixture as in the case of a surrogate or the parent radionuclide of a decay chain. Therefore, the efficiency examples in this appendix account for how the measurement is expressed relative to either the gross activity of the mixture or for an individual radionuclide of the mixture (e.g., total uranium activity in the presence of the various decay progeny).

One of the initial MQOs to examine is the MDC component. The objective in this examination is to select instrumentation such that the MDC for static measurements is a fraction of the I/A level. The surface activity MDC is calculated by converting the instrument's background response in counts per minute (cpm) to surface disintegrations per minute per 100 square centimeters (dpm/100 cm<sup>2</sup>). The conversion is completed using a total efficiency ( $\epsilon_t$ ) that is the product of the instrument efficiency ( $\epsilon_i$ ) and surface efficiency ( $\epsilon_s$ ). This same efficiency is also used to convert a measurement result to surface activity, also in units of dpm/100 cm<sup>2</sup>, to quantify residual contamination levels.

Expanding Equation 3.11 from the main text of this NUREG, assuming equal background and gross count times, the generic static measurement MDC equation is as follows:

$$\text{Static MDC} = \frac{3 + 4.65\sqrt{R_B \times T}}{KT} = \frac{3 + 4.65\sqrt{R_B \times T}}{T \varepsilon_t G} = \frac{3 + 4.65\sqrt{R_B \times T}}{T \varepsilon_i \varepsilon_s G} \quad (\text{Eq. A.1})$$

where:

$R_B$  = background count rate (cpm)

$K$  = proportionality constant that includes the detection efficiency and probe geometry (unitless)

$T$  = measurement count time (typically minutes) – assumes the same length of time is used for background and sample counts

$\varepsilon_t$  = the total detector efficiency (unitless)

$\varepsilon_i$  = the instrument efficiency (unitless)

$\varepsilon_s$  = the surface/source efficiency (unitless)

$G$  = the geometry correction factor for the detector window ( $\text{cm}^2$ ) for becquerels per  $\text{cm}^2$  or as a ratio to  $100 \text{ cm}^2$  for dpm/ $100 \text{ cm}^2$  (unitless)

Similarly, the detector and source efficiency will also have an impact on the scan MDC determination and surface activity calculation, as seen in Equations A.2 and A.3:

$$\text{Scan MDC} = \frac{d' \sqrt{b_i} (60/i)}{\sqrt{p} \varepsilon_i \varepsilon_s G} \quad (\text{Eq. A.2})$$

where:

$d'$  = the index of sensitivity (unitless)

$b_i$  = background counts in the observation interval (counts)

$i$  = observation interval (seconds)

$p$  = surveyor efficiency (unitless)

$$\text{Surface Activity (A)} = \frac{N}{\varepsilon_i \varepsilon_s T G} \quad (\text{Eq. A.3})$$

where:

$N$  = net counts (counts)

$\varepsilon_i$  = the instrument efficiency (unitless)

$\varepsilon_s$  = the surface/source efficiency (unitless)

$T$  = count time (minutes)

$G$  = geometry =  $\frac{\text{Physical Detector Area cm}^2}{100}$

Whether calculating the static MDC (Equation A.1), scan MDC (Equation A.2), or surface activity (Equation A.3), the total efficiency must be estimated to correctly convert raw detector responses in cpm to surface radioactivity units for direct comparison to the applicable I/A level(s). Consider an example where the action level corresponds to a regulatory unrestricted release limit. Detector efficiencies that do not represent the ROCs and over- or under-estimate the detector response will result in a respective increase in the false negative or false positive decision rates. When efficiency is overestimated, the calculated MDC is artificially lowered,

which may lead to the use of a detector that does not satisfy measurement system MQOs for detection capability, and the calculated residual surface activity levels will be underestimated. Conversely, underestimating efficiency, although conservative, may lead to higher false positive occurrences because of inflated surface activity results.

The total efficiency calculation can be simple or complex depending on the number of contaminants, the complexity of the associated decay schemes, and the availability of representative calibration sources. For the simplest cases, where there is a single ROC and a calibration source that is either the same as, or radiologically similar to the ROC, International Organization for Standardization (ISO) 7503-1, "Evaluation of Surface Contamination—Part 1: Beta Emitters and Alpha Emitters," issued in 1988, defines the total efficiency as simply the product of the instrument and surface efficiencies (introduced in Equation A.1) as follows:

$$\epsilon_t = (\epsilon_i)(\epsilon_s) \quad (\text{Eq. A.4})$$

where:

$\epsilon_i$  = the ratio (as a percentage) between the instrument net reading and the  $2\pi$  surface emission rate of a source under given geometrical conditions and the instrument efficiency will be dependent on the energy of the radiations emitted. (Note that the calibration source certificate  $2\pi$  surface emission rate is used in calculating  $\epsilon_i$  rather than the  $4\pi$  total deposited activity.)

and

$\epsilon_s$  = the ratio (as a percentage) between the number of particles of a given type above a given energy emerging from the front face of a source or its window per unit time (surface emission rate) and the number of particles of the same type created or released within the source per unit time.

The separation of the total efficiency into the instrument and surface efficiency components permits the independent assessment of both the energy-dependent intrinsic detector efficiency and the effects of the measurement surface characteristics and overlying, inactive materials (e.g., grease, dirt, moisture) on surface activity measurements. ISO 7503-1:1988 provides default  $\epsilon_s$  values that may be applied when justifiable; otherwise, experimental determination of  $\epsilon_s$  may be required when default conditions are not satisfied. The ISO 7503-1:1988 conditional defaults for  $\epsilon_s$  in the absence of a more precisely known value follow:

- $\epsilon_s = 0.25$  for alpha radiations. Use of this default value assumes that the saturation layer thickness of the contamination itself is less than 5 milligrams per square centimeter ( $\text{mg}/\text{cm}^2$ ) and that surface coverings of any inactive materials are no greater than 50 percent of the saturation thickness.
- $\epsilon_s = 0.25$  for beta maximum radiations greater than 0.15 megaelectron volts (MeV) and less than 0.4 MeV. Use of this default value assumes an inactive material density thickness of no greater than  $2.5 \text{ mg}/\text{cm}^2$ .
- $\epsilon_s = 0.5$  for beta maximum emissions greater than 0.4 MeV. Use of this default value also assumes an inactive material density thickness of no greater than  $2.5 \text{ mg}/\text{cm}^2$ .

The  $\epsilon_i$  component is empirically determined using appropriate National Institute of Standards and Technology (NIST)-traceable calibration sources that represent the ROCs. To determine

applicable calibration sources the following should be considered: establish the types of measurements to be performed, select the associated detectors, and establish the applicable  $\epsilon_s$ ; the radiation emission type, energy, and abundance are characterized for each ROC that will be assessed during scanning or measurement.

Depending on whether a single source or multisource calibration will be performed, different approaches are presented in national and international guidance with respect to calibrations and the determination of instrument efficiencies. For example, ANSI N323AB-2013 (American National Standard for Radiation Protection Instrumentation Test and Calibration, Portable Survey Instruments) indicates that “calibration should include adjustment and/or determination of readings of at least three points selected over the energy range appropriate to the needs of the user application,” and that “single point calibrations are only valid for application to field measurement energies that are greater than the calibration energy.” Guidance in ISO 7503-1:1988 indicates that “in plants and laboratories where different radionuclides with different beta energies are used, it is practical to use only the instrument efficiency for a single beta energy,” and that “it shall, however, be ensured that the beta energy of this reference source is not significantly greater than that of the lowest beta energy to be measured.” Guidance in the ISO 7503-3:2016 notes that “the method of direct calibration of an instrument with respect to a specific radionuclide using a single calibration source made from the same radionuclide can be applied to all radionuclides for which calibration sources are available,” and also notes that “in case of radionuclides with complex emission characteristics or of radionuclides for which no calibration sources are available, a multisource calibration procedure can be applied.” In the case of multisource calibrations, ISO 7503-3:2016 further notes that “the instrument efficiency is measured versus radiation energy using sources emitting mono-energetic radiation,” and that “instrument efficiency values for the radionuclides under consideration are then calculated individually, using the energy and emission probability data relating to the mono-energetic components of the radiation.” The concept of “energy regions” is also presented in ISO 7503-3:2016, where instrument efficiencies are determined by comparison to various calibration sources, where each source is applicable to a specific energy range.

Three examples are provided below to demonstrate progressively more complex single source calibration situations, and to highlight limitations on performing single source calibrations. These examples include scenarios where:

- A single ROC is present, and a single calibration source is used (which is the same radionuclide as the ROC) – See Table A-1,
- Multiple ROCs are present, a single calibration source is used (which is a different radionuclide from all of the ROCs), and the calibration source represents an appropriate energy range for all ROCs – See Table A-2, and
- Multiple ROCs are present, a single alpha calibration source and a single beta calibration source are used (which are both different radionuclides from the ROCs), and one of the calibration sources (beta) is not deemed appropriate for all beta energies from the ROCs – See Table A-3.

For the first example, consider a decommissioning site where technetium (Tc)-99 is the ROC, and a Tc-99 calibration source is available. The ROC characterization in this example is further simplified as Tc-99 has only a single beta-emission decay scheme, unlike other beta-emitting ROCs examined in later examples. Table A-1 provides the information for determining  $\epsilon_t$  using a beta scintillator detector.

**Table A-1 ROC, Calibration Source, Detector Specifications, and Efficiency Calculations**

| ROC Characteristics   |  |
|---|--|
| ROC   | Tc-99  |
| Emission  | beta   |
| Maximum beta energy   | 0.294 MeV  |
| Calibration Source Specifications   |  |
| Calibration source  | Tc-99  |
| Maximum beta energy   | 0.294 MeV  |
| Calibration source area   | 150 cm <sup>2</sup>  |
| Source certificate surface emission rate                                    | 18,500 cpm/150 cm <sup>2</sup>   |
| Detector Specifications   |  |
| Detector type   | Beta Scintillator  |
| Detector geometry   | 100 cm <sup>2</sup>  |
| Detector background   | 400 cpm  |
| Total Efficiency and Static MDC Calculation                                 |  |
| Surface emission rate subtended by the detector                             | $\frac{18,500 \text{ cpm}}{150 \text{ cm}^2} \times 100 \text{ cm}^2 = 12,333 \text{ cpm}$   |
| Detector calibration source net response                                    | 5,703 cpm – 400 cpm = 5,303 cpm  |
| $\epsilon_i$  | $\frac{5,303 \text{ cpm}}{12,333 \text{ cpm}} = 0.43$  |
| $\epsilon_s$  | 0.25   |
| $\epsilon_t$  | 0.43 × 0.25 = 0.11   |
| $MDC = \frac{3+4.65 \times \sqrt{R_B \times T}}{T \epsilon_i \epsilon_s G}$ | $\frac{3+4.65 \times \sqrt{400 \text{ cpm} \times 1 \text{ min}}}{1 \text{ min} \times 0.43 \times 0.25 \times \frac{100 \text{ cm}^2}{100}} = 890 \text{ dpm}/100 \text{ cm}^2$ |

Further ROC characterization is required to address more complex situations in which the ROC efficiency is based on a surrogate calibration source (i.e., the source is a different radionuclide from the ROC) or there are mixtures of ROCs. The characterization provides information for the input parameters to establish the  $\epsilon_i$  for calculating scanning and measurement MDCs and surface activity levels. The full characterization of the applicable ROCs in accordance with the following discussion is necessary to ensure that the selected calibration source conservatively represents the ROC(s). The characterization parameters<sup>1</sup> and the terminology (in parentheses) include the following.

- radiation emission (emission)—the radiation type emitted by a given radionuclide decay (e.g., alpha or beta radiation).
- emission energy (energy/E)—the average ( $E_{AVE}$ ) or maximum ( $E_{MAX}$ ) energy (in MeV) of the emission; as beta emission follows an energy spectrum range, characterization of a given beta decay mode in the general literature will be in terms of an average energy

<sup>1</sup>Data source: <http://www.nndc.bnl.gov/nudat2/>

and a maximum end-point energy. The determination of an appropriate beta  $E_{AVE}/E_{MAX}$  for a specific beta-emitting ROC may require a calculation of a weighted  $E_{AVE}/E_{MAX}$  that will account for the percent of decays (emission intensity as defined below) for a given energy spectrum. Weighted emission energy is defined below and is discussed later in this Appendix. Note: It is acceptable to exclude rare decay modes, defined as less than 0.1 percent of decays, from consideration in the weighted energy calculation.

- emission intensity (I)—percent of decays that result in a given radiation type of emission at a specific energy. Intensity terms may be multiplied by branching ratios, as the examples will illustrate, to account for both the emission type (e.g., alpha or beta emission) and the energies of the respective emission.
- weighted emission energy—for ROCs with variable emission energy per decay, the weighted emission energy is calculated based on the I of the emissions as follows:

$$\sum E_{i...n} \times I_{i...n}.$$

- branching ratio (BR)—the radiation emission decay scheme ratio, as a percentage, for a radionuclide.
- relative fractions (RFs)—either the fractional percentage that a specific radionuclide contributes to the total activity of the mixture or the ratio of other ROC activity relative to the activity of the primary radionuclide such as a surrogate or decay chain parent.

The application of these ROC characterization concepts is demonstrated in Table A-2, which illustrates a gross activity RF for newly processed natural uranium (yellowcake) as the example mixture. This example assumes the output of the measurement DQO is for the quantification of the total uranium alpha activity for comparison with a contamination limit of 5,000 dpm  $\alpha/100 \text{ cm}^2$ . The example also assumes that surrogate calibration sources are used for establishing  $\epsilon_i$ . The Table A-2 parameters assume that only alpha measurements are made.

**Table A-2 ROC, Calibration Source, Detector Specifications, and Efficiency Calculations for Newly Processed Natural Uranium**

| ROC Characteristics               |                     |       |                     |
|-----------------------------------|---------------------|-------|---------------------|
| ROC                               | U-238               | U-235 | U-234               |
| Emission                          | alpha               | alpha | alpha               |
| E (MeV)                           | 4.188               | 4.431 | 4.759               |
| I                                 | 1.00                | 1.00  | 1.00                |
| BR                                | NA                  | NA    | NA                  |
| RF                                | 0.50                | 0.03  | 0.47                |
| Calibration Source Specifications |                     |       |                     |
| Calibration sources               | Th-230 <sup>a</sup> |       | Pu-239              |
| Emission                          | alpha               |       | alpha               |
| E (MeV)                           | 4.663               |       | 5.739               |
| Calibration source area           | 150 cm <sup>2</sup> |       | 150 cm <sup>2</sup> |



|   |   |                                |                    |
|---|---|--------------------------------|--------------------|
| Calibration source certificate surface emission rate                | 38,100 cpm/150 cm <sup>2</sup>  | 53,600 cpm/150 cm <sup>2</sup> |                    |
| Detector Specifications   |   |                                |                    |
| Detector type   | Alpha Scintillator  |                                |                    |
| Detector geometry   | 100 cm <sup>2</sup>   |                                |                    |
| Detector background   | 2 cpm   |                                |                    |
| Total Efficiency and Static MDC Calculation <sup>a</sup>            |   |                                |                    |
| Calibration source surface emission rate subtended by the detector  | $\frac{38,100 \text{ cpm}}{150 \text{ cm}^2} \times 100 \text{ cm}^2 = 25,400 \text{ cpm}$  |                                |                    |
| Detector calibration source net response                            | 10,414 cpm – 2 cpm = 10,412 cpm   |                                |                    |
| $\epsilon_i$  | $\frac{10,412 \text{ cpm}}{25,400 \text{ cpm}} = 0.41$  |                                |                    |
| $\epsilon_s$  | 0.25  |                                |                    |
| Weighted $\epsilon_t$<br>$\sum(\epsilon_i)(\epsilon_s)(RF)$         | U-238   | U-235                          | U-234              |
|   | (0.41)(0.25)(0.49)  | (0.41)(0.25)(0.02)             | (0.41)(0.25)(0.49) |
|   | 0.050 + 0.002 + 0.050   |                                |                    |
|   | = 0.10 <sup>b</sup>   |                                |                    |
| $MDC = \frac{3+4.65\sqrt{R_B \times T}}{T \epsilon_i \epsilon_s G}$ | $\frac{3+4.65\sqrt{2 \text{ cpm} \times 1 \text{ min}}}{1 \text{ min} \times 0.10 \times \frac{100 \text{ cm}^2}{100}} = 93 \text{ dpm}/100 \text{ cm}^2$ |                                |                    |

<sup>a</sup> Th-230 is selected as the calibration source to represent each ROC based on similar alpha emission E.

<sup>b</sup> In this example, because the DQO output is for assessment of total uranium activity, each isotope emits alpha radiation, and the alpha energies are similar. This makes it possible to use the same calibration source to represent each uranium isotope. The efficiency determination can be simplified where the RF term for the total mixture is set to 1.00 and an identical efficiency determined as follows: (0.41)(0.25)(1.00) = 0.10.

Table A-3 expands the prior example and now assumes alpha-plus-beta measurements will be made to quantify the total uranium alpha activity for aged uranium yellowcake (processed natural uranium) with equilibrium ingrowth of the short-lived, beta-emitting progeny of both uranium (U)-238 and U-235 (thorium [Th]-234, protactinium (Pa)-234m, and Th-231). As before, the type of emissions will determine the detector type and provide for  $\epsilon_s$  in terms of the alpha or beta application conditions in ISO 7503-1:1988. This example illustrates the weighted  $E_{MAX}$  calculation for each beta-emitter. The weighted  $E_{MAX}$  will be an input for the calibration sources used and the applicable beta  $\epsilon_s$ . Similarly, although not shown in the example, alpha-emitters may also exhibit various emission energies and intensities, and a single weighted value is used. As the default  $\epsilon_s$  for all alpha-emitters is 0.25, the weighted alpha E will be a consideration only in selecting the appropriate calibration source. Additionally, for the example in Table A-3, the mixture RFs are presented in terms of the total alpha activity for direct comparison of measurement data with the 5,000 dpm  $\alpha/100 \text{ cm}^2$  limit.

Further clarification of the distinction between the relationship of alpha fractions and relative fractions is described as follows. Each uranium isotope decays via an alpha emission. As shown in both Tables A-2 and A-3, the alpha activity RFs of the uranium isotopes, relative to one another, consists of approximately 49 percent (0.49) U-238, 2 percent (0.02) U-235, and 49 percent (0.49) U-238, which sums to the total alpha activity of 100 percent (1.00). The alpha-plus-beta activity will be measured, which allows the detection of the U-238 and U-235 beta-emitting progeny; however, the results are to be reported as uranium total alpha activity

rather than total gross alpha-plus-beta activity. Therefore, each of the beta emission RFs will correspond to that of the respective parent uranium alpha fraction in Table A-3. Note also the additive effect of the beta emissions to the overall alpha fraction, whereby the RFs sum to 2.03.

Another consideration addressed in the Table A-3 example is that the energy of the selected beta calibration source (Tc-99 at  $E_{MAX} = 0.294$  MeV) exceeds energies for several of the beta emissions, and the source cannot be considered reasonably representative of those energies. To be consistent with guidance from ANSI N323AB-2013 and ISO 7503-1:1988, several emissions with energies below Tc-99 are excluded from the efficiency calculation (i.e., all of the Th-234 emissions and 4 of the Th-231 emissions). These excluded emission energies would also not fall within the Tc-99 “energy region” presented in ISO 7503-3:2016. For the purpose of the example, only the emission intensities corresponding to energies near or above the calibration source are utilized for each ROC’s respective efficiency determination. This resulted in a total intensity of zero for Th-234 (i.e., all energies were below the calibration source energy) and a total intensity of 0.84 for Th-231.

The Table A-3 example also introduces a weighting factor (WF) in order to multiplicatively combine the I, BR, and RF parameters for calibration scenarios involving multiple radionuclides and/or decay series. The individual WF,  $\epsilon_i$ , and  $\epsilon_s$  that represent the decay mode, emission type, and energy or intensity of each ROC are then summed to obtain the weighted  $\epsilon_t$ , as shown in Equation A.5:

$$\epsilon_t = (WF_1)(\epsilon_{i1})(\epsilon_{s1}) + (WF_2)(\epsilon_{i2})(\epsilon_{s2}) \dots + \dots (WF_n)(\epsilon_{in})(\epsilon_{sn}) \quad (\text{Eq. A.5})$$

**Table A-3 ROC, Calibration Source, Detector Specifications, and Efficiency Calculations for Aged Processed Natural Uranium**

| ROC Characteristics                                   |       |       |       |                |       |           |      |                   |        |
|---|-------|-------|-------|----------------|-------|-----------|------|-------------------|--------|
| ROC   | U-238 | U-235 | U-234 | Th-234         |       | Pa-234m   |      | Th-231            |        |
| Emission  | alpha | alpha | alpha | beta           |       | beta      |      | beta              |        |
| E (MeV) <sup>a</sup>                                  | 4.188 | 4.431 | 4.759 | $E_{MAX}$      | I     | $E_{MAX}$ | I    | $E_{MAX}$         | I      |
|   |       |       |       | 0.086          | 0.015 | 1.22      | 0.01 | 0.144             | 0.03   |
|   |       |       |       | 0.106          | 0.064 | 1.46      | 0.01 | 0.173             | 0.003  |
|   |       |       |       | 0.107          | 0.14  | 2.27      | 0.98 | 0.208             | 0.12   |
|   |       |       |       | 0.199          | 0.78  |           |      | 0.217             | 0.01   |
|   |       |       |       |                |       |           |      | 0.289             | 0.12   |
|   |       |       |       |                |       |           |      | 0.290             | 0.40   |
|   |       |       |       |                |       |           |      | 0.307             | 0.32   |
|   |       |       |       |                |       |           |      | 0.314             | 0.0017 |
|   |       |       |       |                |       |           |      | 0.333             | 0.0017 |
| Weighted $\beta E_{MAX}^a$<br>$\sum E_{MAX} \times I$ |       |       |       |                |       |           |      |                   |        |
|   |       |       |       | 0.178          |       | 2.25      |      | 0.282             |        |
| I   | 1.00  | 1.00  | 1.00  | 0 <sup>b</sup> |       | ~1        |      | 0.84 <sup>b</sup> |        |
| BR  | NA    | NA    | NA    | NA             |       | NA        |      | NA                |        |
| RF<br>(alpha fraction)                                | 0.49  | 0.02  | 0.49  | 0.49           |       | 0.49      |      | 0.02              |        |

|  |   |                                |                                |  |                     |                      |
|--|---|--------------------------------|--------------------------------|--|---------------------|----------------------|
| WF<br>(weighting<br>factor)  | 0.49  | 0.02                           | 0.49                           | 0  | 0.49                | 0.0168               |
| <b>Calibration Source Specifications</b>                                       |   |                                |                                |  |                     |                      |
| Calibration sources  | Th-230  |                                |                                | Tc-99  |                     |                      |
| Emission   | alpha   |                                |                                | beta   |                     |                      |
| E (MeV)  | 4.663   |                                |                                | 0.294  |                     |                      |
| Calibration source area  | 150 cm <sup>2</sup>   |                                |                                | 150 cm <sup>2</sup>  |                     |                      |
| Source certificate surface emission rate                                       | 38,100 cpm/150 cm <sup>2</sup>  |                                |                                | 18,500 cpm/150 cm <sup>2</sup>   |                     |                      |
| <b>Detector Specifications</b>   |   |                                |                                |  |                     |                      |
| Detector type  | Alpha-Plus-Beta Gas Proportional  |                                |                                |  |                     |                      |
| Detector geometry  | 126 cm <sup>2</sup>   |                                |                                |  |                     |                      |
| Detector background  | 300 cpm   |                                |                                |  |                     |                      |
| <b>Total Efficiency and Static MDC Calculation</b>                             |   |                                |                                |  |                     |                      |
| Surface emission rate subtended by the detector                                | Th-230 Calibration Source   |                                |                                | Tc-99 Calibration Source   |                     |                      |
|  | $\frac{38,100 \text{ cpm}}{150 \text{ cm}^2} \times 126 \text{ cm}^2 = 32,004 \text{ cpm}$  |                                |                                | $\frac{18,500 \text{ cpm}}{150 \text{ cm}^2} \times 126 \text{ cm}^2 = 15,540 \text{ cpm}$ |                     |                      |
| Detector calibration source net response                                       | 13,421 cpm – 300 cpm = 13,121 cpm   |                                |                                | 7,185 cpm – 300 cpm = 6,885 cpm  |                     |                      |
| $\epsilon_i$   | $\frac{13,121 \text{ cpm}}{32,004 \text{ cpm}} = 0.41$  |                                |                                | $\frac{6885 \text{ cpm}}{15,540 \text{ cpm}} = 0.44$                                       |                     |                      |
| $\epsilon_s$   | U-238   | U-235                          | U-234                          | Th-234   | Pa-234 <sup>m</sup> | Th-231               |
|  | 0.25  | 0.25                           | 0.25                           | 0.25   | 0.5                 | 0.25                 |
| Weighted $\epsilon_t$<br>$\Sigma(\epsilon_i)(\epsilon_s)(WF)$                  | $\frac{(0.41)(0.25)}{x(0.49)}$  | $\frac{(0.41)(0.25)}{x(0.02)}$ | $\frac{(0.41)(0.25)}{x(0.49)}$ | (0.44)(0.25)(0)  | (0.44)(0.5)(0.49)   | (0.44)(0.25)(0.0168) |
|  | 0.050   | 0.002                          | 0.050                          | 0.000  | 0.108               | 0.002                |
| <b>= 0.212</b>   |   |                                |                                |  |                     |                      |
| MDC =<br>$\frac{3+4.65 \times \sqrt{R_B \times T}}{T \epsilon_i \epsilon_s G}$ | $\frac{3+4.65 \times \sqrt{300 \text{ cpm} \times 1 \text{ min}}}{1 \text{ min} \times 0.212 \times \frac{126 \text{ cm}^2}{100}} = 313 \text{ dpm}/100 \text{ cm}^2$ |                                |                                |  |                     |                      |

<sup>a</sup>Excludes emission intensities less than 0.1 percent; energies weighted based on emission intensity.

<sup>b</sup>Comprises only radionuclide emission intensities corresponding to energies near or above calibration source energy. This value is used in the WF calculation to multiplicatively combine I, BR, and RF parameters.

The preceding examples demonstrate the application of the emission and energy for selecting detectors and calibration sources and for assigning  $\epsilon_s$ . Additionally, the RF parameter—when multiple ROCs are present at known relative concentration fractions—is demonstrated for calculating a weighted  $\epsilon_t$ . In addition to an RF representing an activity fraction, two other measurement result scenarios are common. One is analogous to a surrogate approach, in which results can be reported in terms of U-238 activity and the ROC RFs represent ratios relative to the U-238. Alternatively, if the measurement result is to be reported as total activity, the RF for each ROC represents a fraction of the total activity. Table A-4 provides a comparison of these RF situations.

**Table A-4 Comparative Relative RFs for Surface Activity Result Reporting for Aged Processed Natural Uranium**

| ROC                 | U-238 | U-235 | U-234 | Th-234 | Pa-234m | Th-231 |
|---------------------|-------|-------|-------|--------|---------|--------|
| RF (U-238 Fraction) | 1.0   | 0.04  | 1.0   | 1.0    | 1.0     | 0.04   |
| RF (Total Activity) | 0.245 | 0.010 | 0.245 | 0.245  | 0.245   | 0.010  |

Sections A-2 and A-3 of this appendix present methods, case studies, and examples of the assessment of factors that complicate the efficiency calculation. These sections also illustrate methods for developing site-specific weighted efficiencies that represent the contaminant mixture scenarios. These case studies expand on the examples above and also the example in Section 5.5 of the main text of this NUREG, which compares theoretical and experimental detector efficiencies for 3-percent enriched uranium contamination. The case studies examine common radiological assessment situations, which include mixtures of beta-emitting and alpha-emitting radionuclides with complex decay schemes, examples where the RF input requires expression as a ratio and not a fraction, accounting for hard-to-detect (HTD) radionuclides in the total weighted detector efficiency, and other factors that may complicate the efficiency calculation. Also, in many cases, there may not be a standard source to match a ROC's characteristics, such as the example in Table A-3 where the Tc-99 source was similar to only one of the three beta-emitting uranium isotope progeny, and thus, an overly conservative representation of the weighted beta energy of the mixture resulted. For such a case, a calibration curve may be prepared. Several case studies in Section A-3 illustrate the calibration curve methodology, and they demonstrate a usable method to determine weighted detection efficiencies for multisource calibrations in lieu of the availability of custom, contaminant-specific calibration sources or for basing detector efficiency on a single source. The usage of a single weighted energy for a given radiation emission allows these methods to be relatively concise. Since radiation emissions often occur with multiple energies being represented (each at a specific intensity), the most comprehensive approach would be to include a single efficiency calculation for each energy followed by summation of all efficiencies. Such an approach is potentially tedious and the usage of a single weighted energy provides for a more streamlined application in field conditions.

As noted in the previous definitions, the weighted emission energy is calculated based on the intensity of the emissions at each energy as  $\sum E_{i...n} \times I_{i...n}$ , where  $E_i$  is the specific energy of an emission, and  $I$  is the intensity of that energy. The summation of all relevant emissions provides a single weighted energy value that can be used in detection efficiency calculations. In the case of beta emissions, a weighted energy could be established using either the average energy ( $E_{AVE}$ ) or the maximum energy ( $E_{MAX}$ ). However, care must be taken to ensure that the

comparison of energies between calibration sources and ROCs is consistent (i.e., only maximum beta energies from a calibration source should be utilized in efficiency calculations using weighted  $E_{MAX}$  and only average beta energies from a calibration source should be utilized in efficiency calculations using weighted  $E_{AVE}$ ). Table A-9 presents both weighted  $E_{AVE}$  and  $E_{MAX}$  values for the radionuclides that are used in the Section A-3 methods and case studies, though the case studies themselves only demonstrate calculations using the  $E_{MAX}$ . It is also worth noting that the National Nuclear Data Center Chart of the Nuclides provides a weighted  $E_{AVE}$  value as the “mean beta- energy” listed under the decay radiation information for each beta emitter.

In order to demonstrate the differences between using a single weighted energy to calculate the detection efficiency and individually determining efficiencies for each respective emission energy (followed by summation), two different examples are provided in Tables A-5 and A-6. Both examples present a calculation of alpha plus beta efficiency for aged processed natural uranium (i.e., yellowcake), similar to the example in Table A-3. However, in these examples it is assumed that a multisource calibration will be used, in contrast to the single source approach shown in Table A-3.

Table A-5 presents an example using aged processed natural uranium, and it utilizes a single weighted  $E_{MAX}$  for both the alpha and beta emissions. Table A-6 presents the same aged process uranium scenario; however, all alpha and beta emissions above an intensity of 0.1% are shown, and a total efficiency ( $\epsilon_t$ ) is calculated for each emission, followed by summation to determine the overall “alpha plus beta” efficiency. In both scenarios, the  $\epsilon_s$  is established based upon the recommended values from ISO 7503-1:1988. For illustrative purposes the  $\epsilon_t$ ,  $\epsilon_i$ , and overall total efficiency values (i.e.,  $\sum \epsilon_{ti}$ , where  $\epsilon_{ti}$  is the total efficiency ( $\epsilon_t$ ) for each ( $i$ ) energy emission) are shown with multiple significant digits in both Table A-5 and A-6.

**Table A-5 ROC, Efficiency Calculations for Aged Processed Natural Uranium**

| Nuclide   | Half-Life (yrs) | Total Intensity | Mean E (keV) <sup>a</sup> | Max. E (keV) <sup>a</sup> | Relative Fraction | $\epsilon_i$    | $\epsilon_s$ | $\epsilon_t^b$ |
|---|-----------------|-----------------|---------------------------|---------------------------|-------------------|-----------------|--------------|----------------|
| <b>Beta Emitters</b>                                      |                 |                 |                           |                           |                   |                 |              |                |
| Th-234  | 6.60E-02        | 100%            | 47.8                      | 178                       | 0.49              | 0.166553        | 0.25         | 0.020403       |
| Pa-234  | 2.21E-06        | 100%            | 809                       | 2,240                     | 0.49              | 0.380000        | 0.50         | 0.093005       |
| Th-231  | 2.91E-03        | 100%            | 78                        | 283                       | 0.02              | 0.242712        | 0.25         | 0.001383       |
| <b>Alpha Emitters</b>                                     |                 |                 |                           |                           |                   |                 |              |                |
| U-238   | 4.47E+09        | 100%            | 4,188                     | N/A                       | 0.49              | 0.288786        | 0.25         | 0.035340       |
| U-234   | 2.46E+05        | 100%            | 4,759                     | N/A                       | 0.49              | 0.387031        | 0.25         | 0.047363       |
| U-235   | 7.04E+08        | 100%            | 4,431                     | N/A                       | 0.02              | 0.336512        | 0.25         | 0.001918       |
| <b>Total Efficiency (<math>\sum \epsilon_{ti}</math>)</b> |                 |                 |                           |                           |                   | <b>0.199412</b> |              |                |

<sup>a</sup>Excludes emission intensities < 0.1%; mean and maximum energies weighted based on emission intensity.

<sup>b</sup>Total efficiency per nuclide is *Total Intensity* × *Relative Fraction* ×  $\epsilon_i$  ×  $\epsilon_s$ .

**Table A-6 ROC, Efficiency Calculations for Aged Processed Natural Uranium**

| Nuclide   | Half-Life (yrs) | Intensity | Mean E (keV) | Max. E (keV) | Relative Fraction | $\epsilon_i$    | $\epsilon_s$ | $\epsilon_t^b$ |
|---|-----------------|-----------|--------------|--------------|-------------------|-----------------|--------------|----------------|
| <b>Beta Emitters</b>  |                 |           |              |              |                   |                 |              |                |
| Th-234  | 6.60E-02        | 1.5%      | 22.3         | 86           | 0.49              | 0.000000        | 0.00         | 0.000000       |
| Th-234  | 6.60E-02        | 6.4%      | 27.7         | 106          | 0.49              | 0.000000        | 0.00         | 0.000000       |
| Th-234  | 6.60E-02        | 14.0%     | 27.8         | 107          | 0.49              | 0.000000        | 0.00         | 0.000000       |
| Th-234  | 6.60E-02        | 78.0%     | 53.6         | 199          | 0.49              | 0.182342        | 0.25         | 0.017423       |
| Pa-234  | 2.21E-06        | 1.0%      | 405.6        | 1224         | 0.49              | 0.372776        | 0.50         | 0.000915       |
| Pa-234  | 2.21E-06        | 0.95%     | 496          | 1459         | 0.49              | 0.380000        | 0.50         | 0.000883       |
| Pa-234  | 2.21E-06        | 97.6%     | 820.5        | 2269         | 0.49              | 0.380000        | 0.50         | 0.090838       |
| Th-231  | 2.91E-03        | 2.6%      | 37.8         | 144.3        | 0.02              | 0.000000        | 0.00         | 0.000000       |
| Th-231  | 2.91E-03        | 0.30%     | 46           | 173.4        | 0.02              | 0.163048        | 0.25         | 0.000002       |
| Th-231  | 2.91E-03        | 12.1%     | 55.9         | 208.1        | 0.02              | 0.189085        | 0.25         | 0.000114       |
| Th-231  | 2.91E-03        | 1.3%      | 58.6         | 217.4        | 0.02              | 0.195920        | 0.25         | 0.000013       |
| Th-231  | 2.91E-03        | 12.0%     | 79.8         | 289.3        | 0.02              | 0.247091        | 0.25         | 0.000148       |
| Th-231  | 2.91E-03        | 40.0%     | 80.1         | 290.2        | 0.02              | 0.247715        | 0.25         | 0.000495       |
| Th-231  | 2.91E-03        | 32.0%     | 85.3         | 307.4        | 0.02              | 0.254103        | 0.25         | 0.000407       |
| Th-231  | 2.91E-03        | 0.17%     | 87.3         | 313.9        | 0.02              | 0.255981        | 0.25         | 0.000002       |
| Th-231  | 2.91E-03        | 0.17%     | 93.1         | 333          | 0.02              | 0.261356        | 0.25         | 0.000002       |
| <b>Alpha Emitters</b>                                       |                 |           |              |              |                   |                 |              |                |
| U-238   | 4.47E+09        | 21.0%     | 4151         | N/A          | 0.49              | 0.280722        | 0.25         | 0.007222       |
| U-238   | 4.47E+09        | 79.0%     | 4198         | N/A          | 0.49              | 0.290896        | 0.25         | 0.028151       |
| U-234   | 2.46E+05        | 0.20%     | 4603.5       | N/A          | 0.49              | 0.365032        | 0.25         | 0.000089       |
| U-234   | 2.46E+05        | 28.4%     | 4722.4       | N/A          | 0.49              | 0.382135        | 0.25         | 0.013304       |
| U-234   | 2.46E+05        | 71.4%     | 4774.6       | N/A          | 0.49              | 0.388980        | 0.25         | 0.034013       |
| U-235   | 7.04E+08        | 0.30%     | 4153         | N/A          | 0.02              | 0.281162        | 0.25         | 0.000004       |
| U-235   | 7.04E+08        | 6.0%      | 4215.8       | N/A          | 0.02              | 0.294663        | 0.25         | 0.000089       |
| U-235   | 7.04E+08        | 0.90%     | 4219         | N/A          | 0.02              | 0.295335        | 0.25         | 0.000013       |
| U-235   | 7.04E+08        | 0.22%     | 4266.2       | N/A          | 0.02              | 0.305074        | 0.25         | 0.000003       |
| U-235   | 7.04E+08        | 0.11%     | 4282.9       | N/A          | 0.02              | 0.308441        | 0.25         | 0.000002       |
| U-235   | 7.04E+08        | 3.5%      | 4322.9       | N/A          | 0.02              | 0.316336        | 0.25         | 0.000056       |
| U-235   | 7.04E+08        | 18.9%     | 4364.3       | N/A          | 0.02              | 0.324256        | 0.25         | 0.000307       |
| U-235   | 7.04E+08        | 57.7%     | 4395.4       | N/A          | 0.02              | 0.330039        | 0.25         | 0.000953       |
| U-235   | 7.04E+08        | 3.1%      | 4414.9       | N/A          | 0.02              | 0.333591        | 0.25         | 0.000052       |
| U-235   | 7.04E+08        | 0.24%     | 4438.5       | N/A          | 0.02              | 0.337815        | 0.25         | 0.000004       |
| U-235   | 7.04E+08        | 1.3%      | 4502.5       | N/A          | 0.02              | 0.348852        | 0.25         | 0.000022       |
| U-235   | 7.04E+08        | 3.8%      | 4556.1       | N/A          | 0.02              | 0.357627        | 0.25         | 0.000068       |
| U-235   | 7.04E+08        | 4.8%      | 4597.4       | N/A          | 0.02              | 0.364098        | 0.25         | 0.000087       |
| <b>Total Efficiency (<math>\Sigma\epsilon_{ti}</math>):</b> |                 |           |              |              |                   | <b>0.195680</b> |              |                |

<sup>a</sup>Excludes emission intensities < 0.1%

<sup>b</sup>Total efficiency per nuclide is Total Intensity × Relative Fraction ×  $\epsilon_i$  ×  $\epsilon_s$ .

In both scenarios shown in Tables A-5 and A-6, the calculated  $\varepsilon_t$  is essentially equal to 0.2. However, the efficiency value calculated from all emission energies, as shown in Table A-6, is slightly lower than the value calculated using a weighted energy (shown in Table A-5). This would be expected, since in Table A-6, the  $\varepsilon_s$  is individually considered for each emission energy, and in some cases the  $\varepsilon_s$  is considered zero for energies that are below those established for the ISO 7503-1:1988 values. However, those energies would have still been considered, to a limited extent, as an element to the single weighted energy value, as shown in Table A-5.

The case study exhibits described in Section A-3 will show only the precalculated weighted energies and not the step for calculating the weighted  $E_{MAX}$ . Additionally, the case studies only utilize a weighted energy efficiency calculation, similar to that shown in Table A-5. However, if desired, the more comprehensive approach shown in Table A-6 could also be applied to the case studies. Prior to the introduction of the case studies, a series of methods and preliminary information to setup the case studies are provided below in Section A-2

## A.2 Methods

American National Standards Institute (ANSI) N13.49, "Performance and Documentation of Radiological Surveys," issued in 2011, states the following:

The DQO process should be used when selecting and calibrating radiological survey instrumentation. Factors to consider include radiation type, radiation energies, minimum detectable concentration (MDC) requirements, and whether qualitative or quantitative survey data are required.

Once these factors are compiled, the project planning team determines the type of measurements to be made and then generates efficiency and MDC values based on site-specific DQOs and detector and measurement types. The planners account for site-specific environmental conditions or other factors that could affect or interfere with (bias) the detector response, such as increased counts (positive bias) from gamma radiation shine or decreased counts because of cold weather voltage plateau shifts (negative bias), to ensure the best decisions. The following are common field survey instruments used for gross alpha and gross beta scanning and surface activity quantification that might be selected (several of them are used in the case studies):

### Gas proportional

- alpha-only, high-voltage (HV) setting to the alpha plateau and 0.4 or 0.8-mg/cm<sup>2</sup> Mylar window density thickness
- beta-only, based on HV setting to the alpha-plus-beta plateau and 3.8-mg/cm<sup>2</sup> density thickness Mylar window to shield alpha contributions
- alpha plus beta, based on beta HV setting to the alpha-plus-beta plateau and 0.4 or 0.8-mg/cm<sup>2</sup> Mylar window density thickness (the 0.4-mg/cm<sup>2</sup> window is preferred when assessing low-energy beta-emitters, such as carbon (C)-14)

### Geiger-Mueller (GM)

- primarily beta

### Zinc Sulfide (ZnS) Scintillators

- alpha only

### Plastic Scintillators (primarily used for beta but also responds to alpha)

- beta, 1.2-mg/cm<sup>2</sup> Mylar window density thickness; additional Mylar layers may be used to eliminate alpha response

### Dual phoswich (ZnS and plastic scintillator)

- alpha
- beta (reduced efficiency compared to gas proportional or plastic scintillator alone)



- 1.2-mg/cm<sup>2</sup> Mylar window density thickness
- simultaneous alpha and beta counting affected by alpha and beta cross-talk when coupled to dual-channel analyzer

As an example of measurement interference, the beta detectors also respond to gamma radiation. However, the gamma counting efficiency is generally low (10–30 counts/minute per microrentgens/hour for cesium (Cs)-137). Furthermore, although the GM and plastic scintillator-based detectors are generally cited as beta detectors, both detectors also respond to alpha radiation. Because the alpha radiation  $\epsilon_i$  for these detectors may be upwards of 40 percent, the user may consider accounting for additional detector response when beta-only measurements have been planned, such as in cases where radon progeny build up on surfaces.

The collection of both shielded and unshielded measurements at each survey area location, or on each item, and within a construction material-specific background reference area can address the additional detector count response from either variable ambient background gamma radiation levels or alpha radiation contributions from radon progeny. The process may be similar to the following:

- (1) Perform static direct measurements of surfaces or items being measured both with and without a beta absorber on the detector face such as a 3/8-inch-thick Plexiglas® shield. These same measurements are also collected on the construction material-specific background surfaces in an appropriate reference area.
- (2) Document both shielded and unshielded gross counts, as well as other applicable variables such as count time, location, surface type, and surface condition.
- (3) Determine the value of N in Equation A.3 by using the appropriate reference material-specific data as follows:

$$N = (R_{U,SU} - R_{S,SU}) - (R_{U,RM} - R_{S,RM}) \quad \text{Eq. A.6}$$

where:

N = net counts

$R_{U,SU}$  = unshielded survey unit count rate

$R_{S,SU}$  = shielded survey unit count rate

$R_{U,RM}$  = unshielded reference area material count rate

$R_{S,RM}$  = reference area material count rate

Alternatively, accept the positive measurement bias.

The case studies include detectors of the types introduced. Although detectors for simultaneous alpha and beta assessment are commercially available, the case studies assume the performance of either alpha-only, alpha-plus-beta, or beta-only measurements. The discrimination into alpha-only, beta-only, or alpha-plus-beta is illustrated using both a dual phoswich and gas proportional detectors. For alpha-only measurements, the gas proportional detector is calibrated and operated on the alpha plateau proportional voltage curve. The high voltage is increased to the alpha-plus-beta plateau region for alpha-plus-beta measurements. The beta-only measurements are also taken at the alpha-plus-beta voltage plateau, but with a

3.8-mg/cm<sup>2</sup> density thickness Mylar window to block the alpha emissions. The higher density Mylar will also reduce the efficiency of the lower energies of the beta spectrum. The plastic scintillator is considered specifically because some consider it a beta-only instrument, though the detector will respond to alpha radiation (when unaccounted for, the alpha radiation may lead to false positive decision errors). Two alpha-plus-beta examples are provided to demonstrate this fact. A GM detector or “frisker” is also considered to compare results to those from the more sensitive detectors.

After the planning team decides whether to assess alpha, beta, or alpha-plus-beta emissions and selects the appropriate detectors for measurements and the detector configuration, the detectors are calibrated to ensure that efficiencies used for surface activity quantification are representative of the ROCs and defensible. As there are no simple rules for estimating  $\epsilon_t$ , multiple factors, including those already introduced, must be considered. The weighted efficiency procedures for calculating the  $\epsilon_t$  begin with the following:

- characterization of the ROCs and, more specifically, the radiation emission (alpha, beta, or both), radiation intensities, parent/progeny relationships, relative fractions for mixtures, half-lives, and other factors
- measurement surface characteristics
- the detector type and detector configuration (e.g., Mylar thickness)
- the availability of standard sources
- how the surface activity will be expressed, which may be either an efficiency/MDC for gross activity or for a specific radionuclide

The case study narratives and exhibits in Section A-3 demonstrate the weighted efficiency procedure for eight scenarios, expanding on the ISO 7503-1:1988 and ROC characterization processes introduced in Tables A-1 through A-3. The case studies, shown in Table A-7, progress in calibration complexity and include the following:

- the different detector models and configurations used in the case studies and shown in Table A-8
  - Ludlum model 43-68 gas proportional detector configured with various Mylar density thickness windows of either 0.4 mg/cm<sup>2</sup> and 0.8 mg/cm<sup>2</sup> for alpha or alpha-plus-beta detection and corresponding HV plateau or 3.8-mg/cm<sup>2</sup> density thickness Mylar windows to block alpha radiation when operating at the alpha-plus-beta plateau
  - Ludlum model 43-92 ZnS(Ag) detector (0.8-mg/cm<sup>2</sup> Mylar window)
  - Ludlum model 44-142 plastic scintillator detector (1.2-mg/cm<sup>2</sup> Mylar window)
  - Ludlum model 43-93 dual phoswich ZnS(Ag)/plastic scintillator detector (1.2-mg/cm<sup>2</sup> Mylar window)
  - Ludlum model 44-9 GM detector
- calibration using sources that are the same radionuclide as the ROC and using surrogate sources

- calibration for radionuclides with a single emission or noncomplex decay scheme
- calibrations for radionuclide mixtures
- calibrations for radionuclides with complex decay schemes
- the resultant calibration efficiencies and MDCs for either gross activity measurements (e.g., for comparison to a gross activity investigation or action level) or for radionuclide-specific measurements (e.g., for comparison to an I/A level of a parent ROC such as Th-232 present with the full decay series)

The radionuclide contaminant combinations include beta-emitters, HTD radionuclides, and mixtures of alpha- and beta-emitters. Both the natural thorium and uranium series are presented (equilibrium is assumed), as are enriched and processed uranium to provide additional guidance and considerations unique to uranium recovery facilities. The last contaminant (for Case 8) is radium in equilibrium with its decay products, which is followed by a discussion of interferences from radon and associated decay products.

**Table A-7 Exhibit Number and Radionuclides of Concern**

| Case No. | ROCs  |
|----------|---|
| 1        | C-14, Tc-99                                 |
| 2        | Ni-63, Co-60, Cs-137                        |
| 3        | Am-241, H-3, Cs-137, Sr/Y-90                |
| 4        | Th-232 plus decay series                    |
| 5        | U-238 plus decay series                     |
| 6        | Enriched uranium                            |
| 7        | Processed uranium in situ recovery facility |
| 8        | Ra-226 plus decay series                    |

Table A-8 lists the ROC mixtures in the case studies for which the  $\epsilon_t$  and MDC values will be calculated, together with the selections for detector type and configuration, radiation emission measured (alpha only, beta only, or alpha plus beta), and how the results are reported in terms of gross activity or radionuclide-specific results. The combinations selected for the case studies are not exhaustive; detector or measurement type options other than those shown in Table A-8 may be acceptable. Those selected demonstrate the kinds of decisions that may be needed during a project.

Table A-9 presents radiation decay data for the beta-emitting case study ROCs and includes the half-life (years), intensity, and both the average and maximum beta energy (kiloelectron volts [keV]) of each radionuclide. Maximum energies—shown as the weighted maximum energy per the process illustrated in Table A-3—are used in the case study exhibits to assign the  $\epsilon_s$  as previously described. Beta radiation data are taken from the National Nuclear Data Center (NNDC) “Chart of Nuclides” Web site maintained by Brookhaven National Laboratory. For radionuclides with complex decay schemes, only emissions with intensities of at least 0.001 (0.1 percent) were considered.

Table A-10 presents radiation decay data for the alpha-emitting case study ROCs and includes the half-life (years), intensity, and weighted average alpha energy (keV) of each radionuclide. All alpha-emitters are assigned an  $\epsilon_s$  of 0.25, so only weighted average energies are presented.

Alpha radiation data are also taken from the NNDC “Chart of Nuclides” Internet site. For radionuclides with complex decay schemes, only emissions with intensities of at least 0.001 (0.1 percent) were considered.

Finally, planners need to consider the overall objective of the measurement (i.e., how the measurement will be compared to the I/A levels. The form of the I/A levels must be considered. That is, the rules for calculating MDC when compared to general gross alpha I/A levels are different than when calculating the MDC from, for example, the uranium series. Table A-11 presents three different categories of I/A levels, and therefore, three different methods for calculating the MDC. As the table describes, the selected category dictates which radionuclides to include in the  $\epsilon_s$  calculation and whether the RF is expressed as a ratio or a fraction. The form of the I/A levels impacts DQO development and detector selection, standard source selection, and other inputs as described in the following case studies.

**Table A-8 Case-Specific Radionuclides, Radiations, and Instrument Inputs**

| Case Study | Radionuclides                        | Measurement Type | Detector                                   | Reported Activity    |
|------------|--------------------------------------|------------------|--|----------------------|
| 1          | C-14, Tc-99                          | Beta-Only        | Gas Proportional                           | Gross Beta           |
|            |                                      |                  | 0.8 mg/cm <sup>2</sup> HV=Alpha+Beta       |                      |
| 2          | Ni-63, Co-60, Cs-137                 | Beta-Only        | Gas Proportional                           | Gross Beta           |
|            |                                      |                  | 0.4 mg/cm <sup>2</sup> HV=Alpha+Beta       |                      |
| 3a         | Am-241, H-3, Cs-137, Sr/Y-90         | Alpha+Beta       | Plastic Scintillator                       | Gross Alpha+Beta     |
| 3b         | Am-241, H-3, Cs-137, Sr/Y-90         | Alpha-Only       | Gas Proportional                           | Gross Alpha          |
|            |                                      |                  | 0.8 mg/cm <sup>2</sup> HV=Alpha            |                      |
|            |                                      | Beta-Only        | Gas Proportional                           | Gross Beta           |
|            |                                      |                  | 3.8 mg/cm <sup>2</sup> HV=Alpha+Beta       |                      |
| 4a         | Th-232 plus decay series (+C)        | Alpha+Beta       | Gas Proportional                           | Gross Th-232+C       |
|            |                                      |                  | 0.8 mg/cm <sup>2</sup> HV=Alpha+Beta       |                      |
| 4b         | Th-232 plus decay series             | Beta-Only        | Gas Proportional                           | Gross Th-232+C       |
|            |                                      |                  | 3.8 mg/cm <sup>2</sup> HV=Alpha+Beta       |                      |
| 4c         | Th-232 plus decay series             | Beta-Only        | Gas Proportional                           | Th-232               |
|            |                                      |                  | 3.8 mg/cm <sup>2</sup> HV=Alpha+Beta       |                      |
| 5a         | Processed uranium—aged yellowcake    | Alpha-Only       | ZnS(Ag) Scintillator                       | Gross total uranium  |
| 5b         | Processed uranium—aged yellowcake    | Beta-Only        | GM   | Gross total uranium  |
| 5c         | Processed uranium—pregnant lixiviant | Alpha-Only       | Dual Phoswich ZnS(Ag)/Plastic Scintillator | Gross alpha          |
| 5d         | Processed uranium—pregnant lixiviant | Beta-Only        | Dual Phoswich ZnS(Ag)/Plastic Scintillator | Gross alpha          |
| 5e         | Unprocessed uranium ore              | Alpha+Beta       | Gas Proportional                           | Gross total uranium  |
|            |                                      |                  | 0.8 mg/cm <sup>2</sup> HV=Alpha+Beta       |                      |
| 6a         | Enriched uranium (20% EU)            | Alpha-Only       | Gas Proportional                           | Gross total uranium  |
|            |                                      |                  | 0.8 mg/cm <sup>2</sup> HV=Alpha            |                      |
| 6b         | Enriched uranium (20% EU), Tc-99     | Alpha+Beta       | Gas Proportional                           | Gross Alpha+Beta     |
|            |                                      |                  | 0.8 mg/cm <sup>2</sup> HV=Alpha+Beta       |                      |
| 7a         | Processed uranium tailings           | Alpha+Beta       | Gas Proportional                           | Gross Alpha+Beta     |
|            |                                      |                  | 0.8 mg/cm <sup>2</sup> HV=Alpha+Beta       |                      |
| 7b         | Processed uranium tailings           | Beta-Only        | GM   | Gross Alpha+Beta     |
| 8a         | Ra-226 plus decay series             | Alpha+Beta       | Gas Proportional                           | Gross total Ra-226+C |
|            |                                      |                  | 0.8 mg/cm <sup>2</sup> HV=Alpha+Beta       |                      |
| 8b         | Ra-226 plus decay series             | Alpha+Beta       | Gas Proportional                           | Ra-226 proxy         |
|            |                                      |                  | 0.8 mg/cm <sup>2</sup> HV=Alpha+Beta       |                      |

**Table A-9 Radiation Data for Beta-Emitters<sup>a</sup>**

| <b>Radionuclide</b> | <b>T1/2<br/>(yr)</b> | <b>Total Beta<br/>Intensity</b> | <b>E<sub>AVG</sub><br/>(keV)<sup>b</sup></b> | <b>E<sub>MAX</sub><br/>(keV)<sup>b</sup></b> |
|---------------------|----------------------|---------------------------------|--|--|
| H-3                 | 1.23E+01             | 1.00                            | 5.69E+00                                     | 1.86E+01                                     |
| C-14                | 5.70E+03             | 1.00                            | 4.95E+01                                     | 1.57E+02                                     |
| Co-60               | 5.27E+00             | 1.00                            | 9.64E+01                                     | 3.18E+02                                     |
| Ni-63               | 1.01E+02             | 1.00                            | 1.74E+01                                     | 6.69E+01                                     |
| Sr-90               | 2.88E+01             | 1.00                            | 1.96E+02                                     | 5.46E+02                                     |
| Y-90                | 7.31E-03             | 1.00                            | 9.34E+02                                     | 2.28E+03                                     |
| Tc-99               | 2.11E+05             | 1.00                            | 8.46E+01                                     | 2.94E+02                                     |
| Cs-137              | 3.01E+01             | 1.00                            | 1.87E+02                                     | 5.49E+02                                     |
| Tl-204              | 3.79E+00             | 0.97                            | 2.44E+02                                     | 7.64E+02                                     |
| Tl-208              | 5.81E-06             | 1.00                            | 5.59E+02                                     | 1.58E+03                                     |
| Pb-210              | 2.22E+01             | 1.00                            | 6.08E+00                                     | 2.44E+01                                     |
| Bi-210              | 1.37E-02             | 1.00                            | 3.89E+02                                     | 1.16E+03                                     |
| Bi-212              | 1.15E-04             | 0.64                            | 7.71E+02                                     | 2.09E+03                                     |
| Bi-214              | 3.79E-05             | 0.99                            | 6.39E+02                                     | 1.77E+03                                     |
| Pb-210              | 2.22E+01             | 1.00                            | 6.08E+00                                     | 2.44E+01                                     |
| Pb-212              | 1.21E-03             | 1.00                            | 1.00E+02                                     | 3.51E+02                                     |
| Pb-214              | 5.10E-05             | 1.00                            | 2.25E+02                                     | 7.19E+02                                     |
| Ra-228              | 5.75E+00             | 1.00                            | 7.24E+00                                     | 2.82E+01                                     |
| Ac-228              | 7.02E-04             | 0.94                            | 3.71E+02                                     | 1.05E+03                                     |
| Th-231              | 2.91E-03             | 1.00                            | 7.79E+01                                     | 2.83E+02                                     |
| Th-234              | 6.60E-02             | 1.00                            | 4.78E+01                                     | 1.78E+02                                     |
| Pa-234              | 2.21E-06             | 1.00                            | 8.09E+02                                     | 2.24E+03                                     |

<sup>a</sup>Source is <http://www.nndc.bnl.gov/chart/> (2016).

<sup>b</sup>Weighted for all emissions with intensities of at least 0.1 percent.

**Table A-10 Radiation Data for Alpha Emitters<sup>a</sup>**

| <b>Radionuclide</b> | <b>T1/2 (yr)</b> | <b>Total Alpha Intensity</b> | <b>E<sub>AVG</sub><sup>b</sup> (keV)</b> |
|---------------------|------------------|------------------------------|--|
| Bi-212              | 1.15E-04         | 0.36                         | 6,052                                    |
| Po-210              | 3.79E-01         | 1.00                         | 5,304                                    |
| Po-212              | 9.48E-15         | 1.00                         | 8,785                                    |
| Po-214              | 5.19E-12         | 1.00                         | 7,686                                    |
| Po-216              | 4.60E-09         | 1.00                         | 6,778                                    |
| Po-218              | 5.89E-06         | 1.00                         | 6,001                                    |
| Rn-222              | 1.05E-02         | 1.00                         | 5,485                                    |
| Ac-227              | 2.18E+01         | 0.01                         | 4,948                                    |
| Ra-224              | 1.00E-02         | 1.00                         | 5,672                                    |
| Ra-226              | 1.60E+03         | 1.00                         | 4,773                                    |
| Th-228              | 1.91E+00         | 1.00                         | 5,402                                    |
| Th-230              | 7.54E+04         | 1.00                         | 4,663                                    |
| Th-232              | 1.40E+10         | 1.00                         | 3,994                                    |
| U-234               | 2.46E+05         | 1.00                         | 4,759                                    |
| U-235               | 7.04E+08         | 1.00                         | 4,431                                    |
| U-238               | 4.47E+09         | 1.00                         | 4,188                                    |
| Am-241              | 4.33E+02         | 1.00                         | 5,487                                    |

<sup>a</sup>Source is <http://www.nndc.bnl.gov/chart/> (2016).

<sup>b</sup>Weighted for all emissions with intensities of at least 0.1 percent.

**Table A-11 Calculation Rules Based on the Form of the I/A Levels**

| I/A Levels                                | Description  | Method   |
|---|--|--|
| General gross radioactivity               | The I/A levels consider only the radiation type with no regard to the source of radiation; for example, 5,000 dpm/100 cm <sup>2</sup> gross beta radiation.      | Only radionuclides in the contaminant that emit the limit-specific radiation type are listed; the RF for each listed radionuclide is assigned as a nonzero fraction, where the sum of the RFs is 1.0.                                      |
| Source-specific gross radioactivity       | The I/A levels consider both the radiation type and the source of radiation; for example, 5,000 dpm/100 cm <sup>2</sup> gross radiation from the uranium series. | All radionuclides in the contaminant are listed regardless of radiation type; the RF for each listed radionuclide is assigned as a nonzero fraction, where the sum of the fractions is 1.0.  |
| Radionuclide-specific gross radioactivity | The I/A levels are focused on one radionuclide even if that radionuclide is one of several contaminants; for example, 5,000 dpm/100 cm <sup>2</sup> of U-238.    | All radionuclides in the contaminant are listed regardless of radiation type; the RF for each listed radionuclide is assigned as a nonzero ratio relative to the target radionuclides where the sum of the ratios may be greater than 1.0. |

Table A-12 presents data for the NIST-traceable calibration sources used to generate the instrument efficiency curves for this appendix. Figures A-1 for alpha-emitters and Figure A-2 for beta-emitters are example curves based on actual empirical data collected using calibrated detectors. However, the efficiencies presented here should not be used to replace detector-specific, source-specific, and environment-specific values for any surface activity assessment project.

**Table A-12 Calibration Source Data<sup>a</sup>**

| Source Radionuclide | Radiation Type | Average Energy (keV) <sup>b</sup> | Maximum Energy (keV) <sup>b</sup> |
|---------------------|----------------|-----------------------------------|-----------------------------------|
| U-238               | Alpha          | 4,188                             | NA                                |
| Th-230              | Alpha          | 4,663                             | NA                                |
| Pu-239              | Alpha          | 5,139                             | NA                                |
| Am-241              | Alpha          | 5,487                             | NA                                |
| Ni-63               | Beta           | 17.425                            | 66.9                              |
| C-14                | Beta           | 49.47                             | 156.5                             |
| Tc-99               | Beta           | 84.6                              | 293.5                             |
| Tl-204              | Beta           | 244.1                             | 763.8                             |
| Sr/Y-90             | Beta           | 564.8                             | 1,413                             |

<sup>a</sup>Source is <http://www.nndc.bnl.gov/chart/> (2016).

<sup>b</sup>Weighted for all emissions with intensities of at least 0.1 percent.

NA = not applicable

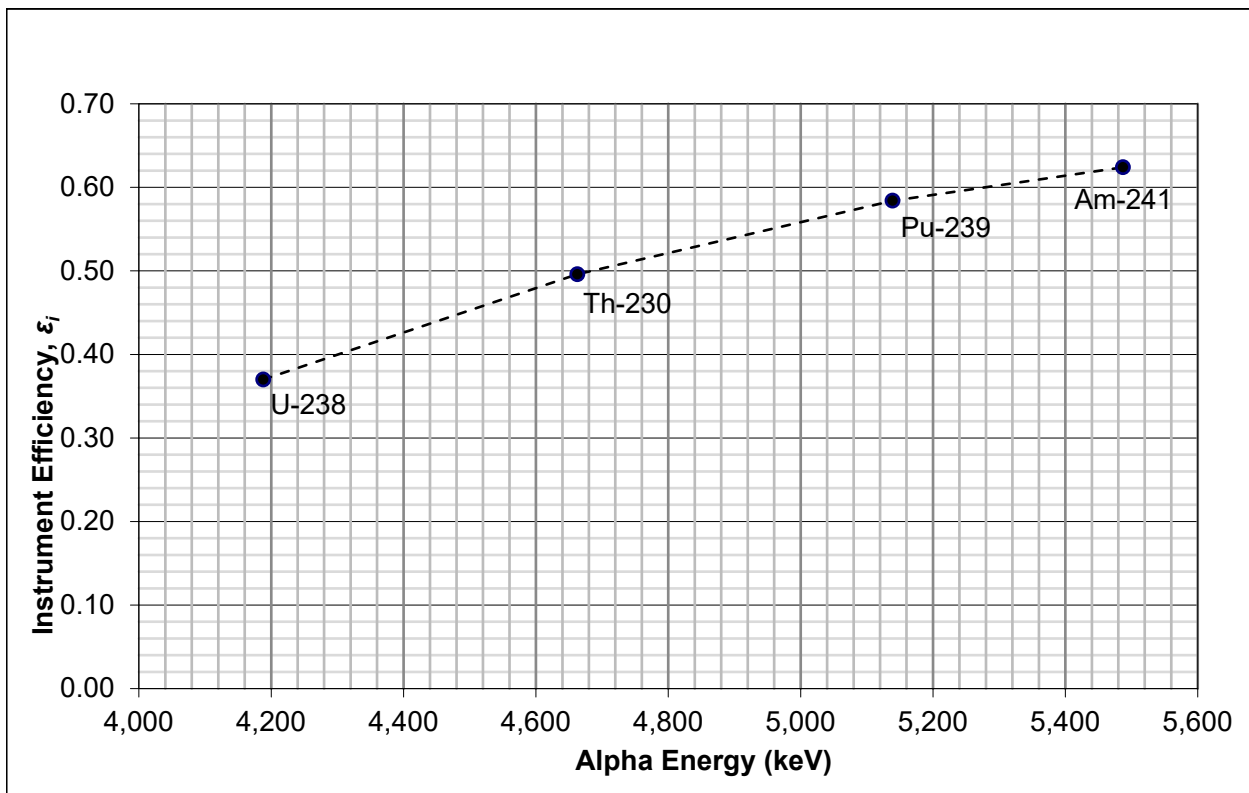


**Figure A-1 Example Alpha Detector Source Calibration Curve**



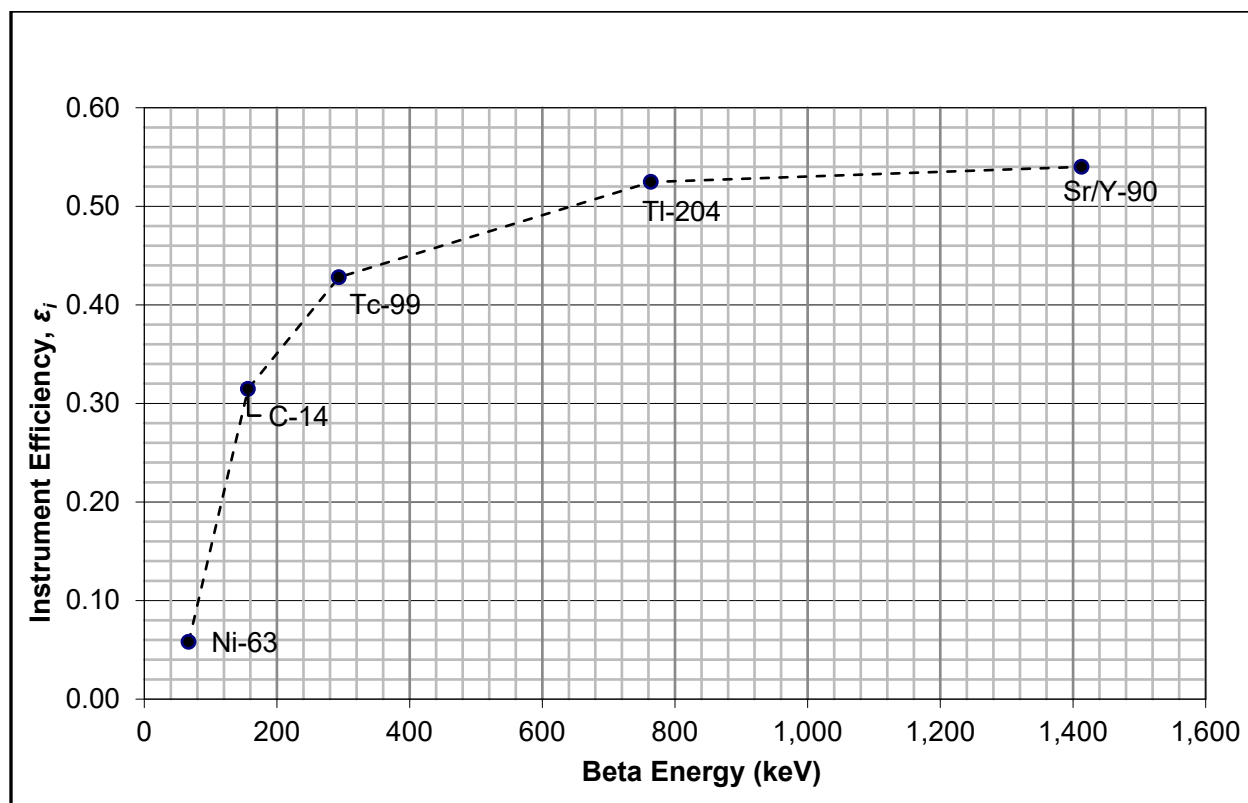


**Figure A-2 Example Beta Detector Source Calibration Curve**

These efficiency curves shown in Figures A-1 and A-2 do not represent the full range of potential radiation energies, so conservative boundary conditions are applied to calculate the  $\epsilon_i$  values in this appendix:

- All alpha radiation with an average energy higher than the most energetic standard is assigned the same efficiency as that standard. For example, all alpha energies above 5,487 keV are assigned the same efficiency as the americium (Am)-241 standard.
- Alpha radiation  $\epsilon_i$  values below that for the high-energy standard were estimated using a second-order polynomial trendline in Excel, which consistently produced an  $R^2 \approx 1.0$ .
- All beta radiation with a maximum energy higher than the most energetic standard is assigned the same efficiency as that standard. For example, all beta energies above 1,413 keV are assigned the same efficiency as the strontium/yttrium (Sr/Y)-90 standard.

All beta energies less than the least energetic standard with a nonzero efficiency are assumed to be HTD and assigned an  $\epsilon_i$  of 0.0. For example, using a gas proportional detector with a 3.8-mg/cm<sup>2</sup> Mylar window thickness, if the ROC maximum beta energy is less than 156.5 keV, an instrument efficiency of 0.0 is assigned. Note this boundary condition is not required for alpha-emitters.

Beta radiation  $\epsilon_i$  values between the low-energy and high-energy standard were estimated using nonlinear interpolation (Equation A.7) given that the efficiency curve does not closely match any regression type considered by Microsoft Excel.

### A.3 Case Studies

This section addresses eight case studies for assessing detection capability (MDCs) and surface activity levels for ROC mixtures—total efficiencies and static MDCs are calculated for each case. Cases 1 and 2 consider various mixtures of beta-emitting fission and activation products. Case 3 is similar to Cases 1 and 2 but also includes an HTD beta-emitter and an alpha-emitter. Case 4 considers the thorium decay series. Case 5 considers the uranium decay series. Cases 6 and 7 consider the presence of 20-percent enriched and processed uranium, respectively. Finally, Case 8 considers radium (Ra)-226 and its decay products. The last case is followed by a discussion of interferences from radon decay products and how those interferences complicate MDC calculations.

#### A.3.1 Case 1—ROCs: Fission and Activation Products

Case 1, the most straightforward, includes two beta-emitting contaminants (C-14 and Tc-99), both of which are directly represented by one of the standard calibration sources listed in Table A-12. The hypothetical I/A level in this case is in terms of general gross beta radioactivity (dpm/100 cm<sup>2</sup> of beta radioactivity), and the RFs will therefore sum to 1.0 and illustrate the application of Equations A.1, A.4, and A.5 for a mixture of fission and activation products.

- The example RFs for C-14 and Tc-99 are 0.6 and 0.4, respectively (60 percent C-14 and 40 percent Tc-99).
- The BR and I of the beta emissions for both ROCs are equal to 1; therefore, the combined WFC-14 = RF C-14 × I C-14 × BR C-14 = (0.6)(1.0)(1.0) = 0.6.
- The combined WF<sub>Tc-99</sub> = RF<sub>Tc-99</sub> × I<sub>Tc-99</sub> × BR<sub>Tc-99</sub> = (0.4)(1.0)(1.0) = 0.4.
- Gross beta measurements will be performed using a gas proportional detector with a 0.8-mg/cm<sup>2</sup> Mylar window. Substituting in Equation A.5 the combined WFs, specific Exhibit 1 values for ε<sub>i</sub>, and the ε<sub>s</sub> of 0.25, the E<sub>MAX</sub> for both betas is less than 0.400 MeV:

$$\epsilon_t = (WF_{C-14})(\epsilon_{iC-14})(\epsilon_{sC-14}) + (WF_{Tc-99})(\epsilon_{iTc-99})(\epsilon_{sTc-99}) = (0.60)(0.31)(0.25) + (0.40)(0.43)(0.25) = \epsilon_t = 0.09$$

Exhibit 1 presents the fully detailed results, noting that contaminant-specific efficiencies do not have to be estimated or interpolated using a beta efficiency calibration curve, but rather can be taken directly from Table A-19 of Exhibit 1 instrument efficiencies for C-14 and Tc-99 and inserted into Equation A.4. For this case, the total efficiency of 0.09 is calculated as shown above. Assuming an average background of 380 cpm over a 1-minute count, and use of the 126-cm<sup>2</sup> gas proportional detector, the gross beta radioactivity static MDC is calculated as follows:

$$\text{Static MDC} = \frac{3 + 4.65 \times \sqrt{380 (1)}}{(1)(0.09)(1.26)} = 826 \text{ dpm/100 cm}^2$$

#### A.3.2 Case 2—ROCs: Mixed Fission and Activation Products

Case 2 is also for a beta-emitting ROC mixture consisting of Co-60, Cs-137, and nickel (Ni)-63—a low-energy beta-emitter (66.9-keV maximum). This case is the first presented that requires interpolated efficiencies. For this example, an Ni-63 standard is available. There are no

standard sources to directly represent cobalt (Co)-60 and Cs-137. Table A-9 provides the beta  $E_{MAX}$  of 318 keV and 594 keV for Co-60 and Cs-137, respectively. In this case, the beta  $E_{MAX}$  for both Co-60 and Cs-137 is between the energies of the Tc-99 and Tl-204 standards. Therefore, the corresponding  $\epsilon_i$  values for both ROCs will be logarithmically interpolated, as shown below for Cs-137, using the Tc-99 and Tl-204  $\epsilon_i$  points on the energy calibration efficiency curve:

$$\log_{10}(\text{Cs-137 } \epsilon_i) = \frac{\log_{10}(\text{TI-204 } \epsilon_i) + [\log_{10}(\text{Tc-99 } \epsilon_i) - \log_{10}(\text{TI-204 } \epsilon_i)] \times [\log_{10}(\text{Cs-137 } E_{MAX}) - \log_{10}(\text{TI-204 } E_{MAX})]}{[\log_{10}(\text{Tc-99 } E_{MAX}) - \log_{10}(\text{TI-204 } E_{MAX})]} \quad \text{Eq. A.7}$$

As in Case 1, the hypothetical I/A levels are for general gross beta radioactivity (dpm/100 cm<sup>2</sup> of beta activity), and the RFs will sum to 1.0. Relative fractions of Co-60, Cs-137, and Ni-63 are 0.50, 0.20, and 0.30, respectively, and gross measurements will be made using a gas proportional detector with a 0.4-mg/cm<sup>2</sup> Mylar window operated on the alpha-plus-beta voltage plateau (essentially all detector response is assumed to be the result of beta interactions). The 0.4-mg/cm<sup>2</sup> Mylar window is selected to measure the low-energy beta from Ni-63—thicker Mylar windows would limit or preclude detection. Note also that the Ni-63  $E_{MAX}$  is less than the 0.150-MeV energy threshold of detectability given in ISO 7503-1:1988.

Exhibit 2 presents results where the total weighted efficiency of 0.11 is calculated, and assuming an average background of 390 cpm for the 126-cm<sup>2</sup> gas proportional detector, the gross beta radioactivity static MDC is 655 dpm/100 cm<sup>2</sup>.

The instrument efficiencies for both Co-60 and Cs-137 shown in Table A-20 of Exhibit 2 were interpolated, noting that the low-energy beta from Ni-63 is below the default surface efficiency threshold of 0.150 MeV associated with a surface efficiency of 0.25, as given in ISO 7503-1:1988. However, the planning team noted that the beta transmission factor was reduced by less than a factor of 4 between the Ni-63 instrument efficiency with the 0.4-mg/cm<sup>2</sup> (Case 2) and 0.8-mg/cm<sup>2</sup> (Case 1) Mylar windows. Based on this and the assumption that surveys were to be performed on smooth surfaces with minimal overlying inactive material, the planning team determined that the default 0.25 surface efficiency would be applied resulting in a low (0.01) but nonzero Ni-63 total efficiency.

### A.3.3 Case Study 3—ROCs: Mixed Fission and Activation Products, HTD, and Am-241

Case 3 is a more complex example that includes the beta-emitting ROCs Cs-137 and Sr/Y-90 and H-3, which is nondetectable with the available detectors ( $\epsilon_i = 0$ ). Additionally, the beta-emitters are commingled with an alpha-emitter, Am-241. Measurement options are the following:

- separate alpha and beta measurements with results independently compared with the Am-241 action level and a gross beta action level followed by application of the unity rule (Equation 4-3 in NUREG-1575, Revision 1, “Multi-Agency Radiation Survey and Site Investigation Manual (MARSSIM),” issued August 2000)
- alpha-plus-beta measurements and data comparison to a gross activity action level (Equation 4-4 in NUREG-1575)

For this case study, separate alpha and beta measurements will be made and the unity rule (NUREG-1575, Equation 4-3) applied when compliance with an I/A level is relevant.

To account for the HTD (H-3), there are also two primary options:

- Modify the action level of one of the detectable contaminants per the surrogate radionuclide methodology (NUREG-1575, Equation 4-1), in which case the efficiency determination will not need to account for the HTD.
- Include the HTD in the gross activity action level and also in the total weighted efficiency determination.

The selected measurement option will be to include the HTD in the total weighted efficiency for gross alpha-plus-beta activity and the corresponding gross activity action level (dpm/100 cm<sup>2</sup> of the combined alpha-plus-beta surface activity for all the ROCs). The ROC RFs would therefore sum to 1.0 and, for this example, are established as H-3 = 0.1, Cs-137 = 0.3, Sr/Y-90 = 0.2, Am-241 = 0.4 (note that Sr-90 and Y-90 are in equilibrium, and each contributes an RF of 0.1).

The measurements are planned using a plastic scintillator with a 1.2-mg/cm<sup>2</sup> Mylar window. The plastic scintillator is specifically selected to demonstrate the detector's response to alpha-emitters, though this instrument is sometimes considered a beta-only detector.

The calibration sources represent both the Am-241 and the Sr-90, in combination with Y-90, and the instrument efficiencies are obtained directly from Exhibit 3a, Table A-21. However, Cs-137 is not represented, and therefore, its  $\epsilon_i$  value must be determined, either via one of the available sources as an analog or interpolation from a beta energy calibration curve. Exhibit 3a and all remaining exhibits use the calibration curve. H-3 is not detectable and is assigned an  $\epsilon_i$  and  $\epsilon_s = 0$  in Exhibit 3a.

Exhibit 3a presents the weighted efficiency and corresponding MDC results in terms of the ROCs' gross alpha-plus-beta activity. The calculated  $\epsilon_t = 0.19$ , and assuming an average background of 540 cpm for the 100-cm<sup>2</sup> plastic scintillator, the gross radioactivity (alpha-plus-beta) static MDC is 596 dpm/100 cm<sup>2</sup>. Note the detector's 0.62  $\epsilon_i$  for the Am-241 alpha emission in Exhibit 3a.

As introduced above, the beta- and alpha-emitters of this scenario may also be assessed independently. That is, there may be separate gross beta activity and gross alpha activity I/A levels. In this case, the weighted beta  $\epsilon_t$  (thus the MDC) would be calculated based on the RF relationship for each beta-emitting ROC relative to its contribution to the beta ROC mixture. Tables A-22 and A-23 of Exhibit 3b consider the same contaminant mixture (H-3, Cs-137, Sr/Y-90, and Am-241) and calculates separate beta and alpha  $\epsilon_t$ s and MDCs. As separate alpha and beta measurements will be performed, the 40-percent RF Am-241 contributed to the ROC mixture is removed, and the RF for each beta-emitting ROC is recalculated based on the respective contribution to the beta mixture with the result of H-3 = 0.17, Cs-137 = 0.50, and Sr/Y-90 = 0.34.<sup>2</sup>

Note that the Exhibit 3b - Beta RFs now sum to 1.0 rather than 0.6 as seen in Exhibit 3a for the alpha-plus-beta measurement. Because a plastic scintillator will respond to alpha emissions, gas proportional detectors will be used. The beta detector will have a 3.8-mg/cm<sup>2</sup> Mylar window that will eliminate the Am-241 alpha response. A separate gas proportional detector, operated at the alpha-only plateau and fitted with a standard 0.8-mg/cm<sup>2</sup> Mylar window, will be used for the Am-241 measurements.

---

<sup>2</sup>RF is 1.01 because of rounding.

Exhibit 3b - Beta presents the weighted beta  $\epsilon_t$  of 0.16, and assuming an average background of 380 cpm for the 126-cm<sup>2</sup> gas proportional detector, the gross beta static MDC is 468 dpm/100 cm<sup>2</sup>.

Exhibit 3b - Alpha presents the weighted alpha  $\epsilon_t$  for Am-241 of 0.12, and assuming an average alpha background of 2 cpm for the 126-cm<sup>2</sup> gas proportional detector, the gross alpha static MDC is 63 dpm/100 cm<sup>2</sup>.

#### A.3.4 Case Study 4—Thorium Series Calibration

Case 4 involves the thorium decay series, which contains multiple alpha and beta emissions. The complexity of the decay scheme requires that the design of the total efficiency calibration method accurately reflects the field measurement method that will be used to assess residual activity on surfaces. The method for developing  $\epsilon_t$  will be based on whether alpha-only, alpha-plus-beta, or beta-only measurements will be used to quantify the surface activity and how the dpm/100 cm<sup>2</sup> measurement results will be expressed. That is, the residual activity may be expressed in terms of either the gross thorium-series radioactivity, or alternatively, it may be normalized to be stated in terms of just the Th-232 activity. Table A-13 shows the measurement type and activity reporting (gross activity versus Th-232) options.

**Table A-13 Activity Reporting Options for Thorium Series**

| Measurement Type | Reported Result              |
|------------------|------------------------------|
| alpha            | Total, gross series activity |
| alpha            | Th-232 activity              |
| beta             | Total, gross series activity |
| beta             | Th-232 activity              |
| alpha plus beta  | Total, gross series activity |
| alpha plus beta  | Th-232 activity              |

The Case Study 4 exhibits illustrate three of the six potential calibration combination scenarios:

- 4a. Alpha-plus-beta measurements for total, gross series activity
- 4b. Beta-only measurements for total, gross series activity
- 4c. Beta-only measurements for Th-232 activity

For Exhibit 4a, as shown in Table A-24, the thorium series alpha-plus-beta emissions will be measured using a 126-cm<sup>2</sup> gas proportional detector with a 0.8-mg/cm<sup>2</sup> Mylar window. The detector will operate in the alpha-plus-beta HV plateau region. The case assumes the Th-232 series is in equilibrium at natural abundances and a multipoint calibration is performed to generate the alpha and beta instrument efficiency curves. As previously discussed, although not specifically shown in this case study exhibit, the beta maximum energies are the weighted energies from Table A-9.

In the exhibit, the RFs appear to sum to 1.1. This is because bismuth (Bi)-212 emits both an alpha (at an intensity of 0.36) and a beta (at an intensity of 0.64) and thus is shown in both the alpha section and beta section. This additional complexity is accurately considered by using a weighting factor (WF), as described in Equation A.5. A combined WF will account for both the intensity and the branching ratio and will sum to 1.0 for the weighted  $\epsilon_t$  determination, as the measurement results are to be reported in terms of total activity for the series. The calculated total efficiency is 0.13, and assuming an average background of 390 cpm for the gas proportional detector, the gross alpha-plus-beta static MDC is 570 dpm/100 cm<sup>2</sup>.

Table A-25 of Exhibit 4b illustrates the total weighted efficiency determination for quantifying the total Th-232 decay series gross activity via measurements of the beta-only emissions. The beta-only measurements may provide more representative results when surface conditions are highly variable and result in greater uncertainty in quantifying the alpha emission component. The weighted  $\epsilon_t$  calculation is shown for a gas proportional detector operated at the alpha-plus-beta plateau with a 3.8-mg/cm<sup>2</sup> Mylar window. The efficiencies for all alpha-emitters are zero when using the Mylar window with a higher density thickness. In this exhibit, the RFs again sum to 1.1 because Bi-212 is listed in both the alpha and beta sections, and the WF sums to 1. With a total efficiency estimate of 0.05, and assuming an average background of 380 cpm for the 126-cm<sup>2</sup> gas proportional detector, the gross beta static MDC is 1,393 dpm/100 cm<sup>2</sup>.

Finally, Table A-26 of Exhibit 4c presents an alternative approach to that used in Exhibit 4b (beta-only measurements) by calculating a  $\epsilon_t$  and the MDC specifically in terms of Th-232. This requires that the RFs are normalized relative to the Th-232 rather than the series gross activity fractions (i.e., the RFs will sum to a value greater than 1.0). If a beta measurement is collected for this instrument configuration, and the 0.53 efficiency is applied, the result is interpreted as dpm/100 cm<sup>2</sup> of Th-232, even though Th-232 is an alpha-emitter. Assuming an average background of 380 cpm for the 126-cm<sup>2</sup> gas proportional detector, the Th-232 static MDC is 139 dpm/100 cm<sup>2</sup>. Note that this result is directly comparable to the gross beta measurement in Exhibit 4b. That is, the static MDC for gross beta (1,393 dpm/100 cm<sup>2</sup>) divided by the sum of the ratios (10) is equal to the Th-232 static MDC of 139 dpm/100 cm<sup>2</sup>.

### **A.3.5 Uranium Recovery Facility Case Studies**

Title 10 of the *Code of Federal Regulations* (10 CFR) Part 20, "Standards for Protection against Radiation," and 10 CFR Part 40, "Domestic Licensing of Source Material," require uranium recovery facilities to conduct environmental monitoring and health physics surveys to protect worker health, the public, and the environment. Regulatory guidance, NUREG-series publications, licensing conditions, Regulatory Guide 8.30, "Health Physics Surveys in Uranium Recovery Facilities," issued May 2002, and Policy and Guidance Directive FC 83-23 provide radiological survey guidance for facilities conducting routine operational and equipment release surveys in support of license termination.

The detector calibration and measurement methods in this section are specific to the scenarios that may be encountered during radiological surveys within uranium recovery facilities. The parameters discussed in the previous multiple ROC case studies for determining the total detector efficiency and subsequent MDC calculations are similarly applied. Their application requires the characterization of the ROC emissions, selection of the measurement methods, and selection of the way in which the residual uranium or other surface activity levels will be expressed.

Ore processing at conventional mills or heap leach facilities results in two radiological streams: (1) the separated uranium isotopes processed into the yellowcake product and (2) tailings/heap piles containing essentially all the long-lived decay series progeny originally present in the ore, beginning with Th-230, as well as a small amount of unrecovered uranium.

For in situ recovery, the pregnant lixiviant extracted for processing contains the uranium isotopes with most of the decay series byproducts remaining in the ore body. Some Th-230 and Ra-226 will be present in both the pregnant lixiviant and the barren lixiviant following ion exchange. The Th-230 and Ra-226 concentrations, and therefore the RFs, will vary between facilities and are evaluated for each site based on process knowledge and analysis of the lixiviant. The type of uranium recovery operation (i.e., conventional mill, heap leach, or in situ recovery) will affect the ROC makeup and associated RFs. Conventional mills and heap leach operations would have both the raw uranium ore, which will include the natural uranium isotopes in secular equilibrium with the complete decay series, and also the separated tailings stream, beginning with Th-230 through the remaining decay series. Additionally, there will be contributions from the unrecovered uranium at concentrations less than 10 percent of the tailings ROCs—nominally 7 percent (NUREG-0706, “Final Generic Environmental Impact Statement,” Volume 3, issued September 1980). Uranium separated from the long-lived progeny with varying ingrowths of the immediate short-lived U-238 decay progeny of Th-234 and Pa-234m may impact the recovery precipitation/filtration, drying, and packaging areas of all three facility types. The amount of ingrowth would depend on time since separation, with equilibrium reached within about 6 months. However, the example methods provided for the applicable uranium recovery case studies assume that any residual processed uranium concentrates impacting surfaces or equipment have been present for longer than 6 months and are consistent with aged yellowcake. Therefore, the specific radioactive materials, or combinations thereof, that have affected an area will determine calibration and measurement methods. Interferences from radon and associated decay products and also gamma radiation shine from nearby material inventories may quite possibly increase the detector background and thus result in increased MDCs for the assessment of surface activity on structural surfaces and equipment.

Use of the DQO process can account for the variations in surface contamination radionuclide makeup that may be encountered. Differences in surface materials and the effects on surface efficiency (e.g., considering smooth versus rough surfaces or differing surface materials on tools and equipment) should also be considered. The DQOs will provide the measurement types required, investigative thresholds, and data assessment methods necessary to maintain a high degree of certainty of a correct radiological release decision, while minimizing the probability of an incorrect decision.

#### *A.3.5.1 Uranium Recovery Facility Mixture Description*

This case study begins with the complete uranium chain of unprocessed ore. Therefore, the initial step, as in the mixed contaminant case studies, is to describe the radionuclide mixture. Table A-14 consolidates the radiation data from Tables A-9 and A-10 for the full uranium chain.

**Table A-14 Radiation Data for Uranium (U-238 and U-235) Decay Series (Unprocessed Ore)<sup>a</sup>**

| Radionuclide        | T1/2 (yr) | Emission | Intensity | E<br>alpha: E <sub>AVE</sub> keV<br>beta: E <sub>MAX</sub> keV <sup>b</sup> |
|---------------------|-----------|----------|-----------|---|
| U-238               | 4.47E+09  | alpha    | 1.00      | 4,188   |
| Th-234              | 6.60E-02  | beta     | 1.00      | 1.78E+02  |
| Pa-234m             | 2.21E-06  | beta     | 1.00      | 2.24E+03  |
| U-234               | 2.46E+05  | alpha    | 1.00      | 4,759   |
| Th-230              | 7.54E+04  | alpha    | 1.00      | 4,663   |
| Ra-226              | 1.60E+03  | alpha    | 1.00      | 4,773   |
| Rn-222              | 1.05E-02  | alpha    | 1.00      | 5,485   |
| Po-218              | 5.89E-06  | alpha    | 1.00      | 6,001   |
| Pb-214              | 5.10E-05  | beta     | 1.00      | 7.19E+02  |
| Bi-214              | 3.79E-05  | beta     | 0.99      | 1.27E+03  |
| Po-214              | 5.19E-12  | alpha    | 1.00      | 7,686   |
| Pb-210              | 2.22E+01  | beta     | 1.00      | 2.44E+01  |
| Bi-210              | 1.37E-02  | beta     | 1.00      | 1.16E+03  |
| Po-210              | 3.79E-01  | alpha    | 1.00      | 5,304   |
| U-235               | 7.04E+08  | alpha    | 1.00      | 4,431   |
| Th-231              | 2.91E-03  | beta     | 1.00      | 2.83E+02  |
| Ac-227 <sup>c</sup> | 2.18E+01  | alpha    | 1.00      | 4,948   |

<sup>a</sup> Source is <http://www.nndc.bnl.gov/chart/> (2016).

<sup>b</sup> Weighted for all emissions with intensities of at least 0.1 percent.

<sup>c</sup> Nuclides in the U-235 decay series below actinium (Ac)-227 are conservatively omitted as minor contributors to total efficiency.

Once the full uranium chain is described, then only those specific radionuclides within a portion of the chain applicable to the other uranium processing scenarios (such as processed uranium or tailing streams) would be evaluated. The alpha-to-beta ratios for each of the uranium processing streams are also considered, as they may prove useful for the qualitative investigations that will be presented. Radionuclides below Ac-227 in the U-235 series are excluded as negligible contributors (less than 0.005) to these total weighted efficiency calculations.

#### A.3.5.2 Case Study 5—Uranium Series Measurement Methods and Calibration

Case 5 examines different uranium decay series mixtures during uranium recovery processing at conventional or heap leach mills and in situ recovery facilities.

The complex radionuclide emissions of the uranium processing streams require DQOs to determine whether alpha, alpha-plus-beta, or beta-only measurements will be used to quantify the surface activity. As in the preceding case studies, the efficiency determination, MDC, and ultimately, the reported surface activity levels can be stated in terms of the gross activity of the applicable components of the decay series (e.g., total gross activity, total uranium activity, or otherwise normalized to be stated in terms of an individual radionuclide such as the U-238 activity).



In general, beta-only measurements are recommended because of the expected dusty environments that may attenuate the alpha radiation beyond what can reasonably be accounted for with the ISO 7503-1:1988 default surface efficiency factor. However, alpha measurements may be necessary to achieve required MDCs when conservative (low activity) I/A levels are adopted, when there are ambient background gamma radiation interferences for beta detectors, or for investigations of anomalous surface activity measurements suspected to be from radon progeny deposition.

Table A-14, together with Tables A-15 and A-16 below, and the exhibits present the radionuclide characteristics for the various uranium recovery process streams. Relative fractions are listed to support weighted efficiency calculations when results are reported as gross total uranium.

**Table A-15 Processed Uranium Ore: Uranium-238 Chain**

| Radionuclide | Emission | Weighted Beta E <sub>MAX</sub> (keV) | Relative Fraction <sup>a</sup> |
|--------------|----------|--------------------------------------|--------------------------------|
| U-238        | Alpha    | --                                   | 0.49                           |
| Th-234       | Beta     | 1.78E+02                             | 0.49                           |
| Pa-234m      | Beta     | 2.24E+03                             | 0.49                           |
| U-235        | Alpha    | --                                   | 0.02                           |
| Th-231       | Beta     | 2.83E+02                             | 0.02                           |
| U-234        | Alpha    | --                                   | 0.49                           |

<sup>a</sup>When the reported activity is gross total uranium, the relative fraction for U-234+U-235+U-238 = 1.0.

**Table A-16 Pregnant Lixiviant**

| Radionuclide | Emission | Weighted Beta E <sub>MAX</sub> (keV) | Relative Fraction <sup>a</sup> |
|--------------|----------|--------------------------------------|--------------------------------|
| U-238        | Alpha    | --                                   | 0.391                          |
| Th-234       | Beta     | 1.78E+02                             | 0.391                          |
| Pa-234m      | Beta     | 2.24E+03                             | 0.391                          |
| U-235        | Alpha    | --                                   | 0.018                          |
| Th-231       | Beta     | 2.83E+02                             | 0.018                          |
| U-234        | Alpha    | --                                   | 0.396                          |
| Th-230       | Alpha    | --                                   | 0.075                          |
| Ra-226       | Alpha    | --                                   | 0.121                          |

<sup>a</sup>When the reported activity is gross total uranium, the relative fraction for U-234+U-235+U-238 = 1.0.

Table A-27 of Exhibit 5a and Table A-28 of Exhibit 5b present the  $\epsilon_t$  and MDC calculation results for assessing total uranium activity from aged yellowcake via alpha and beta measurements using ZnS and GM detectors, respectively. Exhibit 5a presents a total efficiency of 0.08, and assuming an average background of 2 cpm for the 100-cm<sup>2</sup> ZnS detector, the gross total uranium static MDC is 114 dpm/100 cm<sup>2</sup>. Exhibit 5b presents results for the beta-only measurement using the GM, though gross total uranium results are reported to compare directly to ZnS results. The total efficiency of 0.17 is higher than that of the ZnS detector, but the gross total uranium static MDC of 1,518 dpm/100 cm<sup>2</sup> for the GM is much higher than that for the gas proportional detector.

Table A-29 of Exhibit 5c and Table A-30 of Exhibit 5d present the results for a hypothetical scenario involving a previous spill of pregnant lixiviant. The scenario assumes, through process knowledge and prior analyses, that both Th-230 and Ra-226 are each present at 10 percent of the total uranium concentrations. A dual phoswich ZnS/plastic scintillator is modeled so that the project can measure either alpha-only or beta-only activity, though in both cases the reported results are in gross total alpha. Using the alpha-only (ZnS) setting as shown in Exhibit 5c, a total efficiency estimate of 0.09 is calculated, and assuming an average background of 2 cpm for the 100-cm<sup>2</sup> ZnS detector, the gross total alpha static MDC is 111 dpm/100 cm<sup>2</sup>. Exhibit 5d presents results for the beta-only (plastic scintillator) measurement. The total efficiency of 0.09 is the same as the ZnS result, though the gross total alpha static MDC of 902 dpm/100 cm<sup>2</sup> is much higher than that for the ZnS.

Finally, Table A-31 of Exhibit 5e presents results for the measurement of unprocessed uranium ore using a gas proportional detector with 0.8-mg/cm<sup>2</sup> Mylar, and assuming equilibrium conditions in the U-238 and U-235 decay series (U-235 series below Ac-227 are excluded as minor contributors to the overall calculation). As in other cases that report gross total uranium, the RFs for U-234, U-235, and U-238 sum to 1.0, and other radionuclide RFs are scaled accordingly. For this case, the total efficiency of 0.99 is calculated, and assuming an average background of 390 cpm for the 126-cm<sup>2</sup> gas proportional detector, the gross total uranium static MDC is 76 dpm/100 cm<sup>2</sup>.

### **A.3.6 Case Study 6—Enriched Uranium and Enriched Uranium with Tc-99**

Case 6a addresses a contaminant that contains 20-percent enriched uranium (EU), such as may be encountered at a uranium enrichment or fuel processing facility. For Case 6b, Tc-99 is added to the contamination under a scenario in which a facility received and recycled spent nuclear fuel materials. The hypothetical I/A levels are for gross radioactivity (total dpm/100 cm<sup>2</sup> of EU and Tc-99), and the project has planned both alpha-only and an alpha-plus-beta measurement. In Case 6b, RFs will sum to 1.0, and Tc-99 produces 17 percent of the total activity when present. In all exhibits, a gas proportional detector with 0.8-mg/cm<sup>2</sup> Mylar is used. In Exhibit 6a, an alpha-only measurement will be made with no Tc-99 present. Exhibit 6b will measure alpha and beta with Tc-99 present.

Table A-32 of Exhibit 6a presents results for the gross alpha measurements for EU. For this case, the total efficiency of 0.10 is calculated, and assuming an average background of 2 cpm for the 126-cm<sup>2</sup> gas proportional detector, the gross alpha static MDC is 72 dpm/100 cm<sup>2</sup>.

Table A-33 of Exhibit 6b presents results for gross alpha-plus-beta measurement. With a total efficiency estimate of 0.11, and assuming an average background of 390 cpm for the 126-cm<sup>2</sup> gas proportional detector, the gross alpha-plus-beta static MDC is 692 dpm/100 cm<sup>2</sup>.

### A.3.7 Case Study 7—Uranium Tailings

Case 7 is similar to Case 5 but addresses processed uranium tailings, as may be encountered at a conventional uranium recovery facility. The hypothetical I/A levels are for gross radioactivity (total dpm/100 cm<sup>2</sup> activity), and the project has planned to report only alpha-plus-beta measurements. Tailings chain constituents are present at approximately 7 times the total uranium value, so nonuranium radionuclides dominate the measurement. Relative fractions are scaled until the RFs sum to 1.0. The approach here is to use a gas proportional detector with 0.8-mg/cm<sup>2</sup> Mylar to measure alpha-plus-beta radioactivity (Exhibit 7a). In this case, the project does not require individual alpha-only or beta-only measurements. This case also includes beta-only measurements using the GM (Exhibit 7b) but reports them as alpha plus beta for comparison with gas proportional detector results. Table A-17 lists relative fractions used for the uranium mill tailings calculations.

**Table A-17 Tailings Chain**

| Radionuclide | Emission | Beta <sub>MAX</sub><br>(keV) | Relative<br>Fraction <sup>b</sup> |
|--------------|----------|------------------------------|-----------------------------------|
| Th-230       | Alpha    | --                           | 0.0972                            |
| Ra-226       | Alpha    | --                           | 0.0972                            |
| Rn-222       | Alpha    | --                           | 0.0972                            |
| Po-218       | Alpha    | --                           | 0.0972                            |
| Pb-214       | Beta     | 7.19E+02                     | 0.0972                            |
| Bi-214       | Beta     | 1.27E+03                     | 0.0972                            |
| Po-214       | Alpha    | --                           | 0.0972                            |
| Pb-210       | Beta     | 2.44E+01                     | 0.0972                            |
| Bi-210       | Beta     | 1.16E+03                     | 0.0972                            |
| Po-210       | Alpha    | --                           | 0.0972                            |

<sup>a</sup>Tailings will also contain the U-238 chain at concentrations.

<sup>b</sup>Relative fractions are 0.0068 for U-234 and U-238 and 0.0003 for U-235 (U-235 can be excluded as a negligible contributor); total relative fraction, including uranium decay products, sums to 1.0.

Table A-34 of Exhibit 7a presents results for the gross alpha-plus-beta measurements. For this case, the total efficiency of 0.15 is calculated, and assuming an average background of 390 cpm for the 126-cm<sup>2</sup> gas proportional detector, the gross alpha-plus-beta static MDC is 509 dpm/100 cm<sup>2</sup>.

Table A-35 of Exhibit 7b presents results for the beta-only measurement using the GM, though gross alpha-plus-beta results are reported to compare directly to gas proportional detector results. The total efficiency of 0.08 is lower than that of the gas proportional detector, and the alpha-plus-beta static MDC of 3,187 dpm/100 cm<sup>2</sup> for the GM is much higher than that for the gas proportional detector.

### A.3.8 Case Study 8—Byproduct Material, Discrete Radium Sources

Case 8 addresses a site that may contain byproduct materials such as discrete sources of radium. The hypothetical release limit is for gross radioactivity (total dpm/100 cm<sup>2</sup> of Ra-226 and decay

products), and the project has planned only alpha-plus-beta measurements. The approach here is to use a gas proportional detector with 0.8-mg/cm<sup>2</sup> Mylar to measure alpha-plus-beta radioactivity. The project does not require individual alpha-only or beta-only measurements. Radium is assumed to be in equilibrium with all associated decay products.

Table A-36 of Exhibit 8a presents results when the RFs sum to 1.0 and gross alpha-plus-beta results are reported. For this case, the total efficiency of 0.15 is calculated, and assuming an average background of 390 cpm for the 126-cm<sup>2</sup> gas proportional detector, the gross alpha-plus-beta static MDC is 490 dpm/100 cm<sup>2</sup>.

Finally, Table A-37 of Exhibit 8b presents an alternate approach to that used in Exhibit 8a (gross alpha-plus-beta results) by calculating the MDC specifically in terms of Ra-226. This requires that the relative fractions are actually concentration ratios relative to the Ra-226 concentration instead of activity fractions (i.e., Ra-226 RF = 1.0 and all RFs sum to a value greater than 1.0). If an alpha-plus-beta measurement is collected for this instrument configuration and the 1.38 total efficiency is applied, the result is interpreted as dpm/100 cm<sup>2</sup> of Ra-226, even though the detector is responding to all alpha- and beta-emitters. Assuming an average background of 390 cpm for the 126-cm<sup>2</sup> gas proportional detector, the Ra-226 static MDC is 54 dpm/100 cm<sup>2</sup>. This result is directly comparable to the alpha-plus-beta measurement in Exhibit 8a. That is, the static MDC for gross alpha-plus-beta (490 dpm/100 cm<sup>2</sup>) divided by the sum of the ratios (9) is equal to the Ra-226 static MDC of 54 dpm/100 cm<sup>2</sup>.

## **A.4 Radon Progeny Interferences**

Radon progeny deposition will affect buildings and surfaces of all types of facilities (not just those for uranium recovery) to varying degrees. Both short-lived and long-lived progeny may adhere to and build up over time on some surfaces. This discussion addresses both the short- and long-lived progeny. Conventional and heap leach mills, for example, will have radon source terms from stockpiled ores and tailings, while in situ recovery operations will have radon at well heads and radon diffusion into the ore body extraction fluids, which may then impact satellite facilities and the central processing plant. Facilities that do not deal specifically with uranium may also be subject to radon-related interferences given that radon is ubiquitous and tends to accumulate in poorly ventilated areas, and the long-lived progeny can accumulate on surfaces that may be targeted for characterization. For example, longer-lived Pb-210 and progeny may build up on certain metal types—for instance galvanized metals—and rusted metal surfaces, probably because of selective electrostatic or physio-chemical adherence of radon daughter-bearing particulates.

Project planners should develop a plan to deal with false positive decisions caused by radon progeny interferences for facilities where radon interferences or long-lived progeny buildups were not the result of licensed activities. Unfortunately, decommissioning projects are left with limited alternatives, three of which are addressed here: (1) adjustments to the MDC, (2) using short-term decay and barrier shielding, and (3) collecting samples. Table A-18 shows the radiological characteristics of radon and radon progeny including all prominent radionuclides (i.e., BR greater than 0.1 percent) in the decay chain starting with radon (Rn)-222 and ending with polonium (Po)-210. Those progeny associated with long-term activity buildup are in bold and italicized.

### **A.4.1 Account for Radon in the MDC Calculation**

This discussion assumes that radon is a natural constituent of background and that no remedial action will be needed because of elevated radon progeny concentrations on a surface. However, radium or other uranium-series decay products may be present because they are associated with the source material. In these cases, the licensees are responsible for assessing the impact of both naturally occurring and process-related radon (to the extent needed to meet dose criteria and assess measurement data).

**Table A-18 Radon Chain**

| Radionuclide                     | Emission            | Average Beta Energy (keV) <sup>a</sup> | Half-Life <sup>a</sup>   |
|----------------------------------|---------------------|--|--------------------------|
| Rn-222                           | Alpha               | --                                     | 3.8 days                 |
| Po-218                           | Alpha               | --                                     | 3.1 minutes              |
| Pb-214                           | Beta                | 223                                    | 26.8 minutes             |
| Bi-214                           | Beta                | 642                                    | 19.9 minutes             |
| Po-214                           | Alpha               | --                                     | 164.3 μ-sec.             |
| <b><i>Pb-210<sup>b</sup></i></b> | <b><i>Beta</i></b>  | <b><i>6.1</i></b>                      | <b><i>22.2 year</i></b>  |
| <b><i>Bi-210</i></b>             | <b><i>Beta</i></b>  | <b><i>389</i></b>                      | <b><i>5.01 days</i></b>  |
| <b><i>Po-210</i></b>             | <b><i>Alpha</i></b> | <b><i>--</i></b>                       | <b><i>138.4 days</i></b> |

<sup>a</sup>Data source: <http://www.nndc.bnl.gov/nudat2/>

<sup>b</sup>Italicized radionuclides may selectively adhere to surfaces, especially galvanized and rusted metals, and build up over several years.

If radon is attributed to background, decommissioning planners would not adjust the relative activity to account for potentially increased radon concentrations (relative activities apply to the contaminant). The only recourse is to increase  $C_B$  (i.e.,  $R_B \times T$ ), the number of background counts, using Equation A.1. Increasing  $C_B$  is relatively straightforward and prudent if the problem is the long-term buildup of Pb-210 and progeny on, for example, rusty surfaces. Background radiation levels on these surfaces should be relatively stable and may be treated in the same way as any other target medium. If, however, the problem is related to short-term (half-life on the order of hours or less) radon progeny buildup,  $C_B$  may be too variable to be incorporated into a usable MDC calculation. For example, because of radon,  $C_B$  may change dramatically with the weather and time of day. Therefore, the conclusions are as follows:

- Planners can adjust the MDC calculation to include contributions from the long-term buildup of Pb-210 and progeny.
- Adjustments to account for short-term buildup of radon progeny are unlikely to avoid false negative decisions.

#### **A.4.2 Short-Lived Progeny Decay and Barriers**

A common method to address potential false positives from recent radon depositions is to simply wait. The effective half-life of short-term radon progeny is 30 minutes. Additionally, Pb-210 with a half-life of over 22 years, is an HTD and will not contribute to a short-term measurement. An elevated measurement suspected to result from the short-term buildup of radon can be repeated after a few hours. Contamination levels of longer lived radionuclides would not change, while radon levels will drop by roughly 75 percent per hour. The area of interest may be covered during this waiting period to preclude additional buildup via aerial deposition. This obviously will not work and could elevate levels if the radon source is behind the surface of interest (e.g., under a slab-on-grade floor or behind a retaining wall). Therefore, the conclusion is as follows:

- The contaminant should not decay in the short term, while short-term radon depositions will decay at rate of about 75 percent per hour.

- The area of interest may be covered to preclude additional aerial radon progeny deposition, assuming the cover functions to separate the surface from potential radon sources.

### **A.4.3 Sampling**

In the broadest sense, sampling can mean the collection of either a smear sample or a volumetric sample, though in this context both represent a measurement of surface activity. The former applies to interferences from short-lived radon progeny. In this case, the 75 percent per hour rule of thumb that applies to the total measurement (fixed plus removable) also applies to the removable fraction on the smear. The latter applies to interferences from surfaces that may be subject to long-term buildup of Pb-210 and progeny. A scraping of rust, for example, can be analyzed via gamma spectroscopy for Po-210, though close coordination with the laboratory may be required to ensure that sample mass is sufficient to produce reliable results. Therefore, the conclusion is as follows:

- Surfaces potentially affected by short-term radon progeny buildup can be smeared and counted to determine if the 75 percent per hour rule of thumb applies.
- Surfaces potentially affected by long-term radon progeny buildup can be scraped, and the scrapings can be analyzed to identify and quantify Po-210.

These conclusions do not definitively solve the problem of radon progeny interferences, which must be addressed on a project-by-project basis. However, these discussions may offer decommissioning project planners some tools to lower the frequency of false positive decisions related to radon progeny buildup.

### **A.5 Summary**

The case studies presented here provide the basic tenets for managing the many possible scenarios at sites affected by multiple radionuclides. The methods outlined, together with knowledge of the contaminant characteristics and access to appropriate reference sources, should enable the user to develop robust, defensible procedures for determining efficiency and MDCs.

## **A.6 Appendix A References**

American National Standards Institute, ANSI N13.49, "Performance and Documentation of Radiological Surveys," New York, NY, 2011.

American National Standards Institute, ANSI N42.33, "American National Standard for Portable Radiation Detection Instrumentation for Homeland Security," New York, NY, 2007.

International Organization for Standardization, ISO 7503-1, "Evaluation of Surface Contamination—Part 1: Beta Emitters and Alpha Emitters (first edition)," Geneva, Switzerland, 1988.

International Organization for Standardization, ISO 7503-3:2016, "Measurement of Radioactivity—Measurement and Valuation of Surface Contamination—Part 3: Apparatus Calibration," Geneva, Switzerland, 2016.

National Nuclear Data Center, Brookhaven National Laboratory, information extracted from the Chart of Nuclides database, <http://www.nndc.bnl.gov/chart/>.

U.S. Nuclear Regulatory Commission, "Final Generic Environmental Impact Statement," NUREG-0706, Vol. 3, Office of Nuclear Material Safety and Safeguards, September 1980.

U.S. Nuclear Regulatory Commission, "Health Physics Surveys in Uranium Recovery Facilities," Regulatory Guide 8.30, Rev. 1, May 2002. U.S. Nuclear Regulatory Commission, "Multi-Agency Radiation Survey and Site Investigation Manual (MARSSIM)," NUREG-1575, Rev. 1, 2000.

U.S. Nuclear Regulatory Commission, "Termination of Byproduct, Source and Special Nuclear Material Licenses," Policy and Guidance Directive FC 83-23, Office of Nuclear Material Safety and Safeguards, November 4, 1983.

U.S. Nuclear Regulatory Commission, Title 10 of the Code of Federal Regulations (10 CFR) Part 20, "Standards for Protection against Radiation."

U.S. Nuclear Regulatory Commission, Title 10 of the Code of Federal Regulations (10 CFR) Part 40, "Domestic Licensing of Source Material."



## **A.7 APPENDIX A - EXHIBIT OVERVIEW**

This appendix presents 19 exhibits for eight combinations of radiological contaminants (i.e., cases). The appendix is organized by ascending case number; in some cases, multiple exhibits are presented to demonstrate results for different detectors or radiation-type measurement (e.g., beta only or alpha plus beta). The 19 exhibits presented are as follows:

- Exhibit 1. C-14 and Tc-99; Beta Only; Gas Proportional Detector
- Exhibit 2. Ni-63, Co-60, and Cs-137; Beta Only; Gas Proportional Detector
- Exhibit 3a. Am-241, H-3, Cs-137, and SrY-90; Alpha Plus Beta; Plastic Scintillator Detector
- Exhibit 3b - Alpha. Am-241, H-3, Cs-137 and SrY-90; Alpha Only; Gas Proportional Detector
- Exhibit 3b - Beta. Am-241, H-3, Cs-137, and SrY-90; Beta Only; Gas Proportional Detector
- Exhibit 4a. Th-232 Plus Decay Series, Alpha Plus Beta, Gas Proportional Detector
- Exhibit 4b. Th-232 Plus Decay Series, Beta Only, Gas Proportional Detector
- Exhibit 4c. Th-232 Plus Decay Series, Alpha Only, Gas Proportional Detector
- Exhibit 5a. Processed U-Aged Yellowcake, Alpha Only, ZnS Detector
- Exhibit 5b. Processed U-Aged Yellowcake, Beta Only, GM Detector
- Exhibit 5c. Processed U-Pregnant Lixiviant, Alpha Only, Dual Phoswich (ZnS) Detector
- Exhibit 5d. Processed U-Pregnant Lixiviant, Beta Only, Dual Phoswich (Plastic Scintillator) Detector
- Exhibit 5e. Unprocessed U Ore, Alpha Plus Beta, Gas Proportional Detector
- Exhibit 6a. Enriched U, Alpha-Only, Gas Proportional Detector
- Exhibit 6b. Enriched U and Tc-99, Alpha Plus Beta, Gas Proportional Detector
- Exhibit 7a. Processed U Tailings, Alpha Plus Beta, Gas Proportional Detector
- Exhibit 7b. Processed U Tailings, Beta Only, GM Detector
- Exhibit 8a. Ra-226 Plus Decay Series, Alpha Plus Beta, Gas Proportional Detector
- Exhibit 8b. Ra-226 Plus Decay Series, Alpha Plus Beta, Gas Proportional Detector



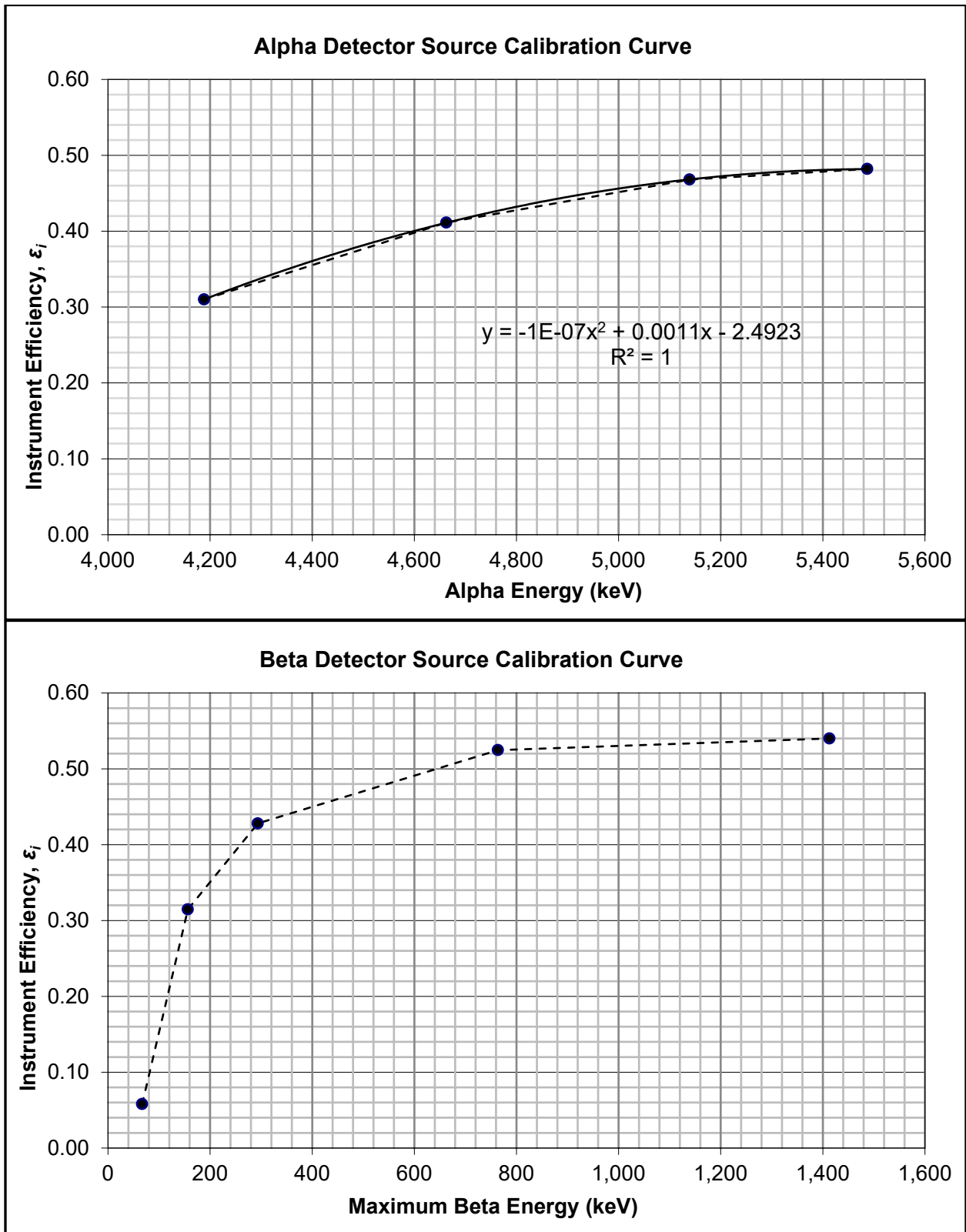


Figure A-3 Exhibit 1. C-14 and Tc-99, Beta-Only, Gas Proportional Detector



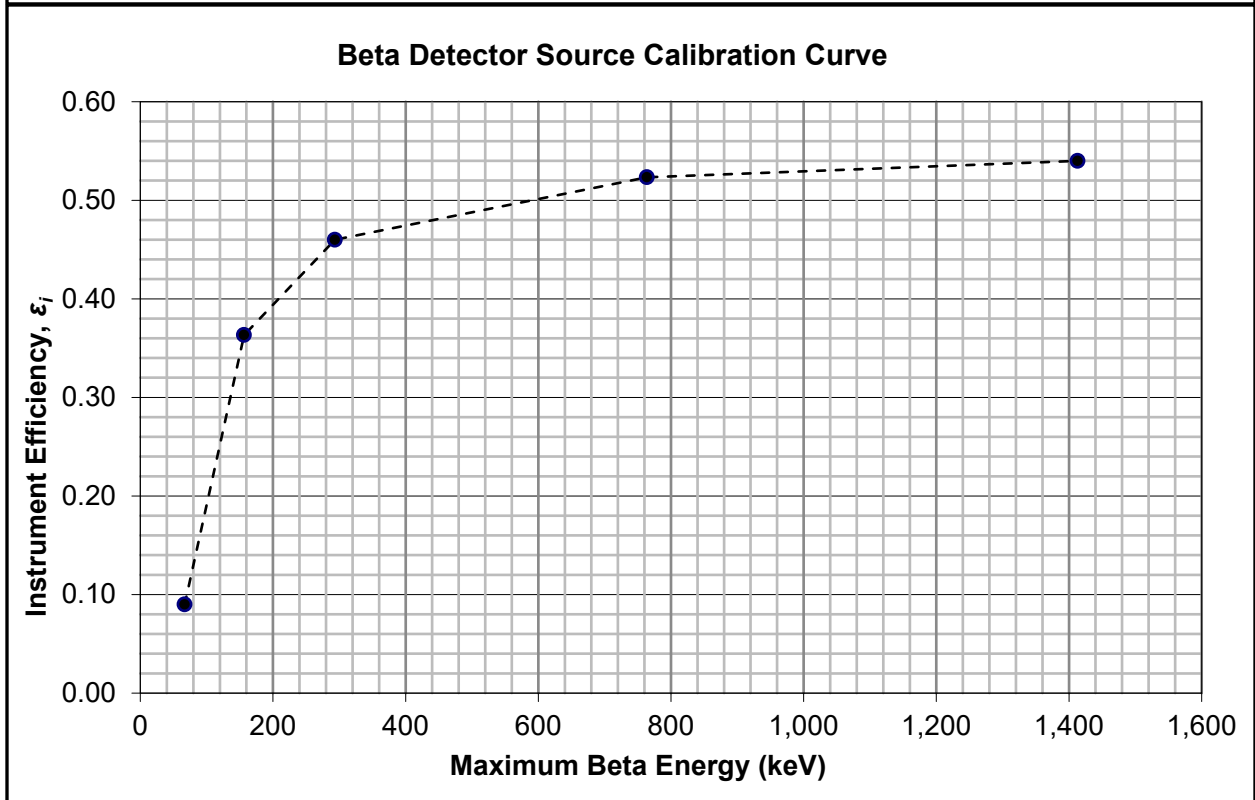
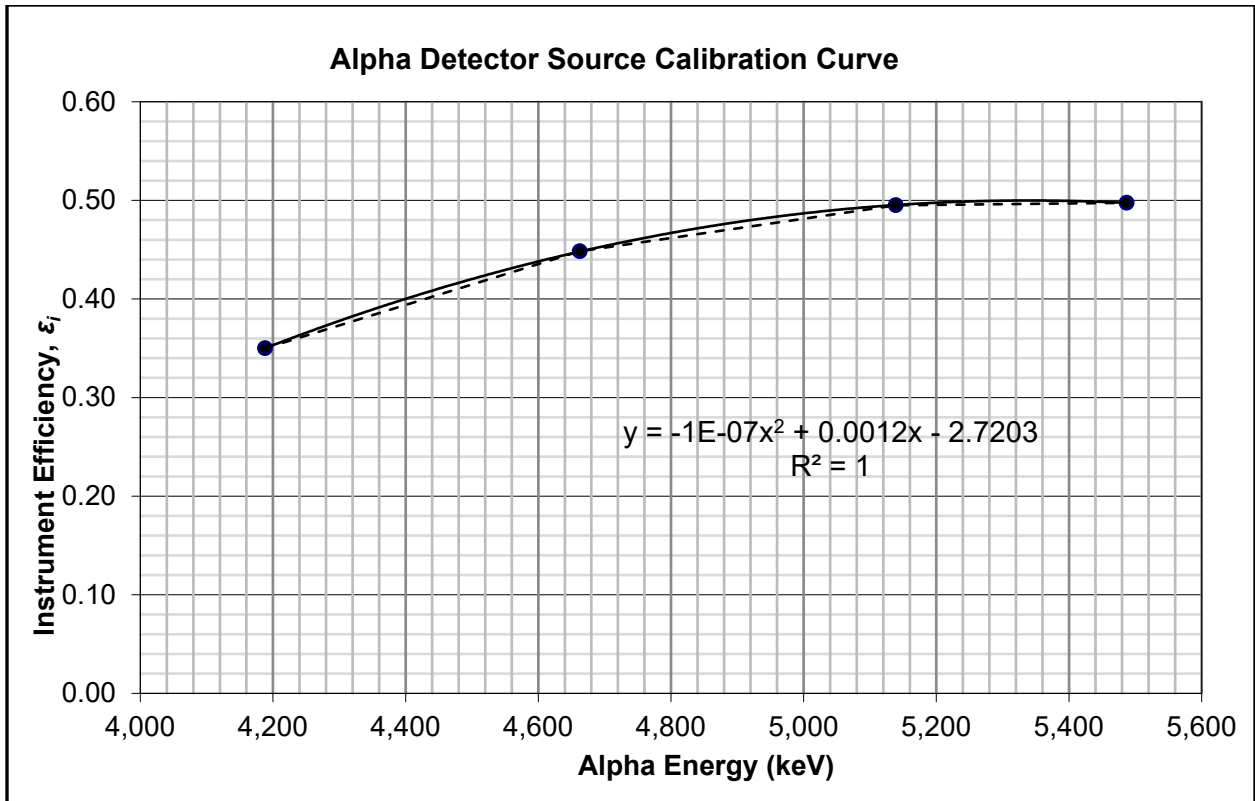
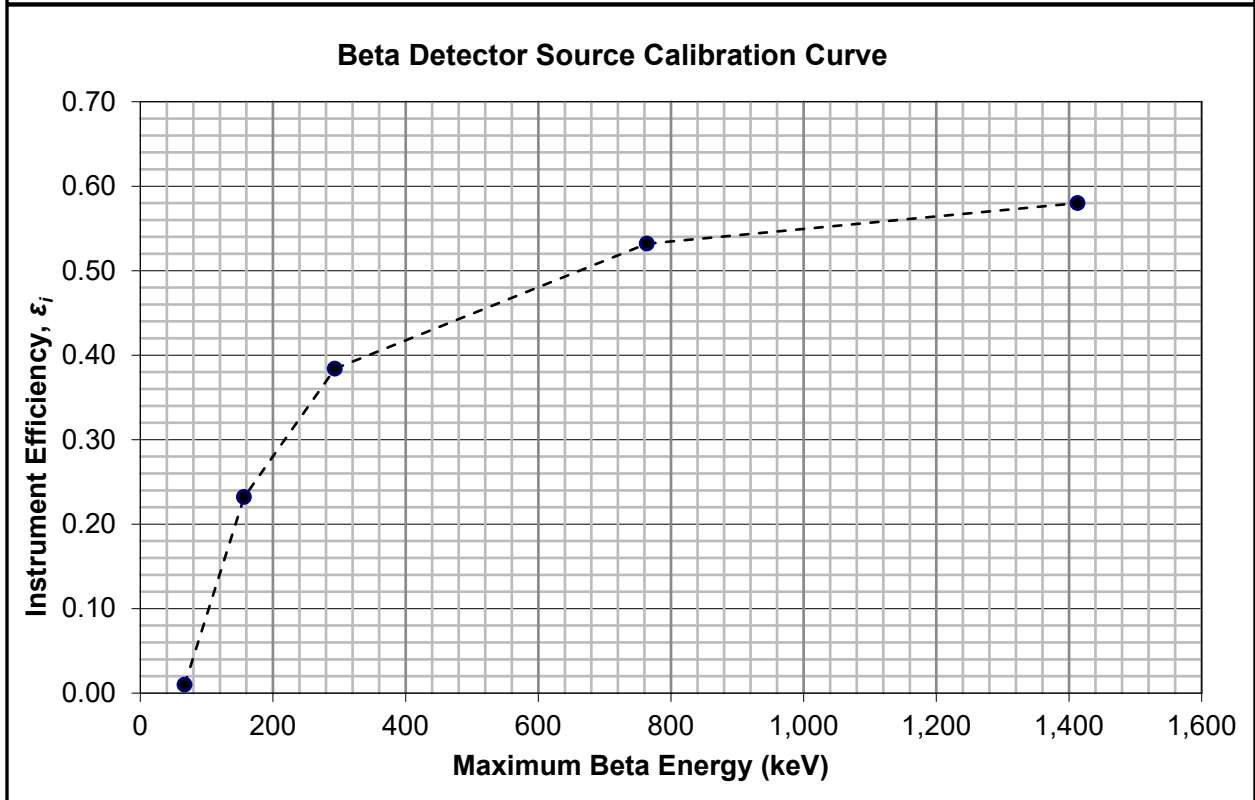
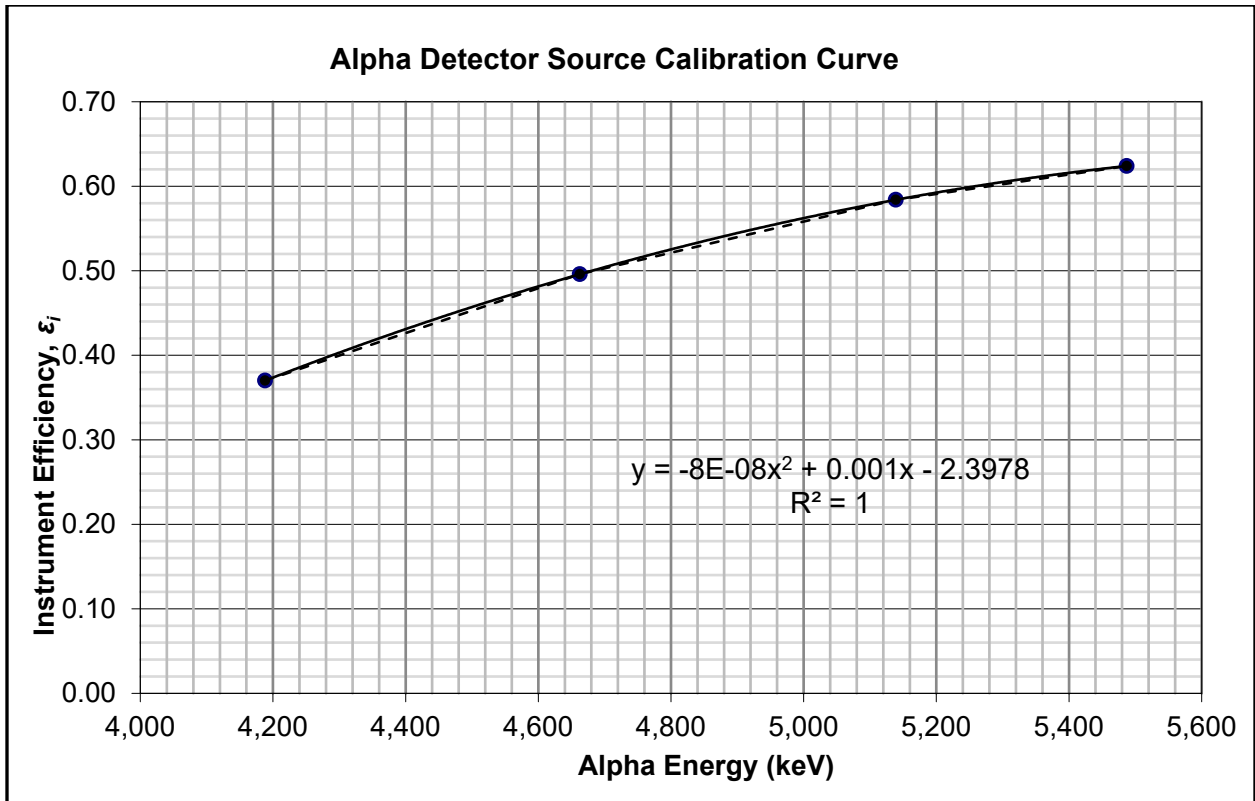


Figure A-4 Exhibit 2. Ni-63, Co-60 and Cs-137, Beta-Only, Gas Proportional Detector





**Figure A-5 Exhibit 3a. Am-241, H-3, Cs-137 and SrY-90, Alpha Plus Beta, Plastic Scintillator Detector**





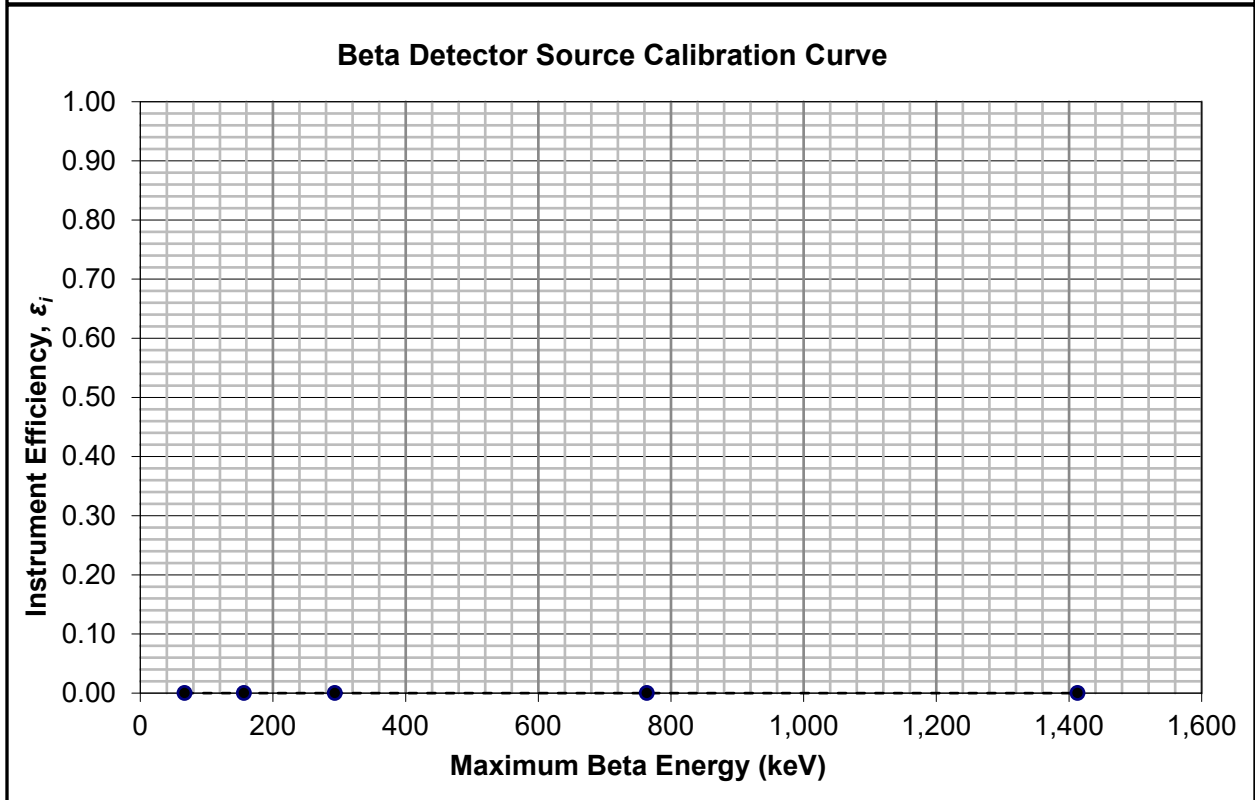
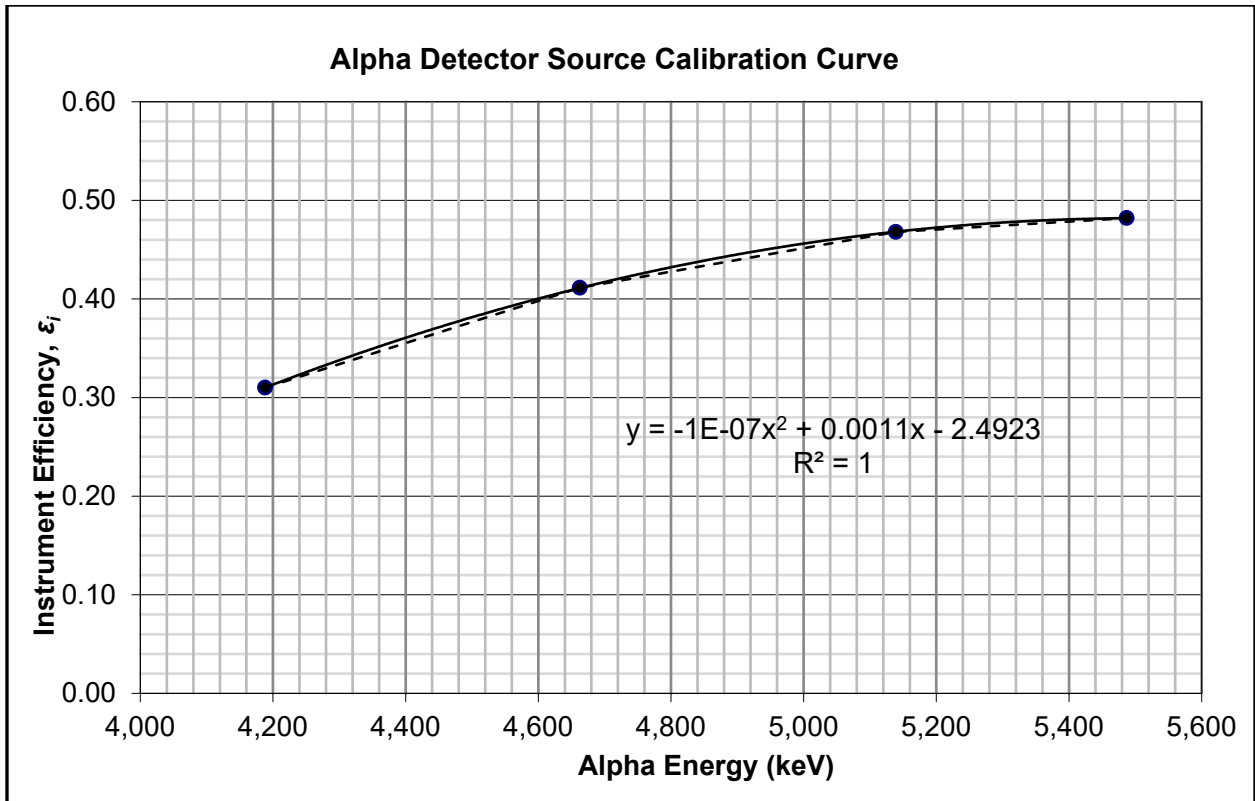


**Figure A-6 Exhibit 3b - Alpha. Am-241, H-3, Cs-137 and SrY-90, Alpha-Only, Gas Proportional Detector**



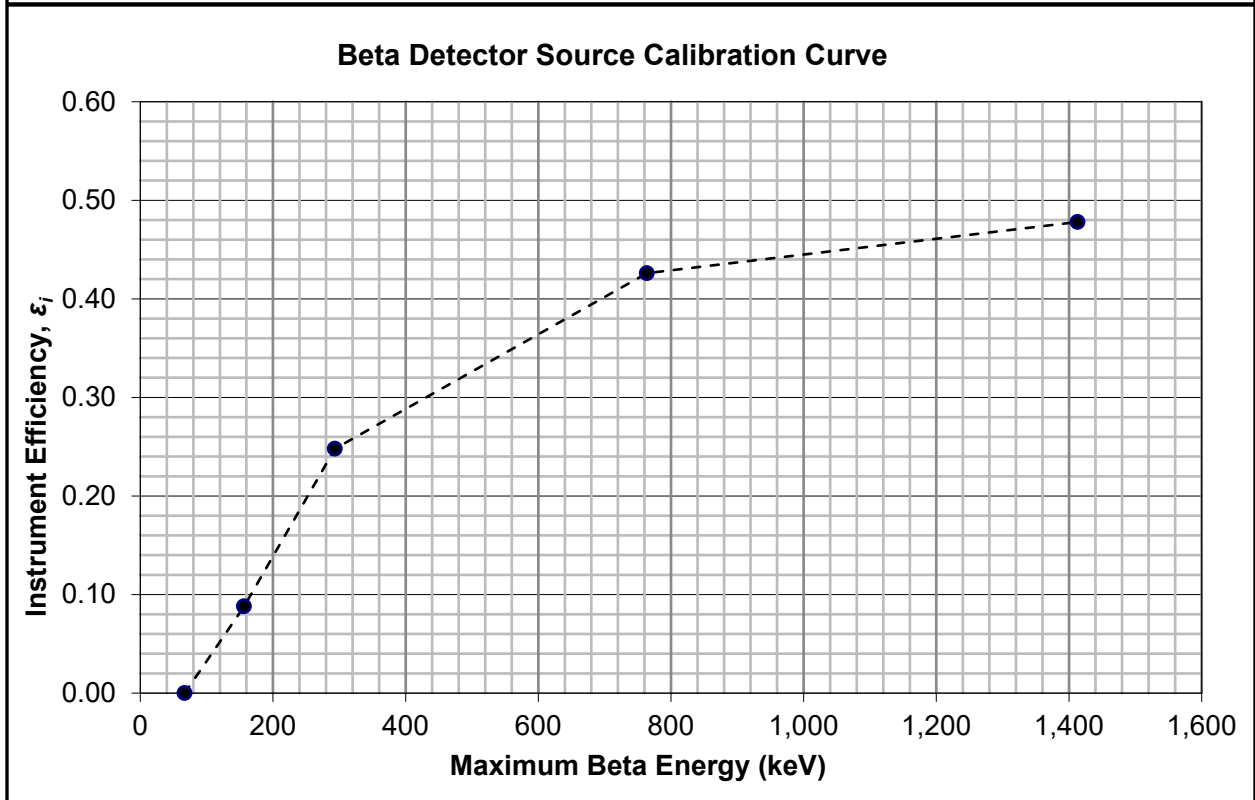
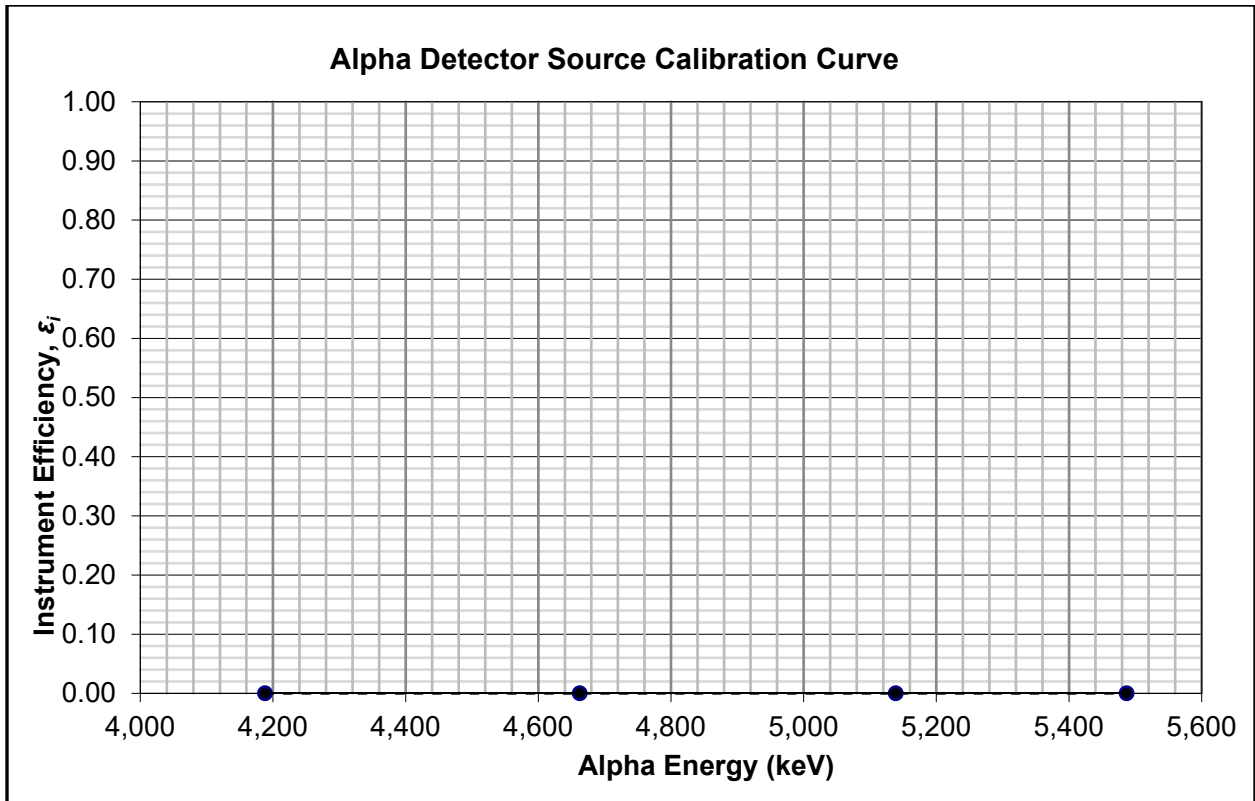


**Figure A-7 Exhibit 3b - Beta. Am-241, H-3, Cs-137, and SrY-90, Beta-Only, Gas Proportional Detector**

**Table A-24 Exhibit 4a. Th-232 Plus Decay Series, Alpha Plus Beta, Gas Proportional Detector**

|                              |       |  |
|------------------------------|-------|--|
| Rateometer/Scaler Model:     | 2221  | <b>Worksheet Results</b>                   |
| Detector Model:              | 43-68 |  |
| Mylar (mg/cm <sup>2</sup> ): | 0.8   |  |
| Voltage Setting (volts):     | 1,750 |  |
| Measured Radiation Type:     | α+β   |  |
|                              |       | Reported Result: Gross α+β                 |
|                              |       | Total Efficiency (Σ ε <sub>i</sub> ): 0.13 |
|                              |       | Static MDC (dpm/100 cm <sup>2</sup> ): 570 |
|                              |       | Scan MDC (dpm/100 cm <sup>2</sup> ): 1,472 |

| Instrument Calibration Data, Source, and MDC Inputs |           |                           |                           |                |  |  |  |  |
|---|-----------|---------------------------|---------------------------|----------------|--|--|--|--|
| Standard Source Inputs                              |           |                           |                           |                | Static and Scan MDC Inputs   |  |  |  |
| Nuclide   | Radiation | Mean E (keV) <sup>a</sup> | Max. E (keV) <sup>a</sup> | ε <sub>i</sub> |  |  |  |  |
| U-238   | Alpha     | 4,188                     | N/A                       | 0.31           | Background (R <sub>b</sub> ) (cpm): 390  |  |  |  |
| Th-230  | Alpha     | 4,663                     | N/A                       | 0.41           | Probe Area (cm <sup>2</sup> ): 126   |  |  |  |
| Pu-239  | Alpha     | 5,139                     | N/A                       | 0.47           | Count Time (t) (min): 1  |  |  |  |
| Am-241  | Alpha     | 5,487                     | N/A                       | 0.48           | Observation Interval (i) (sec): 2  |  |  |  |
| Ni-63   | Beta      | 17.4                      | 66.9                      | 0.06           | Index of Sensitivity (d') (unitless): 1.96   |  |  |  |
| C-14  | Beta      | 49.5                      | 156                       | 0.31           | Surveyor Efficiency (p) (unitless): 0.75   |  |  |  |
| Tc-99   | Beta      | 84.6                      | 294                       | 0.43           | $\text{Static MDC} = \frac{3 + 4.65\sqrt{R_b \times t}}{t \times \epsilon_t \times \frac{\text{Probe Area}}{100}}$                           |  |  |  |
| Tl-204  | Beta      | 244                       | 764                       | 0.52           |  |  |  |  |
| Sr/Y-90   | Beta      | 565                       | 1,413                     | 0.54           | $\text{Scan MDC} = \frac{d' \times \sqrt{R_b \times (i/60)} \times (60/i)}{\sqrt{p} \times \epsilon_t \times \frac{\text{Probe Area}}{100}}$ |  |  |  |

| Weighted Efficiency Input/Output Table |                 |                 |                           |                           |                   |                |                |                             |
|--|-----------------|-----------------|---------------------------|---------------------------|-------------------|----------------|----------------|-----------------------------|
| Nuclide                                | Half-Life (yrs) | Total Intensity | Mean E (keV) <sup>a</sup> | Max. E (keV) <sup>a</sup> | Relative Fraction | ε <sub>i</sub> | ε <sub>s</sub> | ε <sub>t</sub> <sup>b</sup> |
| <b>Beta Emitters</b>                   |                 |                 |                           |                           |                   |                |                |                             |
| Ra-228                                 | 5.75E+00        | 1.00            | 7.2                       | 29                        | 0.10              | 0.00           | 0.25           | 0.00                        |
| Ac-228                                 | 7.02E-04        | 1.00            | 349                       | 1,050                     | 0.10              | 0.53           | 0.50           | 0.03                        |
| Pb-212                                 | 1.21E-03        | 1.00            | 100                       | 351                       | 0.10              | 0.44           | 0.25           | 0.01                        |
| Bi-212                                 | 1.15E-04        | 0.64            | 771                       | 2,090                     | 0.10              | 0.54           | 0.50           | 0.02                        |
| Tl-208                                 | 5.81E-06        | 1.00            | 559                       | 1,580                     | 0.04              | 0.54           | 0.50           | 0.01                        |
|  |                 |                 |                           |                           |                   |                |                |                             |
|  |                 |                 |                           |                           |                   |                |                |                             |
|  |                 |                 |                           |                           |                   |                |                |                             |
|  |                 |                 |                           |                           |                   |                |                |                             |
|  |                 |                 |                           |                           |                   |                |                |                             |
|  |                 |                 |                           |                           |                   |                |                |                             |
|  |                 |                 |                           |                           |                   |                |                |                             |
| <b>Alpha Emitters</b>                  |                 |                 |                           |                           |                   |                |                |                             |
| Th-232                                 | 1.40E+10        | 1.00            | 3,994                     | N/A                       | 0.10              | 0.26           | 0.25           | 0.01                        |
| Th-228                                 | 1.91E+00        | 1.00            | 5,402                     | N/A                       | 0.10              | 0.48           | 0.25           | 0.01                        |
| Ra-224                                 | 1.00E-02        | 1.00            | 5,672                     | N/A                       | 0.10              | 0.48           | 0.25           | 0.01                        |
| Rn-220                                 | 1.76E-06        | 1.00            | 6,287                     | N/A                       | 0.10              | 0.48           | 0.25           | 0.01                        |
| Po-216                                 | 4.60E-09        | 1.00            | 6,778                     | N/A                       | 0.10              | 0.48           | 0.25           | 0.01                        |
| Bi-212                                 | 1.15E-04        | 0.36            | 6,044                     | N/A                       | 0.10              | 0.48           | 0.25           | 0.00                        |
| Po-212                                 | 9.48E-15        | 1.00            | 8,785                     | N/A                       | 0.06              | 0.48           | 0.25           | 0.01                        |
|  |                 |                 |                           |                           |                   |                |                |                             |
|  |                 |                 |                           |                           |                   |                |                |                             |
|  |                 |                 |                           |                           |                   |                |                |                             |
|  |                 |                 |                           |                           |                   |                |                |                             |

<sup>a</sup>Excludes emission intensities < 0.1%; mean and maximum energies weighted based on emission intensity.

<sup>b</sup>Total efficiency per nuclide is Total Intensity × Relative Fraction × ε<sub>i</sub> × ε<sub>s</sub>.

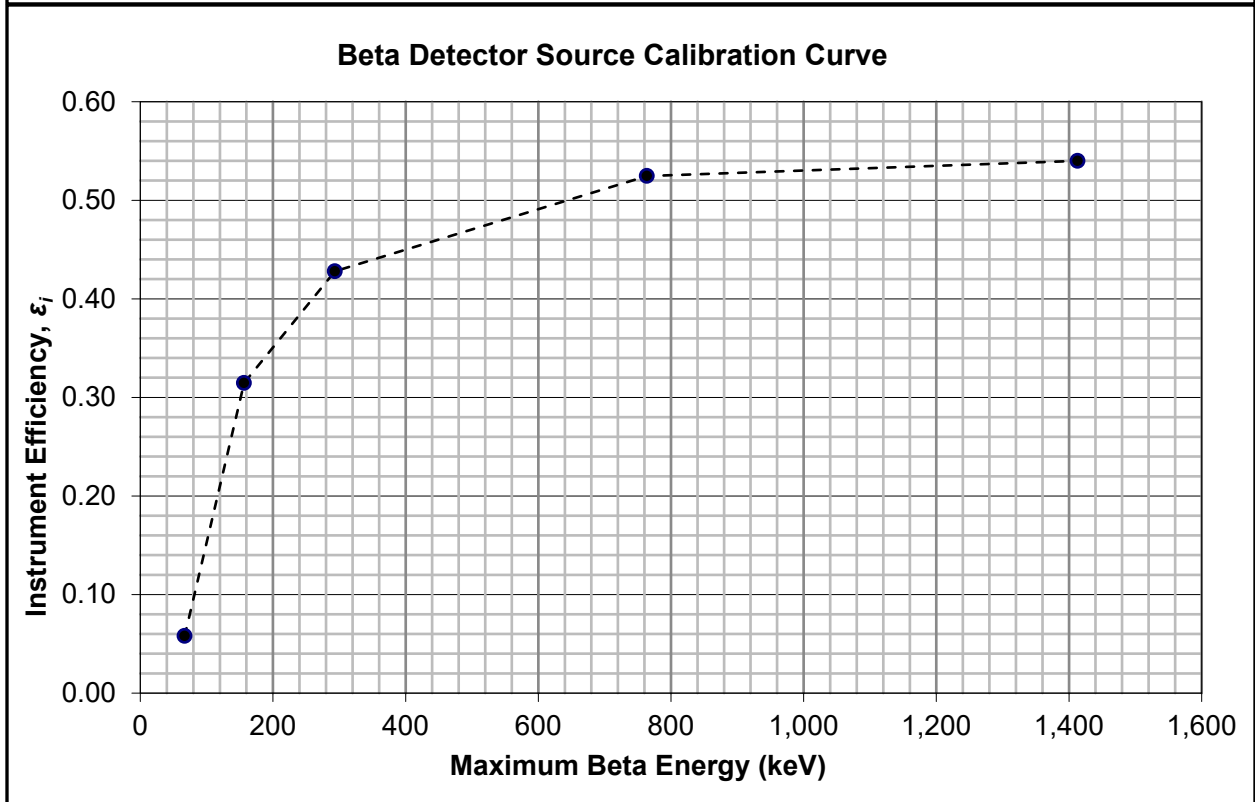
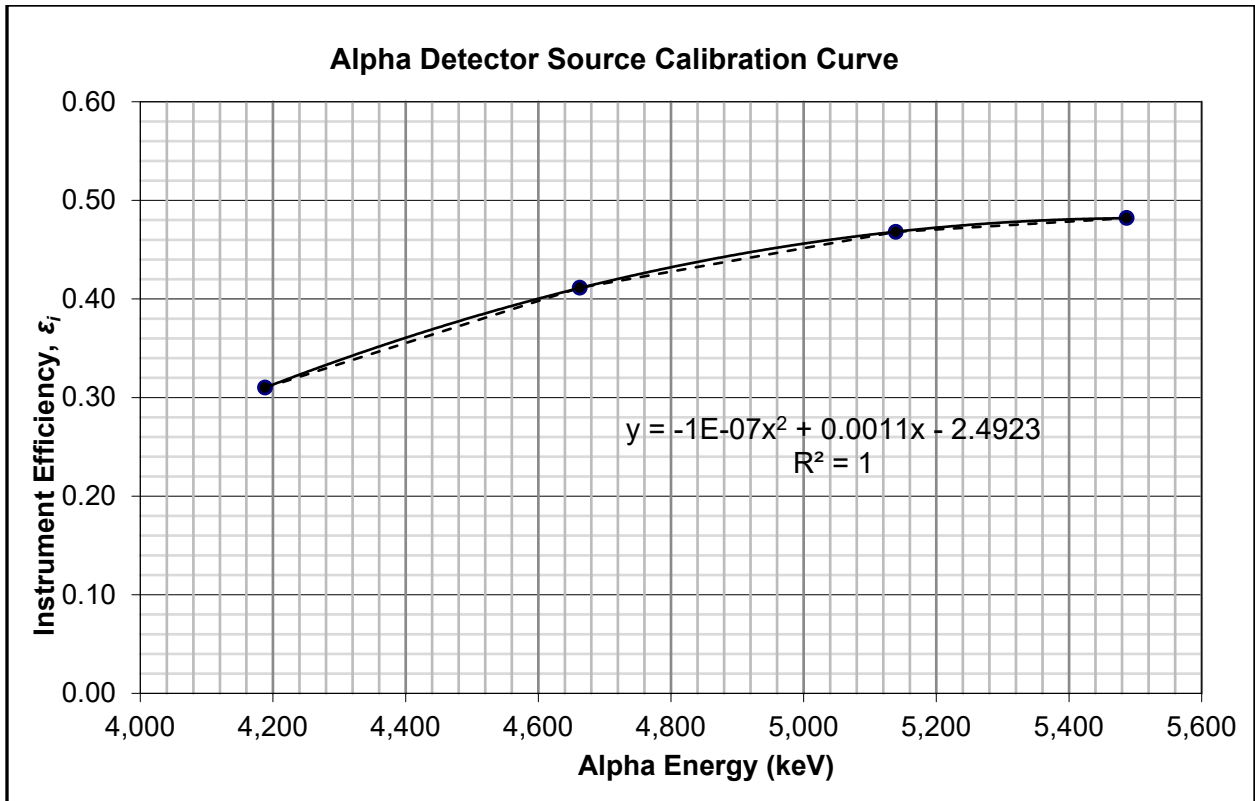


**Figure A-8 Exhibit 4a. Th-232 Plus Decay Series, Alpha Plus Beta, Gas Proportional Detector**

**Table A-25 Exhibit 4b. Th-232 Plus Decay Series, Beta-Only, Gas Proportional Detector**

Ratemeter/Scaler Model: 2221  
 Detector Model: 43-68  
 Mylar (mg/cm<sup>2</sup>): 3.8  
 Voltage Setting (volts): 1,750  
 Measured Radiation Type: β

| Worksheet Results                      |       |
|--|-------|
| Reported Result: Gross α+β             |       |
| Total Efficiency (Σ ε <sub>i</sub> ):  | 0.05  |
| Static MDC (dpm/100 cm <sup>2</sup> ): | 1,393 |
| Scan MDC (dpm/100 cm <sup>2</sup> ):   | 3,594 |

| Instrument Calibration Data, Source, and MDC Inputs |           |                           |                           |                |  |  |
|---|-----------|---------------------------|---------------------------|----------------|--|--|
| Standard Source Inputs                              |           |                           |                           |                | Static and Scan MDC Inputs   |  |
| Nuclide   | Radiation | Mean E (keV) <sup>a</sup> | Max. E (keV) <sup>a</sup> | ε <sub>i</sub> | Background (R <sub>b</sub> ) (cpm): 380  |  |
| U-238   | Alpha     | 4,188                     | N/A                       | 0.00           | Probe Area (cm <sup>2</sup> ): 126   |  |
| Th-230  | Alpha     | 4,663                     | N/A                       | 0.00           | Count Time (t) (min): 1  |  |
| Pu-239  | Alpha     | 5,139                     | N/A                       | 0.00           | Observation Interval (i) (sec): 2  |  |
| Am-241  | Alpha     | 5,487                     | N/A                       | 0.00           | Index of Sensitivity (d') (unitless): 1.96   |  |
| Ni-63   | Beta      | 17.4                      | 66.9                      | 0.00           | Surveyor Efficiency (p) (unitless): 0.75   |  |
| C-14  | Beta      | 49.5                      | 156                       | 0.08           | Static MDC = $\frac{3 + 4.65\sqrt{R_b \times t}}{t \times \epsilon_t \times \frac{Probe\ Area}{100}}$<br>Scan MDC = $\frac{d' \times \sqrt{R_b \times (i/60)} \times (60/i)}{\sqrt{p} \times \epsilon_t \times \frac{Probe\ Area}{100}}$ |  |
| Tc-99   | Beta      | 84.6                      | 294                       | 0.24           |  |  |
| Tl-204  | Beta      | 244                       | 764                       | 0.42           |  |  |
| Sr/Y-90   | Beta      | 565                       | 1,413                     | 0.47           |  |  |

| Weighted Efficiency Input/Output Table |                 |                 |                           |                           |                   |                |                |                             |
|--|-----------------|-----------------|---------------------------|---------------------------|-------------------|----------------|----------------|-----------------------------|
| Nuclide                                | Half-Life (yrs) | Total Intensity | Mean E (keV) <sup>a</sup> | Max. E (keV) <sup>a</sup> | Relative Fraction | ε <sub>i</sub> | ε <sub>s</sub> | ε <sub>t</sub> <sup>b</sup> |
| <b>Beta Emitters</b>                   |                 |                 |                           |                           |                   |                |                |                             |
| Ra-228                                 | 5.75E+00        | 1.00            | 7.2                       | 29                        | 0.10              | 0.00           | 0.25           | 0.00                        |
| Ac-228                                 | 7.02E-04        | 1.00            | 349                       | 1,050                     | 0.10              | 0.45           | 0.50           | 0.02                        |
| Pb-212                                 | 1.21E-03        | 1.00            | 100                       | 351                       | 0.10              | 0.27           | 0.25           | 0.01                        |
| Bi-212                                 | 1.15E-04        | 0.64            | 771                       | 2,090                     | 0.10              | 0.47           | 0.50           | 0.02                        |
| Tl-208                                 | 5.81E-06        | 1.00            | 559                       | 1,580                     | 0.04              | 0.47           | 0.50           | 0.01                        |
|  |                 |                 |                           |                           |                   |                |                |                             |
|  |                 |                 |                           |                           |                   |                |                |                             |
|  |                 |                 |                           |                           |                   |                |                |                             |
|  |                 |                 |                           |                           |                   |                |                |                             |
|  |                 |                 |                           |                           |                   |                |                |                             |
| <b>Alpha Emitters</b>                  |                 |                 |                           |                           |                   |                |                |                             |
| Th-232                                 | 1.40E+10        | 1.00            | 3,994                     | N/A                       | 0.10              | 0.00           | 0.25           | 0.00                        |
| Th-228                                 | 1.91E+00        | 1.00            | 5,402                     | N/A                       | 0.10              | 0.00           | 0.25           | 0.00                        |
| Ra-224                                 | 1.00E-02        | 1.00            | 5,672                     | N/A                       | 0.10              | 0.00           | 0.25           | 0.00                        |
| Rn-220                                 | 1.76E-06        | 1.00            | 6,287                     | N/A                       | 0.10              | 0.00           | 0.25           | 0.00                        |
| Po-216                                 | 4.60E-09        | 1.00            | 6,778                     | N/A                       | 0.10              | 0.00           | 0.25           | 0.00                        |
| Bi-212                                 | 1.15E-04        | 0.36            | 6,044                     | N/A                       | 0.10              | 0.00           | 0.25           | 0.00                        |
| Po-212                                 | 9.48E-15        | 1.00            | 8,785                     | N/A                       | 0.06              | 0.00           | 0.25           | 0.00                        |
|  |                 |                 |                           |                           |                   |                |                |                             |
|  |                 |                 |                           |                           |                   |                |                |                             |

<sup>a</sup>Excludes emission intensities < 0.1%; mean and maximum energies weighted based on emission intensity.

<sup>b</sup>Total efficiency per nuclide is Total Intensity × Relative Fraction × ε<sub>i</sub> × ε<sub>s</sub>.

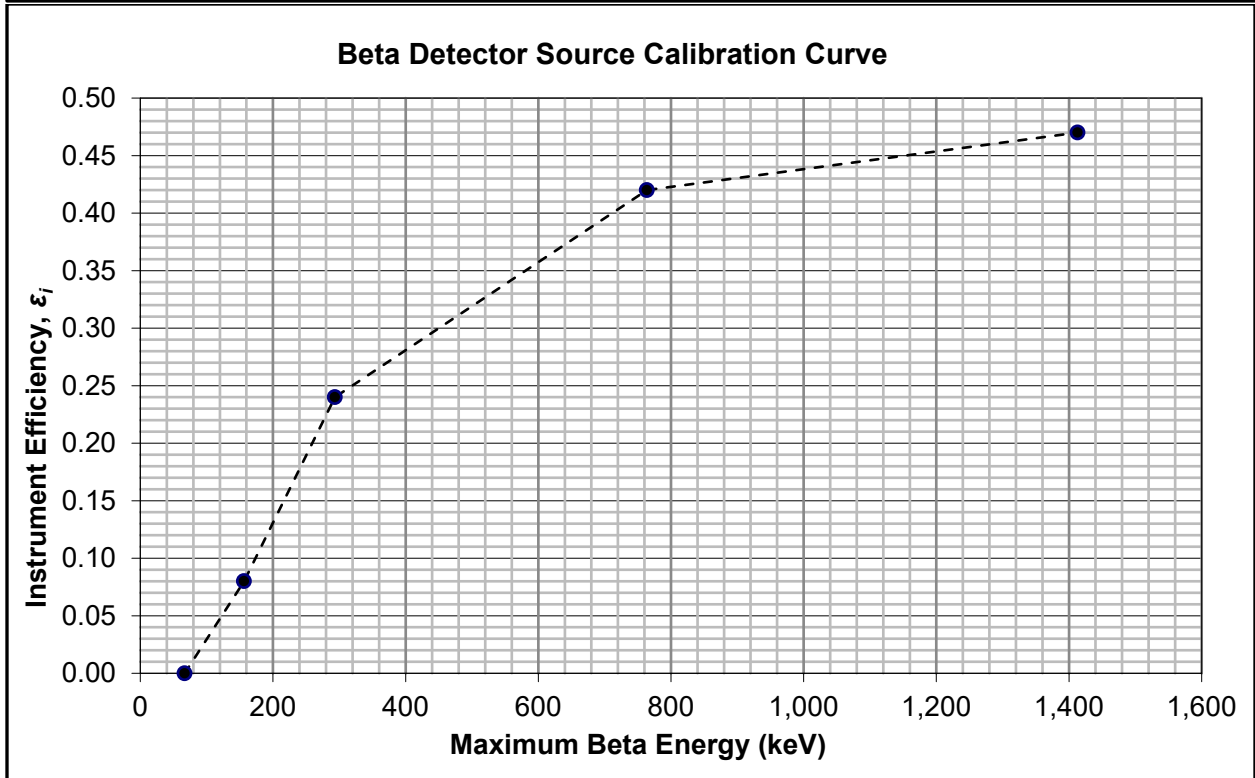
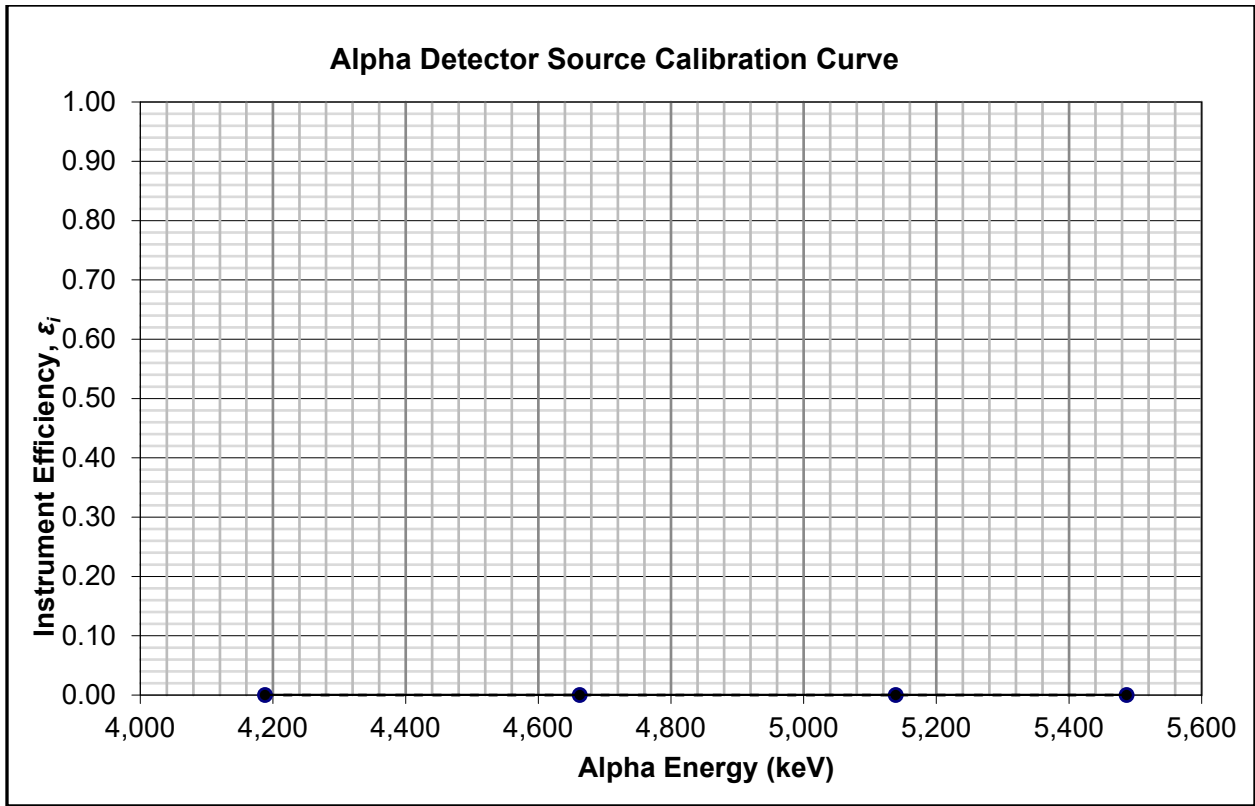


Figure A-9 Exhibit 4b. Th-232 Plus Decay Series, Beta-Only, Gas Proportional Detector

**Table A-26 Exhibit 4c. Th-232 Plus Decay Series, Alpha-Only, Gas Proportional Detector**

**Ratemeter/Scaler Model:** 2221  
**Detector Model:** 43-68  
**Mylar (mg/cm<sup>2</sup>):** 3.8  
**Voltage Setting (volts):** 1,750  
**Measured Radiation Type:** β

| Worksheet Results                      |        |
|--|--------|
| Reported Result:                       | Th-232 |
| Total Efficiency (Σ ε <sub>i</sub> ):  | 0.53   |
| Static MDC (dpm/100 cm <sup>2</sup> ): | 139    |
| Scan MDC (dpm/100 cm <sup>2</sup> ):   | 359    |

| Instrument Calibration Data, Source, and MDC Inputs |           |                           |                           |                |  |  |
|---|-----------|---------------------------|---------------------------|----------------|--|--|
| Standard Source Inputs                              |           |                           |                           |                | Static and Scan MDC Inputs   |  |
| Nuclide   | Radiation | Mean E (keV) <sup>a</sup> | Max. E (keV) <sup>a</sup> | ε <sub>i</sub> |  |  |
| U-238   | Alpha     | 4,188                     | N/A                       | 0.00           | Background (R <sub>b</sub> ) (cpm): 380  |  |
| Th-230  | Alpha     | 4,663                     | N/A                       | 0.00           | Probe Area (cm <sup>2</sup> ): 126   |  |
| Pu-239  | Alpha     | 5,139                     | N/A                       | 0.00           | Count Time (t) (min): 1  |  |
| Am-241  | Alpha     | 5,487                     | N/A                       | 0.00           | Observation Interval (i) (sec): 2  |  |
| Ni-63   | Beta      | 17.4                      | 66.9                      | 0.00           | Index of Sensitivity (d') (unitless): 1.96   |  |
| C-14  | Beta      | 49.5                      | 156                       | 0.08           | Surveyor Efficiency (p) (unitless): 0.75   |  |
| Tc-99   | Beta      | 84.6                      | 294                       | 0.24           | $\text{Static MDC} = \frac{3 + 4.65 \sqrt{R_b \times t}}{t \times \epsilon_t \times \frac{\text{Probe Area}}{100}}$ $\text{Scan MDC} = \frac{d' \times \sqrt{R_b \times (i/60)} \times (60/i)}{\sqrt{p} \times \epsilon_t \times \frac{\text{Probe Area}}{100}}$ |  |
| Tl-204  | Beta      | 244                       | 764                       | 0.42           |  |  |
| Sr/Y-90   | Beta      | 565                       | 1,413                     | 0.47           |  |  |

| Weighted Efficiency Input/Output Table |                 |                 |                           |                           |                   |                |                |                             |
|--|-----------------|-----------------|---------------------------|---------------------------|-------------------|----------------|----------------|-----------------------------|
| Nuclide                                | Half-Life (yrs) | Total Intensity | Mean E (keV) <sup>a</sup> | Max. E (keV) <sup>a</sup> | Relative Fraction | ε <sub>i</sub> | ε <sub>s</sub> | ε <sub>t</sub> <sup>b</sup> |
| <b>Beta Emitters</b>                   |                 |                 |                           |                           |                   |                |                |                             |
| Ra-228                                 | 5.75E+00        | 1.00            | 7.2                       | 29                        | 1.00              | 0.00           | 0.25           | 0.00                        |
| Ac-228                                 | 7.02E-04        | 1.00            | 349                       | 1,050                     | 1.00              | 0.45           | 0.50           | 0.22                        |
| Pb-212                                 | 1.21E-03        | 1.00            | 100                       | 351                       | 1.00              | 0.27           | 0.25           | 0.07                        |
| Bi-212                                 | 1.15E-04        | 0.64            | 771                       | 2,090                     | 1.00              | 0.47           | 0.50           | 0.15                        |
| Tl-208                                 | 5.81E-06        | 1.00            | 559                       | 1,580                     | 0.40              | 0.47           | 0.50           | 0.09                        |
|  |                 |                 |                           |                           |                   |                |                |                             |
|  |                 |                 |                           |                           |                   |                |                |                             |
|  |                 |                 |                           |                           |                   |                |                |                             |
|  |                 |                 |                           |                           |                   |                |                |                             |
|  |                 |                 |                           |                           |                   |                |                |                             |
|  |                 |                 |                           |                           |                   |                |                |                             |
| <b>Alpha Emitters</b>                  |                 |                 |                           |                           |                   |                |                |                             |
| Th-232                                 | 1.40E+10        | 1.00            | 3,994                     | N/A                       | 1.00              | 0.00           | 0.25           | 0.00                        |
| Th-228                                 | 1.91E+00        | 1.00            | 5,402                     | N/A                       | 1.00              | 0.00           | 0.25           | 0.00                        |
| Ra-224                                 | 1.00E-02        | 1.00            | 5,672                     | N/A                       | 1.00              | 0.00           | 0.25           | 0.00                        |
| Rn-220                                 | 1.76E-06        | 1.00            | 6,287                     | N/A                       | 1.00              | 0.00           | 0.25           | 0.00                        |
| Po-216                                 | 4.60E-09        | 1.00            | 6,778                     | N/A                       | 1.00              | 0.00           | 0.25           | 0.00                        |
| Bi-212                                 | 1.15E-04        | 0.36            | 6,044                     | N/A                       | 1.00              | 0.00           | 0.25           | 0.00                        |
| Po-212                                 | 9.48E-15        | 1.00            | 8,785                     | N/A                       | 0.60              | 0.00           | 0.25           | 0.00                        |
|  |                 |                 |                           |                           |                   |                |                |                             |
|  |                 |                 |                           |                           |                   |                |                |                             |
|  |                 |                 |                           |                           |                   |                |                |                             |

<sup>a</sup>Excludes emission intensities < 0.1%; mean and maximum energies weighted based on emission intensity.

<sup>b</sup>Total efficiency per nuclide is Total Intensity × Relative Fraction × ε<sub>i</sub> × ε<sub>s</sub>.



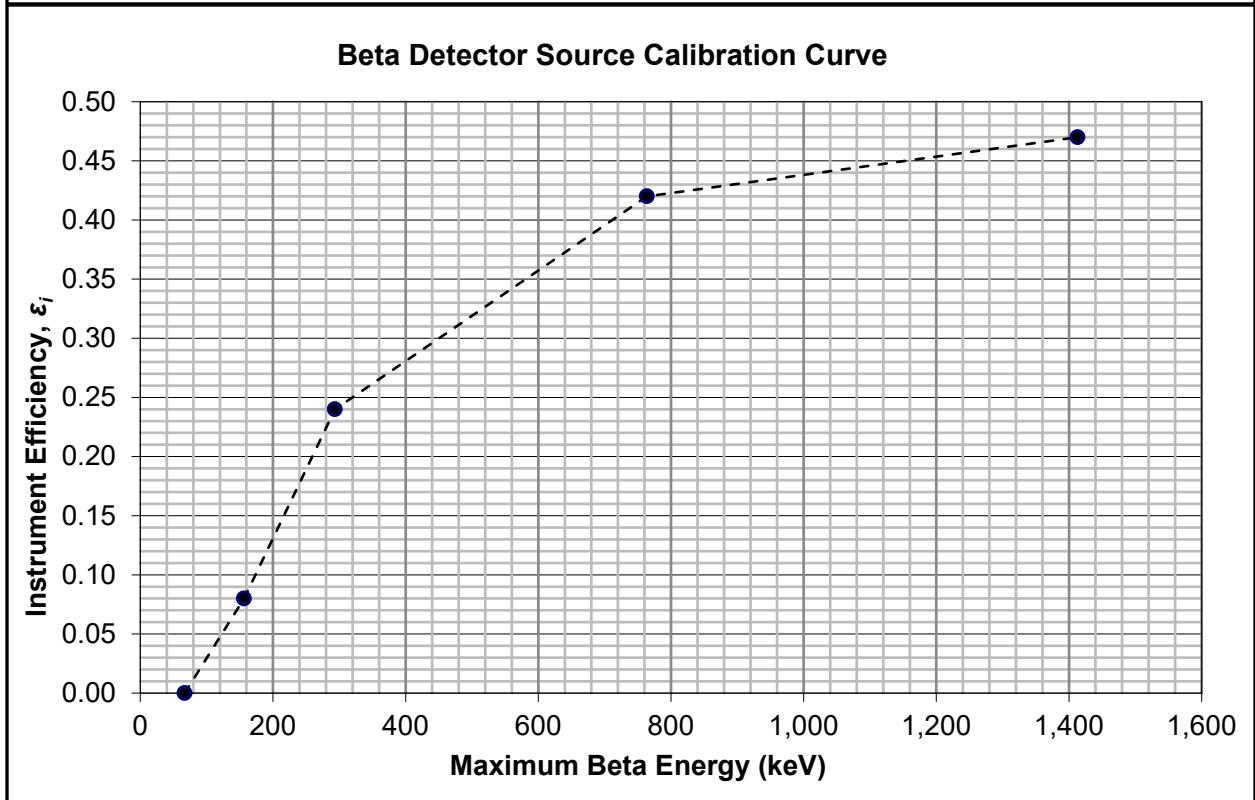
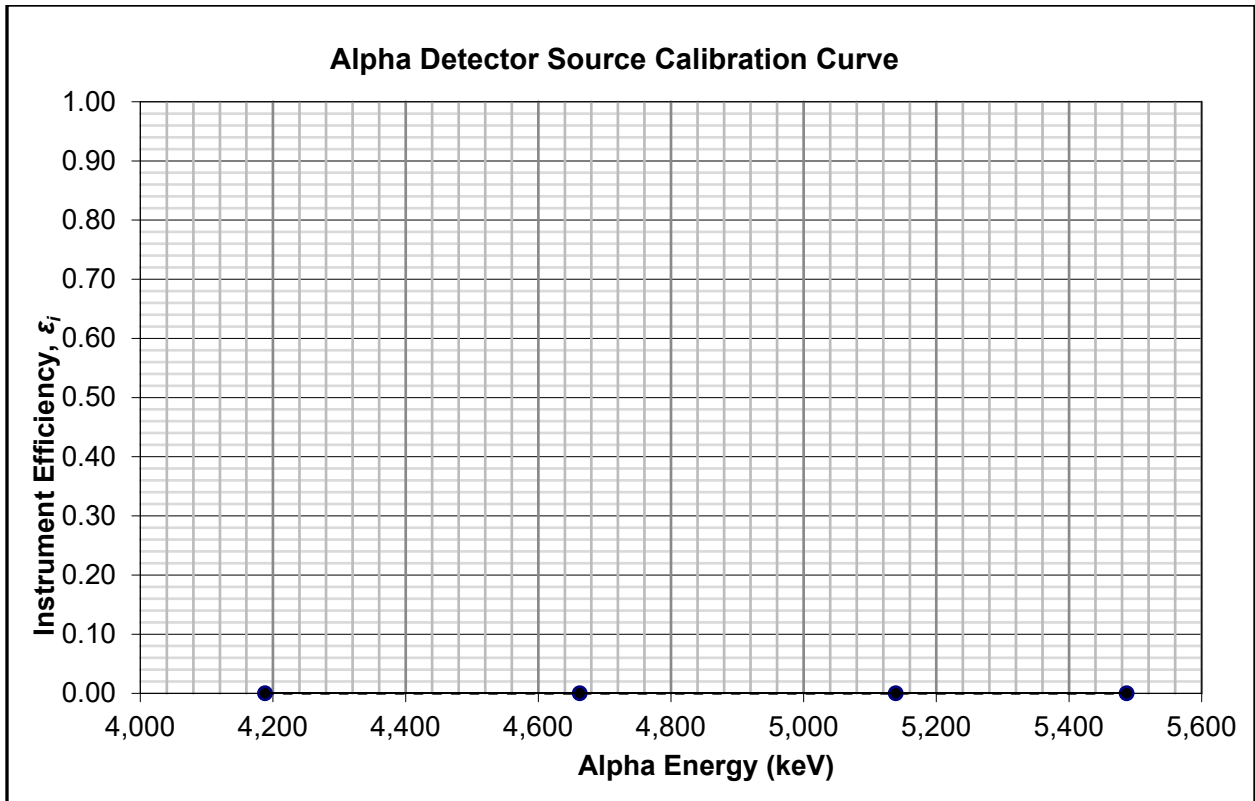


Figure A-10 Exhibit 4c. Th-232 Plus Decay Series, Alpha-Only, Gas Proportional Detector



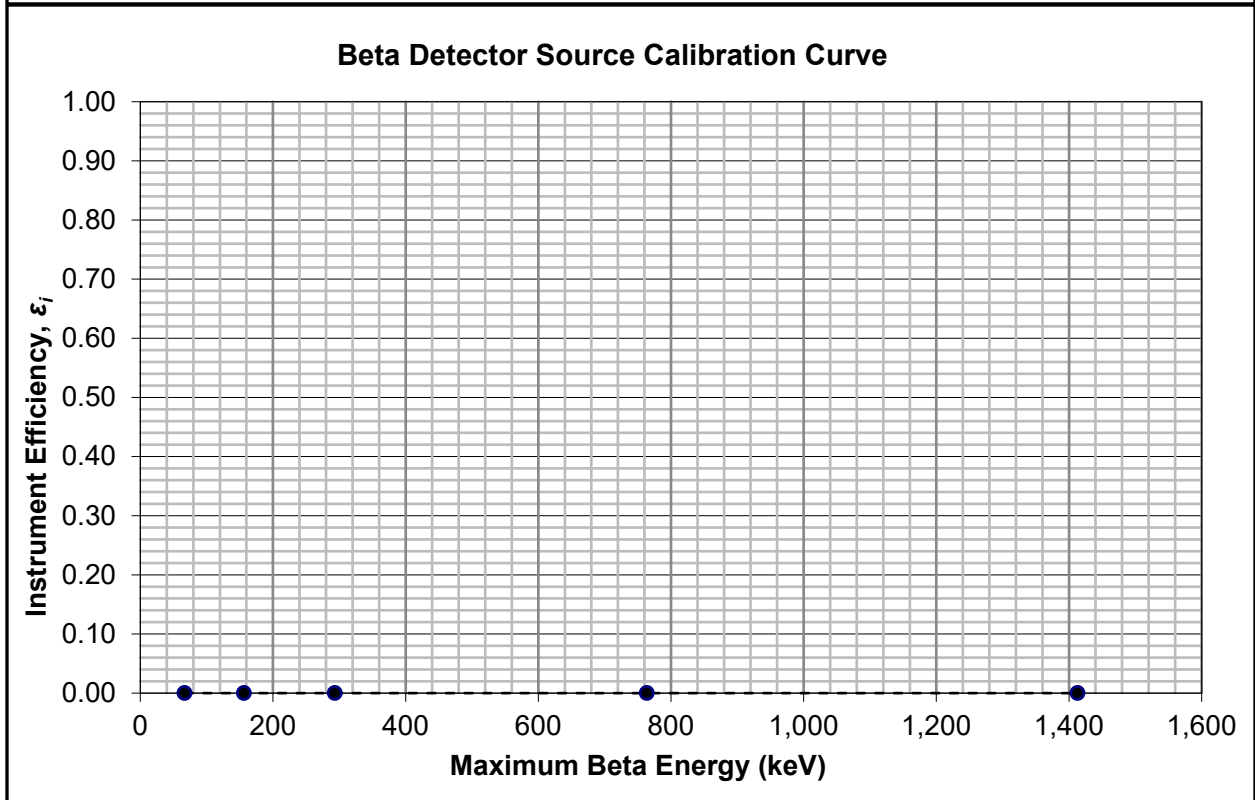
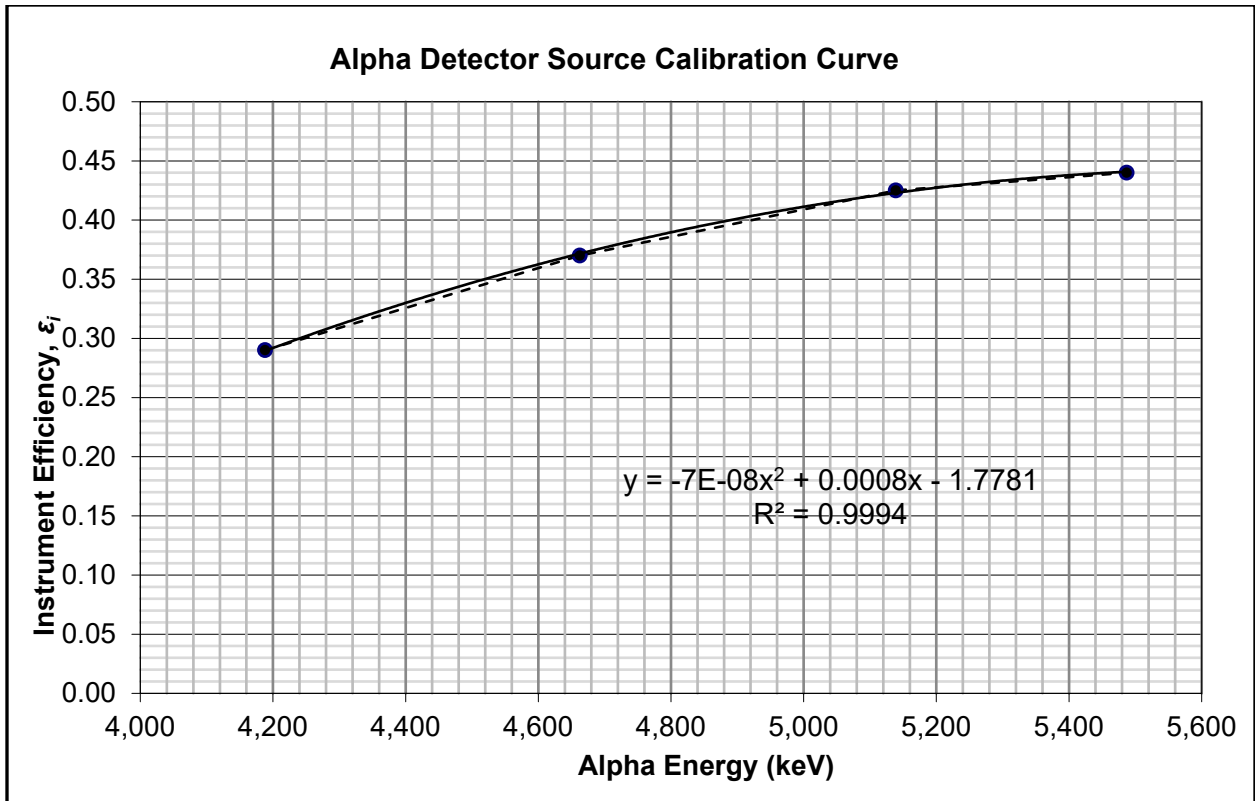


Figure A-11 Exhibit 5a. Processed U-Aged Yellow Cake, Alpha-Only, ZnS Detector



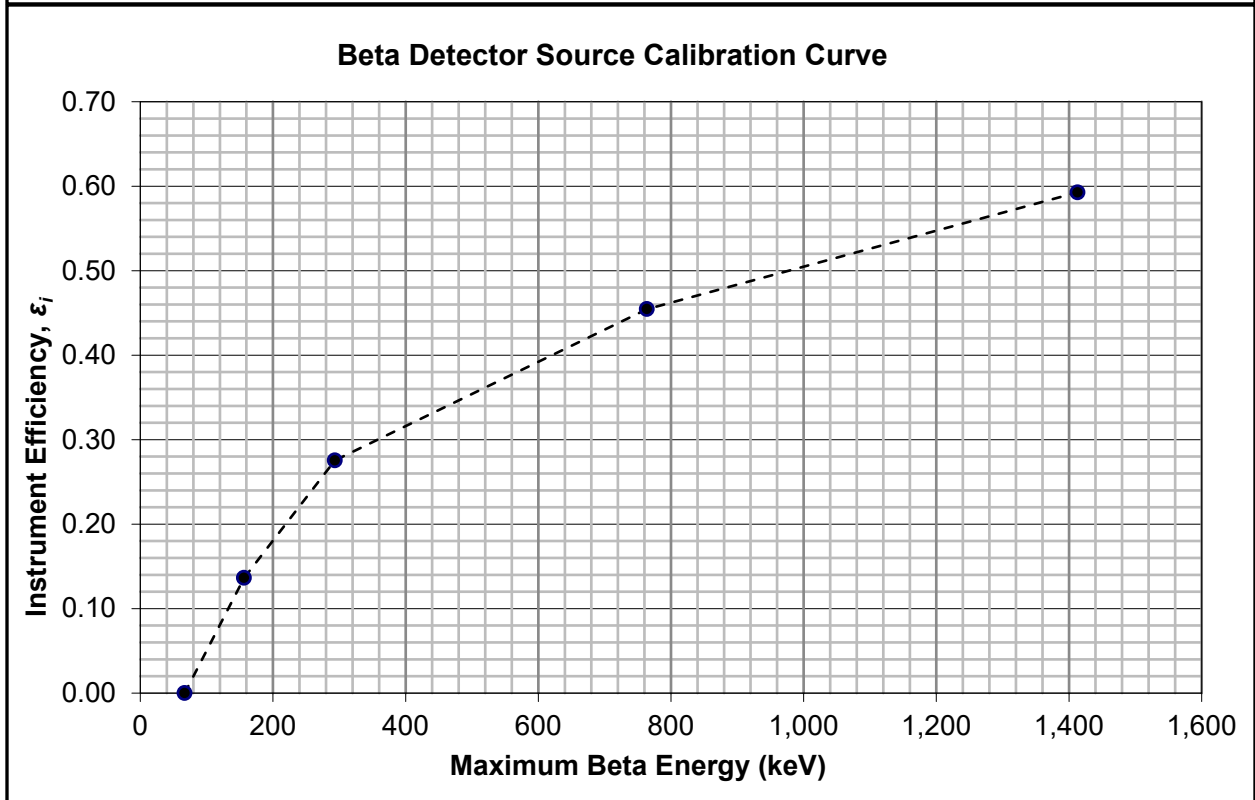
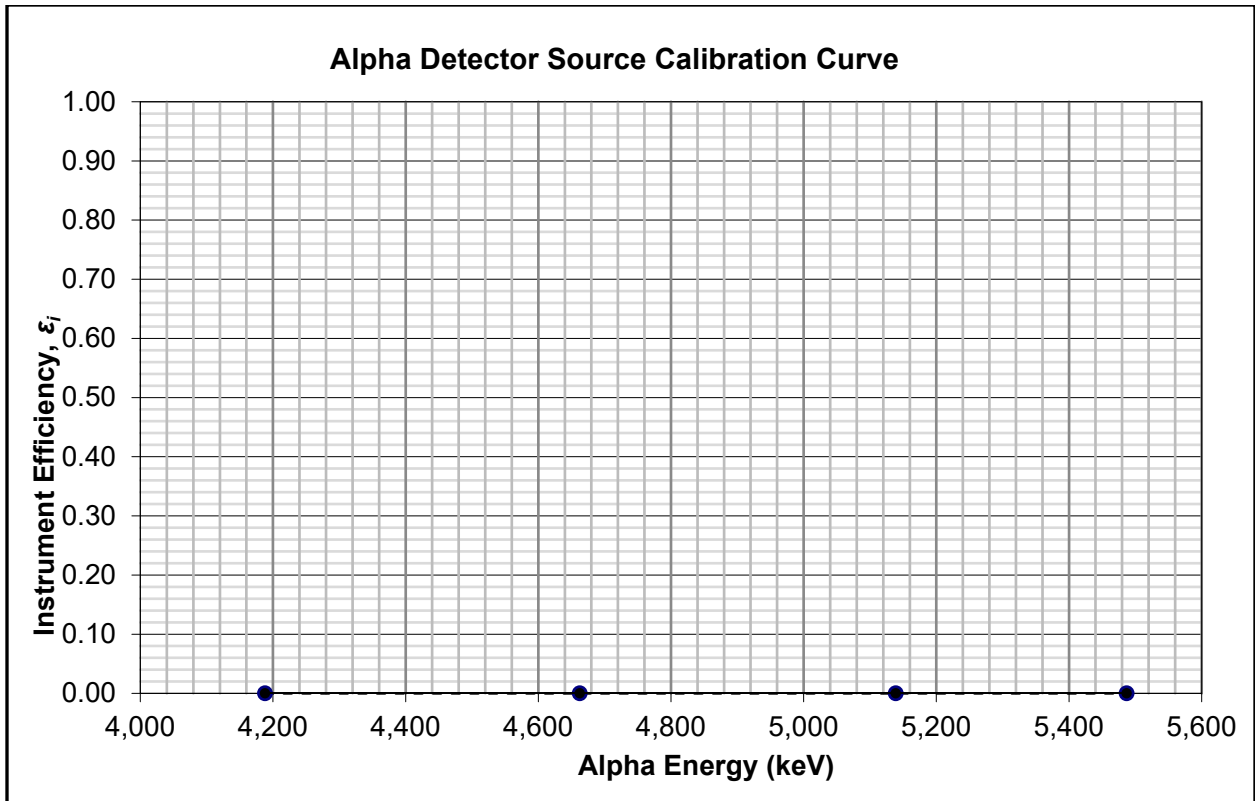


Figure A-12 Exhibit 5b. Processed U-Aged Yellow Cake, Beta-Only, GM Detector

**Table A-29 1 Exhibit 5c. Processed U-Pregnant Lixiviant, Alpha-Only, Dual Phoswich (ZnS) Detector**

|                              |       |
|------------------------------|-------|
| Rateometer/Scaler Model:     | 2221  |
| Detector Model:              | 43-93 |
| Mylar (mg/cm <sup>2</sup> ): | 1.2   |
| Voltage Setting (volts):     | 900   |
| Measured Radiation Type:     | α     |

| Worksheet Results                      |         |
|--|---------|
| Reported Result:                       | Gross α |
| Total Efficiency (Σ ε <sub>i</sub> ):  | 0.09    |
| Static MDC (dpm/100 cm <sup>2</sup> ): | 111     |
| Scan MDC (dpm/100 cm <sup>2</sup> ):   | 798     |

| Instrument Calibration Data, Source, and MDC Inputs |           |                           |                           |                |   |  |  |  |
|---|-----------|---------------------------|---------------------------|----------------|---|--|--|--|
| Standard Source Inputs                              |           |                           |                           |                | Static and Scan MDC Inputs  |  |  |  |
| Nuclide   | Radiation | Mean E (keV) <sup>a</sup> | Max. E (keV) <sup>a</sup> | ε <sub>i</sub> |   |  |  |  |
| U-238   | Alpha     | 4,188                     | N/A                       | 0.29           | Background (R <sub>b</sub> ) (cpm): 2   |  |  |  |
| Th-230  | Alpha     | 4,663                     | N/A                       | 0.37           | Probe Area (cm <sup>2</sup> ): 100  |  |  |  |
| Pu-239  | Alpha     | 5,139                     | N/A                       | 0.43           | Count Time (t) (min): 1   |  |  |  |
| Am-241  | Alpha     | 5,487                     | N/A                       | 0.44           | Observation Interval (i) (sec): 2   |  |  |  |
| Ni-63   | Beta      | 17.4                      | 66.9                      | 0.00           | Prob. of Detection (P) (unitless): 0.9  |  |  |  |
| C-14  | Beta      | 49.5                      | 156                       | 0.00           | Surveyor Efficiency (p) (unitless): N/A   |  |  |  |
| Tc-99   | Beta      | 84.6                      | 294                       | 0.00           | $\text{Static MDC} = \frac{3 + 4.65 \sqrt{R_b \times t}}{t \times \epsilon_t \times \frac{\text{Probe Area}}{100}}$ $\text{Scan MDC} = \frac{[-\ln(1 - P(n \geq 1))]}{\epsilon_i \times \epsilon_s \times \frac{\text{probe area}}{100}} \times (60/i)$ |  |  |  |
| Tl-204  | Beta      | 244                       | 764                       | 0.00           |   |  |  |  |
| Sr/Y-90   | Beta      | 565                       | 1,413                     | 0.00           |   |  |  |  |

| Weighted Efficiency Input/Output Table |                 |                 |                           |                           |                   |                |                |                             |
|--|-----------------|-----------------|---------------------------|---------------------------|-------------------|----------------|----------------|-----------------------------|
| Nuclide                                | Half-Life (yrs) | Total Intensity | Mean E (keV) <sup>a</sup> | Max. E (keV) <sup>a</sup> | Relative Fraction | ε <sub>i</sub> | ε <sub>s</sub> | ε <sub>t</sub> <sup>b</sup> |
| <b>Beta Emitters</b>                   |                 |                 |                           |                           |                   |                |                |                             |
| Th-234                                 | 6.60E-02        | 1.00            | 47.8                      | 178                       | 0.391             | 0.00           | 0.25           | 0.00                        |
| Pa-234                                 | 2.21E-06        | 1.00            | 809                       | 2,240                     | 0.391             | 0.00           | 0.50           | 0.00                        |
| Th-231                                 | 2.91E-03        | 1.00            | 78                        | 283                       | 0.018             | 0.00           | 0.25           | 0.00                        |
|  |                 |                 |                           |                           |                   |                |                |                             |
|  |                 |                 |                           |                           |                   |                |                |                             |
|  |                 |                 |                           |                           |                   |                |                |                             |
|  |                 |                 |                           |                           |                   |                |                |                             |
|  |                 |                 |                           |                           |                   |                |                |                             |
|  |                 |                 |                           |                           |                   |                |                |                             |
| <b>Alpha Emitters</b>                  |                 |                 |                           |                           |                   |                |                |                             |
| U-238                                  | 4.47E+09        | 1.00            | 4,188                     | N/A                       | 0.391             | 0.29           | 0.25           | 0.03                        |
| U-234                                  | 2.46E+05        | 1.00            | 4,759                     | N/A                       | 0.396             | 0.38           | 0.25           | 0.04                        |
| U-235                                  | 7.04E+08        | 1.00            | 4,431                     | N/A                       | 0.018             | 0.34           | 0.25           | 0.00                        |
| Th-230                                 | 7.54E+04        | 1.00            | 4,663                     | N/A                       | 0.075             | 0.37           | 0.25           | 0.01                        |
| Ra-226                                 | 1.60E+03        | 1.00            | 4,773                     | N/A                       | 0.121             | 0.39           | 0.25           | 0.01                        |
|  |                 |                 |                           |                           |                   |                |                |                             |
|  |                 |                 |                           |                           |                   |                |                |                             |
|  |                 |                 |                           |                           |                   |                |                |                             |
|  |                 |                 |                           |                           |                   |                |                |                             |

<sup>a</sup>Excludes emission intensities < 0.1%; mean and maximum energies weighted based on emission intensity.

<sup>b</sup>Total efficiency per nuclide is Total Intensity × Relative Fraction × ε<sub>i</sub> × ε<sub>s</sub>.

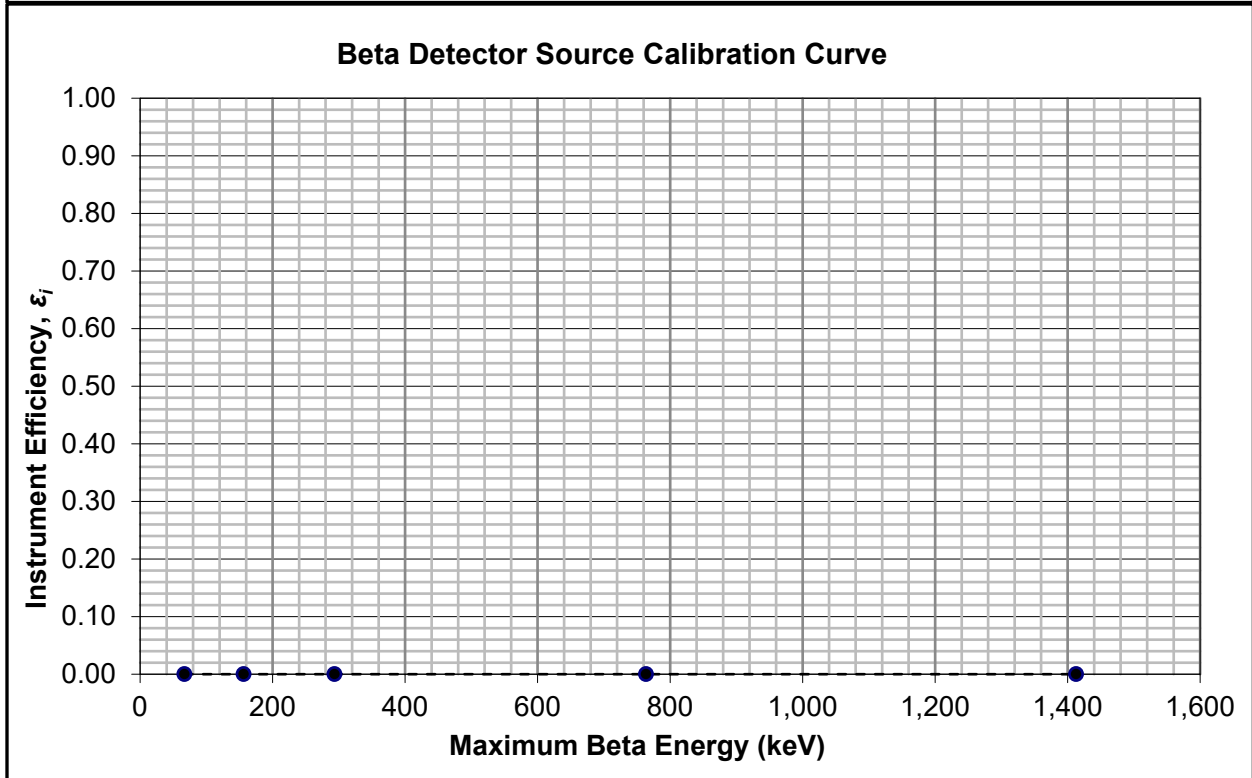
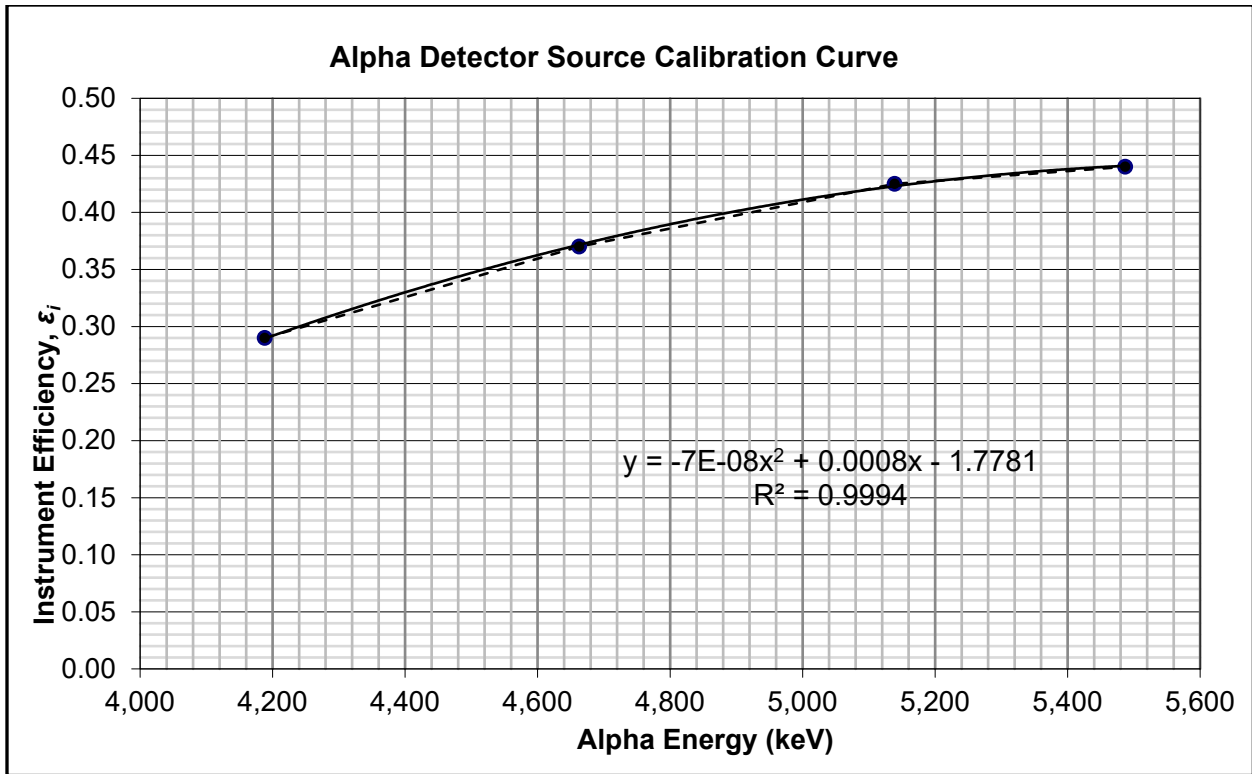


Figure A-13 Exhibit 5c. Processed U-Pregnant Lixiviant, Alpha-Only, Dual Phoswich (ZnS) Detector





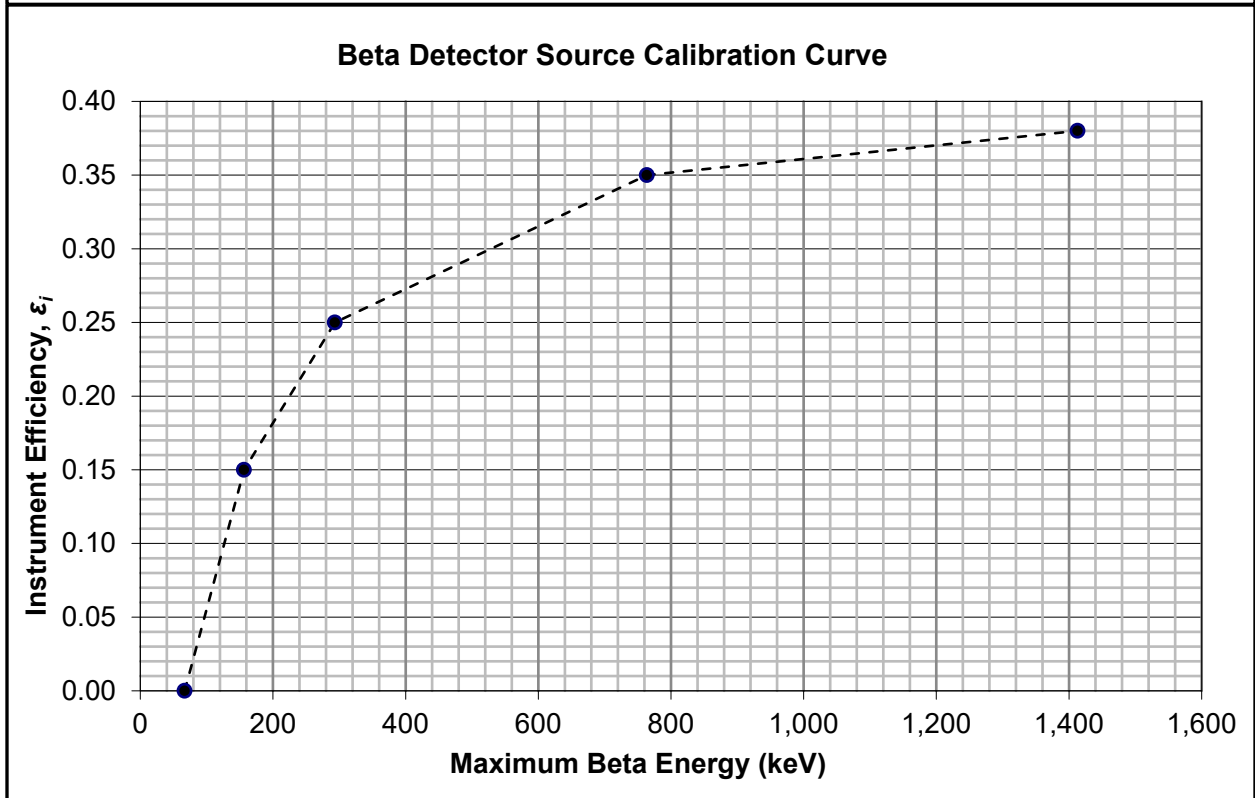
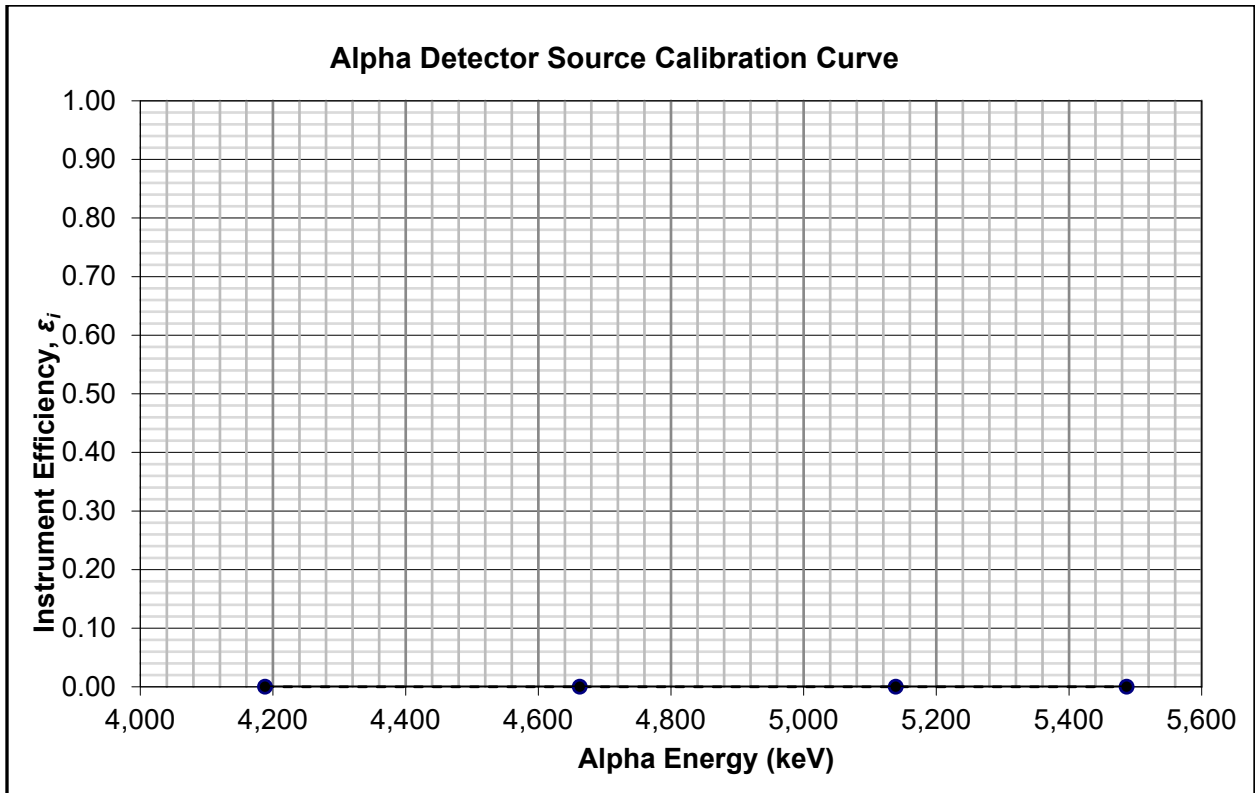


Figure A-14 Exhibit 5d. Processed U-Pregnant Lixiviant, Beta-Only, Dual Phoswich (Plastic Scintillator)

**Table A-31 Exhibit 5e. Unprocessed U Ore, Alpha Plus Beta, Gas Proportional Detector**

|                              |       |
|------------------------------|-------|
| Rateometer/Scaler Model:     | 2221  |
| Detector Model:              | 43-68 |
| Mylar (mg/cm <sup>2</sup> ): | 0.8   |
| Voltage Setting (volts):     | 1,750 |
| Measured Radiation Type:     | α+β   |

| Worksheet Results                      |         |
|--|---------|
| Reported Result:                       | Gross U |
| Total Efficiency (Σ ε <sub>t</sub> ):  | 0.99    |
| Static MDC (dpm/100 cm <sup>2</sup> ): | 76      |
| Scan MDC (dpm/100 cm <sup>2</sup> ):   | 195     |

| Instrument Calibration Data, Source, and MDC Inputs |           |                           |                           |                |   |  |  |  |
|---|-----------|---------------------------|---------------------------|----------------|---|--|--|--|
| Standard Source Inputs                              |           |                           |                           |                | Static and Scan MDC Inputs  |  |  |  |
| Nuclide   | Radiation | Mean E (keV) <sup>a</sup> | Max. E (keV) <sup>a</sup> | ε <sub>i</sub> |   |  |  |  |
| U-238   | Alpha     | 4,188                     | N/A                       | 0.31           | Background (R <sub>b</sub> ) (cpm): 390   |  |  |  |
| Th-230  | Alpha     | 4,663                     | N/A                       | 0.41           | Probe Area (cm <sup>2</sup> ): 126  |  |  |  |
| Pu-239  | Alpha     | 5,139                     | N/A                       | 0.47           | Count Time (t) (min): 1   |  |  |  |
| Am-241  | Alpha     | 5,487                     | N/A                       | 0.48           | Observation Interval (i) (sec): 2   |  |  |  |
| Ni-63   | Beta      | 17.4                      | 66.9                      | 0.06           | Index of Sensitivity (d') (unitless): 1.96  |  |  |  |
| C-14  | Beta      | 49.5                      | 156                       | 0.31           | Surveyor Efficiency (p) (unitless): 0.75  |  |  |  |
| Tc-99   | Beta      | 84.6                      | 294                       | 0.43           | $\text{Static MDC} = \frac{3+4.65\sqrt{R_b \times t}}{t \times \epsilon_t \times \frac{\text{Probe Area}}{100}}$ $\text{Scan MDC} = \frac{d' \times \sqrt{R_b \times (i/60)} \times (60/i)}{\sqrt{p} \times \epsilon_t \times \frac{\text{Probe Area}}{100}}$ |  |  |  |
| Tl-204  | Beta      | 244                       | 764                       | 0.52           |   |  |  |  |
| Sr/Y-90   | Beta      | 565                       | 1,413                     | 0.54           |   |  |  |  |

| Weighted Efficiency Input/Output Table |                 |                 |                           |                           |                   |                |                |                             |
|--|-----------------|-----------------|---------------------------|---------------------------|-------------------|----------------|----------------|-----------------------------|
| Nuclide                                | Half-Life (yrs) | Total Intensity | Mean E (keV) <sup>a</sup> | Max. E (keV) <sup>a</sup> | Relative Fraction | ε <sub>i</sub> | ε <sub>s</sub> | ε <sub>t</sub> <sup>b</sup> |
| <b>Beta Emitters</b>                   |                 |                 |                           |                           |                   |                |                |                             |
| Th-234                                 | 6.60E-02        | 1.00            | 47.8                      | 178                       | 0.49              | 0.33           | 0.25           | 0.04                        |
| Pa-234                                 | 2.21E-06        | 1.00            | 809                       | 2,240                     | 0.49              | 0.54           | 0.50           | 0.13                        |
| Th-231                                 | 2.91E-03        | 1.00            | 78                        | 283                       | 0.02              | 0.42           | 0.25           | 0.00                        |
| Pb-214                                 | 5.10E-05        | 1.00            | 225                       | 719                       | 0.49              | 0.51           | 0.50           | 0.13                        |
| Bi-214                                 | 3.79E-05        | 1.00            | 639                       | 1,770                     | 0.49              | 0.54           | 0.50           | 0.13                        |
| Pb-210                                 | 2.22E+01        | 1.00            | 6                         | 24                        | 0.49              | 0.00           | 0.25           | 0.00                        |
| Bi-210                                 | 1.37E-02        | 1.00            | 389                       | 1,160                     | 0.49              | 0.53           | 0.50           | 0.13                        |
|  |                 |                 |                           |                           |                   |                |                |                             |
|  |                 |                 |                           |                           |                   |                |                |                             |
|  |                 |                 |                           |                           |                   |                |                |                             |
| <b>Alpha Emitters</b>                  |                 |                 |                           |                           |                   |                |                |                             |
| U-238                                  | 4.47E+09        | 1.00            | 4,188                     | N/A                       | 0.49              | 0.31           | 0.25           | 0.04                        |
| U-234                                  | 2.46E+05        | 1.00            | 4,759                     | N/A                       | 0.49              | 0.43           | 0.25           | 0.05                        |
| U-235                                  | 7.04E+08        | 1.00            | 4,431                     | N/A                       | 0.02              | 0.37           | 0.25           | 0.00                        |
| Th-230                                 | 7.54E+04        | 1.00            | 4,663                     | N/A                       | 0.49              | 0.41           | 0.25           | 0.05                        |
| Ra-226                                 | 1.60E+03        | 1.00            | 4,773                     | N/A                       | 0.49              | 0.43           | 0.25           | 0.05                        |
| Rn-222                                 | 1.05E-02        | 1.00            | 5,485                     | N/A                       | 0.49              | 0.48           | 0.25           | 0.06                        |
| Po-214                                 | 5.19E-12        | 1.00            | 7,686                     | N/A                       | 0.49              | 0.48           | 0.25           | 0.06                        |
| Po-210                                 | 3.79E-01        | 1.00            | 5,304                     | N/A                       | 0.49              | 0.48           | 0.25           | 0.06                        |
| Po-218                                 | 5.89E-06        | 1.00            | 6,001                     | N/A                       | 0.49              | 0.48           | 0.25           | 0.06                        |
| Ac-227                                 | 2.18E+01        | 0.01            | 4,948                     | N/A                       | 0.02              | 0.45           | 0.25           | 0.00                        |

<sup>a</sup>Excludes emission intensities < 0.1%; mean and maximum energies weighted based on emission intensity.

<sup>b</sup>Total efficiency per nuclide is Total Intensity × Relative Fraction × ε<sub>i</sub> × ε<sub>s</sub>.

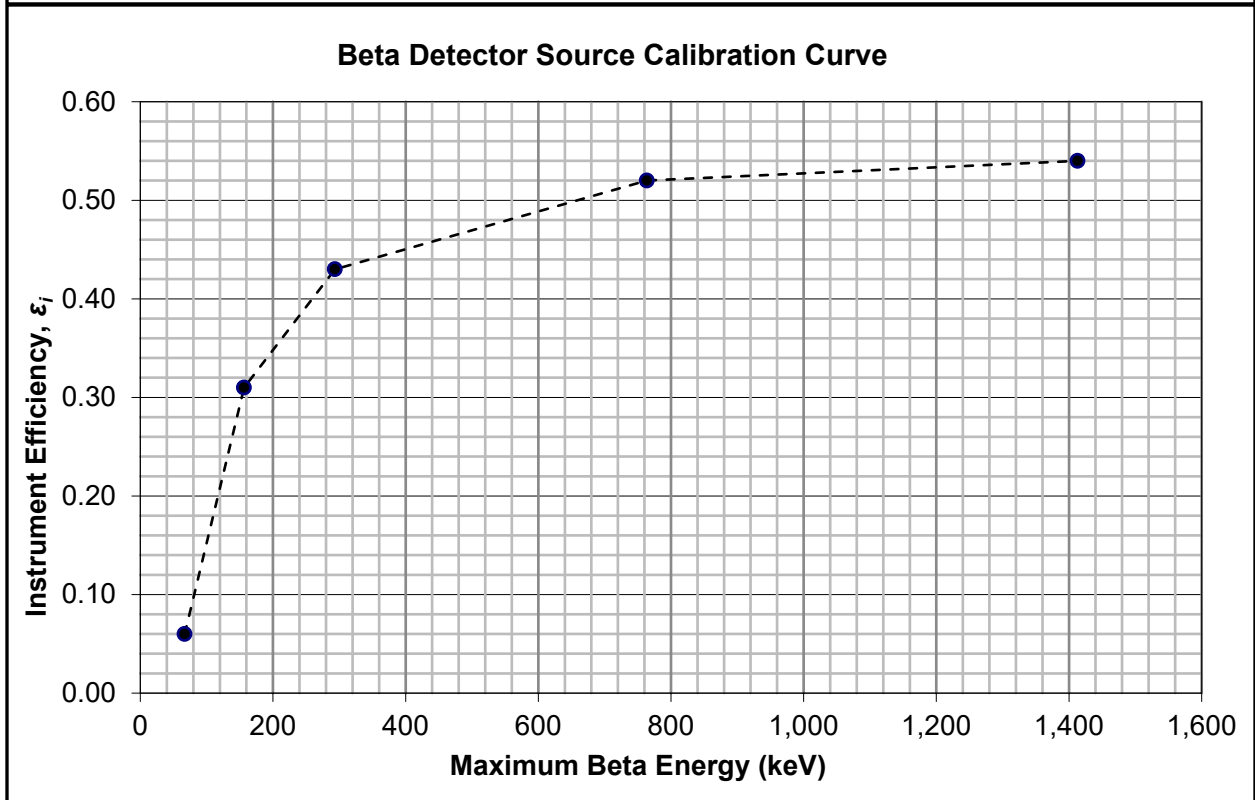
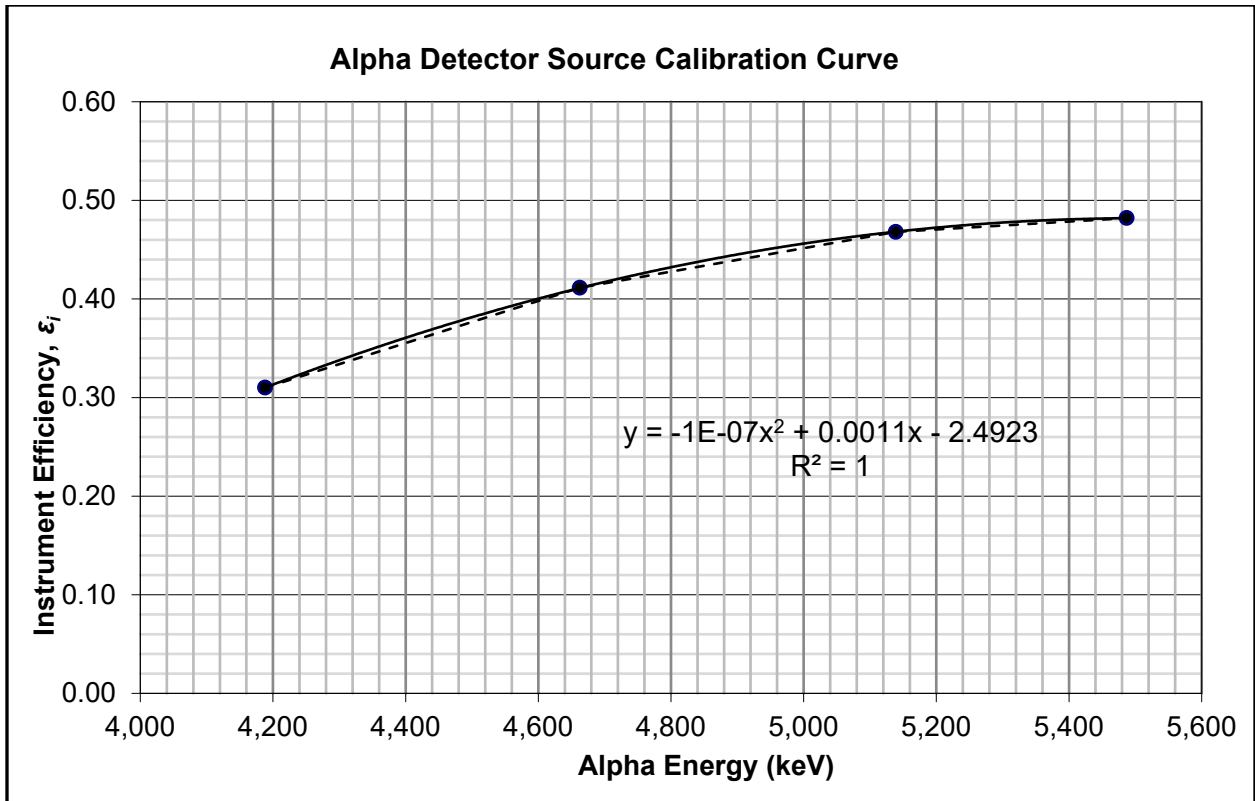


Figure A-15 Exhibit 5e. Unprocessed U Ore, Alpha Plus Beta, Gas Proportional Detector

**Table A-32 Exhibit 6a. Enriched U, Alpha-Only, Gas Proportional Detector**

**Ratemeter/Scaler Model:** 2221  
**Detector Model:** 43-68  
**Mylar (mg/cm<sup>2</sup>):** 0.8  
**Voltage Setting (volts):** 1,300  
**Measured Radiation Type:** α

| Worksheet Results                      |         |
|--|---------|
| Reported Result:                       | Gross U |
| Total Efficiency (Σ ε <sub>t</sub> ):  | 0.10    |
| Static MDC (dpm/100 cm <sup>2</sup> ): | 72      |
| Scan MDC (dpm/100 cm <sup>2</sup> ):   | 523     |

| Instrument Calibration Data, Source, and MDC Inputs |           |                           |                           |                |   |  |  |  |
|---|-----------|---------------------------|---------------------------|----------------|---|--|--|--|
| Standard Source Inputs                              |           |                           |                           |                | Static and Scan MDC Inputs  |  |  |  |
| Nuclide   | Radiation | Mean E (keV) <sup>a</sup> | Max. E (keV) <sup>a</sup> | ε <sub>i</sub> |   |  |  |  |
| U-238   | Alpha     | 4,188                     | N/A                       | 0.31           | Background (R <sub>b</sub> ) (cpm): 2   |  |  |  |
| Th-230  | Alpha     | 4,663                     | N/A                       | 0.41           | Probe Area (cm <sup>2</sup> ): 126  |  |  |  |
| Pu-239  | Alpha     | 5,139                     | N/A                       | 0.47           | Count Time (t) (min): 1   |  |  |  |
| Am-241  | Alpha     | 5,487                     | N/A                       | 0.48           | Observation Interval (i) (sec): 2   |  |  |  |
| Ni-63   | Beta      | 17.4                      | 66.9                      | 0.00           | Prob. of Detection (P) (unitless): 0.9  |  |  |  |
| C-14  | Beta      | 49.5                      | 156                       | 0.00           | Static MDC = $\frac{3+4.65\sqrt{R_b \times t}}{t \times \epsilon_t \times \frac{Probe\ Area}{100}}$<br><br>Scan MDC = $\frac{[-\ln(1-P(n \geq 1))] \times (60/i)}{\epsilon_i \times \epsilon_s \times \frac{probe\ area}{100}}$ |  |  |  |
| Tc-99   | Beta      | 84.6                      | 294                       | 0.00           |   |  |  |  |
| Tl-204  | Beta      | 244                       | 764                       | 0.00           |   |  |  |  |
| Sr/Y-90   | Beta      | 565                       | 1,413                     | 0.00           |   |  |  |  |

| Weighted Efficiency Input/Output Table |                 |                 |                           |                           |                   |                |                |                             |
|--|-----------------|-----------------|---------------------------|---------------------------|-------------------|----------------|----------------|-----------------------------|
| Nuclide                                | Half-Life (yrs) | Total Intensity | Mean E (keV) <sup>a</sup> | Max. E (keV) <sup>a</sup> | Relative Fraction | ε <sub>i</sub> | ε <sub>s</sub> | ε <sub>t</sub> <sup>b</sup> |
| <b>Beta Emitters</b>                   |                 |                 |                           |                           |                   |                |                |                             |
|  |                 |                 |                           |                           |                   |                |                |                             |
|  |                 |                 |                           |                           |                   |                |                |                             |
|  |                 |                 |                           |                           |                   |                |                |                             |
|  |                 |                 |                           |                           |                   |                |                |                             |
|  |                 |                 |                           |                           |                   |                |                |                             |
|  |                 |                 |                           |                           |                   |                |                |                             |
|  |                 |                 |                           |                           |                   |                |                |                             |
|  |                 |                 |                           |                           |                   |                |                |                             |
|  |                 |                 |                           |                           |                   |                |                |                             |
|  |                 |                 |                           |                           |                   |                |                |                             |
|  |                 |                 |                           |                           |                   |                |                |                             |
|  |                 |                 |                           |                           |                   |                |                |                             |
|  |                 |                 |                           |                           |                   |                |                |                             |
|  |                 |                 |                           |                           |                   |                |                |                             |
|  |                 |                 |                           |                           |                   |                |                |                             |
|  |                 |                 |                           |                           |                   |                |                |                             |
|  |                 |                 |                           |                           |                   |                |                |                             |
|  |                 |                 |                           |                           |                   |                |                |                             |
| <b>Alpha Emitters</b>                  |                 |                 |                           |                           |                   |                |                |                             |
| U-238                                  | 4.47E+09        | 1.00            | 4,188                     | N/A                       | 0.03              | 0.31           | 0.25           | 0.00                        |
| U-234                                  | 2.46E+05        | 1.00            | 4,759                     | N/A                       | 0.93              | 0.43           | 0.25           | 0.10                        |
| U-235                                  | 7.04E+08        | 1.00            | 4,431                     | N/A                       | 0.05              | 0.37           | 0.25           | 0.00                        |
|  |                 |                 |                           |                           |                   |                |                |                             |
|  |                 |                 |                           |                           |                   |                |                |                             |
|  |                 |                 |                           |                           |                   |                |                |                             |
|  |                 |                 |                           |                           |                   |                |                |                             |
|  |                 |                 |                           |                           |                   |                |                |                             |
|  |                 |                 |                           |                           |                   |                |                |                             |
|  |                 |                 |                           |                           |                   |                |                |                             |
|  |                 |                 |                           |                           |                   |                |                |                             |
|  |                 |                 |                           |                           |                   |                |                |                             |
|  |                 |                 |                           |                           |                   |                |                |                             |
|  |                 |                 |                           |                           |                   |                |                |                             |
|  |                 |                 |                           |                           |                   |                |                |                             |
|  |                 |                 |                           |                           |                   |                |                |                             |
|  |                 |                 |                           |                           |                   |                |                |                             |
|  |                 |                 |                           |                           |                   |                |                |                             |
|  |                 |                 |                           |                           |                   |                |                |                             |
|  |                 |                 |                           |                           |                   |                |                |                             |
|  |                 |                 |                           |                           |                   |                |                |                             |

<sup>a</sup>Excludes emission intensities < 0.1%; mean and maximum energies weighted based on emission intensity.

<sup>b</sup>Total efficiency per nuclide is Total Intensity × Relative Fraction × ε<sub>i</sub> × ε<sub>s</sub>.

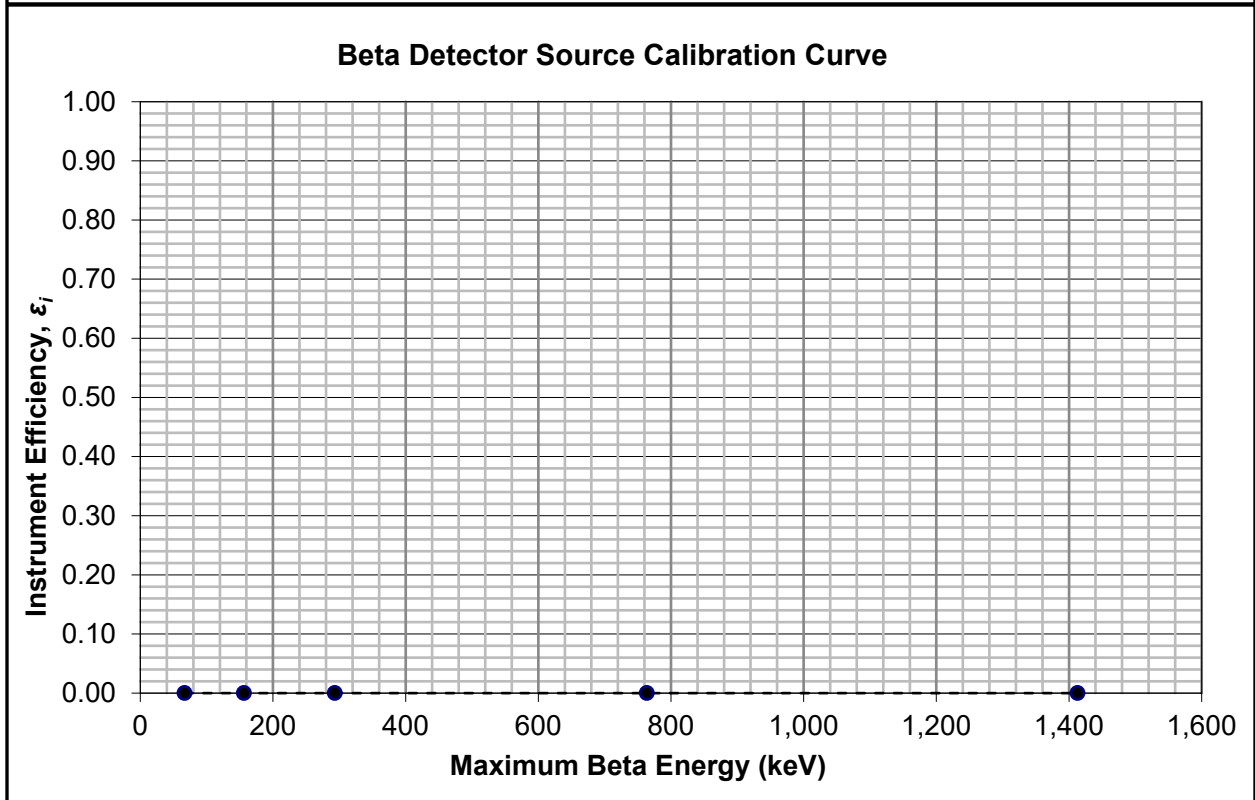
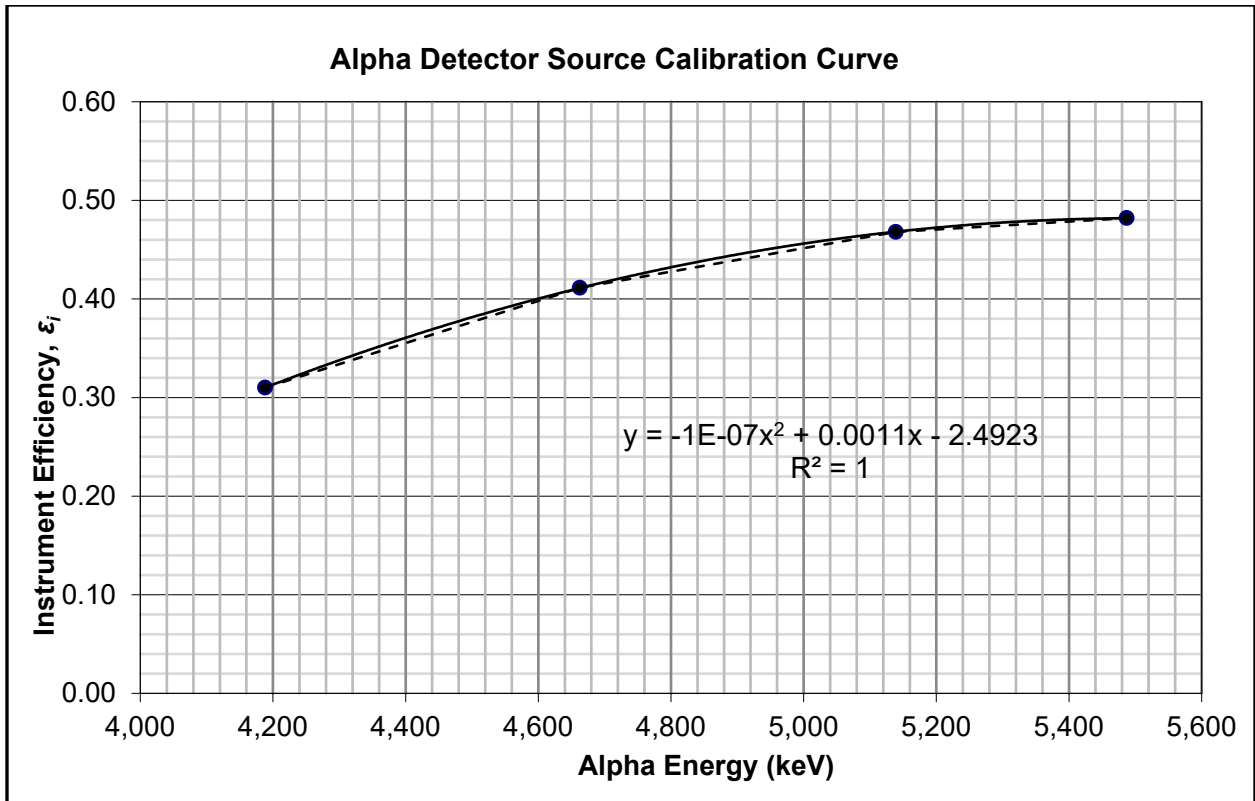


Figure A-16 Exhibit 6a. Enriched U, Alpha-Only, Gas Proportional Detector



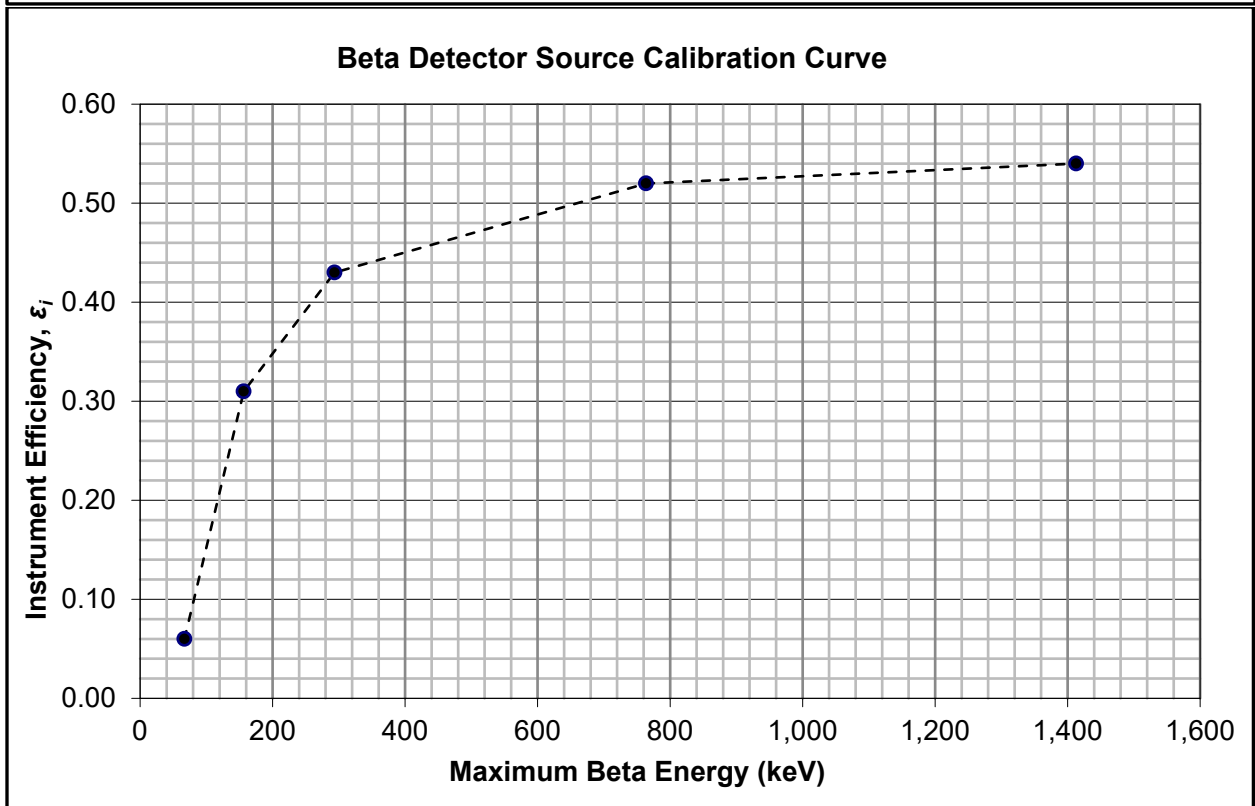
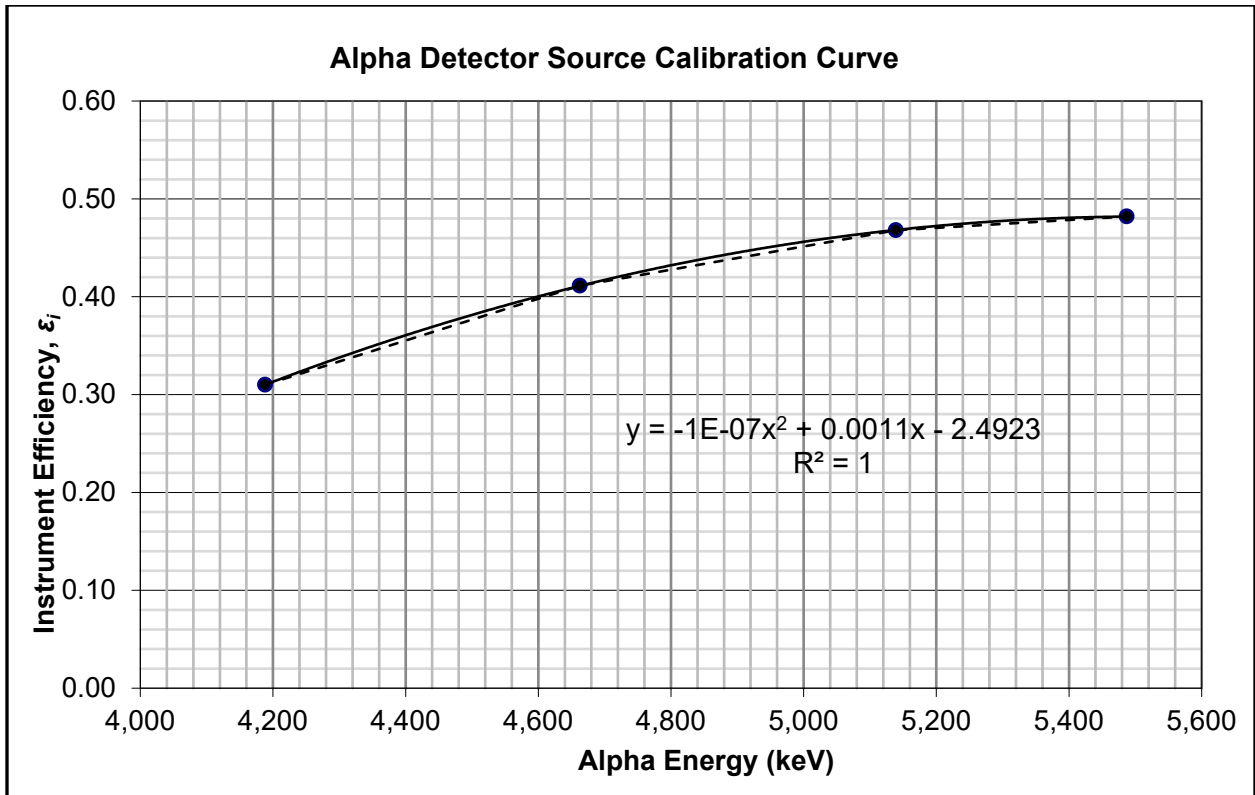


Figure A-17 Exhibit 6b. Enriched U and Tc-99, Alpha Plus Beta, Gas Proportional Detector

**Table A-34 Exhibit 7a. Processed U Tailings, Alpha Plus Beta, Gas Proportional Detector**

|                                   |       |  |
|-----------------------------------|-------|--|
| <b>Ratemeter/Scaler Model:</b>    | 2221  | <b>Worksheet Results</b>                   |
| <b>Detector Model:</b>            | 43-68 |  |
| <b>Mylar (mg/cm<sup>2</sup>):</b> | 0.8   |  |
| <b>Voltage Setting (volts):</b>   | 1,750 |  |
| <b>Measured Radiation Type:</b>   | α+β   |  |
|                                   |       | Reported Result: Gross α+β                 |
|                                   |       | Total Efficiency (Σ ε <sub>i</sub> ): 0.15 |
|                                   |       | Static MDC (dpm/100 cm <sup>2</sup> ): 509 |
|                                   |       | Scan MDC (dpm/100 cm <sup>2</sup> ): 1,313 |

| Instrument Calibration Data, Source, and MDC Inputs  |           |                           |                            |                |
|--|-----------|---------------------------|----------------------------|----------------|
| Standard Source Inputs   |           |                           | Static and Scan MDC Inputs |                |
| Nuclide  | Radiation | Mean E (keV) <sup>a</sup> | Max. E (keV) <sup>a</sup>  | ε <sub>i</sub> |
| U-238  | Alpha     | 4,188                     | N/A                        | 0.31           |
| Th-230   | Alpha     | 4,663                     | N/A                        | 0.41           |
| Pu-239   | Alpha     | 5,139                     | N/A                        | 0.47           |
| Am-241   | Alpha     | 5,487                     | N/A                        | 0.48           |
| Ni-63  | Beta      | 17.4                      | 66.9                       | 0.06           |
| C-14   | Beta      | 49.5                      | 156                        | 0.31           |
| Tc-99  | Beta      | 84.6                      | 294                        | 0.43           |
| Tl-204   | Beta      | 244                       | 764                        | 0.52           |
| Sr/Y-90  | Beta      | 565                       | 1,413                      | 0.54           |
| Background (R <sub>b</sub> ) (cpm): 390  |           |                           |                            |                |
| Probe Area (cm <sup>2</sup> ): 126   |           |                           |                            |                |
| Count Time (t) (min): 1  |           |                           |                            |                |
| Observation Interval (i) (sec): 2  |           |                           |                            |                |
| Index of Sensitivity (d') (unitless): 1.96   |           |                           |                            |                |
| Surveyor Efficiency (p) (unitless): 0.75   |           |                           |                            |                |
| $\text{Static MDC} = \frac{3 + 4.65\sqrt{R_b \times t}}{t \times \epsilon_t \times \frac{\text{Probe Area}}{100}}$                           |           |                           |                            |                |
| $\text{Scan MDC} = \frac{d' \times \sqrt{R_b \times (i/60)} \times (60/i)}{\sqrt{p} \times \epsilon_t \times \frac{\text{Probe Area}}{100}}$ |           |                           |                            |                |

| Weighted Efficiency Input/Output Table |                 |                 |                           |                           |                   |                |                |                             |
|--|-----------------|-----------------|---------------------------|---------------------------|-------------------|----------------|----------------|-----------------------------|
| Nuclide                                | Half-Life (yrs) | Total Intensity | Mean E (keV) <sup>a</sup> | Max. E (keV) <sup>a</sup> | Relative Fraction | ε <sub>i</sub> | ε <sub>s</sub> | ε <sub>t</sub> <sup>b</sup> |
| <b>Beta Emitters</b>                   |                 |                 |                           |                           |                   |                |                |                             |
| Th-234                                 | 6.60E-02        | 1.00            | 47.8                      | 178                       | 0.0068            | 0.33           | 0.25           | 0.00                        |
| Pa-234                                 | 2.21E-06        | 1.00            | 809                       | 2,240                     | 0.0068            | 0.54           | 0.50           | 0.00                        |
| Th-231                                 | 2.91E-03        | 1.00            | 78                        | 283                       | 0.0003            | 0.42           | 0.25           | 0.00                        |
| Pb-214                                 | 5.10E-05        | 1.00            | 225                       | 719                       | 0.0972            | 0.51           | 0.50           | 0.02                        |
| Bi-214                                 | 3.79E-05        | 1.00            | 639                       | 1,770                     | 0.0972            | 0.54           | 0.50           | 0.03                        |
| Pb-210                                 | 2.22E+01        | 1.00            | 6                         | 24                        | 0.0972            | 0.00           | 0.25           | 0.00                        |
| Bi-210                                 | 1.37E-02        | 1.00            | 389                       | 1,160                     | 0.0972            | 0.53           | 0.50           | 0.03                        |
| <b>Alpha Emitters</b>                  |                 |                 |                           |                           |                   |                |                |                             |
| U-238                                  | 4.47E+09        | 1.00            | 4,188                     | N/A                       | 0.0068            | 0.31           | 0.25           | 0.00                        |
| U-234                                  | 2.46E+05        | 1.00            | 4,759                     | N/A                       | 0.0068            | 0.43           | 0.25           | 0.00                        |
| U-235                                  | 7.04E+08        | 1.00            | 4,431                     | N/A                       | 0.0003            | 0.37           | 0.25           | 0.00                        |
| Th-230                                 | 7.54E+04        | 1.00            | 4,663                     | N/A                       | 0.0972            | 0.41           | 0.25           | 0.01                        |
| Ra-226                                 | 1.60E+03        | 1.00            | 4,773                     | N/A                       | 0.0972            | 0.43           | 0.25           | 0.01                        |
| Rn-222                                 | 1.05E-02        | 1.00            | 5,485                     | N/A                       | 0.0972            | 0.48           | 0.25           | 0.01                        |
| Po-214                                 | 5.19E-12        | 1.00            | 7,686                     | N/A                       | 0.0972            | 0.48           | 0.25           | 0.01                        |
| Po-210                                 | 3.79E-01        | 1.00            | 5,304                     | N/A                       | 0.0972            | 0.48           | 0.25           | 0.01                        |
| Po-218                                 | 5.89E-06        | 1.00            | 6,001                     | N/A                       | 0.0972            | 0.48           | 0.25           | 0.01                        |

<sup>a</sup>Excludes emission intensities < 0.1%; mean and maximum energies weighted based on emission intensity.

<sup>b</sup>Total efficiency per nuclide is Total Intensity × Relative Fraction × ε<sub>i</sub> × ε<sub>s</sub>.



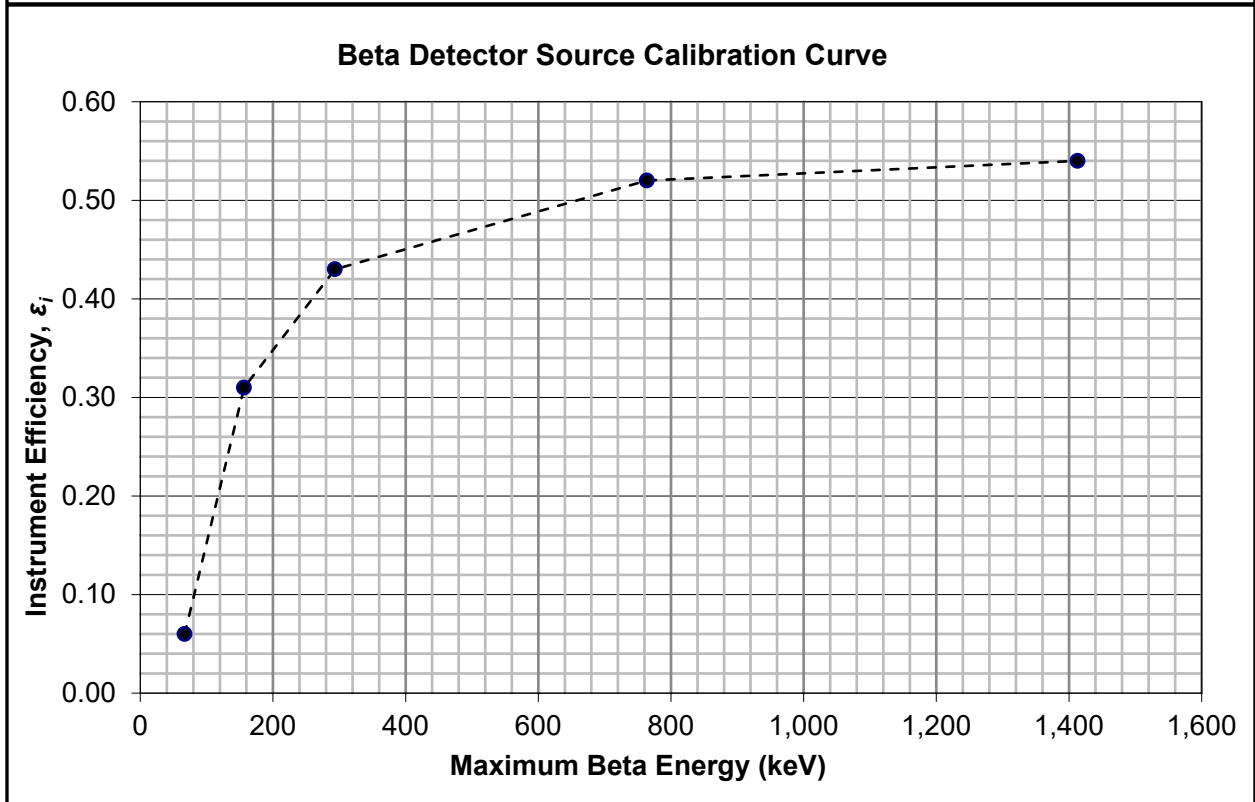
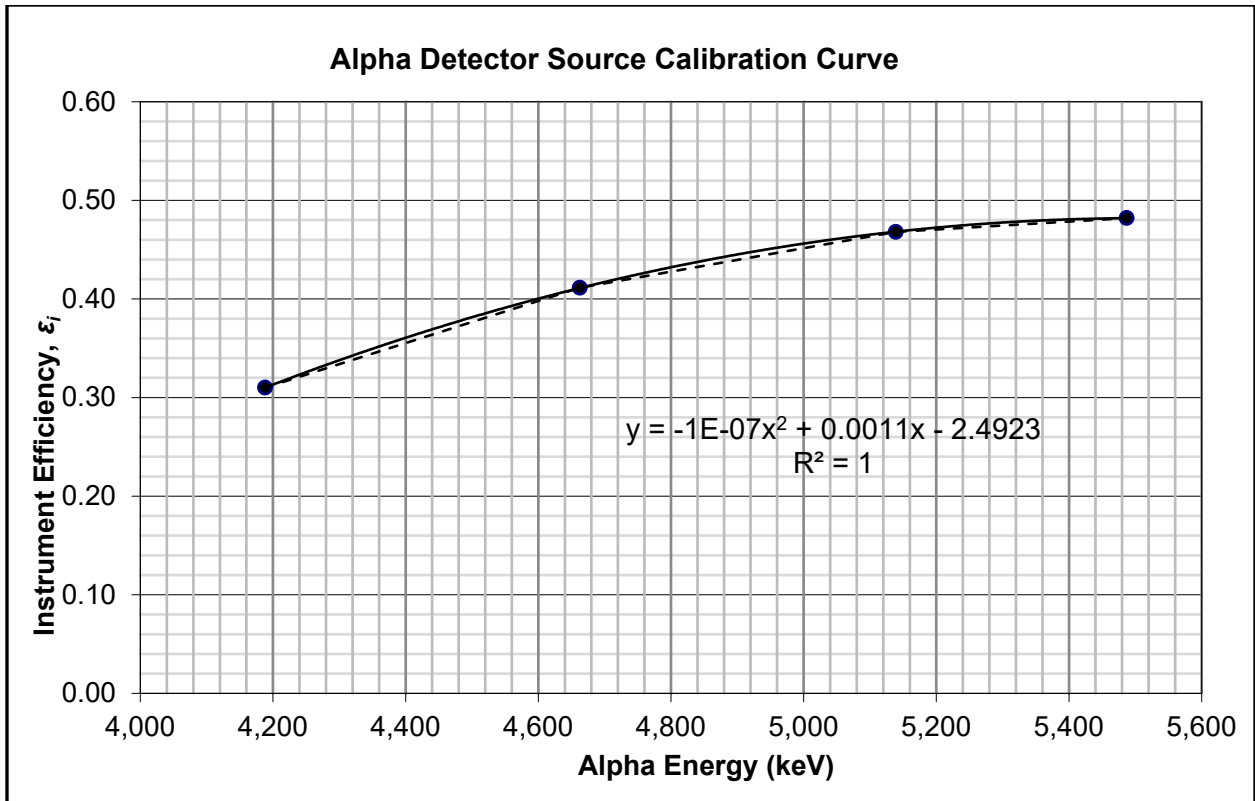


Figure A-18 Exhibit 7a. Processed U Tailings, Alpha Plus Beta, Gas Proportional Detector

**Table A-35 Exhibit 7b. Processed U Tailings, Beta-Only, GM Detector**

**Ratemeter/Scaler Model:** 2221  
**Detector Model:** 44-9  
**Mylar (mg/cm<sup>2</sup>):** 1.7  
**Voltage Setting (volts):** 900  
**Measured Radiation Type:** β

| Worksheet Results                      |           |
|--|-----------|
| Reported Result:                       | Gross α+β |
| Total Efficiency (Σ ε <sub>t</sub> ):  | 0.08      |
| Static MDC (dpm/100 cm <sup>2</sup> ): | 3,187     |
| Scan MDC (dpm/100 cm <sup>2</sup> ):   | 7,843     |

| Instrument Calibration Data, Source, and MDC Inputs |           |                           |                           |                |  |  |  |  |
|---|-----------|---------------------------|---------------------------|----------------|--|--|--|--|
| Standard Source Inputs                              |           |                           |                           |                | Static and Scan MDC Inputs   |  |  |  |
| Nuclide   | Radiation | Mean E (keV) <sup>a</sup> | Max. E (keV) <sup>a</sup> | ε <sub>i</sub> |  |  |  |  |
| U-238   | Alpha     | 4,188                     | N/A                       | 0.00           | Background (R <sub>b</sub> ) (cpm): 60   |  |  |  |
| Th-230  | Alpha     | 4,663                     | N/A                       | 0.00           | Probe Area (cm <sup>2</sup> ): 15.5  |  |  |  |
| Pu-239  | Alpha     | 5,139                     | N/A                       | 0.00           | Count Time (t) (min): 1  |  |  |  |
| Am-241  | Alpha     | 5,487                     | N/A                       | 0.00           | Observation Interval (i) (sec): 2  |  |  |  |
| Ni-63   | Beta      | 17.4                      | 66.9                      | 0.00           | Index of Sensitivity (d') (unitless): 1.96   |  |  |  |
| C-14  | Beta      | 49.5                      | 156                       | 0.14           | Surveyor Efficiency (p) (unitless): 0.75   |  |  |  |
| Tc-99   | Beta      | 84.6                      | 294                       | 0.28           | Static MDC = $\frac{3+4.65\sqrt{R_b \times t}}{t \times \epsilon_t \times \frac{Probe\ Area}{100}}$<br><br>Scan MDC = $\frac{d' \times \sqrt{R_b \times (i/60)} \times (60/i)}{\sqrt{p} \times \epsilon_t \times \frac{Probe\ Area}{100}}$ |  |  |  |
| Tl-204  | Beta      | 244                       | 764                       | 0.45           |  |  |  |  |
| Sr/Y-90   | Beta      | 565                       | 1,413                     | 0.59           |  |  |  |  |

| Weighted Efficiency Input/Output Table |                 |                 |                           |                           |                   |                |                |                             |
|--|-----------------|-----------------|---------------------------|---------------------------|-------------------|----------------|----------------|-----------------------------|
| Nuclide                                | Half-Life (yrs) | Total Intensity | Mean E (keV) <sup>a</sup> | Max. E (keV) <sup>a</sup> | Relative Fraction | ε <sub>i</sub> | ε <sub>s</sub> | ε <sub>t</sub> <sup>b</sup> |
| <b>Beta Emitters</b>                   |                 |                 |                           |                           |                   |                |                |                             |
| Th-234                                 | 6.60E-02        | 1.00            | 47.8                      | 178                       | 0.0068            | 0.16           | 0.25           | 0.00                        |
| Pa-234                                 | 2.21E-06        | 1.00            | 809                       | 2,240                     | 0.0068            | 0.59           | 0.50           | 0.00                        |
| Th-231                                 | 2.91E-03        | 1.00            | 78                        | 283                       | 0.0003            | 0.26           | 0.25           | 0.00                        |
| Pb-214                                 | 5.10E-05        | 1.00            | 225                       | 719                       | 0.0972            | 0.44           | 0.50           | 0.02                        |
| Bi-214                                 | 3.79E-05        | 1.00            | 639                       | 1,770                     | 0.0972            | 0.59           | 0.50           | 0.03                        |
| Pb-210                                 | 2.22E+01        | 1.00            | 6                         | 24                        | 0.0972            | 0.00           | 0.25           | 0.00                        |
| Bi-210                                 | 1.37E-02        | 1.00            | 389                       | 1,160                     | 0.0972            | 0.54           | 0.50           | 0.03                        |
|  |                 |                 |                           |                           |                   |                |                |                             |
|  |                 |                 |                           |                           |                   |                |                |                             |
|  |                 |                 |                           |                           |                   |                |                |                             |
| <b>Alpha Emitters</b>                  |                 |                 |                           |                           |                   |                |                |                             |
| U-238                                  | 4.47E+09        | 1.00            | 4,188                     | N/A                       | 0.0068            | 0.00           | 0.25           | 0.00                        |
| U-234                                  | 2.46E+05        | 1.00            | 4,759                     | N/A                       | 0.0068            | 0.00           | 0.25           | 0.00                        |
| U-235                                  | 7.04E+08        | 1.00            | 4,431                     | N/A                       | 0.0003            | 0.00           | 0.25           | 0.00                        |
| Th-230                                 | 7.54E+04        | 1.00            | 4,663                     | N/A                       | 0.0972            | 0.00           | 0.25           | 0.00                        |
| Ra-226                                 | 1.60E+03        | 1.00            | 4,773                     | N/A                       | 0.0972            | 0.00           | 0.25           | 0.00                        |
| Rn-222                                 | 1.05E-02        | 1.00            | 5,485                     | N/A                       | 0.0972            | 0.00           | 0.25           | 0.00                        |
| Po-214                                 | 5.19E-12        | 1.00            | 7,686                     | N/A                       | 0.0972            | 0.00           | 0.25           | 0.00                        |
| Po-210                                 | 3.79E-01        | 1.00            | 5,304                     | N/A                       | 0.0972            | 0.00           | 0.25           | 0.00                        |
| Po-218                                 | 5.89E-06        | 1.00            | 6,001                     | N/A                       | 0.0972            | 0.00           | 0.25           | 0.00                        |

<sup>a</sup>Excludes emission intensities < 0.1%; mean and maximum energies weighted based on emission intensity.

<sup>b</sup>Total efficiency per nuclide is Total Intensity × Relative Fraction × ε<sub>i</sub> × ε<sub>s</sub>.

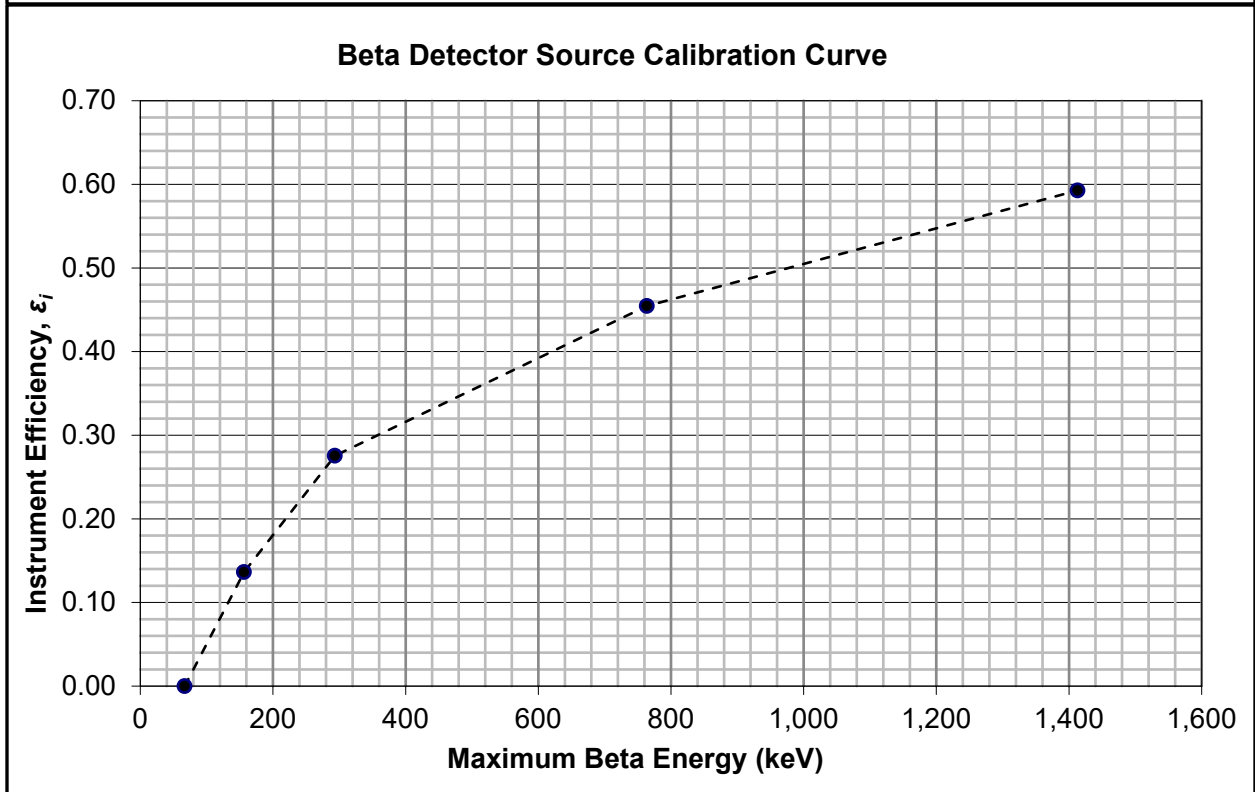
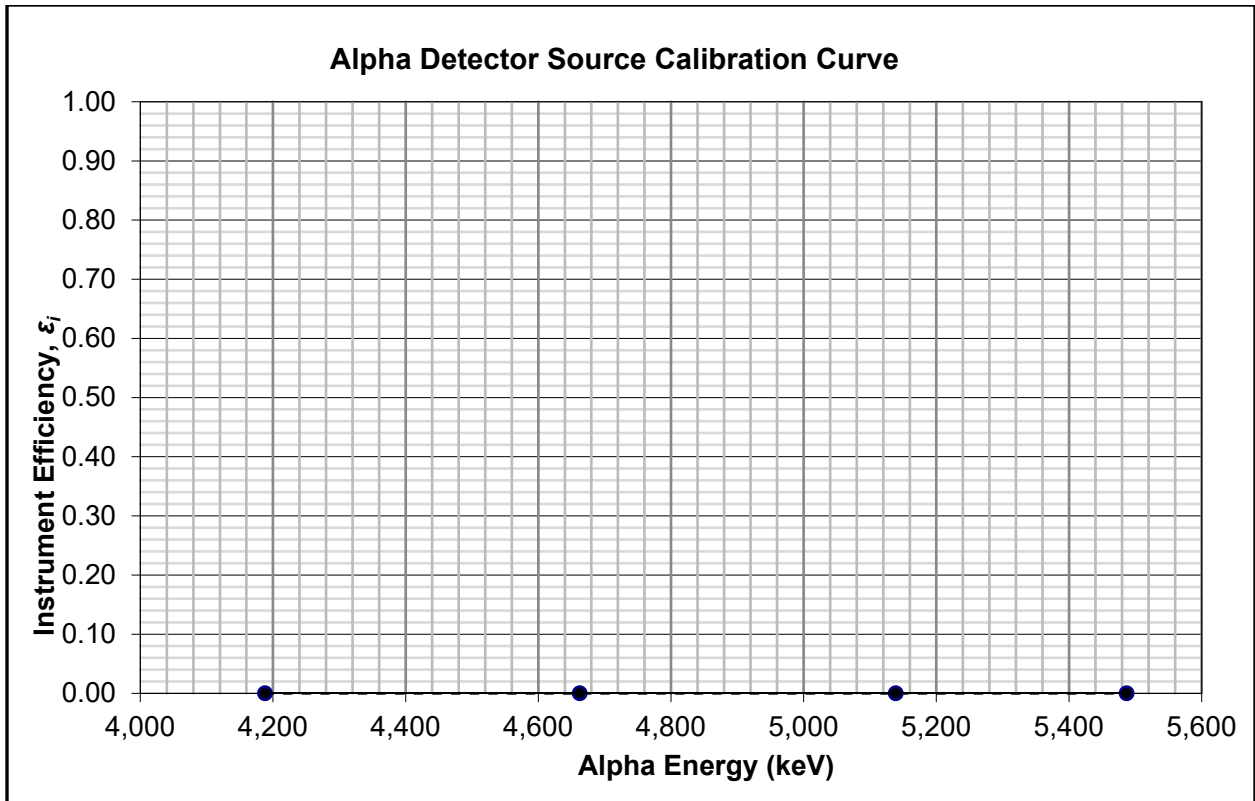
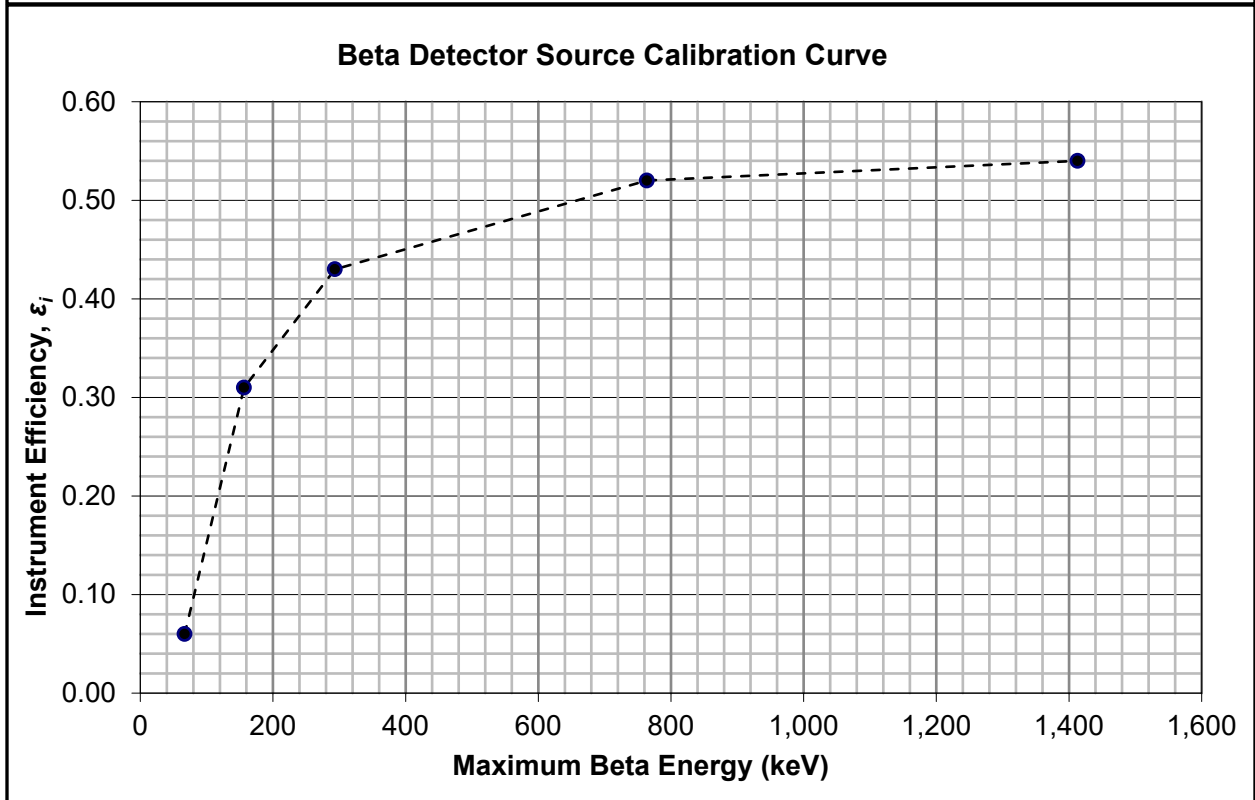
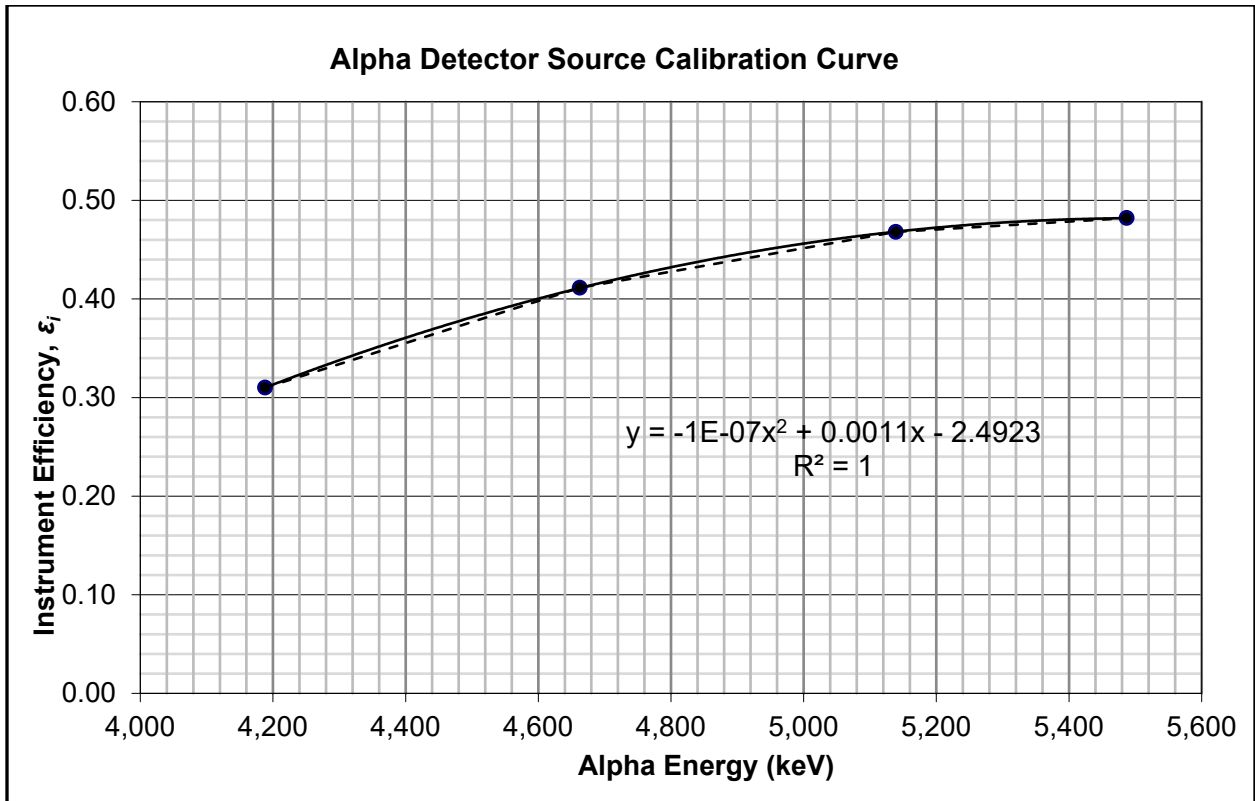


Figure A-19 Exhibit 7b. Processed U Tailings, Beta-Only, GM Detector





**Figure A-20 Exhibit 8a. Ra-226 Plus Decay Series, Alpha Plus Beta, Gas Proportional Detector**



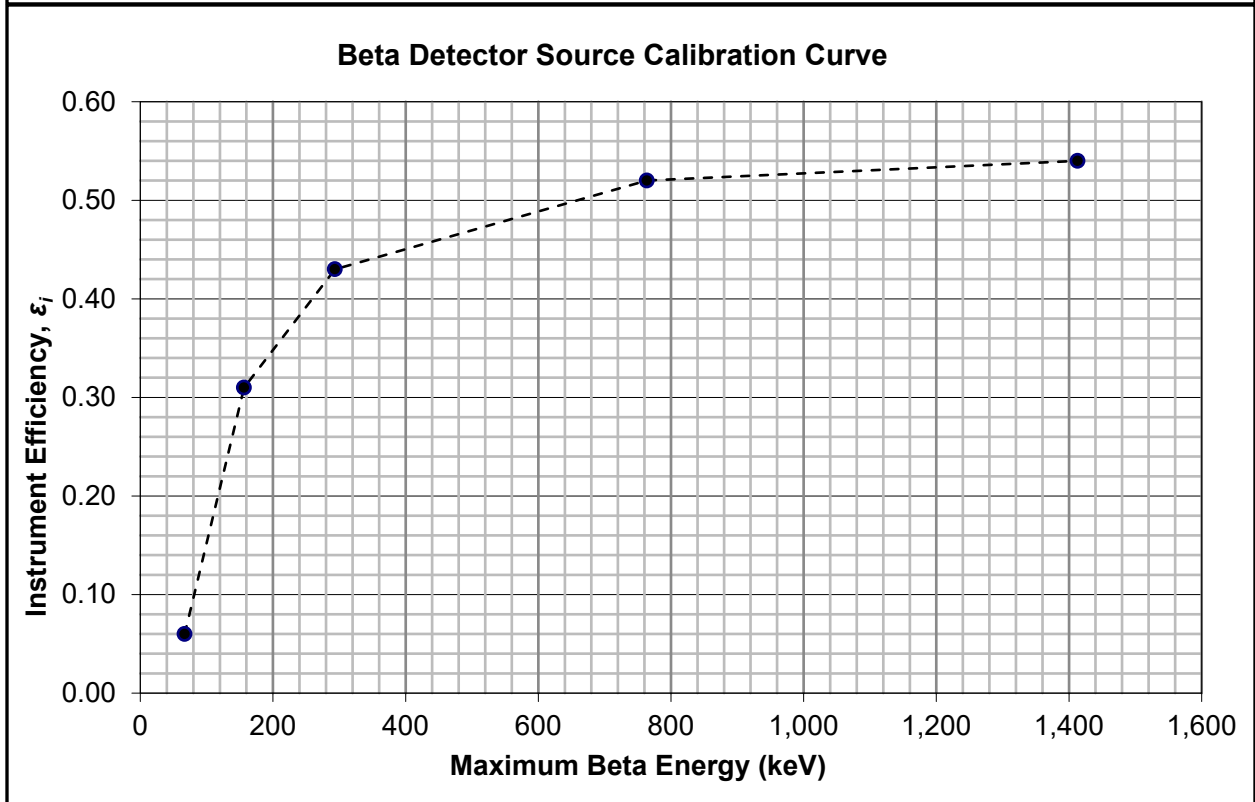
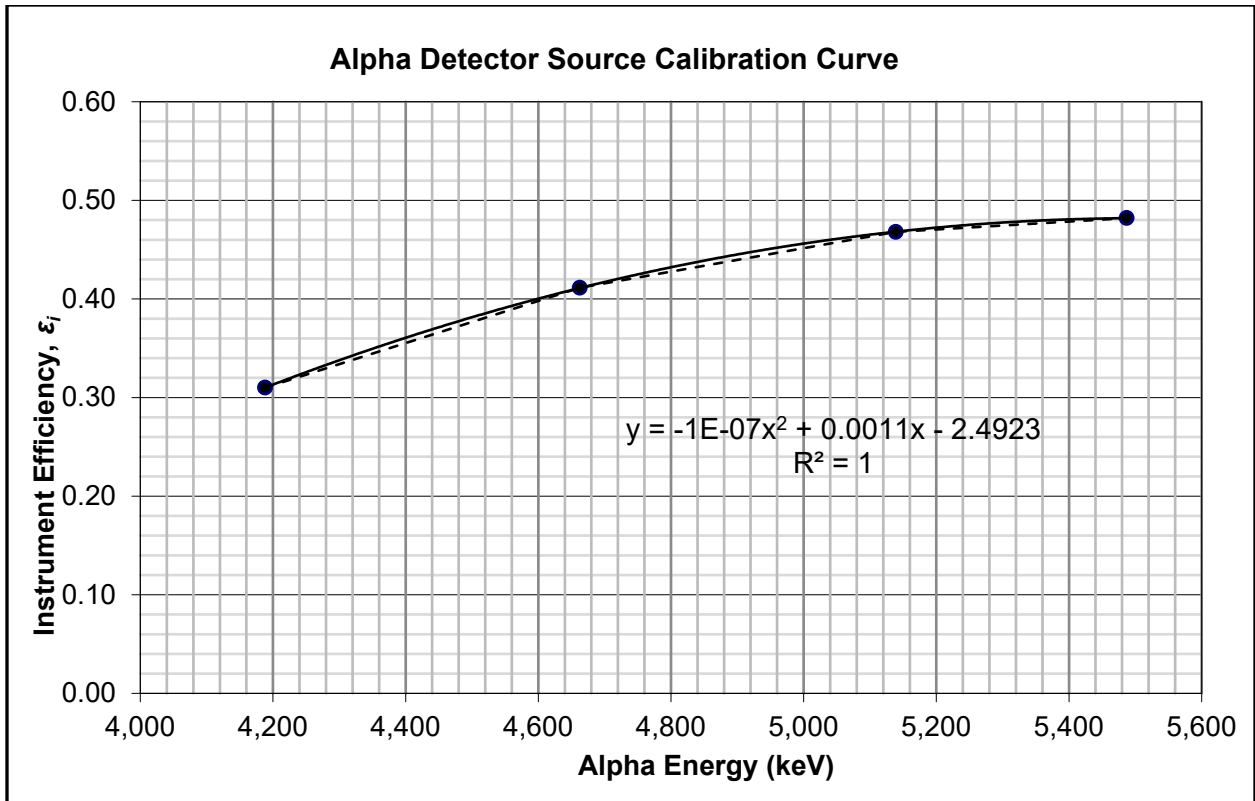


Figure A-21 Exhibit 8b. Ra-226 Plus Decay Series, Alpha Plus Beta, Gas Proportional Detector





**BIBLIOGRAPHIC DATA SHEET**

*(See instructions on the reverse)*

**NUREG-1507, Rev. 1**

2. TITLE AND SUBTITLE

**Minimum Detectable Concentrations with Typical Radiation Survey  
Instruments for Various Contaminants and Field Conditions**

3. DATE REPORT PUBLISHED

| MONTH         | YEAR        |
|---------------|-------------|
| <b>August</b> | <b>2020</b> |

4. FIN OR GRANT NUMBER

5. AUTHOR(S)

E.W. Abelquist, D.A. King, T.J. Vitkus – Oak Ridge Associated  
Universities  
J.P. Clements, A.M. Huffert, B.A. Watson – U.S. Nuclear Regulatory  
Commission

6. TYPE OF REPORT

Technical

7. PERIOD COVERED (Inclusive Dates)

8. PERFORMING ORGANIZATION - NAME AND ADDRESS (If NRC, provide Division, Office or Region, U. S. Nuclear Regulatory Commission, and mailing address; if contractor, provide name and mailing address.)

Division of Decommissioning, Uranium Recovery and Waste Programs  
Office of Nuclear Material Safety and Safeguards  
U.S. Nuclear Regulatory Commission  
Washington, D.C. 20555-0001

9. SPONSORING ORGANIZATION - NAME AND ADDRESS (If NRC, type "Same as above", if contractor, provide NRC Division, Office or Region, U. S. Nuclear Regulatory Commission, and mailing address.)

Division of Decommissioning, Uranium Recovery and Waste Programs  
Office of Nuclear Material Safety and Safeguards  
U.S. Nuclear Regulatory Commission  
Washington, D.C. 20555-0001

10. SUPPLEMENTARY NOTES

11. ABSTRACT (200 words or less)

This document describes and quantitatively evaluates the effects of various factors on the detection sensitivity of commercially available portable field instruments being used to conduct radiological surveys in support of decommissioning. Dose-based criteria, used for compliance with 10 CFR Part 20, Subpart E, are often expressed as concentration-based screening values for structural surface contamination in units of disintegrations per minute per 100 square centimeters and for surface soil contamination in units of picocuries per gram. As described in NUREG 1575, Revision 1, "Multi-Agency Radiation Site Survey and Investigation Manual (MARSSIM)," issued August 2000, radiological survey instruments are used to measure radiation levels that are then directly compared to the release criteria.

Since publication of the original NUREG-1507 in 1998, licensees have increasingly used additional survey instrumentation and data capture tools, including global positioning system (GPS) and geographic information system (GIS) technologies. Survey techniques and calculation methodologies have changed over the interim period along with the introduction of advanced radiation survey instruments. This report introduces some concepts related to these techniques and methodologies along with considerations for detection efficiency calculations, background interferences, signal degradation, and other topics associated with radiation survey instrumentation.

12. KEY WORDS/DESCRIPTORS (List words or phrases that will assist researchers in locating the report.)

Survey Instruments, Radiological Surveys, Decommissioning, MARSSIM, Minimum Detectable Concentration

13. AVAILABILITY STATEMENT

unlimited

14. SECURITY CLASSIFICATION

*(This Page)*

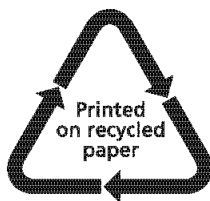
unclassified

*(This Report)*

unclassified

15. NUMBER OF PAGES

16. PRICE



Federal Recycling Program



UNITED STATES  
NUCLEAR REGULATORY COMMISSION  
WASHINGTON, DC 20555-0001  
OFFICIAL BUSINESS



©NRCgov

**NUREG-1507  
Revision 1**

**Minimum Detectable Concentrations with Typical Radiation Survey  
Instruments for Various Contaminants and Field Conditions**

**August 2020**